



HAL
open science

Modulation of Inflammation in Intestinal Epithelial and Immune Cells by N-Acyl Homoserine Lactones and their Synthetic Analogues

Agathe Peyrottes

► **To cite this version:**

Agathe Peyrottes. Modulation of Inflammation in Intestinal Epithelial and Immune Cells by N-Acyl Homoserine Lactones and their Synthetic Analogues. Hépatology and Gastroenterology. Sorbonne Université, 2019. English. NNT : 2019SORUS315 . tel-03400306

HAL Id: tel-03400306

<https://theses.hal.science/tel-03400306>

Submitted on 25 Oct 2021

HAL is a multi-disciplinary open access archive for the deposit and dissemination of scientific research documents, whether they are published or not. The documents may come from teaching and research institutions in France or abroad, or from public or private research centers.

L'archive ouverte pluridisciplinaire **HAL**, est destinée au dépôt et à la diffusion de documents scientifiques de niveau recherche, publiés ou non, émanant des établissements d'enseignement et de recherche français ou étrangers, des laboratoires publics ou privés.

Sorbonne Université

École doctorale 394 – Physiologie, Physiopathologie et Thérapeutique

Thèse de doctorat de Sorbonne Université - Programme Interfaces Pour le Vivant

Présentée et soutenue publiquement le 23 Octobre 2019 par

Agathe Peyrottes

Centre de Recherche St Antoine UMRS938 - Équipe Microbiote, Intestin et Inflammation

Laboratoire des Biomolécules UMR7203 - Équipe Peptides, glycoconjugués et métaux en biologie

Modulation of Inflammation in Intestinal Epithelial and Immune Cells by *N*-Acyl Homoserine Lactones and their Synthetic Analogues

Dirigée par le Dr. Jean-Pierre Grill et le Dr. Jean-Maurice Mallet

Devant un jury composé de :

Philippe Gérard, Directeur de recherche, Rapporteur

Yves Queneau, Directeur de recherche, Rapporteur

Alexandre Escargueil, Professeur, Président du jury

Christine Gravier-Pelletier, Directeur de recherche, Examineur

Jean-Pierre Grill, Maître de Conférence, Examineur

Jean-Maurice Mallet, Directeur de recherche, Examineur

Remerciements

J'adresse mes sincères remerciements aux membres constituant mon jury de thèse. Le Docteur Philippe Gérard et le Docteur Yves Queneau, qui ont aimablement accepté d'être rapporteurs de ma thèse, malgré leurs nombreuses charges professionnelles.

Le Professeur Alexandre Escargueil, qui me fait l'honneur de présider mon jury de thèse.

Le Docteur Gravier-Pelletier, qui a accepté d'examiner mon travail.

Un immense merci à mes directeurs de thèse, le Docteur Jean-Pierre Grill et le Docteur Jean-Maurice Mallet. Merci pour votre encadrement scientifique de grande qualité, vos conseils et vos encouragements. Merci pour votre disponibilité : j'ai toujours trouvé votre porte ouverte pour discuter et construire ce projet ensemble. Merci enfin pour votre soutien sans faille, car ce projet n'a pas été sans difficulté ni déception, la science n'a pas toujours été tendre, mais vous avez su me convaincre de persévérer ou m'aider à rebondir.

Merci au Professeur Philippe Seksik et au Docteur Sandrine Sagan pour m'avoir accueillie dans leurs équipes de recherche et donné les moyens de mener ce projet.

Je ne saurai assez remercier Loïc Brot pour son aide précieuse. Merci de m'avoir formée et aidée avec persévérance au cours de ces trois années. Tant de résultats n'auraient pu être obtenus sans toi ! Merci également à Garance Coquant pour son aide, ses réflexions pertinentes et son enthousiasme. Avec toi je sais que les AHL n'ont pas dit leur dernier mot !

Je remercie très chaleureusement Laurent Cattiaux, pilier de notre équipe de chimie. Tu accomplis un travail de l'ombre fantastique et toujours avec bonne humeur !

Merci au Docteur Véronique Carrière pour son implication en tant que tutrice et dans mon comité de thèse. Merci pour tous ses conseils et son amour des Caco-2/TC7. Je remercie également le Professeur Solange Lavielle pour sa participation à mes comités de suivi de thèse comme expert scientifique.

Je souhaite remercier tous ceux qui m'ont aidée au cours de ces trois années de thèse et ont collaboré de près ou de loin à ce projet : le Docteur Dominique Rainteau et Lydie Humbert en spectrométrie de masse, qui ont toléré avec bonne humeur mes expériences interminables ; le Docteur Sophie Thenet et Doriane Aguanno, qui m'ont initiée aux mystères de l'imagerie sur cellules fixées, de FIJI et du traitement d'images ; le Docteur Lorraine Montel et le Docteur Jacques Fattaccioli à l'IPGG pour leur aide et leur savoir-faire en imagerie sur cellules vivantes ; le Docteur Olivier Buriez pour ses conseils en voltamétrie cyclique.

Enfin un chaleureux merci à tous les membres passés et présents, permanents ou non, de mes deux laboratoires. Les chimistes : Sylvestre Bachollet, Nicolas Delsuc, Blaise Dumas, Lucas Henry, Manon Isaac, Emilie Mathieu, Pascal Matton, Antonio Mazzoleni, Roxanne Ornstein, et Amandine Vincent. Les biologistes : Luisa De Sordi, Cécilia Landman, Aonghus Lavelle, Sarah Layani, Ingrid Lema, Paul McLellan, Marielle Moreau, Cyriane Oeuvray, Barbara Postal, Elodie Quévrain, Nathalie Rolhion, Marjolène Straube, Elodie Tauziet, Sothea Touch et Margaux Wieckowski. Merci à nos gestionnaires Eliane Moulinié, Karine Gherdi et Valerica Mandrea.

Un tendre merci à mes parents qui m'ont toujours fait confiance et me soutiennent patiemment depuis que j'ai quitté le cocon familial. Merci à mon « petit » frère, mais grand par la taille et le talent ! Je m'efforce d'être un bon exemple, et je suis certaine que tu seras un médecin merveilleux.

Merci Adam, compagnon affectueux et toujours positif, rentré du bout du monde pour de futures aventures.

Pour finir, une pensée à tous ceux partis trop tôt à mon goût, et dont j'espère être digne.

Abstract

IBD are chronic intestinal disorders leading to bowel damages and increased intestinal cancer risk. Their pathogenesis involves many factors : dysregulation of immunity to commensal bacteria and changes in the microbiota composition called dysbiosis. These pathologies are soaring extremely fast.

The importance of host-bacteria dialog has drawn attention to the bacterial communication named Quorum Sensing. Driven by *N*-acyl-homoserine lactones (AHL) in Gram-negative bacteria, QS had never been studied in the human gut microbiota. Our team identified up to 14 AHL through LC-MS/MS, among which a doubly unsaturated AHL of formula 3oxoC₁₂:2-HSL. This AHL correlated to patients' IBD status : healthy controls and patients in remission exhibited high levels, while patients with active disease showed no or little amounts of the biomarker. It has otherwise been shown that a natural AHL of close structure (3oxoC₁₂-HSL) can interfere with inflammation in mammalian epithelial and immune cells. Its mechanism of action remains yet unknown.

Using the natural 3oxoC₁₂-HSL as a template, we studied the effects, stability and metabolism of the two AHL on intestinal epithelial cells, macrophages and bacteria strains. To explore further their mechanism of action we developed several tagged-molecules for cell imaging and pull-down assays.

Finally, we performed a Structure-Activity-Relationship study to evaluate the impact of chemical modifications on the biological activity of natural AHL and the patterns retaining anti-inflammatory activity. This study highlighted several improved analogues.

Résumé

Les MICI sont caractérisées par l'inflammation chronique de l'épithélium intestinal et mettent en jeu des facteurs multiples : environnement, prédisposition génétique, perturbations immunitaires et déséquilibre du microbiote appelé dysbiose. Leur prévalence a fortement augmenté au cours des dernières décennies.

L'importance de la relation hôte-microbiote implique le mode de communication bactérienne appelé *Quorum Sensing*. Basé sur les *N*-Acyl Homoserine Lactones (AHL) chez les bactéries Gram négatif, celui-ci n'avait jamais été étudié dans le microbiote intestinal humain. Notre équipe a identifié par LC/MS 14 AHL dans des échantillons fécaux, dont une AHL insaturée (3oxoC₁₂:2-HSL). Celle-ci montre des corrélations avec le statut médical du donneur car présente chez les donneurs sains et les patients en rémission, mais significativement diminuée ou absente chez les malades en poussée.

En parallèle, il est connu qu'une AHL de structure proche (3oxoC₁₂-HSL) peut moduler la réponse inflammatoire et immunitaire de l'hôte. Néanmoins son mécanisme d'action reste encore incertain.

En utilisant la 3oxoC₁₂-HSL comme modèle, nous avons étudié les effets biologiques, la stabilité et le métabolisme des deux AHLs dans des cellules épithéliales de l'intestin, des cellules immunitaires et des souches bactériennes. Afin d'explorer plus en avant leur mécanisme d'action, nous avons développé des molécules marquées pour l'imagerie et la recherche de récepteurs.

Enfin, nous avons développé des analogues bio-inspirés pour étudier la relation structure-effets des AHL. Cette étude a mis en évidence plusieurs analogues plus actifs que les molécules naturelles.

List of Abbreviations

2-HQ : 2-hydroxyquinoline (PON inhibitor)

5-FITC : Fluorescein 5-isothiocyanate

5-FTSC : Fluorescein 5-thiosemicarbazide

5-HL : 5-hydroxy-6*E/Z*,11*Z*,14*Z*-eicosatetraenoic acid, 1,5-lactone

Acac : Acetylacetone

AcCN (or MeCN) : acetonitrile

ACH : Aminocyclohexanol

AcOH : Acetic acid

ACP : Acyl-acyl carrier protein

AHL : *N*-Acyl Homoserine Lactone

AI : Auto-Inducer

AIEC : Adherent-invasive *E. coli*

AIP : Auto-inducing peptide

AJ : Adherent junction

AP-2 : Adaptor protein 2

AQP : Aquaporin

a.u. : arbitrary units

BCA assay : Bicinchoninic Acid assay (also known as Smith assay)

BMDM : Bone-marrow derived macrophage

Boc : *tert*-butyloxycarbonyl protecting group

BSA : Bovine Serum Albumin

CAI : Cholerae autoinducer

Caspase : Cysteine-**asp**artic proteases

CD : Crohn's Disease

Cox : Cyclooxygenase

CSP : Competence stimulating peptide

CuAAC : Copper-catalysed azide-alkyne cycloaddition

Cyhex : Cyclohexane

DABCO : 1,4-diazabicyclo[2.2.2]octane

DAPI : 4',6-diamidino-2-phenylindole

DC : Dendritic cell

DCC : *N,N'*-Dicyclohexylcarbodiimide

DCF : 2',7'-dichlorofluorescein

ESI : Electrospray ionisation

H₂-DCF : 2',7'-dichlorodihydrofluorescein

H₂-DCFDA : 2',7'-dichlorodihydrofluorescein diacetate

DCM : Dichloromethane

DIPEA (or DIEA) : *N,N*-Diisopropylethylamine

DKP : Diketopiperazine

DMAP : 4-Dimethylaminopyridine

DMEM : Dulbecco's Modified Eagle's minimum essential Medium also known as Dulbecco's Modified Eagle's Medium

DMF : Dimethylformamide

DMSO : Dimethyl sulfoxide

DNA / cDNA : Deoxyribonucleic acid / coding Deoxyribonucleic acid

DPBS : Dulbecco's phosphate buffer saline

EDC : 1-Ethyl-3-(3-dimethylaminopropyl)carbodiimide

EDTA : Ethylene-diamine-tetraacetic acid

ELISA : Enzyme Linked Immunosorbent Assay

Equiv : Equivalent

ER : Endoplasmic reticulum

Et₃N : Triethylamine

EtOAc : Ethyl Acetate

EtOH : Ethanol

FCS : Foetal Calf Serum

FITC : Fluorescein isothiocyanate

FISH : Fluorescent *In Situ* Hybridization

FSTC : Fluorescein thiosemicarbazide

GAPDH : Glyceraldehyde 3-phosphate dehydrogenase

GI : Gastro-intestinal

GM-CSF : Granulocyte-macrophage colony-stimulating factor

GPCR : G-protein coupled receptor

GTP : Guanosine-5'-triphosphate

HATU : 1-[Bis(dimethylamino)methylene]-1H-1,2,3-triazolo[4,5-b]pyridinium 3-oxide hexafluorophosphate, Hexafluorophosphate Azabenzotriazole Tetramethyl Uronium

HAQ : 4-hydroxy-2-alkylquinolines

HHQ : 4-hydroxy-2-heptylquinoline

HPLC : High Performance Liquid Chromatography

HRP : Horseradish peroxidase

HS : Homoserine

HSL : Homoserine Lactone

HTH domain : Helix-Turn-Helix domain

HTL : Homoserine-thiolactone

IBD : Inflammatory Bowel Disease

IL : Interleukin

IFN- γ : Interferon gamma

IP3 : Inositol triphosphate

IQGAP1 : Ras GTPase-Activating-like Protein (also known as p195)

JAM : Junctional adhesion molecule

KO : Knock-out

LB medium : Lysogeny Broth or Luria-Bertani medium

LC : Liquid Chromatography

LDH : Lactate dehydrogenase

LogP : Partition coefficient between 1-octanol and water

LPS : Lipopolysaccharide

MAPK (or MAP kinases) : Mitogen-activated protein kinases

MEF : Mouse embryonic fibroblasts

MeOH : Methanol

MIP : Macrophage inflammatory protein

MS : Mass Spectrometry

NaAscb : Sodium ascorbate

NADH : Nicotinamide adenine dinucleotide

NBD : Nitrobenzofurazan *aka* 7-nitro-1,2,3-benzoxadiazole

NBD-Cl : 4-chloro-7-nitro-1,2,3-benzoxadiazole

NEAA : Non-Essential Amino Acids

NFκB : Nuclear factor kappa B

NHS : *N*-Hydroxysuccinimide

NMR : Nuclear magnetic resonance

NOD2 : Nucleotide-binding oligomerisation domain 2

PAMP : Pathogen-associated molecular pattern

PARP : Poly(ADP-ribose) polymerase

PBMC : Peripheral blood mononuclear cell

PBS : Phosphate Buffer Solution or Saline

PCR : Polymerase Chain Reaction

qPCR: Quantitative PCR

PFA : *para*formaldehyde

PGE : Prostaglandin

PON: Paraoxonase

PPAR : Peroxisome proliferator-activated receptor

ppm : Parts per million

PQS : Pseudomonas Quinolone signal

PRR : Pathogen recognition receptor

QQ : Quorum quenching

QS : Quorum sensing

ROS : Reactive oxygen species

r.t. : room temperature

RT-PCR : Real-Time PCR

SAM : S-adenosyl methionine

SCFA : Short-chain fatty acid

SEM : Standard error to the mean

T2R38 : Taste Receptor 2 Member 38

TA : Tetramic Acid

TBA-BF₄ : Tetrabutylammonium tetrafluoroborate

TER : Transepithelial resistance

TFA : Trifluoroacetic acid

TJ : Tight junction

TLC : Thin layer chromatography

TLR : Toll-like receptor

TMB : Tetramethylbenzidine

TNF- α : Tumor necrosis factor alpha

TPSA : Topological polar surface area

UC : Ulcerative Colitis

WT : Wild-type

ZO-1 : Zonula occludens 1

Table of Contents

REMERCIEMENTS	I
ABSTRACT	5
RESUME.....	6
LIST OF ABBREVIATIONS	7
INTRODUCTION	16
1. INFLAMMATORY BOWEL DISEASES : AN INTRODUCTION	16
1.1. General description of IBD.....	16
1.2. Pathophysiology of Inflammatory Bowel Diseases.....	19
1.2.1. Genetic factors in IBD.....	19
1.2.2. Environmental factors in IBD.....	22
1.2.3. IBD and microbiota : a complex interplay.....	23
1.2.3.1. Healthy or normal gut microbiota.....	23
1.2.3.2. Role of the microbiota	27
1.2.3.3. Characterising the intestinal dysbiosis in Inflammatory Bowel Diseases.....	28
2. INTRODUCTION TO MICROBIOLOGY AND ITS RELATION TO THE HUMAN GUT ECOSYSTEM.....	30
2.1. The Quorum Sensing.....	30
2.1.1. Discovery and main characteristics of the Quorum Sensing	31
2.1.1.1. General mechanism(s) of the bacterial QS	31
2.1.1.2. The Quorum System of <i>Vibrio fischeri</i> : a paradigm for LuxI/LuxR-type quorum sensing systems	32
2.1.2. Overview of QS signaling molecules	34
2.1.2.1. Type-1 autoinducers (AI-1).....	34
2.1.2.2. Type-2 autoinducers (AI-2).....	36
2.1.2.3. Type 3 autoinducers (AI-3).....	38
2.1.2.4. Other signaling molecules in Quorum Sensing.....	38
2.1.2.4.1. Cholerae autoinducer (CAI)	38
2.1.2.4.2. 3-hydroxy palmitic acid methyl ester (3OH-PAME).....	39
2.1.2.4.3. The Pseudomonas Quinolone Signal (PQS).....	39
2.1.2.4.4. The Diketopiperazines (DKP).....	40
2.1.2.4.5. The γ -butyrolactone	41
2.1.2.4.6. Auto-inducing peptides (AIP).....	42
2.1.2.5. Summary table of presented QS molecules	42
2.1.3. Interspecies Communication and Signaling	43
2.2. Interkingdom Signaling : Effects of N-Acyl Homoserine Lactones on Eukaryotic cells.....	44
2.2.1. AHL penetration into cells.....	44
2.2.2. Apoptosis.....	45
2.2.3. Immunomodulatory effects and inflammation	46
2.2.3.1. 3oxoC ₁₂ -HSL is a chemoattractant per se for neutrophils.....	47
2.2.3.2. AHL effects on immune cell functions	48
2.2.3.3. Inflammatory properties on epithelia	50
2.2.4. Morphological changes in cells.....	51
2.2.4.1. Tight and adherent junctions of the gut epithelium.....	51
2.2.4.2. Cell migration and wound healing	52
2.2.5. Quorum quenching.....	53
2.2.6. AHL receptors	55
2.3. State of the art in our laboratory.....	57
2.3.1. Are there AHLs in the intestinal ecosystem?	58
2.3.2. Objectives of the project.....	60

MATERIALS AND METHODS	61
1. EXPERIMENTAL PROCEDURES AND PROTOCOLS EMPLOYED IN BIOLOGY	61
1.1. Cell culture	61
1.1.1. The Caco-2/TC7 cell line	61
1.1.2. The Raw 264.7 cell line	62
1.1.3. The bacterial reporter strain <i>E. coli</i> pSB1075	63
1.1.4. Bactericidal assay	64
1.2. Evaluation of the biological activity of molecules in mammal cells	64
1.2.1. Caco-2/TC7 stimulation with cytokines	64
1.2.2. Raw 264.7 stimulation with LPS and IFN- γ	65
1.2.3. Measurement of protein concentration in cell lysate	65
1.2.4. Human cytokines quantification by ELISA	65
1.2.5. Quantification of murine cytokines	66
1.2.6. Cytotoxicity assay	66
1.3. RNA extraction, Reverse transcription and Quantitative PCR	67
1.4. Biological activity of molecules on bacterial reporter strain <i>E. coli</i> pSB1075	69
1.5. Immunofluorescence experiments	69
1.5.1. Fixed-cells imaging	69
1.5.2. Live-cell imaging	70
1.6. Reactive Oxygen Species production in Caco-2/TC7 cells	70
1.7. Statistical analysis	70
2. MASS SPECTROMETRY : TANDEM LC/MS-MS	71
2.1. Evaluation of AHL half-life in cell culture medium at 20°C	71
2.2. Cell preparation for assessment of kinetics of AHL entry in cells	71
2.3. AHL detection by tandem HPLC-MS/MS	72
3. MATERIAL AND METHODS IN CHEMISTRY	74
3.1. Convention for atom numbering in <i>N</i> -acyl homoserine lactones and their analogues	74
3.2. Experimental procedures for synthesis and physicochemical characterization of natural AHLs, intermediates and non-natural analogues	74
3.3. Synthetic procedures for the preparation of AHL probes	99
4. ANALYTICAL TECHNIQUES	109
4.1. Electrochemistry and cyclic voltammetry	109
4.2. Spectrometry	110
4.3. Molecule characterisation (NMR, MS and HRMS)	110
PART I : BIOLOGICAL STUDIES OF TWO NATURAL <i>N</i>-ACYL HOMOSERINE LACTONES.....	112
1. DESCRIPTION AND PREPARATION OF THE MOLECULES	112
1.1. The saturated 3oxoC ₁₂ -HSL	112
1.2. The unsaturated 3oxoC _{12:2} -HSL	113
2. COMPARED BIOLOGICAL EFFECTS AND PROPERTIES OF THE MOLECULES	115
2.1. Results on our biological models	115
2.1.1. Establishment of stimulation protocols	115
2.1.2. Natural AHLs can modulate the secretion of pro-inflammatory cytokines in Caco-2/TC7 and Raw 264.7 cell lines	118
2.1.2.1. Caco-2/TC7 and Raw 264.7 cells have different tolerances towards AHLs in range 1-100 μ M	118
2.1.2.2. AHLs have a bi-modal action over IL-8 secretion by Caco-2/TC7 cells	120
2.1.2.3. Timing and chronology in AHL treatments	122
2.1.2.4. AHLs have mild effects on IL-6 secretion by Raw 264.7 cells	125
2.1.2.5. Other pro-inflammatory cytokines : IL-1 β and TNF- α	126
2.1.3. No mRNA modulation is observed in Caco-2/TC7 cells submitted to AHLs	128
2.1.4. AHLs and secretion of anti-inflammatory cytokines	128
2.1.5. AHLs and bacteria	130
2.1.6. Discussion	132
2.2. Stability & metabolism of AHLs	136

2.2.1.	Degradation of AHLs in biological media	136
2.2.1.1.	AHLs are degraded into two major by-products	136
2.2.1.2.	pH-dependent stability in biological medium	137
2.2.1.3.	Biological study of tetramic acid from the 3oxoC ₁₂ -HSL	139
2.2.2.	Enzymatic degradation and extracellular metabolism of AHLs	142
2.2.2.1.	PON mRNA expression in the studied cell lines	142
2.2.2.2.	Influence of the inhibition of Paraoxonases on AHL effects	145
2.2.3.	Intracellular AHL metabolism : entry and cellular fate	152
2.2.4.	Hydrolysed AHLs and bacteria	157
2.2.5.	Discussion	160
2.3.	<i>Insight into the AHL mechanism of action : cell imaging and receptor investigation</i>	162
2.3.1.	Mapping AHLs in epithelial intestinal cells	162
2.3.1.1.	Use of a commercially available fluorescent molecule	162
2.3.1.2.	Development and evaluation of new molecules	170
2.3.1.2.1.	Development of a clickable AHL	170
2.3.1.2.2.	The nitrobenzofurazan: a smaller fluorescent probe	174
2.3.1.2.3.	Design of potentially fixable naphthalimide-based fluorescent probes	178
2.3.1.3.	Conclusions on cell-imaging	185
2.3.2.	Design of a biotin-tagged AHL	188
2.4.	<i>AHL, Reactive oxygen species and iron</i>	191

PART II : STRUCTURE ACTIVITY RELATIONSHIP STUDY & PHARMACOMODULATION..... 197

1.	CONSTRUCTION OF A LIBRARY OF SYNTHETIC NATURAL AND NON-NATURAL COMPOUNDS	197
1.1.	<i>Natural N-Acyl-Homoserine Lactones</i>	198
1.2.	<i>Introduction to AHLs non-natural analogues</i>	200
2.	STRUCTURE ACTIVITY RELATIONSHIP STUDY	203
2.1.	<i>Compared results on mammalian cell lines</i>	203
2.1.1.	Importance of the keto group	203
2.1.2.	Importance of the acyl chain	206
2.1.2.1.	Shorter acyl chains	206
2.1.2.2.	Longer acyl chains	208
2.1.2.3.	Discussion on acyl chain effects	209
2.1.3.	Importance of the cyclic headgroup	211
2.1.3.1.	Chirality and AHL activity	211
2.1.3.2.	Thiolactones	213
2.1.3.3.	The aminocyclohexanol series	215
2.1.3.4.	Aromatic headgroups	217
2.1.3.4.1.	The methoxy-anilide analogues	217
2.1.3.4.2.	The amino-chlorophenol analogue	219
2.1.3.5.	Miscellaneous : diverse compounds	221
2.1.4.	Discussion on AHL modifications	223
2.2.	<i>Further investigation on two hit candidates</i>	225
2.3.	<i>Development of a dimeric AHL</i>	226
2.4.	<i>Results on bacteria strains</i>	228
2.4.1.	Results on LasR bioassay	229
2.4.1.1.	Ketone effects	229
2.4.1.2.	Influence of the acyl chain length	230
2.4.1.3.	Substitution of the headgroup	231
2.4.2.	Bactericidal properties of selected compounds	232
2.4.3.	Investigation of inhibitors	233
2.4.4.	Discussion on the bacterial properties of the analogue library	235

CONCLUSIONS & PERSPECTIVES 239

LIST OF FIGURES 242

LIST OF SCHEMES 246

LIST OF TABLES	247
REFERENCES	248
ANNEXES	273
<i>A.1. Synthesis</i>	273
<i>A.2. Usual Biochemical Assays</i>	277
<i>A.3. Scientific communications related to this PhD work</i>	279
<i>A.4. NMR characterisation of the 3oxoC₁₂:2-HSL as provided by the commercial supplier DIVERCHIM.</i> ..	290

Introduction

1. Inflammatory Bowel Diseases : an introduction

1.1. General description of IBD

Inflammatory Bowel diseases (IBD) are idiopathic disorders affecting the gastrointestinal tract. During IBD, genetically susceptible patients exhibit an abnormal mucosal immune response to commensal microbiota, response which causes chronic and relapsing inflammation of the gut mucosa. The most prevalent forms of IBD are Crohn's Disease (*CD*) and Ulcerative Colitis (*UC*). IBD are non-life threatening diseases but can significantly alter the patient's quality of life, with a median onset age from 15 to 30 years old.¹

Both IBD subsets are characterised by a chronic and relapsing inflammation of the intestinal mucosa that can evolve into harsh complications and consequences (among which an increased neoplastic risk²). Patients usually undergo disease flare-ups punctuated with remissions phases.^{1,3} Despite common features, these pathologies are two distinguishable diseases (Table 1).

	Crohn's Disease	Ulcerative Colitis
<i>Age (years)</i>	15 - 35	20 – 30 and 50+
<i>Diarrhea</i>	Very frequent	In most
<i>Bleeding</i>	May occur	Very frequent
<i>Mucus</i>	Occurs	Frequent
<i>Pain</i>	Frequent	Variable
<i>Anal lesions</i>	Common	Occasional
<i>Scope appearance</i>	Mucosa inflamed or normal, +/- aphthous ulcers	Mucosa inflamed with oedema, contact bleeding, ulceration
<i>Histology</i>	Transmural inflammation, deep ulceration, fissuring, granuloma, patchy involvement	Mucosal inflammation, Goblet cell depletion, crypt abscess, superficial ulceration

Table 1 - Overview of compared clinical, endoscopic and histological characteristics in patients with IBD

Crohn's disease is generally diagnosed around the age of 25-30 during a first flare up or complication, but it can also be observed in paediatric and geriatric patients (about one sixth of

patients are diagnosed before the age of fifteen). Although a vast majority of cases start in the terminal ileum and the right colon⁴, the disease can literally affect any segment of the digestive tract from mouth to tail end. Clinically, Crohn's disease presents most often with abdominal cramps, diarrhea, delayed growth (in teens), weight loss, fever and anaemia.⁵ Some patients may also develop extra-intestinal presentations such as arthritis or skin lesions.^{6,7} CD is characterised by transmural and discontinuous breaches.⁸ The persisting inflammation can provoke complications including fistulae, abscesses, stricture and stenosis that may require surgical treatment. There a total cumulated risk of 50% at 20 years after diagnosis.⁹⁻¹³ The Montreal index (Table 2) has defined a classification of Crohn's disease according to three criteria that are the age at diagnosis (staged A1 to A3), the localisation of breaches (staged L1 to L3) and the inflammatory phenotype (staged B1 to B3).¹⁴ Approximately one third of patients present L1 stage at diagnosis, one third with L2 and one third with L3-stage, but the phenotype changes throughout the disease's evolution in time.

<i>Age at diagnosis</i>	A1 : below 16 y A2 : between 17 and 40 y A3 : older than 40 y
<i>Localisation of lesions</i>	L1 : ileal L2 : colonic L3 : ileocolonic L4 : isolated upper disease*
<i>Phenotype</i>	B1 : non-stricturing, non-penetrating B2 : structuring B3 : penetrating p : perianal disease modifier#

Table 2 - Montreal Classification for Crohn's Disease

* L4 is a modifier added to L1-L3 when presence of concomitant upper gastrointestinal disease¹⁵. # added to B1-B3 when presence of concomitant perianal disease. Adapted from Satsangi et al.¹⁴

In contrast, Ulcerative Colitis presents as a continuous and uninterrupted colonic mucosal inflammation restricted to the large intestine, that starts at the rectum and extends proximally to the colon.^{1,16,17} Ulcerative Colitis is globally more prevalent than Crohn's disease^{1,18}, and presents with a bimodal pattern of incidence : an onset peak that affects subjects from 15 to 30 years old, and a second smaller peak touching subjects between 50 and 70. Common symptoms in UC are bloody diarrhea mixed with mucus, with or without a rectal syndrome. There is a Montreal classification of extent and severity for ulcerative colitis too, presented in Table 3.¹⁴ Globally, 30% percent of patients present stage E1 UC at diagnosis,

40% stage E2 and the remaining 30% are E3. The lesions and breaches spread out during the course of the disease in 20% of cases.¹⁹

<i>Grading Extent</i>		<i>Anatomy</i>
E1	<i>Ulcerative proctitis</i>	Involvement limited to the rectum
E2	<i>Left sided UC (distal UC)</i>	Involvement limited to a portion of the colorectum distal to the splenic flexure
E3	<i>Extensive UC (pancolitis)</i>	Involvement extends proximal to the splenic flexure
<i>Severity</i>		<i>Definition</i>
S0	<i>Clinical remission</i>	Asymptomatic
S1	<i>Mild UC</i>	Passage of ≤ 4 stools/day (with or without blood), absence of any systemic illness, and normal inflammatory markers (ESR)
S2	<i>Moderate UC</i>	Passage of ≥ 4 stools/day but with minimal signs of systemic toxicity
S3	<i>Severe UC</i>	Passage of ≥ 6 bloody stools/day, pulse rate ≥ 90 beats/min, temperature $\geq 37.5^{\circ}\text{C}$, haemoglobin ≤ 10.5 g/100 ml, and ESR ≥ 30 mm/h

Table 3 - Montreal Classification of extent and severity for Ulcerative Colitis

Adapted from Satsangi et al.¹⁴

In epidemiology, diseases are studied both in terms of prevalence and incidence. The incidence rate regards the number of new cases for a given population and time length, while the prevalence counts the total number of cases for a given population and time length. IBD incidence and prevalence vary greatly from a geographic area to another, with the highest incidence and prevalence rates found in northern Europe and North America.^{1,18} Over the period 1990-2016 the prevalence of IBD exceeded 0.3% of the total population in North America, Oceania and some European countries¹⁸ (over 135.6 cases per 100 000 people for CD in Canada, the USA, Australia, New Zealand, Germany, Hungary, the Netherlands and Scandinavia; over 198 cases per 100 000 people for UC in Canada, the USA, Germany, Hungary, the Netherlands and Scandinavia). Over the same span of time, the incidence for CD exceeded 6.38 cases per 100 000 people-years in the USA, Canada, Australia, the UK, Italy, Hungary, the Netherlands, Denmark, Sweden and Finland, while it exceeded 7.71 cases per 100 000 people-years for UC in the USA, Canada, Australia, the UK, Hungary, the Netherlands, Denmark, Sweden, Norway, Finland and Lithuania.¹⁸ Since 1990, several studies of temporal

trends have reported stable or decreasing incidences of IBD for North America and Europe.^{18,20,21} Opposite this, the prevalence of IBD in newly industrialised countries is low, but the predicted incidence is expected to rise as their lifestyle shifts towards that of westernised countries.

These epidemiologic observations have drawn attention to the impact of genetics and lifestyle on the IBD aetiology, and more specifically those of Western countries.²² Overall, the soaring prevalence of these diseases will bring ever increasing burdens and challenges to the global healthcare system.

1.2. Pathophysiology of Inflammatory Bowel Diseases

If the aetiology of Inflammatory Bowel Diseases is still unclear, it is commonly admitted that they are multifactor pathologies arising from a combination of genetic susceptibilities and environmental factors, which trigger an inappropriate mucosal immune response.²³

1.2.1. Genetic factors in IBD

The involvement of genetics in IBD has been suspected for almost 70 years from the observation of familial aggregation. The rate of clustering is 2-14% in patients with CD reporting a family history of CD and 5–16% for report of any type of IBD ; 7–11% in patients with UC reporting family history of UC and 8–14% for any type of IBD.^{24–28}

The degree of familial clustering of a pathology (λ_s) can be expressed as the ratio (or percentage) of the risk of siblings over the reported prevalence in population. Literature reports λ_s ratio ranging from 15 to 42 for CD^{24,25,29,30} and 7–17 for UC.^{25,30} In comparison with other highly complex disorders, type-1 diabetes has λ_s equal to 15, type-2 diabetes and schizophrenia have $\lambda_s < 10$, and coeliac disease has λ_s ratio ranging from 7 to 30.

Large concordance studies in twins have since brought new evidence to confirm the relative importance of inherited and environmental factors in the aetiology of IBD. Theoretically, a pathology that would depend entirely on genetic factors should have a concordance in monozygotic twins (identical twins) close to a 100%, while its concordance in dizygotic (non-

identical twins) would decrease to 50%. On the opposite side, a disease entirely free from inherited factors would express similar concordance in both homozygotic and dizygotic twins. Studies in Northern Europe (Sweden^{31,32}, Denmark³³ and the UK³⁴) found concordance rates between 20 and 50% for CD in identical twins, and lower than 10% for non-identical twins. Concordance rates for UC were lower, ranging 14–19% in monozygotic twins and 0–7% in dizygotic twins.

Orholm *et al.* furthermore demonstrated that the risk of developing CD for a first-degree relative to CD-patients was 10 times higher than in population, while the risk of UC in UC-relative was 8 times higher.²⁵

The identification of susceptibility genes for IBD started with the discovery of mutations in the *NOD2* gene located on chromosome 16 in CD patients.³⁵ This gene encodes the NOD2 protein for *Nucleotide-binding Oligomerization Domain-containing protein 2*, but also known as *Caspase Recruitment Domain-containing protein 15* (CARD15) or *Inflammatory Bowel Disease protein 1* (IBD1). This protein is involved in the immune response as an intracellular pattern-recognition receptor (PRR) and can sense intracellular bacterial molecules such as the muramyl dipeptide present in the peptidoglycans forming the bacterial cell wall, especially of Gram-positive bacteria.^{36,37} NOD2 protein can be found in many cell types, including macrophages, monocytes, dendritic cells, B- and T-lymphocytes, and intestinal epithelial cells. NOD2 polymorphisms are associated with increased susceptibility to CD, but not UC. NOD2 mutations are extensively associated with European ancestry CD : about 30% of patients of European decent carry at least one of the three identified polymorphisms, when these variants are rare in patients of African origin and absent in patients of Asian ancestry.^{38–41} Mutated NOD2 carriers more often present with ileal disease and are more prone to develop strictures and fistulae.

Other than NOD2, autophagy gene mutations and especially that of *ATG16L1*, have been associated with CD.⁴² Located on chromosome 2, this gene is expressed in intestinal epithelial cells, antigen-presenting cells, B cells and CD4+/CD8+ T cells. It is involved with two other partners in the formation of a complex necessary for autophagosome formation, which role is essentially in pathogen clearance. Several studies have identified significant associations between the rs2241880 variant of *ATG16L1* and CD ; individuals with CD and the *ATG16L1*

risk variant presented with defective autophagy mechanisms.^{43–45}

Another main autophagy gene has been linked to Crohn's disease: the *IRGM* gene located on chromosome 5. This gene is involved in autophagy against intracellular pathogens, such as *Toxoplasma gondii*, *Mycobacterium tuberculosis* or *Salmonella typhimurium*.^{46–48} The association of single-nucleotide polymorphisms (SNPs) in NOD2, ATG16L1 and IRGM with CD stress how innate immune defects are central features in CD, but not in UC.

As previously demonstrated by twin concordance studies, genetic predispositions seem to have a more modest contribution in ulcerative colitis than in Crohn's disease. Nevertheless, some susceptibility loci could be identified for UC as well, such as polymorphisms in *PTPN2*, *HERC2* and *ECM11*.^{49,50} The anti-inflammatory cytokine IL-10 has also drawn a lot of attention towards its involvement in intestinal immune regulation and colitis. It was demonstrated that IL-10 deficient mice spontaneously developed enterocolitis.^{51–53} In parallel, important defects in IL-10 signaling in the lamina propria cells from patients with UC have been described.

Finally some polymorphisms have been associated with both CD and UC, among which the most significant ones were related to the interleukin IL-23R gene. IL-23 is a regulatory cytokine secreted by CD4+ T cells, CD8+ T cells, activated macrophages, dendritic cells, natural killer cells (NK cells) and NKT-cells⁵⁴, that may be involved in chronic inflammation.^{55–58} The functional IL-23 is an heterodimeric cytokine, composed of IL12p40 and IL23-specific p19 subunit. IL-23 expression is particularly enriched in the intestine, and it can suppress the regulatory T-cell responses in the gut, hence favouring inflammation. Consequently, increased levels on IL-17 have been observed in the lamina propria of UC patients.⁵⁹

Genetic polymorphisms within the interleukin-23 receptor (IL23R), IL12B and STAT3 have been significantly associated with both CD and UC ^{60,61}, although the mechanisms by which these SNPs interfere with gene function and affect IBD pathogenesis is still unclear.

Overall recent analyses have reported a total of 163 IBD risk loci ⁶² accounting for up to 71 associations (when only 71 susceptibility loci had been identified in 2012 ⁶³). The candidate genes within these loci implicate a broad array of genes, but unsurprisingly many are related to immune response mechanisms, cytokine production and cytokine receptors...etc. A large number – 110 out of 163 – of these loci are associated with both UC and CD, with more or less heterogenous effects. Among the remaining mutations, 30 are identified as CD-specific are 23 as UC-specific. Furthermore, 70% of the loci (113 out of 163) have also been identified in other

complex diseases, including immune disorders (e.g. type-1 diabetes, psoriasis and ankylosing spondylitis) and immunodeficiencies leading to severe infections.^{64,65}

Despite the large number of loci identified, it seems they account for 20% only of the genetic susceptibility to IBD.⁶⁶

1.2.2. Environmental factors in IBD

The imperfect concordance observed in monozygotic twins studies suggests an important role for environmental factors and lifestyle in Inflammatory Bowel Disease. These data are further supported by several epidemiologic observations :

- First, the existence of north-south, east-west and urban-rural gradients in incidence rates and prevalence of IBD is observed worldwide,⁶⁷
- Ethnic groups previously less affected by IBD such as Asians and Hispanics,⁶⁸ nowadays exhibit increased incidence rates that correlate with their change in lifestyle towards westernization,
- Increased incidence rates in immigrants from low incidence regions that moved in countries with a high incidence, within a single generation timespan.^{69,70}

Many environmental factors have been pointed out at the moment : less women breastfeeding⁷¹, improved domestic hygiene and sanitation⁷², quality of drinkable tap water⁷³, air pollution exposure⁷⁴, western diet⁷⁵ high in sugars and polyunsaturated fats but low in fibres... But no strict cause-consequence relation could be demonstrated, only correlations. Only two environmental factors have been clearly identified up to date : tobacco consumption and appendectomy.

Current cigarette smoking at time of disease has been shown to be protective in ulcerative colitis against non-smoking.^{76,77} UC patients who are smokers tend to have a milder course of disease, and disease activity tends to increase in patients that quit smoking⁷⁸ while ex-smokers have more chances of developing UC.⁷⁷ Surprisingly, smoking has totally the opposite effect on Crohn's disease, where it tends to increase both the risks of relapse and of surgical intervention.⁷⁹⁻⁸¹

Early appendicectomy before the age of 20 years old for acute appendicitis has been shown to be protective against UC.^{82,83} In the case of Crohn's Disease, many different opinions have been expressed in the literature, but the overall trend seems to support the theory that appendicectomy increases the risk of developing CD.^{84,85}

1.2.3. IBD and microbiota : a complex interplay

There is abundant data supporting the intricate link between IBD and microbiota. Antibiotics have for instance been reported to induce remission in active CD patients and to play a role in the prevention of post-operative recurrence in CD.⁸⁶ 16S rRNA sequencing in children has demonstrated differences in microbiota between IBD and non-IBD paediatric patients.⁸⁷

Microbiota is intended as the microorganisms inhabiting a defined ecological niche. The intestinal microbiota encompasses bacteria, archaea, fungi and viruses, all of which make up diverse ecosystems within us and live in symbiosis with their host. It is commonly admitted that the human gut contains up to 10^{14} bacteria, an estimate 10-fold more than the number of eukaryotic cells in our organism.⁸⁸ The intestinal microbiota begins to establish at birth and during early infancy, when the GI tract is colonised by microorganisms from diverse taxa among which *Bifidobacterium*, *Lactobacillus* and *Enterobacteriaceae*, that are acquired from many sources such as the mother's vaginal microbiota (if the infant is born naturally and not by C-section), skin and faecal microbiota of parents, siblings, classmates or breast milk.⁸⁹ The microbiota is then shaped by host genetics, microbial exposure, diet, medical treatments and other environmental pressures, to reach its final structure around the age of three years old.⁹⁰ Gut microbes are adapted to a certain type of lifestyle such as a diet⁹¹, and extreme diet changes may result in wide alterations of the microbiota composition.⁹²

1.2.3.1. Healthy or normal gut microbiota

The definition of a healthy microbiota remains unclear and elusive despite the enormous progresses achieved along the past decades. This imprecision is largely imputable to culture-based difficulties to identify and grow the anaerobic bacteria that make up the majority of our

gut microbiota, but also to the new sequencing methods which, if they brought numerous answers, have unveiled a bacterial complexity and diversity we were previously unaware of.

The knowledge of the human gut microbiota was for long limited to the bacterial strains that could be cultivated in the laboratory. The development of the first anaerobic techniques – pioneered by Hungate and Freter^{93,94} – opened the field to the discovery of a large number of micro-organisms. The dominant cultivable genera then identified were the following: *Bacteroides*, *Eubacterium*, *Peptostreptococcus*, *Ruminococcus*, *Bifidobacterium*, *Fusobacterium* and *Clostridium* (Table 4).

Bacterial genus	Moore 1974 ⁹⁵	Finegold 1983 ⁹⁶
<i>Bacteroides</i>	30	56
<i>Eubacterium</i>	26	14
<i>Bifidobacterium</i>	11	4
<i>Peptostreptococcus</i>	9	4
<i>Fusobacterium</i>	8	0,1
<i>Ruminococcus</i>	4	9
<i>Clostridium</i>	2	2
<i>Lactobacillus</i>	2	6
<i>Streptococcus</i>	2	6
Others	3	1

Table 4 - First identified dominant cultivable bacterial genera

Based solely on the known and cultivable micro-organisms, it was believed for several decades that the human microbiota held only 400 species, among which 25 to 40 species made up the dominant microbiota of each individual.

The advent of new high throughput sequencing methods, bioinformatics, and the improvement of anaerobic culture broadened our knowledge of the gut microbiota. The Human Microbiome Project was one of the first large-scale studies to provide thorough data on the human microbiome. It was observed that a healthy human gut is likely to be comprised of more than a 1000 bacterial species and as much as 10¹¹ bacteria per gram of colonic content.⁹⁷ In contrast a taxonomic approach could only identify 70-100 known species.

Following this project, several groups attempted to set up a definition of a “core” human microbiome. Li and co-workers compared the microbial diversity of different body sites ; the vaginal microbiota revealed to be the least diverse, while oral and skin were the most complex ones, closely followed by the gut microbiota.⁹⁸ Similarly, the group of B. A. Méthe analysed phyla abundance over the body sites by exploiting the data from the Human Microbiome

Project.⁹⁷ Its conclusions joined that of Li : stool samples mainly contained representatives of phyla Bacteroidetes, Firmicutes, and Proteobacteria. Results may however differ based on the analytic technique used for sequencing (16S rRNA versus Whole Genome Sequencing).

From these analyses emerged a definition of the common core of the distal gut microbiota, that is predominantly composed of phyla Bacteroidetes and Firmicutes, closely followed by Actinobacteria (*Collinsella*, *Bifidobacteria*, *Atopobium*), Verrucomicrobia (*Akkermansia*) and Proteobacteria.^{99–101} The Bacteroidetes phylum consists of Gram-negative bacteria ; its most important representatives in the gut ecosystem are genera *Bacteroides* and *Prevotella*. On the opposite Firmicutes are Gram-positive bacteria, largely represented by orders *Lactobacillales* and *Clostridiales* (*Eubacterium*, *Ruminococcus*, *Clostridium*, *Faecalibacterium*, *Butyrivibrio*).

Recent studies have not only described a phylogenetic core¹⁰⁰ (Table 5), but also a metagenomic core¹⁰², of the human gut microbiota composed of some sixty bacterial species from the main previous phyla.

Phylum		Representation (%)	Dominant genera
Firmicutes	<i>Clostridium</i> cluster XIVa	14 - 31	<i>Eubacterium</i> , <i>Clostridium</i> , <i>Butyrivibrio</i>
	<i>Clostridium</i> cluster IV (or <i>Clostridium leptum</i>)	16 – 22	<i>Faecalibacterium prausnitzii</i> , <i>Ruminococcus albus</i> <i>Ruminococcus flavefaciens</i>
Bacteroidetes		9 – 42	<i>Bacteroides</i> , <i>Prevotella</i> , <i>Parabacteroides</i>
Actinobacteria		1 – 10	<i>Bifidobacterium</i> , <i>Collinsella-Atopobium</i>
Verrucomicrobia		N/A	<i>Akkermansia muciniphila</i>

Table 5 - Main bacterial phyla in the gut microbiota as identified by recent studies

Less than 0.1% of the gut microbiota is made of overt pathogens (e.g. *Campylobacter jejuni*, *Salmonella enterica*, and *Vibrio cholera*), but opportunistic pathogens such as *Bacteroides thetaiotamicron* or *Bacteroides fragilis* have also been identified in an analysis of the Human Microbiome Project by Huttenhower et al.¹⁰³ These were respectively detected in 46% and 16% of stool samples. *Escherichia coli* accounted for 0.1% or more of the microbiota in only 15% of stools.

The proportion of each phylum is individual specific, but it is possible to cluster people according to species and functional composition of their microbiome. Arumugam and co-workers classified healthy adult into three groups that appeared to be independent of nationality and gender.¹⁰⁴ They suggested a classification of individuals over three preferred ecological

configurations of the gut microbiota called “*enterotypes*” : Enterotypes 1 contain a high proportion of genera *Bacteroides*, Enterotypes 2 have a high proportion of *Prevotella*, and Enterotypes 3 show a high proportion of *Ruminococcus*. The concept was confirmed by other studies^{105,106}, and similar clusters were observed in other mammals such as pigs and mice.^{107,108} This definition of enterotypes was recently completed by Vandeputte *et al*, who reported *Ruminococcus* enterotype to consistently present a high cell count, while they could describe two subtypes of the *Bacteroides* enterotype based on the raw cell count of donors (low cell count / high cell count).¹⁰⁹

Most bacteria of the human body are located in the gastro-intestinal tract, and 70% of them inhabit the colon.¹¹⁰ The composition and density of the human gut microbiota changes along the length of the GI tract from oesophagus and stomach to small intestine, large intestine and colon with the variations of pH, chemical, nutritional and immunological gradients. These variations have been demonstrated by comparing the microbial composition found in upper GI tract analysed by biopsies and the composition found in stool samples that would better mirror the lower tract microbiota.^{97,111} The bacterial composition of the microbiota in the small intestine increases in diversity and complexity from proximal to distal direction (from duodenum to jejunum and ileum) and reaches its climax in the large intestine ; the small intestine is characterised by high levels of oxygen and antimicrobial agents combined to a short transit time, conditions that limit bacterial growth and favour the rapidly-growing, facultative anaerobes with high adhesion ability to mucus and/or epithelium.⁹¹ Microbiological data is scarce for this region of the GI tract (hard to routinely sample), but it appears that genus *Streptococcus* is dominant in duodenum and jejunum.^{112,113} On the opposite, ecological colonic conditions allow the development of a dense and rich bacterial community, most of which are anaerobes and thrive on the undigested complex carbohydrates (the *fibres*).¹¹⁴ The dominant microbiota in the large intestine includes Firmicutes and Bacteroidetes.

In addition to longitudinal variations, our microbiome also varies axially from lumen to mucosal surfaces.^{101,115} Studies have shown that the phylum Firmicutes was largely predominant in the mucosa-associated microbiota (sampled by biopsy) compared to the luminal one (sampled by stool analysis), where Bacteroidetes would dominate.^{101,116,117}

1.2.3.2. Role of the microbiota

The gut microbiota is a beneficial “organ” to its host due to its multiple implications in metabolism, epithelial integrity, antimicrobial protection and maturation of the immune system.

Bacteria provide the host with nutrients and vitamins and some of their microbial metabolites are strongly involved in our metabolism and regulation of the glucose and lipid homeostasis. Colonic bacteria for instance, can degrade complex carbohydrates otherwise undigested to generate short-chain fatty acids (SCFAs) which are saturated aliphatic acids consisting of one to six carbons, among which acetate, propionate and butyrate are the most abundant.^{118,119} These are absorbed by intestinal epithelial cells and participate in the regulation of cellular processes and metabolism, e.g. gene expression, proliferation, differentiation, and apoptosis.^{120–122} Gut bacteria can also synthesize essential vitamins : vitamin B12 is produced by lactic acid bacteria^{123,124}, folate by *Bifidobacteria*¹²⁵, but also indoles, vitamin K, biotin, riboflavin, thiamine...etc. Non-reabsorbed bile acids are metabolized by colonic bacteria into secondary biliary acids.¹²⁶ These many examples of bacterial components are mostly recognised by human G-protein-coupled receptors (GPCRs), resulting in hormone secretion by enteroendocrine cells.^{127–130}

Several microbial species have been identified for their role in epithelial integrity, among which *A. muciniphila*, *L. plantarum*, *R. gnavus*, *F. prausnitzii* and *B. thetaiotaomicron*.^{131–136} These could modulate epithelial and mucus properties, as well as their turnover.

Right beneath the intestinal epithelial cells (IECs) lining the gut mucosa, is located the most extensive human lymphoid compartment : the gut-associated lymphoid tissue (GALT). The GALT is rich in immune cells associated with innate and adaptive immunity. It is involved in maintaining the homeostasis at the intestinal interface between host and microbiota, by differentiating commensal micro-organisms from their pathogen counterparts.^{137,138} The intestinal bacteria participate to teach the GALT via their constant interactions with dendritic cells (DCs) and IECs through recognition of pathogen-associated molecular patterns (PAMPs) by innate immune receptors named PRRs for Pattern Recognition Receptors (a group of receptors including NOD and TLRs). PAMPs can include lipopolysaccharides (LPS) from Gram-negative bacteria and other molecular patterns such as peptidoglycans and flagellin ; these can for instance trigger the onset of low-grade intestinal inflammation and insulin resistance in obese or diabetic patients.^{139–141} It has notably been shown that bacteria are

required for maturation of the immune system. Segmented filamentous bacteria (SFB), a class of commensal bacteria, have several effects : they are required for Th17 cells differentiation in the lamina propria¹⁴², and stimulate the postnatal maturation of the GALT, as well as other immune-stimulatory properties.¹²² *Bacteroides fragilis* are needed for the expansion of CD4+ T cells and their conversion into regulatory T cells via secretion of polysaccharide A^{143,144} ; germ-free animals otherwise lack expansion of the CD4+ population. The physical colonization of the gut epithelium by commensal bacteria is furthermore protective against pathogens for they compete for attachment sites and nutrients, and can also secrete antimicrobial agents.¹⁴⁵

Finally, the gut microbiota has the property to stimulate its host for production of native antimicrobial substances : cathelicidins, C-type lectins, defensins and IgAs.

1.2.3.3. Characterising the intestinal dysbiosis in Inflammatory Bowel Diseases

A dysbiosis can be described as “an unfavourable alteration of the microbiota composition” resulting in a host-microbiota relationship breakdown.¹⁴⁶ It is now clear that alterations of normally balanced microbial populations can be linked to gastrointestinal pathologies susceptibilities, and many studies have observed a dysbiosis in patients suffering from active IBD (both CD and UC). The main characteristics of this IBD-linked dysbiosis are summarised below in Table 6.^{22,147–151}

CHARACTERISTICS	DESCRIPTION
Instable microbial composition over time	Loss of microbial richness Decrease in α -diversity
Changes in the microbial composition	Decrease species richness within genus <i>Bacteroides</i> and phylum Firmicutes Increase in Gammaproteobacteria Decrease in Clostridia, Ruminococcaceae, <i>Bifidobacterium</i> , <i>Lactobacillus</i> Decrease in group <i>Clostridium leptum</i> and especially in <i>F. prausnitzii</i>
Increase in some groups not observed in controls	Presence of <i>AIEC</i> (adherent-invasive E. coli) Presence of <i>Fusobacterium</i>
Changes in microbial functions	Decrease in SCFAs, especially butyrate Decrease in butanoate and propanoate metabolism Decrease in amino acids biosynthesis Increase in auxotrophy Increase in amino acids and sulfate transport Increased oxidative stress Increase in type II secretion system, secretion of toxins

Table 6 - General features of dysbiosis in IBD

An overall reduction in the gut microbial diversity is observed in IBD, where the microflora is constituted of fewer species and presents an instability of composition over time, even in patients in remission.¹⁵² Firmicutes in particular have decreased, while in contrast Bacteroidetes, Proteobacteria and Actinobacteria have increased.^{153,154} The decrease in Firmicutes – reported to reach up to 10 or 100-fold based on surgical resections¹⁵⁴ – is strongly linked to the loss of clostridial clusters.^{79,137} These two groups are main butyrate-producers ; butyrate is an essential energy source for intestinal epithelial cells, but has also anti-inflammatory properties on the mucosa. Genera associated with mucosal protection and anti-inflammatory properties such as *Faecalibacterium* are therefore affected and lowered.^{155,156} At the same time, bacteria from the Enterobacteriaceae family are relatively expanded in the mucosal environment (compared to the lumen).¹⁵⁷ These are mostly facultative anaerobes and Gram-negative bacteria, such as the adherent-invasive *E. coli*. Intestinal colonisation by *E. coli* and especially AIEC has mainly been reported in CD cases, and the ratio *F. Prausnitzii/E.coli* could be used as a marker of dysbiosis and a predictor of CD recurrence, although a clear causal relationship has yet to be demonstrated.¹⁵⁸

Due to a damaged epithelial barrier resulting from inflammation, IBD patients tend to have higher counts of mucosa-associated bacteria than healthy controls.^{159,160} Quantitatively, *in situ* fluorescent hybridisation techniques revealed the presence of bacteria in the mucus layer of 30% of biopsies from IBD patients, where they were observed in only 3% of healthy controls.¹⁶¹ These observations are associated to the increased number of mucolytic bacteria such as *Ruminococcus gnavus* and *Ruminococcus torques* found in the dysbiotic microflora of colonic IBD compared to controls.¹⁶²

In parallel, recent studies have described a quantitative – not relative – raw decrease in cell count in samples from patients suffering from Crohn’s Disease.¹⁰⁹

Other than bacteria, the intestinal fungal populations are also affected in patients with IBD. Sokol *et al.* demonstrated dramatic imbalance in the fungal microbiota of IBD patients versus HS. Concomitant analysis of both fungal and bacterial modifications in IBD revealed important correlations, suggesting the “*existence of disease-specific interkingdom alterations*”.¹⁶³

Some studies have investigated the chronologic intricate links between dysbiosis and the onset of IBD. In animal models, the pre-existence of a microbiota seems to be a prerequisite

to the development of colitis (be it spontaneous or induced).¹⁶⁴ Experiments conducted on germ-free mice have shown that the introduction of a dysbiotic microbiota in immunologically deficient organisms was a driver for colitis. Furthermore, an unbalanced microbiota could also induce colitis in otherwise healthy wild-type individuals.

From a human point of view, it was shown that a lower diversity could be measured in healthy twin compared to their affected twin in discordant UC twin pairs study, suggesting that dysbiosis may precede the onset of the pathology.¹⁵³

The complex interplay between IBD and its dysbiotic microbiota can be summarized into two broad categories. First, the microbiota from IBD patients shows an enhanced capacity to manage oxidative stress and to promote virulence factors, both leading to enhanced inflammation ; second, the modified microbial ecosystem has a lower ability to produce its own nutrients.

2. Introduction to microbiology and its relation to the human gut ecosystem

2.1. The Quorum Sensing

For a very long time bacteria were considered as individual and isolated organisms. This point of view changed when the idea of microbial interactions was suggested. It was then postulated that microorganisms did not always behave as lonely individuals, but could exhibit community behaviours and even form “*societies*”.¹⁶⁵

Living as a community demands interactions, that drive a need for communication between members of the group in order to transfer the appropriate information. Hence many microorganisms have developed communication mechanisms based on the punctual secretion of diffusible chemical messengers.^{166,167} These molecules are used to mediate several processes such as regulating the colony density or metabolites production, synchronizing behaviours or phenotypes.

The molecules used by microorganisms will hereafter be referred to as signal messengers, to differentiate them from hormones, a term more commonly used for many-cell organisms and

describing molecules secreted within an organism, when signal molecules are released in the surrounding medium such as water, soil, air, biological matter, etc.

The cell to cell communication therefore relies on the exchange of chemical signal molecules between cells ; driven by the Quorum Sensing (QS), it depends on the bacterial density within the colony.

2.1.1. Discovery and main characteristics of the Quorum Sensing

Quorum Sensing was discovered in the 1970s, while studying the bioluminescence emitted by the marine bacteria *Vibrio fischeri*.^{168,169} This bacterium lives in symbiosis with its host, the Hawaiian bobtail squid *Euprymna scolopes*,¹⁷⁰ which benefits from the bioluminescence which allows it to mask its own shadow by mimicking sun/moon radiations in the ocean to avoid predation. This phenomenon is termed counterillumination.^{171,172} The bacteria on the other hand, benefits from a nutrients-rich environment and favourable growing conditions. *V. fischeri* has also been described to live symbiotically in the light organ of the fish *Monocentris japonicus*, which uses the light produced to attract a mate. Many other uses of *V. fischeri* bioluminescence have been reported, such as attracting prey or warding off predators.¹⁶⁸

When *V. fischeri* lives freely in open water in a state of low bacterial concentration, it does not emit bioluminescence as the signal molecules produced diffuse freely into the water. However, when the bacteria colonise the squid's luminescent organ (photophores) they can grow and multiply to reach the bacterial concentration threshold that triggers the expression of genes involved in the bioluminescence emission.¹⁷³ The signal messenger involved was first isolated in Gram-negative bacteria in 1981 and named Auto-Inducer type 1 (AI-1).¹⁷⁴ It was identified as a *N*-Acyl Homoserine Lactone (AHL). The gene encoding the main enzyme from the AHL biosynthesis pathway was discovered in 1984,^{175,176} while the name Quorum Sensing was first used a decade later.

2.1.1.1. General mechanism(s) of the bacterial QS

The bacterial Quorum Sensing is a signaling mechanism empowering the intercellular communication within members of a same strain/kind, but also between different species.^{177,178} It is based on molecules named chemical messengers or signal messengers, synthesized by

enzymes whose activation relies on the bacterial density within a colony and the correlated concentration of signal messengers in the close environment surrounding the bacteria.¹⁷⁹

When the bacterial density rises, the chemical messenger concentration rises as well¹⁸⁰ – in an environment of appropriate shape and conformation (preferably a sealed enclosure as open media favour the diffusion of molecules) – to reach a critical threshold or *quorum* above which the bacterial population is considered to be “quorate” and starts behaving as a community instead of scattered individuals to exhibit synchronised behaviours or phenotypes. Common orders of magnitude for quorum range approximately from picomolar to micromolar concentrations.

When the signal messenger concentration goes above the quorum, the molecules bind and activate their cognate protein receptors to form complexes that will act as transcription factors. The latter will alter gene expression levels to initiate a range of behaviours that will benefit the bacterial community. In the case of type-1 autoinducers, a second downstream phenomenon is activated : the quorum amplifies the production of signal molecules (mechanism called a positive retroactive loop), which exacerbates the phenomenon (hence the name of *autoinducer*).

QS-regulated phenotypes may vary broadly from one bacterial specie to another, but among the most common ones are the formation of biofilms¹⁸¹, the sporulation¹⁸², the induction of bioluminescence¹⁷⁹, the expression of virulence factors¹⁸³, the synthesis of antibiotics and other extracellular products^{184,185}, some DNA transfer or fluctuations of the mobility/motility...

2.1.1.2. The Quorum System of *Vibrio fischeri* : a paradigm for LuxI/LuxR-type quorum sensing systems

In *Vibrio fischeri*, the *luxI* gene enclosed in the operon LuxICDABE encodes for the LuxI synthase that synthesizes the signal messenger *N*-(3-oxo-hexanoyl)-homoserine lactone (abbreviated OHHL or 3oxoC₆-HSL).^{174,176} The gene *luxR* encodes the LuxR AHL receptor, that after interaction with the OHHL to form a stable complex will act as a transcription factor and bind upstream of the LuxICDABE operon.¹⁸⁶ Its binding induces transcription of components of the luciferase system and the exponential increase in LuxI synthesis to enter a powerful positive feedback loop.¹⁸⁷

Below quorum concentration, the LuxR protein is unstable and degrades rapidly; productive ligand-protein interaction and binding can only occur at high ligand concentrations, hence at high bacterial densities.^{187,188}

Since, many other types of signal messengers involved in QS in both Gram-negative and Gram-positive bacteria have been described, but the LuxI/LuxR system from *V. Fischeri* is still viewed as a reference model to describe similar LuxI/LuxR-type systems (Table 7).

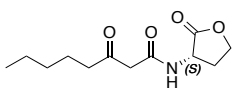
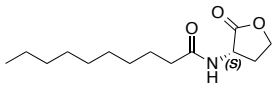
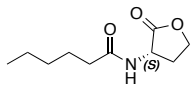
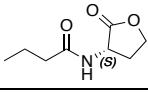
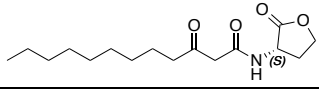
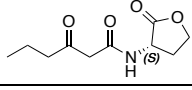
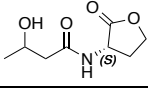
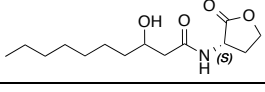
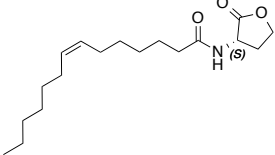
Bacterium	AHL(s) produced	Nomenclature used in this work	LuxI/LuxR homologues
<i>Agrobacterium tumefaciens</i>		3oxoC ₈ -HSL	TraI/TraR
<i>Burkholderia cenocepacia</i>		C ₈ -HSL	CepI/CepR
<i>Chromobacterium violaceum</i>		C ₆ -HSL	CviI/CviR
<i>Pseudomonas aeruginosa</i>		C ₄ -HSL	RhII/RhIR
		3oxoC ₁₂ -HSL	LasI/LasR; QscR ^a
<i>Vibrio fischeri</i>		3oxoC ₆ -HSL	LuxI/LuxR
<i>Vibrio harveyi</i>		3OHC ₄ -HSL	LuxM/LuxN ^b
<i>Acidovorax radices</i> N35		3OHC ₁₀ -HSL	AraI/AraR
<i>Rhodobacter sphaeroides</i>		7- <i>cis</i> -C ₁₄ -HSL	CerI/CerR ¹⁸⁹

Table 7 - Some examples of LuxI/LuxR-type AHL systems

^a QscR is an orphan receptor responding to 3oxoC₁₂-HSL. ^b LuxM and LuxN genes show however no homology with the usual LuxI/LuxR genes. Adapted and completed from Blackwell et al. ¹⁸⁸.

It was later shown that *V. fischeri* possesses two other quorum sensing systems governed by duets AinS/AinR and LuxS/LuxPQ.¹⁷⁰ AinS uses the AHL *N*-octanoyl-homoserine lactone (C₈-HSL), while LuxS relies on the furanosyl borate diester (AI-2, *see further*).

2.1.2. Overview of QS signaling molecules

Bacterial QS is based on and regulated by the emission and reception of low molecular weight chemical messengers called autoinducers. Some molecules can be recognised only by members of the same species, while other molecules are not specie-specific.¹⁹⁰ Their structures and biosynthetic pathways vary from one bacterial strain to another, but they can generally be classified into broad classes, based on common molecular features.^{191,192}

2.1.2.1. Type-1 autoinducers (AI-1)

Type-1 autoinducers are made up of *N*-Acyl Homoserine Lactones (Figure 1). These molecules consist in a hydrophobic fatty acyl chain of variable length – usually 4 to 18 carbons¹⁹³ - attached in α -position to a homoserine lactone ring unsubstituted at β - and γ -positions. The third carbon from the acyl chain can exhibit variable degrees of oxidation, being linked either to a proton, a hydroxyl group or a doubly-bound oxygen to form a ketone. Type-1 autoinducers also include some “nearly-AHL” compounds such as the *p*-coumaroyl-HSL,¹⁹⁴ the cinnamoyl-homoserine lactone also known as aryl-HSL¹⁹⁵, and the isovaleryl-homoserine lactone (Figure 2).¹⁹⁶

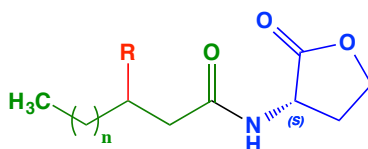


Figure 1 - General structure of *N*-acyl homoserine lactones

Blue : the α -*N*-acylated homoserine lactone headgroup. Green : the fatty acyl chain ($n = 0 \dots 14$). Red : diverse oxidation patterns of the 3-position ($R = O, OH, H$).

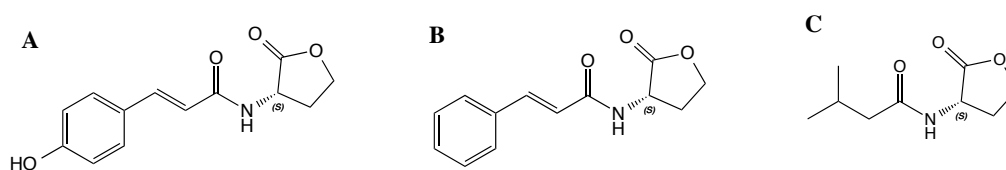


Figure 2 - Non-conventional forms of type-1 autoinducers

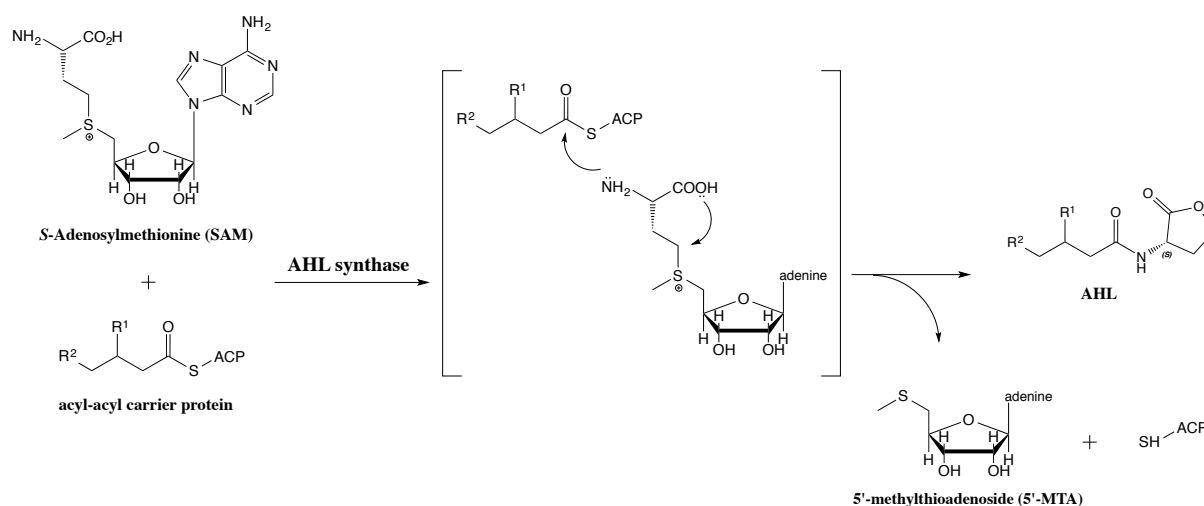
A : *p*-coumaroyl-HSL. **B** : aryl-HSL. **C** : isovaleryl-HSL.

AHL are mostly produced and detected by Gram-negative bacteria from phylum *Proteobacteria*^{197,198}; more than 70 known species of Gram-negative bacteria employ AHL as autoinducers.¹⁹⁹ AHL-based quorum sensing was also observed in cyanobacteria.^{200,201}

The AHLs are secreted in the outer environment where they accumulate. Hydrophilic short-chained AHL passively diffuse through the bacterial outer membrane, while the more hydrophobic long-chained AHL are actively secreted in the surrounding environment.²⁰² At low cell densities, AHL passively diffuse down a concentration gradient, while at high densities they accumulate until extra- and intracellular levels are roughly equivalent (ca. 10 nM).¹⁸⁰

The surrogate enzyme for AHL biosynthesis by bacteria is the AHL synthase. It is encoded by three gene families that have been named according to the three autoinducer genes originally identified in *V. fischeri*: *luxI*, *ainS*, and *hdtS*.²⁰³

The LuxI AHL synthase family is the best known to date, and the key steps of its biosynthetic pathway have been fully elucidated²⁰⁴ (Scheme 1): the AHL synthase LuxI catalyses the amide bond formation between the fatty chain from an acyl-acyl carrier protein (acyl-ACP) and the amino group of a S-adenosyl-methionine (SAM). The lactone head of the AHL is then formed by release of 5'-methylthioadenosine (5'-MTA).



Scheme 1 - Biosynthesis of AHL as catalysed by LuxI-type AHL synthases

Inspired from Galloway et al.¹⁹⁸

Type and production of the secreted AHL also depends on the available carbon sources present in the bacteria environment. For instance, the bacterium *Methylobacterium extorquens* AM1 can only produce AHLs when it grows under methylotrophic conditions.²⁰⁵

AHL receptors are intracellular and encoded by orthologous genes from the *luxR* family. Effective concentrations for AHL impact range from 0.1 to 400 nM.¹⁸⁰ Named LuxR or LuxR-like receptors, these proteins are transcriptional regulators. At low cell and AHL densities, the N-terminal region of the LuxR protein folds back onto its HTH domain, thus blocking DNA binding. But when the type-1 autoinducer concentration increases, the N-terminal part of the receptor can bind specifically to the signal messenger with high affinity, so that the HTH domain is available for DNA binding and activates transcription.¹⁷⁰

2.1.2.2. Type-2 autoinducers (AI-2)

Type-2 autoinducers were identified more recently than AI-1, in the Gram-negative bacterium *V. harveyi* where AHL-deficient strains of the bacterium still managed to emit bioluminescence despite lacking the natural AI-1 3OHC₄-HSL.²⁰⁶ These non-specie-specific molecules seem to allow cross-kingdom communication between Gram-negative and Gram-positive bacteria^{167,207,208}; bacteria could in particular sense the presence of non-mate members. Some organisms have developed mutations to hijack the AI-2 communication network: *Escherichia coli* and *Salmonella typhimurium* can activate a special enzyme dedicated to the intracellular import of AI-2,²⁰⁹ while some hosts are able to secrete an AI-2 mimic.²¹⁰

Only two type-2 autoinducers have been identified to date (Figure 3): the (2*S*,4*S*)-2-methyl-2,3,3',4-tetrahydroxy-tetrahydrofuran-borate (*S*-THMF-borate or furanosyl diester borate) found for instance in *Vibrio harveyi*, and the (2*R*,4*S*)-2-methyl-2,3,3',4-tetrahydroxytetrahydrofuran (*R*-THMF) found in *Salmonella typhimirium*.^{207,211}

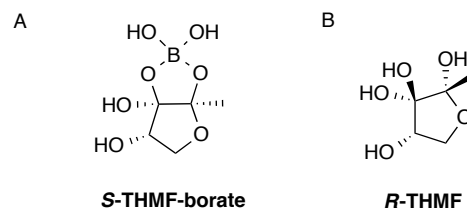
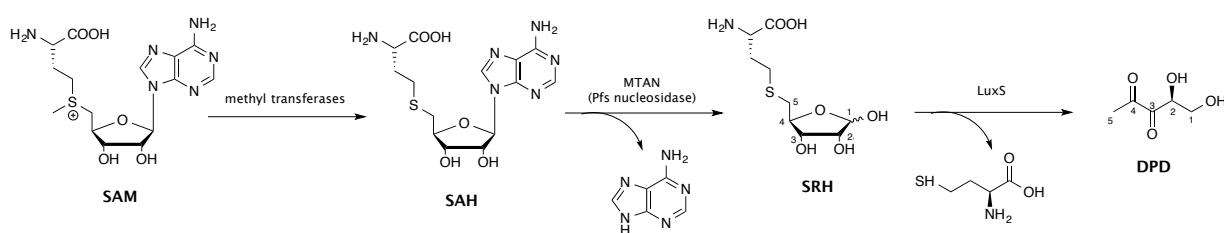


Figure 3 - Type-2 autoinducers (*S*-THMF-borate (A) and (*R*-THMF (B)

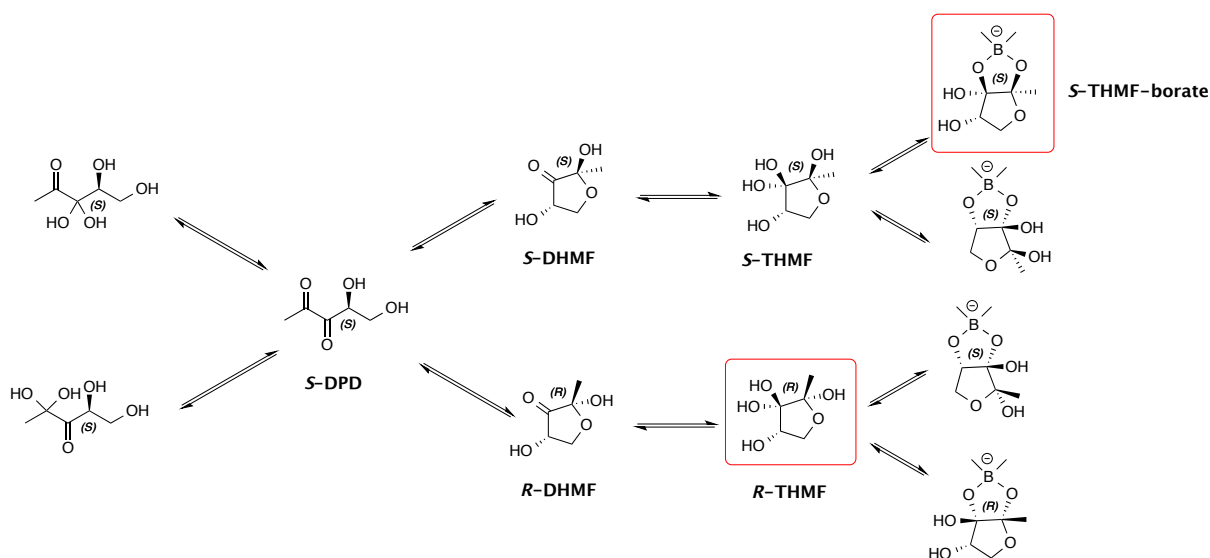
The furanosyl borate diester AI-2 is produced from SAM (S-Adenosylmethionine) - an essential cofactor for nucleic acid and protein synthesis – through an enzymatic pathway involving at least the 3 enzymes MetF, MetE and AI-2 synthase.²¹²

AI-2 synthase is the key-enzyme in the AI-2 biosynthesis ; it is encoded by a member of the *luxS* gene family, found to date in over 70 bacterial species.^{206,213} The *luxS* gene is an absolute requirement for production of type-2 autoinducers : in case of inactivation, AI-2 production totally shuts down.²¹⁴

The AI-2 synthase catalyses the removal of homocysteine from S-Ribosylhomoserine (SRH) to afford an AI-2 precursor named DPD or 4,5-dihydroxy-2,3-pentanedione (Scheme 2), which later undergoes spontaneous rearrangement to form several DPD derivatives that co-exist in equilibrium and can convert one into another.²⁰⁹ This is known as the “AI-2 pool” (Scheme 3).²¹⁵ Spontaneous cyclization of DPD can then produce enantiomers *S*-DHMF and *R*-DHMF, which later hydrate to generate four others compounds. Finally, boronate ester formation from DPD will only occur if the borate concentration in solution is high enough to form the four final compounds.



Scheme 2 - Biosynthesis of DPD involving LuxS



Scheme 3 - Complex equilibria involving DPD and its derivatives in the AI-2 pool system

Elements in red boxes are known type-2 autoinducer molecules. Adapted from Galloway et al.¹⁹⁸

It is worth noting that it is thought that the LuxS enzyme has a metabolic role in cells, other than its involvement in AI-2 biosynthesis, which could explain its widespread conservation among bacteria.^{206,208}

After its synthesis, AI-2 is actively transported across the bacterial outer membrane to join its receptor. This receptor belongs to a two-member complex: in the case of *V. harveyi*, the AI-2 is recognised by receptor LuxP that will itself afterward interact with protein LuxQ. The latter acts as a histidine kinase whenever the AI-2 concentration is low, inducing downstream intracellular phosphorylations to inhibit the LuxR activity. This mechanism favours the expression of AphA, a low cell density regulator, leading to changes in the regulation of up to a hundred genes.

If the bacterial density is high, all QS molecules from *V. harveyi* (AI-2, CAI-1 and 3OHC₄-HSL) accumulate in the medium and bind to their respective receptors (LuxPQ, CqsS and LuxN). Ligand binding promotes the phosphatase behaviour of the receptor proteins, reversing the phosphorylation flow towards the upstream path that will favour LuxR over AphA and induce bioluminescence.²¹⁶

2.1.2.3. Type 3 autoinducers (AI-3)

A third type of autoinducers has been reported to date, and is called AI-3 for type-3 autoinducer. It was first encountered in the enterohemorrhagic intestinal pathogen *Escherichia coli* (EHEC), that produces it in response to epinephrine and norepinephrine presence in the bacteria environment.²¹⁷⁻²¹⁹ Because epinephrine and norepinephrine are AI-3 agonists, it is supposed the autoinducer has an aromatic structure. Little is known about type-3 autoinducer, and whether gene *luxS* might be involved in its biosynthesis is still unclear.²²⁰

2.1.2.4. Other signaling molecules in Quorum Sensing

2.1.2.4.1. Cholerae autoinducer (CAI)

Cholerae autoinducer-1 or CAI-1 is a class of signaling molecules secreted by members of genus *Vibrio*, with a role in the regulation of virulence factor secretion (Figure 4). The full chemical name of these molecules is (*S*)-3-hydroxytridecan-4-one, and they appear to be

biosynthesized by enzyme CsqA and sensed by receptor protein CsqS (standing for *Cholerae quorum sensing Autoinducer/Sensor*).^{221–223} Only the (*S*)-enantiomer is naturally found in *V. cholerae* supernatants, and literature reports the (*R*)-isomer is about twice less active.²²⁴

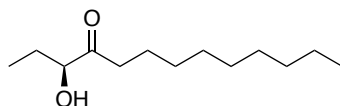


Figure 4 - Chemical structures of *Cholerae* autoinducer-1 (CAI-1) from *Vibrio cholerae*

2.1.2.4.2. 3-hydroxy palmitic acid methyl ester (3OH-PAME)

The 3-hydroxy palmitic acid methyl ester (Figure 5) is a volatile quorum sensing molecule secreted by soil bacterium *Ralstonia solanaceum* (genus *Pseudomonas*), whose purpose is the expression of virulence factors.²²⁵ Its biosynthesis is governed by a SAM-dependent methyl transferase that turns 3-hydroxypalmitic acid into 3-hydroxypalmitic acid methyl ester, and is encoded by gene *phcB*.^{226,227}

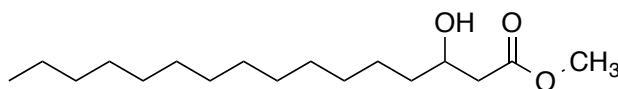


Figure 5 - Molecular structure of 3-hydroxypalmitic acid methyl ester

2.1.2.4.3. The *Pseudomonas* Quinolone Signal (PQS)

The *Pseudomonas* Quinolone Signal, or PQS, is a signaling system present in bacteria from genus *Pseudomonas* and based on molecule 2-heptyl-3-hydroxy-4-quinolone.²²⁸ *Pseudomonas* bacteria are Gram-negative microorganisms and strict aerobes, whose most notorious member is the opportunistic human pathogen *Pseudomonas aeruginosa* that affects prominently patients with cystic fibrosis (a lethal inherited lung disorder).

PQS is synthesized from precursor 4-hydroxy-2-heptylquinoline (HHQ), itself a member of 4-hydroxy-2-alkylquinolines (HAQ) a group of molecules produced by the enzyme encoded by operon *pqsABCDE* and gene *pqsH* (Figure 6).^{229–231} The quinolones are sensed by a LuxR-type transcriptional regulator named PqsR for which both HHQ and PQS act as inducers, although

PQS has much better affinity for the receptor and is about 100 times more active than HHQ.^{232,233} PqsR is also involved in the PQS regulation as it links to the *pqsABCDE* operon region and regulates its expression in an autoregulatory fashion.

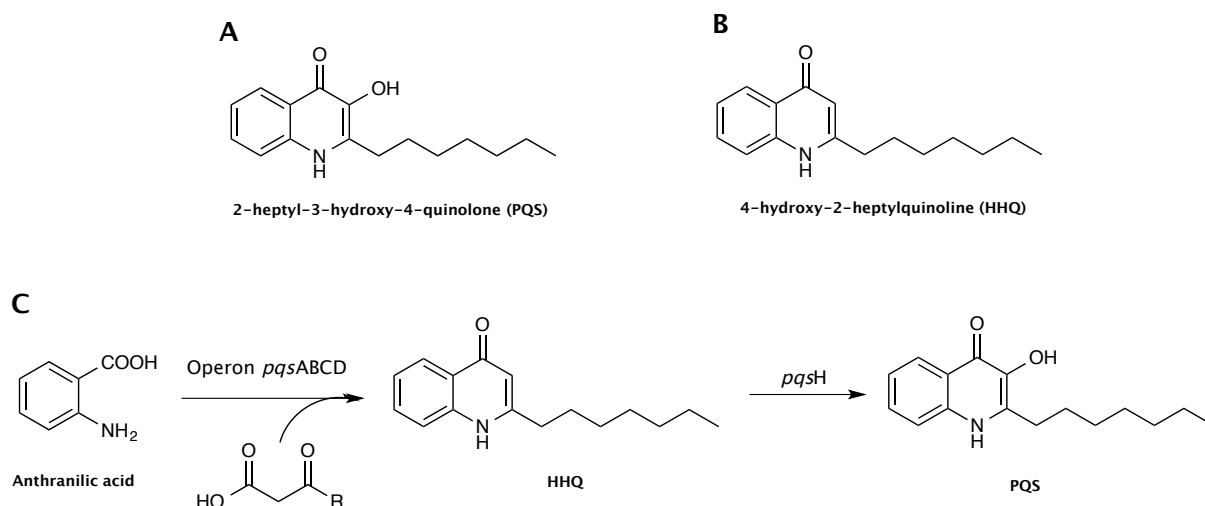


Figure 6 - Pseudomonas Quinolone Signal (PQS) biosynthetic pathway

Adapted from Dubern et al.²³¹

Pseudomonas aeruginosa harbours a hierarchical circuit composed of several QS types.²³⁴ On top of PQS the bacterium can synthesize two type-1 autoinducers, 3oxoC₁₂-HSL and C₄-HSL, thanks to two pairs of LuxI/LuxR-type homologues respectively named LasI/LasR and RhII/RhIR. The two QS paths work in tandem to control virulence factor and biofilm production in the pathogen. The 3oxoC₁₂-HSL is the primary AHL from *P. aeruginosa*, and appears to be at the top of its QS hierarchy²³⁵: it initiates the signaling cascade by inducing the transcription of virulence factors at high cell density, and also activates the expression of *rhlI* and *rhlR*. The AHL-dependent QS regulator LasR also controls the transcription of *pqsH* and the expression of *pqsR*.^{236,237}

Mutations of *pqsR* induce lower levels of secreted pyocyanin, elastase, exoprotein and 3oxoC₁₂-HSL in *P. aeruginosa*.

2.1.2.4.4. The Diketopiperazines (DKP)

Few 2,5-diketopiperazines have been described to date.²³⁸ Their chemical structure is characterized by a core 6-membered piperazine ring grafted with amino acid sidechains at

carbons 2 and 5 (Figure 7). They have been observed in several Proteobacteria among which are *P. aeruginosa*, *Proteus mirabilis*, *Enterobacter agglomerans*. The DKPs are quite ubiquitous as they can activate AHL receptors, exhibit anti-fungal properties, and also activate genes encoding for membrane proteins and toxins.²³⁹

Given that DKPs incorporate natural amino acids, it is expected they exhibit a (*L*)-configuration.²³⁸ Recent work from Bofinger *et al.* has qualified this belief by demonstrating some bacteria produced mixed DKP isomers with different ratios.²⁴⁰ *C. sakazakii* for instance produces high amounts of cyclo(*L*-Pro-*L*-Leu), but also cyclo(*D*-Pro-*D*-Leu) and cyclo(*D*-Pro-*L*-Leu). The authors attributed the presence of diverse isomers to the bacteria use of *D*-amino acids and to DKP epimerisation.

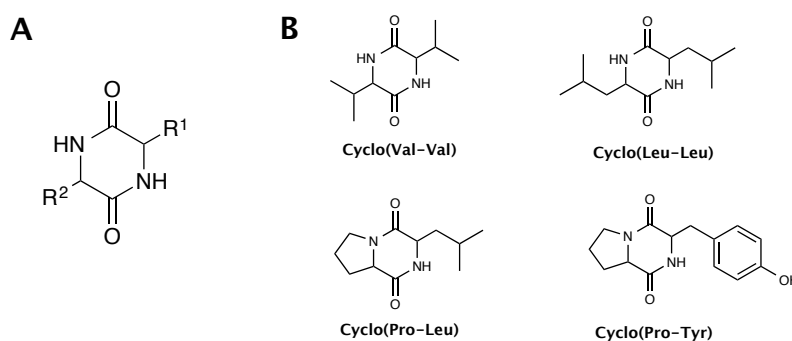


Figure 7 - Molecular structure of DKPs

A : General molecular structure with putative side chains R¹ and R². **B** : DKPs examples, without representation of stereochemistry.^{238–240}

2.1.2.4.5. The γ -butyrolactone

The γ -butyrolactone is a small 5-membered ring molecule very similar to the lactone headgroup of *N*-acyl homoserine lactones (Figure 8). It is produced by Gram-positive bacteria such as genus *Streptomyces* through diverse genes : *scgA* and *scgX* are involved in its biosynthesis, while *scgR* encodes for its protein receptor.²⁴¹

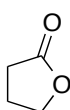


Figure 8 – Chemical structure of γ -butyrolactone

2.1.2.4.6. Auto-inducing peptides (AIP)

Gram-positive bacteria use Auto-inducing peptides (Figure 9) as molecular signals.²⁴² Similarly to other QS molecules, these will bind their cognate receptor only when the AIP extracellular concentration is high to activate target genes via a succession of phosphorylations.^{243,244}

AIPs are peptides containing a thiolactone (sulphur equivalent of lactones), and composed of 7 to 9 amino acids among which a mandatory cysteine which will play a central part in allowing covalent binding to the peptide C-terminal to form a cyclic thioester.²⁴⁵

Among AIPs are the CSP (Competence Stimulating Peptide) known to regulate DNA absorption in *Streptococcus*, the GBAP (Gelatinase Biosynthesis Activating Pheromone) in *Enterococcus faecalis* that regulates virulence factors, and the Auto-inducing peptides I-IV in *Staphylococcus aureus* that control its virulence factor production.

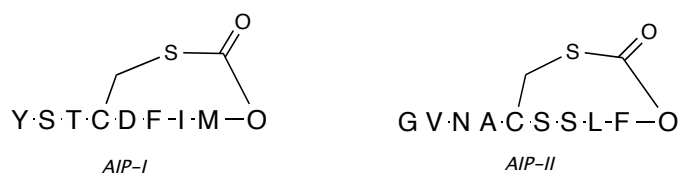


Figure 9 - Auto-inducing peptides I and II from *Staphylococcus aureus*

2.1.2.5. Summary table of presented QS molecules

Gram type	Molecule	Producing organism	Example of QS-regulated phenotype
Gram -	AI-1	<i>Proteobacteria</i>	Biofilm, bioluminescence
	AI-3	Entero-haemorrhagic <i>Escherichia. coli</i>	Unknown
	CAI	<i>Vibrio</i>	Virulence factors
	3OH-PAME	<i>Ralstonia</i>	Virulence factors
	PQS	<i>Pseudomonas</i>	Virulence factors
	DKP	<i>Proteobacteria</i>	Membrane protein, toxins
Gram +	γ -butyrolactone	<i>Streptomyces</i>	Antibiotic synthesis
	AIP	<i>Firmicutes</i>	
Gram + & -	AI-2	Bacteria	Bioluminescence, inter-species communication

Table 8 - Summary table of exposed Quorum Sensing molecules

2.1.3. Interspecies Communication and Signaling

At times it is useful for a bacterial colony to disrupt the quorum sensing from another competing group of bacteria. Several strategies have been observed. *S. aureus* for instance, uses QS to control its own *agr* virulence, but also to inhibit the virulence factors in other competing *S. aureus* groups.²⁴⁶ *P. aureofaciens* regulates antibiotic production via an AHL circuit, and this mechanism allows it to sense the presence of competing bacteria and respond by secreting antibacterial compounds.²⁴⁷ The soil bacterium *B. subtilis* produces an enzyme called AiiA that can inactivate the AHL of commensal soil bacterium *Erwinia carotovora*. The latter uses quorum sensing to colonise plants and also to regulate antibiotic production. AiiA from *B. subtilis* renders *E. carotovora* incapable of antibiotic and colonisation factors production.²⁴⁸

Other bacteria have chosen to join forces and collaborate. This strategy does not always rely on the “universal” type-2 auto-inducer. Visser and co-workers for instance demonstrated that the addition of AHL from *P. aeruginosa* to *B. cepacia* colonies induced the expression of virulence factors. They hypothesized that interspecies communication in a dual population of mixed *P. aeruginosa* and *B. cepacia* co-ordinately regulates virulence factors and influences the infection progression.²⁴⁹

Finally, certain non-AHL-producing bacteria have developed strategies to hijack the Quorum Sensing of others. The SdiA receptor is an orphan LuxR-type AHL receptor, encountered for instance in *Escherichia*, *Salmonella*, *Klebsiella*, *Enterobacter* and *Citrobacter*.^{250–252} Thanks to SdiA these bacteria can sense a wide panel of type-1 autoinducers, although they are not equipped with a LuxI homologue or any other member of the AHL synthases family.

These elements prove the importance of Quorum Sensing and AHL-based QS in interspecies communication and interactions, but certainly also the host-bacteria relationship. A strong implication in human microbiome and especially the intestinal microbiota must be expected. To date, data on such ecosystems are rather scarce and have mainly focused on intestinal pathogens. For instance, pathogenic bacteria *Yersinia enterocolitica* and *Y. pseudotuberculosis* possess two hierarchical LuxI/LuxR-type systems able to synthesize several AHLs^{253–255}, while *Pseudomonas aeruginosa* - whose quorum sensing has been extensively studied – can be found in the intestinal ecosystem.²⁵⁶

2.2. Interkingdom Signaling : Effects of *N*-Acyl Homoserine Lactones on Eukaryotic cells

The cells from the two kingdoms of Eukaryotes and Prokaryotes have co-existed and co-evolved alongside another for thousands of years, during which they have adapted to the signal molecules secreted by the other. QS molecules are now known to influence gene expression and other behaviours in Eukaryotic cells, a phenomenon called “*interkingdom signaling*”.²⁵⁷ Microbiota-derived SCFAs and GABA neurotransmitter from *Lactobacilli* have for instance neuropharmacological properties^{258–260}, while the mammalian hormone epinephrine has been described to substitute for autoinducer in the quorum sensing system of enterohemorrhagic *Escherichia coli* with impacts on the bacterium motility and virulence expression.^{217,261} Bacteria are also able of sensing an array of human peptide hormones such as somatostatin and gastrin.^{262,263}

Most studies to date on the effects of AHLs on mammal cells have focused on the well-known type-1 autoinducers from *P. aeruginosa* 3oxoC₁₂-HSL and C₄-HSL, but also 3oxoC₆-HSL from *V. fischeri*.

Pseudomonas aeruginosa is a highly adaptable Gram-negative pathogen, known to infect a large panel of host species, among which humans. In humans it provokes acute and chronic infections, especially in immune-compromised individuals such as cystic fibrosis patients, or those presenting with compromised epithelial barrier.^{264–268} The bacterium Quorum Sensing is one of the most extensively studied to date ; it is composed of three hierarchical networks whose successive interactions control the expression of virulence factors such as elastase, proteases, exotoxin A, pyocyanin, but also biofilm formation.^{269–272} Up to 10% of *P. aeruginosa* genome is controlled by QS, which makes its understanding vital to counteract effects on infected hosts.²⁷³ Furthermore, this bacterium causes a heavy burden on the medical community due to its widespread antibiotic resistance.

2.2.1. AHL penetration into cells

AHL are amphiphilic molecules, with a hydrophobic/lipophilic acyl chain and a hydrophilic/lipophobic lactone headgroup. It has been shown that these properties allow the

3oxoC₁₂-HSL to diffuse freely through the cell membrane of Prokaryotic and Eukaryotic cells, as do short-chained AHL in bacteria, while long-chained are actively transported.

Williams *et al.* demonstrated autoinducers could efficiently enter mammalian cells by transfecting cells with constructs of QS receptors coupled to a bioluminescence gene.²⁷⁴ The luminescence mapping demonstrated that the presence of cognate autoinducer drove the constructs to the nucleus. These data suggest that bacterial autoinducers can penetrate into mammalian cells, and that autoinducer binding is required for proper protein folding, addressing and functionality of bacterial receptors.

Pursuing the same goal, Ritchie *et al.* employed a radioactive 3oxoC₁₂-HSL to track and localise the autoinducer penetration in cells.²⁷⁵ The group observed an extremely fast (within minutes) and unregulated entry of the molecule, which also reached its maximum level very quickly, while the intracellular concentration was proportional to the extracellular levels. The intracellular localisation was mainly cytoplasmic (low proportions of nucleic and membrane-bound molecule), although this could also reflect the relative capacities of the different cell compartments.

2.2.2. Apoptosis

Upon exposure to 3oxoC₁₂-HSL, apoptosis has been observed in several human cell types including breast carcinoma cells, neutrophils, macrophages, fibroblasts and vascular endothelial cells ; however the phenomenon seems to be cell-type specific, as epithelial cells can resist it.²⁷⁶ Apoptosis induction appears dose-dependent and molecule specific, as other AHLs such as C₄-HSL did not provoke it. In particular, the oxo-moiety and the (*S*)-form of the lactone headgroup seem required for induction of apoptosis in macrophages.²⁷⁷

The exposure of human cells to 3oxoC₁₂-HSL activates several signalling pathways associated with apoptosis ; the apoptosis caused by 3oxoC₁₂-HSL has notably been linked to the modulation of signalling in mitochondria and the endoplasmic reticulum (ER), two organelles involved in the regulation of intracellular stress response. Upon treatment with AHL, dramatic morphological changes of these organelles are observed in bone-marrow derived macrophages (BMDM), including mitochondrial swelling and ER distortion.²⁷⁸ Triggering the ER-stress

pathway leads to Ca^{2+} release in the cytosol within minutes and downstream apoptosis, but also changes in ER protein synthesis rate through inactivation of $\text{eIF2}\alpha$.²⁷⁸

The mitochondrial apoptotic events are driven by caspase-3/9 activation and subsequent PARP cleavage,^{278,279} a biochemical marker of apoptosis.²⁸⁰ Kravchenko *et al.* confirmed this property was intrinsically connected to the lactone integrity of AHL, as neither its degradation products nor a lactam synthetic analogue were able to induce PARP cleavage in macrophages and lung epithelial cells.²⁷⁸ The activation of effector caspase-3 was also reported in airway epithelial cells²⁸¹, fibroblasts^{282,283}, intestinal epithelial cells²⁸⁴, breast carcinoma cells²⁷⁹, lymphoma cells²⁸⁵, lung carcinoma cells²⁸⁶, colorectal carcinoma cells²⁸⁶, and leucocytes.²⁷⁶⁻²⁷⁸

ER stress-responsive proteins inositol-requiring enzyme 1 α and X-box binding protein 1 are required to observe AHL-induced cell death in MEFs.²⁸³ Neely *et al.* showed that 3oxoC₁₂-HSL at 50 and 100 μM could induce MOMP and cytochrome *c* release in MEFs by itself, and that effector caspase-3/7 and initiator caspase-8 were essential for AHL-induced pro-apoptotic effects. This suggests the molecule may trigger the mitochondria-dependent intrinsic apoptosis pathway. On the opposite, previous studies had rather implicated caspase-8 and the extrinsic pathway in reported AHL-induced apoptosis.^{276,281,282,285} For comparison, the intrinsic pathway is activated by intracellular signals upon cell stress and depends on mitochondrial proteins release while the extrinsic pathway is activated by extracellular ligands binding to cell-surface death receptors.

Li *et al.* reported the partial inhibition of the Akt/PKB pathway and down-regulation of STAT3 activity in breast carcinoma cells upon treatment with 50-100 μM of AHL for 48h, with the JAK/STAT pathway likely involved in mediating the pro-apoptotic effects of the AHL.²⁷⁹ Likewise, Taguchi *et al.* observed the molecule could suppress Akt activation by blocking its phosphorylation in undifferentiated intestinal epithelial cells.²⁸⁴

2.2.3. Immunomodulatory effects and inflammation

The concept that AHLs may directly influence the host immune system originates from Telford *et al.* landmark paper.²⁸⁷ Since then, the literature dealing with the immunomodulatory properties of the 3oxoC₁₂-HSL on mammal cells has often seemed inconsistent as it reports both pro- and anti-inflammatory host response upon exposure to the molecule. These apparently

contradictory effects mostly rely on the diversity of experimental conditions implemented, such as the cell type, the AHL concentration, and the inflammatory status of resting versus stimulated cells.

The effects of the AHL 3oxoC₁₂-HSL on human cells have been explored on various cell types, and a wide range of observations have been reported including pro-apoptotic effects (cf. above), pro-inflammatory behaviour and immunomodulation (cf. *Introduction - 2.2.3*), haemodynamic effects²⁸⁸, and tight junctions perturbation (cf. *Introduction - 2.2.4.1*). Overall the molecule appears to exert direct pro-inflammatory functions at concentrations over 100µM on fibroblasts and lung epithelial cells, but also indirect effects from apoptosis induction and phagocytosis modulation. On the other hand, it shows anti-inflammatory properties on stimulated immune cells at concentrations below 100µM.

The effects on the immune system suggest a scenario where *P. aeruginosa* and 3oxoC₁₂-HSL respectively reach high cell density and high concentration during infection, which weakens the host's adaptive immune response and leads to increased bacterial persistence. This hypothesis could help explain why the bacterium provokes chronic infections in cystic fibrosis lungs or in diabetic wounds.

2.2.3.1. 3oxoC₁₂-HSL is a chemoattractant per se for neutrophils

Neutrophils are immune cells that usually appear at early stage of infection and become activated upon sensing bacteria and bacterial product, or under certain immune stimuli. This activation mediates the execution of specialised immune functions such as chemotaxis, phagocytosis and production of reactive oxygen species (ROS). AHLs such as 3oxoC₁₂-HSL and 3oxoC₁₀-HSL were shown to act as chemoattractants for human neutrophils and to induce their migration to the site of “infection” (here the AHL site) in a dose-dependent manner.^{289,290} Interestingly, this property was limited to long-chain and ketone-bearing AHL only, as C₄-HSL and C₁₂-HSL were not effective chemoattractants. Comparatively to some “usual” chemoattractants for human neutrophils that are chemokines, cytokines (e.g. IL-8 and GM-CSF), leukotriene B₄ or bacterial products, higher concentrations of AHL (100µM) were required for chemotaxis. Concomitantly to neutrophil migration, the authors observed cytoskeletal F-actin accumulation in the leading edge of neutrophils, via an increase of the F-actin to G-actin ratio and the activation of Rho GTPases Rac1 and Cdc42.²⁸⁹

On the opposite, Khambati *et al.* described antagonising AHL effects on chemotaxis in murine mast cells.²⁹¹ Molecules 3oxoC₁₂-HSL and C₁₂-HSL could both modulate mast cell function by the inhibition of degranulation and mediator release. The first AHL especially, seriously attenuated chemotaxis in mast cells. This property is of particular interest in the context of inflammatory bowel diseases, where an excessive activation of mast cells has been described.²⁹²

2.2.3.2. AHL effects on immune cell functions

In a pioneer paper, Telford *et al.* reported AHL 3oxoC₁₂-HSL could inhibit the secretion of cytokines IL-12 and TNF- α in LPS-stimulated macrophages. The molecule could inhibit the proliferation of T-cells as well, and the release of IL-2 *in vitro*.^{287,293} These observations led the authors to hypothesize that AHL might shift the host protective T-helper type-1 (Th1) response towards a pathogen protective T-helper type-2 (Th2) response.

The assumption was later unvalidated when several groups investigated the expression and function of T-cells TLRs after exposure to 3oxoC₁₂-HSL. TLRs play an important role in immunity as they mediate the activation of innate immune responses to infection by recognizing PAMPs. They initiate signaling cascades to activate NF κ B and the IRFs to provoke increased pro-inflammatory gene expression and fight back the infection.

Ritchie *et al.* explored the molecule effects on well-defined *in vitro* antigen-specific CD4 T cell response and mouse models.^{294,295} They analysed the variations in IFN- γ and IL-4 as markers of specific Th1 and Th2 responses. The AHL effects resulted neither from T-cell toxicity nor T-cell death ; exposure to 1-5 μ M affected early events in the T-cell activation (within 1-2 h) and resulted in decreased secretion of IFN- γ and IL-4 in both primary and secondary stimulation. It also appeared that rather than favouring a Th1/Th2 population imbalance, the 3oxoC₁₂-HSL inhibited the development and differentiation of all effector CD4 T-cells regardless of their Th1 or Th2 nature, and that the potency of the inhibition was correlated to the affinity of the antigen to which the T-cells were responding. More generally, the capacity of the 3oxoC₁₂-HSL to inhibit activation and proliferation of T-cells (and dendritic cells) had also been reported by Smith *et al.*²⁹⁶

Lu *et al.* determined whether the AHL had (a) direct(s) effect(s) on the immune function and expression of TLRs in monocytes. CD14⁺ monocytes were obtained from PBMCs from blood donors and exposed to 3oxoC₁₂-HSL at 10-100μM for 12 h ; upon exposure their IL-12 secretion was inhibited and proliferation blocked, TLR2 and 4 mRNA expressions were reduced, while TLR5 mRNA expression was increased in a dose-dependent manner. Although TLR2 and 4 protein levels were reduced, TLR5 protein expression was unchanged.

Bao *et al.* similarly investigated the expression and function of T-cells TLRs after exposure to 3oxoC₁₂-HSL, but their finding were quite the opposite of previous ones.²⁹⁷ PBMCs were treated with 1-100μM of the molecule for 12h, resulting in dose-dependent decrease in monocyte TNF-α secretion. In contrast with the findings from Ritchie *et al.* the authors observed concentration-dependent increase in T-cell growth rate and proliferation after 12h incubation with 1-100μM 3oxoC₁₂-HSL. It also appeared that the AHL could upregulate TL2 and TLR4 mRNA and protein expression at 10-100μM ; the TLR2 upregulation was significantly higher than that of TLR4.

Macrophages are other important effector cells of the immune response. Upon migration into tissues, the circulating monocytes differentiate into macrophages or dendritic cells (DCs). Macrophages are recruited to the site of infection by neutrophils ; they exhibit strong phagocytic activity and secrete many cytokines, among which pro-inflammatory cytokines to stimulate other immune cells to fight against infection. Vikström *et al.* studied the influence of human macrophage treatment with 100μM 3oxoC₁₂-HSL on their phagocytic activity, production of ROS and activation of p38 and p42/44 MAPK signaling pathways.²⁹⁸ Briefly, the macrophages were incubated with heat-killed *Saccharomyces cerevisiae* yeast cells in a 1:10 cell/yeast ratio to induce response in macrophages. Thirty minutes AHL exposure (resp. 1h) increased the phagocytic activity by 1.8 fold (resp. 1.6), but had no effect on ROS production. It was also shown that the 3oxoC₁₂-HSL activated the p38 MAPK but not the p42/44 MAPK signaling pathway, and that the AHL effects on phagocytosis could be inhibited by specific blocking of p38 MAPK activation with 10μM SB203580.

Multiple studies have reported molecule 3oxoC₁₂-HSL to decrease LPS-induced secretion of pro-inflammatory cytokine TNF-α in macrophages^{287,293,299,300}, although this effect is not consistently observed.^{278,301} Similarly, mice immunisation with AHL-protein conjugate increased their subsequent survival when exposed to *P. aeruginosa* which would suggest pro-inflammatory effects of the 3oxoC₁₂-HSL.³⁰²

Glucksam-Galnoy *et al.* investigated the immunomodulatory effects of the 3oxoC₁₂-HSL on the IL-10 and TNF- α cytokine secretion in murine macrophage cell line Raw 264.7. Their experiments revealed inhibitory effects of the AHL on the secretion of the pro-inflammatory cytokine TNF- α correlated to an increase in secretion of anti-inflammatory cytokine IL-10.³⁰³ The results were confirmed by quantitative real-time PCR, with a 3.5-fold increase of IL-10 mRNA levels upon treatment with 50 μ M 3oxoC₁₂-HSL. They also demonstrated that the immunosuppressive properties of the 3oxoC₁₂-HSL were independent of the TLR activated, as LPS- or imiquimod-induced stimulation resulted in similar increases of the IL-10 secretion. Because IL-10 can downregulate many pro-inflammatory cytokines (among which TNF- α , IFN- γ , IL-1 α , IL-1 β and IL-6³⁰⁴⁻³⁰⁷) the authors hypothesized 3oxoC₁₂-HSL could indirectly modulate the release of a wide array of pro-inflammatory cytokines.

2.2.3.3. Inflammatory properties on epithelia

It has long been shown that Quorum sensing molecules may modify the innate immune mechanism of airway epithelia. As early as in 1995, Di Mango *et al.* studied the influence of *P. aeruginosa* products on respiratory epithelial cells IL-8 secretion.³⁰⁸ The 3oxoC₁₂-HSL was found to stimulate IL-8 production in a dose-dependent manner ; it had moderate effects at 30 μ M, but much stronger effects at 100 μ M.

Smith *et al.* demonstrated that the 3oxoC₁₂-HSL could strongly stimulate both IL-8 mRNA and IL-8 protein in human fibroblasts and lung epithelial cells *in vitro* (resp. cell lines L828 and 16HBE).³⁰⁹ Stimulation of epithelial cells with 100 μ M induced a 15-fold IL-8 mRNA increase within 2h, while IL-8 levels in supernatants rose between 4h and 24h, with a climax at 8h (14-fold induction). Similar results were observed on fibroblasts, although with milder effects. The second *P. aeruginosa* auto-inducer C₄-HSL was used as a negative control, and elicited no response compared to resting cells. The IL-8 produced from these 3oxoC₁₂-HSL-stimulated cells proved functionally active and induced chemotaxis of neutrophils. The mechanism for IL-8 induction was partly elucidated, as the authors proved transcription factors NF- κ B and AP-2 to be essential for maximal induction. The activation of NF- κ B and subsequent production of IL-8 were found to be regulated by a MAP kinase pathway.

The group similarly studied the effects of 3oxoC₁₂-HSL on primary normal human lung fibroblasts and showed the molecule induced cyclooxygenase Cox-2, a seminal proinflammatory enzyme associated with inflammatory infiltrate, fever and pain.³¹⁰ An 8-fold induction in mRNA and a 35-fold increase in protein for Cox-2 were observed upon exposure to 100µM AHL. The increase in mRNA levels occurred from 4h after incubation start, with a maximum induction at 8h. Effects were much milder with 10µM concentration. In contrast, the expression of Cox-1 was not modulated by the AHL. Here as well 3oxoC₁₂-HSL activation of the transcription factor NF-κB was required for the induction of Cox-2. Concomitantly, the AHL also caused an increase in the expression of microsomal PGE synthase and PGE₂ in human lung fibroblasts and epithelial cells, but had no effect on the expression of the cytosolic PGE synthase.

Similar observations were made on skin injections with purified 3oxoC₁₂-HSL in mice. Dermal injections induced Cox-2, IL-1, IL-6, macrophage inflammatory protein 2 (MIP-2), monocyte chemotactic protein 1, MIP-1β, inducible protein 10, and T-cell activation gene 3.²⁹⁶ These results were confirmed by Shiner *et al.* who demonstrated a 3oxoC₁₂-HSL-induced pro-inflammatory response in human endothelial cells and mouse fibroblasts.³¹¹

2.2.4. Morphological changes in cells

2.2.4.1. Tight and adherent junctions of the gut epithelium

Epithelial cells lining the gut mucosa compose the interface between two compartments : the gut lumen and the lamina propria. They provide both physical and immunological barriers to prevent the mutual interpenetration of these compartments. The physical barrier relies on epithelial cell-to-cell adhesions that prevent pathogens and food constituents passage to the lamina propria. These are called tight junctions (TJ) and adherent junctions (AJ).³¹² Both junctional models associate with the actin cytoskeleton ; adherent junctions consist of the transmembrane protein E-cadherin and intracellular components p120-catenin, β-catenin and α-catenin, that initiate cell-cell contacts and mediate the maturation and maintenance of the contact. Tight junctions on the other hand, consist of the transmembrane proteins occludin and claudin, as well as the cytoplasmic scaffolding proteins ZO-1, -2, and -3 ; their role consists of regulating the paracellular pathways for ionic movements in between cells.

Vikström *et al.* demonstrated a modulation of the junctional integrity of polarised epithelial cells (Caco-2 cultured as a monolayer on Transwell filters) by 3oxoC₁₂-HSL. The QS molecule can disrupt the tight junctions in a time-dependent manner at 100-300µM, as proved by decreased transepithelial electrical resistance (TER), increased paracellular flux of solutes and diverse-sized dextran, reorganisation of F-actin and decreased expression and distribution of both occluding and ZO-1 proteins.³¹³ The AHL activated p38 and p42/44 MAPK; its effects on epithelial integrity were partly prevented upon inhibition of these kinases. Similar results were obtained on adherent junctions : at 200µM the molecule down-regulated the expression of proteins E-cadherin and β-catenin and altered their distribution in the cell monolayer. Junctional complexes occludin/ZO-1, JAM/ZO-1 and E-cadherin/β-catenin were also disrupted and their expression and distribution modified, with an overall increased permeability.³¹⁴

2.2.4.2. Cell migration and wound healing

Epithelial cells undergo wound-healing processes after epithelial injuries that may appear during IBD. These rely on the equilibrium between migration, proliferation and differentiation of the cells within the wounded region.³¹⁵ They are controlled by small GTPases of the Rho family such as Rho, Rac, and Cdc42.^{316,317}

Human cells can also adapt to environmental stresses by adjusting their volume ; this mechanism relies on membrane-spanning water channels called aquaporins (AQP) that facilitate the transport of small uncharged solutes and water through the cell membrane. To exert their functions aquaporins interact with the cytoskeleton and signaling cascades to influence cell morphology via volume modulation, movement and migration.³¹⁸ The aquaporin AQP9 has especially been identified for its critical role in the inflammatory response of human leukocytes during bacterial infection with increased expression in patients suffering from infectious endocarditis or systemic inflammatory response syndrome. Holm *et al.* studied the influence 3oxoC₁₂-HSL on cell morphology and AQP9 characteristics in human primary macrophages isolated from healthy blood donors.³¹⁹ The authors observed the AHL enhanced cell volume, area and protrusive activity ; these processes seem mediated by water fluxes across the cell membrane through AQP9 as shown by the upregulated expression of the aquaporin mRNA, proteins levels and in cell imaging. By doing so the AHL manipulates AQP characteristics that are important for proper macrophage functions during infection.

Losa *et al.* reported multiple effects of molecule 3oxoC₁₂-HSL on human airway epithelial cells, among which are morphological alterations and loss of gap junction conductivity in nonpolarized cells. Other QS molecules (PQS, C₄-HSL and (*R*)-3oxoC₁₂-HSL) were used as negative controls and proved ineffective. The effects were however not observed on polarised cells cultured on Transwell filters due to differential expression of AHL-degrading enzymes.

Finally, Karlsson *et al.* demonstrated 3oxoC₁₂-HSL could modulate Caco-2 cells migration rate in wound healing assays, in a dose- and time-dependent manner, regardless of substrate coating type.³²⁰ At high concentration (200µM) the molecule inhibited cell migration after long treatments (24, 48 and 72h) whereas doses 50 and 100µM only returned lowered effects. Surprisingly, low doses (1.5 – 12 µM) of molecule had opposed effects and promoted the cell migration.

2.2.5. Quorum quenching

Quorum Quenching (QQ) is the capacity to inhibit Quorum Sensing by blocking the signal transduction. The blockade can happen at three levels : first, the production of signal molecules by synthases can be impaired or abolished ; then the ligand recognition by receptors can be blocked, for instance with competing analogues ; finally, the auto-inducer can be degraded before reaching the receptor active site and performing its function. Regarding *N*-Acyl Homoserine Lactones, the third strategy relies heavily on enzymatic degradation : acylases (also known as amidases) can cleave the amide bond linking headgroup and acyl tail, lactonases can hydrolyse the lactone ring into an open-form ester, and oxydoreductases which can modify the oxidation pattern of the acyl chain at carbon-3 and terminal carbon.^{321–325} Degradation by acylases and oxydoreductases is irreversible, while hydrolysis by lactonases can be reversed under very acidic conditions (pH < 2).

In AHL-producing bacteria, the existence of QQ enzymes is supposed to help tune the concentration of signal molecules in the environment, to ensure it follows the bacterial density as closely as possible. *Pseudomonas aeruginosa* for instance produces an acylase named PvdQ which can hydrolyse long-chain AHLs, and especially its own auto-inducer 3oxoC₁₂-HSL.³²⁶

In non-AHL-producing bacteria however, the Quorum Quenching is rather a defensive behaviour to impair surrounding and competing bacteria, or simply prevent toxicity from

AHLs. Indeed, a degradation product named tetramic acid from the 3oxoC₁₂-HSL of *P. aeruginosa* has been described as bactericidal on Gram-positive bacteria, which should therefore prevent its formation.^{327–330}

Eukaryotes and especially mammals can secrete quorum quenching enzymes as well. The most studied representatives in this arsenal are lactonases called Paraoxonases or PONs. These are native mammalian enzymes, highly conserved across species (they are found in rat, rabbit, mouse, human...), with calcium-dependent hydrolase activity toward a fairly broad range of ester substrates such as arylesters, phosphotriesters, lactones and cyclic carbonate esters.^{331,332} The PONs are thought to be involved in drug metabolism, inactivation and clearance, and especially inhibition of lipid oxidation of lipoprotein (LDL), but also protection from cardiovascular diseases, metabolic disorders, cancer and infections.^{333,334} Their name indeed originates from the ability of PON1 to hydrolyse the pesticide paraoxon.

The mammalian PONs are classified into three subgroups numbered PON-1 to PON-3, that share 60% to 70% homology in their amino acid sequences and present with overlapping substrate specificities.³³⁵ Phylogenetic data suggest the mammalian paraoxonases originate from bacterial lactonases with quorum quenching activity, acquired through horizontal transfer.³³⁶

PONs have many substrates, but few inhibitor are known to date. The 2-hydroxyquinoline or 2-HQ is a competitive PON inhibitor (Figure 10). It contains a lactam moiety (a cyclic amide), that has been described as resisting hydrolysis by PONs and inhibits their hydrolysing functions.³³²

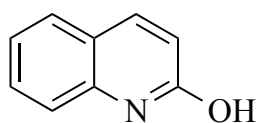


Figure 10 - Structure of PON inhibitor 2-hydroxyquinoline (2-HQ)

CAS number [59-31-4], empirical formula C₉H₇NO, molecular weight 145.16 g/mol.

2.2.6. AHL receptors

The AHL perception mechanism in mammalian cells is still fairly unclear. To date, no mammalian homolog of bacterial receptors to AHLs has been described, and the global assumption favours the idea of a different set of recognition proteins that could sense the bacterial autoinducers. It has been shown that the AHLs were not recognised by the classical PRRs from the innate immune system like other microbial molecules.²⁷⁸ Studies primarily tend to identify signal transduction pathways : some intermediates or final AHL-targets have been described, for instance NF- κ B and AP-2, which mediate the direct pro-inflammatory effects of the molecule. But it is unlikely that these mammalian transcription factors could be regulated by bacterial lipid-based compounds. Similarly, MAP kinases have been associated to AHL-mediated effects but not in all cell types (not in breast cancer cells for instance ²⁷⁹), which prevents MAPK from being universal mammalian AHL-receptors.

Considering the diversity of AHL effects reported, the hypothesis of at least two distinct eukaryotic receptors is regarded as quite likely. One putative receptor would be located at or close by the cell membrane and could mediate apoptosis induction via inositol triphosphate (IP3) and Ca²⁺ release ; prospective candidates are the G-protein coupled receptors. GPCRs are a large and versatile superfamily of membrane proteins, known to bind a large number of hormones and up to 40% of all therapeutic drugs. The assumption of a second AHL-receptor is based on the observation that blocking the AHL-mediated apoptosis induction in human fibroblast had no effect on the molecule-induced immunomodulation.³¹¹ This second receptor might be intracellular and located close to the nucleus ; proteins of the peroxisome proliferator-activated receptor (PPAR) family have for example been suggested.

In 2008, Jahoor *et al.* identified the peroxisome proliferator-activated receptor beta/delta and gamma (resp. PPAR β/δ and PPAR γ) as potential AHL receptors.³³⁷ Based on reported effects of the AHLs, the group made the hypothesis of an uncharacterised receptor accounting for the inflammatory properties of the molecule, which they supposed to be an intracellular protein. They examined the expression of a panel of nuclear hormone receptors in AHL-stimulated fibroblasts and lung epithelium cells : PPAR β/δ and PPAR γ were identified as the best candidates. The PPARs are attractive candidates as they respond to ligands of relatively

disparate structures and are associated with inflammatory gene regulation. When ligand-free, the PPARs bind to DNA and form complexes with co-repressor proteins, so that target genes are repressed. Ligand binding provokes structural changes that facilitate interactions with co-activators and promote the transcription of target genes. PPAR β has the broadest expression pattern (skin, gut, placenta, skeletal muscle, adipose tissue, and brain) while the PPAR γ two isoforms are found in the adipose tissue, the gut, brain, vascular cells, and specific kinds of immune and inflammatory cells.

The transcriptional activity of PPAR γ was proved inhibited by 3oxoC₁₂-HSL in a dose-dependent manner, both in the presence and absence of the PPAR γ agonist rosiglitazone ; on the opposite, PPAR β/δ activity increased in a dose-specific manner. Control C₄-HSL was ineffective at all doses on both PPARs activity. The 3oxoC₁₂-HSL could also inhibit the DNA binding activity of PPAR γ , and antagonise the anti-inflammatory trans-repression of cytokines expression by rosiglitazone, thereby potentiating the expression of pro-inflammatory genes.

However, AHL-recognition by PPARs does not account for all reported AHL effects in mammalian cells, among which the *I κ B α* induction, that all nuclear receptor agonist have failed to mediate.

Other candidate mammalian AHL receptors are the G-protein coupled receptors, and among these, member 38 of the bitter taste receptor family (T2R38). The gustatory system has evolved as a gatekeeper, determining food to ingest or not. In particular, bitterness sensing plays a central role in avoiding toxic substances. T2R38 (gene *Tas2R38*) is the most widely studied of the bitter taste receptor family, as it is extensively distributed along the gastrointestinal tract from tongue to distal end.^{338,339} In the lower GI tract, T2R38 is suspected of playing a role in eliciting immune responses to toxic compounds or pathogens in digestive diseases and metabolic conditions ; indeed *Tas2R38* polymorphisms have been linked to increased susceptibility to infections and colorectal cancer.^{340,341}

Humans possess 25 known bitter taste receptors to date, that can recognize hundreds (if not thousands) of bitter compounds.³⁴² As a result, the selectivity of T2Rs differs enormously among receptors. The human T2R38 can recognize a fairly extensive spectrum of compounds

with common structural motifs, a property that raises concerns regarding its AHL specificity.^{343–345}

A third potential mammalian AHL partner is the IQ-motif-containing GTPase-activating protein IQGAP1, which was identified as a putative human target in epithelial cells by means of a biotin-labelled 3oxoC₁₂-HSL coupled to LC-MS/MS by Karlsson *et al.*³²⁰ IQGAP1 is localised in the leading edge of migrating cells.^{346,347} As a scaffolding protein, it contains multiple domains for protein-binding : interactions with actin, myosin, β -catenin, E-cadherin, calmodulin, and MAPK have been reported.^{348,349} It plays a central role in cell morphology, vesicle trafficking and migration.³⁴⁷ IQGAP1 has been shown to directly interact with and stabilise the Rho-family GTPases, Rac1, and Cdc42 in their GTP-bound state.³⁵⁰ The hypothesis of a scaffolding protein as AHL partner is sensible, considering those proteins integrate signaling pathways by mediating critical rearrangement in the cytoskeleton and cell morphogenesis among which are chemotaxis. These effects were reported as modulated by AHL in the previous section. Unfortunately, we still lack concrete evidence at the moment to entirely validate IQGAP1 as an identified 3oxoC₁₂-HSL protein partner.

The interactions of 3oxoC₁₂-HSL with several partners located in several cell compartments, passive diffusion and entering into the cytoplasm, do not technically exclude each other. It has, for instance previously been shown that some lipid-based molecules, such as chemoattractant leukotriene B₄, can bind to both the cell surface receptor LTB₄, and nuclear PPAR.

2.3. State of the art in our laboratory

Previous literature has demonstrated intricate interactions between Quorum Sensing molecules and mammalian cells. Although studied in many bacterial ecosystems, these molecules had until recently never been identified in the human intestinal microbiota.³⁵¹ Yet, given the compositional changes observed among bacteria during dysbiosis, changes in the Quorum Sensing molecular patterns could be expected as well. Indeed, one of the most

important consequences of the IBD-linked dysbiosis is a decreased ratio [Firmicutes over Bacteroidetes]. Keeping in mind that Bacteroidetes are Gram-negative bacteria – the bacterial subset using *N*-Acyl Homoserine Lactones as autoinducers – a differential expression pattern of AHLs was suggested in the intestinal ecosystem of IBD patients.

To assess this hypothesis, our group first examined the presence of *N*-Acyl Homoserine Lactones in intestinal samples from IBD patients, before performing their characterisation. These results have been published.³⁵²

2.3.1. Are there AHLs in the intestinal ecosystem?

To answer this question, 75 faecal samples from 49 IBD patients and 26 healthy donors (HD) were collected. Among these patients 22 had Crohn's disease, while 27 had Ulcerative colitis, and 24 samples were collected during flares while 25 were collected during remissions. Diverse extraction and preparation steps were performed on these samples, which were eventually analysed by mass spectrometry HPLC/MS-MS. It revealed the presence of 14 different AHLs, with diverse distributions among samples (Figure 11). Among these, one AHL identified with *m/z* ratio at 294.2 was prominent and appeared in 40% samples, while all other AHLs were found in less than 10 samples. Thanks to HPLC, fractions containing the desired AHL were harvested to perform high resolution mass spectrometry and obtain its precise mass. The mass of protonated AHL $[M+H]^+$ revealed to be 294.1700 *m/z*, which corresponds to formula $C_{16}H_{24}O_4N$. This formula was attributed to a doubly unsaturated AHL with a 12-carbon-long acyl chain and oxo pattern at carbon-3, that is to say a 3oxoC₁₂:2-HSL. However, the localisation of carbon double bonds could not precisely be assessed due to extremely low quantities. The newly identified AHL proved active on Quorum sensing as confirmed testing on NTL4 biosensor.

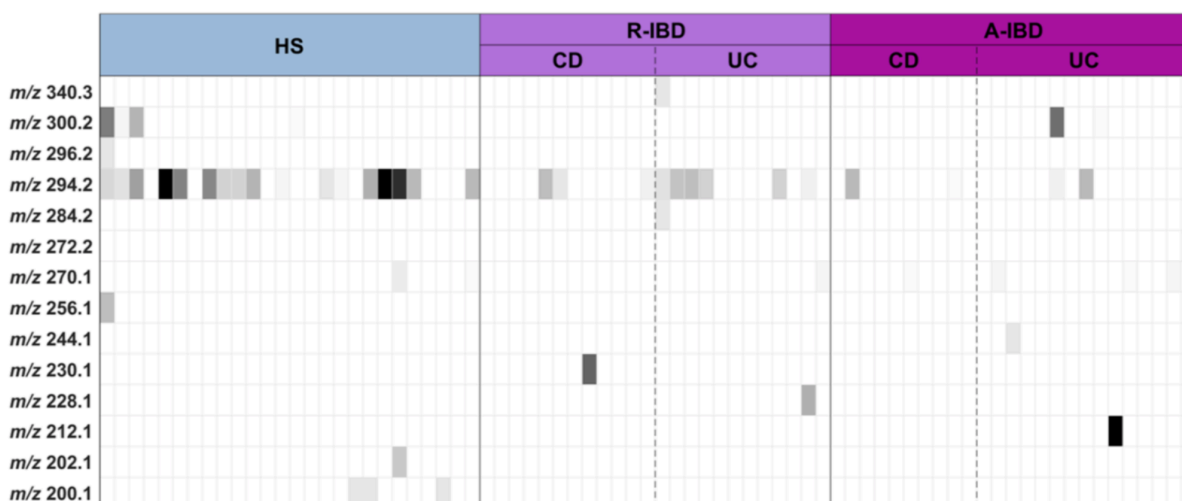


Figure 11 – Heatmap of found AHLs in faecal samples from IBD patients and healthy subjects as identified by their m/z ratio and the medical status of the donor

Extracted from Landman et al.³⁵². The grey colour indicates the AHL concentration, with white the lowest to black the highest. HS : healthy subject, R-IBD : IBD patient in remission, A-IBD : active IBD, CD : Crohn’s Disease, UC : Ulcerative Colitis.

Unsaturated AHLs are not commonly found in the realm of bacteria, where saturated AHLs dominate. Though, the marine *Roseobacter* clade is a well-known producer of mono- and di-unsaturated AHLs with chains ranging from medium to long (10 to 18 carbons).^{353–355} The common feature among all these unsaturated AHLs concerning their oxidation pattern at carbon-3 : they all carry either an hydroxyl moiety or a proton. But none harbours a ketone. This observation makes our newly described AHL 3oxoC₁₂:2-HSL even more remarkable as it is the first doubly unsaturated oxo-AHL that has been described.

Correlations between the newly identified AHL and the donors’ medical status were investigated. It appeared the molecule was significantly lowered in IBD patients in flare-up (4 out of 25 samples, 16%) or remission (37.5%) compared to healthy donors (65.4%). Its faecal concentration was also significantly decreased in IBD patients with active disease (average 0.25 nmol/g feces) or in remission, in comparison to healthy subjects (2.62 nmol/g feces).

It was further demonstrated that the 3oxoC₁₂:2-HSL correlates with normobiosis, and hence absence of disease. Principle component analysis (PCA) of data from microbiota sequencing revealed different distributions depending on the absence or presence of 3oxoC₁₂:2-HSL : some groups were decreased and other increased in presence of the molecule. In

particular, the presence of 3oxoC₁₂:2-HSL was associated with higher counts of Firmicutes and lower counts of *E. coli*. These findings make the 3oxoC₁₂:2-HSL a good biomarker of intestinal health, but do not provide any direct information regarding its biological activity.

2.3.2. Objectives of the project

This PhD was funded by the *Interfaces Pour le Vivant* scholarship program, to carry out a frontier project between Biology and Chemistry.

It is the very first time that AHLs have been extracted from human intestinal samples. Previous studies have reported the *P. aeruginosa* AHL 3oxoC₁₂-HSL is recognised and active on human lung epithelial cells. Similar results must be demonstrated on intestinal epithelial cells.

The human gut microbiota is a highly complex system with bacteria that are difficult to culture in the lab. As a result, it has been impossible to identify with certainty the strain(s) producing these AHLs in the intestinal ecosystem. Thus, we chose to focus our study on the 3oxoC₁₂-HSL and 3oxoC₁₂:2-HSL only, employed as representative AHL frameworks.

Building on these two structurally close molecules, our first objective was to study their respective biological properties on intestinal inflammation during IBD. A large array of markers were examined, including toxicity, modulation of cytokines expression and secretion, and ROS production.

In a second step, the AHLs stability to chemical and enzymological degradation was studied, and their cellular metabolism was investigated. This study revealed a complex mechanism involving equilibrium between several metabolites. These findings led us to develop chemically modified AHLs and fluorescent tools for cell imaging, in order to obtain a better insight into the AHL mechanism of action.

As our biological results exposed AHLs complexities and limitations, the last part of this project focused on the development of a library of bio-inspired AHL analogues. These compounds were dedicated to the identification of structural traits beneficial to AHL activity, and revealed several promising candidates.

Materials and Methods

1. Experimental procedures and protocols employed in Biology

Penicillin-streptomycin antibiotics, non-essential amino acids (NEAA) and L-glutamine were from Invitrogen (Thermo Fisher Scientific, Waltham, Massachusetts, USA). Dulbecco's Phosphate Buffered Saline (DPBS 10X), high glucose Dulbecco's modified Eagle's medium DMEM GlutaMAX 4.5 g/L glucose, Dulbecco's modified Eagle's medium DMEM and red-phenol-free DMEM were from Gibco (Thermo Fisher Scientific, Waltham, Massachusetts, USA). Foetal calf serum was from GE Healthcare (Life Science, South Logan, Utah, USA).

2-hydroxyquinoline (CAS [59-31-4]), 3oxoC₁₂-HSL, probenecid, H₂-DCFDA and sterile DMSO were bought from Sigma. 3oxoC₁₂:2-HSL was synthesized on request by Diverchim (Roissy-en-France, France). γ -butyrolactone, was from TCI Chemicals (Tokyo, Japan). AHL-FITC was from Cayman Chemicals.

All absorbance and luminescence assays were read on a SpectraMax M5_e Molecular Devices® spectrometer.

1.1. Cell culture

1.1.1. The Caco-2/TC7 cell line

The Caco-2 cell line derived from a human colon adenocarcinoma represents a cell culture model of enterocytes lining the small intestine epithelium.³⁵⁶ Caco-2/TC7 cell line is a clonal population of the human colon carcinoma-derived Caco-2 cells, which reproduces to a high degree and homogeneously most of the morphological and functional characteristics of normal human enterocytes.^{357,358}

Caco-2/TC7 cells display contact inhibition property leading to the arrest of growth when cells reach confluence (Figure 12), leading to the establishment of a cell monolayer. During the exponential growth phase (from seeding to confluence), cells remain undifferentiated. At confluence, they become spontaneously (in the absence of differentiation inducers) and

progressively differentiated and polarised.^{356,357} The differentiation process, which is a growth-related mechanism, is maximal at late confluency (stationary phase of the growth curve).

Cells develop an apical brush border harbouring microvilli and endowed with characteristic enterocytic enzymes such as hydrolases.³⁵⁷

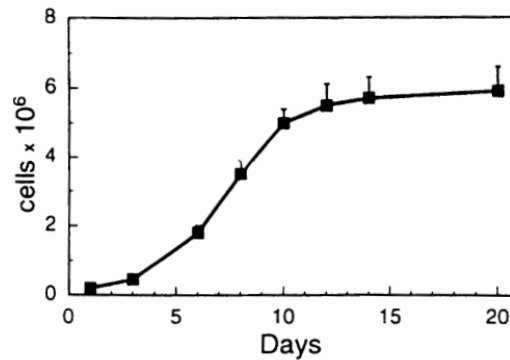


Figure 12 - Growth curve of Caco-2 cells showing the exponential growth phase, the arrest of growth at confluence, and the stationary phase where differentiation occurs.

Note that growth kinetic may vary according to seeding conditions. Caco-2/TC7 cells display similar growth curve. Figure extracted from Pignata et al.³⁵⁹

In accordance with published literature, Caco-2/TC7 cells in our experiments were seeded at 10^5 cells/well (equivalent to $10\text{-}12 \times 10^3$ cells/cm²) in 6-well plastic culture plates.³⁵⁷ The cells were maintained in high glucose medium (high glucose Dulbecco's modified Eagle's medium DMEM GlutaMAX 4.5 g/L glucose) supplemented with 20% heat-inactivated foetal calf serum, 1% non-essential amino acids NEAA and 1% penicillin-streptomycin. The cells were cultured at 37°C in 10% CO₂/air atmosphere. Medium was changed every day. In these conditions, the cells showed confluency at day 6. On day 17 the cells were serum-starved, and they were used on day 18.

1.1.2. The Raw 264.7 cell line

The Raw 264.7 cell line are murine macrophage/monocyte-like cells derived from Abelson leukaemia virus transformed cell line originating from BALB/c mice. This cell line is very often used as an *in vitro* macrophage model. Raw 264.7 cells are capable to perform phagocytosis and pinocytosis, can kill target cells by antibody-dependent cytotoxicity and secrete an broad array of inflammatory cytokines as well as nitric oxide (NO). Raw 264.7 cells

are furthermore a very practical cell line : the cells grow fast, appreciate small diameter wells, and demand to be used before confluency. These conditions make them good suitors for compound screening.

Taciak *et al.* demonstrated the functional, morphological, phenotypic and genetic stability of Raw 264.7 cells from passage 10 till passage 30³⁶⁰ ; hence we used cells between passages 13 and 26 for our studies.

Raw 264.7 cells from ATCC were used. They were cultured in Dulbecco's modified Eagle's medium DMEM supplemented with 10% heat-inactivated foetal calf serum and 1% 200 mM L-glutamine, and maintained at 37°C with 5% CO₂/air atmosphere. Medium was changed every other day.

1.1.3. The bacterial reporter strain *E. coli* pSB1075

A bacterial Quorum-Sensing reporter strain was used to study the capacity of molecules to be recognised by the *Pseudomonas aeruginosa* AHL receptor LasR and induce downstream activation. To do so, the strain *Escherichia coli* pSB1075 was employed.

The enterobacterium *Escherichia coli* does not naturally produce AHLs and does not possess any orphan AHL receptor either. This bioluminescent strain has been engineered by addition of a pSB1075 plasmid. This plasmid contains genes coding for both tetracycline resistance and expression of the AHL receptor LasR from bacterium *Pseudomonas aeruginosa*, as well as a fusion gene derived from the LasR promotor and the luxCDABE gene from *Photobacterium luminescens*. The bacterial strain was grown in LB medium supplemented with 5 µg/ml tetracycline to exert a selective pressure and ensure the desired strain alone was expanded. The fusion gene included in the plasmid gives the bacteria the capacity to emit bioluminescence whenever the LasR receptor becomes activated, and provides the user with a robust assay for molecular screening. The LasR receptor from *P. aeruginosa* is well-suited for recognition of long-chain AHL, especially its natural partner the 3-oxoC₁₂-HSL which elicit the highest bioluminescent response. On opposite, short-chain AHLs such as C₄-HSL cannot elicit bioluminescence.

Briefly, bacterial culture was started on day 0 in 10 ml LB medium supplemented with 5 µg/ml tetracycline and maintained 24h at 37°C and 70 rpm agitation. On day 1, the culture was diluted to 1/100 (P1) in 10 ml LB medium supplemented with 5 µg/ml tetracycline and maintained 24h at 37°C and 70rpm agitation. On day 2, the experiment took place : a bacteria suspension extemporaneously diluted to the 1/10 in LB medium supplemented with 5 µg/ml tetracycline (P2) was distributed in a black opaque 96-well plate and incubated for 4h with a range of AHL concentrations or controls until the resulting luminescence was read at endpoint. All experiments were performed in triplicates.

1.1.4. Bactericidal assay

E. coli strain K12 was put into culture on agar gel at day 0, and one colony transferred to liquid bacterial culture medium LYBHI on day 1. On day 2 the colony was diluted to 1/100 in LYBHI medium and expanded for 18h before plating in opaque 96-well plate. Into each well were distributed LYBHI, controls or increasing doses of tested molecules, and bacteria. Absorbance at 600nm was read at starting time ($t = 0$) and after 18-hour incubation. Raw absorbance values were corrected using absorbance of bacteria-free solutions. All experiments were performed twice, each with 4 replicates.

1.2. Evaluation of the biological activity of molecules in mammal cells

1.2.1. Caco-2/TC7 stimulation with cytokines

Caco-2/TC7 cells were seeded in 6-well plates at 100 000 cells/well and cultured for 18 days. On day 17, the cells were serum-starved – meaning the cell medium was replaced with a medium deprived of FCS - and used on day 18.

The stimulation medium was composed of starvation medium (DMEM GlutaMAX, 1% NEAA, 1% penicillin-streptomycin) with 100 µM 2-HQ. The cells were incubated for 18 h at 37°C with 2ml of stimulation medium containing 0,1% DMSO (negative control) or stimulation medium containing the tested compounds at desired concentrations, with or without a pro-inflammatory cytokine to induce inflammation. We used either IL-1β at 25 ng/ml or a combination of TNF-α and IFN-γ at 50 ng/ml each. After 18 h, the supernatants were collected, and stored at -80°C

before ELISA. Cells were washed with 1 ml PBS 1X/well, and lysed in 100 μ L PBS 1X containing 1% triton X-100. Cells were harvested by scraping, and stored at -80°C before protein quantification. LDH assay was performed straight away before freezing.

All cell experiments were realised in triplicate.

1.2.2. Raw 264.7 stimulation with LPS and IFN- γ

Raw 264.7 cells were seeded in 12-well plates at 75 000 cells/well, or 24-well plates at 40 000 cells/well, upon reaching 80-90% confluence after 3 days. For stimulation, the cells were incubated for 6 h at 37°C with 750 μ L (resp. 500 μ L) of cell medium enriched with 100 μ M 2-HQ, containing 0,1% DMSO (negative control) or the tested compounds at desired concentrations, with or without LPS (10 ng/ml) and IFN- γ (20 U/ml) to establish inflammation. After 6 h, the supernatants were collected, and stored at -80°C before ELISA. Cells were harvested by scraping them in 100 μ L PBS 1X/well and stored at -80°C before protein quantification. LDH assay was performed straight away before freezing.

All experiments were done in triplicate.

1.2.3. Measurement of protein concentration in cell lysate

Protein concentrations were determined in cell lysates using bicinchoninic acid (BCA) protein assay reagents and bovine serum albumin (BSA) as standard according to the manufacturer's instructions (Uptima-Interchim, Montluçon, France).

1.2.4. Human cytokines quantification by ELISA

Levels of the pro-inflammatory cytokine IL-8 produced by cells were determined in cell supernatants and/or cell lysates using commercially available IL-8 detection ELISA kit (DuoSet Human CXCL8/IL-8, ref. DY208) provided by R&D Systems (Minneapolis, Minnesota, USA) according to the manufacturer instructions. Levels of human cytokine IL-1 β were determined in cell supernatants and/or cell lysates using commercially available "Human IL-1 β ELISA Set" kit provided by BD Biosciences (ref. 557953) according to the manufacturer instructions.

Levels of human cytokine IL-10 were determined in cell supernatants and/or cell lysates using commercially available “Human IL-10 Uncoated ELISA” kit provided by Invitrogen (ThermoFisher, ref. 88-7106) according to the manufacturer instructions.

All cytokines levels were first normalized to the protein content determined in the corresponding cell lysates. Then, to compare experiments they could be further normalized using the activated control condition (DMSO + cytokines) as a 100% response.

1.2.5. Quantification of murine cytokines

Levels of murine cytokines IL-6, TNF- α and IL-10 produced by cells were determined in cell supernatants or cell lysates using commercially available “BD OptEIA Mouse IL-6 ELISA Set” kit from BD Biosciences (San Jose, California, USA, ref. 555240), “DuoSet Mouse TNF- α ” from R&D Systems (Minneapolis, MN, USA, ref. DY410-05) and “DuoSet Mouse IL-10” from R&D Systems (ref. DY417-05), respectively. All ELISA kits were employed according to the manufacturer instructions.

Cytokines levels were first normalized to the protein content determined in the corresponding cell lysates. To compare experiments they could be further normalized using the activated control condition (DMSO + cytokines) as a 100% response.

1.2.6. Cytotoxicity assay

Cytotoxicity of tested compounds and controls, with or without pro-inflammatory cytokines, was assessed using lactate dehydrogenase (LDH) release assay, which follows the release of LDH in cell supernatant, a good indicator of membrane damage. A compound was considered cytotoxic when its LDH ratio was over 10%.

Two methods could be used to perform the assay : measurement with a pyruvate/NADH solution (Sigma), or using the Cytotoxicity Detection Kit^{PLUS} (LDH) from Roche (Sigma-Aldrich).

For the Pyruvate/NADH method, a solution of pyruvate/NADH was prepared with 4.1 mg pyruvic acid (0.62 mM) and 7.7 mg NADH (0.18 mM) in 60 ml 0.1M PBS (pH 7.4).

For measurement of the LDH concentration in supernatant, 800µL of NADH was added to 200µL of supernatant into a plastic cuvette, and decrease in absorbance at 340 nm was monitored for 1 min. For measurement of the LDH concentration in cell lysate, 800µL of NADH was added to 10µL of supernatant and 190µL 0.1M PBS into a plastic cuvette, and decrease in absorbance at 340 nm was monitored for 1 min. The percentage of LDH released in the supernatant was calculated as the ratio of corrected slopes in the supernatant and cell lysate.

With the Cytotoxicity Detection Kit^{PLUS} (LDH – Roche – ref. 04744934001), levels of LDH were determined in supernatants and cell lysates by means of the absorbance-based test according to the manufacturer instructions. A percentage of cytotoxicity could be establish with the formula:

$$\%_{LDH} = \frac{DO_{sample} - DO_{low\ control}}{DO_{high\ control} - DO_{low\ control}} \times 100$$

1.3. RNA extraction, Reverse transcription and Quantitative PCR

For RNA extraction, all cells were seeded in 6-well plates. Caco-2/TC7 cells were seeded at 100 000 cells/well and cultured for 18 days, while Raw 264.7 cells were seeded at 110 000 cells/well and cultured to reach 80% confluence.

The cells were treated with the tested compounds at desired concentrations, with or without 100µM 2-HQ, during 4 or 6h for Caco-2/TC7 and Raw 264.7 cells respectively.

After incubation the medium was removed, the plates placed on ice and the cells washed with 1ml/well ice-cold PBS and then scrapped in 1ml ice-cold PBS before being transferred to an Eppendorf conical tube. The samples were centrifuged at 4°C for 10 min at 250g. The supernatant was removed and discarded, while the pellets were stored overnight at -80°C before RNA extraction.

RNA extraction was performed via TRIzol reagent method according to manufacturer instructions (ThermoFisher). Concentration and purity of extracted RNAs were measured on a NanodropTM spectrophotometer (ThermoFisher Scientific). 1µg of RNA was then retro-transcribed to cDNA with kit “High Capacity cDNA Reverse Transcription Kit with RNase

inhibitor” from Applied BioSystem, and according the manufacturer’s instructions. Afterwards, cDNA was stored at -20°C.

On the following day cDNA was diluted to 1/75 in extra-pure water qPCR-grade and analysed with the SYBRGreen Master Mix (Applied Biosystems) according to the supplier’s instructions (Table 9). Forward and reverse primers 10X (Table 10) were from Eurogentec (Belgium). qPCR experiment was performed on a Step One Plus Real Time PCR system (Applied Biosystems, Life Technologies, Foster City, California, USA) with settings: DNA denaturation for 10 minutes at 95°C, followed by 40-50 cycles of dehybridization of primers (15 s, 95°C) and annealing (1 min, 60°C). The $2^{-\Delta\Delta Ct}$ method has been used to analyse the data, and Glyceraldehyde- 3-Phosphate Dehydrogenase (GAPDH) was used as a housekeeping gene. All conditions had three biological replicate and two technical replicates, while two negative controls were included for each gene, without any DNA sample.

Reagent	Volume/well (µL)	Final concentration
SYBRGreen Master Mix	6.25	-
cDNA 1/75 (0.67 ng/µL)	2.5	0.134 ng/µL
Forward primer 1X (10 µM)	0.25	200 nM
Reverse primer 1X (10 µM)	0.25	200 nM
H ₂ O DEPC	3.25	-
Total	12.5	-

Table 9 - qPCR well content

Gene	Forward primer	Reverse primer
<i>Mouse PON1</i>	5'-GATGGATCTGGACGAGAGAGAGAC-3'	5'-TAATACTCAAGAAACCCTTGC-3'
<i>Mouse PON2</i>	5'-CAGTAAGCGTGGAAAAATACTTG-3'	5'-GAATCAAACCCTTCTGCCAC-3'
<i>Mouse PON3</i>	5'-CACTGCTTATCTTTATGTCGTG-3'	5'-GAAGCACAGAGCCGTTGTTC-3'
<i>Mouse GAPDH</i>	5'-TGACCAGAGTCCATGCCATCACTC-3'	5'-ATGACCTTGCCACAGCCTTGG-3'
<i>Human PON1</i>	5'-TGCCTAATGGACTGGCTTTC-3'	5'-GTGATGCCCAATTCCAACAC-3'
<i>Human PON2</i>	5'-TCCACACTGCCACCTGATTA-3'	5'-GTGCAAAGCTGTGGAGTCCT-3'
<i>Human PON3</i>	5'-GAATGCCTCTCGAGAAGTGG-3'	5'-TAAAAGCCAGCCCACTAGGA-3'
<i>Human GAPDH</i>	5'-TGACCAGAGTCCATGCCATCACTC-3'	5'-ATGACCTTGCCACAGCCTTGG-3'
<i>Human IL-8</i>	5'-AGACAGCAGAGCACACAAGC-3'	5'-ATGGTTCCTTCCGGTGGT-3'
<i>Human IL-1β</i>	5'-CTGTCCTGCGTGTGAAAGA-3'	5'-TTGGGTAATTTTTGGGATCTACA-3'
<i>Human IL-10</i>	5'-GCCTAACATGCTTCGAGATC-3'	5'-TGATGTCTGGGTCTTGGTTC-3'
<i>Human TNF-α</i>	5'-CAGCCTCTTCTCCTCCTGA-3'	5'-GCCAGAGGGCTGATTAGAGA-3'

Table 10 - Primers sequences for qPCR

1.4. Biological activity of molecules on bacterial reporter strain *E. coli* pSB1075

Enterobacterium Escherichia coli does not naturally produce AHLs. This bioluminescent strain has been engineered by addition of a pSB1075 plasmid containing genes encoding for tetracycline resistance and expression of the AHL receptor *LasR*, as well as a fusion gene from the *LasR* promoter and the *luxCDABE* gene from *Photobacterium luminescens*.

On day 1, a 1/100 dilution of the bacterial strain (P1) was grown for 24h at 37°C under agitation (70 rpm) in LB medium containing 5 µg/ml tetracycline (selective pressure). On day 2, P1 was diluted to the 1/10 in the same medium to obtain P2. In a black 96-well plate were placed 200 µL of P2 and 10 µL of compound (medium, water and DMSO for negative controls, short-chained C₄-HSL for positive control, and the sample to test at desired concentration). The plate was incubated for 4 hours at 37°C under 70 rpm agitation. Luminescence was then read at all wavelengths (integration time 200 ms) on a microplate reader.

For competitive assays the culture protocol was similar, but bacteria were submitted to pre-incubation with either 1, 10 or 100 nM 3-oxoC₁₂-HSL for various time length (1, 2, 6 or 16h) before dilution to obtain P2 and classic incubation with the tested compound at desired concentrations.

1.5. Immunofluorescence experiments

1.5.1. Fixed-cells imaging

Caco-2/TC7 cells were seeded in 12-well plates on round coverslips diameter 12 mm at 75 000 cells per well and grown for 4 days. On day 5 the cells were incubated for 1h or 24h with the desired compounds in starvation medium. After incubation the supernatants were removed and cells rinsed twice with 1ml cold PBS 1X enriched with 1mM CaCl₂ and 0.5mM MgCl₂. The cells were fixed in PFA 4% for 20 min (1 ml/well) and rinsed with PBS again (x2). The cells were then incubated in humid chambers with DABCO 100 mg/ml in PBS 1X (60µL/coverslip). The coverslips were rinsed in milli-Q H₂O to remove excess DABCO, briefly drained and mounted on slides in DAPI-enriched Mowiol (5ng/ml) or ProLong™ Gold Antifade Mountant with DAPI (ThermoFisher, ref. P36931).

Slides were observed within 6h and on the following day to assess signal fading, on a Zeiss AxioImager2 epifluorescence microscope with structured light (Apotome2, Zeiss), camera and Zen software (2.3 Blue Edition) at magnification X63. Pictures are post-treated with Fiji software.

1.5.2. Live-cell imaging

Caco-2/TC7 cells were seeded in 4-well microslides with glass bottom from IBIDI (ref. 80427, IBIDI GmbH, Gräfeifing, Germany) at 40 000 cells/ml and 600 μ L/well, and grown for 4 days. On day 5 the cells were incubated for 1h in starvation medium. Once incubation completed, the supernatants were removed and the wells rinsed twice with red-phenol-free DMEM. The cells were observed straight away using a Leica confocal laser scanning microscope at magnification X63. Pictures are post-treated with Fiji software.

1.6. Reactive Oxygen Species production in Caco-2/TC7 cells

Caco-2/TC7 cells were seeded in 12-well black microplates with *ibiTreat* glass bottom from IBIDI (ref. 82406) at 75 000 cells per well (150 000 cells/ml and 500 μ L/well) and grown for 4 days. On day 5 the cells were incubated for 30 min with freshly prepared 50 μ M H₂-DCFDA in starvation medium. At completion, the supernatants were removed and the cells rinsed once with sterile PBS 1X. Afterwards solution in red-phenol-free DMEM containing increasing doses of AHL or controls were deposited in triplicates and the cells incubated at 37°C over 24h. Fluorescence was read at regular intervals on a FluoStar spectrometer, with excitation wavelength 485 nm, emission wavelength 535 nm and gain set at 1000.

1.7. Statistical analysis

All data are represented as mean \pm SEM of *n* independent experiments and were tested for gaussian distribution. Statistical significant was examined by mean of Student *t*-test, one-way ANOVA, two-way ANOVA or Kruskal-Wallis test depending on the data set, associated with post-test (Tukey's or Dunn's multiple comparison test). Differences were considered significant where $p < 0.05$. All statistical analysis were realised using software Prism 6.0, GraphPad.

2. Mass Spectrometry : Tandem LC/MS-MS

2.1. Evaluation of AHL half-life in cell culture medium at 20°C

The 3oxoC₁₂-HSL (resp. the 3oxoC₁₂:2-HSL) was dissolved at 5 or 15 μM in DMEM GlutaMax and the solution stirred at room temperature. Samples (1 ml) were taken at intervals over 24 h. The samples were extracted twice with 1ml EtOAc, then acidified with 1M HCl solution to decrease pH to approx. to 4-5, and finally extracted a third time with 1ml EtOAc. All aqueous and organics phases were stored at -80°C before treatment and analysis.

For mass spectrometry sample preparation, the organic extracts and aqueous phases were evaporated under a nitrogen stream at 50°C. The residues were dissolved in 250 μL MeOH (HPLC grade) and placed in 2ml MS vials (Agilent Technologies, Garches, France) equipped with 250μL inserts (Agilent Technologies).

2.2. Cell preparation for assessment of kinetics of AHL entry in cells

Caco-2/TC7 were plated in 6-well plates at 100 000 cells/well and grown for 18 days. On the 17th day their medium was changed to a starvation medium. On day 18 they were incubated with 1 ml/well of starvation medium containing 15 μM 3oxoC₁₂-HSL, with or without 100μM 2-HQ. At regular intervals, the supernatant of selected wells was removed and placed in 1.5 ml Eppendorf microtube, while the cells were scrapped in 500 μL ice-cold PBS 1X and lysed by sonication. All samples were then extracted twice with EtOAc (500 μL for supernatants and 300 μL for cell lysates) using vortex and 3 min centrifugation at 5000 rpm. The aqueous phase was then acidified with 20 μL of 1M HCl solution to bring down pH to 4, and extracted with EtOAc once more according the same protocol. All aqueous and organics phases were stored at -80°C before treatment and analysis.

For mass spectrometry sample preparation, the organic extracts and aqueous phases were evaporated under a nitrogen stream at 50°C. The residues were dissolved in 250 μL MeOH (HPLC grade) and placed in 2ml MS vials (Agilent Technologies) equipped with 250μL inserts (Agilent Technologies).

2.3. AHL detection by tandem HPLC-MS/MS

Because it allows quantitation and detection of very low quantities, mass spectrometry has become widely used in AHL sensing and identification through recent years. Early methods involved GC-MS and capillary electrophoresis, but HPLC coupled mass spectrometry has now established as gold standard.^{361–363} In this technique, the inverse phase liquid chromatography allows separation of compounds base on hydrophobicity : the more polar molecules exit the column first. Hence the retention time of diverse *N*-Acyl Homoserine Lactones is imposed by their acyl chain length, its saturation and the oxidation pattern at carbon-3.^{364,365} Separated components are then directly injected into the mass spectrometer. Mass spectrometry is an analytical technique based on ionisation of a given sample, which once charged is submitted to an electric or magnetic field. Components of the sample have different deflections depending on their masse-to-charge ratio m/z , which can be detected to sort and identify them.

The regular mass spectrometry technique however does not allow differentiation between compounds of the same masse-to-charge ratio. To do so, one can use tandem mass spectrometry which enables multiple rounds of mass spectrometry. With tandem MS/MS, it is possible to isolate compounds of interest based on their given masse-to-charge ratio, and then to fragment them in order to identify these fragments. AHLs have a well-known pattern of fragmentation, studied both on standard molecules and bacterial supernatant extracts.^{365–368} They typically break at the amide bound according two paths : the charge is either carried by the lactone ring giving a specific m/z ratio of 102, or it is carried by the chain fragment to give a m/z ratio of $[M+X-101]^+$, where X is typically a proton, a sodium ion, an ammonium... etc.

During our experiments, the chromatographic separation of compounds was carried out on a Zorbax eclipse XDB-C18 column (Agilent Technology) fitted on an Agilent 1100 tandem HPLC-MS/MS system (Massy, France). The column's temperature was maintained at 45°C. Five microliters of the compound solution were injected. The mobile phases consisted of (A) water with 0.1% formic acid and (B) acetonitrile with 0.1% formic acid in an 80:20 starting ratio, respectively. The linear gradient for AHL elution was programmed as follows : after increasing B in A from 20% to 40% for 5 minutes and from 40% to 95% for 15 minutes, the gradient was then kept constant over 10 minutes before 5 min re-equilibration for an overall 35 min run. Separation was achieved at a flow rate of 0.4 mL/min.

This method allowed for the separation of AHLs based on their hydrophobicity depending on the length of the acyl side chain, the nature of the substitution on the third carbon, the presence of unsaturation and the lactone headgroup integrity.³⁶⁹

Mass spectra were obtained using an API® 2,000 Q-Trap (AB-Sciex, Concord, Ontario, Canada) equipped with a TurboIon electrospray set in the positive mode with nitrogen as nebuliser gas. The ion source temperature was set at 350°C. Declustering and entrance potentials were set at 60 V and 5000 V, respectively. Data were acquired by the Analyst® software (version 1.4.2, AB-Sciex) in the multiple reaction monitoring mode. As described in the literature, identification of an AHL (designated by m/z of the precursor ion $[M+H]^+$) was defined by the presence at the same retention time of the precursor ion and the two possible product ions: $[M+H -101]^+$ corresponding to neutral loss and $m/z = 102$ corresponding to the lactone moiety.³⁶⁵ Other adducts were also observed, principally with ammonium ions.

The AHL quantification was expressed in micromoles per litre after calibration with commercially available 3oxoC₁₂-HSL and normalisation relative to the internal standard *N*-butyryl-*L*-homoserine-lactone-d₅ (C₄-d₅-HSL, Cayman Chemicals).

3. Material and Methods in Chemistry

Unless otherwise stated, all reactions were performed under argon atmosphere in dry glassware. Reagents were purchased from commercial suppliers Sigma-Aldrich and TCI Chemicals, and used without further purification.

Flash Chromatography was performed on pre-packed silica gel columns (SiOH irregular silica gel 40-63 μ m) from CHROMABOND® Flash (Macherey-Nagel, Düren, Germany) fitted on an automated SPOT platform from *ArMen*.

Thin Layer Chromatography was performed on aluminium sheets covered with silica gel 60 F₂₅₄ (Millipore, Merck) and revealed with potassium permanganate (KMnO₄), iodine on silica, bromocresol green or under UV light (254 nm or 365 nm).

3.1. Convention for atom numbering in *N*-acyl homoserine lactones and their analogues

In the following molecular description, the atom numbering for AHL and their analogues will be as described on Figure 13, unless otherwise stated.

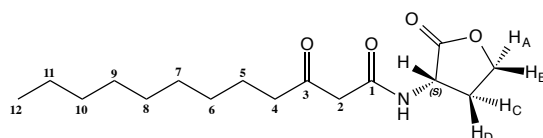


Figure 13 - Atom numbering convention for natural AHL and synthetic analogues

3.2. Experimental procedures for synthesis and physicochemical characterization of natural AHLs, intermediates and non-natural analogues

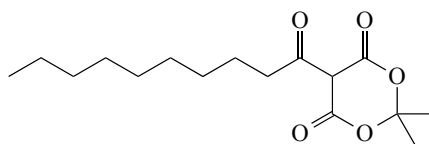
General procedure for the preparation of Meldrum's acid derivatives 3a-c³⁰⁰ (GP1)

The appropriate carboxylic acid (1.0 equiv) was dissolved in DCM (1.5 ml/mmol acid) at r.t. To the mixture were successively added DCC (1.1 equiv), DMAP (1.05 equiv) and Meldrum's acid (1.0 equiv).

The reaction was stirred overnight at r.t. under argon atmosphere. Follow-up of the reaction was achieved by TLC in 1:1 EtOAc/cyclohexane, and revealed with iodine.

At completion, the reaction mixture was filtered to eliminate precipitated DCU and the filter-cake thoroughly washed with dichloromethane. The filtrate was collected and solvent removed under vacuum. The resulting oil was diluted in EtOAc and the organic phase was extracted with 1M HCl (x2), while the aqueous phase was washed with EtOAc (x2). Combined organics were dried on MgSO₄, before removing the solvent under vacuum. The crude product, obtained as an oil, was directly engaged in the following step.

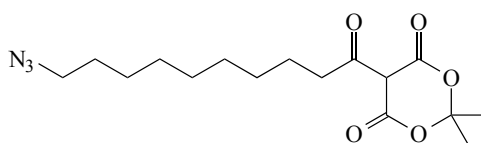
2,2-dimethyl-5-(1-oxodecyl)-1,3-dioxane-4,6-dione **3a** [182359-65-5]



C₁₆H₂₆O₅
(Mw: 298.38)

Prepared by GP1 with 94% yield. ¹H NMR (300 MHz, CDCl₃) : δ 3.12 – 3.03 (m, 2H, C(4)**H**₂), 1.74 (s, 6H, OC(**CH**₃)₂O), 1.45 – 1.24 (m, 14H, C(5)**H**₂ to C(11)**H**₂), 0.91 – 0.86 (m, 3H, C(12)**H**₃). ¹³C NMR (75 MHz, CDCl₃) : δ 198.3 (ketone), 170.6 (ester), 160.2 (ester), 104.7 (OC(CH₃)₂O), 91.2, 35.7, 31.8, 29.4, 26.8, 26.2, 22.7, 14.1 (C(12)). R_f (1:3 EtOAc/Cyhex) : 0.22.

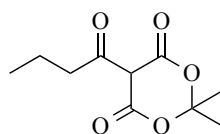
Azido 2,2-dimethyl-5-(1-oxodecyl)-1,3-dioxane-4,6-dione **3b** [no CAS]



C₁₆H₂₅N₃O₅
(Mw: 339.39)

Prepared by GP1 with 87% yield. ¹H NMR (300 MHz, CDCl₃) : 3.24 (t, *J* = 6.9 Hz, 2H, C(12)**H**₂), 3.08 – 3.02 (m, 2H, C(4)**H**₂), 2.12 (s, 1H, C(2)**H**), 1.72 (s, 6H, C(**CH**₃)₂), 1.62 – 1.54 (m, 4H, C(5)**H**₂ and C(6)**H**₂), 1.31 – 1.28 (m, 10H, C(7)**H**₂ to C(11)**H**₂). ¹³C NMR (75 MHz, CDCl₃) : δ 198.3 (ketone), 170.7 (ester), 160.3 (ester), 104.9 (C₂), 91.4 (OC(CH₃)₂O), 51.6 (C₁₂), 43.9 (C₄), 35.8 (C₅), 29.4, 29.2, 28.9, 26.9 ((**CH**₃)₂), 26.8, 26.2, 23.9. R_f (1:3 EtOAc/Cyhex) : 0.25.

2,2-dimethyl-5-(1-oxobutyl)-1,3-dioxane-4,6-dione **3c** [72546-06-6]



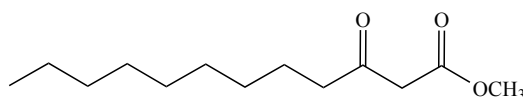
C₁₀H₁₄O₅
(Mw: 214.22)

Prepared by GP1 with 71% yield. ¹H NMR (300 MHz, CDCl₃) : 3.00 – 2.92 (m, 2H, C(4)**H**₂), 1.72 – 1.59 (m, 8H, C(**CH**₃)₂ and C(5)**H**₂), 0.94 (t, *J* = 7.4 Hz, 3H, C(6)**H**₂). ¹³C NMR (75 MHz, CDCl₃) : δ 197.9 (C₃), 170.5 (ester), 160.1 (ester), 104.7 (C₂), 91.3 (OC(CH₃)₂O), 37.4 (C₄), 26.7 ((CH₃)₂), 19.5 (C₅), 13.8 (C₆). R_f(1:4 EtOAc/Cyhex) : 0.15.

General procedure for the methanolysis of the Meldrum's acid derivative **4a-c³⁷⁰ (GP2)**

The Meldrum's acid derivative **3a-c** (1.0 equiv) was dissolved in excess methanol and the reaction flask equipped with reflux apparatus under argon atmosphere. The reaction was refluxed for 2 hours, then heating was stopped and the mixture left to cool down spontaneously to r.t. and stirred overnight. Advancement of the reaction was followed by TLC in 1:1 EtOAc/cyclohexane and revealed in iodine. At completion solvent was removed under vacuum and the oily product engaged crude in the following step.

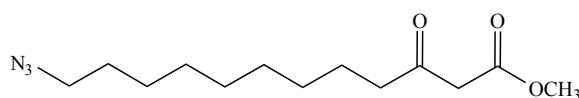
Methyl 3-oxododecanoate **4a** [76835-64-8]



C₁₃H₂₄O₃
(Mw = 228.33)

Prepared by GP2 with 96% yield. ¹H NMR (300 MHz, CDCl₃) : δ 3.75 (s, 3H, OCH₃), 3.46 (s, 2H, C(2)**H**₂), 2.54 (t, *J* = 7.4 Hz, 2H, C(4)**H**₂), 1.59 (d, *J* = 7.4 Hz, 2H, C(5)**H**₂), 1.28 (s, 12H, C(6)**H**₂ to C(11)**H**₂), 0.92 – 0.87 (m, 3H, C(12)**H**₃). ¹³C NMR (75 MHz, CDCl₃) : δ 202.9 (C₃), 167.7 (C₁), 52.3 (OCH₃), 49.0 (C₂), 43.1, 31.9, 29.4, 29.4, 29.2, 29.0, 23.5, 22.7, 14.1 (C₁₂). R_f (1:3 EtOAc/Cyhex) : 0.55.

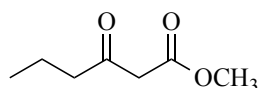
12-azido-3-oxododecanoic acid methyl ester **4b** [1421598-01-7]



C₁₃H₂₄N₃O₃
(Mw = 269.34)

Prepared by GP2 with 81% yield. ^1H NMR (300 MHz, CDCl_3) : δ 3.71 (s, 3H, OCH_3), 3.42 (s, 2H, $\text{C}(2)\text{H}_2$), 3.22 (t, $J = 6.9$ Hz, 2H, $\text{C}(12)\text{H}_2$), 2.50 (t, $J = 7.3$ Hz, 2H, $\text{C}(4)\text{H}_2$), 1.55 (q, $J = 6.8$ Hz, 2H, $\text{C}(5)\text{H}_2$), 1.27 (t, $J = 4.7$ Hz, 12H, $\text{C}(6)\text{H}_2$ to $\text{C}(11)\text{H}_2$). ^{13}C NMR (75 MHz, CDCl_3) : δ 202.9 (ketone), 167.8 (ester), 52.4 (OCH_3), 51.6 (CH_2N_3), 49.1 (C_2), 43.1, 29.4, 29.3, 29.1, 29.0, 28.9, 26.8, 23.5. R_f (1:3 EtOAc/Cyhex) : 0.6.

3-oxo-hexanoic acid methyl ester 4c [30414-54-1]



$\text{C}_7\text{H}_{12}\text{O}_3$
(Mw: 144.17)

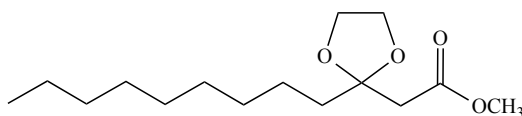
Prepared by GP2 with 49% yield. ^1H NMR (300 MHz, CDCl_3) : δ 3.59 (s, 3H, OCH_3), 3.33 (s, 2H, $\text{C}(2)\text{H}_2$), 2.39 (t, $J = 7.2$ Hz, 2H, $\text{C}(4)\text{H}_2$), 1.49 (h, $J = 7.3$ Hz, 2H, $\text{C}(5)\text{H}_2$), 0.79 (t, $J = 7.4$ Hz, 3H, $\text{C}(6)\text{H}_3$). ^{13}C NMR (75 MHz, CDCl_3) : δ 202.6 (C_3), 167.77 (C_1), 52.0 (OCH_3), 48.8 (C_2), 44.7 (C_4), 16.7 (C_5), 13.3 (C_6). R_f (1:4 EtOAc/Cyhex) : 0.55.

General procedure for installation of ketal at the C_3 position 5a-c³⁷¹ (GP3)

The 3-ketomethyl ester **4a-c** (1.0 equiv) was diluted in toluene (approx. 1 ml/mmol ester) and were successively added camphorsulfonic acid (0.2 equiv), trimethylorthoformate (5.0 equiv) and ethylene glycol (8.9 equiv). The reaction mixture was heated to 80°C for 3 hours, then left to cool down spontaneously and stirred overnight at r.t. Advancement of the reaction was followed by TLC in 1:6 EtOAc/cyclohexane and revealed with iodine. At completion toluene was removed under vacuum and the resulting oil was dissolved in DCM. The organic phase was extracted with sat. NaHCO_3 solution (x3) while the aqueous layer was washed DCM. The combined organics were dried over MgSO_4 and the solvent removed under vacuum.

If necessary, the oily product could be purified by Flash Chromatography on a silica column using a gradient elution from 1:8 to 1:2 EtOAc/cyclohexane.

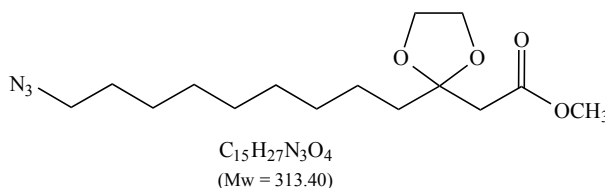
2-nonyl-1,3-dioxolane-2-acetic acid methyl ester 5a [109873-29-2]



$\text{C}_{15}\text{H}_{28}\text{O}_4$
(Mw = 272.38)

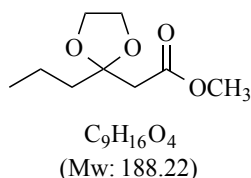
Prepared by GP3 with 95% yield. ^1H NMR (300 MHz, CDCl_3) : δ 4.01 – 3.95 (m, 4H, $\text{OCH}_2\text{CH}_2\text{O}$), 3.70 (s, 3H, OCH_3), 2.67 (s, 2H, $\text{C}(2)\text{H}_2$), 1.83 – 1.76 (m, 2H, $\text{C}(4)\text{H}_2$), 1.41 – 1.36 (m, 2H, $\text{C}(5)\text{H}_2$), 1.28 (d, $J = 5.4$ Hz, 12H, $\text{C}(6)\text{H}_2$ to $\text{C}(11)\text{H}_2$), 0.91 – 0.85 (m, 3H, $\text{C}(12)\text{H}_3$). ^{13}C NMR (75 MHz, CDCl_3): δ 170.1 (C_1), 109.4 (C_3), 65.10 (ketal), 51.72 (OCH_3), 42.4, 37.8 (C_2), 31.9, 29.7, 29.6, 29.5, 29.3, 23.5, 22.7, 14.1 (C_{12}). R_f (1:8 EtOAc/Cyhex) : 0.31.

2-(9-azido)nonyl-1,3-dioxolane-2-acetic acid methyl ester **5b** [No CAS]



Prepared by GP3 with 93% yield. ^1H NMR (300 MHz, CDCl_3) : δ 4.00 – 3.93 (m, 4H, $\text{OCH}_2\text{CH}_2\text{O}$), 3.67 (d, $J = 0.9$ Hz, 3H, OCH_3), 3.23 (t, $J = 6.9$ Hz, 2H, $\text{C}(12)\text{H}_2$), 2.64 (s, 2H, $\text{C}(2)\text{H}_2$), 1.80 – 1.74 (m, 2H, $\text{C}(4)\text{H}_2$), 1.61 – 1.55 (m, 2H, $\text{C}(5)\text{H}_2$), 1.28 (d, $J = 5.3$ Hz, 12H, $\text{C}(6)\text{H}_2$ to $\text{C}(11)\text{H}_2$). ^{13}C NMR (75 MHz, CDCl_3) : δ 170.2 (C_1), 109.5 (C_3), 65.2 (ketal), 51.9 (OCH_3), 51.6 (C_{12}), 42.5, 37.8 (C_2), 29.7, 29.5, 29.5, 29.2, 28.9, 26.8, 23.6. R_f (1:4 EtOAc/Cyhex) : 0.45.

2-propyl-1,3-dioxolane-2-acetic acid methyl ester **5c** [1083287-07-3]



Prepared by GP3 with 66% yield. ^1H NMR (300 MHz, CDCl_3) : δ 3.92 – 3.78 (m, 4H, $\text{OCH}_2\text{CH}_2\text{O}$), 3.56 (s, 3H, OCH_3), 2.53 (s, 2H, $\text{C}(2)\text{H}_2$), 1.70 – 1.60 (m, 2H, $\text{C}(4)\text{H}_2$), 1.36 – 1.21 (m, 2H, $\text{C}(5)\text{H}_2$), 0.80 (t, $J = 7.4$ Hz, 3H, $\text{C}(6)\text{H}_3$). ^{13}C NMR (75 MHz, CDCl_3) : δ 169.8 (C_1), 109.1 (C_3), 64.9 (ketal), 51.5 (OCH_3), 42.2 (C_2), 39.8 (C_4), 16.7 (C_5), 14.0 (C_6). R_f (1:2 EtOAc/Cyhex) : 0.64.

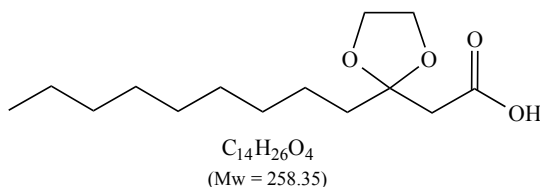
General procedure for the basic hydrolysis of methyl ester **6a-c**^{301,372} (**GP4**)

The ketal-protected methyl ester **5a-c** (1.0 equiv) was dissolved in THF (1.25 ml/mmol ester) and 1M NaOH solution (approx. 2.5 equiv) added. The reaction mix was brought to reflux for 3 hours.

Advancement of the reaction was followed by TLC in 1:8 EtOAc/cyclohexane and revealed with iodine.

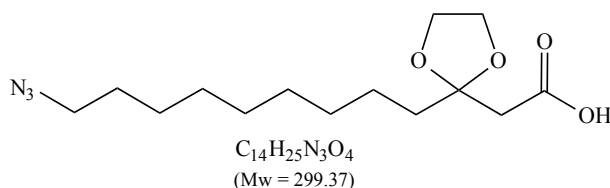
At completion and after the reaction mixture had cooled down to r.t., pH was adjusted to 4-5 with 1M HCl. The organic phase was extracted with DCM (x3). The combined organics were dried over MgSO₄ and the solvent removed under vacuum to afford the desired product as an oil.

2-nonyl-1,3-dioxolane-2-acetic acid **6a** [596104-60-8]



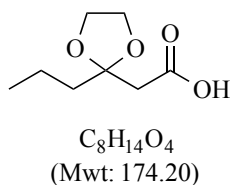
Prepared by GP4 with 95% yield. ¹H NMR (300 MHz, CDCl₃) : δ 10.93 (s, 1H, OH), 4.06 – 3.99 (m, 4H, OCH₂CH₂O), 2.72 (s, 2H, C(2)H₂), 1.85 – 1.78 (m, 2H, C(4)H₂), 1.43-1.37 (m, 2H, C(5)H₂) 1.29 (d, *J* = 5.2 Hz, 12H, C(6)H₂ to C(11)H₂), 0.92 – 0.87 (m, 3H, C(12)H₃). ¹³C NMR (75 MHz, CDCl₃) : δ 174.6 (C₁), 109.3 (C₃), 65.1 (OCH₂CH₂O), 42.4, 37.6 (C₂), 31.9, 29.7, 29.5, 29.3, 26.9, 23.5, 22.7, 14.1 (C₁₂). Does not migrate under usual TLC conditions.

2-(9-azido)nonyl-1,3-dioxolane-2-acetic acid **6b** [1421598-02-8]



Prepared by GP4 with 97% yield. ¹H NMR (300 MHz, CDCl₃) : δ 8.77 (s, 1H, OH), 4.07-3.93 (m, 4H, OCH₂CH₂O), 3.24 (t, *J* = 6.9 Hz, 2H, C(12)H₂), 2.68 (s, 2H, C(2)H₂), 1.95-1.82 (m, 2H, C(4)H₂), 1.61-1.55 (m, 2H, C(5)H₂), 1.29 (d, *J* = 6.5 Hz, 12H, C(6)H₂ to C(11)H₂). ¹³C NMR (75 MHz, CDCl₃) : δ 174.3 (C₁), 109.4 (C₃), 65.2 (acetal), 51.6 (C₁₂), 42.5, 37.7 (C₂), 29.7, 29.5, 29.5, 29.2, 28.9, 26.2, 23.6. Does not migrate under usual TLC conditions.

2-propyl-1,3-dioxolane-2-acetic acid **6c** [5735-99-9]



Prepared by GP4 with 90% yield. ¹H NMR (300 MHz, CDCl₃) : δ 10.27 – 9.96 (m, 1H, OH), 3.96 – 3.82 (m, 4H, OCH₂CH₂O), 2.59 (s, 2H, C(2)H₂), 1.74 – 1.64 (m, 2H, C(4)H₂), 1.40-1.24 (m, 2H, C(5)H₂), 0.82 (t, *J* = 7.4 Hz, 3H, C(6)H₃). ¹³C NMR (75 MHz, CDCl₃) : δ 174.8 (C₁), 109.1 (C₃), 65.0 (OCH₂CH₂O), 42.2 (C₂), 39.7 (C₄), 16.7 (C₅), 14.0 (C₆). Does not migrate under usual TLC conditions.

General EDC- and DMAP-mediated ketoamides preparation with various headgroup installation^{373,374} (GP5)

For general headgroups, the ketal-protected carboxylic acid **6a** (1.0 equiv) was dissolved in DCM (approx. 7 ml/mmol acid) and were successively added EDC (1.2 equiv), DMAP (1.7 equiv) and the appropriate amino headgroup (1.3 equiv).

For (S)-(-)-(α)-amino-(γ)-butyrolactone, the ketal-protected acid **6a-c** (1.0 equiv) and EDC (1.1 equiv) were dissolved in DCM (approx. 2 ml/mmol of substrate) under argon atmosphere, and left to stir at r.t. for 20 min. Then (S)-(-)-(α)-amino-(γ)-butyrolactone hydrochloride (1.3 equiv) and DMAP (1.7 equiv) in DCM (approx. 2 ml/mmol of substrate) were added. The reaction was stirred for 12-22 hours under argon atmosphere at r.t.

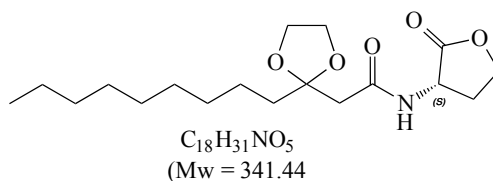
Advancement of the reaction was followed by TLC in EtOAc/cyclohexane mix and revelation achieved with iodine, UV light, potassium permanganate or bromocresol green depending on the headgroup nature. At completion, more DCM was added (13 ml/mmol of substrate) and the organic layer was washed with 1M HCl (x3). The phases were separated, the combined organics were dried over MgSO₄ and solvent removed under vacuum to afford the desired compound as an oil. If necessary, the product could be purified by Flash Chromatography on a silica column.

Alternative EDC- and Et₃N-mediated procedure for ketoamides preparation from (S)-(-)-(α)-amino-(γ)-butyrolactone (GP5 bis)

To a stirred solution of (S)-(-)-(α)-amino-(γ)-butyrolactone hydrochloride (0.91 equiv) in DCM (approx. 6 ml/mmol of substrate) were successively added Et₃N (1.0 equiv), the protected acid **6a** (1.0 equiv) and EDC (1.37 equiv). The reaction was stirred at r.t. for 40 hours.

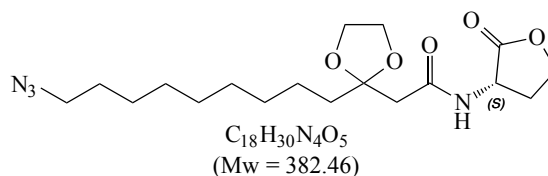
Advancement of the reaction was followed by TLC in 1:2 EtOAc/Cyhex and revelation with iodine, potassium permanganate and UV light. At completion, the mixture was evaporated *in vacuo* to dryness. The residue was partitioned between water (8 ml/mmol of substrate) and EtOAc (17 ml/mmol of substrate), and the organic layer was successively washed with sat. NaHCO₃ (x2) and brine (x2). The organic layer was dried over MgSO₄ and evaporated to dryness to yield the desired compound as an oil. If necessary, the product could be purified by Flash Chromatography on a silica column.

(S)-2-(2-nonyl-1,3-dioxolan-2-yl)-N-(2-oxotetrahydrofuran-3-yl)acetamide 7a [182359-61-1]



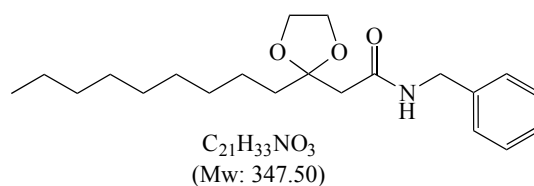
Prepared by both GP5 and GP5bis with respective yields 88% and 91%. 1H NMR (300 MHz, $CDCl_3$) : δ 6.99 (d, $J = 6.3$ Hz, 1H, **NH**), 4.58 (ddd, $J = 11.6, 8.6, 6.3$ Hz, 1H, **C α H**), 4.46 (td, $J = 9.1, 1.3$ Hz, 1H, **H_A**), 4.27 (ddd, $J = 11.2, 9.1, 5.9$ Hz, 1H, **H_B**), 4.11 – 3.96 (m, 4H, **OCH₂CH₂O**), 2.80 (dddd, $J = 12.5, 8.7, 5.9, 1.3$ Hz, 1H, **H_D**), 2.64 (s, 2H, **C(2)H₂**), 2.13 (dtd, $J = 12.5, 11.3, 8.8$ Hz, 1H, **H_C**), 1.71 – 1.65 (m, 2H, **C(4)H₂**), 1.39 – 1.33 (m, 2H, **C(5)H₂**), 1.27 (d, $J = 7.0$ Hz, 12H, **C(6)H₂** to **C(11)H₂**), 0.91 – 0.84 (m, 3H, **C(12)H₃**). ^{13}C NMR (75 MHz, $CDCl_3$) : δ 175.4 (**C₁**), 170. (ester), 109.8 (**C₃**), 66.1 (**CH_AH_B**), 65.3 (**CH₂** acetal), 65.1 (**CH₂** acetal), 49.1 (**CH**), 44.3, 37.7 (**C₂**), 32.0, 30.5 (**CH_CH_D**), 29.8, 29.7, 29.7, 29.5, 23.9, 22.8, 14.3 (**C₁₂**). R_f (4:1 EtOAc/Cychex) : 0.35. HRMS (ESI) : exact mass calculated for $C_{18}H_{31}NO_5Na$ ($[M+Na]^+$) : 362.2094. Found : 364.2095.

12-azido-3-(1,3-dioxolane)-N-((3S)-tetrahydro-2-oxo-3-furanyl)dodecanamide 7b [No CAS]



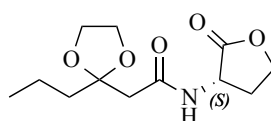
Prepared by GP5 with 69% yield. 1H NMR (300 MHz, $CDCl_3$) : δ 6.99 (d, $J = 6.4$ Hz, 1H, **NH**), 4.57 (ddd, $J = 11.6, 8.7, 6.4$ Hz, 1H, **C α H**), 4.45 (td, $J = 9.1, 1.3$ Hz, 1H, **H_A**), 4.26 (ddd, $J = 11.1, 9.1, 5.9$ Hz, 1H, **H_B**), 4.08 – 3.95 (m, 4H, **OCH₂CH₂O**), 3.24 (t, $J = 6.9$ Hz, 2H, **C(12)H₂**), 2.84 – 2.73 (m, 1H, **H_D**), 2.63 (s, 2H, **C(2)H₂**), 2.13 (dtd, $J = 12.5, 11.4, 8.9$ Hz, 1H, **H_C**), 1.71 – 1.65 (m, 2H, **C(4)H₂**), 1.63–1.53 (m, 2H, **C(5)H₂**), 1.38 – 1.28 (m, 12H, **C(6)H₂** to **C(11)H₂**). ^{13}C NMR (75 MHz, $CDCl_3$) : δ 175.3 (**C₁**), 169.9 (ester), 109.7 (**C₃**), 66.0 (**CH_AH_B**), 65.2 (**CH₂** acetal), 65.1 (**CH₂** acetal), 51.6 (**C₁₂**), 49.1 (**CH**), 44.3, 37.6 (**C₂**), 30.4 (**CH_CH_D**), 29.7, 29.5, 29.5, 29.2, 28.9, 26.8, 23.8. R_f (2:1 EtOAc/Cychex) : 0.20. HRMS (ESI) : exact mass calculated for $C_{18}H_{30}N_4O_4Na$ ($[M+Na]^+$) : 405.2108. Found : 405.2110.

N-benzyl-2-(2-nonyl-1,3-dioxalan-2-yl)acetamide 7c [No CAS]



Prepared by GP5 with 50% yield. ^1H NMR (300 MHz, CDCl_3) : δ 7.36 – 7.31 (m, 1H, **NH**), 7.29 (td, $J = 4.4, 2.3$ Hz, 4H, *m*- and *o*-aromatic H), 6.74 (t, $J = 5.9$ Hz, 1H, *p*-aromatic H), 4.45 (d, $J = 5.8$ Hz, 2H, **NHCH₂**), 3.97 – 3.85 (m, 4H, **OCH₂CH₂O**), 2.61 (s, 2H, **C(2)H₂**), 1.70 – 1.63 (m, 2H, **C(4)H₂**), 1.36 (ddd, $J = 11.7, 6.4, 3.2$ Hz, 2H, **C(5)H₂**), 1.25 (s, 12H, **C(6)H₂** to **C(11)H₂**), 0.90 – 0.85 (m, 3H, **C(12)H₃**). ^{13}C NMR (75 MHz, CDCl_3) : δ 169.1 (**C₁**), 138.7 (aromatic C), 128.8 (2 aromatic C), 127.9 (2 aromatic C), 127.5 (aromatic C), 109.9 (**C₃**), 65.02 (ketal), 44.7, 37.5, 32.0, 29.8, 29.7, 29.7, 29.4, 23.8, 22.8, 14.3 (**C₁₂**). R_f (1:1 EtOAc/Cychex) : 0.58. HRMS (ESI) : exact mass calculated for $\text{C}_{21}\text{H}_{33}\text{NO}_3\text{H}$ ($[\text{M}+\text{H}]^+$) : 348.2533. Found : 348.2533.

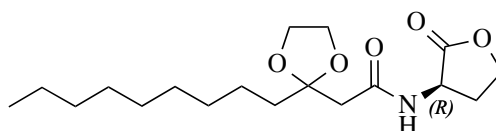
2-propyl-*N*-[(3*S*)-tetrahydro-2-oxo-3-furanyl]-1,3-dioxolane-2-acetamide **7d** [1083287-09-5]



$\text{C}_{12}\text{H}_{19}\text{NO}_5$
(Mw: 257.29)

Prepared by GP5 with 52% yield. ^1H NMR (300 MHz, CDCl_3) : δ 7.01 (d, $J = 6.6$ Hz, 1H, **NH**), 4.57 (ddd, $J = 11.5, 8.7, 6.5$ Hz, 1H, **C α H**), 4.44 (td, $J = 9.1, 1.3$ Hz, 1H, **H_A**), 4.25 (ddd, $J = 11.1, 9.2, 6.0$ Hz, 1H, **H_A**), 4.09 – 3.93 (m, 4H, **OCH₂CH₂O**), 2.77 (dddd, $J = 12.5, 8.7, 6.0, 1.4$ Hz, 1H, **H_D**), 2.62 (s, 2H, **C(2)H₂**), 2.14 (dtd, $J = 12.4, 11.3, 8.9$ Hz, 1H, **H_C**), 1.70 – 1.62 (m, 2H, **C(4)H₂**), 1.46 – 1.32 (m, 2H, **C(5)H₂**), 0.90 (m, $J = 7.3$ Hz, 3H, **C(12)H₃**). ^{13}C NMR (75 MHz, CDCl_3) : δ 175.4 (**C₁**), 169.9 (ester), 109.6 (**C₃**), 66.0 (**CH_AH_B**), 65.2 (**CH₂** acetal), 65.1 (**CH₂** acetal), 49.0 (**CH**), 44.3 (**CH_CH_D**), 39.8, 30.3, 17.1 (**C₅**), 14.3 (**C₆**). R_f (1:1 EtOAc/Cychex) : 0.10. HRMS (ESI) : exact mass calculated for $\text{C}_{12}\text{H}_{19}\text{NO}_5\text{Na}$ ($[\text{M}+\text{Na}]^+$) : 280.1155. Found : 280.1156.

(*R*)-2-(2-nonyl-1,3-dioxolan-2-yl)-*N*-(2-oxotetrahydrofuran-3-yl)acetamide **7e** [No CAS]

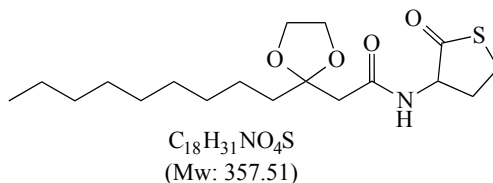


$\text{C}_{18}\text{H}_{31}\text{NO}_5$
Mw: 341.45

Prepared by GP5 with 23% yield. ^1H NMR (300 MHz, CDCl_3) : δ 7.01 (d, $J = 6.5$ Hz, 1H, **NH**), 4.57 (ddd, $J = 11.5, 8.7, 6.5$ Hz, 1H, **C α H**), 4.43 (td, $J = 9.1, 1.4$ Hz, 1H, **H_A**), 4.25 (ddd, $J = 11.1, 9.2, 6.0$ Hz, 1H, **H_B**), 4.08 – 3.93 (m, 4H, **OCH₂CH₂O**), 2.81 – 2.70 (m, 1H, **H_D**), 2.62 (s, 2H, **C(2)H₂**), 2.21 – 2.05 (m, 1H, **H_C**), 1.70 – 1.62 (m, 2H, **C(4)H₂**), 1.38 – 1.30 (m, 2H, **C(5)H₂**), 1.24 (d, $J = 6.4$ Hz, 12H, **C(6)H₂** to **C(11)H₂**), 0.88 – 0.82 (m, 3H, **C(12)H₃**). ^{13}C NMR (75 MHz, CDCl_3) : δ 175.4 (**C₁**), 169.9 (ester), 109.7 (**C₃**), 66.0 (**CH_AH_B**), 65.2 (**CH₂** acetal), 65.1 (**CH₂** acetal), 49.0 (**CH**), 44.3 (**C₂**), 37.6, 32.0,

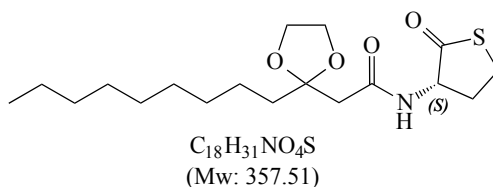
30.3, 29.8 (CH₂H_D), 29.6, 29.6, 29.4, 23.8, 22.7, 14.2 (C₁₂). R_f (3:1 EtOAc/Cyhex) : 0.25. HRMS (ESI): exact mass calculated for C₁₈H₃₁NO₅Na ([M+Na]⁺) : 364.2094. Found : 364.2095.

2-nonyl-N-(3-tetrahydro-2-oxo-3-thienyl)-1,3-dioxalane-2-acetamide 7f [No CAS]



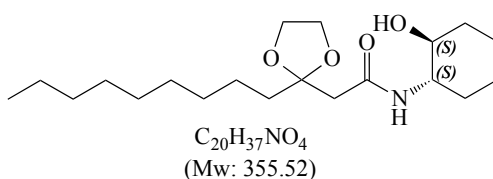
Prepared by modified GP5 with 53% yield. ¹H NMR (300 MHz, CDCl₃) : δ 6.89 (d, *J* = 6.6 Hz, 1H, NH), 4.56 (dt, *J* = 13.1, 6.7 Hz, 1H, C_αH), 4.10 – 3.93 (m, 4H, OCH₂CH₂O), 3.34 (td, *J* = 11.7, 5.1 Hz, 1H, H_B), 3.22 (ddd, *J* = 11.4, 7.1, 1.3 Hz, 1H, H_A), 2.86 (dddd, *J* = 12.1, 6.7, 5.1, 1.4 Hz, 1H, H_C), 2.61 (s, 2H, C(2)H₂), 1.92 (qd, *J* = 12.4, 7.0 Hz, 1H, H_D), 1.70 – 1.62 (m, 2H, C(4)H₂), 1.38 – 1.32 (m, 2H, C(5)H₂), 1.23 (s, 12H, C(6)H₂ to C(11)H₂), 0.90 – 0.81 (m, 3H, C(12)H₃). ¹³C NMR (75 MHz, CDCl₃): δ 205.3 (C=O), 169.8 (C₁), 109.8 (C₃), 65.2 (OCH₂CH₂O), 65.0 (OCH₂CH₂O), 59.3 (CH), 44.4, 37.6 (C₂), 32.0, 31.9, 29.8, 29.6, 29.6, 29.4, 27.6, 23.8, 22.8, 14.2 (C₁₂). R_f (1:1 EtOAc/Cyhex) : 0.31. HRMS (ESI) : exact mass calculated for C₁₈H₃₁NO₄SH ([M+H]⁺) : 358.2047. Found : 358.2047.

2-nonyl-N-(3(S)-tetrahydro-2-oxo-3-thienyl)-1,3-dioxalane-2-acetamide 7g [429675-24-1]



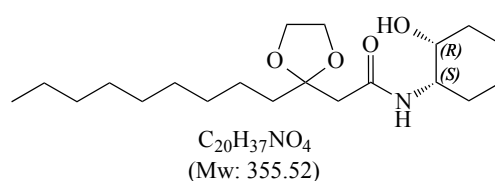
Prepared by GP5bis with 64% yield. ¹H NMR (300 MHz, CDCl₃) : δ 6.89 (d, *J* = 6.6 Hz, 1H, NH), 4.56 (dt, *J* = 13.1, 6.7 Hz, 1H, H), 4.10 – 3.93 (m, 4H, OCH₂CH₂O), 3.34 (td, *J* = 11.7, 5.1 Hz, 1H, H_B), 3.22 (ddd, *J* = 11.4, 7.1, 1.3 Hz, 1H, H_A), 2.86 (dddd, *J* = 12.1, 6.7, 5.1, 1.4 Hz, 1H, H_C), 2.61 (s, 2H, C(2)H₂), 1.92 (qd, *J* = 12.4, 7.0 Hz, 1H, H_D), 1.70 – 1.62 (m, 2H, C(4)H₂), 1.38 – 1.32 (m, 2H, C(5)H₂), 1.23 (s, 12H, C(6)H₂ to C(11)H₂), 0.90 – 0.81 (m, 3H, C(12)H₃). ¹³C NMR (75 MHz, CDCl₃) : δ 205.3 (C=O), 169.8 (C₁), 109.8 (C₃), 65.2 (OCH₂CH₂O), 65.0 (OCH₂CH₂O), 59.3 (CH), 44.4, 37.6 (C₂), 32.0, 31.9, 29.8, 29.6, 29.6, 29.4, 27.6, 23.8, 22.8, 14.2 (C₁₂). R_f (1:1 EtOAc/Cyhex) : 0.31. HRMS (ESI) : exact mass calculated for C₁₈H₃₁NO₄SH ([M+H]⁺) : 358.2047. Found : 358.2047.

N-((1S,2S)-2-hydroxycyclohexyl)-2-(2-nonyl-1,3-dioxalan-2-yl)acetamide 7h [No CAS]



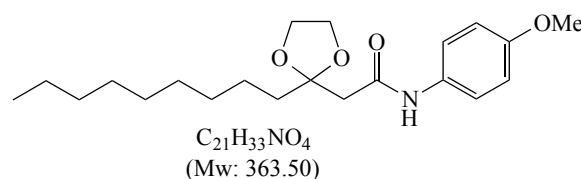
Prepared by GP5 with 54% yield. ^1H NMR (300 MHz, CDCl_3) : δ 6.47 (d, $J = 7.5$ Hz, 1H, NH), 3.96 (p, $J = 3.7, 3.1$ Hz, 4H), 3.66 – 3.53 (m, 1H, NHCHC(OH)H), 3.28 (td, $J = 9.9, 4.3$ Hz, 1H, NHCH), 2.63 - 2.49 (m, 2H, C(2)H₂), 2.01 (ddd, $J = 11.9, 4.9, 2.5$ Hz, 1H, NHCHC(H)H_{eq}), 1.89 (dq, $J = 14.3, 4.6, 3.3$ Hz, 1H, NHCHC(H)H_{ax}), 1.73 – 1.59 (m, 4H, C(4)H₂ and NHCHCH(OH)CH₂), 1.35 – 1.27 (m, 2H, C(5)H₂), 1.21 (s, 16H, C(6)H₂ to C(11)H₂ and NHCHCH₂CH₂CH₂CH₂C(OH)H), 0.83 (t, $J = 6.7$ Hz, 3H, C(12)H₃). ^{13}C NMR (75 MHz, CDCl_3) : δ 171.0 (C₁), 109.9 (C₃), 75.3 (CHOH), 65.0 (ketal), 65.0 (ketal), 55.5 (NHCH), 44.6 (C₂), 37.5, 34.4, 31.9 (C₄), 31.4 (C₅), 29.7, 29.6, 29.6, 29.4, 24.6, 24.06, 23.7, 22.7, 14.2 (C₁₂). R_f (2:1 EtOAc/Cyhex) : 0.15. MS (ESI): exact mass calculated for C₂₀H₃₇NO₄Na ([M+Na]⁺) : 355.5. Found : 378.1.

N-((1*S*,2*R*)-2-hydroxycyclohexyl)-2-(2-nonyl-1,3-dioxolan-2-yl)acetamide **7i** [No CAS]



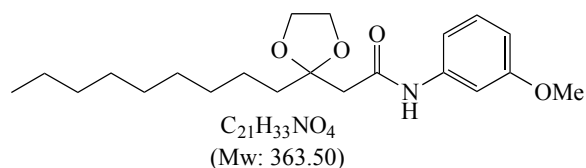
Prepared by GP5 with 51% yield. ^1H NMR (300 MHz, CDCl_3) : δ 6.70 (d, $J = 8.1$ Hz, 1H, NH), 4.01 – 3.96 (m, 4H, ketal), 3.95 – 3.87 (m, 2H, NHCHC(OH)H and NHCH), 2.56 (d, $J = 2.7$ Hz, 2H, C(2)H₂), 2.37 (s, 1H), 1.71 – 1.57 (m, 7H), 1.38 (ddd, $J = 14.3, 6.9, 4.0$ Hz, 4H), 1.24 (d, $J = 2.2$ Hz, 12H, C(6)H₂ to C(11)H₂), 0.89 – 0.83 (m, 3H, C(12)H₃). ^{13}C NMR (75 MHz, CDCl_3) : δ 169.3 (C₁), 110.0 (C₃), 69.5 (CHOH), 65.1 (ketal), 50.8 (NHCH), 44.8 (C₂), 37.5, 32.0, 31.5, 29.8, 29.6, 29.4, 27.4, 23.8, 23.5, 22.8, 20.5, 14.2 (C₁₂). R_f (3:1 EtOAc/Cyhex) : 0.26. HRMS (ESI) : exact mass calculated for C₂₀H₃₇NO₄Na ([M+Na]⁺) : 378.2615. Found : 378.2615.

N-(4-methoxyphenyl)-2-nonyl-1,3-Dioxolane-2-acetamide **7j** [1391732-32-3]



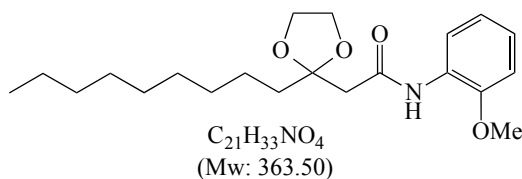
Prepared by GP5 with quantitative yield. ^1H NMR (300 MHz, CDCl_3) : δ 8.22 (s, 1H, NH), 7.48 – 7.41 (m, 2H, CCHCHCOMe), 6.91 – 6.84 (m, 2H, CCHCHCOMe), 4.08 – 4.01 (m, 4H, OCH₂CH₂O), 3.81 (s, 3H, OCH₃), 2.73 (d, $J = 1.5$ Hz, 2H, C(2)H₂), 1.78 – 1.72 (m, 2H, C(4)H₂), 1.41 (dt, $J = 10.8, 5.9$ Hz, 2H, C(5)H₂), 1.28 (d, $J = 4.1$ Hz, 12H, C(6)H₂ to C(11)H₂), 0.89 (td, $J = 6.6, 2.1$ Hz, 3H, C(12)H₃). ^{13}C NMR (75 MHz, CDCl_3) : δ 167.1 (C₁), 156.2 (COMe), 131.2 (NHC), 121.5 (CCHCHCOMe), 114.1 (CCHCHCOMe), 109.8 (C₃), 65.1 (acetal), 55.5 (OCH₃), 45.5 (C₂), 42.2, 37.5, 31.9, 29.5, 29.5, 29.3, 23.7, 22.7, 14.1 (C₁₂). R_f (1:2 EtOAc/Cyhex) : 0.7.

N-(3-methoxyphenyl)-2-nonyl-1,3-Dioxolane-2-acetamide **7k** [1391732-30-1]



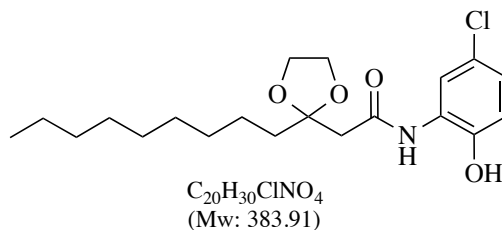
Prepared by GP5 with 88% yield. 1H NMR (300 MHz, $CDCl_3$) : δ 8.35 (s, 1H, NH), 7.33 (t, $J = 2.2$ Hz, 1H, CCHCOMe), 7.22 (t, $J = 8.1$ Hz, 1H, CCHCHCHCOMe), 6.99 (ddd, $J = 8.1, 2.0, 0.9$ Hz, 1H, CCHCHCHCOMe), 6.67 (ddd, $J = 8.3, 2.5, 0.9$ Hz, 1H, CCHCHCHCOMe), 4.03 (m, 4H, OCH_2CH_2O), 3.82 (s, 3H, OCH_3), 2.74 (s, 2H, $C(2)H_2$), 1.78 – 1.71 (m, 2H, $C(4)H_2$), 1.44 – 1.38 (m, 2H, $C(5)H_2$), 1.29 – 1.26 (m, 12H, $C(6)H_2$ to $C(11)H_2$), 0.91 – 0.87 (m, 3H, $C(12)H_3$). ^{13}C NMR (75 MHz, $CDCl_3$) : δ 167.3 (C_1), 160.2 (COMe), 139.3 (NHC), 129.6 (NHCCHCOMe), 111.8 (aromatic), 109.9 (aromatic), 105.5 (aromatic), 65.0 (acetal), 55.3 (OCH_3), 45.8 (C_2), 42.2, 37.6, 31.9, 29.7, 29.5, 29.3, 23.7, 22.7, 14.1 (C_{12}). R_f (1:2 EtOAc/Cyhex) : 0.5.

N-(2-methoxyphenyl)-2-nonyl-1,3-Dioxolane-2-acetamide **7l** [1403677-57-5]



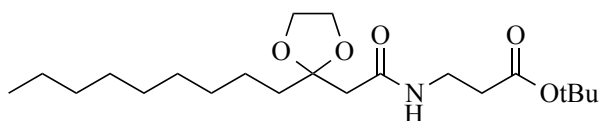
Prepared by GP5 with 71% yield. 1H NMR (300 MHz, $CDCl_3$) : δ 8.84 (s, 1H, NH), 8.37 (dd, $J = 7.9, 1.8$ Hz, 1H, CCOMeCH), 7.06-6.92 (m, 2H, CCHCHCHCH), 6.87 (dd, $J = 7.9, 1.6$ Hz, 1H, CCHCH), 4.04 (qd, $J = 3.3, 1.8$ Hz, 4H, OCH_2CH_2O), 3.89 (s, 3H, OCH_3), 2.76 (s, 2H, $C(2)H_2$), 1.82 – 1.68 (m, 4H, $C(4)H_2C(5)H_2$), 1.29 – 1.23 (m, 12H, $C(6)H_2$ to $C(11)H_2$), 0.89 – 0.85 (m, 3H, $C(12)H_3$). ^{13}C NMR (75 MHz, $CDCl_3$) : δ 167.3 (C_1), 148.2 (COMe), 128.1 (NHC), 123.6 (aromatic), 121.3 (aromatic), 120.1 (aromatic), 110.1 (aromatic), 100.1 (C_3), 65.2 (acetal), 56.0 (OCH_3), 46.0 (C_2), 37.9, 32.0, 29.8, 29.7, 29.6, 29.4, 23.9, 22.8, 14.3 (C_{12}). R_f (1:4 EtOAc/Cyhex) : 0.31.

N-(5-chloro-2-hydroxyphenyl)-2-(2-nonyl-1,3-dioxolan-2-yl)acetamide **7m** [No CAS]



Prepared by GP5 with 37% yield. ^1H NMR (300 MHz, CDCl_3) : δ 8.78 (s, 1H, OH), 8.67 (s, 1H, NH), 7.07 (dd, $J = 8.7, 12.5$ Hz, 1H, aromatic), 6.98 (d, $J = 2.5$ Hz, 1H, aromatic), 6.94 (d, $J = 8.7$ Hz, 1H, aromatic), 4.07 (s, 4H, $\text{OCH}_2\text{CH}_2\text{O}$), 2.80 (s, 2H, C(2) H_2), 1.75 – 1.69 (m, 2H, C(4) H_2), 1.43 – 1.36 (m, 2H, C(5) H_2), 1.28 – 1.25 (m, 12H, C(6) H_2 to C(11) H_2), 0.90 – 0.85 (m, 3H, C(12) H_3). ^{13}C NMR (75 MHz, CDCl_3) : δ 169.8 (C_1), 147.7 (COH), 127.0 (NHC), 126.7 (CCl), 124.9 (aromatic), 121.9 (aromatic), 121.2 (aromatic), 109.8 (C_3), 65.3 (acetal), 44.7 (C_2), 37.7, 32.0, 29.7, 29.6, 29.4, 23.8, 22.8, 14.3 (C_{12}). R_f (1:4 EtOAc/Cyhex) : 0.14. HRMS (ESI) : exact mass calculated for $\text{C}_{20}\text{H}_{30}\text{ClNO}_4\text{H}$ ($[\text{M}+\text{H}^+]$) : 384.1936. Found : 384.1936.

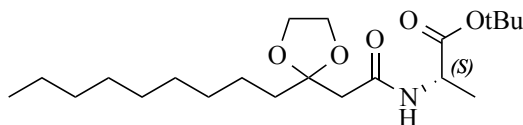
tert-butyl 3-(2-(2-nonyl-1,3-dioxolan-2-yl)acetamido)propanoate **10a** [No CAS]



$\text{C}_{21}\text{H}_{39}\text{NO}_5$
(Mw: 385.55)

Prepared by GP5 and GP5 bis, with 77% and 65% yield respectively. ^1H NMR (300 MHz, CDCl_3) : δ 6.92 - 6.78 (m, 1H, C(O)NH), 3.96 (s, 4H, ketal), 3.46 (q, $J = 6.1$ Hz, 2H, C(O)NHCH $_2$), 2.53 (s, 2H, C(2) H_2), 2.43 (dd, $J = 6.5, 5.7$ Hz, 2H, CH $_2$ C(O)O t Bu), 1.68 – 1.60 (m, 2H, C(4) H_2), 1.44 (s, 9H, *tert*-butyl), 1.38 – 1.30 (m, 2H, C(5) H_2), 1.23 (d, $J = 2.1$ Hz, 12H, C(6) H_2 to C(11) H_2), 0.90 – 0.82 (m, 3H, C(12) H_3). ^{13}C NMR (75 MHz, CDCl_3) : δ 171.8 (C_1), 169.1 (C(O)O t Bu), 109.8 (C_3), 81.0 (OC(CH $_3$) $_3$), 65.0 (ketal), 44.6 (C_2), 37.45 (C_4), 35.4 (NHCH $_2$ CH $_2$), 35.0 (NHCH $_2$ CH $_2$), 32.0, 29.8, 29.7, 29.6, 29.4, 28.2, 23.8, 22.8, 14.2 (C_{12}).

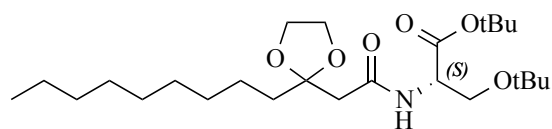
tert-butyl (2-(2-nonyl-1,3-dioxolan-2-yl)acetyl)alaninate **10b** [No CAS]



$\text{C}_{21}\text{H}_{39}\text{NO}_5$
(Mw: 385.55)

Prepared by GP5 with 45% yield. ^1H NMR (300 MHz, CDCl_3) : δ 6.98 (d, $J = 7.6$ Hz, 1H, C(O)NH), 4.47 (p, $J = 7.2$ Hz, 1H, C(O)NHCH), 4.07 - 3.95 (m, 4H, ketal), 2.57 (s, 2H, C(2) H_2), 1.72 – 1.64 (m, 2H, C(4) H_2), 1.45 (s, 9H, C(O)O t Bu), 1.35 (d, $J = 7.1$ Hz, 3H, NHCHCH $_3$), 1.24 (d, $J = 2.2$ Hz, 14H, C(5) H_2 to C(11) H_2), 0.89 - 0.83 (m, 3H, C(12) H_3). ^{13}C NMR (75 MHz, CDCl_3) : δ 172.4 (C(O)O t Bu), 168.5 (C_1), 109.9 (C_3), 81.9 (C(O)OC(CH $_3$) $_3$), 65.1 (ketal), 48.6 (C(O)NHCH), 44.6 (C_2), 37.5 (C_4), 32.0, 29.8, 29.6, 29.4, 28.1 (C(O)OC(CH $_3$) $_3$), 23.9, 22.8, 18.8 (NHCHCH $_3$), 14.2 (C_{12}).

tert-butyl O-(tert-butyl)-N-(2-(2-nonyl-1,3-dioxolan-2-yl)acetyl)serinate 10c [No CAS]

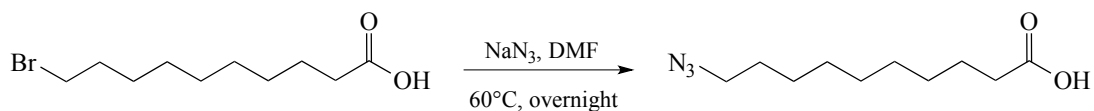


C₂₅H₄₇NO₆
(Mw: 457.65)

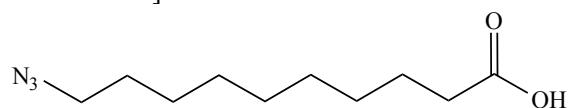
Prepared by GP5 with 72% yield. ¹H NMR (300 MHz, CDCl₃) : δ 7.21 (d, *J* = 8.2 Hz, 1H, C(O)NH), 4.56 (dt, *J* = 8.2, 3.0 Hz, 1H, C(O)NHCH), 4.07 - 3.90 (m, 4H, ketal), 3.71 (dd, *J* = 8.7, 3.0 Hz, 1H, C(O)NHCHCH_CH_D), 3.48 (dd, *J* = 8.7, 3.0 Hz, 1H, C(O)NHCHCH_CH_D), 2.65 - 2.50 (m, 2H, C(2)H₂), 1.71 - 1.62 (m, 2H, C(4)H₂), 1.42 (s, 9H, C(O)O^tBu), 1.38 - 1.15 (m, 14H, C(5)H₂ to C(11)H₂), 1.10 (s, 9H, CH₂O^tBu), 0.83 (m, 3H, C(12)H₃). ¹³C NMR (75 MHz, CDCl₃) : δ 169.6 (C(O)O^tBu), 168.8 (C₁), 109.9 (C₃), 81.7 (C(O)OC(CH₃)₃), 73.0 (CH₂OC(CH₃)₃), 65.1 (ketal), 65.1 (ketal), 62.5 (NHCHCH₂O^tBu), 53.2 (C(O)NHCH), 44.5 (C₂), 37.7 (C₄), 32.0, 29.9, 29.7, 29.7, 29.4, 28.2 (C(O)OC(CH₃)₃), 27.5 (CH₂OC(CH₃)₃), 23.8, 22.8, 14.2 (C₁₂).

Procedure for the synthesis of terminal azido-carboxylic acids³⁷⁵

The appropriate bromocarboxylic acid (1.0 equiv) and sodium azide (1.5 equiv) were dissolved in DMF (5 ml/mmol of carboxylic acid). The reaction was heated to 60°C and stirred overnight under argon atmosphere. After completion, the solvent was removed under reduced pressure. The resulting oil was dissolved in a 1:1:1 (v/v/v) mixture of EtOAc, H₂O and brine. Organics were extracted with EtOAc (x3) and washed with half-saturated brine (x2) before drying over MgSO₄. Solvent were removed under vacuo to afford product as an oil.



10-azidodecanoic acid 14 [186788-32-9]



C₁₀H₁₉N₃O₂
(Mw = 213.28)

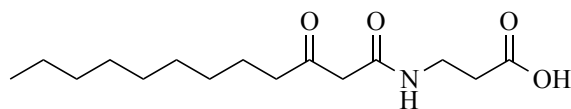
Prepared with quantitative yield. ¹H NMR (300 MHz, CDCl₃) : δ 3.24 (t, *J* = 6.9 Hz, 2H, C(10)H₂), 2.33 (t, *J* = 7.5 Hz, 2H, C(2)H₂), 1.60 (dt, *J* = 10.1, 6.9 Hz, 4H, C(3)H₂ and C(9)H₂), 1.30 (m, 10H, C(4)H₂

to C(8)H₂). ¹³C NMR (75 MHz, CDCl₃) : δ 180.3 (acid), 51.6 (C₁₀), 34.2 (C₂), 29.4, 29.2, 29.2, 29.1, 28.9, 26.8, 24.8.

General procedure for removal of acetal protecting group³⁷⁶ (GP6)

The protected AHL or analogue precursor (1.0 equiv) was dissolved in TFA (4 ml/mmol substrate) and water (1ml/mmol of substrate). DCM could be added if necessary to enhance solubility (up to 10 ml/mmol of substrate). The reaction was stirred at r.t. under argon atmosphere until TLC analysis in EtOAc/CycHex showed the complete consumption of the starting material (overnight). The reaction was quenched by addition of sat. NaHCO₃ solution and NaHCO_{3(s)} until pH was lowered to 4-5, and the organic layer was extracted with DCM (x3). The combined organics were dried over MgSO₄ and solvent removed *in vacuo*. If necessary, the product could be purified by Flash Chromatography on a silica column.

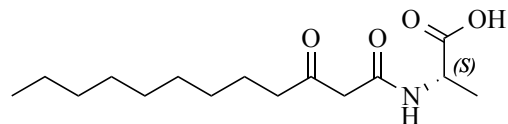
(2-(2-nonyl-1,3-dioxolan-2-yl)acetyl)-β-alanine 11a [No CAS]



C₁₅H₂₇NO₄
(Mw: 285.38)

Prepared by GP6 with 59% yield. ¹H NMR (300 MHz, CDCl₃) : δ 7.44 (s, 1H, NH), 3.56 (q, *J* = 6.1 Hz, 2H, C(O)NHCH₂CH₂), 3.40 (s, 2H, C(2)H₂), 2.62 (t, *J* = 6.1 Hz, 2H, C(O)NHCH₂CH₂), 2.53 (t, *J* = 7.4 Hz, 2H, C(4)H₂), 1.57 (t, *J* = 7.1 Hz, 2H, C(5)H₂), 1.26 (t, *J* = 2.2 Hz, 12H, C(6)H₂ to C(11)H₂), 0.91 – 0.83 (m, 3H, C(12)H₂). HRMS (ESI) : exact mass calculated for C₁₅H₂₇NO₄Na ([M+Na]⁺) : 308.1832. Found : 308.1834.

(2-(2-nonyl-1,3-dioxolan-2-yl)acetyl)alanine 11b [No CAS]

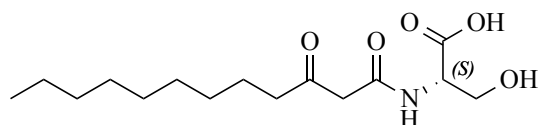


C₁₅H₂₇NO₄
(Mw: 285.38)

Prepared by GP6 with 83% yield. ¹H NMR (300 MHz, CDCl₃) : δ 10.10 (s, 1H, OH), 7.80 (d, *J* = 7.1 Hz, 1H, C(O)NH), 4.56 (p, *J* = 7.2 Hz, 1H, C(O)NHCH), 3.47 (s, 2H, C(2)H₂), 2.52 (t, *J* = 7.4 Hz, 2H, C(4)H₂), 1.56 (p, *J* = 7.1 Hz, 2H, C(5)H₂), 1.46 (d, *J* = 7.2 Hz, 3H, NHCHCH₃), 1.24 (t, *J* = 2.4 Hz,

12H, C(6)**H**₂ to C(11)**H**₂), 0.86 (t, *J* = 6.5 Hz, 3H, C(12)**H**₃). ¹³C NMR (75 MHz, CDCl₃) : δ 206.9 (C₃), 176.0 (COOH), 166.6 (C₁), 48.4 (C(O)NHCH), 48.2 (C₂), 43.9 (C₄), 32.0, 29.8, 29.5, 29.4, 29.1, 23.4, 22.8, 17.9 (NHCHCH₃), 14.2 (C₁₂). HRMS (ESI) : exact mass calculated for C₁₅H₂₇NO₄Na ([M+Na]⁺): 308.1832. Found : 308.1834.

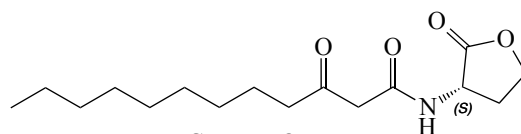
(2-(2-nonyl-1,3-dioxolan-2-yl)acetyl)serine **11c** [No CAS]



C₁₅H₂₇NO₅
(Mw: 301.38)

Obtained by GP6 with 99% yield. ¹H NMR (300 MHz, CDCl₃) : δ 8.10 – 7.90 (m, 1H, C(O)NH), 7.59 – 7.28 (m, 2H, COOH and OH), 4.54 (d, *J* = 8.1 Hz, 1H, C(O)NHCH), 4.11 - 3.76 (m, 2H, C(O)NHCHCH₂**H**_D), 3.52 (s, 2H, C(2)**H**₂), 2.53 (t, *J* = 7.4 Hz, 2H, C(4)**H**₂), 1.51 (dd, *J* = 13.8, 6.9 Hz, 2H, C(5)**H**₂), 1.25 (s, 12H, C(6)**H**₂ to C(11)**H**₂), 0.87 (t, *J* = 6.6 Hz, 3H, C(12)**H**₃). ¹³C NMR (75 MHz, CDCl₃) : δ 207.1 (C₃), 173.8 (COOH), 167.9 (C₁), 62.5 (NHCHCH₂OH), 55.1 (C(O)NHCH), 49.4 (C₂), 43.8 (C₄), 32.0, 29.8, 29.7, 29.5, 29.3, 23.6, 22.8, 14.2 (C₁₂). HRMS (ESI) : exact mass calculated for C₁₅H₂₇NO₅Na ([M+Na]⁺) : 324.1781. Found : 324.1783.

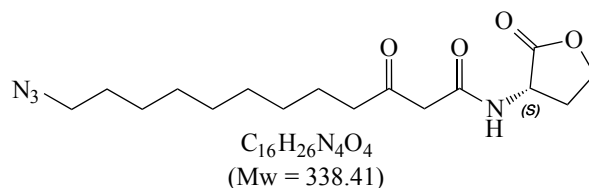
N-(3(S)-oxododecanoyl)homoserine lactone **1** (= **15a**) [168982-69-2]



C₁₆H₂₇NO₄
(Mw = 297.39)

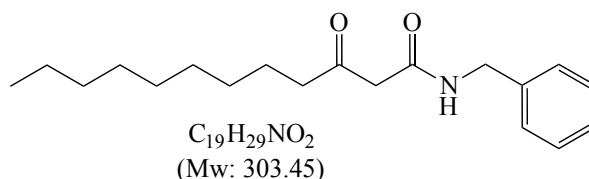
Prepared by GP6 with 98% yield. ¹H NMR (300 MHz, CDCl₃) : δ 7.68 (d, *J* = 6.6 Hz, 1H, NH), 4.59 (ddd, *J* = 11.5, 8.7, 6.6 Hz, 1H, C_α**H**), 4.48 (td, *J* = 9.1, 1.4 Hz, 1H, **H**_A), 4.27 (ddd, *J* = 11.1, 9.1, 6.0 Hz, 1H, **H**_B), 3.47 (s, 2H, C(2)**H**₂), 2.76 (dddd, *J* = 12.6, 8.8, 6.0, 1.4 Hz, 1H, **H**_C), 2.52 (t, *J* = 7.3 Hz, 2H, C(4)**H**₂), 2.30-2.15 (m, 1H, **H**_D), 1.57 (d, *J* = 6.9 Hz, 2H, C(5)**H**₂), 1.26 (t, *J* = 3.1 Hz, 12H, C(6)**H**₂ to C(11)**H**₂), 0.90-0.85 (m, 3H, C(12)**H**₃). ¹³C NMR (75 MHz, CDCl₃) : δ 206.8 (C₃), 174.8 (ester), 166.4 (C₁), 66.0 (CH_A**H**_B), 49.2 (C_α), 48.1 (C₂), 44.1, 32.0, 30.0, 29.5, 29.5, 29.4, 29.1, 23.5, 22.8, 14.2 (C₁₂). R_f (2:1 EtOAc/Cyhex) : 0.35. HRMS (ESI): exact mass calculated for C₁₆H₂₇NO₄Na ([M+Na]⁺): 320.1832. Found : 320.1834.

12-azido-3-oxo-*N*-((3*S*)-tetrahydro-2-oxo-3-furanyl)dodecanamide **15b** [1175052-13-7]



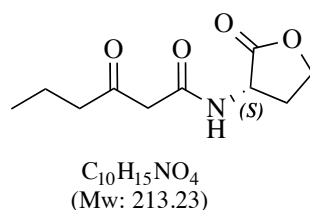
Prepared by GP6 with 87% yield. 1H NMR (300 MHz, $CDCl_3$) : δ 7.61 (d, $J = 4.9$ Hz, 1H, NH), 4.58 (ddd, $J = 11.5, 8.7, 6.5$ Hz, 1H, $C_\alpha H$), 4.47 (td, $J = 9.1, 1.5$ Hz, 1H, H_A), 4.27 (ddd, $J = 11.0, 9.3, 6.1$ Hz, 1H, H_B), 3.46 (s, 2H, $C(2)H_2$), 3.25 (t, $J = 6.9$ Hz, 2H, $C(12)H_2$), 2.76 (dddd, $J = 12.6, 8.7, 6.0, 1.5$ Hz, 1H, H_D), 2.52 (t, $J = 7.3$ Hz, 2H, $C(4)H_2$), 2.22 (dtd, $J = 12.5, 11.2, 8.9$ Hz, 1H, H_C), 1.59 (t, $J = 6.6$ Hz, 2H, $C(5)H_2$), 1.37 – 1.27 (m, 12H, $C(6)H_2$ to $C(11)H_2$). ^{13}C NMR (75 MHz, $CDCl_3$) : δ 210.6 (C_3), 168.5 (ester), 166.0 (C_1), 66.0 ($CH_A H_B$), 51.6 (C_{12}), 49.2 (C_2), 48.2, 44.1, 30.1 ($CH_C H_D$), 29.4, 29.3, 29.2, 29.1, 27.0, 26.8, 23.5. HRMS (ESI) : exact mass calculated for $C_{16}H_{26}N_4O_4Na$ ($[M+Na]^+$): 361.1846. Found : 361.1848.

3-oxo-*N*-(phenylmethyl)-dodecanamide **15c** [1449574-85-9]



Prepared by GP6 with quantitative yield. 1H NMR (300 MHz, $CDCl_3$) : δ 7.38 – 7.26 (m, 5H, aromatic), 4.47 (d, $J = 5.7$ Hz, 2H, $NHCH_2C$), 3.44 (s, 2H, $C(2)H_2$), 2.52 (t, $J = 7.3$ Hz, 2H, $C(4)H_2$), 1.57 (p, $J = 7.0$ Hz, 2H, $C(5)H_2$), 1.34 – 1.20 (m, 12H, $C(6)H_2$ to $C(11)H_2$), 0.91 – 0.84 (m, 3H, $C(12)H_3$). ^{13}C NMR (75 MHz, $CDCl_3$) : δ 207.4 (C_3), 165.6 (C_1), 139.7 ($NHCH_2C$), 128.8 (aromatic x2), 127.9 (aromatic x2), 127.6 (aromatic x1), 48.7 ($NHCH_2C$), 44.2 (C_2), 43.7, 32.0, 29.5, 29.5, 29.4, 29.1, 23.5, 22.8, 14.3 (C_{12}). R_f (1:1 EtOAc/CycHex) : 0.66. HRMS (ESI): exact mass calculated for $C_{19}H_{29}NO_2Na$ ($[M+Na]^+$): 326.2091. Found : 326.2091.

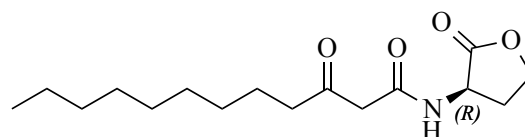
(*S*)-3-oxo-*N*-(2-oxotetrahydrofuran-3-yl)hexanamide **15d** [143537-62-6]



Prepared by GP6 with 40% yield. 1H NMR (300 MHz, $CDCl_3$) : δ 7.67 (d, $J = 6.7$ Hz, 1H, NH), 4.59 (ddd, $J = 11.4, 8.8, 6.8$ Hz, 1H, $C_\alpha H$), 4.45 (td, $J = 9.1, 1.5$ Hz, 1H, $CH_A H_B$), 4.26 (ddd, $J = 10.9, 9.2,$

6.1 Hz, 1H, CH_AH_B), 3.45 (s, 2H, C(2)H₂), 2.70 (dddd, $J = 12.6, 8.9, 6.2, 1.5$ Hz, 1H, CH_CH_D), 2.50 (t, $J = 7.3$ Hz, 2H, C(4)H₂), 2.24 (dtd, $J = 12.5, 11.2, 8.9$ Hz, 1H, CH_CH_D), 1.59 (h, $J = 7.4$ Hz, 2H, C(5)H₂), 0.90 (t, $J = 7.4$ Hz, 3H, C(6)H₃). ¹³C NMR (75 MHz, CDCl₃) : δ 206.4 (C₃), 175.1 (lactone), 166.6 (C₁), 66.0 (CH_AH_B), 49.1 (C_α), 48.6 (C₂), 45.7 (C₄), 29.7 (CH_CH_D), 16.9 (C₅), 13.6 (C₆). R_f (3:1 EtOAc/CycHex) : 0.28. HRMS (ESI) : exact mass calculated for C₁₀H₁₅NO₄H ([M+H]⁺) : 214.1075. Found : 214.1074.

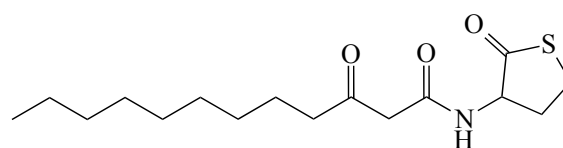
N-(3(R)-oxododecanoyl)homoserine lactone **15e** [886755-08-4]



C₁₆H₂₇NO₄
(Mw: 297.40)

Prepared by GP6 with 87% yield. ¹H NMR (300 MHz, CDCl₃) : δ 7.67 (d, $J = 6.7$ Hz, 1H, NH), 4.59 (ddd, $J = 11.4, 8.8, 6.7$ Hz, 1H, C_αH), 4.46 (td, $J = 9.1, 1.5$ Hz, 1H, H_A), 4.27 (ddd, $J = 11.0, 9.2, 6.1$ Hz, 1H, H_B), 3.46 (s, 2H, C(2)H₂), 2.79 – 2.68 (m, 1H, H_C), 2.52 (t, $J = 7.4$ Hz, 2H, C(4)H₂), 2.23 (dtd, $J = 12.4, 11.2, 8.9$ Hz, 1H, H_D), 1.57 (p, $J = 7.1$ Hz, 2H, C(5)H₂), 1.25 (t, $J = 3.0$ Hz, 12H, C(6)H₂ to C(11)H₂), 0.90-0.83 (m, 3H, C(12)H₃). ¹³C NMR (75 MHz, CDCl₃) : δ 206.7 (C₃), 175.0 (ester), 166.5 (C₁), 66.0 (CH_AH_B), 49.2 (NHCH), 48.3 (C₂), 44.0, 32.0, 29.9, 29.5, 29.5, 29.4, 29.1, 23.5, 22.8, 14.2 (C₁₂). R_f (2:1 EtOAc/Cyhex) : 0.35. HRMS (ESI) : exact mass calculated for C₁₆H₂₇NO₄H ([M+H]⁺) : 298.2013. Found : 298.2014.

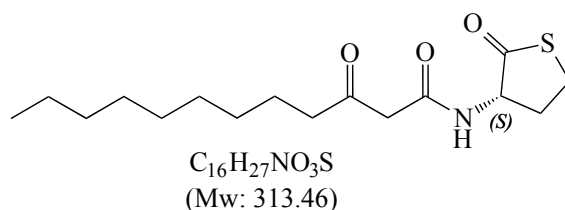
3-oxo-N-(tetrahydro-2-oxo-3-thienyl)-dodecanamide **15f** [663883-93-0]



C₁₆H₂₇NO₃S
(Mw: 313.46)

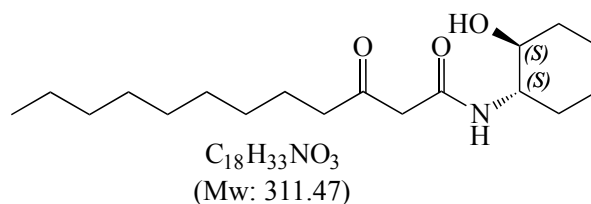
Prepared by GP6 with quantitative yield. ¹H NMR (300 MHz, CDCl₃) : δ 7.47 (s, 1H, NH), 4.58 (dt, $J = 13.2, 6.8$ Hz, 1H, C_αH), 3.45 (s, 2H, C(2)H₂), 3.40 – 3.22 (m, 2H, CH_AH_B), 2.86 (dddd, $J = 12.2, 6.7, 5.1, 1.5$ Hz, 1H, H_D), 2.52 (t, $J = 7.4$ Hz, 2H, C(4)H₂), 2.01 (qd, $J = 12.4, 7.1$ Hz, 1H, H_C), 1.62 – 1.55 (m, 2H, C(5)H₂), 1.26 (t, $J = 2.8$ Hz, 12H, C(6)H₂ to C(11)H₂), 0.91 – 0.84 (m, 3H, C(12)H₃). ¹³C NMR (75 MHz, CDCl₃) : δ 206.8 (C₃), 204.7 (thioester), 166.4 (C₁), 59.4 (C_α), 48.3, 44.1, 32.0, 31.7, 29.5, 29.5, 29.4, 29.1, 27.6, 23.5, 22.8, 14.2 (C₁₂). HRMS (ESI) : exact mass calculated for C₁₆H₂₇NO₃Na ([M+Na]⁺) : 336.1604. Found : 336.1605.

3-oxo-N-[(3S)-tetrahydro-2-oxo-3-thienyl]-dodecanamide 15g [177158-29-1]



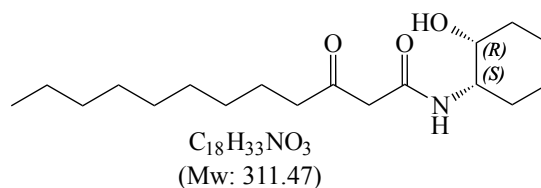
Prepared by GP6 with quantitative yield. 1H NMR (300 MHz, $CDCl_3$) : δ 7.48 (d, $J = 6.6$ Hz, 1H, NH), 4.58 (dt, $J = 13.3, 6.6$ Hz, 1H, $C_\alpha H$), 3.45 (s, 2H, C(2) H_2), 3.35 (td, $J = 11.5, 5.1$ Hz, 1H, CH_A), 3.25 (ddd, $J = 11.5, 7.1, 1.5$ Hz, 1H, CH_B), 2.84 (dddd, $J = 12.4, 6.7, 5.1, 1.5$ Hz, 1H, H_D), 2.52 (t, $J = 7.3$ Hz, 2H, C(4) H_2), 2.01 (qd, $J = 12.4, 7.1$ Hz, 1H, H_C), 1.57 (t, $J = 7.3$ Hz, 2H, C(5) H_2), 1.25 (t, $J = 3.1$ Hz, 12H, C(6) H_2 to C(11) H_2), 0.91 – 0.82 (m, 3H, C(12) H_3). ^{13}C NMR (75 MHz, $CDCl_3$) : δ 206.7 (C_3), 204.7 (thioester), 166.4 (C_1), 59.4 (C_α), 48.4 (CS), 44.1 (C_2), 32.0, 31.6, 29.5, 29.5, 29.4, 29.1, 27.6, 23.5, 22.8, 14.2 (C_{12}). HRMS (ESI) : exact mass calculated for $C_{16}H_{27}NO_3SH$ ($[M+H]^+$) : 314.1784. Found : 314.1785.

N-[(1S,2S)-2-hydroxycyclohexyl]-3-oxo-dodecanamide 15h [886755-19-7]



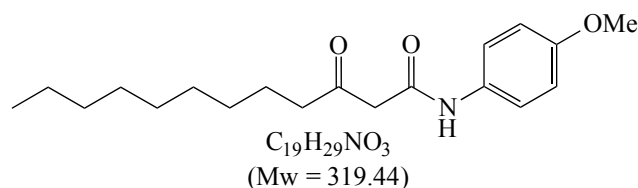
Prepared by GP6 with 54% yield. 1H NMR (300 MHz, $CDCl_3$) : δ 7.17 (d, $J = 7.4$ Hz, 1H, NH), 3.65 (dddd, $J = 11.2, 9.1, 7.4, 4.3$ Hz, 1H, NHCHC(OH) H_{ax}), 3.41 (s, 2H, C(2) H_2), 3.38 – 3.27 (m, 1H, NHCH), 2.51 (t, $J = 7.3$ Hz, 2H, C(4) H_2), 2.09 – 1.99 (m, 1H, NHCHC(H) H_{eq}), 1.95 (tdd, $J = 7.4, 3.9, 2.3$ Hz, 1H, NHCHC(H) H_{ax}), 1.71 (ddt, $J = 8.8, 5.6, 2.7$ Hz, 2H, NHCHCH(OH) CH_2), 1.56 (p, $J = 6.9$ Hz, 2H, C(5) H_2), 1.36 – 1.16 (m, 16H, C(6) H_2 to C(11) H_2 and NHCHCH $_2$ CH $_2$ CH $_2$ CH $_2$ C(OH)H), 0.90 – 0.81 (m, 3H, C(12) H_3). ^{13}C NMR (75 MHz, $CDCl_3$) : δ 207.6 (C_3), 167.4 (C_1), 75.2 (CHOH), 55.9 (NHCH), 48.6 (C_2), 44.1, 34.4, 32.0, 31.4, 29.5, 29.5, 29.4, 29.1, 24.7, 24.1, 23.5, 22.8, 14.2 (C_{12}). HRMS (ESI) : exact mass calculated for $C_{18}H_{33}NO_3Na$ ($[M+Na]^+$) : 334.2353. Found : 334.2353.

N-[(1S,2R)-2-hydroxycyclohexyl]-3-oxo-dodecanamide 15i [897031-37-7]



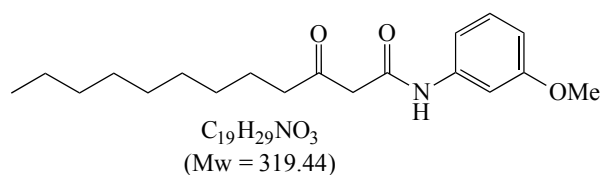
Prepared by GP6 with 67% yield. ^1H NMR (300 MHz, CDCl_3) : δ 7.25 – 7.14 (m, 1H, NH), 3.98 (ddd, $J = 8.2, 6.2, 2.7$ Hz, 1H, NHCH), 3.92 (dt, $J = 5.8, 2.6$ Hz, 1H, NHCHC(OH)H_{eq}), 3.40 (d, $J = 1.5$ Hz, 2H, C(2)H₂), 2.52 (t, $J = 7.3$ Hz, 2H, C(4)H₂), 2.20 – 2.08 (m, 2H), 1.68 – 1.53 (m, 6H), 1.42 (ttt, $J = 11.5, 5.5, 5.0, 2.8$ Hz, 2H), 1.26 (d, $J = 3.5$ Hz, 12H, C(6)H₂ to C(11)H₂), 0.91 – 0.83 (m, 3H, C(12)H₃). ^{13}C NMR (75 MHz, CDCl_3) : δ 207.3 (C₃), 165.8 (C₁), 69.4 (COH), 51.2 (NHCH), 49.2 (C₂), 44.1, 32.0, 31.5, 29.5, 29.5, 29.4, 29.2, 27.3, 23.5, 23.5, 22.8, 20.4, 14.2 (C₁₂). R_f (3:1 EtOAc/CycHex) : 0.38. HRMS (ESI) : exact mass calculated for C₁₈H₃₃NO₃H ([M+H]⁺) : 312.2533. Found : 312.2534.

N-(4-methoxyphenyl)-3-oxododecanamide **15j** [1391732-24-3]



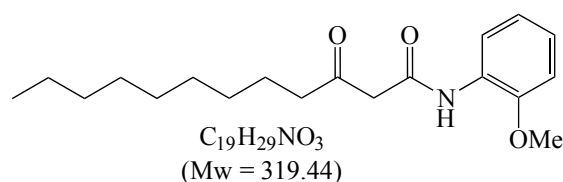
Prepared by GP6 with 75% yield. ^1H NMR (300 MHz, CDCl_3) : δ 9.03 (s, 1H, NH), 7.49-7.40 (m, 2H, NHCCHCHCOMeCHCH), 6.91-6.82 (m, 2H, NHCCHCHCOMeCHCH), 3.79 (s, 3H, OCH₃), 3.55 (s, 2H, C(2)H₂), 2.57 (t, $J = 7.3$ Hz, 2H, C(4)H₂), 1.61 (q, $J = 8.2, 7.7$ Hz, 2H, C(5)H₂), 1.26 (s, 14H, C(6)H₂ to C(11)H₂), 0.90-0.85 (m, 3H, C(12)H₃). ^{13}C NMR (75 MHz, CDCl_3) : δ 208.2 (C₃), 163.4 (C₁), 156.7 (NHC(CH)₂COMe), 130.8 (NHCCH), 122.0 (2 aromatic), 114.3 (2 aromatic), 55.6 (OCH₃), 48.9 (C₂), 44.4, 32.0, 29.5, 29.5, 29.4, 29.1, 23.6, 22.8, 14.2 (C₁₂). R_f (1:3 EtOAc/Cyhex) : 0.4. HRMS (ESI): exact mass calculated for C₁₉H₂₉NO₃Na ([M+Na]⁺) : 342.2040. Found : 342.2040.

N-(3-methoxyphenyl)-3-oxododecanamide **15k** [1391732-22-1]



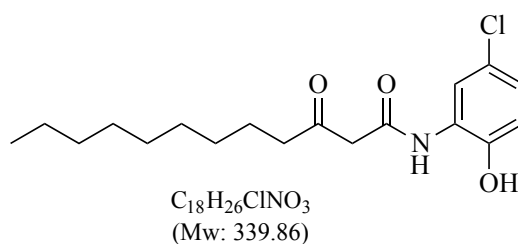
Prepared by GP6 with 66% yield. ^1H NMR (300 MHz, CDCl_3) : δ 9.19 (s, 1H, NH), 7.30 (t, $J = 2.2$ Hz, 1H, NHCCHCOMe), 7.23 (t, $J = 8.1$ Hz, 1H, NHCCHCHCH), 7.06 (ddd, $J = 8.1, 2.0, 1.0$ Hz, 1H, NHCCHCHCH), 6.69 (ddd, $J = 8.3, 2.5, 0.9$ Hz, 1H, NHCCHCHCHCOMe), 3.82 (s, 3H, OCH₃), 3.57 (s, 2H, C(2)H₂), 2.59 (t, $J = 7.3$ Hz, 2H, C(4)H₂), 1.67-1.57 (m, 2H, C(5)H₂), 1.30 (d, $J = 8.0$ Hz, 12H, C(6)H₂ to C(11)H₂), 0.92-0.88 (m, 3H, C(12)H₃). ^{13}C NMR (75 MHz, CDCl_3) : δ 208.0 (C₃), 163.5 (C₁), 160.1 (NHCCHCOMe), 138.7 (NHCCH), 129.7 (NHCCHCHCH), 112.3 (NHCCHCHCHCOMe), 110.4 (NHCCHCOMe), 105.7 (NHCCHCH), 55.3 (OCH₃), 48.9 (C₂), 44.3 (C₄), 31.9, 29.4, 29.3, 29.2, 29.0, 23.3, 22.7, 14.1 (C₁₂). R_f (1:1 EtOAc/Cyhex) : 0.63. HRMS (ESI) : exact mass calculated for C₁₉H₂₉NO₃Na ([M+Na]⁺) : 342.2040. Found : 342.2040.

N-(2-methoxyphenyl)-3-oxododecanamide **15l** [1198116-42-5]



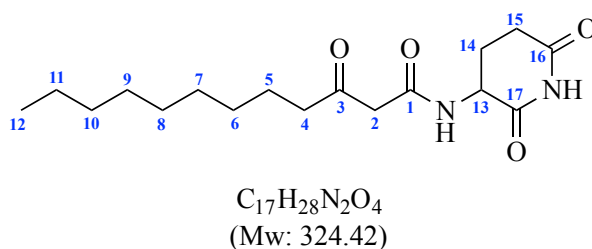
Prepared by GP6 with 51% yield. 1H NMR (300 MHz, $CDCl_3$): δ 9.33 (s, 1H, NH), 8.34 (dd, J = 8.0, 1.7 Hz, 1H, aromatic), 7.08 (td, J = 7.8, 1.7 Hz, 1H, aromatic), 7.00 – 6.89 (m, 2H, aromatic), 3.94 (s, 3H, OCH_3), 3.60 (s, 2H, C(2) H_2), 2.61 (t, J = 7.4 Hz, 2H, C(4) H_2), 1.69 – 1.61 (m, 2H, C(5) H_2), 1.33 – 1.26 (m, 12H, C(6) H_2 to C(11) H_2), 0.93 – 0.87 (m, 3H, C(12) H_3). ^{13}C NMR (75 MHz, $CDCl_3$): δ 207.1 (C_3), 163.6 (C_1), 148.5 (NHCCOMe), 127.5 (NHCCOMe), 124.2 (aromatic), 121.1 (aromatic), 120.3 (aromatic), 110.2 (aromatic), 56.0 (OCH_3), 50.2 (C_2), 44.2 (C_4), 32.0, 29.5, 29.4, 29.2, 27.1, 23.6, 22.8, 14.2 (C_{12}). R_f (3:7 EtOAc/Cycchex) : 0.6. HRMS (ESI) : exact mass calculated for $C_{19}H_{29}NO_3Na$ ($[M+Na]^+$) : 342.2040. Found : 342.2040.

N-(5-chloro-2-hydroxyphenyl)-3-oxododecanamide **15m** [663883-68-9]



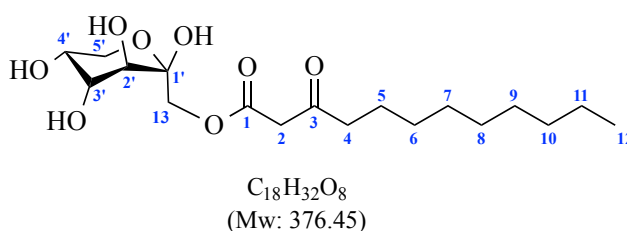
Prepared by GP6 with 98% yield. 1H NMR (300 MHz, MeOD- d_4): δ 8.01 (d, J = 2.5 Hz, 1H, aromatic H), 6.94 (dd, J = 8.6, 2.6 Hz, 1H, aromatic H), 6.84 – 6.76 (m, 1H, aromatic H), 3.64 (dd, J = 5.5, 3.3 Hz, 1H, C(2)H enol-form), 2.60 (t, J = 7.3 Hz, 2H, C(4) H_2), 1.59 (p, J = 7.2 Hz, 2H, C(5) H_2), 1.34 – 1.26 (m, 12H, C(6) H_2 to C(11) H_2), 0.92 – 0.87 (m, 3H, C(12) H_3). ^{13}C NMR (75 MHz, MeOD- d_4): δ 207.4 (C_3), 167.6 (C_1), 147.6 (COH), 128.3 (aromatic C), 125.5 (aromatic CH), 124.9 (aromatic C), 122.5 (aromatic CH), 117.0 (aromatic CH), 42.0 (C_2), 33.0 (C_4), 30.6, 30.5, 30.4, 30.1, 24.5, 23.7, 14.4 (C_{12}). HRMS (ESI) : exact mass calculated for $C_{18}H_{26}ClNO_3H$ ($[M+H]^+$) : 340.1674. Found : 340.1673.

N-(2,6-dioxopiperidin-3-yl)-3-oxododecanamide **32** [No Cas]



Prepared by GP6 with 93% yield. ^1H NMR (300 MHz, CDCl_3) : δ 8.65 (s, 1H, C(17)NHC(18)), 7.80 (d, $J = 6.6$ Hz, 1H, C(1)NH), 4.63 (ddd, $J = 12.8, 6.6, 5.1$ Hz, 1H, C(13)H), 3.47 (s, 2H, C(2)H₂), 2.79 – 2.68 (m, 2H, C(15)H₂), 2.53 (t, $J = 7.4$ Hz, 2H, C(4)H₂), 2.44 (dtd, $J = 13.0, 5.0, 2.9$ Hz, 1H, C(14)HH'), 1.94 (qd, $J = 12.7, 6.0$ Hz, 1H, C(14)HH'), 1.57 (p, $J = 7.0$ Hz, 2H, C(5)H₂), 1.25 (t, $J = 3.4$ Hz, 12H, C(6)H₂ to C(11)H₂), 0.90 – 0.82 (m, 3H, C(12)H₃). ^{13}C NMR (75 MHz, CDCl_3) : δ 206.7 (C₃), 171.9 (C₁₇), 171.4 (C₁₆), 166.5 (C₁), 50.7 (C₁₃), 48.6 (C₂), 44.0, 32.0, 31.3, 29.5, 29.5, 29.4, 29.1, 24.8, 23.5, 22.8, 14.2 (C₁₂). R_f (2:1 EtOAc/CycHex) : 0.16. HRMS (ESI) : exact mass calculated for C₁₇H₂₈N₂O₄Na ([M+Na]⁺) : 347.1941. Found : 347.1942.

Compound 34 [No CAS]



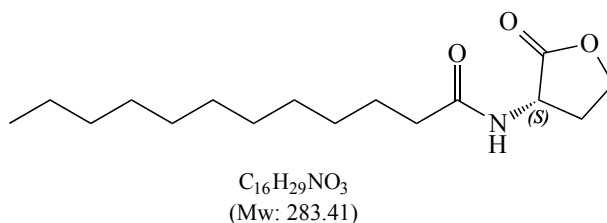
Prepared by GP6 with 87% yield. ^1H NMR (300 MHz, 1:1 MeOD/ CDCl_3) : δ 4.34 – 3.44 (m, 5H, carbohydrate protons), 2.61 – 2.50 (m, 2H), 1.59 – 1.52 (m, 2H), 1.25 (q, $J = 4.6, 4.1$ Hz, 16H), 0.87 – 0.83 (m, 3H, C(12)H₃). ^{13}C NMR (75 MHz, 1:1 MeOD/ CDCl_3) : δ 206.5, 170.5, 71.5, 71.1, 70.6, 70.3, 69.5, 69.3, 43.9, 32.7, 30.2, 30.2, 30.1, 29.8, 24.6, 24.2, 23.4, 14.6. HRMS (ESI) : exact mass calculated for C₁₈H₃₂O₈Na ([M+Na]⁺) : 399.1989. Found : 399.1989.

Procedure for synthesis of non 3-substituted AHLs³⁷⁷

To a stirred solution of (*S*)-(-)-(α)-amino-(γ)-butyrolactone hydrochloride (1.0 equiv) in DCM (approx. 2ml/mmol of substrate) were added Et₃N (2.2 equiv) and the appropriate acyl chloride (1.0 equiv), on an ice bath. After dissolution, the ice bath was removed and the mixture allowed to rise to r.t. It was then stirred overnight at r.t. At completion the reaction mixture was washed with 1M HCL (x2) and brine (x2), dried over MgSO₄ and the solvents removed under *vacuo* to afford the desired product.

If necessary, the product could be purified by Flash Chromatography on a silica column using EtOAc/Cyhex.

N-[(3*S*)-tetrahydro-2-oxo-3-furanyl]-dodecanamide 27 [137173-46-7]



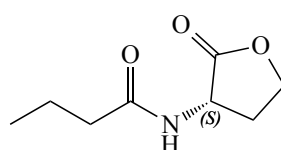
Prepared with 61% yield. ^1H NMR (300 MHz, CDCl_3) : δ 6.08 – 5.95 (m, 1H, **NH**), 4.60 – 4.50 (m, 1H, **C α H**), 4.47 (td, $J = 9.2, 1.3$ Hz, 1H, **H $_A$**), 4.28 (ddd, $J = 11.3, 9.3, 5.8$ Hz, 1H, **H $_B$**), 2.92 – 2.81 (m, 1H, **H $_C$**), 2.28 – 2.20 (m, 2H, **C(2)H $_2$**), 2.12 (dtd, $J = 12.5, 11.5, 8.8$ Hz, 1H, **H $_D$**), 1.62 (q, $J = 7.0$ Hz, 2H, **C(3)H $_2$**), 1.32 – 1.24 (m, 16H, **C(4)H $_2$** to **C(11)H $_2$**), 0.92 – 0.83 (m, 3H, **C(12)H $_3$**). ^{13}C NMR (75 MHz, CDCl_3) : δ 173.9 (ester), 168.4 (**C $_1$**), 66.3 (**CH $_A$ H $_B$**), 49.4 (**NHCH**), 36.4 (**C $_2$**), 32.1, 30.9 (**CH $_C$ H $_D$**), 29.7, 29.6, 29.5, 29.5, 29.4, 25.6, 22.8, 14.3 (**C $_{12}$**). R_f (2:1 EtOAc/Cyhex) : 0.4. HRMS (ESI) : exact mass calculated for $\text{C}_{16}\text{H}_{29}\text{NO}_3\text{Na}$ ($[\text{M}+\text{Na}]^+$) : 306.2040. Found : 306.2041.

EDC- and DMAP-mediated ketoamides preparation from butyric acid and (*S*)-(-)-(α)-amino-(γ)-butyrolactone

Butyric acid (1.0 equiv) and EDC.HCl (1.1 equiv) were dissolved in DCM (approx. 2 ml/mmol of substrate) under argon atmosphere, and left to stir at r.t. for 20 min. Then (*S*)-(-)-(α)-amino-(γ)-butyrolactone hydrochloride (1.3 equiv) and DMAP (1.7 equiv) in DCM (approx. 2 ml/mmol of substrate) were added. The reaction was stirred overnight under argon atmosphere at r.t.

Advancement of the reaction was followed by TLC in 2:1 EtOAc/cyclohexane mix and revelation achieved with iodine on silica. At completion the organic layer was washed with 1M HCl (x3). The phases were separated, the combined organics were dried over MgSO_4 and solvent removed under vacuum to afford desired compound. If necessary, the product could be purified by Flash Chromatography on a silica column.

N-butanoyl-L-homoserine lactone **28** [67605-85-0]



$\text{C}_8\text{H}_{13}\text{NO}_3$
(Mw: 171.20)

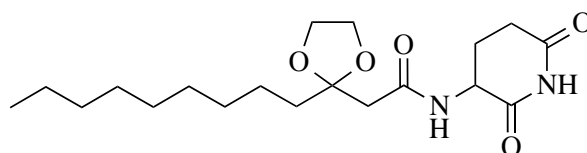
Prepared with 16% yield. ^1H NMR (300 MHz, CDCl_3) : δ 6.45 (d, $J = 6.5$ Hz, 1H, **NH**), 4.59 (ddd, $J = 11.5, 8.7, 6.5$ Hz, 1H, **C α H**), 4.44 (td, $J = 9.1, 1.4$ Hz, 1H, **H $_A$**), 4.26 (ddd, $J = 11.1, 9.2, 6.0$ Hz, 1H, **H $_B$**), 2.76 (dddd, $J = 12.5, 8.7, 6.0, 1.4$ Hz, 1H, **H $_D$**), 2.25 – 2.18 (m, 2H, **C(2)H $_2$**), 2.17 – 2.07 (m, 1H, **H $_C$**), 1.65 (h, $J = 7.4$ Hz, 2H, **C(3)H $_2$**), 0.93 (t, $J = 7.4$ Hz, 3H, **C(4)H $_3$**). ^{13}C NMR (75 MHz, CDCl_3) : δ 175.9 (ester), 173.8 (**C $_1$**), 66.2 (**CH $_A$ H $_B$**), 49.1 (**C α**), 38.1 (**CH $_C$ H $_D$**), 30.3 (**C $_2$**), 19.0 (**C $_3$**), 13.8 (**C $_4$**). HRMS (ESI) : exact mass calculated for $\text{C}_8\text{H}_{13}\text{NO}_3\text{H}$ ($[\text{M}+\text{H}]^+$) : 172.0968. Found : 172.0968.

Procedure for HATU- and DIPEA-mediated ketoamides preparation from 3-aminopiperidine-2,6-dione hydrochloride

The ketal-protected acid **6a** (1.0 equiv) and HATU (1 equiv) were dissolved in MeCN (approx. 5 ml/mmol of substrate) under argon atmosphere, and left to stir at r.t. for 20 min. Then 3-aminopiperidine-2,6-dione hydrochloride (1 equiv) and DIPEA (1 equiv) were added, and the mixture was stirred overnight.

Advancement of the reaction was followed by TLC in 6:1 EtOAc/Cyhex and revelation was achieved with iodine. At completion, the solvent was removed and the resulting oil was diluted in EtOAc and successively extracted with H₂O and brine. The organic layer was dried over MgSO₄ and evaporated to dryness to yield the keto-protected AHL analogue. If necessary, the product could be purified by Flash Chromatography on a silica column.

N-(2,6-dioxopiperidin-3-yl)-2-(2-nonyl-1,3-dioxolan-2-yl)acetamide **31** [No CAS]



C₁₉H₃₂N₂O₅
Mw: 368.47

Prepared with 57% yield. ¹H NMR (300 MHz, CDCl₃) : δ 8.91 (s, 1H, NH), 7.28 (s, 1H, NH), 4.61 (ddd, *J* = 12.2, 6.6, 5.1 Hz, 1H, NHCH), 4.11 – 3.92 (m, 4H, ketal), 2.76 – 2.69 (m, 2H, CHCH₂CH₂C(O)), 2.66 (d, *J* = 6.0 Hz, 2H, C(2)H₂), 2.48 – 2.37 (m, 1H, CHCHH'CH₂C(O)), 1.95 – 1.73 (m, 1H, CHCHH'CH₂C(O)), 1.66 (dd, *J* = 10.6, 5.3 Hz, 2H, C(4)H₂), 1.38 – 1.31 (m, 2H, C(5)H₂), 1.24 (d, *J* = 5.4 Hz, 12H, C(6)H₂ to C(11)H₂), 0.85 (t, *J* = 6.5 Hz, 3H, C(12)H₃). R_f (6:1 EtOAc/Cyhex): 0.29. HRMS (ESI) : exact mass calculated for C₁₉H₃₂N₂O₅Na ([M+Na⁺]) : 391.2203. Found : 391.2567.

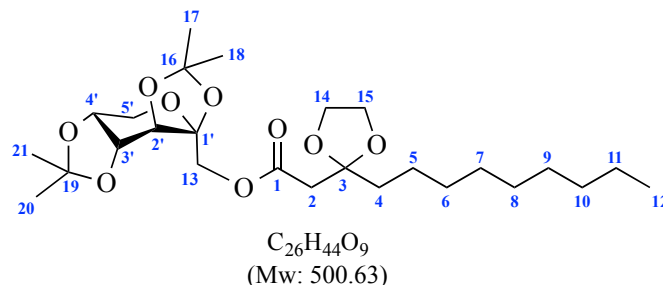
Procedure for EDC- and DMAP-mediated ketoamides preparation from protected sugars

The ketal-protected acid **6a** (1.0 equiv) and EDC.HCl (2.0 equiv) were dissolved in DCM (approx. 5 ml/mmol of substrate) under argon atmosphere, and left to stir at r.t. for 20 min. Then the protected 2,3:4,5-Di-*O*-isopropylidene-β-*D*-fructopyranose (1.1 equiv) and DMAP (1.0 equiv) were added, and the mixture was stirred overnight.

Advancement of the reaction was followed by TLC in 1:3 EtOAc/cyclohexane and revelation was achieved with EtOH/H₂SO₄. At completion, organics were extracted with H₂O and brine, and the aqueous layer washed with more DCM. The combined organic layers were dried over MgSO₄ and

evaporated to dryness to yield the keto-protected AHL analogue. If necessary, the product could be purified by Flash Chromatography on a silica column.

Compound 33 [No CAS]



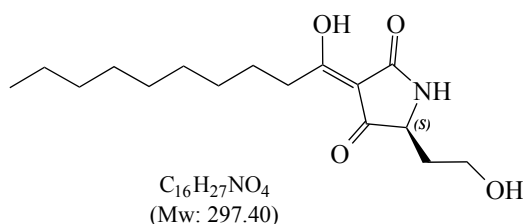
Prepared with 60% yield. 1H NMR (300 MHz, $CDCl_3$): δ 4.58 (dd, $J = 8.0, 2.6$ Hz, 1H), 4.37 – 4.30 (m, 2H, OC(13)**H**₂), 4.22 (ddd, $J = 8.0, 1.9, 0.8$ Hz, 1H), 4.07 (d, $J = 11.8$ Hz, 1H), 3.98 – 3.92 (m, 4H, OC(14)**H**₂C(15)**H**₂O), 3.89 (dd, $J = 13.0, 1.9$ Hz, 1H), 3.74 (dd, $J = 13.0, 0.8$ Hz, 1H), 2.68 (s, 2H, C(2)**H**₂), 1.82 – 1.74 (m, 2H, C(4)**H**₂), 1.52 (s, 3H, **CH**₃ isopropyl), 1.46 (s, 3H, **CH**₃ isopropyl), 1.40 (d, $J = 1.4$ Hz, 4H), 1.32 (s, 3H, **CH**₃ isopropyl), 1.30 – 1.19 (m, 12H), 0.90 – 0.82 (m, 3H, C(12)**H**₃). ^{13}C NMR (75 MHz, $CDCl_3$): δ 168.9 (C₁), 109.5 (C₃), 109.2, 108.8, 101.6, 70.9, 70.5, 70.2, 65.4, 65.3, 65.2, 61.3, 42.5 (C₄), 38.0 (C₂), 32.0, 29.8, 29.7, 29.6, 29.4, 26.6, 26.0, 25.3, 24.2, 23.6, 22.8, 14.2 (C₁₂). R_f (1:3 EtOAc/Cyhex) : 0.44. HRMS (ESI) : exact mass calculated for $C_{26}H_{44}O_9NH_4$ ($[M+NH_4]^+$): 518.3324. Found : 518.3325.

Synthesis of 3-acyltetramic acids (TA) from 3oxoC₁₂-HSL^{328,329}

A solution of 0.5 M sodium methoxide in methanol (1.0 equiv) was added to a stirred solution of **1** (1.0 equiv) in methanol (3 ml/mmol of substrate) under argon atmosphere. The reaction mixture was stirred for 3 hours at 55°C and then overnight at 50°C. The mixture was cooled to r.t. and then passed through an acidic ion exchange resin (Amberlite IR120 H⁺ donor). The resin was eluted with MeOH, the eluents combined and concentrated *in vacuo* to afford the desired tetramic acid as a solid.

If necessary, the product could be purified by Flash Chromatography on a silica column using a gradient elution from 2:1 EtOAc/Cyhex to 8:2 EtOAc/MeOH.

(3Z,5S)-3-(1-hydroxydecylidene)-5-(2-hydroxyethyl)-2,4-pyrrolidinedione 8 [847997-19-7]



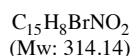
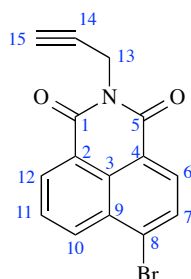
Prepared with 73% yield. ^1H NMR (300 MHz, CDCl_3) : δ 8.00 – 8.51 (m, 1H), 7.12 (s, 1H), 3.90 – 3.98 (m, 1H), 3.83 (ddd, $J=19, 11, 5$ Hz, 2H), 2.77 – 2.95 (m, 2H), 2.04 – 2.16 (m, 1H), 1.70 – 1.82 (m, 1H), 1.64 (p, $J=8$ Hz, 2H), 1.21 – 1.37 (m, 12H), 0.82 – 0.89 (m, 3H). ^{13}C NMR (75 MHz, CDCl_3) : δ 195.8, 189.9, 175.3, 100.6, 61.7, 60.6, 34.3, 33.1, 32.0, 29.4, 29.1, 26.0, 22.8, 14.2. R_f (1:4 MeOH/EtOAc) : 0.25. HRMS (ESI) : exact mass calculated for $\text{C}_{16}\text{H}_{27}\text{NO}_4\text{Na}$ ($[\text{M}+\text{Na}]^+$) : 320.1832. Found : 320.1834.

General procedure for the hydrolysis of *N*-acyl homoserine lactone into *N*-acyl homoserine²⁵⁰ (GP7)

The desired closed-ring *N*-Acyl Homoserine lactone was solubilised at 100 μM in 1 ml 0.1 M sodium carbonate buffer ($\text{NaHCO}_3/\text{Na}_2\text{CO}_3$) pH 9.0 and stirred at 40 $^\circ\text{C}$ and 500 rpm for 2 hours. Complete hydrolysis was verified by TLC spotting and eluted in 3:1 EtOAc/Cyhex and revealed with iodine over silica. No further purification was realised.

3.3. Synthetic procedures for the preparation of AHL probes

Synthesis of 4-bromo-*N*-propargyl-8-naphthalimide **19** [1236253-27-2]

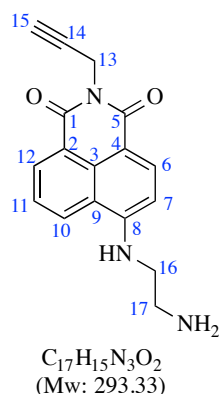


A suspension of 4-bromo-1,8-naphthalic anhydride (1.0 equiv) and propargylamine (1.5 equiv) was refluxed in ethanol for 8 hours. At completion, the mixture was concentrated under vacuo, and the resulting slush was dissolved in DCM and washed with 0.2 M NaOH. The organic layer was dried over MgSO_4 , and solvent removed under vacuo to afford the desired product as a pale yellow solid with 93% yield.

^1H NMR (300 MHz, CDCl_3) : δ 8.70 (dd, $J = 7.3, 1.1$ Hz, 1H, C(10)**H**), 8.60 (dd, $J = 8.5, 1.2$ Hz, 1H, C(12)**H**), 8.46 (d, $J = 7.9$ Hz, 1H, C(6)**H**), 8.06 (d, $J = 7.9$ Hz, 1H, C(7)**H**), 7.87 (dd, $J = 8.5, 7.3$ Hz, 1H, C(11)**H**), 4.95 (d, $J = 2.5$ Hz, 2H, C(13)**H**₂), 2.20 (t, $J = 2.5$ Hz, 1H, C(15)**H**). ^{13}C NMR (75 MHz,

CDCl₃) : δ 163.0 (C₁ and C₅), 157.8 (C₈), 133.9 (C₇), 132.6 (C₆), 131.8 (C₁₀), 131.4 (C₁₂) 131.0 (C₃), 128.3 (C₁₁), 122.0 (C₉), 78.4 (C₁₄), 70.9 (C₁₅), 29.7 (C₁₃).

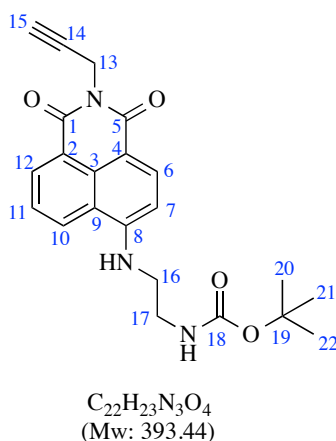
Synthesis of 4-(1,2-diaminethyl)-*N*-propargyl-8-naphthalimide **20** [1807605-66-8]



4-bromo-*N*-propargyl-8-naphthalimide **19** (1.0 equiv) and ethylenediamine (10 equiv) were suspended in 20 ml EtOH and brought to reflux for 72 hours. At completion the reaction mixture was concentrated under vacuo and the resulting solid was washed with water. The filter-cake was collected and dried, before being used crude in the following step. Synthesized with 89% yield.

¹H NMR (300 MHz, DMSO-d₆) : δ 8.73 (dd, J = 8.4, 1.1 Hz, 1H, C(12)**H**), 8.44 (dd, J = 7.4, 1.0 Hz, 1H, C(10)**H**), 8.26 (d, J = 8.6 Hz, 1H, C(6)**H**), 7.68 (dd, J = 8.4, 7.3 Hz, 1H, C(11)**H**), 6.81 (d, J = 8.7 Hz, 1H, C(7)**H**), 4.73 (d, J = 2.5 Hz, 2H, C(13)**H**₂), 3.38 (t, J = 6.5 Hz, 2H, C(16)**H**₂), 3.07 (t, J = 2.4 Hz, 2H, C(17)**H**₂), 2.87 (t, J = 6.5 Hz, 1H, C(15)**H**). ¹³C NMR (75 MHz, DMSO-d₆) : δ 163.0 (C₅), 162.0 (C₁), 151.2 (C₈), 134.5 (C₆), 130.9 (C₁₀), 129.4 (C₃), 129.1 (C₁₂), 124.2 (C₁₁), 121.4 (C₂), 120.1 (C₉), 107.0 (C₄), 104.0 (C₇), 79.9 (C₁₄), 72.5 (C₁₅), 46.3 (C₁₆), 40.0 (C₁₇), 28.6 (C₁₃).

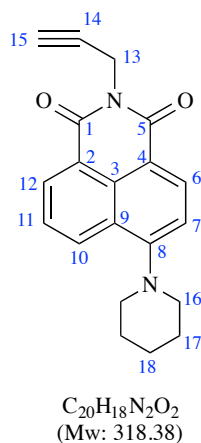
Synthesis of 4-[*tert*-butyl(2-aminoethyl)carbamate]-*N*-propargyl-8-naphthalimide **21** [No CAS]



Crude 4-(1,2-diaminethyl)-*N*-propargyl-8-naphthalimide **20** (1.0 equiv) was dissolved in a 1:1 mixture of MeCN and THF, and placed on an ice bath. Boc₂O (1.2 equiv) was then added and the reaction allowed to go back to r.t. Stirred at r.t. for 2-3 hours. After completion the solvent was removed under vacuo. The resulting oil was dissolved in EtOAc and extracted with saturated NaHCO₃ (x3) and brine. The combined organics were dried over MgSO₄ and concentrated to afford the product as an orange solid. Purified by Flash Chromatography with gradient elution from 100:0 to 95:5 DCM/EtOH. Synthesized with 78% yield.

¹H NMR (300 MHz, CDCl₃) : δ 8.51 (dd, *J* = 7.4, 1.2 Hz, 1H, C(10)**H**), 8.38 (d, *J* = 8.4 Hz, 1H, C(6)**H**), 8.22 (dt, *J* = 7.6, 1.6 Hz, 1H, C(12)**H**), 7.54 (dd, *J* = 8.4, 7.3 Hz, 1H, C(11)**H**), 7.07 (t, *J* = 3.8 Hz, 1H, C(17)**H**₂NHCO), 6.50 (d, *J* = 8.5 Hz, 1H, C(7)**H**), 5.34 (t, *J* = 6.3 Hz, 1H, NHC(16)**H**₂), 4.93 (d, *J* = 2.5 Hz, 2H, C(13)**H**₂), 3.64 (dt, *J* = 10.0, 5.0 Hz, 2H, C(16)**H**₂), 3.47 – 3.38 (m, 2H, C(17)**H**₂), 2.17 (t, *J* = 2.4 Hz, 1H, C(15)**H**), 1.47 (s, 9H, C(20)**H**₃ and C(21)**H**₃ and C(22)**H**₃). ¹³C NMR (75 MHz, CDCl₃) : δ 164.1 (C₅), 163.4 (C₁), 158.7 (C₁₈), 150.6 (C₈), 135.1 (C₆), 131.5 (C₁₀), 129.9 (C₃), 127.5 (C₁₂), 124.7 (C₁₁), 122.4 (C₂), 120.4 (C₉), 109.3 (C₄), 103.5 (C₇), 80.7 (C₁₉), 79.5 (C₁₄), 70.1 (C₁₅), 46.8 (C₁₆), 39.6 (C₁₇), 29.3 (C₁₃), 28.5 (C₂₀, C₂₁ and C₂₂). R_f (20:1 DCM/EtOH) : 0.57. HRMS (ESI) : exact mass calculated for C₂₂H₂₃N₃O₄H ([M+H]⁺) : 394.1761. Found : 394.1761.

Synthesis of 4-piperidinyl-*N*-propargyl-8-naphthalimide **24** [1361506-98-0]



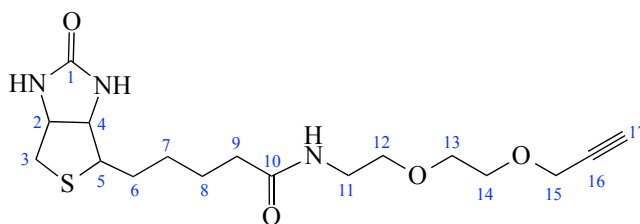
4-bromo-*N*-propargyl-8-naphthalimide **19** (1.0 equiv, 496 mg) was dissolved in 10 ml piperidine and stirred at 100°C for 4 hours. At completion, the mixture was concentrated under vacuo, and the resulting oil was dissolved in DCM and washed with water (x3). The organic layer was dried over MgSO₄, and solvent removed under vacuo to give a crude dark yellow solid. Purified by Flash chromatography in 10:0 to 4:6 DCM/MeOH to afford the desired product with 86% yield.

^1H NMR (300 MHz, CDCl_3) : δ 8.59 (dd, $J = 7.3, 1.2$ Hz, 1H, C(10)**H**), 8.51 (d, $J = 8.1$ Hz, 1H, C(6)**H**), 8.39 (dd, $J = 8.5, 1.2$ Hz, 1H, C(12)**H**), 7.67 (dd, $J = 8.4, 7.3$ Hz, 1H, C(11)**H**), 7.17 (d, $J = 8.1$ Hz, 1H, C(7)**H**), 4.94 (d, $J = 2.5$ Hz, 2H, C(13)**H**₂), 3.27 – 3.17 (m, 4H, 2 x C(16)**H**₂), 2.16 (t, $J = 2.5$ Hz, 1H, C(15)**H**), 1.89 (dq, $J = 11.0, 5.5, 5.1$ Hz, 4H, 2 x C(17)**H**₂), 1.72 (tt, $J = 6.8, 4.2$ Hz, 2H, C(18)**H**₂). ^{13}C NMR (75 MHz, CDCl_3) : δ 163.9 (C₅), 163.4 (C₁), 157.8 (C₈), 133.2 (C₆), 131.5 (C₁₀), 131.2 (C₁₂), 130.1 (C₃), 126.4 (C₂), 125.5 (C₁₁), 122.9 (C₉), 115.5 (C₄), 114.9 (C₇), 79.1 (C₁₄), 70.3 (C₁₅), 54.7 (C₁₆), 29.4 (C₁₃), 26.3 (C₁₇), 24.5 (C₁₈). R_f (10:0 DCM/MeOH) : 0.51.

Synthesis of compound 27 by the NHS-mediated coupling of biotin to linker³⁷⁸

To a stirred solution of biotin (1.0 equiv) in DMF (approx. 5 ml/mmol biotin) were added NHS (1.1 equiv) and EDC (1.49 equiv). The solution was stirred at r.t. for 24 hrs. DIPEA (6.1 equiv) and 2-[2-(2-propynyloxy)ethoxy]ethylamine (0.5 equiv) were then added and stirring pursued overnight at r.t. before refluxing the reaction for 6 hrs. At completion, the reaction mixture was evaporated to dryness before being purified by Flash chromatography in MeOH/ CHCl_3 to afford the desired compound as an oil.

(3a*S*,4*S*,6a*R*)-hexahydro-2-oxo-*N*-[2-[2-(2-propyn-1-yloxy)ethoxy]ethyl]-1*H*-thieno[3,4-*d*]imidazole-4-pentanamide 27 [2227450-68-0]



$\text{C}_{17}\text{H}_{27}\text{N}_3\text{O}_4\text{S}$
(Mw: 369.48)

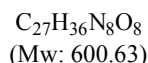
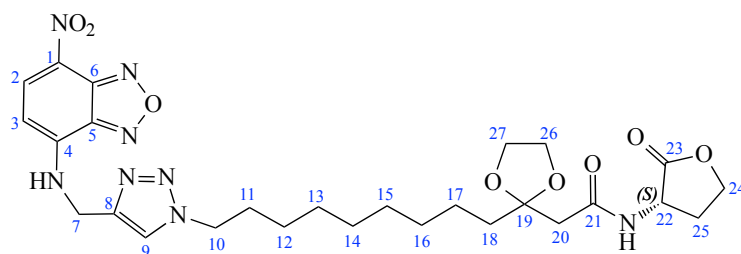
Prepared with quantitative yield. ^1H NMR (300 MHz, $\text{DMSO-}d_6$) : δ 7.82 (t, $J = 5.6$ Hz, 1H, **NH** amide), 6.42 – 6.33 (m, 2H, **NH** urea), 4.34 – 4.28 (m, 1H, C(2)**H**), 4.16 – 4.10 (m, 3H, C(4)**H** and C(15)**H**₂), 3.54 (tt, $J = 4.8, 2.7$ Hz, 4H), 3.38 (m, 4H), 3.18 (d, $J = 5.8$ Hz, 1H, C(5)**H**), 3.09 (ddd, $J = 8.5, 6.1, 4.3$ Hz, 1H, C(17)**H**), 2.82 (dd, $J = 12.4, 5.0$ Hz, 1H, C(3)**HH'**), 2.57 (d, $J = 12.4$ Hz, 1H, C(3)**HH''**), 2.06 (t, $J = 7.4$ Hz, 2H, C(9)**H**₂), 1.68 – 1.40 (m, 4H, C(8)**H**₂ and C(6)**H**₂), 1.37 – 1.24 (m, 2H, C(7)**H**₂). ^{13}C NMR (75 MHz, $\text{DMSO-}d_6$) : δ 172.3 (C₁₀), 162.8 (C₁), 81.8 (C₁₇), 77.2 (C₁₆), 69.3, 69.2, 68.5, 61.1, 59.2, 57.6, 55.5, 38.5, 35.1, 28.2, 28.1, 25.3. R_f (1:10 MeOH/ CHCl_3) : 0.32. HRMS (ESI) : exact mass calculated for $\text{C}_{17}\text{H}_{27}\text{N}_3\text{O}_4\text{SNa}$ ($[\text{M}+\text{Na}]^+$) : 392.1614. Found : 392.1616.

General procedure for copper-mediated azide-alkyne cycloaddition (Click Chemistry) in aqueous conditions³⁷⁹ (GP8)

A freshly prepared solution of CuSO₄ (0.492 equiv) and sodium ascorbate (0.984 equiv) in H₂O (3 ml/mmol ascorbate) was added to a stirred solution of the azide-containing molecule **7b** (1.95 equiv) and the alkyne reagent (1.0 equiv) in DMF (1:9 H₂O/DMF, v/v). The mixture was stirred overnight at room temperature.

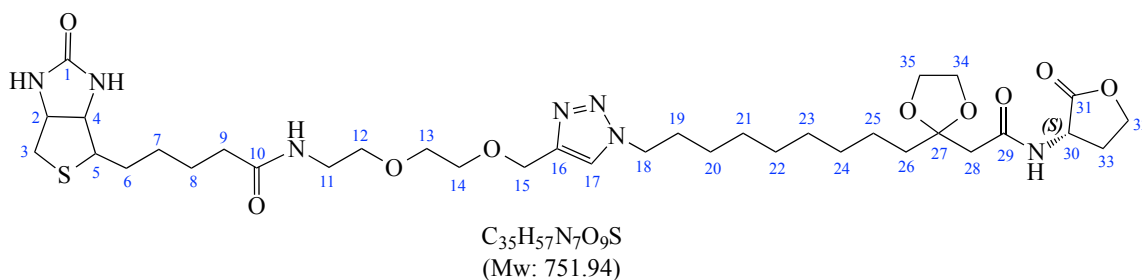
At completion, solvents were removed under vacuum. The oil was diluted in 0.1M aqueous EDTA solution, and organics extracted with DCM (x3). Combined organics washed with 0.1M EDTA (x2) and dried over MgSO₄. Solvent removed under *vacuo* to afford the desired product.

Protected NBD-tagged AHL probe 17



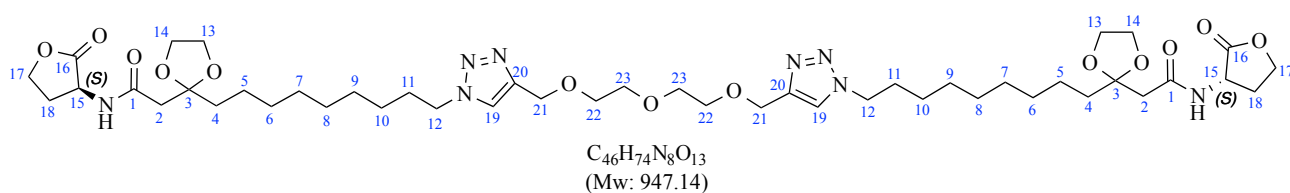
Prepared by GP8 with 81% yield. Purified by Flash Chromatography with gradient elution from 100:0 to 80:20 DCM/MeOH. ¹H NMR (300 MHz, CDCl₃) : δ 8.48 (d, *J* = 8.6 Hz, 1H, C(2)**H**), 7.65 (s, 1H, C(9)**H**), 7.18 (t, *J* = 5.7 Hz, 1H, NBD-N**H**), 7.06 (d, *J* = 6.7 Hz, 1H, C(21)**NH**), 6.39 (d, *J* = 8.6 Hz, 1H, C(3)**H**), 4.83 (d, *J* = 5.7 Hz, 2H, C(7)**H**₂), 4.58 (ddd, *J* = 11.5, 8.8, 6.6 Hz, 1H, C(24)**H**_A**H**_B), 4.46 (td, *J* = 9.1, 1.4 Hz, 1H, C(22)**H**), 4.37 (t, *J* = 7.1 Hz, 2H, C(10)**H**₂), 4.28 (ddd, *J* = 11.0, 9.3, 6.1 Hz, 1H, C(24)**H**_A**H**_B), 4.10 – 3.95 (m, 4H, C(26)**H**₂C(27)**H**₂), 2.76 (dddd, *J* = 12.5, 8.8, 6.0, 1.4 Hz, 1H, C(25)**H**_C**H**_D), 2.64 (s, 2H, C(20)**H**₂), 2.20 (dtd, *J* = 12.5, 11.2, 8.9 Hz, 1H, C(25)**H**_C**H**_D), 1.90 (p, *J* = 7.3 Hz, 2H, C(18)**H**₂), 1.72 – 1.63 (m, 2H, C(17)**H**₂), 1.31 – 1.21 (m, 12H, C(16)**H**₂ to C(11)**H**₂). ¹³C NMR (75 MHz, CDCl₃) : δ 175.4 (C₂₃), 170.0 (C₂₁), 144.5 (aromatic), 143.6 (aromatic), 136.5 (aromatic), 123.4, 109.7 (C₁₉), 99.8 (C₉), 66.1, 65.2-65.1 (C₂₆₋₂₇), 50.7 (C₁₀), 49.1 (C₂₂), 44.3 (C₂₄), 39.6, 37.4, 31.1, 30.1, 30.0, 29.4, 29.0, 28.9, 28.7, 26.2, 23.6. R_f (95:5 DCM/MeOH) : 0.53. HRMS (ESI) : exact mass calculated for C₂₇H₃₆N₈O₈Na ([M+Na]⁺) : 623.2548. Found : 623.2549.

Protected biotin-tagged AHL probe **28**



Prepared by GP8 with 66% yield. 1H NMR (300 MHz, DMSO- d_6): δ 8.17 (d, $J = 7.9$ Hz, 1H, NH keto-amide), 8.07 (s, 1H, C(17)H), 7.85 (t, $J = 5.6$ Hz, 1H, NH amide), 6.38 (d, $J = 17.4$ Hz, 2H, urea from biotin), 4.50 (s, 2H, C(15)H₂), 4.49 - 4.43 (m, 1H, C(32)H_AH_B), 4.32 (dq, $J = 7.1, 5.3$ Hz, 4H, C(4)H and C(30)H and C(18)H₂), 4.24 - 4.16 (m, 1H, C(32) H_AH_B), 4.15 - 4.09 (m, 1H, C(2)H), 3.94 - 3.80 (m, 4H, ketal), 3.56 - 3.48 (m, 8H, C(O)NHCH₂CH₂OCH₂CH₂O), 3.17 (q, $J = 5.8$ Hz, 2H), 3.12 - 3.05 (m, 1H, NHCHCHS), 2.81 (dd, $J = 12.4, 5.1$ Hz, 1H, C(H)(H')S), 2.59 (s, 1H, C(H)(H')S), 2.40 (s, 2H, C(2)H₂), 2.38 - 2.25 (m, 1H, H_C), 2.21 - 2.10 (m, 1H, H_D), 2.05 (t, $J = 7.4$ Hz, 2H, CH₂C(O)NH), 1.80 (q, $J = 7.0$ Hz, 2H), 1.65 (dd, $J = 10.5, 5.1$ Hz, 2H), 1.48 (q, $J = 5.3, 3.1$ Hz, 2H), 1.22 (m, 14H). ^{13}C NMR (75 MHz, DMSO- d_6): δ 175.3, 172.3, 168.3, 162.8, 143.9, 123.8, 109.1, 69.5, 69.2, 68.9, 65.3, 64.4, 63.6, 61.1, 59.3, 55.5, 49.3, 48.0, 43.4, 37.1, 35.9, 35.1, 29.8, 29.2, 28.9, 28.8, 28.4, 28.2, 28.2, 28.1, 25.9, 25.3, 23.0. R_f (9:1 DCM/MeOH) : 0.45. HRMS (ESI) : exact mass calculated for C₃₅H₅₇N₇O₉SNa ([M+Na]⁺) : 774.3831. Found : 774.3838.

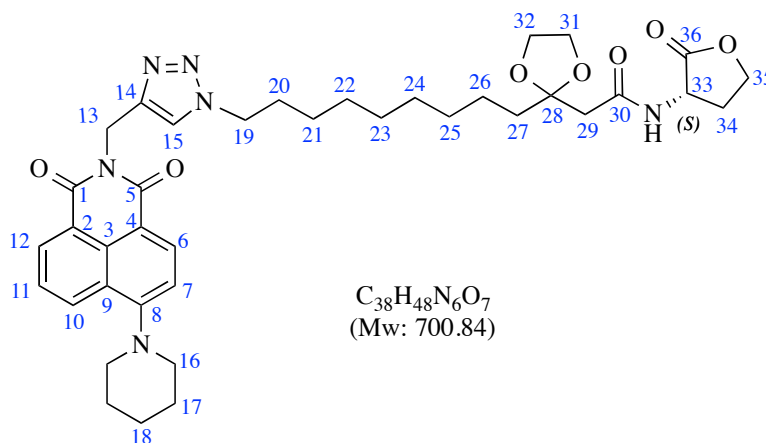
Protected dimeric AHL **35** [No CAS]:



Prepared by GP8 with 70% yield. 1H NMR (300 MHz, CDCl₃): δ 7.55 (s, 2H, C(19)H), 7.03 (d, $J = 6.5$ Hz, 2H, NH), 4.67 (s, 4H, C(21)H₂), 4.56 (ddd, $J = 11.6, 8.7, 6.5$ Hz, 2H, C(15)H), 4.44 (td, $J = 9.1, 1.3$ Hz, 2H, C(17)H_A), 4.35 - 4.27 (m, 4H, C(12)H₂), 4.27 - 4.19 (m, 2H, C(17)H_B), 4.10 - 3.93 (m, 8H, OC(13)H₂C(14)H₂O), 3.71 - 3.61 (m, 8H, OC(22)H₂C(23)H₂O), 2.75 (dddd, $J = 14.3, 8.7, 6.0, 1.4$ Hz, 2H, C(18)H_C), 2.62 (s, 4H, C(2)H₂), 2.23 - 2.06 (m, 2H, C(18)H_D), 1.86 (t, $J = 7.1$ Hz, 4H, C(4)H₂), 1.71 - 1.62 (m, 4H, C(5)H₂), 1.26 (d, $J = 14.4$ Hz, 24H, C(6)H₂ to C(11)H₂). ^{13}C NMR (75 MHz, CDCl₃): δ 175.3 (C₁₆), 169.8 (C₁), 145.1 (C₂₀), 122.5 (C₁₉), 109.6 (C₃), 70.6, 69.7, 66.0, 65.2 (glycol), 65.01 (glycol), 64.8, 50.4 (C₁₂), 49.0 (C₁₅), 44.3 (C₁₇), 37.5 (C₂), 30.4, 30.2, 29.6, 29.4, 29.3, 29.0, 26.5,

23.7. R_f (100% EtOAc) : 0.14. HRMS (ESI) : exact mass calculated for C₄₆H₇₄N₈O₁₃Na ([M+Na]⁺): 969.5268 . Found : 969.5274 .

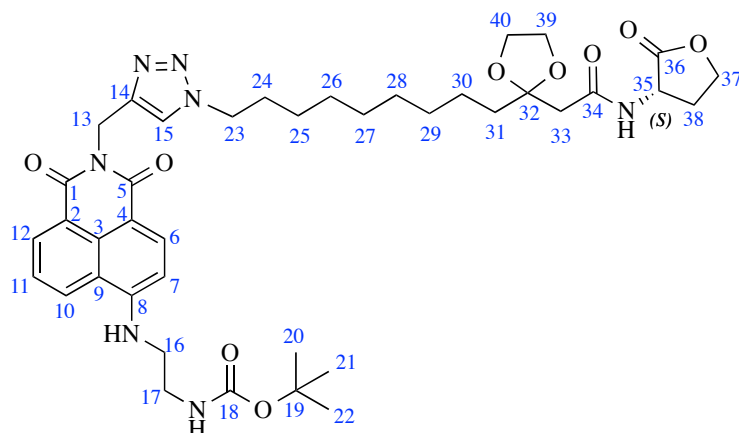
Copper-mediated azide-alkyne cycloaddition of 4-piperidinyl-*N*-propargyl-8-naphthalimide **20 and **7b** in non-aqueous conditions**



4-piperidinyl-*N*-propargyl-8-naphthalimide **20** (2.0 equiv), **7b** (1.0 equiv) and CuI (0.5 equiv) were dissolved in anhydrous THF (approx. 10ml/mmol substrate). Then was added DIPEA (2.0 equiv). The reaction was stirred overnight at r.t. At completion solvent was removed under vacuo, and the resulting product dissolved in DCM and extracted with 0.1 M EDTA (x3). The recombined organics were dried over MgSO₄ and concentrated. The crude product was purified by Flash Chromatography with DCM/MeOH to afford the desired product **25** with 69% yield.

¹H NMR (300 MHz, CDCl₃) : δ 8.53 (dd, *J* = 7.3, 1.2 Hz, 1H, C(10)**H**), 8.45 (d, *J* = 8.1 Hz, 1H, C(6)**H**), 8.34 (dd, *J* = 8.4, 1.2 Hz, 1H, C(12)**H**), 7.66 – 7.60 (m, 1H, C(11)**H**), 7.59 (s, 1H, C(15)**H**), 7.13 (d, *J* = 8.2 Hz, 1H, C(7)**H**), 7.06 (d, *J* = 6.6 Hz, 1H, NH), 5.45 (s, 2H, C(13)**H**₂), 4.56 (ddd, *J* = 11.5, 8.7, 6.6 Hz, 1H, C(33)**H**), 4.43 (td, *J* = 9.0, 1.4 Hz, 1H, C(35)**H**_B), 4.29 – 4.18 (m, 3H, C(35)**H**_A and C(19)**H**₂), 4.06 – 3.91 (acetal), 3.25 – 3.13 (m, 4H, 2 x C(16)**H**₂), 2.78 – 2.67 (m, 1H, C(34)**H**_C), 2.60 (s, 2H, C(29)**H**₂), 2.23 – 2.08 (m, 1H, C(34)**H**_D), 1.83 (dt, *J* = 14.4, 6.8 Hz, 6H, 2 x C(17)**H**₂ and C(27)**H**₂), 1.73 – 1.60 (m, 4H, C(18)**H**₂ and C(26)**H**₂), 1.27 – 1.17 (m, 12H, C(20)**H**₂ to C(25)**H**₂). ¹³C NMR (75 MHz, CDCl₃) : δ 175.3 (C₃₆), 169.8 (C₃₀), 164.3 (C₅), 163.8 (C₁), 157.6 (C₈), 133.0 (C₆), 131.3 (C₁₁), 130.9 (C₁₀), 130.1 (C₃) 126.2 (C₂), 125.4 (C₁₂), 123.0 (C₉), 115.6 (C₄), 114.7 (C₇), 109.6 (C₂₈), 100.0 (C₁₅), 66.0 (C₁₄), 65.2 (acetal), 65.0 (acetal), 54.6 (C₁₆), 50.3 (C₁₉), 49.0 (C₃₃), 44.3 (C₃₅), 37.5 (C₂₉), 35.2 (C₃₄), 30.3 (C₂₇), 30.1, 29.5, 29.3 (C₁₃), 28.9, 26.4, 26.3 (C₁₇), 24.4 (C₁₈), 23.6. R_f (100:5 DCM/EtOH) : 0.52. HRMS (ESI) : exact mass calculated for C₃₈H₄₈N₆O₇Na ([M+Na]⁺) : 723.3477. Found : 723.3480.

Copper-mediated azide-alkyne cycloaddition of 4-[*tert*-butyl(2-aminoethyl)carbamate]-*N*-propargyl-8-naphthalimide **21 and **7b** in non-aqueous conditions**



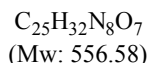
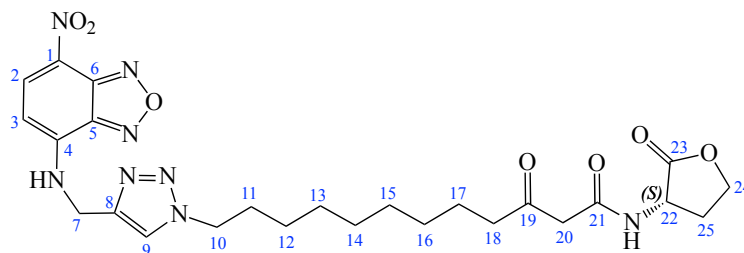
C₄₀H₅₃N₇O₉
(Mw: 775.90)

4-[*tert*-butyl(2-aminoethyl)carbamate]-*N*-propargyl-8-naphthalimide **21** (2.0 equiv), **7b** (1.0 equiv) and CuI (0.5 equiv) were dissolved in anhydrous THF (approx. 10ml/mmol substrate). Then was added DIPEA (2.0 equiv). The reaction was stirred overnight at r.t. At completion solvent was removed under vacuo, and the resulting product dissolved in DCM and extracted with 0.1 M EDTA (x3). The combined organics were dried over MgSO₄ and concentrated. The crude product was purified by Flash Chromatography with DCM/MeOH to afford the desired product **22** with 96% yield.

¹H NMR (300 MHz, CDCl₃) : δ 8.21 (d, *J* = 8.4 Hz, 1H, C(6)**H**), 7.97 (d, *J* = 7.2 Hz, 1H, C(10)**H**), 7.81 – 7.72 (m, 2H, C(12)**H** and C(15)**H**), 7.28 (d, *J* = 5.4 Hz, 1H, C(17)**NHC**(18)), 7.03 (d, *J* = 6.5 Hz, 1H, C(34)**NH**), 6.93 (t, *J* = 7.8 Hz, 1H, C(11)**H**), 6.52 (d, *J* = 8.4 Hz, 1H, C(7)**H**), 6.23 (t, *J* = 5.6 Hz, 1H, C(8)**NHC**(16)), 5.43 (s, 2H, C(13)**H**₂), 4.57 (ddd, *J* = 11.5, 8.7, 6.5 Hz, 1H, C(35)**H**), 4.44 (td, *J* = 9.0, 1.4 Hz, 1H, C(37)**H**_A**H**_B), 4.33 (t, *J* = 7.3 Hz, 2H, C(23)**H**₂), 4.25 (ddd, *J* = 11.0, 9.3, 6.0 Hz, 1H, C(37)**H**_A**H**_B), 4.07 – 3.92 (m, 4H, ketal), 3.59 (s, 2H, C(16)**H**₂), 3.53 – 3.49 (m, 2H, C(17)**H**₂), 2.75 (dddd, *J* = 12.4, 8.6, 6.0, 1.4 Hz, 1H, C(38)**H**_C**H**_D), 2.61 (s, 2H, C(33)**H**₂), 2.16 (tdd, *J* = 12.3, 10.0, 7.1 Hz, 1H, C(38)**H**_A**H**_B), 1.89 (p, *J* = 7.1 Hz, 2H, C(31)**H**₂), 1.64 (dd, *J* = 10.4, 5.5 Hz, 2H, C(30)**H**₂), 1.43 (s, 9H, C(20)**H**₃**C**(21)**H**₃**C**(22)**H**₃), 1.29 – 1.21 (m, 12H, C(29)**H**₂ to C(24)**H**₂). ¹³C NMR (75 MHz, CDCl₃) : δ 175.32(C₃₆), 169.9 (C₃₄), 164.5 (C₅), 163.7 (C₁), 157.6 (C₁₈), 151.3 (C₈), 134.6 (C₆), 130.5 (C₁₀), 129.4 (C₃), 127.4 (C₁₂), 124.0 (C₁₁), 121.7 (C₂), 120.3 (C₉), 109.7 (C₃₂), 108.7 (C₄), 103.6 (C₇), 94.9 (C₁₅), 79.6 (C₁₉), 66.0 (C₁₄), 65.2 (ketal), 65.1 (ketal), 50.6 (C₂₃), 49.0 (C₃₅), 47.9 (C₁₆), 45.2, 44.3 (C₃₇), 39.7 (C₁₇), 37.6 (C₃₈), 34.7, 30.3, 30.2, 29.6, 29.3, 29.3, 29.0, 28.6 (C₂₀, C₂₁, and C₂₂), 26.6, 23.7. R_f (20:1 DCM/EtOH) : 0.38. HRMS (ESI) : exact mass calculated for C₄₀H₅₃N₇O₉Na ([M+Na]⁺): 798.3797. Found : 798.3801.

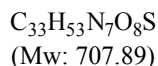
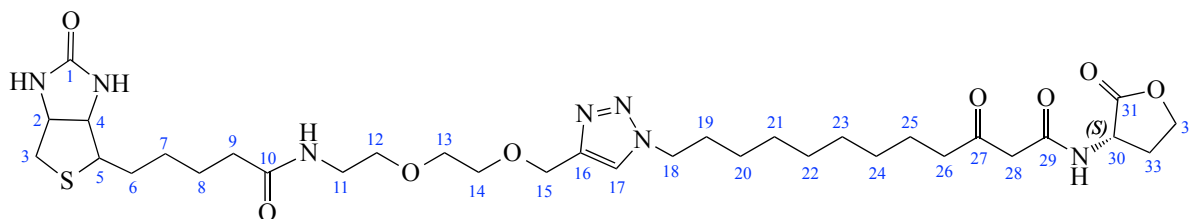
General procedure for removal of acetal protecting group on AHL probes³⁷⁶ (GP6)

NBD-tagged 3oxoC₁₂-HSL 18



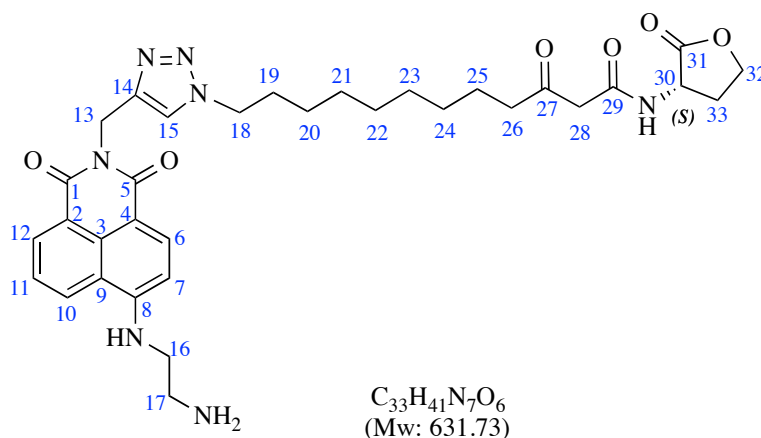
Prepared by GP6 with 99% yield. ¹H NMR (300 MHz, MeOD-*d*₄) : δ 8.49 (dd, *J* = 8.8, 3.1 Hz, 1H, NH), 8.02 (s, 1H, C(9)H), 6.44 (d, *J* = 8.7 Hz, 2H, C(2)HC(3)H), 4.83 (d, *J* = 5.7 Hz, 2H, C(7)H₂), 4.61 (dd, *J* = 11.0, 9.1 Hz, 1H, C(22)H), 4.46 (td, *J* = 9.0, 1.9 Hz, 1H, C(24)H_AH_B), 4.38 (t, *J* = 7.1 Hz, 2H, C(10)H₂), 4.33 - 4.24 (m, 1H, C(24)H_AH_B), 2.56 (dd, *J* = 9.3, 5.1 Hz, 3H, C(20)H₂ and C(25)H_CH_D), 2.37 - 2.20 (m, 1H, C(25)H_CH_D), 1.87 (t, *J* = 7.0 Hz, 2H, C(18)H₂), 1.51 (t, *J* = 7.1 Hz, 2H, C(17)H₂), 1.29 (s, 12H, C(16)H₂ to C(11)H₂). HPLC (5% MeCN+0.1%TFA to 100% MeCN+0.1% TFA in H₂O+0.1% TFA, over 10 min) : RT = 7.198 min. HRMS (ESI) : exact mass calculated for C₂₅H₃₂N₈O₇Na ([M+Na]⁺) : 579.2286. Found : 579.2286.

Biotin-tagged 3oxoC₁₂-HSL 29



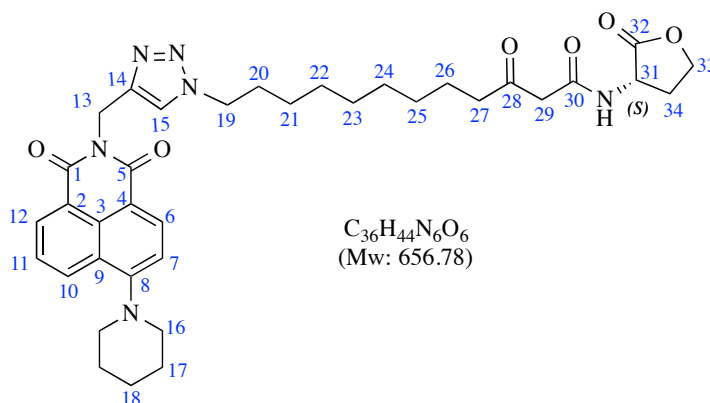
Prepared by GP6 with 98% yield. ¹H NMR (300 MHz, DMSO-*d*₆) : δ 8.59 (d, *J* = 7.9 Hz, 1H, NH keto-amide), 8.08 (s, 1H, C(17)H), 7.84 (t, *J* = 5.7 Hz, 1H, NH amide), 6.38 (d, *J* = 18.0 Hz, 2H, biotin urea), 4.61 - 4.53 (m, 1H, C(30)H), 4.51 (s, 2H, C(15)H₂), 4.33 (h, *J* = 6.8 Hz, 4H, C(4)H, C(32)H_AH_B and C(18)H₂), 4.20 (ddd, *J* = 10.5, 8.7, 6.4 Hz, 1H, C(32)H_AH_B), 4.12 (t, *J* = 6.2 Hz, 1H, C(2)H), 3.55 - 3.49 (m, 8H, C(11)H₂C(12)H₂OC(13)H₂C(14)H₂O), 3.38 (t, *J* = 5.9 Hz, 2H, C(26)H₂), 3.33 (s, 2H, C(28)H₂), 3.17 (q, *J* = 5.8 Hz, 2H), 3.08 (dt, *J* = 8.6, 5.8 Hz, 1H, C(5)H), 2.81 (dd, *J* = 12.4, 5.1 Hz, 1H, C(3)HH'), 2.73 (p, *J* = 1.9 Hz, 1H, C(3)HH'), 2.27 (p, *J* = 1.9 Hz, 1H, C(33)H_CH_D), 2.16 (td, *J* = 11.2, 9.0 Hz, 1H, C(33)H_CH_D), 2.05 (t, *J* = 7.3 Hz, 2H, C(9)H₂), 1.80 (q, *J* = 7.1 Hz, 2H), 1.46 (dt, *J* = 14.6, 6.9 Hz, 4H), 1.30 - 1.18 (m, 12H). HRMS (ESI) : exact mass calculated for C₃₃H₅₃N₇O₈SH ([M+H]⁺) : 708.3749. Found : 708.3750.

(S)-2-((2-((1-(10,12-dioxo-12-((2-oxotetrahydrofuran-3-yl)amino)dodecyl)-1H-1,2,3-triazol-4-yl)methyl)-1,3-dioxo-2,3-dihydro-1H-benzo[de]isoquinolin-6-yl)amino)ethan-1-aminium 2,2,2-trifluoroacetate **23** [No CAS]



Prepared by GP6 with 61% yield. MS (ESI) : exact mass calculated for $C_{33}H_{42}N_7O_6Na$ ($[M-TFA+Na]^+$): 655.0. Found : 654.9.

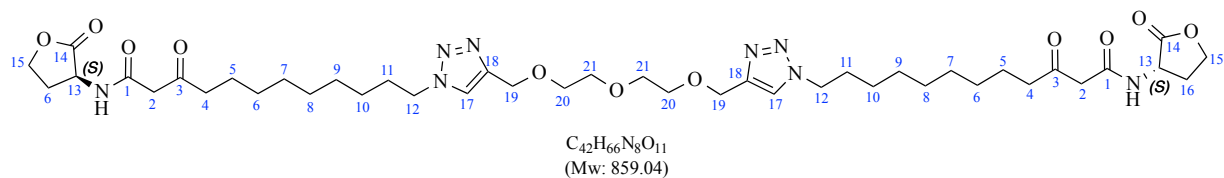
(S)-12-(4-((1,3-dioxo-6-(piperidin-1-yl)-1H-benzo[de]isoquinolin-2(3H)-yl)methyl)-1H-1,2,3-triazol-1-yl)-3-oxo-N-(2-oxotetrahydrofuran-3-yl)dodecanamide **26** [No CAS]



Prepared by GP6 with 70% yield. 1H NMR (300 MHz, $CDCl_3$) : δ 8.56 (dd, $J = 7.3, 1.2$ Hz, 1H, C(10)**H**), 8.48 (d, $J = 8.1$ Hz, 1H, C(6)**H**), 8.37 (dd, $J = 8.5, 1.2$ Hz, 1H, C(12)**H**), 7.81 (d, $J = 6.7$ Hz, 1H, NH), 7.65 (dd, $J = 8.5, 7.3$ Hz, 1H, C(11)**H**), 7.61 (s, 1H, C(15)**H**), 7.15 (d, $J = 8.1$ Hz, 1H, C(7)**H**), 5.47 (s, 2H, C(13)**H**₂), 4.61 (ddd, $J = 11.4, 8.8, 6.7$ Hz, 1H, C(31)**H**), 4.46 (td, $J = 9.1, 1.5$ Hz, 1H, C(33)**H**_B), 4.31 – 4.21 (m, 3H, C(33)**H**_A and C(19)**H**₂), 3.48 (s, 2H, C(29)**H**₂), 3.25 – 3.17 (m, 4H, 2 x C(16)**H**₂), 2.73 (dddd, $J = 12.5, 8.8, 6.1, 1.5$ Hz, 1H, C(34)**H**_C), 2.50 (t, $J = 7.3$ Hz, 2H, C(27)**H**₂), 2.35 – 2.19 (m, 1H, C(34)**H**_D), 1.85 (tt, $J = 9.3, 4.3$ Hz, 6H, 2 x C(17)**H**₂ and C(26)**H**₂), 1.71 (tt, $J = 8.5, 4.1$ Hz, 2H, C(25)**H**₂), 1.53 (t, $J = 7.2$ Hz, 2H, C(18)**H**₂), 1.26 – 1.20 (m, 12H, C(24)**H**₂ to C(20)**H**₂). ^{13}C NMR (75 MHz, $CDCl_3$) : δ 206.4 (C₂₈), 174.9 (C₃₂), 166.6 (C₃₀), 164.4 (C₅), 163.9 (C₁), 157.7 (C₈), 144.0 (C₂), 133.1 (C₆), 131.4 (C₁₁), 131.0 (C₁₀), 130.2 (C₃), 126.4 (C₉), 125.5 (C₁₂), 123.2 (C₁₅), 123.0 (C₉), 115.7 (C₄), 114.8 (C₇), 66.0 (C₁₄), 54.7 (C₁₆), 50.3 (C₁₉), 49.2 (C₃₁), 48.6 (C₃₃), 43.7 (C₂₉), 35.3, 30.2, 29.8,

29.0, 29.0, 28.8, 28.7, 26.3, 24.5, 23.3. HRMS (ESI) : exact mass calculated for C₃₆H₄₄N₆O₆H ([M+H]⁺): 657.3395. Found : 657.3387.

Dimeric AHL 36 (No CAS)



Prepared by GP6 with quantitative yield. ¹H NMR (300 MHz, CDCl₃) : δ 7.76 (d, *J* = 6.7 Hz, 2H, NH), 7.58 (s, 2H, C(17)H), 4.68 (s, 4H, C(19)H₂), 4.64 - 4.54 (m, 2H, C(13)H), 4.47 (td, *J* = 9.1, 1.5 Hz, 2H, C(15)H_A), 4.33 (t, *J* = 7.2 Hz, 4H, C(12)H₂), 4.30 - 4.22 (m, 2H, C(15)H_B), 3.73 - 3.63 (m, 8H, OC(20)H₂C(21)H₂O), 3.47 (s, 4H, C(2)H₂), 2.74 (dddd, *J* = 12.5, 8.8, 6.1, 1.5 Hz, 2H, C(16)H_C), 2.52 (t, *J* = 7.3 Hz, 4H, C(4)H₂), 2.25 (dtd, *J* = 12.5, 11.2, 8.9 Hz, 2H, C(16)H_D), 1.90 (s, 4H), 1.60 - 1.53 (m, 4H), 1.29 - 1.24 (m, 20H). ¹³C NMR (75 MHz, CDCl₃) : δ 206.5 (C₃), 174.8 (C₁₄), 166.6 (C₁), 145.2 (C₁₈), 122.7 (C₁₇), 70.6, 69.8, 66.0, 64.8, 50.5 (C₁₂), 49.2 (C₁₃), 48.5 (C₂), 43.9 (C₁₅), 30.3, 29.9, 29.1, 29.1, 28.9, 28.9, 26.5, 23.4. HRMS (ESI) : exact mass calculated for C₄₂H₆₆N₈O₁₁Na ([M+Na]⁺) : 881.4743. Found : 881.4754.

4. Analytical techniques

4.1. Electrochemistry and cyclic voltammetry

Cyclic voltammetry measurements were recorded in a heat-dried glass reactor containing 4 ml of TBA-BF₄ 0.1M in anhydrous MeCN. The Reference electrode was made of saturated KCl, the counter electrode was a platinum disk electrode, and a glassy carbon electrode diameter 1mm was used as working electrode. The working electrode was carefully polished between each run. The scan rate was 0.1 V.s⁻¹. FeCl₃ and ligand **15c** were employed at 2mM in MeCN. Electrodes were cleaned and solutions degassed between each scan to ensure homogeneity of results.

4.2. Spectrometry

UV-visible spectra were recorded at room temperature on a Jasco FP-8300 spectrometer, using 1 cm path length quartz cuvettes. Analysed compounds were resuspended in sterile PBS 1X. Concentration was 1 μ M for fluorescein-containing compounds, and 10 μ M for all other fluorescent molecules. PBS 1X was consequently used to establish blank and baseline spectra.

4.3. Molecule characterisation (NMR, MS and HRMS)

NMR spectra were recorded on a Bruker Advance 300 MHz spectrometer operating at 300 MHz for ^1H NMR and 75 MHz for ^{13}C NMR. Commercial deuterated NMR solvents were bought Eurisotop. All chemical shifts (δ) for ^1H and ^{13}C spectra are reported in parts per million (ppm) relative to the internal residual solvent signals, and coupling constants (J) are in Hertz (Hz). The NMR signal multiplicities are abbreviated as follows: singlet (s), doublet (d), doublet of doublets (dd), triplet (t), doublet of triplets (dt), quartet (q), quintet (qt), multiplet (m), broad signal (br).

Routine mass spectrometry spectra were acquired on a AB Sciex API 3000 LC-MS/MS spectrometer at the Ecole Nationale Supérieure de Chimie de Paris (ENSCP) platform. High resolution mass spectrometry analysis was performed at the Institut Parisien de Chimie Moléculaire (FR 2769) of Sorbone Université, from 10 μ g/ml stock solutions prepared in high purity mass spectrometry solvents and using an electrospray source.

Part I : Biological studies of two natural

N-Acyl Homoserine Lactones

1. Description and preparation of the molecules

1.1. The saturated 3oxoC₁₂-HSL

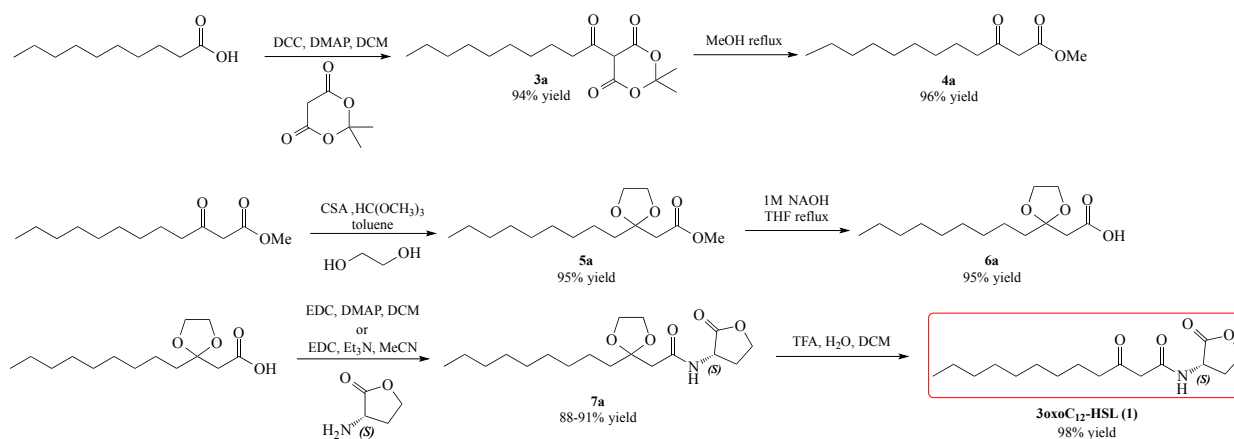
The saturated AHL compound **1** is a commercially available molecule ; it was also synthesized in-house for this work. The synthetic strategy has been adapted from published literature, enhanced with modifications to increase yields, ease purification steps and offer more flexibility (Scheme 4).^{300,370–372,376}

The usual AHL synthetic strategy used to rely on two steps performed in a one-pot manner : first, the coupling of an appropriate carboxylic acid with Meldrum's derivative ; then, the immediate coupling of the resulting intermediate with the headgroup (*S*)-(-)- α -amino- γ -butyrolactone. This method shows several drawbacks among which are the difficult purification after the second step (it affords many undesired by-products), low overall yields (about 30% according our in-house experience), and demands a large quantity of the lactone headgroup which is a fairly expensive reagent.

Our most important modification consisted in the introduction of 5 additional steps, including ketone protection and deprotection. The ketone-protected intermediates are less polar than their counterparts with free ketones, which makes them more suitable for purification with silica gel chromatography under usual and mild conditions. This allows higher post-purification yields and purity. Furthermore, the protection of the ketone inhibits the keto/enol equilibrium of ketoamides and blocks the intermediate in a single configuration, making purification and characterisation easier. Our synthetic strategy affords building block **6a** in good yields, and the latter can then be derivatised to prepare a very large array of molecules.

Briefly, our synthesis started with decanoic acid and its coupling to Meldrum's acid. The resulting derivative was refluxed in methanol to perform hydrolysis and obtain dodecanoic acid

methyl ester. The ketone was protected as a ketal with ethylene glycol, and the terminal ester hydrolysed to afford the carboxylic acid. To this acid was coupled the appropriate headgroup (*S*)-(-)- α -amino- γ -butyrolactone. The final step consisted in deprotection of the ketone, to afford AHL **1**. The overall yield was 70-73% depending on the chosen method for lactone headgroup coupling.



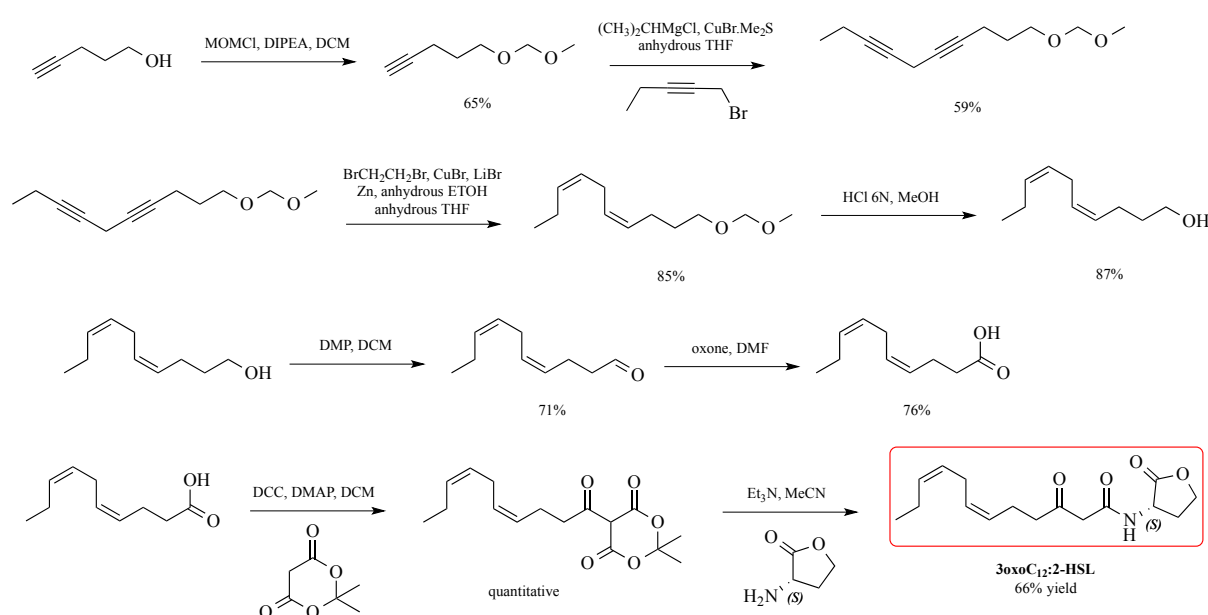
Scheme 4 - General synthesis of 3oxoC₁₂-HSL (1)

1.2. The unsaturated 3oxoC₁₂:2-HSL

Previous work in our team had highlighted the importance of an unknown doubly-unsaturated AHL, with a 12-carbon long acyl chain, and a keto group at C₃-position. Such a description gives rise to no less than 63 position isomers for the insaturations, without considering the additional variation arising from the (*E*) and (*Z*) configurational isomerism of the double bonds. Facing such a very large amount of possible structures, a choice was made to synthesize only one isomer to perform extensive biological studies. The isomer choice was rationalised and the position of the insaturations inspired from the naturally arising pattern of ω -3/ ω -6 in fatty acyl chains. Hence the insaturations were located at carbons 6 and 9 of the acyl chain to give rise to a 3oxoC₁₂:2-HSL that will hereafter be named compound **2**.

The development of the synthetic strategy for this molecule was done in-house, but the larger scale synthesis was externalised to a dedicated private company. Briefly, the synthesis first focuses on connecting two 5-atom and alkyne-containing molecules in order to build up a 10-

carbon acyl chain containing two triple bonds located in positions ω -3 and ω -6 and a terminal MOM-protected alcohol. These triple bonds are then reduced to two double bonds with (*Z*) configurations. The alcohol is deprotected, first oxidised to an aldehyde by means of Dess-Martin periodinane, and then to a carboxylic acid with oxone. The obtained carboxylic acid is then coupled to Meldrum's acid, and the resulting derivative reacted with (*S*)-(-)- α -amino- γ -butyrolactone to obtain the desired final compound with an overall 10% yield (Scheme 5). This compound will hereafter be named 3oxoC₁₂:2-HSL to indicate its close structure to AHL **1** and the presence of two insaturations, and will carry the number **2**.



Scheme 5 - General synthesis of 3oxoC₁₂:2-HSL (2**)**

The resulting 3oxoC₁₂:2-HSL was used for biological studies and systematically compared to its saturated counterpart AHL **1**. However, due to the little amount of **2** available to us and its high price, molecule 3oxoC₁₂-HSL was often favoured as a general frame to model AHL carrying a long acyl chain. It is both cheaper in terms of commercial sourcing, and easier to access by chemical synthesis. AHL **1** was also preferred to perform larger scope studies such as stability and metabolism, cell imaging or protein interactions.

2. Compared biological effects and properties of the molecules

2.1. Results on our biological models

2.1.1. Establishment of stimulation protocols

To mimic the inflammatory status of IBD patients during flare, we developed a protocol to study the cytokine release of cells in situation of active inflammation, and its eventual modulation by the natural AHLs 3oxoC₁₂-HSL and 3oxoC₁₂:2-HSL.

Inflammation was induced in cells seeded and cultured in microwell plates by addition of pro-inflammatory cytokines ; controls or tested molecules at diverse concentrations were added at the same time as cytokines. The whole system was incubated at 37°C for 18 hours (Caco-2/TC7 cells) or 6h (Raw 264.7 cells). DMSO 0.1% being used as vehicle to the tested molecules, it was also chosen as a positive control condition of active inflammation. An enzymatic inhibitor called 2-hydroxyquinoline (2-HQ) was added to the reaction mix ; its purpose will be detailed further in this manuscript.

As stated, DMSO is employed as vehicle to prepare highly concentrated AHL stock solutions because these molecules are poorly soluble in aqueous media, even at 37°C.³⁸⁰ AHL stability in DMSO was verified : no degradation of the molecules was observed in 200mM stock solutions conserved for several weeks in pure sterile DMSO at -80°C.

IL-1 β was chosen to induce inflammation in Caco-2/TC7 cell line based on literature where lung epithelial cells but also Caco-2 cells are stimulated with this interleukin.^{309,381–383} Several concentrations were tested : 10, 15, 20 and 25 ng/ml ; the optimal concentration of 25 ng/ml was retained as it induced sufficient inflammatory response (17-fold IL-8 secretion increase versus resting cells) and no cytotoxicity was observed with this dose as tested by LDH release in cell supernatant (Figure 14). This choice is coherent with literature.

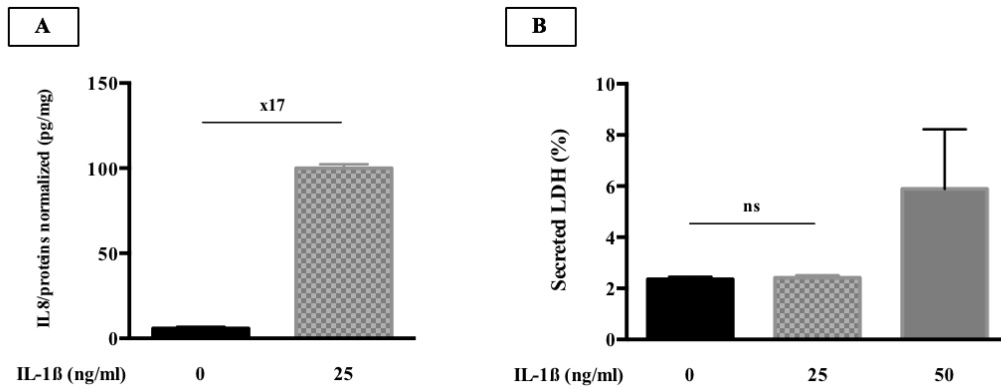


Figure 14 - Effects of diverse IL-1 β doses on IL-8 secretion (A) and cytotoxicity (B) in Caco-2/TC7 cells
 The points are the mean value of different replicates \pm SEM. ns: no significant difference.

Alternatively, we also tested an activation method based on a combination of human cytokines IFN- γ and TNF- α , each at 50 ng/ml. Some groups report utilisation of a combination of IL-1 β and IFN- γ /TNF- α at respective concentrations 25/50/50 ng/ml.³⁸³ We found that IL-1 β alone at 25 ng/ml or IFN- γ /TNF- α each at 50 ng/ml was sufficient to induce reasonable inflammation, and both methods returned comparable inflammatory induction in our intestinal epithelial cell model (Figure 15).

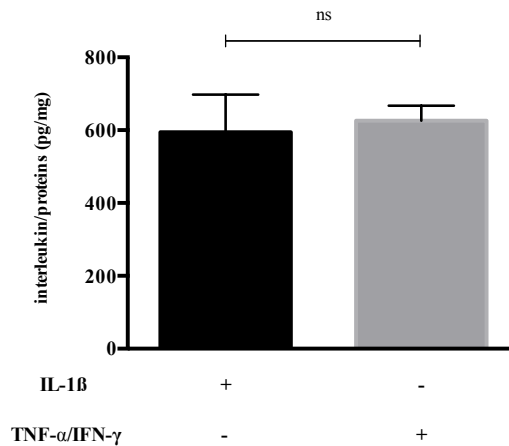


Figure 15 - Compared inflammation inductions in Caco-2/TC7 cells with 25 ng/ml IL-1 β stimulation versus combined TNF- α and IFN- γ at 50 ng/ml each

The points are the mean value of different replicates (n = 6) \pm SEM. ns: no significant difference in levels of secreted IL-8 between the two cytokine conditions.

Inflammation was stimulated in Raw 264.7 cells by means of combined bacterial LPS and murine IFN- γ , at respective concentrations 10 ng/ml and 20 U/ml. Each chemokine alone

poorly activates the macrophages, while their combination fully potentializes the inflammatory secretion (Figure 16).

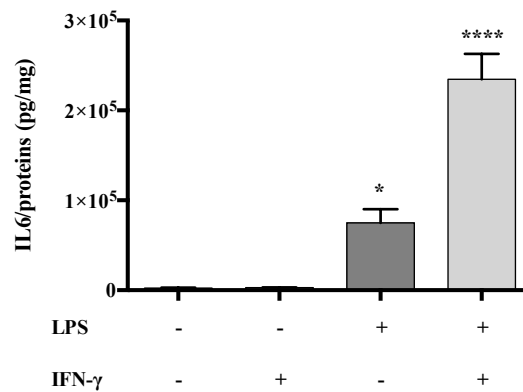


Figure 16 - Compared effects of activating cocktails on Raw 264.7 macrophages

The cells were incubated for 6h with diverse cocktails containing combinations of DMEM, LPS at 10 ng/ml and/or IFN- γ at 20 U/ml. The points are the mean value of different replicates (n = 6) \pm SEM. *p < 0.05, ****p < 0.0001 compared to DMEM alone, ANOVA (p < 0.0001), Tukey's post-test.

Finally, the influence on inflammatory response of vehicle DMSO and auxiliary 2-HQ was examined in both cell lines (Figure 17). No statistical difference was observed on cytokines responses whether the cells were incubated with or without 0.1% DMSO and 100 μ M 2-HQ, under resting or activated conditions.

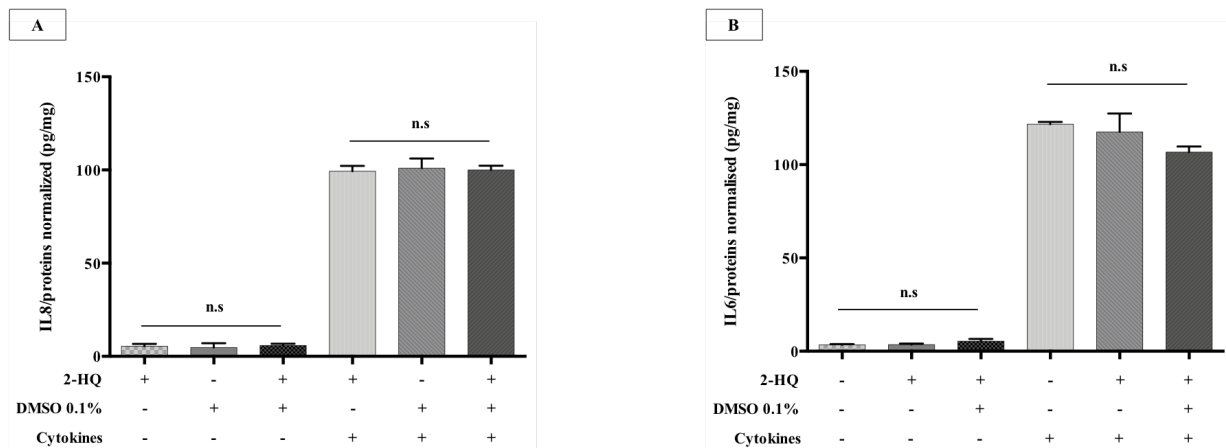


Figure 17 - Effects of DMSO 0,1% and inhibitor 2-HQ on the inflammatory response of Caco-2/TC7 cells (A) and Raw 264.7 macrophages (B)

The points are the mean value of different replicates \pm SEM. n.s : non-significant difference between conditions.

2.1.2. Natural AHLs can modulate the secretion of pro-inflammatory cytokines in *Caco-2/TC7* and *Raw 264.7* cell lines

We evaluated the capacity of the natural AHLs 3oxoC₁₂-HSL and 3oxoC₁₂:2-HSL to modulate the secretion of a selection of pro-inflammatory cytokines in cell lines *Caco-2/TC7* and *Raw 264.7*. Using ELISA, we studied the release of human interleukins IL-8 and IL-1 β by *Caco-2/TC7* cells, while murine IL-6 and TNF- α were measured for *Raw 264.7* macrophages. For each replicate, the raw secretion was divided by the protein load in the well, to compare replicates without bias. In each experiment, the ratio [secreted cytokine over amount of proteins] from the control condition DMSO 0.1% was used as a 100% induction reference.

2.1.2.1. *Caco-2/TC7* and *Raw 264.7* cells have different tolerances towards AHLs in range 1-100 μ M

The toxicity of controls and AHL treatment on the two cell lines was evaluated by means of the ratio [secreted LDH in supernatant over cytosolic LDH], expressed as a percentage. A ratio over 10% was considered cytotoxic.

In *Caco-2/TC7* cells, both **1** and **2** are well tolerated in the range 1 – 100 μ M under resting and stimulated concentrations (Figure 18). The secreted LDH does not exceed 2.5% for the saturated AHL **1** and 1.5% for unsaturated **2**, which is even lower than the control DMSO 0.1% alone (4% secreted LDH).

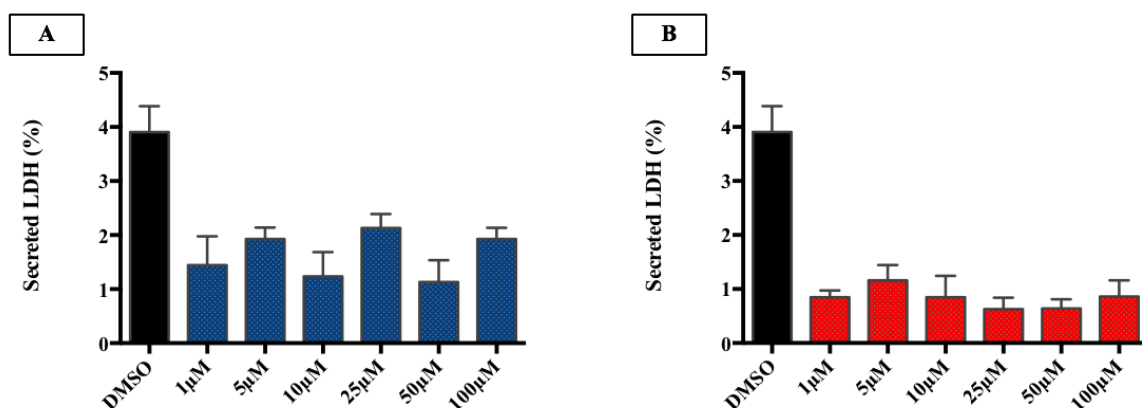


Figure 18 – Cytotoxicity of AHL treatment on *Caco-2/TC7* cells in stimulated state as measured by LDH release Cells were treated with increasing doses of 3oxoC₁₂-HSL (**A**) or 3oxoC₁₂:2-HSL (**B**). The points are the mean value of different replicates (n \geq 3) \pm SEM. No statistical difference between AHL conditions.

To explore the drop of cytotoxicity observed upon addition of AHLs, the effects of combined 25 ng/ml IL-1 β and 0.1% DMSO were explored (Figure 19). It appeared each compound alone had no or little effect on cytotoxicity, whereas their combination provoked a moderate increase in LDH release (3.8 % vs 2.4 % in basal condition). The AHLs hence seem to compensate this increase in toxicity.

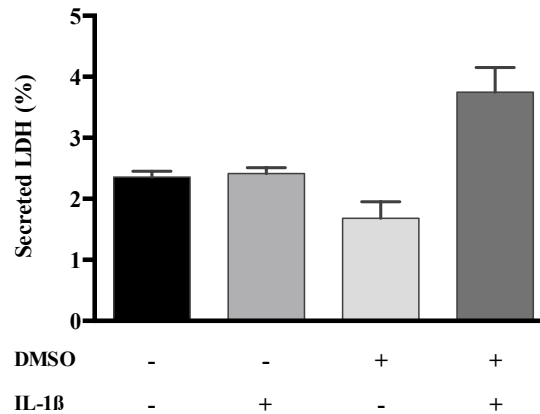


Figure 19 - Effects of addition of IL-1 β and DMSO on cytotoxicity in Caco-2/TC7 cells

IL-1 β was administered at 25 ng/ml and DMSO as 0.1% of final volume. The points represent the mean value of different replicates \pm SEM.

In the Raw 264.7 cell line, an increase in LDH was observed from 50 μ M with both AHLs and the 10% threshold was exceeded at 100 μ M (Figure 20). This phenomenon appeared in both resting and activated states. Hence, in the following experiments the tested AHL dosage was reduced from 1-100 μ M to 1-50 μ M, as compared to the Caco-2/TC7 line.

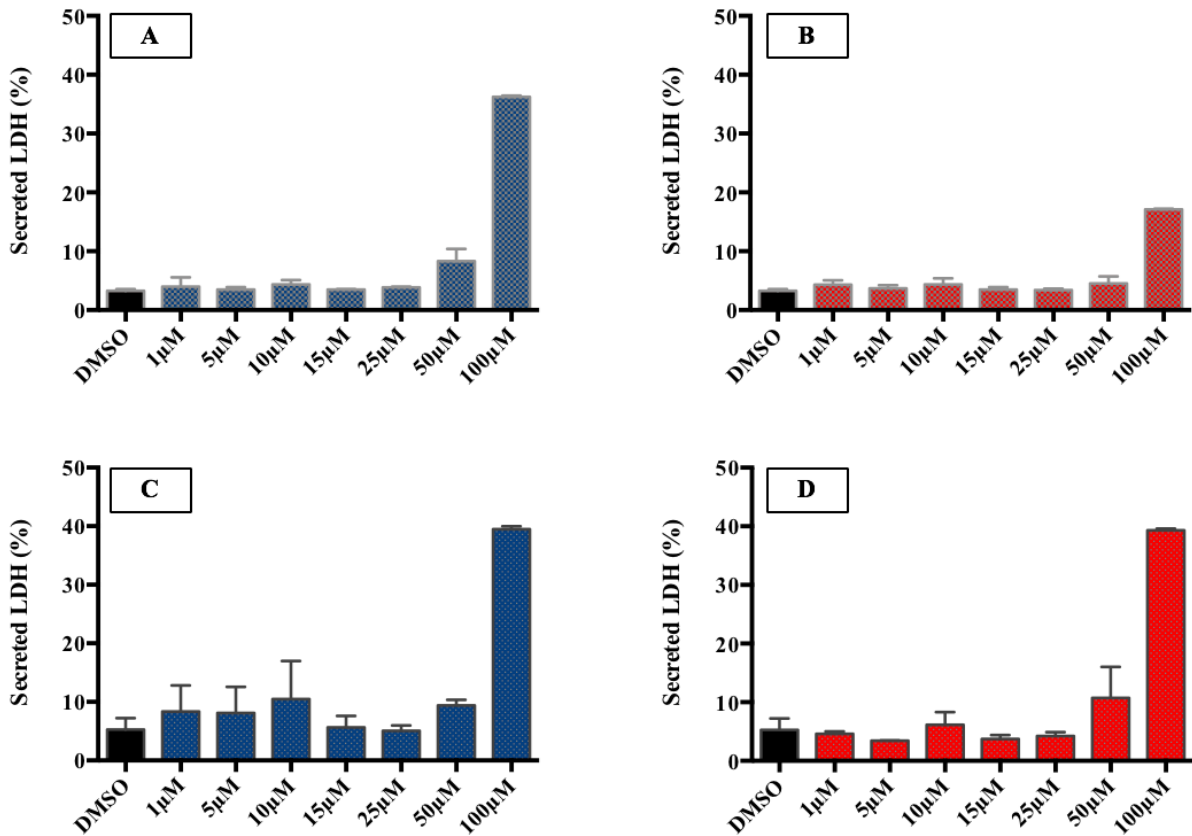


Figure 20 - Cytotoxicity of AHL treatment on Raw 264.7 cells in resting and stimulated states as measured by LDH release

Cells were treated with increasing doses of 3oxoC₁₂-HSL in resting and activated states (resp. A and C) or 3oxoC₁₂:2-HSL (resp. B and D). The points are the mean value of different replicates (n = 3) ± SEM.

2.1.2.2. AHLs have a bi-modal action over IL-8 secretion by Caco-2/TC7 cells

With IL-1β activation, the natural AHLs 3oxoC₁₂-HSL and 3oxoC₁₂:2-HSL both present a bell-shaped activity curve on IL-8 secretion (Figure 21), with significant anti-inflammatory action at low concentration (resp. 5µM and 25µM) and pro-inflammatory effect at high concentration (over 100µM). The two molecules exhibit a similar magnitude of anti-inflammatory potential, with respective average reduction of 27,6% and 25,6% of IL-8 secretion compared to DMSO control.

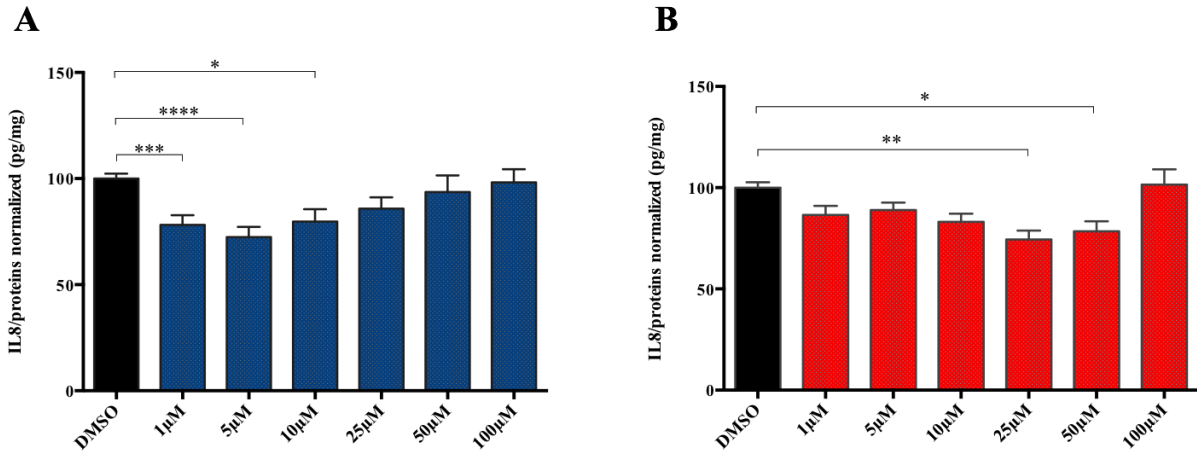


Figure 21 - IL-8 secretory response of IL-1 β activated Caco-2/TC7 cells in presence of AHL 3oxoC12-HSL (A) and 3oxoC12:2-HSL (B)

The cells are exposed to a range of AHL concentrations for 18h with IL-1 β to induce inflammation. The amount of secreted IL-8 is normalized to the control activated DMSO. The points are the mean value of different replicates ($n > 10$) \pm SEM. * $p < 0.05$, ** $p < 0.01$, *** $p < 0.001$, **** $p < 0.0001$ vs control, one-way ANOVA ($p < 0.0001$), Tukey's post-test.

However no statistically significant modulation was observed on resting cells, when the Caco-2/TC7 did not undergo inflammatory stress (Figure 22). Only a slight tendency suggests a decreased IL-8 secretion upon exposure to 5 μ M 3oxoC12-HSL and 25 μ M 3oxoC12:2-HSL in resting cells.

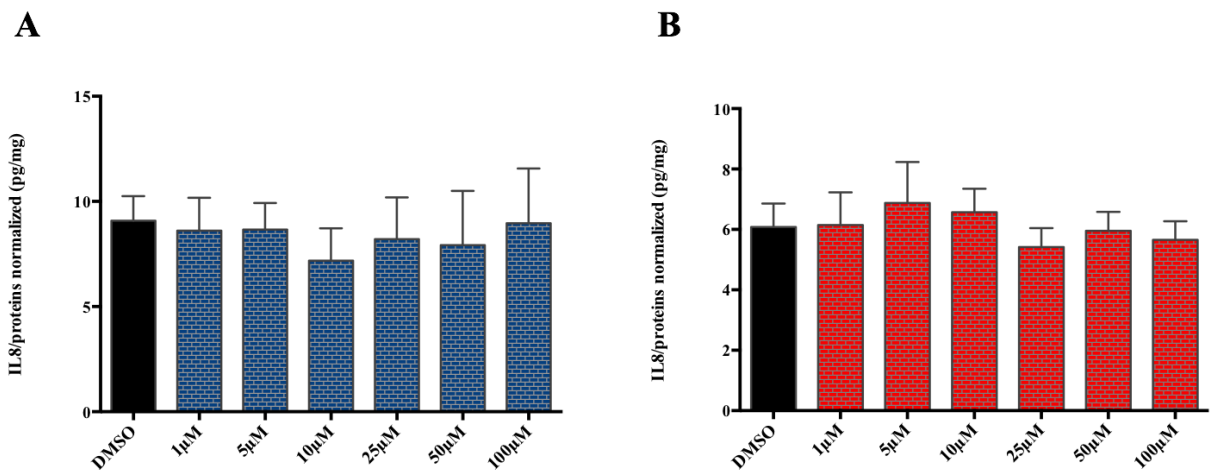


Figure 22 - IL-8 secretory response of resting Caco-2/TC7 cells in presence of AHL 3oxoC12-HSL (A) and 3oxoC12:2-HSL (B)

The cells are exposed to a range of AHL concentrations for 18h without inflammatory stimulus. The amount of secreted IL-8 is normalized to the control activated DMSO. The points are the mean value of different replicates ($n > 10$) \pm SEM. No statistical difference vs control, one-way ANOVA ($p > 0.9$), Tukey's post-test.

This pattern of a dual behaviour was similarly investigated under stimulation with combined IFN- γ /TNF- α . Again, bell-shape activity curves were observed, characterized by anti-inflammatory behaviour at low concentration and rather pro-inflammatory action above 50 μ M (Figure 23). With the saturated AHL **1**, the IL-8 secretion in supernatant was significantly reduced at 5 and 10 μ M, with respective diminution of 24 and 23% compared to control. The unsaturated AHL **2** demonstrated a maximum reduction of 34% at 10 μ M, however without reaching significance (number *n* of replicates was too low).

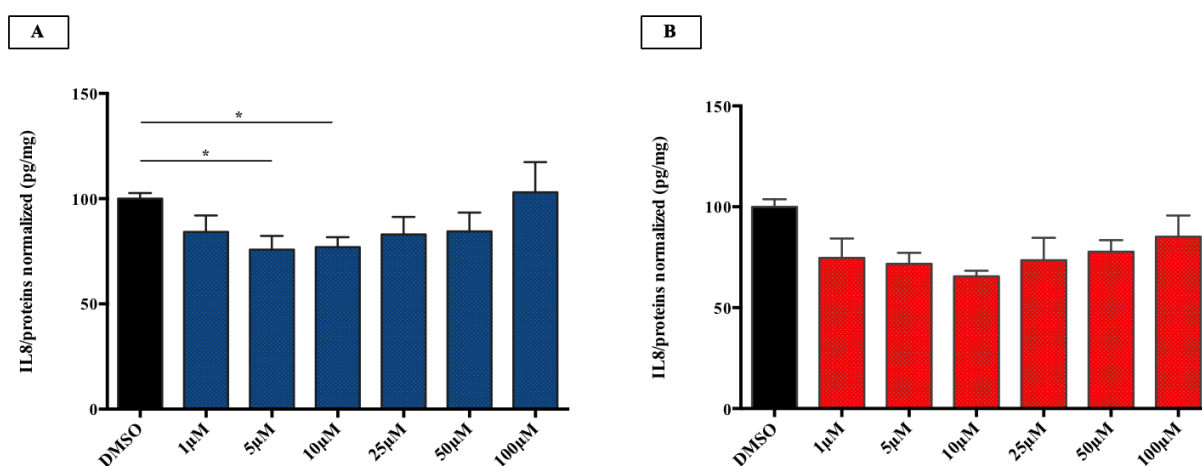


Figure 23 - IL-8 secretory response of TNF- α /IFN- γ activated Caco-2/TC7 cells in presence of AHL 3oxoC₁₂-HSL (A) and 3oxoC₁₂:2-HSL (B)

The cells are exposed to a range of AHL concentrations for 18h with combined TNF- α /IFN- γ to induce inflammation. The amount of secreted IL-8 is normalized to the control activated DMSO. The points are the mean value of different replicates (**A** : *n* > 14, **B** : *n* = 6) \pm SEM. **p* < 0.05 vs control, Kruskal-Wallis test (**A** : *p* = 0.0060, **B** : *p* = 0.0908), Dunn's post-test.

2.1.2.3. Timing and chronology in AHL treatments

It was decided to perform a 18-hour incubation of Caco-2/TC7 cells with AHLs for technical and practical matters : early experiments examined the IL-8 secretion after 6h, and the levels were too low to be detected using our usual IL-8 ELISA kit. Hence the incubation was extended overnight to 18 hours, as DiMango and co-workers reported a maximum IL-8 induction in lung epithelial cells in range 8-24h after beginning of incubation.³⁰⁸

To obtain an insight in the AHL action kinetics, we have examined the IL-8 production at short times (3h) after incubation with increasing doses of 3oxoC₁₂-HSL. But to ensure

sufficient concentration for detection, the ELISA dosage was performed on intracellular samples ; on average, after the 3-hour incubation 5-10 pg/ml were measured in supernatant versus 90-100 pg/ml in cell lysates. The profile of [IL-8 over total proteins] was similar to those obtained with IL-8 secreted in supernatant after 18h (Figure 24), but the potency of AHL **1** was not as important (20% IL-8 reduction versus 27% under regular conditions). These results indicate that AHL-mediated events happen early after exposure, and their effects can last for several hours.

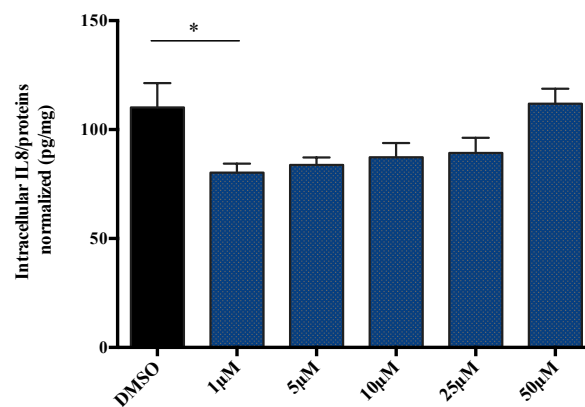


Figure 24 – Intracellular IL-8 secretory response of activated Caco-2/TC7 cells after 3-hour incubation in presence of increasing doses of 3oxoC₁₂-HSL

The amount of dosed IL-8 is normalized to the control activated DMSO. The points are the mean value of different replicates (n = 9) ± SEM. *p < 0.05 vs control, one-way ANOVA (p = 0.0051), Tukey's post-test.

Given that we observed AHL-effects as soon as 3 h after the start of incubation, we wondered if pre-incubating Caco-2/TC7 cells with the most active doses of 3oxoC₁₂-HSL before applying the inflammatory stimulus could potentialize the molecule's anti-inflammatory properties at low concentration, or extend its range of activity. A 4-hour pre-incubation was chosen, and the cells were split into three different groups : one control group received 0.1% DMSO, and two test groups received 5 or 10µM 3oxoC₁₂-HSL for pre-incubation. After 4 hours, cell media were removed and the wells were rinsed with PBS. Then, the cells were all treated according the usual protocol for biological assay with increasing doses of **1** or controls, and cytokines.

The results were positive on DMSO control conditions with or without cytokines : a dose-dependent reduction of IL-8 secretion was observed with increasing concentration of 3oxoC₁₂-HSL used during pre-incubation (Figure 25). In resting state, the pre-incubation with 5µM AHL **1** induced twice less IL-8 than in the absence of AHL pre-incubation. With 10µM, the IL-8

secretion was decreased by 2.5-fold. Under cytokine activation, the drops were respectively 1.2- and 1.4-fold.

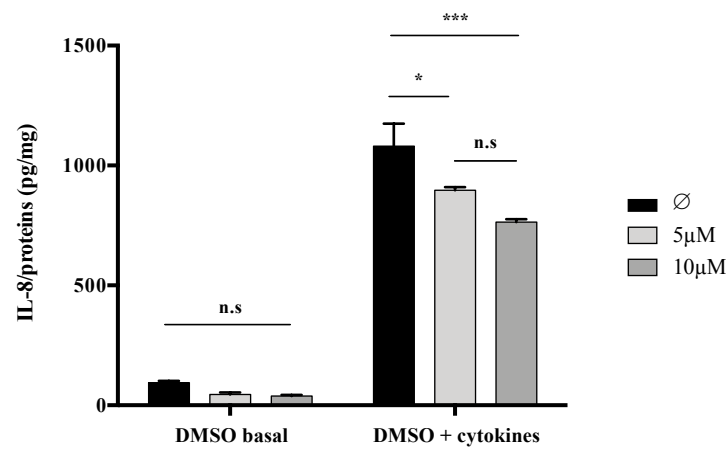


Figure 25 - IL-8 secretory response of resting or activated Caco-2/TC7 cells with DMSO 0.1% after successive 4-hour pre-incubation with DMSO 0.1%, 5µM or 10µM 3oxoC₁₂-HSL and 18-hour incubation in presence of increasing doses of 3oxoC₁₂-HSL

The amount of IL-8 is normalized to protein concentration. The points are the mean value of different replicates (n = 3) ± SEM. *p < 0.05, ***p < 0.001 vs control, two-way ANOVA (p = 0.0017), Tukey's post-test.

However, where the cells received AHL during the 18-hour incubation, the positive effects of pre-incubation seemed abolished. No significant difference was observed between cells that received a 5µM pre-incubation and those that did not, except at 100µM.

A beneficial trend appears on Figure 26 where we compare the normalised results from 5µM-preincubated cells to the global normalised results collected across our usual experiments without incubation (77,74% vs. 103,1%). It is difficult to infer strong conclusions from this pilot experiment due to its small number of replicates, but it would be worth repeating to find out if positive results with 5µM preincubation remain consistent.

Unfortunately, the cells that received a 10µM pre-incubation showed increased cytotoxicity.

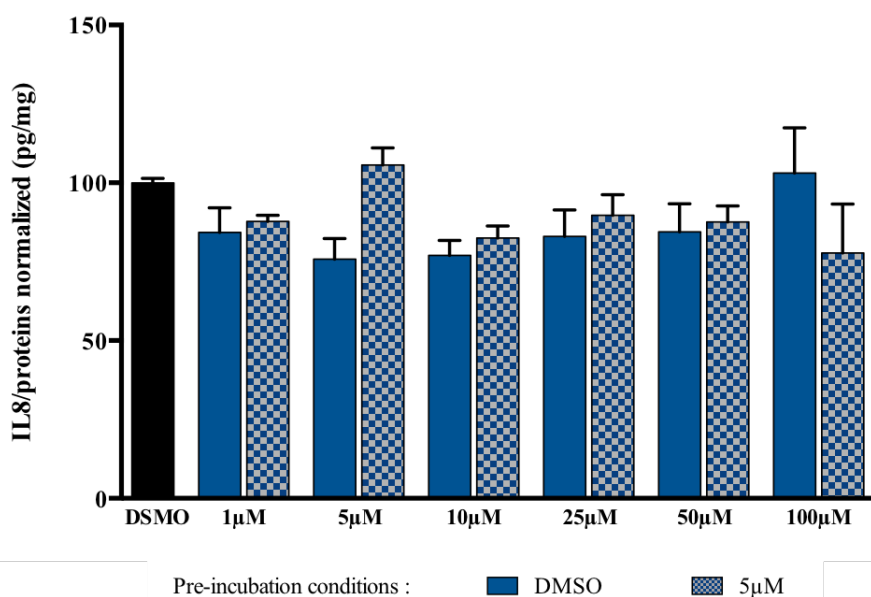


Figure 26 - Compared IL-8 secretory response of activated Caco-2/TC7 cells after successive 4-hour incubation and 18-hour incubation in presence of increasing doses of 3oxoC₁₂-HSL

Comparison of normalized data with the general data collected over multiple experiments (n > 10). The points represent different replicates ± SEM.

2.1.2.4. AHLs have mild effects on IL-6 secretion by Raw 264.7 cells

In the Raw 264.7 cell line, the first studied cytokine was murine IL-6 secreted in supernatants (Figure 27). No trend nor significant effect was observed on resting cells. On activated cells however, the characteristic bell-shape activity curve was identified again, with 15µM as most anti-inflammatory active concentration for both AHLs: respectively 17% and 29% decrease of IL-6 secretion for 3oxoC₁₂-HSL and 3oxoC₁₂:2-HSL compared to control DMSO. Yet, no significant difference was observed compared to that control, and only trends can be inverted from these results.

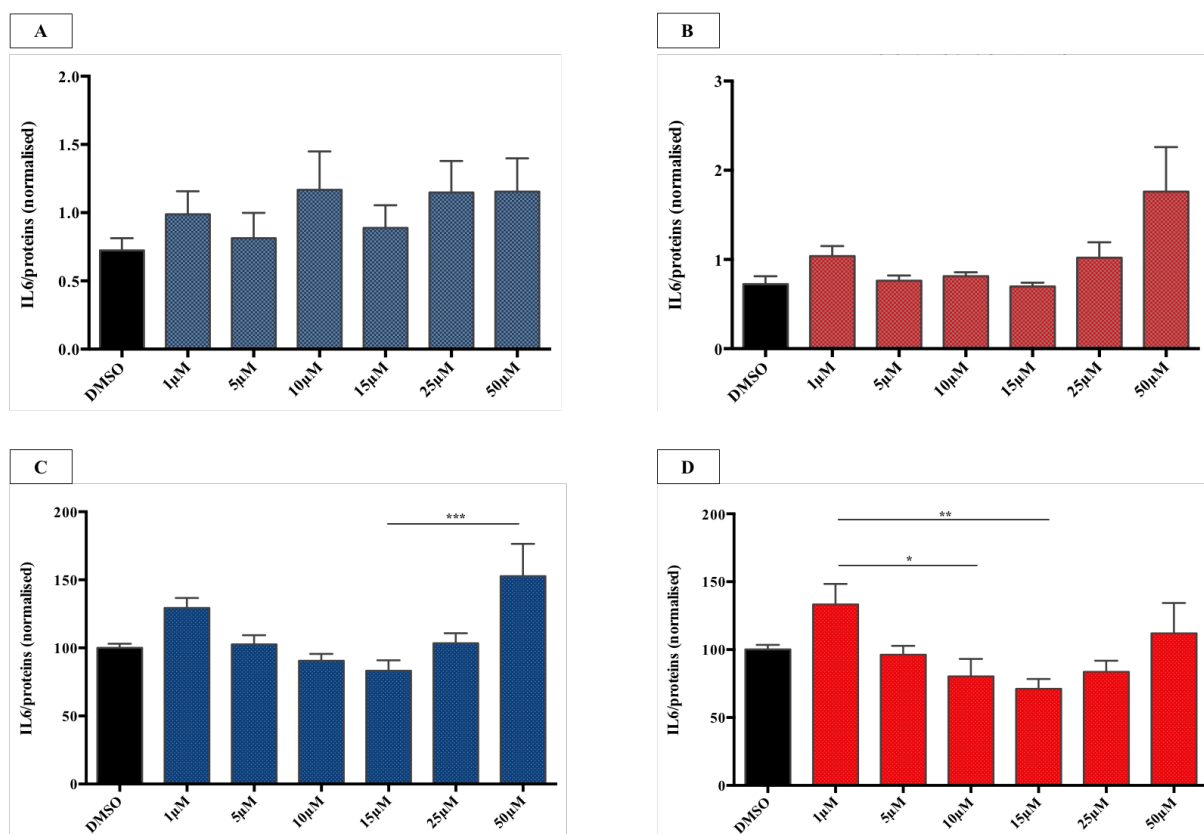


Figure 27 - IL-6 secretory response of LPS/IFN- γ activated Raw 264.7 murine macrophages in presence of AHLs

Cells were treated with increasing doses of 3oxoC₁₂-HSL in resting and activated states (resp. **A** and **C**) or 3oxoC₁₂:2-HSL (resp. **B** and **D**). The points are the mean value of different replicates ($n \geq 6$) \pm SEM. No statistical difference vs control with Tukey's post-test, yet positive one-way ANOVA (**C** : $p < 0.0001$, **D** : $p = 0.0067$).

2.1.2.5. Other pro-inflammatory cytokines : IL-1 β and TNF- α

Other pro-inflammatory cytokines were investigated in our cell models: IL-1 β in Caco-2/TC7 cells only, and TNF- α in both cell lines.

The secretion of IL-1 β in Caco-2/TC7 supernatants is scarce and erratic, but the intracellular levels of IL-1 β proteins were found to reach as much as 1500 pg/mg of proteins (Figure 28). Little variation was observed intracellularly with increasing doses of 3oxoC₁₂-HSL and statistical significance was not reached. The unsaturated AHL 3oxoC₁₂:2-HSL however demonstrated lower levels of intracellular IL-1 β , although the trend was unclear and would require further investigation.

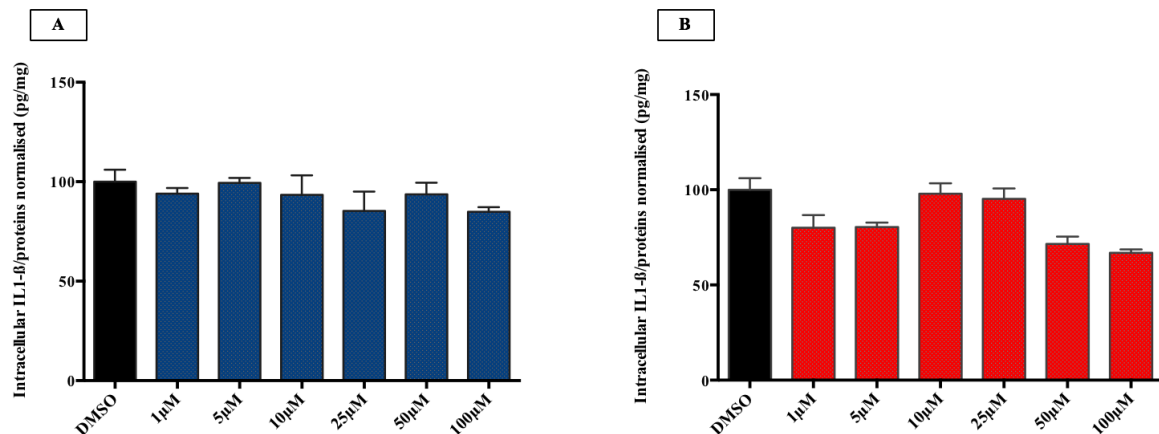


Figure 28 - IL-1 β secretory response of TNF- α /IFN- γ activated Caco-2/TC7 cells in presence of AHL 3oxoC₁₂-HSL (A) and 3oxoC₁₂:2-HSL (B)

The cells are exposed to a range of AHL concentrations for 18h with combined TNF- α /IFN- γ to induce inflammation. The amount of secreted IL-8 is normalized to the control activated DMSO. The points are the mean value of different replicates (n = 3) \pm SEM. **A** : Kruskal-Wallis test (n.s.), Dunn's post-test. **B** : Kruskal-Wallis test (p < 0.05), Dunn's post-test.

Caco-2/TC7 cells were also screened for TNF- α , but it appeared the intracellular and secreted levels were extremely low. This observation was confirmed in qPCR analysis, where human TNF- α mRNA were barely detected and exhibited very late amplification times. Raw 264.7 cells on the opposite were much more prone to secrete this cytokine (Figure 29). The usual bell-shape curve was observed with the saturated AHL **1**, with 37% decrease in secretion at 25 μ M compared to control ; the unsaturated AHL **2** was even more powerful with respective reduction of 31%, 38% and 54% at concentrations 15, 25 and 50 μ M. For the first time, a clear dose-dependent response was observed in the range of studied concentrations.

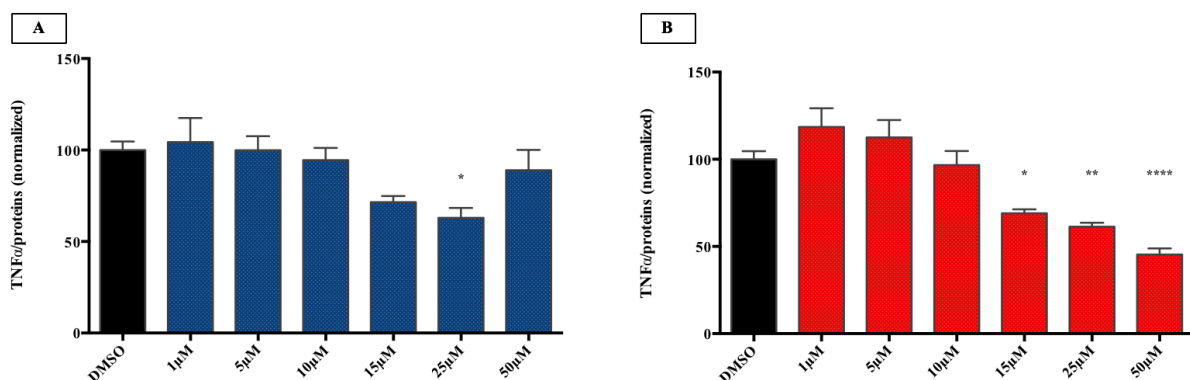


Figure 29 – TNF- α secretory response of LPS/IFN- γ activated Raw 264.7 murine macrophages in presence of AHLs

Cells were stimulated and treated with increasing doses of 3oxoC₁₂-HSL (A) or 3oxoC₁₂:2-HSL (B). The points are the mean value of different replicates (n = 9) \pm SEM. *p < 0.05, **p < 0.01, ****p < 0.0001. **A** : one-way ANOVA (p = 0.0023), Tukey's post-test. **B** : one-way ANOVA (p < 0.0001), Tukey's post-test.

2.1.3. No mRNA modulation is observed in Caco-2/TC7 cells submitted to AHLs

Following our observations on IL-8 secretion, Caco-2/TC7 cells were tested for IL-8 mRNA expression in the presence of AHLs. Surprisingly, no frank modulation was observed (Figure 30A), but only a trend where 4h treatments with 5 μ M 3oxoC₁₂-HSL or 25 μ M 3oxoC₁₂:2-HSL combined to cytokines induced slight and non-statistically significant decreases in IL-8 mRNA levels. Similarly, no modulation of human IL-1 β mRNA levels was observed (Figure 30B) which in that case concurs with our observations on protein levels.

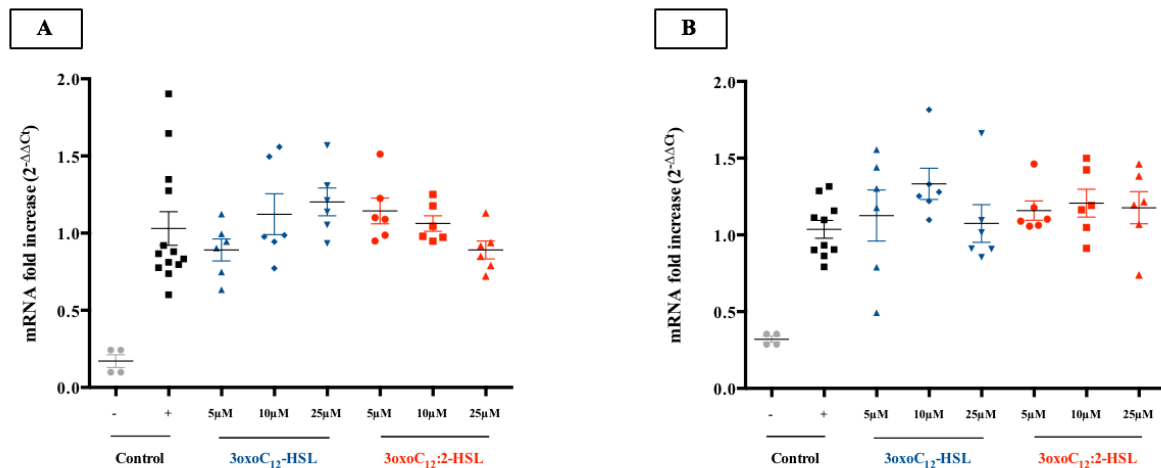


Figure 30 - Human mRNA levels for cytokines IL-8 (A) and IL-1 β (B) in Caco-2/TC7 cells after 4h incubation with AHLs

Activated cells treated with increasing doses of 3oxoC₁₂-HSL or 3oxoC₁₂:2-HSL. 2^{-ΔΔCt} calculated proportionally to house-keeping gene human GAPDH. The points represent different replicates (n \geq 6) \pm SEM.

2.1.4. AHLs and secretion of anti-inflammatory cytokines

Caco-2/TC7 cells were screened for human IL-10, but the results were not conclusive. Very little mRNA expression of human IL-10 was observed at 4h, and secretion of protein IL-10 was scarce and heterogenous after 18 hours incubation: in supernatants the protein levels barely reached 10 pg/ml, while intracellular levels culminated at 30 pg/ml.

Raw 264.7 macrophages are much better producers of anti-inflammatory interleukin-10. Levels of murine IL-10 were measured in supernatants after 6-hour incubation and concentrations about 400-800 pg/ml were observed in resting cells, while LPS/IFN- γ activated macrophages secreted up to 80000–160000 pg/ml of mouse IL-10. At first sight, AHLs at

concentrations 1 – 25 μ M do not affect the secretion of murine IL-10 in comparison to control condition DMSO 0.1% ; concentration 50 μ M however induced increased IL-10 release in supernatant with both compounds (Figure 31). AHL **1** led to a 60% increase in IL-10 secretion, while **2** induced a 34% increase.

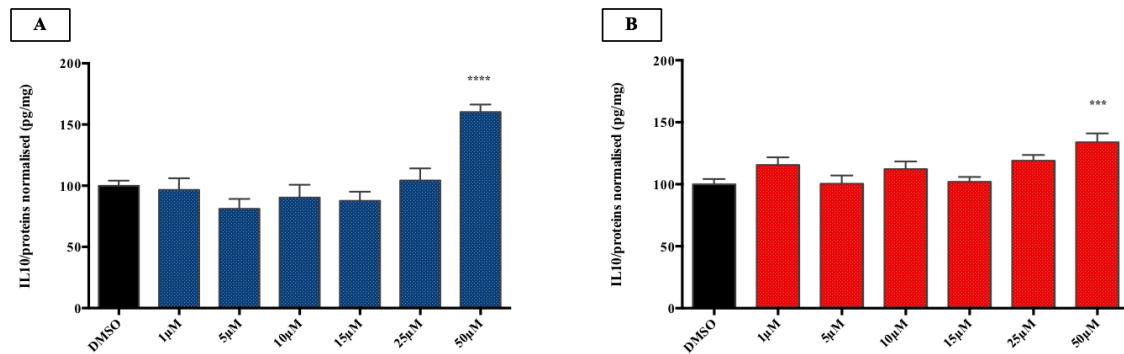


Figure 31 – IL-10 secretory response of LPS/IFN- γ activated Raw 264.7 murine macrophages in presence of AHLs

Cells were stimulated and treated with increasing doses of 3oxoC₁₂-HSL (A) or 3oxoC_{12:2}-HSL (B). The points are the mean value of different replicates (n = 9) \pm SEM. ***p < 0.001, ****p < 0.0001 compared to positive control activated DMSO 0.1%. A: one-way ANOVA (p < 0.0001), Tukey's post-test ; 50 μ M is also significantly different to all other doses 1-25 μ M. B: one-way ANOVA (p = 0.0004), Tukey's post-test ; 50 μ M is also significantly different to doses 5 and 15 μ M.

If AHLs do not seem to affect macrophage anti-inflammatory secretion by direct modulation of IL-10, they could perhaps exert their effect by balancing the ratio [anti-inflammatory cytokines over pro-inflammatory cytokines]. To explore this hypothesis, we examined the ratio [IL-10 (pg/mg) over TNF- α (pg/mg)] in activated Raw 264.7 cells (Figure 32). Both cytokines were dosed on the same experiment to prevent biases due to cell minimal variations from one passage to another. The IL-10/TNF- α ratio seems unaffected by the AHLs at doses 1-10 μ M. From 15 μ M we can observe a trend towards increasing ratios, that reaches statistical significance at 50 μ M. The 3oxoC₁₂-HSL induces an approximative 3-fold increase in IL-10/TNF- α ratio (exact value is 2.75) while the 3oxoC_{12:2}-HSL leads to a 2-fold augmentation (exact value 2.18). This difference in potency results primarily from the higher IL-10 secretion observed in presence of AHL **1** compared to **2**.

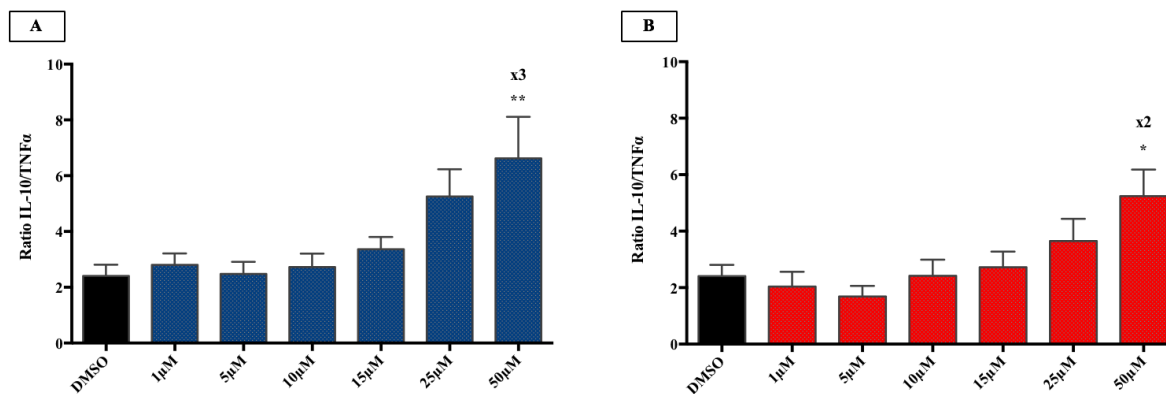


Figure 32 – Ratio of secreted IL-10 over secreted TNF- α in response to LPS/IFN- γ inflammatory stimulus in Raw 264.7 murine macrophages in presence of AHLs

Cells were stimulated and treated with increasing doses of 3oxoC₁₂-HSL (A) or 3oxoC₁₂:2-HSL (B). The points are the mean value of different replicates (n = 9) \pm SEM. *p < 0.05, **p < 0.01 compared to positive control activated DMSO 0.1%. **A:** one-way ANOVA (p = 0.0005), Tukey's post-test ; 50 μ M is also significantly different to doses 1-10 μ M. **B:** one-way ANOVA (p = 0.0029), Tukey's post-test ; 50 μ M is also significantly different to doses 1-10 μ M. These experiments were realised by Miss Garance COQUANT.

2.1.5. AHLs and bacteria

The two long-chain AHLs 3oxoC₁₂-HSL and 3oxoC₁₂:2-HSL were tested on the bacteria reporter strain *E. coli* pSB1075 to assess their interaction with the *P. aeruginosa* receptor LasR and its resulting activation by lecture of luminescence. The emitted bioluminescence (in arbitrary units) was then plotted against the AHL concentration in logarithmic units to invert agonistic activation curves and constants. Among these, the half maximum effective concentrations (EC₅₀) of the two C₁₂ AHL were calculated: the 3oxoC₁₂-HSL was the most effective with an EC₅₀ of 9 nM, while the 3oxoC₁₂:2-HSL exhibited an EC₅₀ about eleven times higher, of 100 nM (Figure 33). Several other commercial short- and long-chain AHLs were used as controls to characterise the QS reporter model and verify the receptor chain-length specificity (Table 11). As expected, the *Pseudomonas aeruginosa* LasR recognises preferably rather long-chain AHL, here compounds with 10- to 14-carbon chains. On the opposite, short-chain molecules C₄-HSL and C₇-HSL does not elicit response. The substitution at carbon 3 seems to matter as well ; compound 3-OH-C₁₂-HSL was a weaker agonist than AHL **1** from which it only differs in oxidation status at C₃ (respective hydroxyl versus keto group).

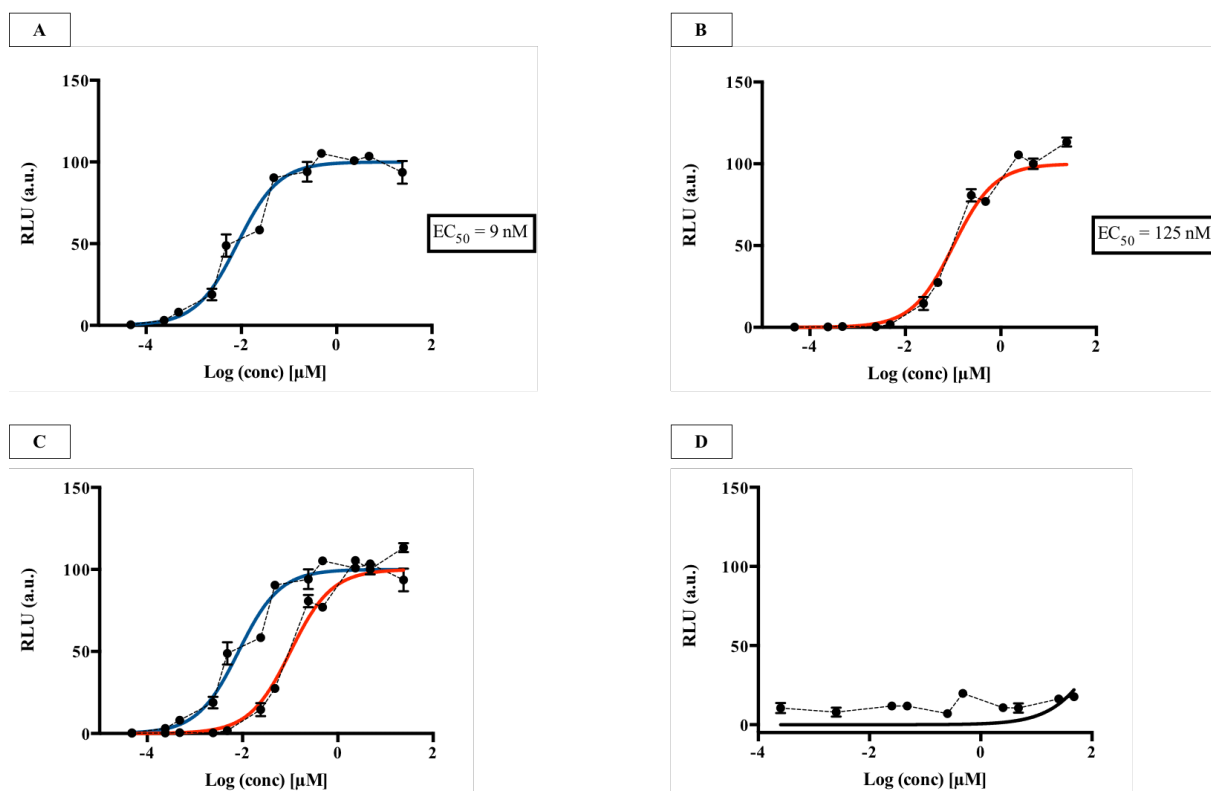


Figure 33 - Emission of luminescence by the bacteria reporter strain *E. coli* pSB1075 in presence of a range of concentrations of AHLs

A: incubation with the 3oxoC₁₂-HSL. **B:** incubation with the 3oxoC₁₂:2-HSL. **C:** compared effects of the two C₁₂-HSL. **D:** control incubation with the C₄-HSL. Incubation 4h at 37°C and 70 rpm agitation. The points are the mean value of different replicates (n > 3) ± SEM.

Compound	EC ₅₀ (μM)	95% CI (μM)	Activation (%)
(S)-3oxoC ₁₂ -HSL	0.009	0.007 – 0.012	100
(S)-3oxoC ₁₂ :2-HSL	0.102	0.081 – 0.127	100
(S)-C ₄ -HSL	> 1000	-	-
(S)-C ₇ -HSL	> 1000	-	-
(S)-3oxoC ₁₀ -HSL	0.092	0.051 – 0.167	100
(S)-3-OH-C ₁₂ -HSL	1.800	1.245 – 2.602	100
(S)-3oxoC ₁₄ -HSL	0.401	0.271 – 0.592	95

Table 11 - Summary properties of diverse natural and commercial AHLs

Potential bactericidal effects of AHL **1** and **2** were studied, to ensure the apparent decrease in EC₅₀ observed with **2** was not due to bacterial death. AHLs **1** and **2** in range 1-100μM demonstrated no effect on bacterial survival after 18-hour incubation : the recorded absorbances are similar to those observed with LYBHI medium alone and LYBHI complemented with 0.1% DMSO (Figure 34). Hence we can conclude that **2** is really a weaker agonist than **1**, with decrease capacity to bind/accommodate the LasR receptor from *Pseudomonas aeruginosa*. Passador and co-workers had previously reported a lowered EC₅₀ on

a *lasB* construct from *P. aeruginosa* with a mono-unsaturated AHL in ω -6 (10 μ M vs. 7 μ M for native AHL **1**). The authors hypothesized that free rotation of the acyl chain was a requirement for proper receptor activation. With such a point of view, it would then seem logical that AHL **2** exhibited an even more impaired EC₅₀ given that it harbours two insaturations that further reduce its rotatability.

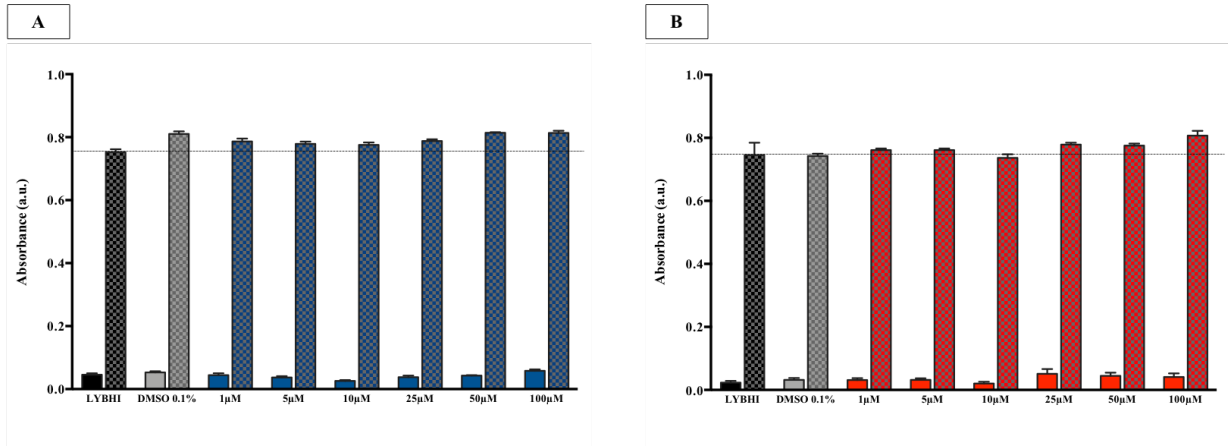


Figure 34 - Compared survival and growth of *E. coli* strain K12 incubated with controls or increasing doses of **1 (A) or **2** (B) as read by absorbance at 600nm**

Absorbance was read on a SpectraMax spectrophotometer. The points are the mean of several independent replicates (n = 6) \pm SEM.

2.1.6. Discussion

It seems quite important first to examine the dosage of AHL employed in our experiments and its biological relevance. AHL have been identified *in vivo* in an array of fluids from human sputum to bacterial biofilms, and now in feces as reported by our team. Undirect samplings (not close to the cells) return very low concentrations maybe because it is only an insight of the actual levels or due to technical bias : concentrations ranging from 1 to 20 nM are detected in the sputum of patients with cystic fibrosis³⁸⁴, while 0.2 to 2 nM/g of feces are found in samples from IBD patients. On the opposite very high concentrations are measured in *Pseudomonas aeruginosa* biofilms: levels as high as 300-600 μ M have been reported by Charlton et al.³⁸⁵ and biofilms have been identified in the lung of cystic fibrosis patients.^{386,387} However the goal of our study is neither to study AHLs in fluid samples nor in organs/models where a bacterial infection is fully established. What we aim at is to explore AHLs effects in organs not yet under infection but undergoing inflammation and in contact with a dysbiotic

microbiota, hence where pathogens could thrive. In this regard, it has been described that planktonic *P. aeruginosa* secreted AHL at low micromolar concentrations³⁸⁸, which is incidentally the range of concentration detected in a murine model of *P. aeruginosa* acute lung infection (1-20 μ M).³⁰² Hence we thought relevant to broaden this range to 1-100 μ M, which could be the levels of AHLs intestinal cells from a IBD patient would encounter in a non-infected but inflammatory and dysbiotic state.

Overall our goal was to study the effects of C₁₂ AHLs in the context of primary inflammation and immediate immune response. This aim lead our choice in the studied cytokines: IL-8 and IL-6 are known pro-inflammatory interleukins involved in early events in immunity. IL-8 acts as a chemoattractant to recruit neutrophils to the site of activation and create an inflammatory infiltrate. IL-6 combined to IL-1 β (and TGF- β , but not necessarily) induces differentiation of naïve T cells into Th17 lymphocytes ; this subset of lymphocytes secretes IL-17 (especially subtype IL-17A), an interleukin that itself promotes secretion of IL-6, IL-8 and TNF- α .^{389,390} Inflammation in IBD - and more generally auto-immune diseases such as psoriasis and ankylosing spondylitis - have furthermore been shown to belong to a model of IL-17/Th17 inflammation. Hence a panel composed of IL-8, IL-6, IL-1 β and TNF- α seemed relevant in the scope of our study.

Through literature it appears that cell tolerance to AHLs is highly variable and dependent on the chosen cell line, epithelial cells being the most resistant. Tateda et *al.* for instance described a rapid (within 2 hours) loss of viability in mouse bone-marrow derived macrophages (BMDMs) incubated with 25 μ M **1** and higher concentrations, but also in mouse macrophages P388D1 (confirmed by Horikawa et *al.*²⁷⁷), human macrophages U-937 and neutrophils.²⁷⁶ We however have not observed such cytotoxicity in concentrations ranging 1-50 μ M, despite a 6-hour-long incubation. On the opposite, the same group observed no significant cell death in human lung epithelial cells CCL-185 nor human epithelial cells Hep-2, which in that case is in line with our findings on gut epithelial cells Caco-2/TC7. Similarly, Telford et *al.* found no toxicity as assayed by LDH release in Jurkat E6.1 cells in range 0.1-100 μ M.²⁸⁷

The capacity of 3oxoC₁₂-HSL **1** to negatively modulate response in immune cells had already been reported, although our results are not always in accordance with published

literature. Kravchenko *et al.* observed reduced LPS-induced levels of TNF- α and IL-12 β mRNA in BMDMs co-incubated with LPS and 3oxoC₁₂-HSL.²⁹⁹ These results were confirmed at protein level by several groups in diverse macrophage cell lines, among which Raw 264.7 cells.^{287,300,301,303,391} The range of effective 3oxoC₁₂-HSL concentration varied from 15 to 50 μ M, which is of the same order of magnitude as our reports.

To the best of our knowledge, Chhabra *et al.* are the only group to have studied the effects of unsaturated AHLs on mammalian cells. Although their assay dealt with splenocyte proliferation, it is worth noting that mono-unsaturated AHL showed loss of activity comparatively to the 3oxoC₁₂-HSL : molecules with a terminal unsaturation exhibited a two-fold increase in IC₅₀, while those with a double-bond further down the chain had an average 4-fold increase in IC₅₀. These results suggest a lower affinity in unsaturated AHLs compared to their saturated counterpart, which corroborates our results on hIL-8 and mL-6 secretion where both AHL **1** and **2** have similar inductions but at different concentrations.

Our findings on IL-10 secretion in macrophages are in accordance with published results from Glucksam-Galnoy and co-workers.³⁰³ The group reported an IL-10 secretion increase in LPS-stimulated Raw 264.7 cells in presence of 50 μ M 3oxoC₁₂-HSL over a 5h incubation ; at 50 μ M they observed a 3.2-fold increase where we only report a 0.6-fold increase. An hypothesis to explain this difference could lay within our different stimulation protocols (LPS vs. combined LPS and IFN- γ). The group confirmed the results in mouse peritoneal macrophages, a more physiological setting of primary macrophages. Glucksam-Galnoy *et al.* also studied the involvement of PPAR γ -mediated mechanisms in the AHL-modulation of cytokines TNF- α and IL-10. Using PPAR γ agonist ciglitazone, the authors demonstrated that the inhibition of TNF- α could occur via PPAR γ , but that the increase in IL-10 took place via a PPAR γ -independent mechanism. This duality of pathways defends the idea it exists more than one mammalian receptor to AHLs, which could explain the bell-shaped activity curves we observed during our experiments. The observed AHL effects would then be the result of a balance between these receptors, each with different affinities and mechanisms. Passive diffusion of the AHLs through the cell membrane is not excluded either. As mentioned in *Part I - 2.2.1*, the auto-inducers can penetrate mammalian cells to reach a putative intracellular partner. In this regard, the difference in acyl chain structure between **1** and **2** may modulate their respective penetration rates. Computation predicts AHL **2** to be less lipophilic, more hydrophilic and less flexible than its saturated counterpart **1**. These elements can affect its cell penetration capacity. It is our

assumption that such decreased cell penetration could explain the difference observed in terms of most active concentration between the two molecules. If this assumption was verified, it would yet remain to prove the existence of an intracellular partner accounting for the AHL-mediated anti-inflammatory properties at low concentration.

There is not much reports on AHLs and inflammation in epithelial cells, and most of these employed different cell lines and protocols from our experiments. Smith *et al.* have worked extensively on the effects of 3oxoC₁₂-HSL in human lung fibroblasts and epithelial cells. Among others, the group demonstrated that AHL **1** was a strong inducer of both IL-8 mRNA and protein IL-8 through NF-κB transcription factor. However, their experiments were all conducted on resting cells, while ours deal with cytokine-activated cells. Surprisingly, the group reports IL-8 secretion with 100μM **1** almost as important as with 20 ng/ml IL-1β, which is very different from our own observations. We worked on a different cell line, and strict comparisons are hence hard to establish, but the novelty of our study resides in the description of AHL anti-inflammatory effects on epithelial cells undergoing a cytokine stress. Some have suggested that the ability of AHL 3oxoC₁₂-HSL to moderate pro-inflammatory cytokines in macrophages was not opposed to a putative mechanism acting through cross-talk of the unfolded protein response (UPR) and modulation of the NF-κB through an ER (endoplasmic reticulum) pathway. More work will be required to validate such an hypothesis in epithelial cells.

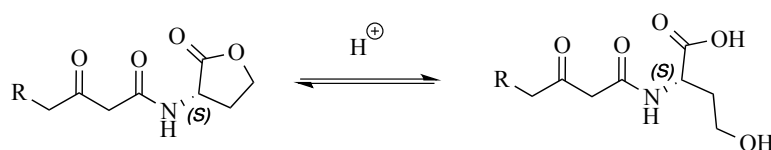
Overall, we were able to show that AHLs **1** and **2** exhibit anti-inflammatory properties on secretion of several cytokines and in two different cell lines. These effects, observed at protein level, were restricted to the low micromolar range and were not observed at the mRNA level. AHLs prove efficient when added concomitantly to the inflammatory stimulus, and pilot results suggest a benefit could be found in cell pre-incubation with low dosage of AHLs. If such results were obtained, it could maybe pave the way to a future use of AHLs as long-term treatment for IBD patients in order to extend remission between flares, during low-grade inflammation rather than acute episodes. Indeed, we have not tested AHLs in a model of pre-established inflammation and hence cannot tell if these molecules would be efficient enough to reverse long-term inflammatory damages.

2.2. Stability & metabolism of AHLs

2.2.1. Degradation of AHLs in biological media

2.2.1.1. AHLs are degraded into two major by-products

N-Acyl Homoserine lactones are not very stable molecules at biological pH, essentially from the presence of a lactone moiety. These molecules can undergo two main degrading phenomena : the hydrolysis of the lactone ring to produce an acyclic headgroup containing a carboxylic acid and an alcohol (Scheme 6), and a spontaneous rearrangement to produce a tetramic acid (Scheme 7).



Scheme 6 – Hydrolysis of AHL into open-form corresponding acyl homoserine

The hydrolysis of the lactone ring is a phenomenon that can happen under two environmental pressures. First, living cells and organisms can secrete degrading enzymes that will catalyse lactonolysis reactions to produce open-ring AHL equivalents, that we will name 3oxoC₁₂-HS for **Homoserine** (as opposed to HSL for Homoserine Lactone) in the case of AHL 1. Such enzymes are called lactonases ; in particular, human cells do secrete a family of lactone-hydrolysing enzymes called Paraoxonases or PON. There are three members in this family: PON-1, PON-2, and PON-3.³⁹²

Secondly, the hydrolysis can be pH-dependent like the saponification of a regular ester. Due to their ring-conformation, lactones are however much more prone to degradation at lower pH than conventional esters : indeed, the ring locks the ester bonds C=O and O-C in a trans conformation which impairs stereoelectronic stabilisation (Figure 35).³⁹³ For instance, the calculated/predicted pKa for *L*-Homoserine lactone is 7.33 ; hence, biological pH is high enough to provoke hydrolysis of AHLs.

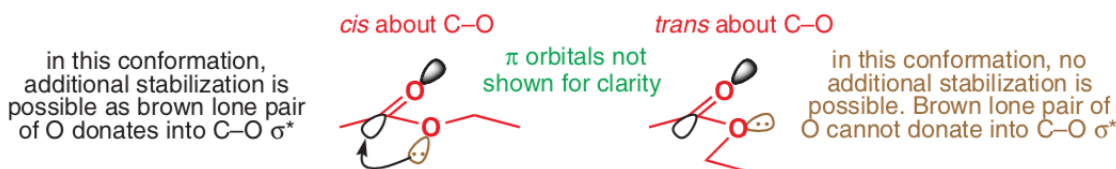
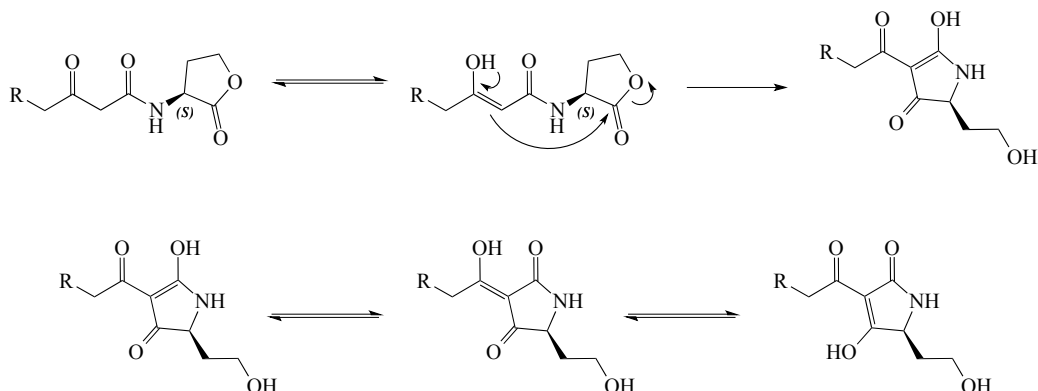


Figure 35 – Stereoelectronic effects in esters depend on their spatial conformation

Extracted from Clayden *et al.*³⁹³

AHLs **1** and **2** belong to the specific class of *N*-3-oxoacyl homoserine lactones as they harbour a ketone at carbon 3. These β -ketoamides exist as an equilibrium between a keto-form and an enol-form, and can undergo an irreversible and non-enzymatic Claisen-like mechanism at biological pH to be degraded into tetramic acids (Scheme 7). The resulting compounds are a class of molecules containing a 2,4-pyrrolidinedione ring system branched to an acyl chain.



Scheme 7 - Irreversible conversion of AHLs into tetramic acids

2.2.1.2. pH-dependent stability in biological medium

We first studied the stability of AHLs **1** and **2** in non-conditioned cell-free DMEM at room temperature. Solutions of known initial AHL concentrations were maintained with stirring over 24 h and samples taken at regular intervals. These samples were extracted with ethyl acetate, acidified to pH 4 with 1M HCl, and extracted again with EtOAc. The two resulting organic phases and the aqueous phase were then evaporated to dryness and retaken in fresh HPLC-grade methanol before analysis in tandem mass spectrometry LC-MS/MS. A deuterated short-chain AHL C_4 - d_5 -HSL was added to the samples at constant concentration to be used as internal standard for quantitation. The quantitation was itself performed using a standard curve of solutions with known 3-oxo C_{12} -HSL concentrations and constant C_4 - d_5 -HSL doses (Figure

36), from which a linear regression plotting the ratio $AUC_{\text{AHL}}/AUC_{\text{standard}}$ against concentration could be inverted.

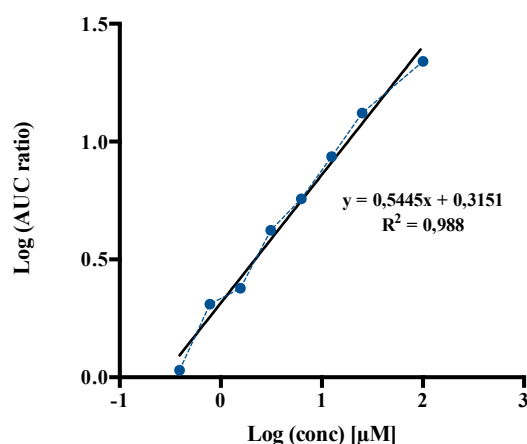


Figure 36 - Standard curve for 3oxoC₁₂-HSL ranging from 300 nM to 100 µM in tandem LC-MS/MS
 AUC : Area Under the Curve. Fitting curve obtained with the Linear Regression model, Prism, GraphPad.

Both AHLs **1** and **2** decay over time to produce two degradation compounds (Figure 37). From this data we interpolated kinetics constant for each AHL, using a one-phase decay/association non-linear interpolation model on Prism, GraphPad (Table 12). It appears saturated AHL **1** has a slightly shorter half-life than the unsaturated AHL **2**. The degradation of AHL follows an apparent first order kinetic mechanism, and is independent from initial concentration. Overall, both AHLs hydrolyse in cell medium within hours ; the open form is largely predominant over the tetramic acid that never exceeded 9% of total matter amount in our experiments.

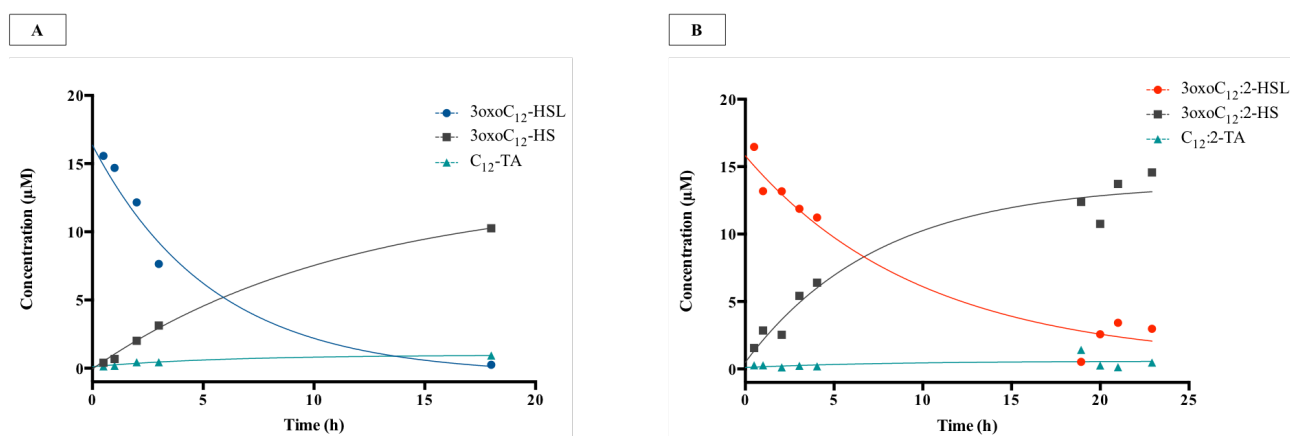


Figure 37 - Compared kinetics for AHL decay and degradation products apparition

15µM initial AHL concentration diluted in non-conditioned cell-free DMEM Glutamax at r.t. with stirring.
A: 3oxoC₁₂-HSL ; **B:** 3oxoC_{12:2}-HSL.

We wish to emphasize these kinetic data are informative but not entirely relevant to our assays, which take place at 37°C. The aqueous medium is furthermore enriched with cell-secreted soluble components. Indeed, temperature positively influences the kinetics of chemical reactions. This element was confirmed by Yates and co-workers, who explored the effects of temperature, pH, and AHL acyl chain length on AHL rates of hydrolysis.³⁹⁴ The authors reported that extended acyl chains increased the stability of AHLs at a given pH, i.e. AHLs with short acyl chains (C₃-C₄) were completely hydrolysed at lower pH than AHLs with longer acyl chains (C₆-C₈). Chain effects may explain the unexpected difference in half-life between AHLs **1** and **2**. Yates *et al.* also explored the influence of AHL hydrolysis with pH : the medium should acidify upon AHL hydrolysis due to the production of new carboxylic acids ; we chose to neglect this factor as we performed all experiments in buffered cell medium and at low concentration.

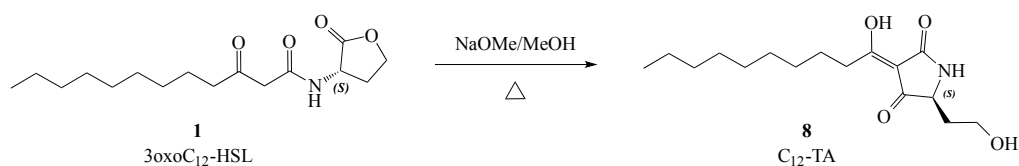
<i>Initial condition</i>	3oxoC₁₂-HSL 15μM	3oxoC₁₂:2-HSL 15μM
k_{app} (h⁻¹)	0,1842	0,1453
t_{1/2} (h)	3,762	4,769

Table 12 - First order kinetic constants for AHL degradation in cell-free medium at r.t.

2.2.1.3. Biological study of tetramic acid from the 3oxoC₁₂-HSL

Despite its low proportion, the tetramic acid **8** derived from 3oxoC₁₂-HSL (abbreviated C₁₂-TA) was investigated for biological activity in our cell and bacterial models. The molecule full name is (5*S*,3*Z*)-3-(1-hydroxydecylidene)-5-(2-hydroxyethyl)pyrrolidine-2,4-dione.

As seen with kinetics experiments, the TA production in biological medium is slow. As a consequence, it was rather easier to synthesize molecule **8** from precursor AHL **1** than to isolate it from samples. Briefly, chemically synthesized **1** (*Part I - 1.1*) was solubilized in a 0.5 M sodium methoxide solution in methanol and heated. The reaction was quenched via an acidic ion exchange resin to afford the desired tetramic acid **8** (Scheme 8).



Scheme 8 - Preparation of tetramic acid **8 from precursor 3oxoC₁₂-HSL**

Usual synthetic methodology from literature.^{328,329}

The tetramic acid **8** was tested on Caco-2/TC7 and Raw 264.7 cells, and both *E. coli* strains pSB1075 and K12. Compared to positive control DMSO, the molecule has no effect or is pro-inflammatory at all concentrations in both cell lines (Figure 38). No effect was observed either in resting Caco-2/TC7 cells (data not shown). Regarding toxicity, tetramic acid **8** is highly toxic from 50 μ M and over on Raw 264.7 cells, which explains the soaring TNF- α secretion observed at this concentration. Surprisingly, the molecule is also cytotoxic from 50 μ M and over in Caco-2/TC7 cells, while this cell-line is often less susceptible to toxicity. Overall, our results suggest that tetramic acid **8** cannot be accountable for the observed modulatory effects obtained upon cell incubation with AHLs.

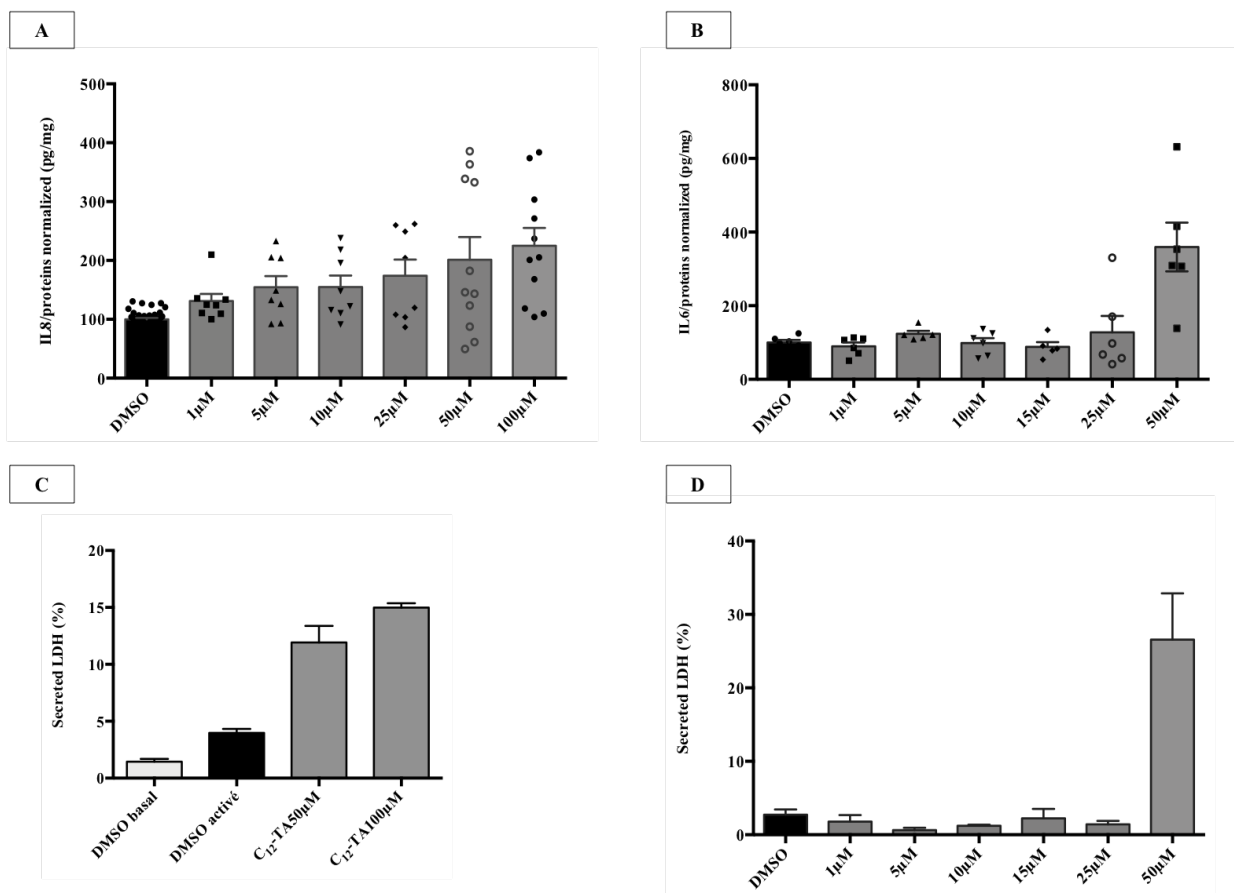


Figure 38 - Compared biological effects of tetramic acid **8 on cell lines Caco-2/TC7 cells and Raw 264.7 macrophages**

A (resp. **B**) : IL-8 response of Caco-2/TC7 cells (resp. IL-6 response of Raw 264.7 cells) to stimulation in presence of increasing doses of tetramic acid **8**. **C** (resp. **D**): secreted LDH in Caco-2/TC7 cells (resp. Raw 264.7 cells) to stimulation in presence of increasing doses of tetramic acid **8**. The points are the mean value of different replicates ($n \geq 3$) \pm SEM.

Tetramic acid **8** was also tested on the reporter strain *E. coli* pSB1075 (Figure 39). Surprisingly and although it is a degradation product, the molecule can act as an agonist of the

LasR receptor, but is weaker than precursor 3oxoC₁₂-HSL with an apparent EC₅₀ 300-fold greater (2.7 μM for **8** vs. 9 nM for **1**).

Compound **8** was finally tested for its bactericidal properties. No effect on bacterial growth of *E. Coli* strain K12 was observed over 18h (Figure 40). This result is in accordance with literature where the tetramic acid from 3oxoC₁₂-HSL (**8**) had been reported to possess antibacterial/antibiotic activity on selected Gram-positive strains, but not on most Gram-negative strains.^{327–330} Lowery *et al.* hypothesized the sensibility of Gram-positive vs Gram-negative bacteria resides in their different outer membrane, and especially in the absence of LPS.³²⁷ The authors studied two LPS-defective mutant strains *E. coli* Δ*imp* and D22, and indeed C₁₂-TA showed respective minimum inhibitory concentrations (MIC) of 25 and 50 μM. On the opposite *E. coli* strain K12 had no detectable MIC in their range of tested concentrations (below 100 μM), which is in line with our own findings.

Although surprising, it was also demonstrated that tetramic acid from 3oxoC₁₂-HSL could act as an antibiotic agent on its own producer, *Pseudomonas aeruginosa*. At high concentration (over 100 μM), Honda *et al.* observed decreased viability of *P. aeruginosa* after 5-hour incubation in presence of its tetramic acid in a concentration-dependent fashion. The group further demonstrated that the ratio [bacteria over tetramic acid] was critical for the activity of **8** against *P. aeruginosa*. Indeed, bacterial cultures at 10⁹ CFU/ml were protected from the antibacterial effects of the tetramic acid, while cultures at 10⁶ CFU/ml showed loss of viability.

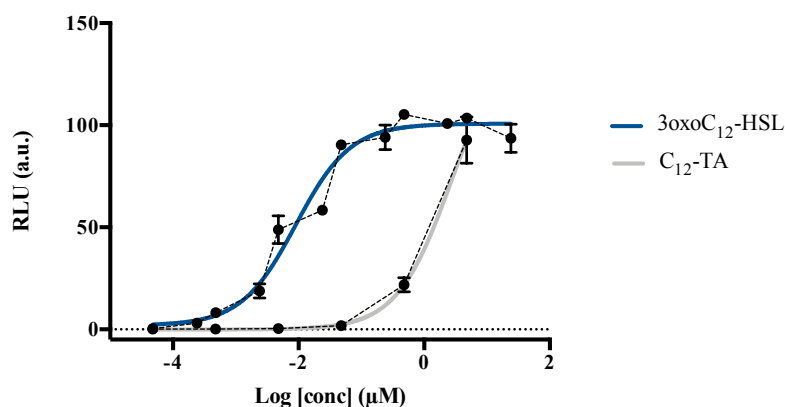


Figure 39 - Compared emission of luminescence by the bacteria reporter strain *E. coli* pSB1075 in presence of a range of AHL and tetramic acid concentrations

The 3oxoC₁₂-HSL **1** is the blue line ; the tetramic acid **8** is the grey line. Incubation 4h at 37°C and 70 rpm agitation. The points are the mean value of different replicates (n ≥ 3) ± SEM.

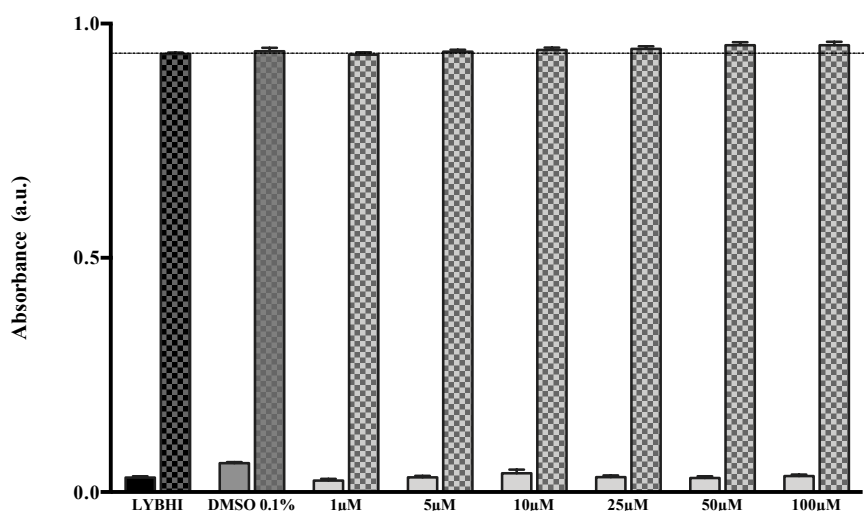


Figure 40 - Survival assay of *E. coli* strain K12 in presence of increasing doses of tetramic acid 8

Plain lines are $t = 0\text{h}$, dashed lines are $t = 18\text{h}$. Bacteria maintained in LYBHI medium under 37°C and 70 rpm agitation. Pure LYBHI medium and medium complemented with 0.1% DMSO were used as controls. The points are the mean value of different replicates ($n = 6$) \pm SEM. No significant difference observed.

2.2.2. Enzymatic degradation and extracellular metabolism of AHLs

From the previous section, we can hypothesize that the AHL-mediated immunomodulatory effects are either due to the closed lactone-ring molecule, or its open-form counterpart, given that molecule **8** is rather inactive or pro-inflammatory. The open-form homoserine can arise from both enzymatic and pH-dependent hydrolysis, but the time scales of these phenomena are very different. As reported in *Introduction - 2.2.1* AHL **1** may enter cells within minutes, which makes its pH-dependent hydrolysis in the extracellular compartment statistically unfavoured given it shows an apparent half-life time over 3h in cell-free biological medium. Cells however possess lactone-hydrolysing enzymes such as paraoxonases, that can be intracellular resident or secreted in the extracellular compartment.

2.2.2.1. PON mRNA expression in the studied cell lines

Total mRNA were extracted from cells after 4h incubation under various conditions. The mRNA were then converted to cDNA via RT-PCR, and the latter analysed by quantitative PCR. Relative mRNA levels among conditions were calculated by the $2^{-\Delta\Delta\text{Ct}}$ method. It appeared both human PON-2 and 3 mRNA were present in Caco-2/TC7 cells, while human

PON-1 was scarce or absent (it showed late C_t times and very poor amplification comparatively to the two other PON isoforms). This data is only partially in accordance with published literature, as Shamir *et al.* reported the three PONs mRNA were found at similar levels in Caco-2 cells.³⁹⁵ In Raw 264.7 macrophages, murine PON-3 mRNA alone could be detected.

It was thus hypothesized that using a competitive PON inhibitor would increase the half-life of undegraded AHLs in cell supernatant before their enzymatic lactonolysis. The chosen inhibitor was the 2-hydroxyquinoline or 2-HQ.³³² Our cell experiments were conducted in presence of 100µM 2-HQ as reported in literature.³⁹⁶

PON-2 was of special interest for us since it appears to be the most active isoform on 3oxoC₁₂-HSL among PON family members, as reported by Teiber *et al.*³³⁵ The group compared the specific activities of several purified PON proteins for 5-HL (best known substrate for PON-2 at the time of their study) and 3oxoC₁₂-HSL (Table 13). All three PONs could hydrolyse the AHL, but PON-2 revealed to be the most efficient at all AHL concentrations. PON-2 is expressed in most human tissues including the intestine, as opposed to PON-1 that is highly expressed in the liver.^{334,397} Shamir *et al.* observed that – although the three PONs mRNA were found at same levels in their Caco-2 model – the PON-2 protein levels were significantly higher than those of PON-1 and -3, with equal amounts of PON-2 protein distributed between plasma membrane and cytosol. The group also reported that post-confluency differentiated polarised Caco-2 cells could secrete PONs in their surrounding medium ; PON-2 was specifically found in apical supernatant (physiologically corresponding to the gut lumen), while PON-1 was only addressed in basolateral supernatant (corresponding to lamina propria and circulation). PON-3 protein was found in both compartments, but its expression levels were 3-fold lower than those of PON-2 in the upper medium.

PROTEIN	Specific activity for hydrolysis (nmol.min ⁻¹ .mg ⁻¹)		
	10µM 5-HL	10µM (S)-3oxoC ₁₂ -HSL	25µM (S)-3oxoC ₁₂ -HSL
Human PON-1 _{192Q}	29 500 ± 1 700	224 ± 17	790 ± 55
Human PON-1 _{192R}	36 800 ± 4 000	334 ± 19	1 586 ± 77
Human PON-2	3 100 ± 300	7 647 ± 373	13 371 ± 943
Human PON-3	22 100 ± 2 500	100 ± 10	320 ± 19

Table 13 - Compared specific activities of several purified PON proteins for 5-HL and 3oxoC₁₂-HSL hydrolysis
Adapted from Teiber *et al.*³³⁵ Values are means ± SD (n = 3 to 4). The two considered PON-1 proteins are two isoforms differentiated by a 192Q/R polymorphism.

Based on this data, it appeared necessary to verify the innocuity of 2-HQ but also DMSO and cytokines on PON-2 mRNA levels in Caco-2/TC7 cells (Figure 41). No significant difference was observed between expression in resting cells with medium alone and cells with medium containing 0.1% DMSO, 100 μ M 2-HQ, cytokines, or their combinations. To the best of our knowledge, these results are in concordance with current published literature where no modulation of PON mRNA expression by 2-HQ has ever been reported.

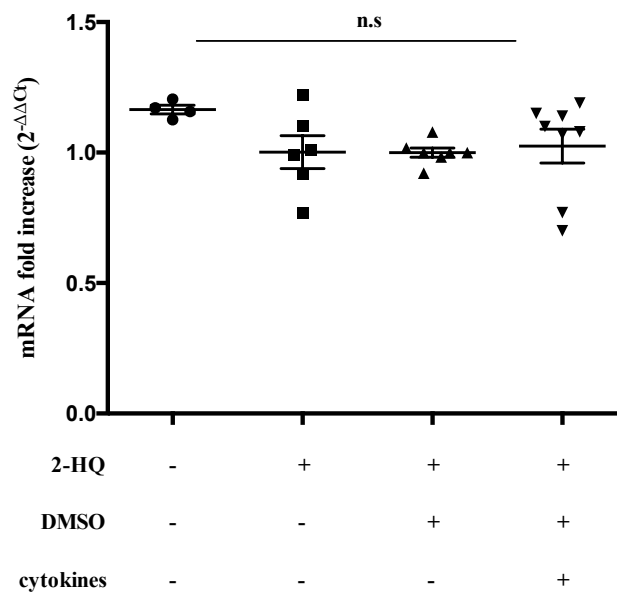


Figure 41 - Influence of 0.1% DMSO, PON inhibitor 2-HQ and cytokines on Caco-2/TC7 cells PON-2 mRNA expression

2^{-ΔΔCt} calculated proportionally to house-keeping gene human GAPDH. The points represent different replicates (n ≥ 4) ± SEM. No significant difference between conditions.

Could AHL inflammatory properties rely on a PON modulation? To elucidate this hypothesis, AHL effects over PON-2 and PON-3 mRNA levels in Caco-2/TC7 cells were investigated. For both AHL 1 and 2 we studied the influence of increasing concentrations ranging from 1 to 100 μ M in presence of 2-HQ and DMSO on resting cells : no significant difference was observed with control (Figure 42). Similarly, AHL effects were investigated when combined to cytokines. The concentration window was narrowed down to range 5 – 25 μ M where the main anti-inflammatory effects are observed.

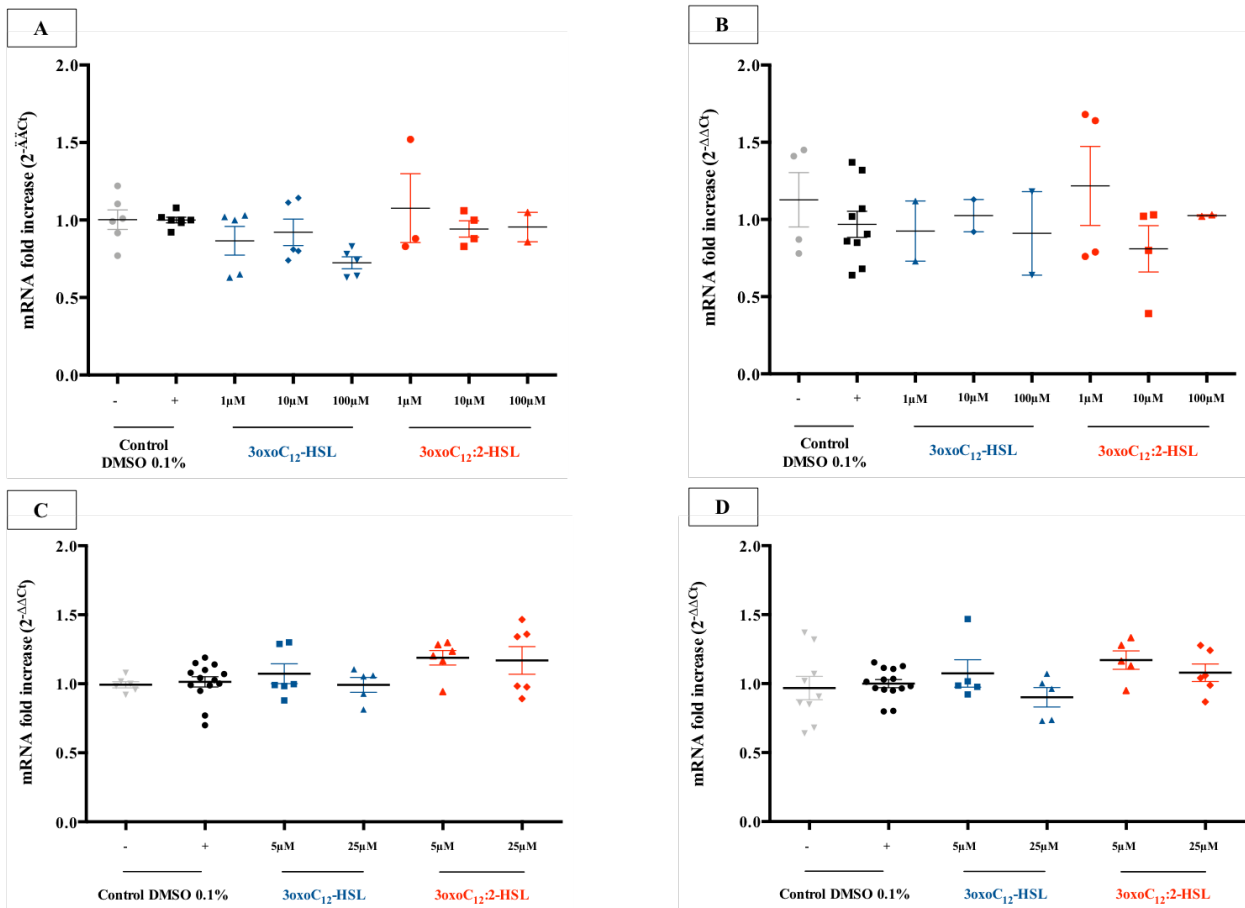


Figure 42 – Compared effects of increasing doses of AHLs 1 and 2 under various conditions on Caco-2/TC7 cells PON-2 and -3 mRNA expression

2-HQ added at 100 μM in all conditions. **A** (resp. **B**) : human PON-2 (resp. PON-3) mRNA levels on resting cells. **C** (resp. **D**) : human PON-2 (resp. PON-3) mRNA levels on cytokines-activated cells. $2^{-\Delta\Delta C_t}$ calculated proportionally to house-keeping gene human GAPDH. The points represent different replicates ($n \geq 2$) \pm SEM. No significant difference between conditions.

2.2.2.2. Influence of the inhibition of Paraoxonases on AHL effects

To investigate further the influence and intricate links between AHLs and Paraoxonases, the Caco-2/TC7 cell experiments were repeated without PON inhibitor. The removal of 2-HQ resulted in decreased anti-inflammatory effects at low micromolar concentration, while the pro-inflammatory effects observed at higher concentration were conserved. Similar observations were made on both cell lines Raw 264.7 and Caco-2/TC7 (Figure 43).

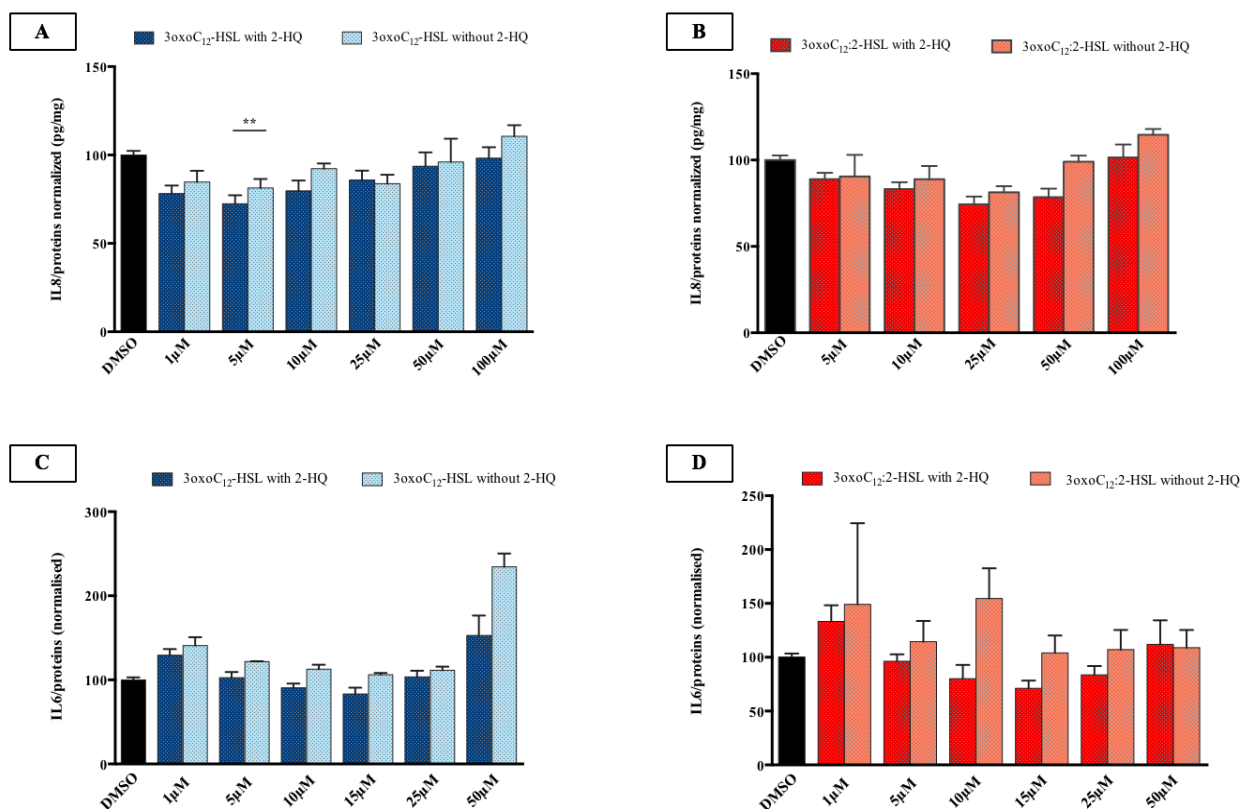
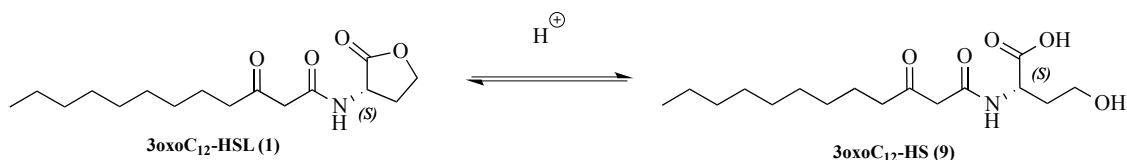


Figure 43 - Compared biological responses to AHLs in presence or absence of PON inhibitor 2-hydroxyquinoline

Caco-2/TC7 cells (A & B) or Raw 264.7 macrophages (C & D) were exposed to increasing concentrations of 3oxoC₁₂-HSL (A & C) or 3oxoC₁₂:2-HSL (B & D) in presence or absence of 2-HQ according previously exposed protocols. Means of separate replicates ± SEM (n ≥ 3). ANOVA, Tukey's post-test.

As the 2-hydroxyquinoline itself has no effect on the inflammatory response of cells (cf. Part I - 2.1.1), the loss of effect could possibly be attributed to the larger amount of AHL hydrolysed in cell medium when the PON inhibitor is removed. At physiological pH, the open-form homoserine headgroup exists as a carboxylate anion because the pKa of its carboxylic acid has been estimated about 3 (based on serine pKa). At physiological pH, the hydrolysed molecule hence contains a charged hydrophilic headgroup that might hinder its cell penetration.

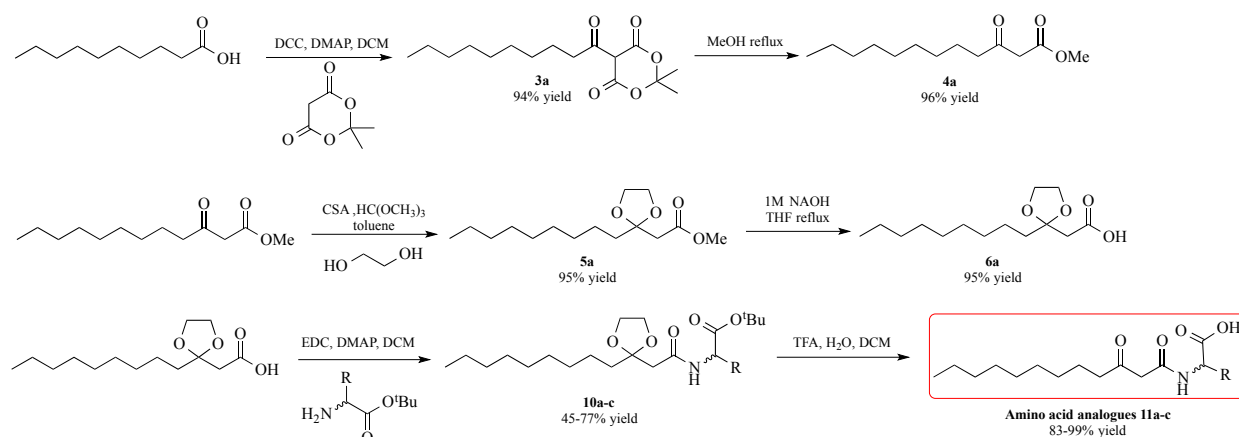
It is chemically easy to synthesize the 3oxoC₁₂-HS **9** by basic hydrolysis of precursor AHL **1** (Scheme 9). But difficulties arise upon testing this molecule under biological conditions. As stated previously, the pKa of HSL/HS species is 7.33 in case of 3oxoC₁₂-HSL, which is about biological pH. Hence under such conditions, if we were to dissolve **9** into cell medium, the molecule would not exist as a single specie but as an equilibrium between **1** and **9**. It is then hard to decipher from which compound the observed effects result.



Scheme 9 – Equilibrium between closed- and open-ring forms *3oxoC₁₂-HSL* and *3oxoC₁₂-HS*

In order to circumvent this technical problem, AHL analogues with amino acid headgroups were synthesized to model the action of open-form *3oxoC₁₂-HS* (**9**). Three different amino acids were chosen for coupling : serine, alanine, and β -alanine. Serine is structurally close to homoserine – it misses only one *CH₂* - and could mimic appropriately its behaviour and interactions, while its shorter chain makes the cyclisation quite unfavoured.

The strategy employed for the synthesis of non-natural AHL analogues with amino acid-inspired headgroups was based on that of natural AHL **1** (Scheme 4), coupled to a *tert*-butyl ester protecting group strategy (Scheme 10).

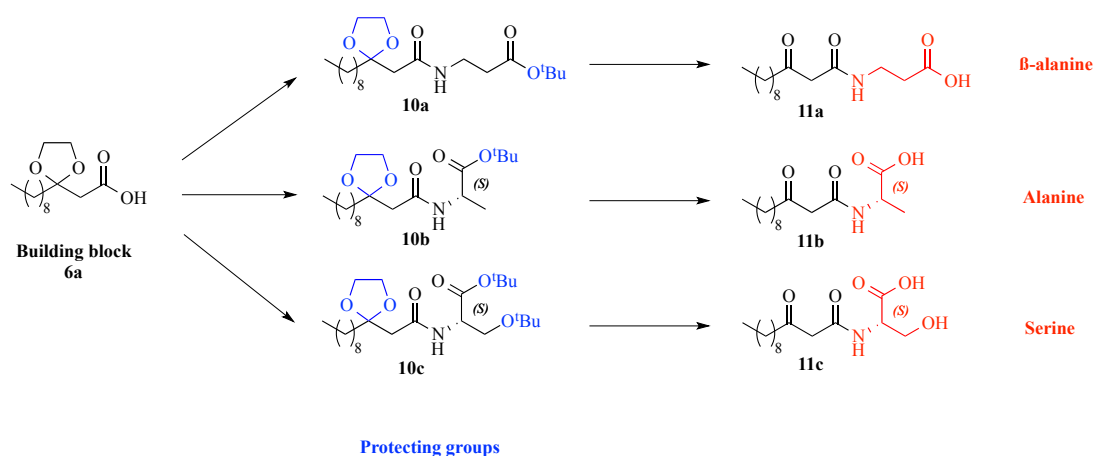


Scheme 10 - Synthetic pathway for preparation of AHL analogues **11a-c** bearing amino acid headgroups

a: β -alanine. **b:** alanine. **c:** serine.

Amino acids naturally offer at least two reacting sites – the *O*-terminal carboxylic acid and the *N*-terminal amine – and sometimes more depending on the nature of the amino acid sidechain. In order to perform the coupling between the acyl chain donor **6a** carboxylic acid and the amine from the amino acid, the *O*-terminal and any extra reacting site had to be protected. *Tert*-butyl esters are common carboxylic acid protecting groups and were chosen for their stability under basic treatments and the ease to remove them under strong acidic conditions

such as 90% TFA. The later property especially allows to deprotect both the amino acid and the C₃-ketone in a single step (Scheme 11).



Scheme 11 - Common TFA deprotection step of O'Bu- and ketal-protected chemical functions

To understand why the cyclisation of a serine analogue is quite unlikely, we have to compare the inner structures of serine and homoserine. The cyclisation of the two amino acids into lactones is under kinetic control, and their respective kinetics are fairly different. The kinetic control relies on the relative level of the activation energy barrier ΔG^\ddagger , which itself depends on the enthalpy of activation ΔH^\ddagger , the temperature T, and the entropy of activation ΔS^\ddagger as shown in the following equation:

$$\Delta G^\ddagger = \Delta H^\ddagger - T\Delta S^\ddagger$$

Equation 1 – Activation energy barriers

ΔH^\ddagger tells us about the energy needed to bring atoms close enough to react, against strains and repulsive electronic forces ; ΔS^\ddagger describes how easy an ordered transition state can be formed from a randomly structured and rotating molecule. Five-membered ring formation is often considered fastest of all as there is no ring strain and end-atoms to bring together are not too significantly far apart (small ΔH^\ddagger and large enough ΔS^\ddagger). Four-membered ring formation however, is much impaired due to an important ring strain (large ΔH^\ddagger) combined to a low ΔS^\ddagger (fewer potential conformation meaning greater organisation).

Alanine with its minimal sidechain, was chosen to study the importance of the terminal alcohol group on the side chain – absent in alanine and present in serine. While finally, β-

alanine was synthesized to investigate the necessity of a ring-shaped headgroup versus an extended structure (hence versus alanine itself). The comparison between the molecules was rationalised by computing their theoretical physical properties with the ADME databank tool of the Swiss institute of Bioinformatics and the free online-available software *Molinspiration* (Table 14). Among others we compared topological polar surface areas (TPSA), flexibility by the number of rotatable bonds, lipophilicity and water solubility. The TPSA of a molecule is the surface sum over all polar atoms ; it is commonly admitted that molecules with a TPSA greater than 140 Å² are poorly cell-permeable. As it appears, all molecules have a TPSA lower than 140 Å², but those of **9** and **11c** are significantly greater, suggesting an impaired cell-penetration capacity.

The lipophilicity of **1** is strongly impacted when the molecule gets hydrolysed. Based on these predictions, compound **9** is about 200 times less lipophilic than the native 3oxoC₁₂-HSL. As computed, molecule **11c** reasonably mimics the physical properties of **9**, although it is less lipophilic by one log unit.

<i>Molecule</i>	<i>Num. rotatable bonds</i>	<i>Num. H-bond acceptors</i>	<i>Num. H-bond donors</i>	<i>TPSA (Å²)</i>	<i>Log P_{ow} (miLogP model)</i>	<i>Water solubility class</i>
3oxoC ₁₂ -HSL (1)	12	4	1	72.47	2.16	Moderately soluble
3oxoC ₁₂ -HS (9)	15	5	3	103.70	0.20	Soluble
3oxoC ₁₂ -serine (11c)	14	5	3	103.70	-0.79	Soluble
3oxoC ₁₂ -alanine (11b)	13	4	2	83.47	0.19	Soluble
3oxoC ₁₂ -β-alanine (11a)	14	4	2	83.47	0.13	Moderately soluble

Table 14 – Compared predicted physical properties of 3oxoC₁₂-HSL, 3oxoC₁₂-HS, and amino acid analogues
For molecules **9** and **11a-c**, the calculations were made using their carboxylate anion form, which predominates at physiological pH.

The three analogues **11a-c** were tested on the Raw 264.7 murine cell line in stimulatory conditions and compared to natural AHL **1**, all other parameters otherwise similar.

Monitoring the TNF-α response, it appeared that the serine analogue returned a significantly reduced response compared to the natural molecule. The bell-shape response curve was majorly abrogated towards a non-active behaviour (Figure 44). The difference in potency was especially marked at 15 and 25μM, concentrations at which **1** reaches maximum potency in our

macrophage model. At 15 μ M where AHL **1** induces a 29% decrease in TNF- α secretion compared to DMSO, the serine analogue induces only a 7% decrease ; at 25 μ M the difference is even 37% to 4% respective decreases compared to control. With the hypothesis that serine analogue **11c** is a reasonable model for compound **9**, these results suggest what would be observed upon macrophage assay with the hydrolysed form of AHL **1**. It seems that the drastic loss of lipophilicity negatively impacts the AHL activity, maybe due to impaired cell-penetration.

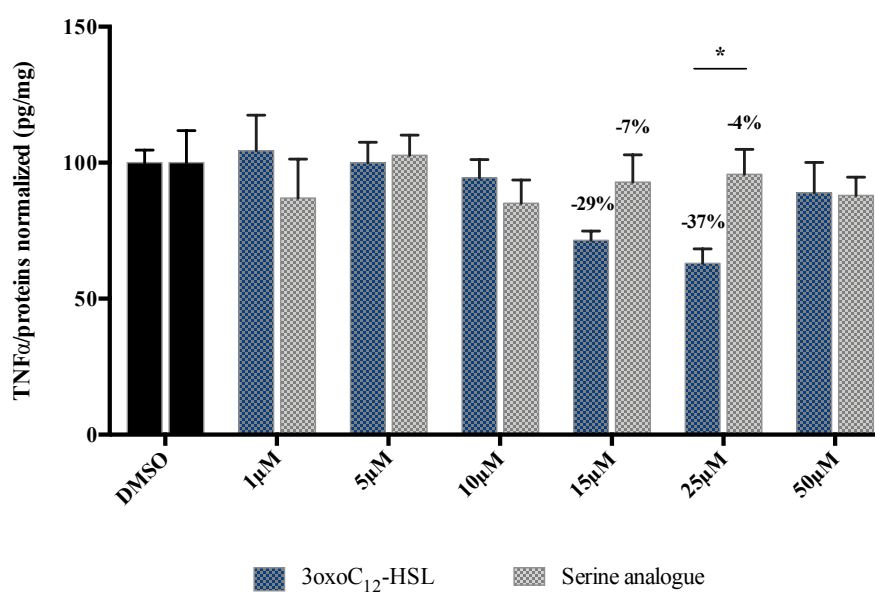


Figure 44 – Compared TNF- α responses of LPS/IFN- γ stimulated Raw 264.7 macrophages in presence of natural molecule 3oxoC₁₂-HSL (1**) and analogue 3oxoC₁₂-serine (**11c**)**

Raw 264.7 cells were incubated for 6h in presence of cytokines, 100 μ M 2-HQ and increasing concentrations of molecules. The points are the mean of different replicates ($n \geq 6$) \pm SEM. * $p < 0,05$. Two-way ANOVA, Tukey's post-test.

Similarly, the Raw cells responses to analogues with an alanine and β -alanine headgroup were analysed. Compound **11b** retained a reasonable share of the original AHL activity (about 86%), especially at 25 μ M where a 32%-decreased TNF- α secretion was observed (vs. 37% for AHL **1**). Compared to analogue **11c** which had lost activity, it only lacks an hydroxyl group.

The β -alanine analogue **11a** showed no activity in our model, neither anti-inflammatory nor pro-inflammatory ; responses at all doses were in the range of control DMSO. **11a** and **11b** are position isomers : their chemical formulas are identical but their layouts differ, hence giving them different properties. In particular, **11a** is much more flexible than **11b** due to its extended geometry ; from our observations it seems this conformation has a negative impact (Table 14).

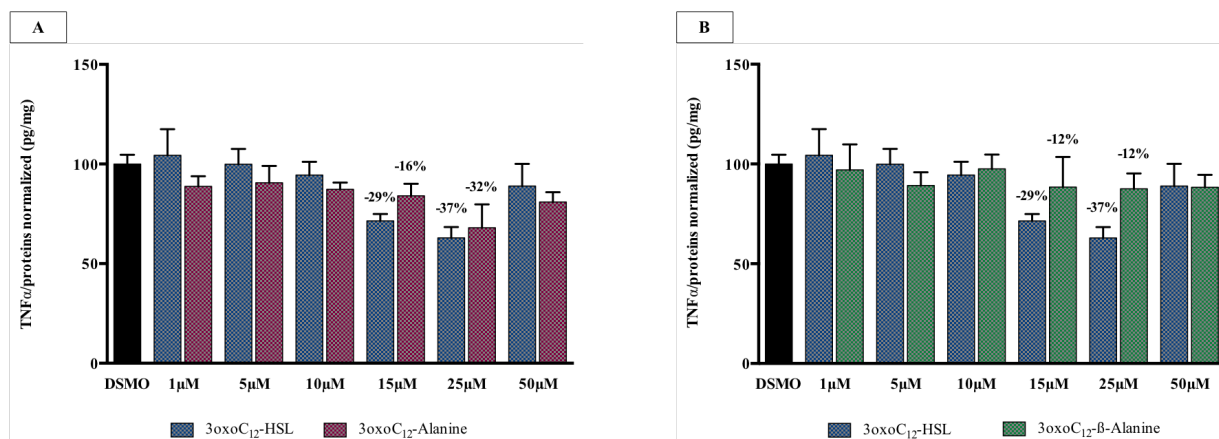


Figure 45 - Compared TNF- α responses of LPS/IFN- γ stimulated Raw 264.7 macrophages in presence of natural molecule 3oxoC₁₂-HSL (1) and analogues 11a-b

A: comparison with 3oxoC₁₂-alanine **11b**. **B:** comparison with 3oxoC₁₂- β -alanine **11a**. Raw 264.7 cells were incubated for 6h in presence of cytokines, 100 μ M 2-HQ and increasing concentrations of molecules. The points are the mean of different replicates ($n \geq 6$) \pm SEM. No significant difference. Two-way ANOVA, Tukey's post-test.

In terms of cell toxicity, the three analogues **11a-c** have very different effects (Figure 46). While the alanine analogue **11b** is non-toxic at all concentrations, its linear counterpart **11a** shows great cytotoxicity from 15 μ M and above. The serine analogue **11c** is toxic from 50 μ M, a behaviour resembling that of natural AHL **1**, which shows increased secreted LDH at 50 μ M and is toxic at 100 μ M.

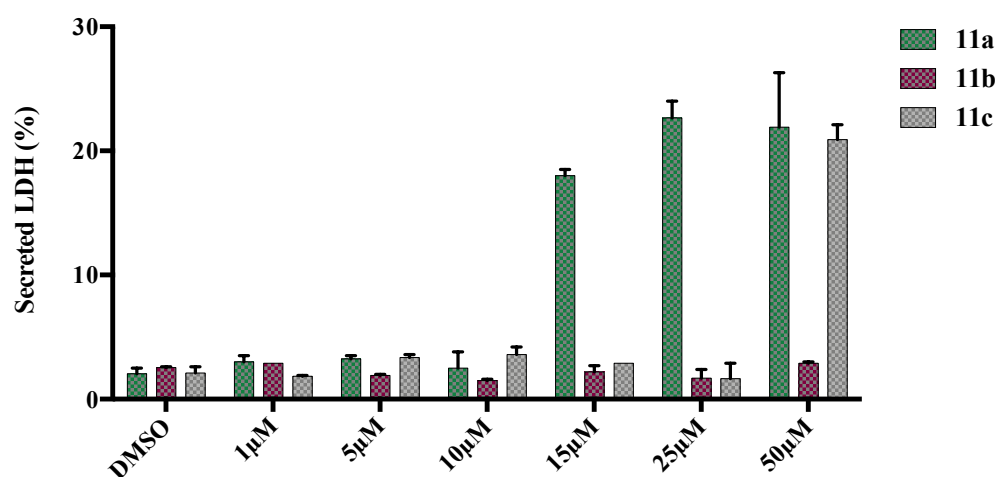


Figure 46 - Compared LDH secretion (%) of LPS/IFN- γ stimulated Raw 264.7 macrophages in presence of analogues 11a-b

Raw 264.7 cells were incubated for 6h in presence of cytokines, 100 μ M 2-HQ, control DMSO or increasing concentrations of molecules. The points are the mean of different replicates ($n = 3$) \pm SEM.

2.2.3. Intracellular AHL metabolism : entry and cellular fate

We then formally evaluated the entry of natural AHL **1** in Caco-2/TC7 cells. First, we compared the fate of molecules in supernatant when exposed to cells or equivalent preconditioned medium. Preconditioned medium is complete Caco-2/TC7 cell medium that has been exposed to cells for 24h and then collected, thus containing all cell-secreted components such as enzymes, proteins...etc. Briefly, solutions of initial concentration 15 μ M in 3oxoC₁₂-HSL were prepared each in the appropriate medium (fresh or preconditioned), with 100 μ M 2-HQ. The fresh solution was added to a flask containing 18-day-old past-confluence Caco-2/TC7 cells, while the solution in preconditioned medium was placed in an empty sterile flask. Both flasks were then incubated at 37°C and samples of supernatant taken over 24h. Extraction method was similar to that reported in *Part I - 2.2.1.2*. The sample composition was analysed by tandem LC-MS/MS to follow the evolution of AHL **1** and its degradation products **8** and **9** quantities over time (Figure 47).

Tetramic acid **8** was detected at very low concentrations in both conditions, which is in accordance with our previous observations. Overall, closed-ring AHL **1** decreased over time while open-form **9** increased. The time frames of these phenomena and the concentrations recorded were however significantly different from one condition to another.

In preconditioned medium, the decrease in molecule **1** exhibited apparent half-life and kinetic constant of 2.3 h and 0.2990 h⁻¹ ; these kinetic parameters are different from those observed at r.t. in cell-free medium and express an increased rate of AHL hydrolysis that can be attributed – at least partially - to the rise in temperature. The apparent rate of formation of hydrolysed molecule **9** is fairly concordant, with a kinetic constant of 0.3404 h⁻¹ and a half-life about 2h. Concentration in **9** plummets at 9.3 μ M.

In the solution exposed to cells, the decrease in AHL **1** is approximately 7 times faster with a half-life of 0.35h. However the formation of hydrolysed **9** is not augmented but rather diminished with a plateau at 3.4 μ M. This difference between the two conditions expresses the passage of AHL from the extracellular to the intracellular compartment. This phenomenon is very fast and probably happens within minutes after cell exposure to AHLs as described in literature by Ritchie and co-workers.²⁷⁵

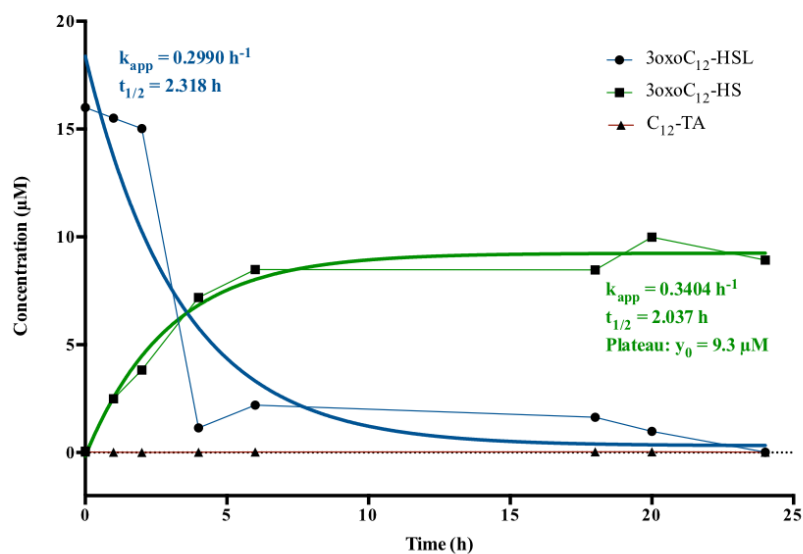
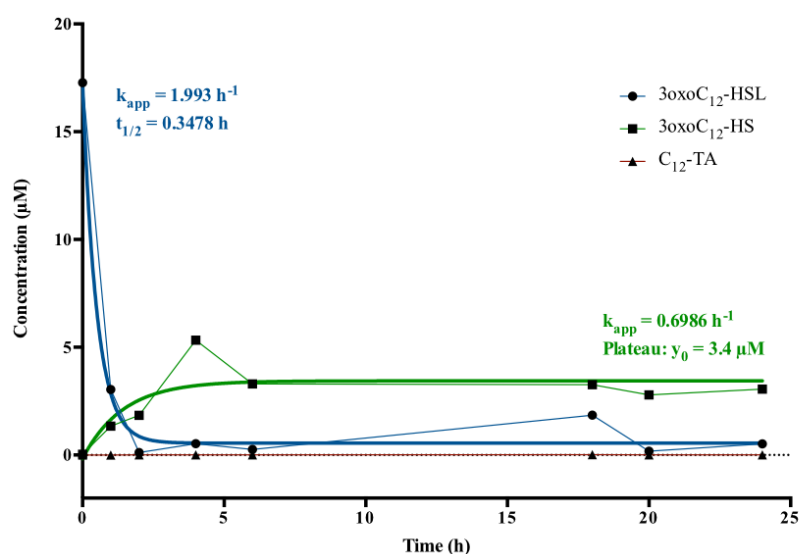
A**B**

Figure 47 - 24-hour time evolution of supernatant load in 3oxoC₁₂-HSL, 3oxoC₁₂-HS and C₁₂-TA

A : 15µM 3oxoC₁₂-HSL incubated in preconditioned medium. **B** : 15µM 3oxoC₁₂-HSL incubated in presence of Caco-2/TC7 cells. Both flasks, of similar model, were enriched with 100µM 2-HQ and maintained at 37°C in the same incubator. Analyses performed by LC-MS/MS in presence of internal AHL standard C₄-d₅-HSL.

We must signal the analysis of samples by tandem LC-MS/MS is not perfect. Indeed on Figure 47A were no cell is present, the total concentration of matter recovered at 24h is not 15µM (initial concentration in AHL) but 9.2µM, i.e. 62% of the expected theoretical concentration. This difference results from several factors. First, the AHL can interact with different elements such as proteins or plastic cell culture flasks that will “hide” the molecule.

Then, our mass analysis technique is based on *a priori* selection of molecular fragments : we cannot find what we are not looking for. Hence, supposing AHLs may degrade by mechanisms other than lactonolysis and tetramic acid formation, we would miss those metabolites.

Despite these drawbacks, the results from conditions **A** and **B** in Figure 47 remain significantly different. Indeed in condition **B** we recover $3.4\mu\text{M}$; using the previously calculated error of 62%, we would then expect a total theoretical concentration of $5.5\mu\text{M}$. This result still remains significantly different from both experimental and theoretical results for the **A** condition (resp. 9.2 and $15\mu\text{M}$).

In a second experiment, we analysed the AHL load of the intracellular compartment. Similarly to the previous conditions, a fresh solution of $15\mu\text{M}$ 3oxoC₁₂-HSL was incubated on Caco-2/TC7 cells at 37°C and samples of both supernatant and cell lysate were collected over 24h. The experiment repeated twice : once in presence of $100\mu\text{M}$ 2-HQ, the second time without the PON inhibitor.

The first important conclusion to draw from these experiments is the partition of 2-hydroxyquinoline between the extra- and intracellular compartments : over 24h the proportions of inhibitor remained constant (Figure 48), with an average 10% of total 2-HQ amount entering cells while 90% remained in supernatants. The entry and saturation of the molecule in cells is extremely fast as we observe it from sampling at 5min. Thus, it is highly probable that the secreted PONs are efficiently inhibited in the extracellular medium. On the opposite, the intracellular compartment contains a much greater load in PONs and 10 times less inhibitor : the inhibition is comparatively poor in the cell cytosol.

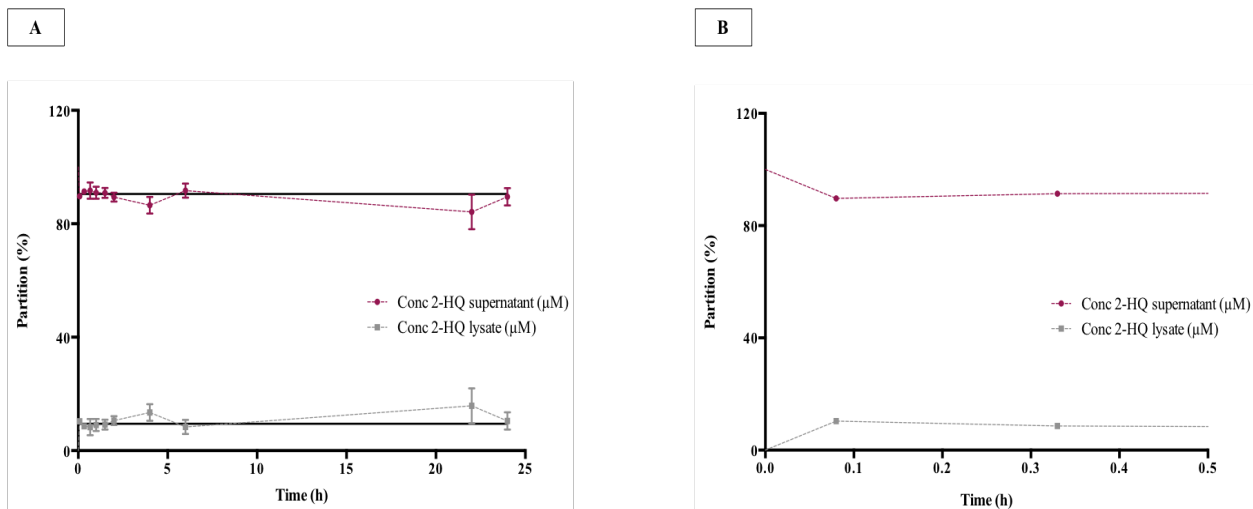


Figure 48 - Partition of PON inhibitor 2-hydroxyquinoline between the extra- and intracellular compartments
At all times (A) and magnification on the first 30 min (B).

We then examined the proportions of matter that stayed in solution or entered cells depending on the presence or absence of 2-HQ (Figure 49). With the PON inhibitor 50% of the matter enters cells within 5 min, and about 90% is located in cell lysates after 1h of time. In comparison, without 2-HQ only 18% of total matter is found intracellularly after 5 min, and the proportion of matter found inside cells will plummet about 60% after 45 min. These results are concordant with our findings from the extracellular experiment and confirm the hypothesis according which the inhibition of PON hydrolysis promotes the maintenance of AHL integrity and thereby their penetration into cells.

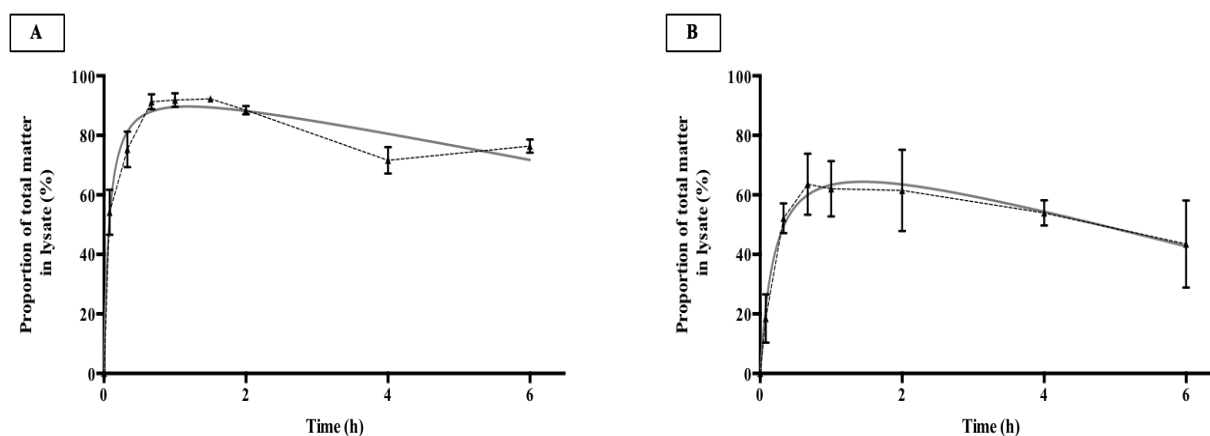


Figure 49 – Compared proportions of total amount of molecules found in total cell lysate over time
Total amount of molecules means AHL, hydrolysed AHL and tetramic acid. **A** : experiment in presence of 100µM 2-HQ. **B** : experiment without 2-HQ.

Finally, following our findings of a poor PON inhibition in cells, we studied the proportional repartition of closed-ring 3oxoC₁₂-HSL and open-form 3oxoC₁₂-HS. It appears that, if the integrity of the homoserine ring is needed to promote the cell entry of AHLs, they are rapidly hydrolysed into their homoserine counterpart **9** (Figure 50). Indeed by mapping the proportions of **1** and **9** found in total cell lysates we can observe that the open-form molecule becomes prevalent within minutes after cell penetration and will be the major form over longer timespan. Only timing seemed affected as the absence of 2-hydroxyquinoline retards the maximum of HSL proportion from 5 min to 20 min. Otherwise, no frank difference in profiles was observed with or without 2-HQ, which was expected considering the small proportion of inhibitor found intracellularly. Overall the homoserine form dominates in cell cytosol representing between 60 and 95% of total matter found in cell lysates.

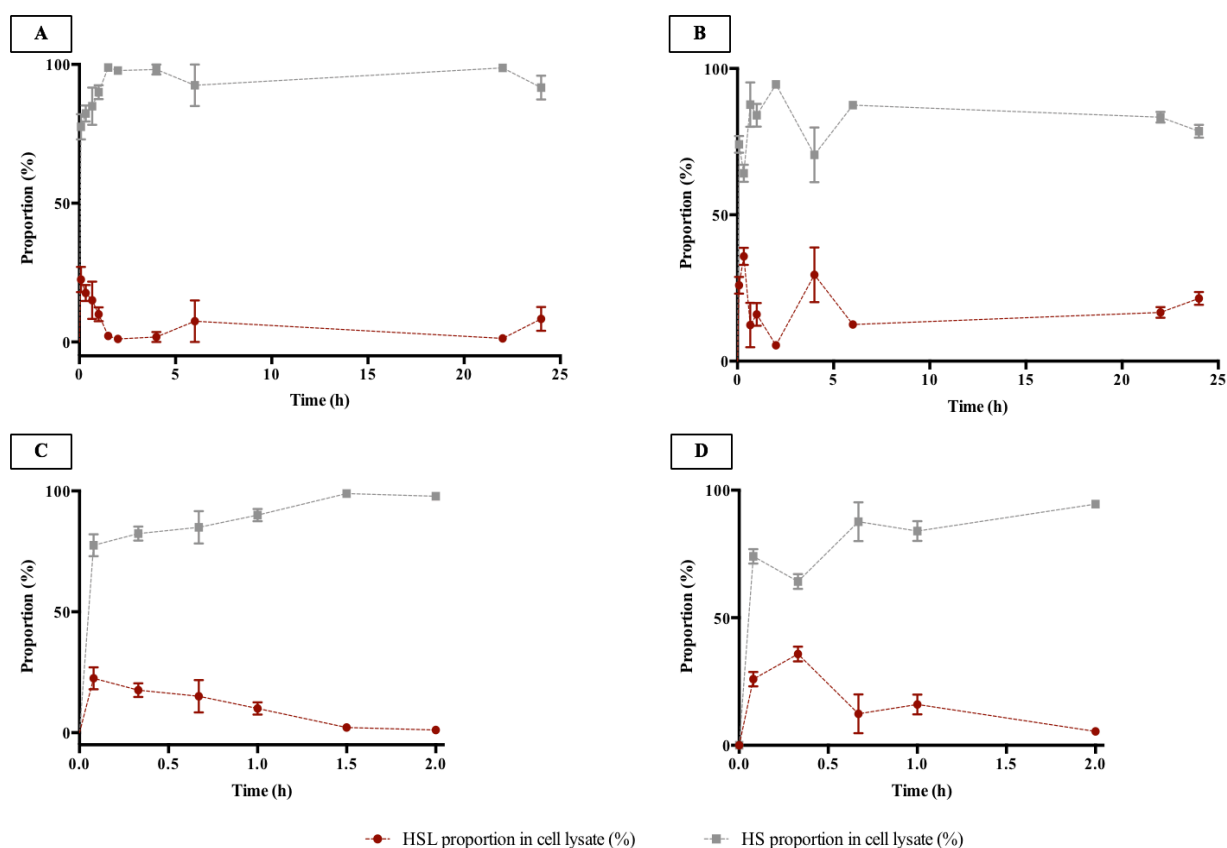


Figure 50 – Proportions of homoserine lactone and homoserine forms found in Caco-2/TC7 cell lysates over time

A and **B** show the complete profile over 24h ; **C** and **D** are the truncated profiles over short time span. **A** and **C** are results with 100 μM 2-HQ ; **B** and **D** are results in absence of PON inhibitor. All cells maintained at 37°C in the same incubator. Points are the mean of different replicates (n = 3) ± SEM.

2.2.4. Hydrolysed AHLs and bacteria

The hydrolysed 3oxoC₁₂-HS and 3oxoC₁₂:2-HS were prepared by basic hydrolysis of their parent compounds. Completion of hydrolysis was verified by thin layer chromatography (TLC) in cyclohexane/ethyl acetate and revealed with iodine (Figure 51). The parent AHL is polar but migrates with increasing proportions of polar eluent in the eluting mix (here EtOAc), from a 1:1 polar/apolar ratio to a 3:1 ratio. The hydrolysed molecule remains stuck on the base line despite the increase in eluent polarity. The presence of a single spot ensures the purity of a product, while the “co-spotting” line is a verification for co-eluting troubleshooting.

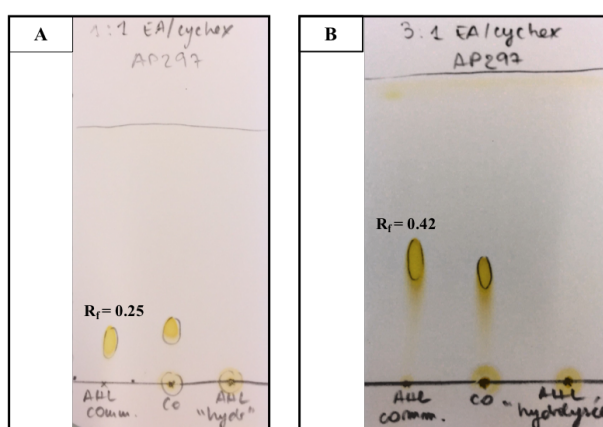


Figure 51 – Silica gel TLC plates of 3oxoC₁₂-HSL and 3oxoC₁₂-HS

The plates were eluted in 1:1 EtOAc/Cyhex (A) or 3:1 EtOAc/Cyhex (B) and revealed with iodine on silica. The retention factor (R_f) is calculated as the ratio [height of the compound spot] over [height of the elution front].

3oxoC₁₂-HS and 3oxoC₁₂:2-HS were tested on bacteria reporter strain *E. coli* pSB1075 to evaluate their capacity as LasR agonists (Figure 52). Surprisingly, the two molecules induced very different profiles. The 3oxoC₁₂:2-HS does not induce bioluminescence, even after 4h. The 3oxoC₁₂-HS however, is recognised by the receptor, but gives weaker signals than its parent AHL at given time and concentration which indicates an impaired capacity to activate LasR. After 4 hours, we could read an EC₅₀ of 300 nM for 3oxoC₁₂-HS versus 9 nM for 3oxoC₁₂-HSL in the same conditions ; this corresponds to a 33-fold decrease in affinity. This result is not in accordance with literature which described no activity of hydrolysed autoinducers on their cognate receptor.^{248,394} This unexpected observation may result from the capacity of 3oxoC₁₂-HS to recyclize into a lactone : Yates *et al.* indeed demonstrated the open-form AHL would completely return to lactone at pH 2.³⁹⁴ Given that bacterial metabolism tends to acidify the

surrounding medium, it is highly possible that part of the open-form molecules have recycled over the 4-hour incubation, giving rise to little bioluminescence.

Regarding the absence of LasR activation with compound 3oxoC₁₂:2-HS, one could suppose this molecule is impaired both by its hydrolysed headgroup and its unsaturated acyl chain. Indeed, 3oxoC₁₂:2-HSL (**2**) already exhibits a 11-fold increase in EC₅₀ versus **1**, with an EC₅₀ of 100 nM. Assuming the hydrolysis of the lactone headgroup induces an additional 33-fold increase in EC₅₀, it would reach an estimate 3.37 μM, a value out of the range of our experiment.

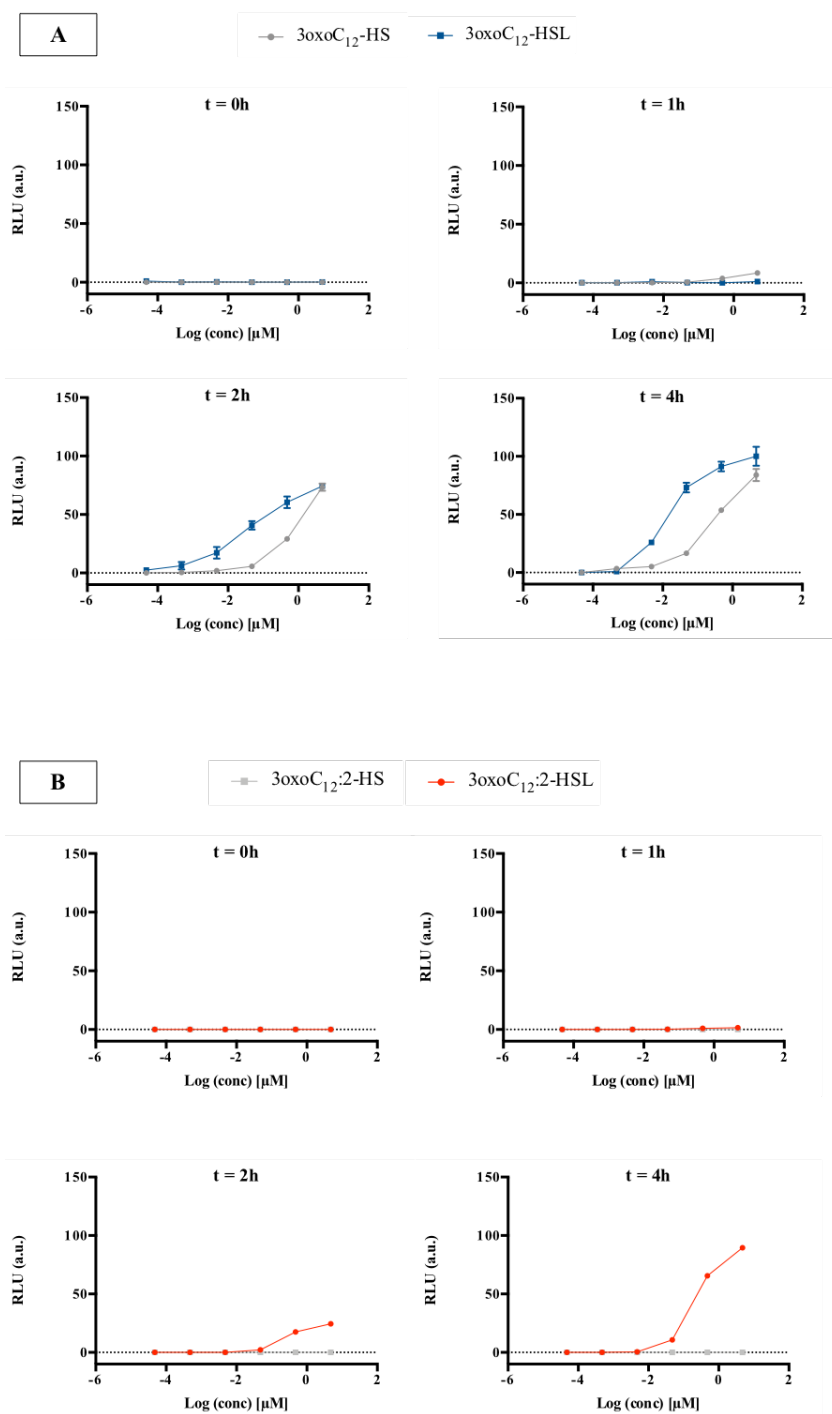


Figure 52 - Time evolution from 0 to 4h of the bioluminescence emitted by strain *E. coli* pSB1075 in presence of increasing doses of autoinducers and their hydrolysed derivatives

A : 3oxoC₁₂-HSL and 3oxoC₁₂-HS. **B** : 3oxoC₁₂:2-HSL and 3oxoC₁₂:2-HS.

The necessity of a ring-shaped headgroup for LasR activation is further confirmed by testing amino acid analogues **11a-c** in the *E. coli* pSB1075 bioassay. As shown on Figure 53, the three compounds cannot elicit bioluminescence in the range of tested concentrations.

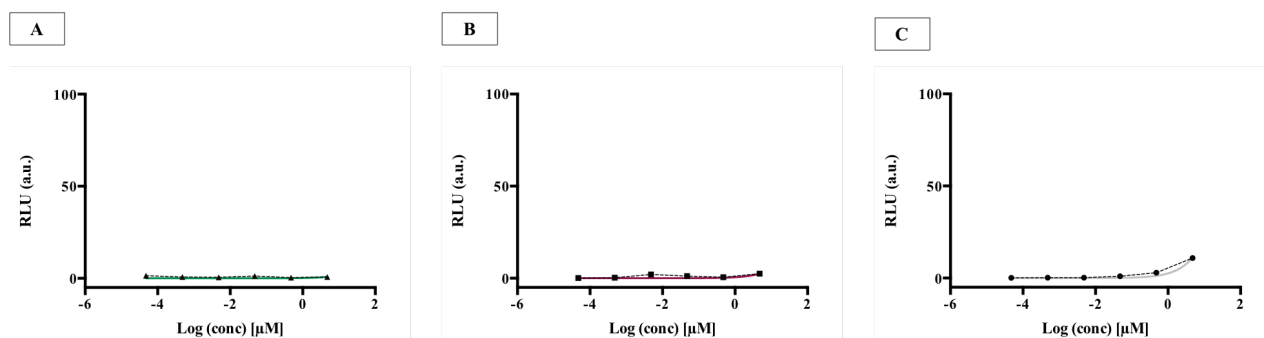


Figure 53 – Bioluminescence emitted by strain *E. coli* pSB1075 in presence of increasing doses of AHL analogues with amino acid headgroups

A : 3oxoC₁₂-β-alanine **11a.** **B :** 3oxoC₁₂-alanine **11b.** **C :** 3oxoC₁₂-serine **11c.**

2.2.5. Discussion

As signal molecules, it is not unexpected that acyl homoserine lactones tend to be degraded once secreted in their surroundings. Indeed, via AHL-sensing bacteria can detect the presence (or absence) of other members in the colony. Hence it is important that AHL get degraded to ensure their concentration closely reflects the dynamics of the bacterial population through time. A mammalian host is no different environment and Losa et al. demonstrated parallel evolutions between 3oxoC₁₂-HSL concentration and bacterial load in aspirates from intubated patients colonised by *P. aeruginosa*.³⁹⁸

To date, few groups studied the time evolution of AHL concentrations in mammalian cell supernatant. Our experiments showed an average half-life of 0.3478 h⁻¹ (21 min) when AHL **1** was incubated at 37°C on 18-day-old Caco-2/TC7 cells. This result is concordant with findings from Losa and co-workers who reported an approximate half-life of 30 minutes for compound 3oxoC₁₂-HSL incubated on 20-day-old polarised bronchial epithelial cells.

Our research went further as we studied the intracellular metabolism of AHLs. Once in the inner compartment, the molecule is not protected anymore from hydrolysis by the PON inhibitor, and the hydrolysed form 3oxoC₁₂-HS becomes predominant within minutes after the AHL entry in cells, to accumulate inside the cell across our experiment. Kravchenko et al. made similar findings after 3oxoC₁₂-HSL incubation on macrophages and extraction of supernatants and pellets with ethyl acetate.²⁷⁸ The author observed that the cellular fractions contained about 10 times more hydrolysed form than lactone, while the closed-ring AHL remained dominant in supernatants. Their results were later confirmed by Horke et al. on several PON2-producing

cell lines.³⁹⁹ We report here concordant results on the Caco-2/TC7 cell line, with an intracellular 3oxoC₁₂-HS load oscillating from 65% to 95% over 24h.

Where other groups chose to work directly with hydrolysed AHL to study its cell effects, we imagined an equivalent model, the 3oxoC₁₂-serine **11c**, to ensure the unicity of the chemical species at biological pH. This analogue exhibited seriously decreased effects in biological assay, among which an incapacity to downregulate TNF- α secretion in Raw 264.7 macrophages. Assuming that **11c** is a fair model of AHL **1**, this loss of activity is in accordance with findings from Kravchenko et al. who report 3oxoC₁₂-HS is unable to induce phosphorylation of p38 and eIF2 α or cleavage of PPAR γ , where these were described effects of intact 3oxoC₁₂-HSL.²⁷⁸ The alanine analogue **11b** however, less hydrophilic and more prone to cell penetration, retained reasonable biological activity. Furthermore we have shown that absence of PON inhibitor reduced but did not abolish the AHL-effect, while several groups have shown that KO-mice for PON or drosophila lacking paraoxonases were prone to bacterial infection.^{400,401} So what is the intricate link between PON, AHL and their hydrolysis?

It is our feeling that PON are required intracellularly for AHL activity, while their extracellular presence will prevent AHL cell penetration and hence decrease the observed effects. This belief is supported by three different studies.^{286,399,402} Both teams demonstrated that 3oxoC₁₂-HSL cellular effects were reversed after incubation with PON inhibitor TQ416, hence suggesting that AHL require PON-mediated intracellular hydrolysis to perform their function. This is coherent with our own observations: we employ a PON inhibitor that is highly efficient in the extracellular environment, but poorly distributed in the inner compartment, thus we observe a high rate of intracellular AHL hydrolysis. Once hydrolysed, the homoserine form becomes trapped inside the cell due to its high hydrophilicity which does not allow it to cross the cell membrane back ; the hydrolysed molecule can now directly interact with its putative receptor(s) or indirectly mediate its varied effects. On the opposite, in absence of PON inhibitor in the outer compartment, the rate of hydrolysis is increased in the cell medium and the hydrolysed AHL cannot cross the cell membrane in. A low dosage of molecules will eventually manage to enter the cell, but not enough to reach full efficacy ; the AHL effects are blunted. Our hypothesis does not refute the statement made by several groups that the structural integrity of the lactone ring is required for to mediate its effects on mammalian cells ^{278,300} ; but we would rather believe that the lactone is required to mediate AHL penetration into cells, like a pro-drug. Which compound is the active form inside cells remains to be proved.

Unfortunately, our study of degradations of molecule 3oxoC₁₂-HSL could not be fully extensive, and we were forced to make some assumptions.

Based on literature⁴⁰³, it was assumed that the rate of racemisation of **1** from the (*S*)-stereoisomer to the (*R*)-stereoisomer was sufficiently slow to be neglected, compared to its rate of degradation into compounds **9** and **8**.

We have focused our study on a particular kind of enzymes, the paraoxonases, that act by lactonolysis of the AHL headgroup. However, AHLs could be metabolised by many other enzymes. Such quorum-quenching enzymes are wide-spread among bacteria, and analogues might be found in mammals. Among others, AHL could be degraded by acylases to release a free HSL and a carboxylic acid, by oxidoreductases that would change the C₃ pattern (for instance transform the ketone into an hydroxyl group), or by cytochrome P450 monooxygenase CYP102A to add extra hydroxyl groups along the acyl chain. Hence, there are many plausible possibilities of degradation in mammalian cells which we have not thoroughly investigated and would need to be considered. One may also imagine the development of heavy-atom-labelled AHL in order to follow its full *in vivo* and *in vitro* metabolism by mass spectrometry.

2.3. Insight into the AHL mechanism of action : cell imaging and receptor investigation

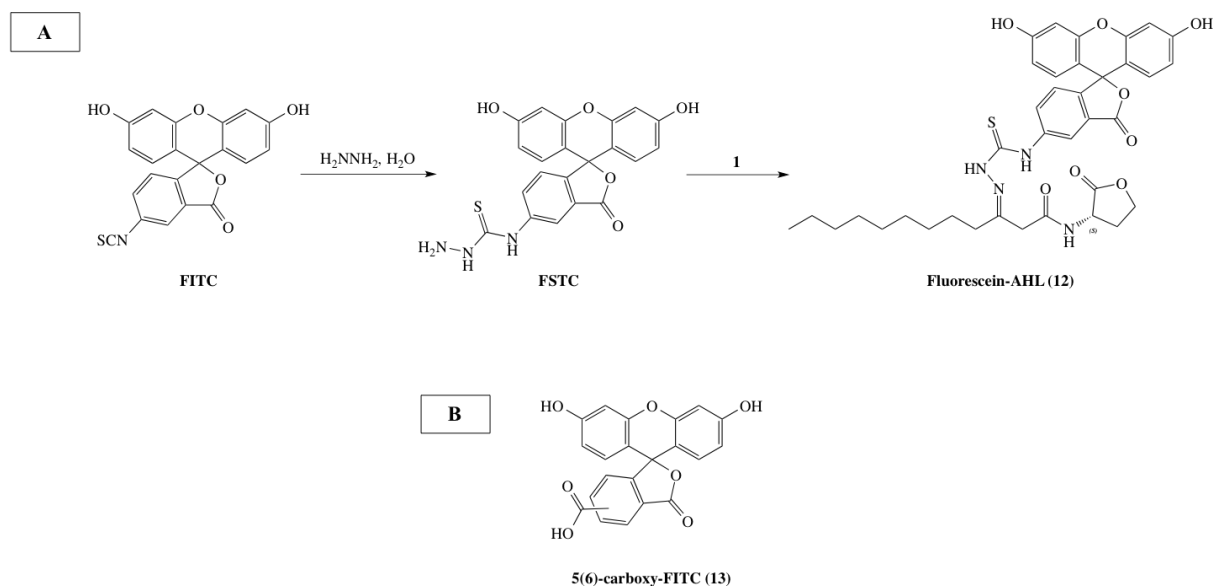
As presented in *Introduction - 2.2.6* the existence of one or more specific mammalian receptors for AHLs is yet to prove. Several tracks have been investigated in literature, among which IQGAP-1 protein, PPAR γ and bitter taste receptor T2R38. We have here mainly tried to develop tools for the study of AHL-protein interactions by designing several tagged 3oxoC₁₂-HSL.

2.3.1. Mapping AHLs in epithelial intestinal cells

2.3.1.1. Use of a commercially available fluorescent molecule

We started performing cell imaging with the commercially available fluorescein-tagged AHL **12** provided by Cayman Chemicals ; molecule 5(6)-carboxy-FITC **13** was used as

fluorescent control. Compound **12** derives from the coupling of fluorophore fluorescein thiosemicarbazide (FSTC) onto the ketone of natural 3oxoC₁₂-HSL (**1**) to form an imine. The Fluorescein thiosemicarbazide can itself be prepared from fluorescein isothiocyanate (FITC) by reaction with hydrazine (Scheme 12).

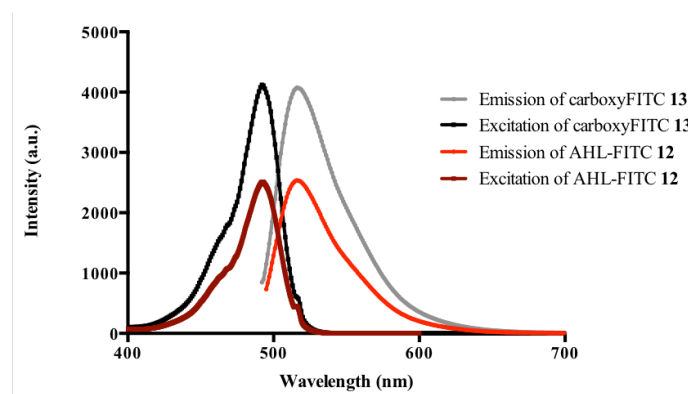


Scheme 12 - Fluorescein-tagged AHL and control

A : synthetic steps for preparation of FSTC from FITC and hydrazine, followed by coupling with **1** to produce **12**.

B : structure of control fluorophore **13**.

The absorbance and fluorescence spectra of **12** and **13** were recorded and compared in order to assess the influence of the AHL-coupling on the spectral properties of fluorescein in aqueous medium (Figure 54). No difference was observed in terms of emission/excitation wavelengths and Stokes shift ; the intensity of fluorescence were however significantly different, with an average 38% reduction of maximum emission intensity in **12** versus **13** (resp. 2536 units vs. 4074 units).



Molecule	λ_{em} (nm)	λ_{ex} (nm)	Stokes shift (nm)	Max emission
AHL-FITC 12	516	492	24	2536
CarboxyFITC 13	516	492	24	4074

Figure 54 - Spectral properties of fluorescent molecules 12 and 13

Spectra were recorded at r.t. using solutions of 1 μ M in PBS 1X.

The two molecules were first tested on Caco-2/TC7 cells under the usual assay, to examine their activity and especially their toxicity. As shown on Figure 55, it appears none of the molecule is toxic on intestinal epithelial cells after 18-hour incubation at 10 μ M, a concentration 10 times higher than that employed for imaging assays. While the control probe carboxyFITC 13 is overall inactive on cells, the tagged AHL 12 exhibits a decrease in IL-8 secretion at 5 and 10 μ M. This behaviour resembles that of natural compound 1, although with decreased potency.

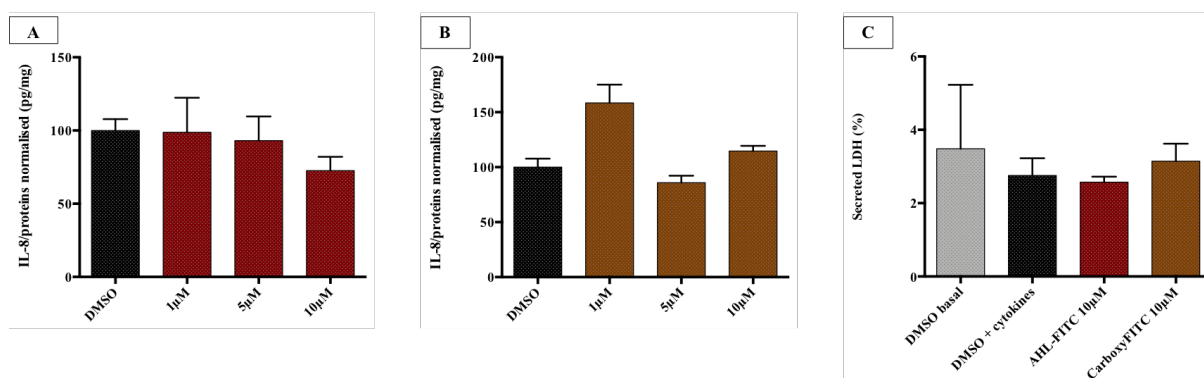


Figure 55 – Biological activity on Caco-2/TC7 cells in presence of fluorescent molecules 12 and 13

18-day-old cells were incubated 18h with cytokines and increasing doses of the molecules according the established protocol. **A** : IL-8 response after incubation with AHL-FITC 12. **B** : IL-8 response after incubation with control probe carboxyFITC 13. **C** : compared levels of secreted LDH. Points are the mean of several replicates (n = 6) \pm SEM. No significant difference observed.

Our first imaging experiments were realised on fixed Caco-2/TC7 cells. Cells grown on cover glass were incubated for 1h with **12** or control molecule 5(6)-carboxy-FITC **13**, rinsed with PBS 1X, fixed using paraformaldehyde (PFA), permeabilised if necessary and mounted on slides. Nuclei were stained with the DNA-binding agent DAPI.

The age of the cells rapidly appeared as a determinant factor, as **12** would not enter post-confluent Caco-2/TC7 cells while signal was observed upon incubation in 90%-confluent cells. Hence all our following imaging experiments were achieved on 80-90% confluent cells.

Observation of **12** in fixed cells returned very heterogenous results: signal was sometimes found in the nucleus, and others at a perinuclear localisation as condensed dots that might be small vesicles (Figure 56). Control **13** was itself also found in cell nuclei, which questions the specificity of the location of **12** in fixed cells. Moreover the observation was particularly tedious, with a rapidly fading signal that tended to diffuse within hours. We hypothesized that the cell fixation might denaturise the active site of the molecule, thus releasing it in the cell where it could freely diffuse. Based on this belief, we moved towards live-cell imaging.

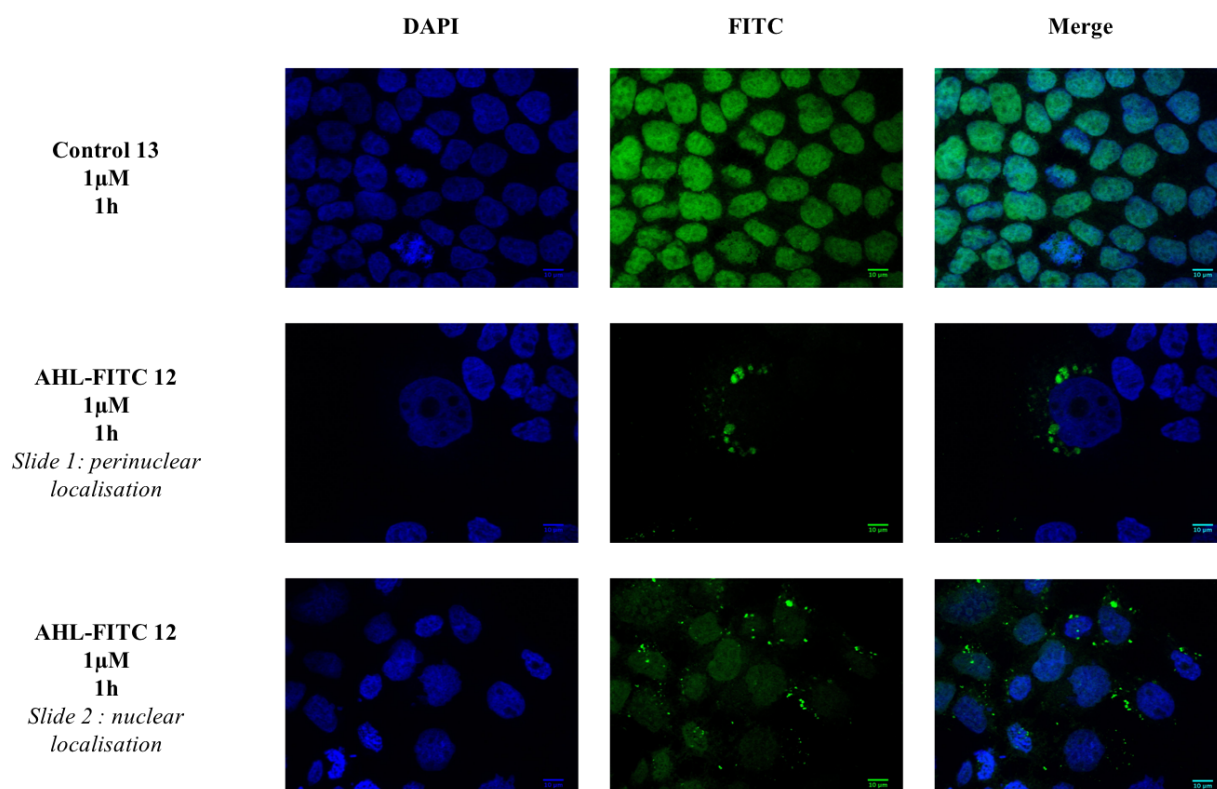


Figure 56 - Fixed-cell imaging of control fluorophore 13 and FITC-tagged 3oxoC₁₂-HSL 12

4-day-old Caco-2/TC7 cells at 80-90% confluent were incubated with 1 μ M of desired molecule for 1h. Mounted in DAPI-containing Mowiol. Observed with an epifluorescence microscope. Image processing achieved with FIJI.

Cells in live-imaging received similar incubation treatment to the fixed ones ; the incubating medium was then removed, the cells rinsed and the medium replaced with phenol-red-free DMEM to avoid perturbing microscopy signals. A confocal microscope was used for observation. The results in live-cell imaging are drastically different from those on fixed cells : the signal is localised at the cell outer membrane, and none is observed in the nucleus (Figure 57). To visualize the location of signal in cell islets, we can plot linear and surface signal intensity profiles. High intensities of light are localised at cell membrane while the inner cell compartment appears dark on surface plots ; similarly linear profiles show high intensity peaks cell membrane crossing, alternating with low intensity zones.

The live-cell imaging results presented in Figures 57 & 58 were realised in collaboration with Dr. Lorraine Montel and Dr. Jacques Fattaccioli, at the Pierre-Gilles de Gennes Institute for microfluidics.

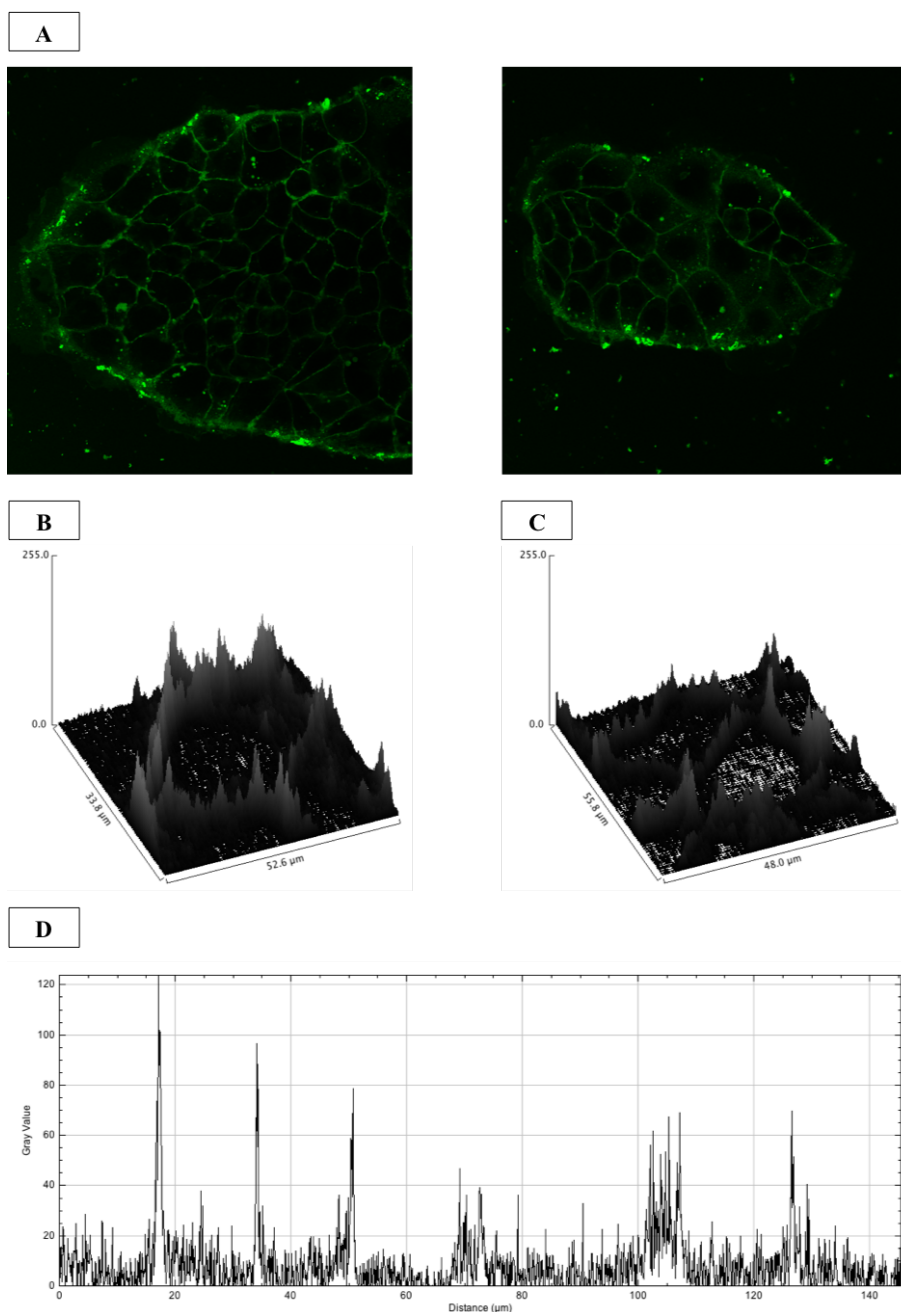


Figure 57 – Live-cell imaging with AHL-FITC 12

4-day-old Caco-2/TC7 cells at 80-90% confluency were incubated with 1 μM of 12 for 1h. Observed with a laser-scanning confocal microscope. Image processing achieved with FIJI. **A:** confocal microscopy images. **B:** one-cell surface plot. **C:** two-cells surface plot. **D:** Linear profile plot.

Meanwhile, control molecule **13** was tested under the same conditions. It returned weak and non-specific signal, hence confirming the observations with **12** are not biased by the addition of FITC on the AHL. To further assess the specificity of **12** for a putative AHL receptor, we set up competition experiments with natural AHLs **1** and **2**: the cells were incubated for 1h with a combination of 1 μM **12** and increasing concentrations of **1** or **2** (ratio fluorescent molecule/competitor 1:20 to 1:100). With image processing we could retrieve mean grey values

and integrated intensities over the surface from the obtained pictures (Figure 58). At ratio 1:20, saturated AHL 1 strongly disrupts the fluorescence from **12**, reducing the average intensity by 88%. The unsaturated AHL **2** however is not quite as efficient : ratio 1:20 does not induce any modification of signal intensity, ratio 1:50 reduces the fluorescence approximately by 20%, and ratio 1:100 reduces the signal by 50%. Similarly, the mean grey value of conditions with 3oxoC₁₂-HSL co-incubation are significantly decreased compared to control **12** alone ; co-incubation with **2** however returns a dose-dependent decrease of mean grey value, but does not reach the levels obtained with the saturated AHL **1**.

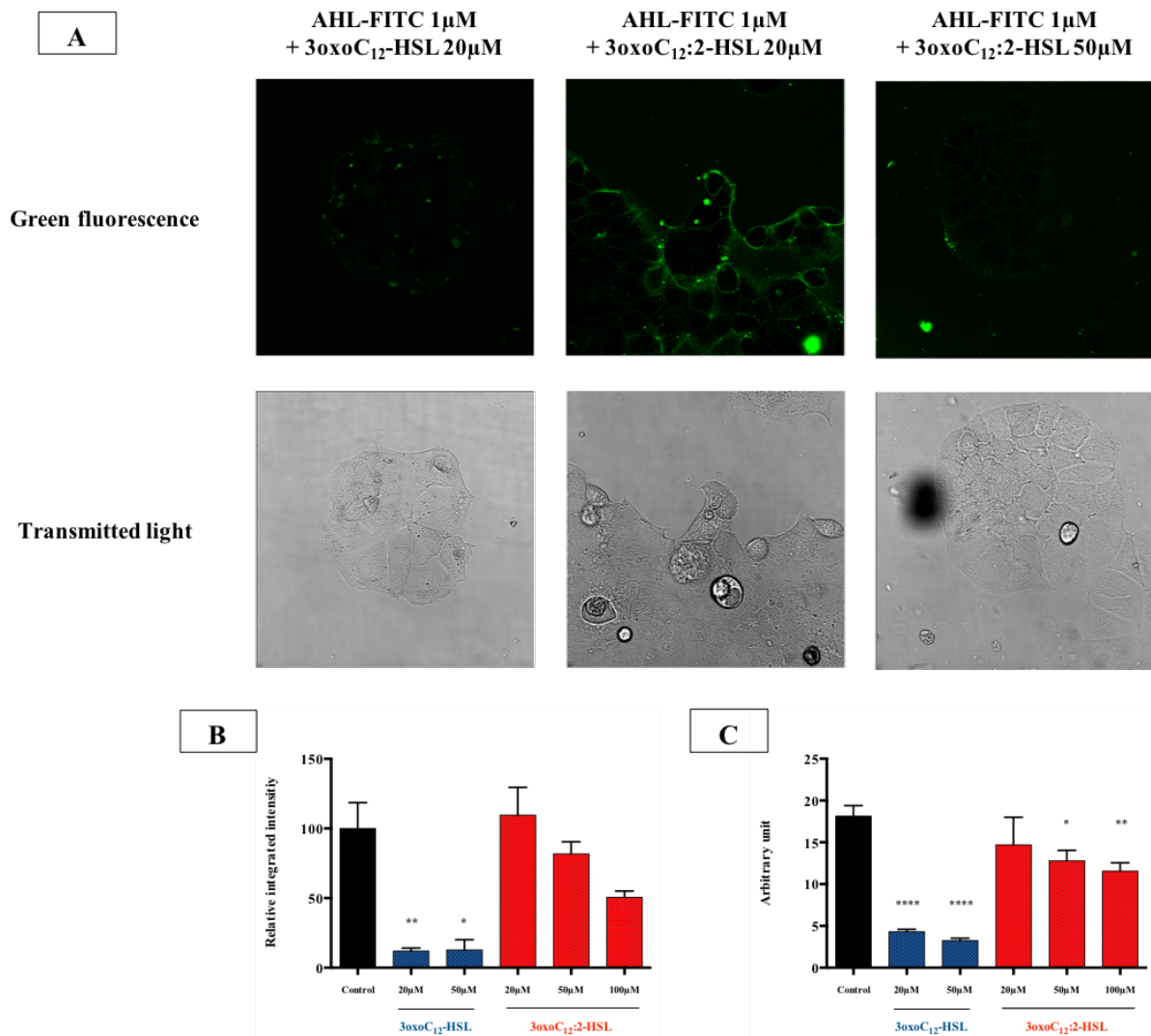


Figure 58 – Competition assay between AHL-FITC 12 and non-tagged AHLs 1 and 2

4-day-old Caco-2/TC7 cells in phenol-red-free DMEM. **A** : compared images (green fluorescence & transmitted light) for several competition conditions. **B** : compared relative integrated densities for control condition 1μM AHL-FITC 12 and several competition conditions. **C** : compared mean grey values for control condition 1μM AHL-FITC 12 and several competition conditions. *p < 0.05, **p < 0.001 compared to control condition. One-way ANOVA (**B** : p = 0.0020 ; **C** : p < 0.0001), Holm-Sidak's (**B**) or Dunnett's (**C**) post-test.

The residence time of fluorescent molecule **12** was examined, and fluorescence compared after 1h and 24h incubation. The signal appears weakened after longer incubation times (Figure 59) : the localisation of fluorescence seems to be unchanged at cell membrane, but the residual integrated intensity is about 50%. The mean grey however is not significantly affected. The diminished signal could be due to the degradation of molecule **12** (hydrolysis of the imine bond) or its efflux out of the cell. Because we rinsed cells before observation, it was impossible to evaluate if the residual fluorescence in the outer cell compartment was increased at 24h compared to 1h.

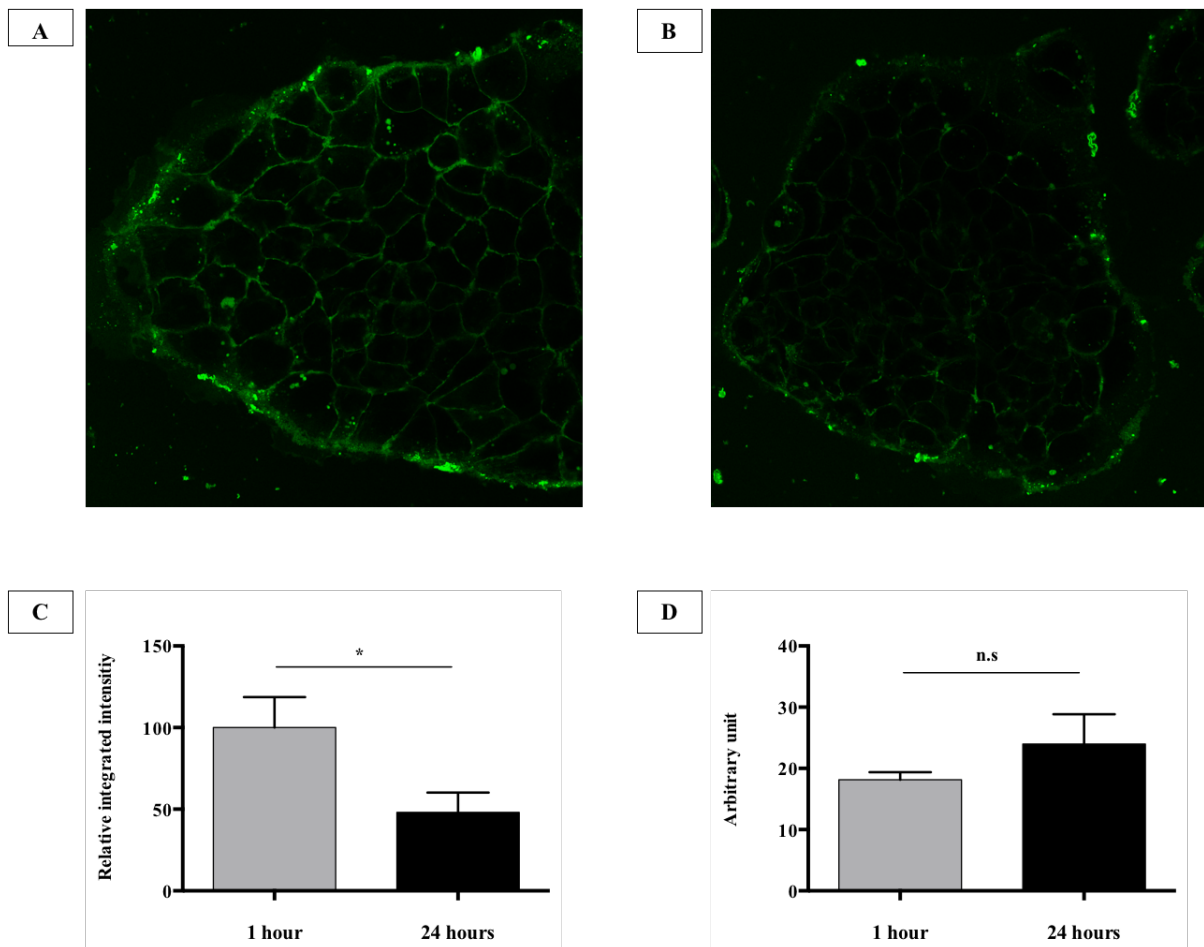


Figure 59 – Compared results with 1μM AHL-FITC 12 after 1h or 24h incubation time

4-day-old Caco-2/TC7 cells in phenol-red-free DMEM. **A** (resp. **B**) : observed green fluorescence with 1μM AHL-FITC 12 after 1h incubation time (resp. 24h). **C** : compared relative integrated densities for 1μM AHL-FITC 12 after 1h or 24h incubation. **D** : compared mean grey values for 1μM AHL-FITC 12 after 1h or 24h incubation. *p < 0.05 compared to control condition. Unpaired two-tailed t test with Welch's correction (**C**: p = 0.0339 ; **D** : p > 0.05).

2.3.1.2. Development and evaluation of new molecules

The previous section has highlighted some drawbacks of the commercial AHL-FITC **12**, which is composed of a fluorescent probe much larger than the AHL itself, is attached via ketone-modification, and faces diffusion issues despite PFA-fixation that allow it to reach the nucleus and bias our results. Kravchenko *et al.* have especially identified the integrity of the headgroup and the C₃-ketone as requirements for AHL activity in mammals.²⁷⁸

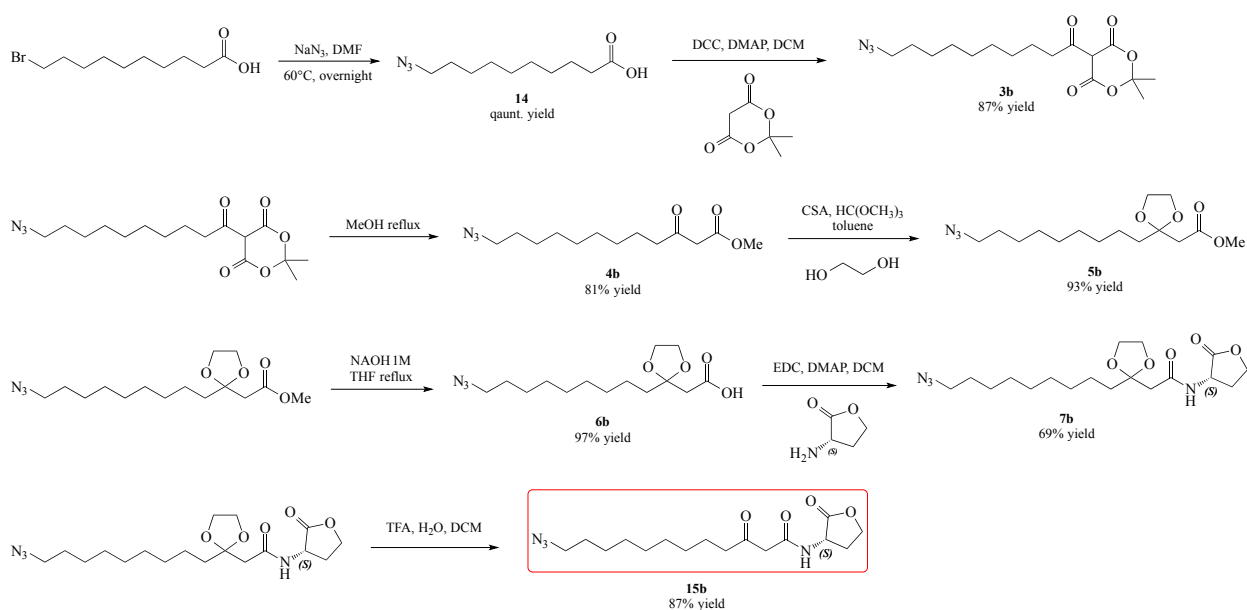
To tackle these limitations we imagined the development of a readily clickable AHL, modified at its acyl chain rather than headgroup or C₃-ketone. To this newly designed molecule, we coupled several probes : first a nitrobenzofurazan (NBD) that unlike the fluorescein offers both the advantages of a small size and high lipophilicity, then a series of modified naphthalimide probes to attempt to develop fixable probes.

2.3.1.2.1. Development of a clickable AHL

Cu^I-catalysed azide-alkyne 1,3-dipolar cycloaddition (CuAAC) chemistry, also known as click chemistry, is a powerful technic for synthesis of five-membered heterocycles and bioconjugation. It offers minimal modification of the parent compounds, that are equipped with bio-orthogonal alkyne or azide tag. The mechanism of this reaction is based on a two-copper catalytic cycle to regioselectively afford the 1,4-isomer under room temperature and short time span.⁴⁰⁴⁻⁴⁰⁶ The main drawback of this reaction resides in the amount of copper needed to perform it *in cellulo*, that ranges in the cytotoxic dosage. In comparison, the Huisgen's non-catalysed 1,3-dipolar cycloaddition affords a mixture of 1,4- and 1,5-isomers, requires high temperature (100°C) and proceeds rather slowly.

We chose to tag the AHL chain with an azide group, placing the alkyne group on probes. Because it only consists in carbons the addition of an alkyne moiety to the acyl chain of AHL **1** might be considered a more conservative modification than an azide group. Previous studies have nevertheless demonstrated the superiority of azido-compounds over alkyne-compounds for background signal reduction.⁴⁰⁷ The synthetic strategy for preparation of a clickable-AHL relies heavily of the synthesis of natural AHL **1**. Only one additional step is required, a nucleophilic substitution to turn the starting bromo-carboxylic acid into an azido-carboxylic

acid. After what, the added chemical group will remain untouched along the course of the synthetic path, to afford final compound **15b** (Scheme 13). The overall yield is 38%.



Scheme 13 - Synthetic path for preparation of non-natural analogue 12-azido-3oxoC₁₂-HSL (15b**)**

The analogue **15b**, whose structure is very close to **1**, was evaluated for its activity on cell and bacteria models according our established protocols. In the Caco-2/TC7 cell line the analogue retains the typical bell-shaped activity curve of natural AHLs (Figure 60A) with anti-inflammatory activity at low concentration ($5\mu\text{M}$) of similar magnitude to that of molecule **1** (Figure 61). In the range of tested concentrations, only dosage $1\mu\text{M}$ returned an IL-8 response significantly different from that of 3oxoC₁₂-HSL. No toxicity was otherwise observed as proved by the low levels of secreted LDH (Figure 60C): the molecule shows an average 1.6% liberated LDH after 18h treatment with $100\mu\text{M}$ alone, and 1.9% after treatment combined to IL-1 β . On the opposite, molecule **15b** is very poorly tolerated by Raw 264.7 macrophages with pro-inflammatory IL-6 secretion at all concentrations and increased cytotoxicity from $25\mu\text{M}$ and above (Figure 60B & D).

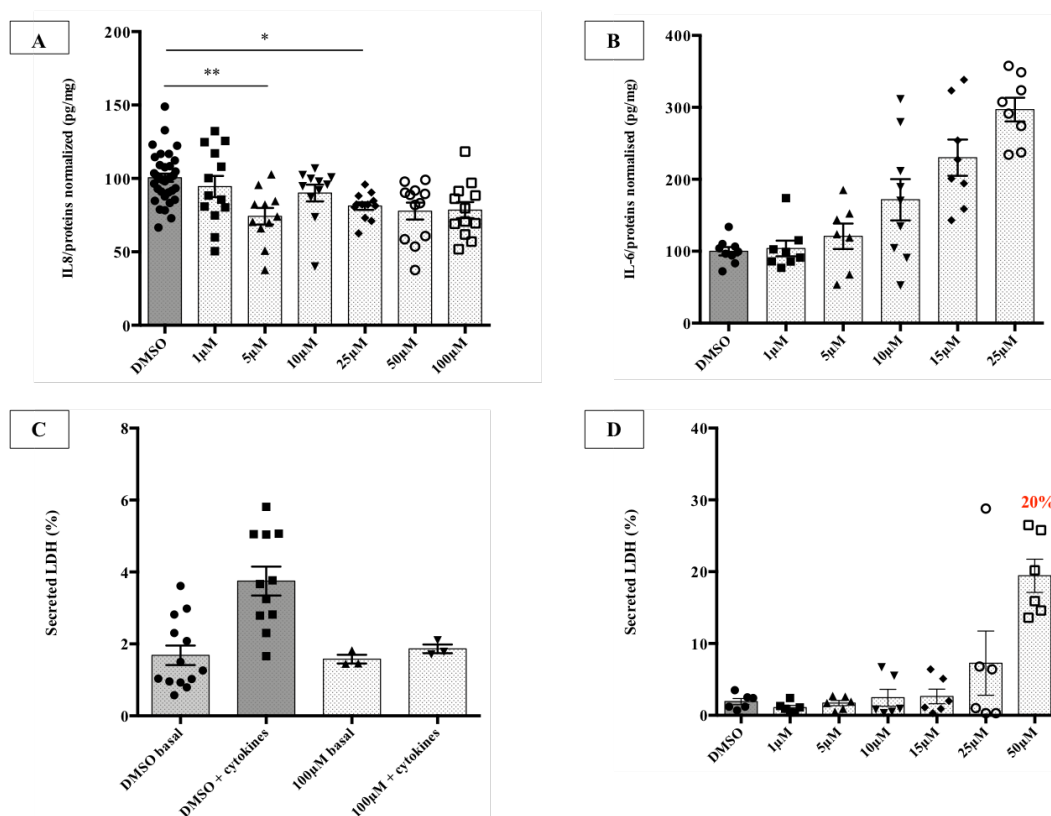


Figure 60 – Biological activity of clickable analogue 15b

A (resp. **B**) : human IL-8 (resp. murine IL-6) response of cytokine-stimulated Caco-2/TC7 (resp. Raw 264.7) cells treated for 18 h (resp. 6 h) with increasing dose of analogue **15b**. **C** (resp. **D**) : secreted LDH (%) of Caco-2/TC7 (resp. Raw 264.7) cells in presence of cytokines and increasing dose of analogue **15b**. The bars represent the mean of several replicates ($n \geq 3$) \pm SEM, illustrated by dots. * $p < 0.05$ compared to DMSO, one-way ANOVA **A** : $p < 0.0001$), Tukey's post-test.

Our findings are only partly in accordance with published results from Garner *et al.* who studied the effects of analogue **15b** and its alkynyl counterpart on phosphorylation patterns in BDMD.⁴⁰⁸ The group reported similar activity of natural AHL **1** and synthetic **15b** on their biological model, whereas the alkynyl compound and the (*R*)-isoform returned negative results. The authors hypothesized that the addition of azido moiety might create extra hydrogen bonds or Van der Waals interactions capable of aiding the analogue binding to the putative AHL receptor(s). These similarities are in line with our observations in Caco-2/TC7 cells, but not with those in Raw 264.7 macrophages that should however share more features with BDMD. These data suggest the use of analogue **15b** for cell study may need to be restricted to the Caco-2/TC7 cell line or other epithelial cell lines.

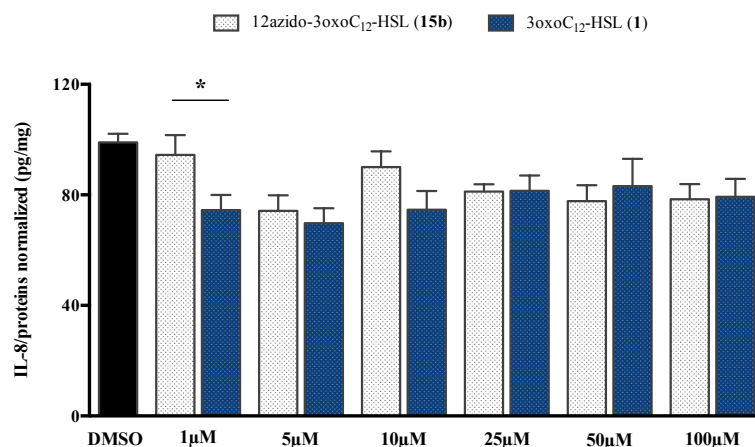


Figure 61 – Compared IL-8 response of cytokine-stimulated Caco-2/TC7 cells incubated with increasing doses of analogue 15b (in white) or natural 3oxoC₁₂-HSL 1

Established stimulatory protocol. *p = 0.0369, unpaired two-tailed t-test with Welch’s correction.

Activity of **15b** was eventually examined in bacterial lines. In terms of bacteria survival (Figure 62), no effect of the analogue was observed after 18-hour incubation. The activation of LasR receptor however appeared impaired compared to **1**, with an EC₅₀ of 430nM (vs. 9nM) that revealed a weaker agonist. These results are corroborate the findings from Garner et al. who also tested the impact of **15b** as a potential *P. aeruginosa* autoinducer using the luminescent reporter strain PAO-JP2.⁴⁰⁸ Although their bacteria reporter line differs from ours, the authors reached similar conclusions: the analogue demonstrated impaired activity, with an approximate 2-fold reduction of luminescence.

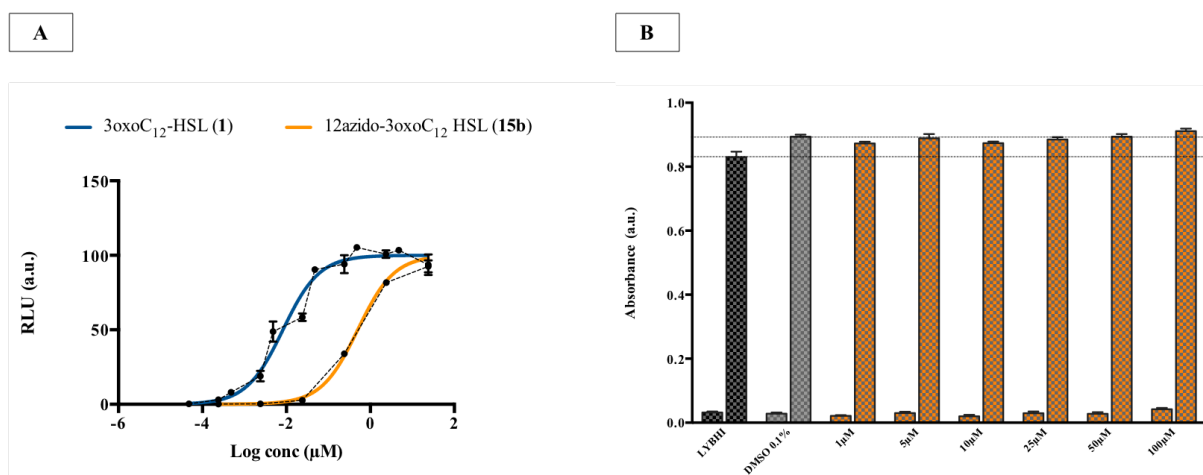
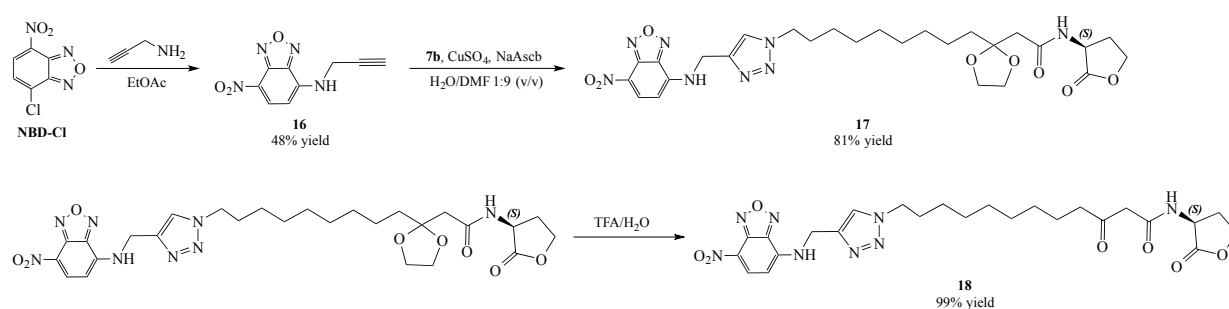


Figure 62 - Analogue 15b activity in bacteria lines

Established protocols. **A** : luminescent reporter assay for activation in *E. coli* pSB1075 strain. **B** : bactericidal assay in *E. coli* strain K12.

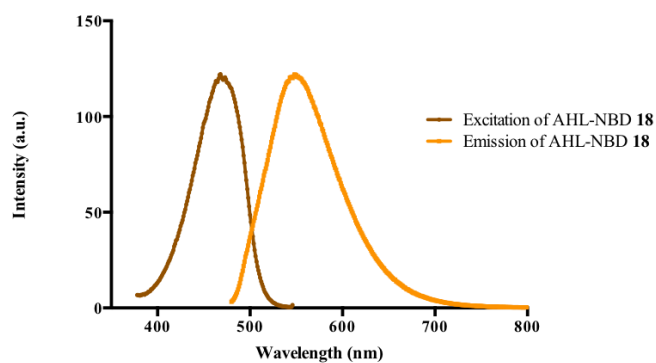
2.3.1.2.2. The nitrobenzofurazan: a smaller fluorescent probe

A first tagged AHL was synthesized using the small fluorescent probe nitrobenzofurazan (NBD). Starting with commercially available chlorine-grafted nitrobenzofurazan NBD-Cl, we developed a three-step synthesis for the preparation of NBD-tagged AHL **18** (Scheme 14). Briefly, NBD-Cl was reacted with propargylamine to afford intermediate **16**. On top of introducing an alkynyl group, the propargylamine was chosen as a minimal spacer to branch the AHL and the probe and minimize as much as possible the size of the final compound. **16** was then coupled with **7b** under aqueous conditions to afford **17**, whose ketone was then deprotected to give final “AHL-NBD” **18**.



Scheme 14 - Three-step synthesis of NBD-tagged AHL 18

The absorbance and fluorescence spectra of **18** were recorded in order to assess the spectral properties of coupled-NBD in aqueous medium (Figure 63). Pure NBD-Cl is poorly fluorescent, but once coupled it exhibits a green fluorescence with $\lambda_{em} = 548$ nm. The maximum emission intensity is rather low compared to fluorescein (122 vs. over 2000) due to the aqueous environment ; very hydrophilic, it is to expect that NBD fluorescence would be much stronger in a lipophile environment.



Molecule	λ_{em} (nm)	λ_{ex} (nm)	Stokes shift (nm)	Max. emission intensity
AHL-NBD 18	548	468	80	122

Figure 63 - Spectral properties of fluorescent molecule 18

Spectra were recorded at r.t. using solutions of 10 μ M in PBS 1X.

The two molecules were first tested on Caco-2/TC7 cells under the usual assay, to examine their activity and toxicity. As shown on Figure 64, it appears none of the molecule is toxic on intestinal epithelial cells after 18-hour incubation at 10 μ M, a concentration 10 times higher than that employed for imaging assays. While the control probe NBD-Cl has pro-inflammatory effects on cells, the NBD-tagged AHL 18 exhibits a decrease in IL-8 secretion at 10 μ M. This behaviour resembles that of natural compound 1, although with decreased potency.

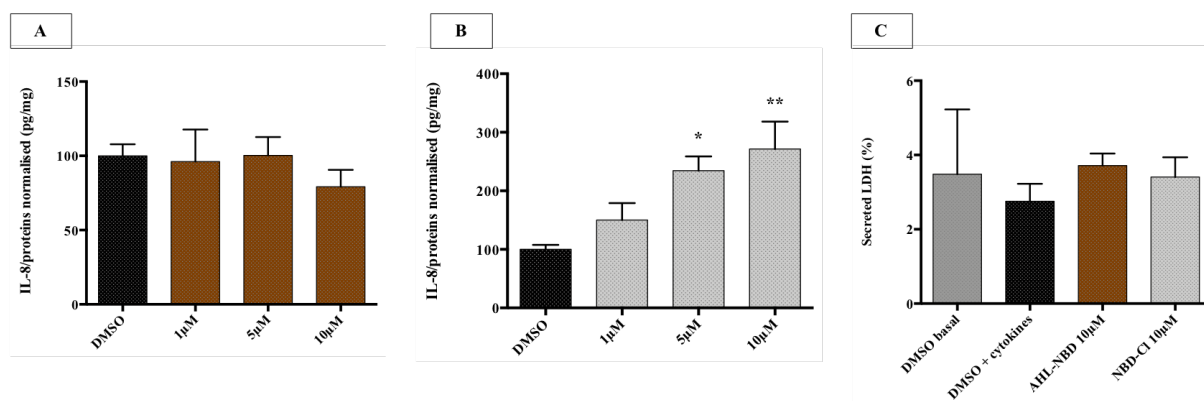


Figure 64 - Biological activity on Caco-2/TC7 cells in presence of fluorescent molecules AHL-NBD (18) and NBD-Cl

18-day-old cells were incubated 18h with cytokines and increasing doses of the molecules according the established protocol. **A** : IL-8 response after incubation with AHL-NBD 18. **B** : IL-8 response after incubation with control NBD-Cl. **C** : compared levels of secreted LDH. Points are the mean of several replicates (n = 6) \pm SEM. **A** & **C** : no significant difference observed. **B** : *p < 0.05, **p < 0.01 compared to DMSO, one-way ANOVA (p = 0.009), Tukey's post-test.

The AHL-NBD was tested on both fixed and live cells. In fixed cells weak signal was observed in nuclei with both AHL-NBD **18** and control NBD-Cl without any specificity, thereby demonstrating this molecule is ill-adapted to the fixed-cell technique (results not shown). Compound **18** was tested in live cells according to the protocol established with AHL-FITC **12**, at 1 μ M and for incubation times 1h or 24h (Figure 65). The resulting signal was much weaker, heterogenous, and did not stain the cell membrane but was rather diffuse in the cytoplasm without penetrating the nucleus that remained deep dark. Control NBD-Cl returned similar images, which questions the selectivity of **18** for a putative AHL receptor. Quantification of integrated signal density and mean grey values confirmed this hypothesis by showing no significant difference between compound **18** and control, regardless of the incubation time (1h or 24h).

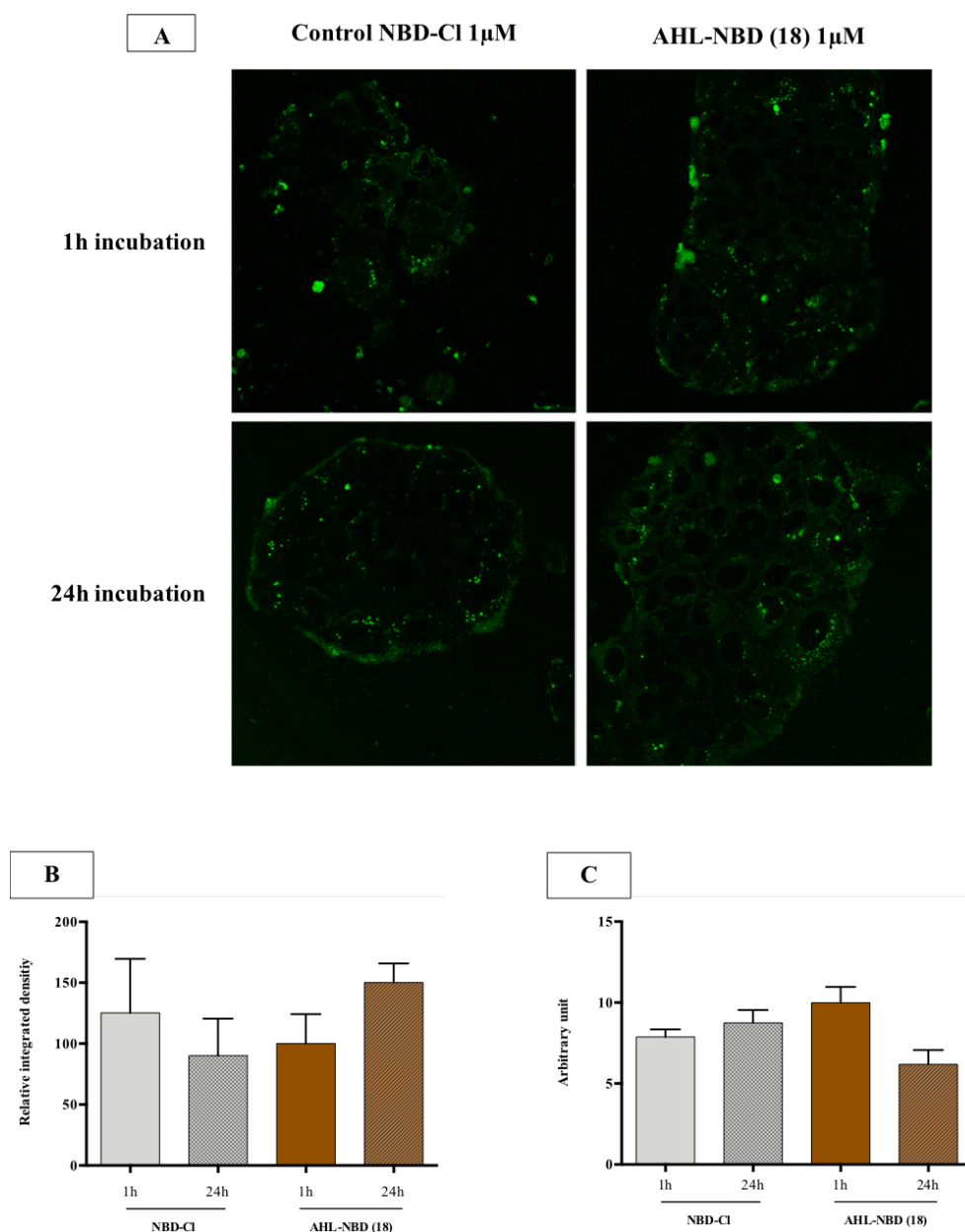


Figure 65 - Compared results with 1 μ M AHL-NBD 18 or 1 μ M control NBD-Cl after 1h or 24h incubation time
4-day-old Caco-2/TC7 cells in phenol-red-free DMEM. **A** : compared green fluorescence with 1 μ M AHL-NBD **18** or 1 μ M control NBD-Cl after 1h incubation time (resp. 24h). **B** : compared relative integrated densities with 1 μ M AHL-NBD **18** or 1 μ M control NBD-Cl after 1h incubation time (resp. 24h). **C** : compared mean grey values with 1 μ M AHL-NBD **18** or 1 μ M control NBD-Cl after 1h incubation time (resp. 24h). No significant difference between conditions.

To further investigate the selectivity of AHL-NBD, we performed a competition assay by co-incubating 1 μ M **18** with 50 μ M of 3oxoC₁₂-HSL **1** during 1h. The resulting images showed no difference in terms of integrated density and mean grey value with the images obtained with 1 μ M AHL-NBD alone (Figure 66). Hence, it appears the NBD-tagged AHL does not target an AHL partner, but its localisation would rather be driven by interactions of the fluorophore alone.

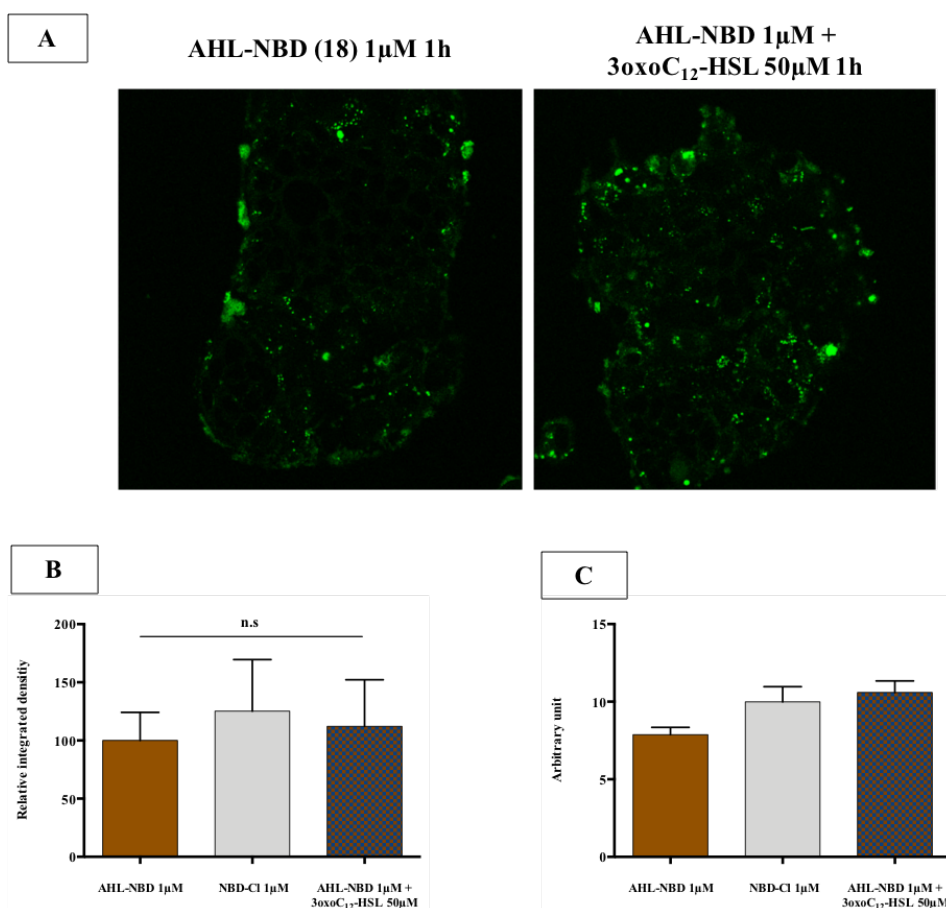


Figure 66 - Compared results with 1 μ M AHL-NBD 18, 1 μ M control NBD-Cl or 1 μ M AHL-NBD combined to 50 μ M 3oxoC₁₂-HSL after 1h incubation time

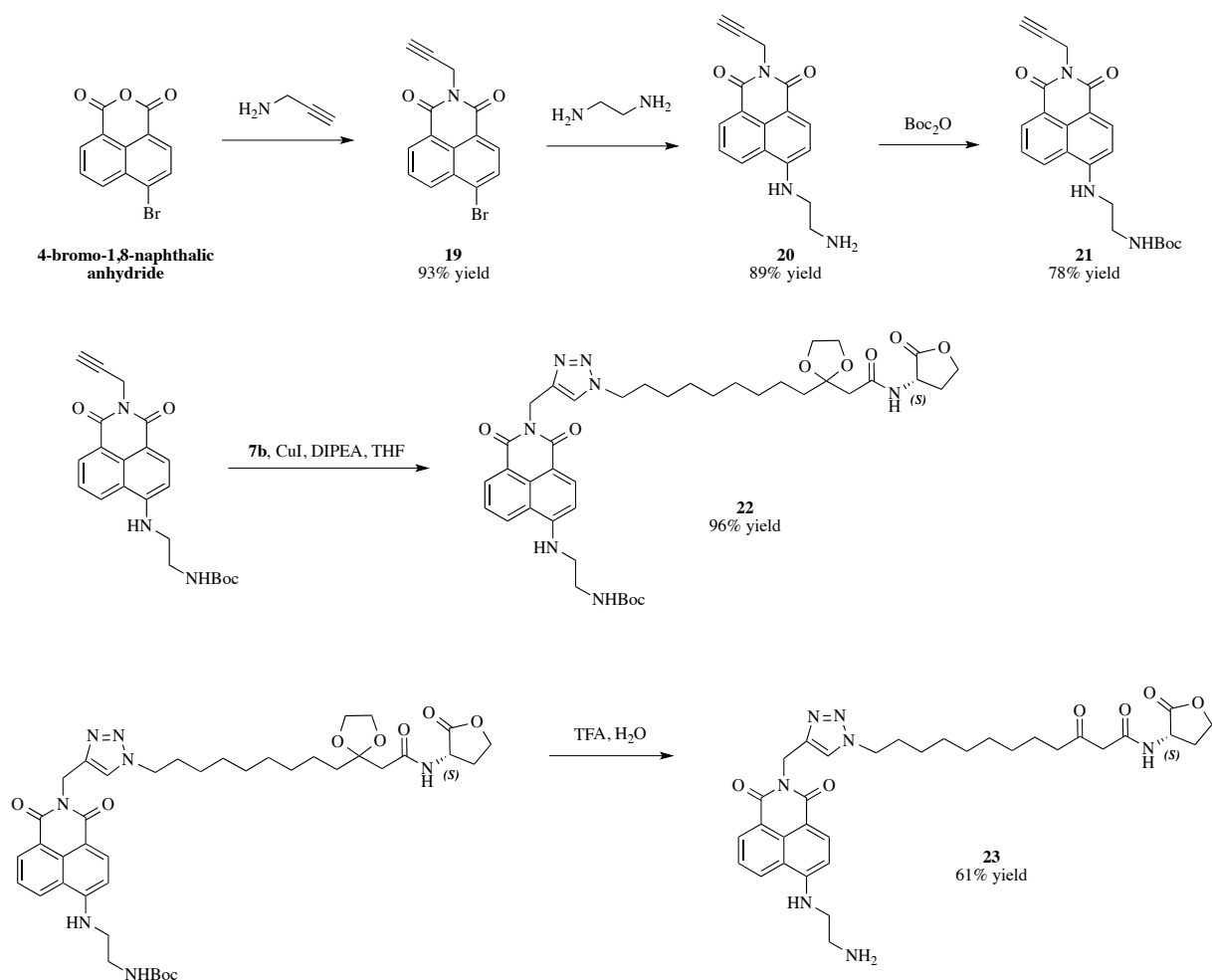
4-day-old Caco-2/TC7 cells in phenol-red-free DMEM. **A** : compared green fluorescence with 1 μ M AHL-NBD **18** or 1 μ M AHL-NBD combined to 50 μ M 3oxoC₁₂-HSL after 1h incubation time. **B** : compared relative integrated densities with 1 μ M AHL-NBD **18** or 1 μ M AHL-NBD combined to 50 μ M 3oxoC₁₂-HSL after 1h incubation time (n.s : no significant difference between conditions). **C** : compared mean grey values with 1 μ M AHL-NBD **18** or 1 μ M AHL-NBD combined to 50 μ M 3oxoC₁₂-HSL after 1h incubation time.

2.3.1.2.3. Design of potentially fixable naphthalimide-based fluorescent probes

A third family of fluorescent probes was developed, based on 4-bromo-naphthalimide. This fluorophore has several advantages : it is of intermediate size between nitrobenzofurazan and fluorescein ; it remains a rather lipophilic compound but conserves decent signal intensity in aqueous media ; and presence of a bromine atom allows a range of substitution to modulate fluorescence properties or use as a handle for further binding. Especially, we imagined the preparation of a potentially-fixable probe, carrying a free primary amine.

Cell-fixation is used in histology to preserve biological tissues from decay. Chemical fixation with aldehydes is most commonly used. Aldehydes are crosslinking fixatives meaning they perform their function by creating covalent bonds between proteins in tissue to anchor soluble proteins to the cytoskeleton and rigidify the whole cell structure. The crosslinking process starts primarily with residues of the basic amino acid lysine, which presents a lysyl side chain of formula $(\text{CH}_2)_4\text{NH}_2$. We thought to mimic this side chain by introducing an ethylamine $((\text{CH}_2)_2\text{NH}_2)$ chain on a naphthalimide probe.

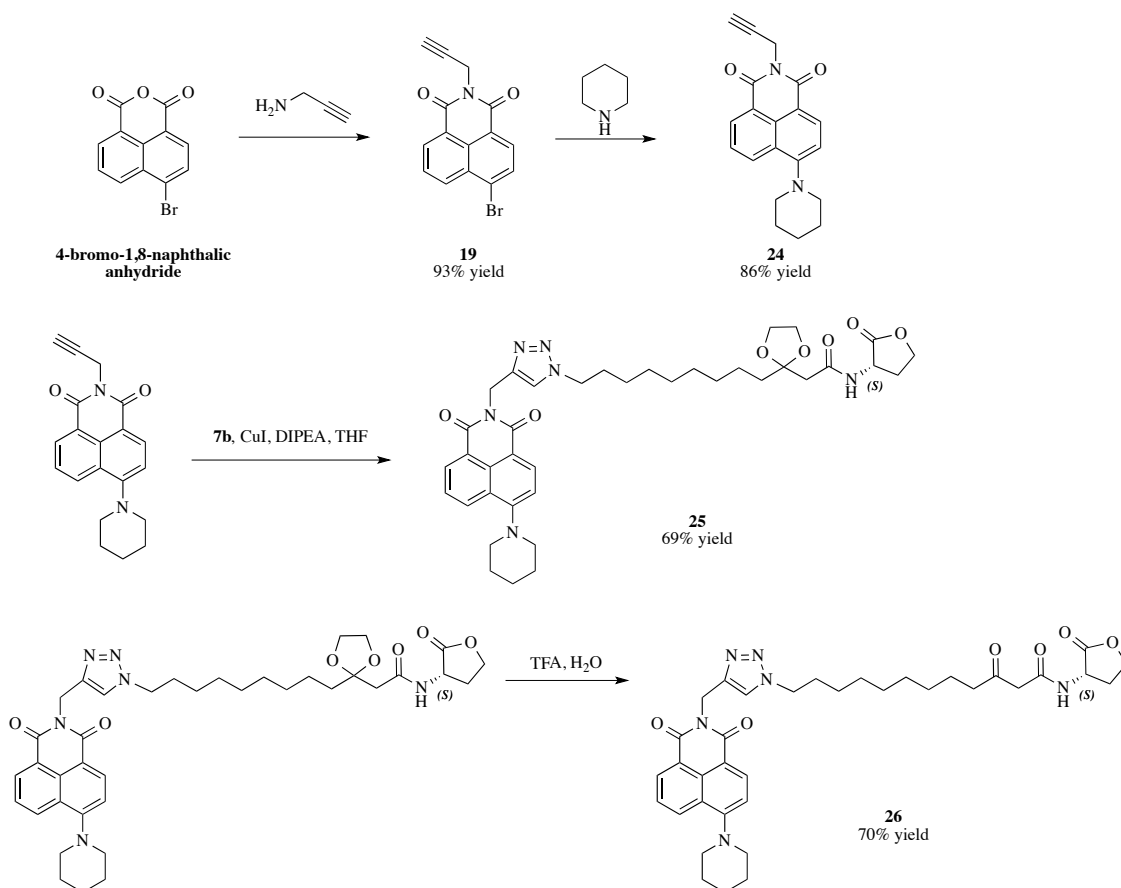
The synthetic strategy (Scheme 15) proceeds from 4-bromo-1,8-naphthalic anhydride, which is turned into an alkyl-containing 1,8-naphthalimide derivative using propargylamine. The bromine is then substituted with ethylenediamine. The resulting naphthalimide carries a free primary amine that should be protected ; a Boc-strategy was chosen because it can be removed by TFA treatment, which is also the condition used to deprotect the ketone for the AHL. The protected molecule can then be clicked with compound **7b**, before a final deprotection step.



Scheme 15 - Synthetic path for the preparation of a naphthalimide-tagged AHL with a free primary amine (compound **23)**

Overall yield is 38%.

In parallel, a similar synthesis was performed with piperidine instead of ethylenediamine, and the resulting naphthalimide clicked to **7b** and deprotected (Scheme 16). The piperidine probe would later be used as a non-fixable control, as it carries non free primary amine.



Scheme 16 - Synthetic path for the preparation of a 4-piperidinyl-naphthalimide-tagged AHL (compound 26)
Overall yield is 39%.

The absorbance and fluorescence spectra of **23** and **26** were recorded in order to assess the spectral properties of AHL-coupled naphthalimides in aqueous medium, and the influence of a free amine versus its protected counterpart (Figure 67). Molecules **20** and **24** were used as free probe controls, respectively. These show quite different properties, that can be attributed to their diverse amine patterns. Their emission wavelengths are close, but their maximum intensities differ by a two-fold (385 vs. 756 a.u. respectively). A significant variation in their excitation wavelengths is also observed.

Coupling the probes to the azido-AHL has very surprisingly opposed effects on their spectral properties, depending on the presence or absence of a free amine. In case of free-amine probe **20**, the AHL-tagged **23** exhibits higher intensities both in emission and excitation spectra, without significant modification of characteristic wavelengths and Stokes shift. The properties of piperidine-probe **24** are however much more impacted by coupling as the signal intensities collapse in compound **26**.

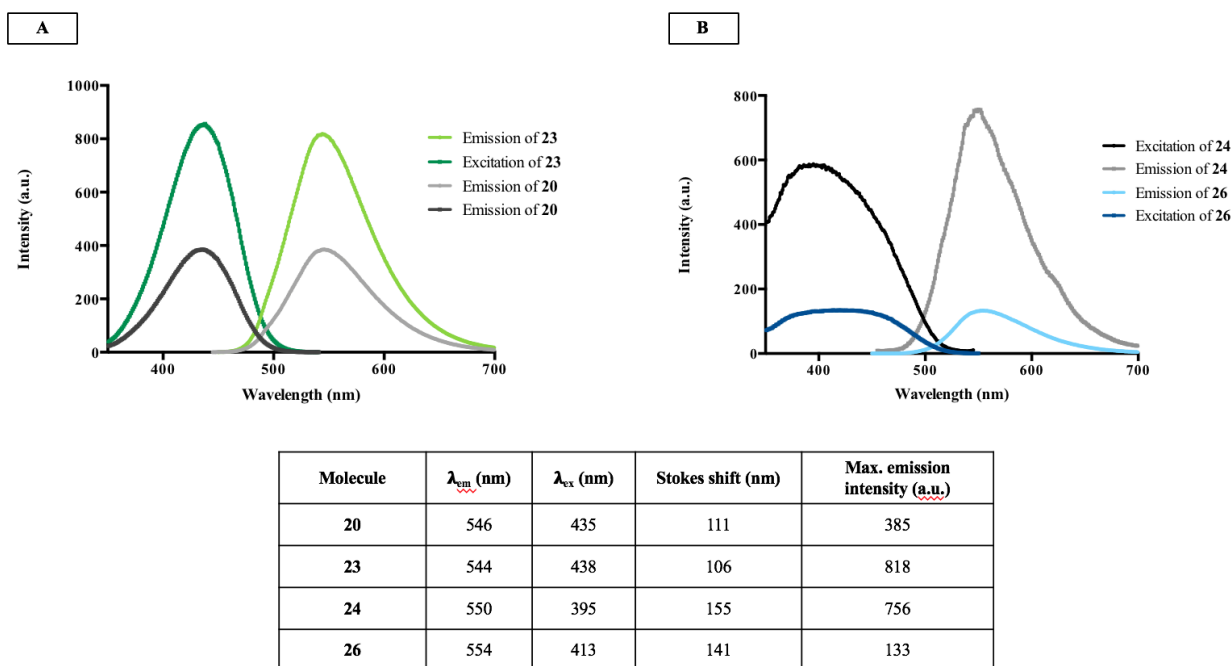


Figure 67 - Spectral properties of fluorescent molecules 20, 23, 24 and 26

Spectra were recorded at r.t. using solutions of 10 μ M in PBS 1X.

Compounds **23** and **26**, and their respective AHL-free controls **20** and **24**, were successively tested under fixed- and live-cell conditions. In both cases, 4-day-old Caco-2/TC7 cells at 80-90% confluence were employed and exposed to compounds for 1h.

Cells were fixed with PFA, incubated with the antifading agent DABCO and mounted with DAPI-enriched Prolong Gold (Figure 68). The results are quite different from those obtained with AHL-FITC **12**. Molecules **23** and **26** are observed in the nucleus but also the cytoplasm, where it may accumulate in small vesicles hence the dotted aspect in the perinuclear area. Overall, the molecules are excluded from the cell membrane. Piperidine-tagged **26** gives stronger signal than **23**; its behaviour is also frankly different from its control, which cannot be observed despite its capacity to emit stronger maximum emission signal as observed in Figure 67. However its cell penetration is rather inhomogeneous, as some cells are marked while others remained completely dark. On the opposite control **20** penetrates cells and is observed in nuclei, although its signal is weaker than that of AHL-tagged counterpart **23**. Given that Figure 67 demonstrates molecule **20** has a lower maximum emission intensity than **23**, it is hard to conclude whether the reduced signal we observe results from the fact that fewer controls than tagged-molecules could penetrate the cells or simply from their different emission capacities.

Based only on our results in fixed-cells, it seems that piperidine-naphthalimide-AHL **26** - but not free-amine **23** - could be a fair AHL probe. The molecule shows significantly different signal than AHL-free control, indicating that the fluorophore alone cannot enter the cells (or is rapidly removed) when the AHL-tagged counterpart is not. Questions remain regarding the selectivity of **26** for putative AHL receptor(s), which we tried to answer by live-cell imaging.

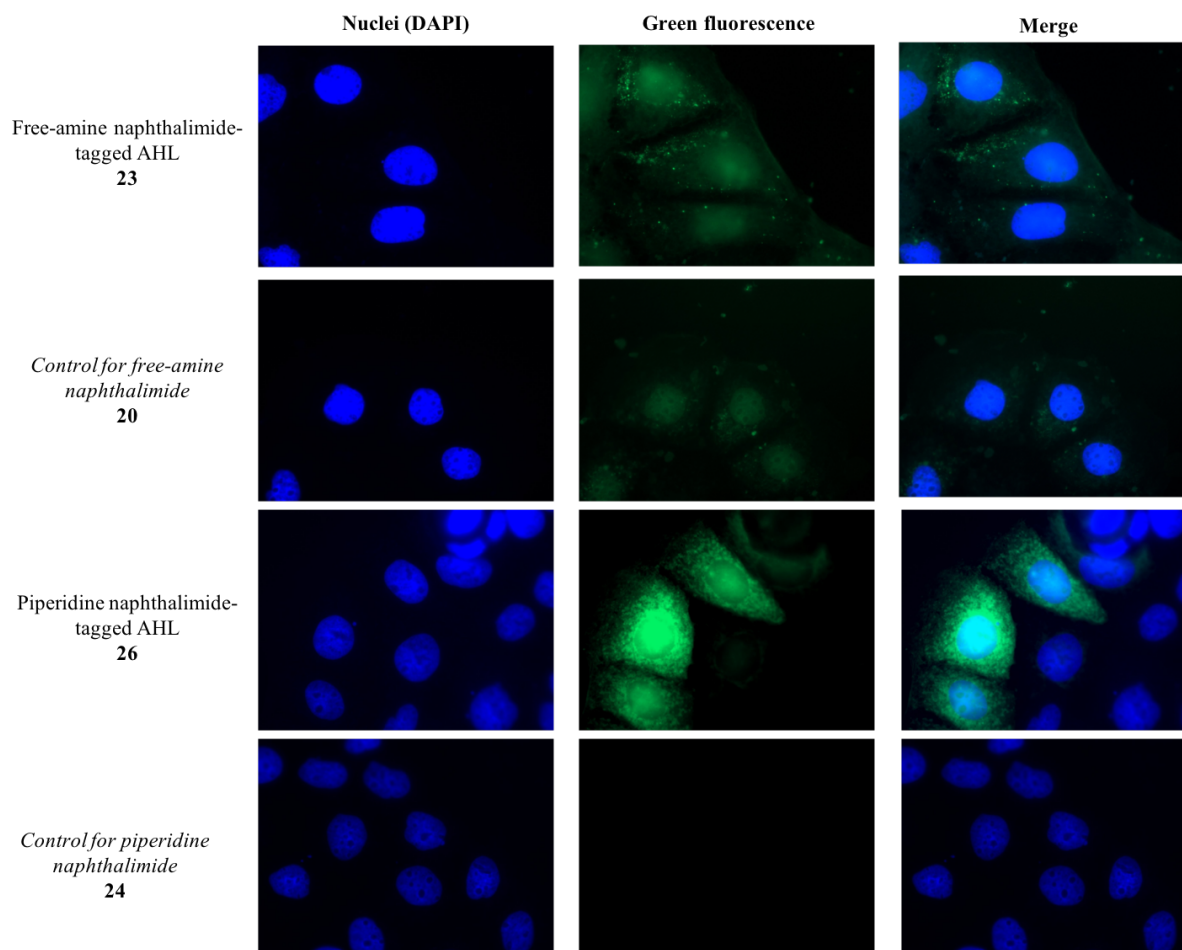


Figure 68 - Fixed-cell imaging of naphthalimide-tagged AHLs 23 (A) and 26 (B) and their respective controls 20 and 24

4-day-old Caco-2/TC7 cells at 80-90% confluent were incubated with 1 μ M of desired molecule for 1h. Mounted in DAPI-containing Prolong Gold. Observed with epifluorescence microscope. Image processing achieved with FIJI.

Molecule **23** and its control **20** returned very little signal in live-cell imaging (Figure 69A & B) ; **20** can barely be observed, while **23** gives weak and diffuse fluorescence, observed with difficulties in the cytosol of Caco-2/TC7 cells. It is hard to explain why **23** and **20** can be observed in fixed cells and not in live cells. An hypothesis we have made concerns the protonation of the free primary amine they harbour : in live cells and under physiological pH, this amine will be protonated (NH_3^+), which might affect the molecule cell penetration, time of

intracellular residency or efflux, especially as the cells keep on processing the xenobiotics while we observe them. On the opposite in fixed cells the amount of molecule that managed to penetrate the inner cellular compartment is blocked by fixation, furthermore as we incubate the cells with DABCO. This organic compound is a highly nucleophilic amine used as a scavenger to protect fluorophores from fading by quenching reactive oxygen species.

Consistently with our observations in fixed cells, molecule **26** exhibits good fluorescence signal versus its control **24** (Figure 69C & D). The molecule is mostly observed in the cytosol and especially the perinuclear area ; comparatively to fixed cells, less signal is observed in the nucleus, which suggests that part of the molecule may diffuse under fixed-cell conditions. The signal is however more homogenous in live cells, where almost all cells are consistently marked, as opposed to fixed cells.

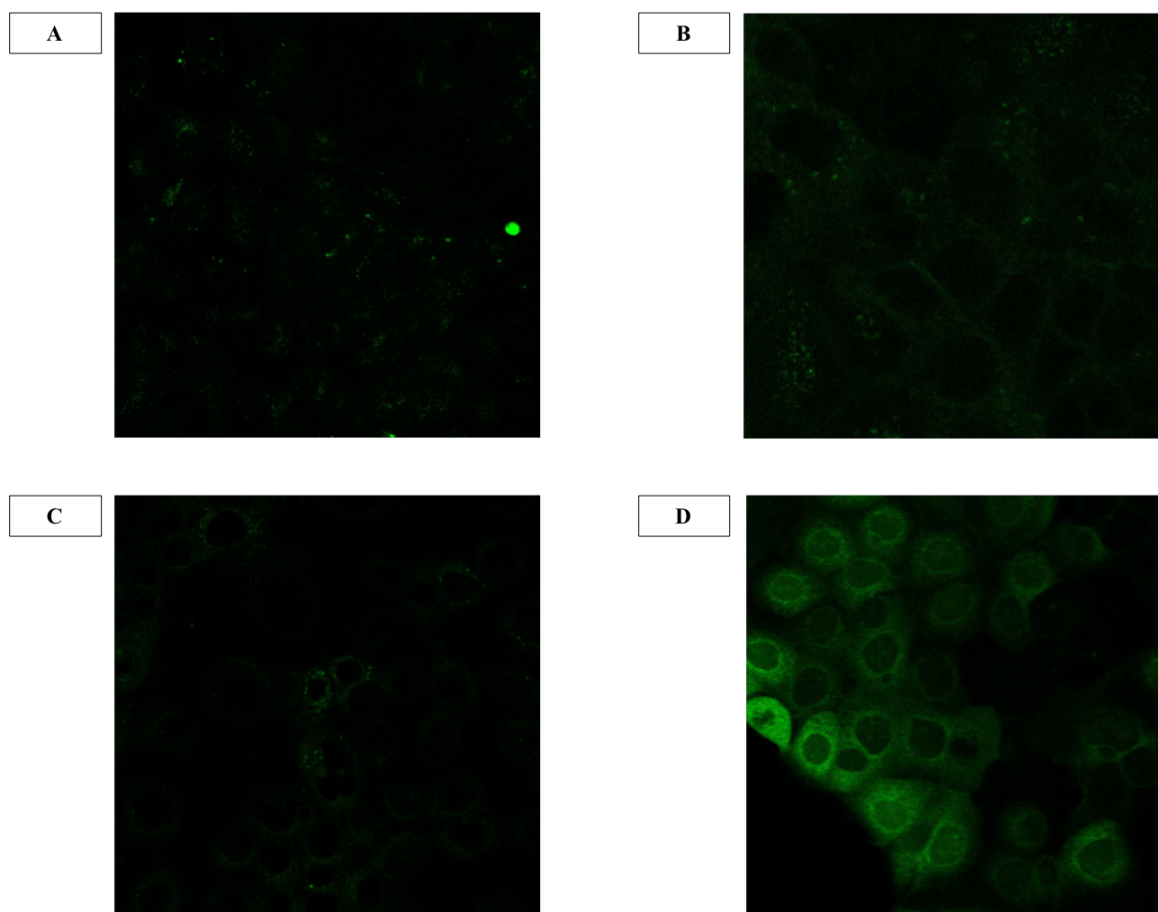


Figure 69 - Live-cell imaging of molecules 20 (A), 23 (B), 24 (C) and 26 (D)

4-day-old Caco-2/TC7 cells at 80-90% confluence were incubated with 5 μ M of desired molecule for 1h. Observed with a Leica confocal microscope in phenol-red-free DMEM. Image processing achieved with FIJI.

2.3.1.3. Conclusions on cell-imaging

To date few groups have reported working with the commercial AHL-FITC **12** and only Vikström and co-workers did so in Caco-2 cells, which makes comparisons scarce.

The existence of a membrane receptor was first suggested by Shiner et *al.* in 2006.³¹¹ The authors demonstrated AHL interactions with membranes on artificial models and natural T-cells.⁴⁰⁹ The 3oxoC₁₂-HSL especially interacted with the lymphocytes in a cooperative binding mode, thus suggesting the existence of an AHL membrane receptor.

In 2012 Vikström and co-workers identified IQGAP1 as AHL partner in Caco-2 cells by means of pulled-down assay and laser scan microscopy.³²⁰ Their images were obtained on Caco-2 monolayers treated with 1µM AHL-FITC for 1 to 60 min. In their report green signal appeared as soon as 5 min and localizes primarily in the cell nuclei throughout the experiment. At 20 min a faint stain of the cellular outer membrane is (hardly) perceptible, but disappears at 60 min. Based on this transient stain, the authors concluded on colocalization of FITC-tagged AHL **12** with the IQGAP1 immunostaining.

Using fixed Caco-2/TC7 cells marked under similar conditions with probe **12**, we were not able to reproduce those results ; only nuclei or the perinuclear area appeared stained with green fluorescence in our model. Comparison with control carboxy-FITC **13** rose even more questions, as it returned similar staining to **12**. As far as we know, no other group has provided evidence of AHL-FITC lack of specificity on fixed cells using a closely related AHL-free fluorophore.

To prove specificity, Gaida et *al.* have however performed competitive assay of AHL-FITC with native AHL **1** under cytofluorometric conditions : they were able to displace binding of **12** with **1** (ratio of molecules not provided but AHL-FITC is employed at 100µM in their experiments...).⁴¹⁰ This result joins our observations on live Caco-2/TC7 cells, under which conditions we report a specificity of FITC-tagged AHL **12** versus its carboxyFITC counterpart **13** (no signal was observed with control), but also quenching of the green fluorescence from a 1:20 ratio of **12** versus **1**. These result was not entirely reproduced using the unsaturated AHL **2** as competitor, which induced signal decrease but was not able to abrogate it entirely despite a ratio of 1:100 **12/2**. Higher ratios were not investigated by fear of toxicity.

The incapacity of **2** to displace AHL-FITC was quite unexpected. Though, Caco-2/TC7 cell assays have demonstrated that AHL **2** may either bind the putative AHL receptor(s) with less affinity than **1** or penetrate cells less efficiently, given that both molecules exhibit similar potencies but at different concentrations (5 and 25 μ M respectively). We would have expected to find this 5-fold difference in the fluorescent competitive assays, and yet we did not. We have formulated two hypotheses to explain this unpredictable result: either the addition of FITC - instead of hindering the AHL activity - provides new stabilizing interactions that favour its binding to AHL partner(s) ; or the decreased affinity of **2** has dynamic consequences, meaning that its interactions are slower than those of molecule **1** and 1h is a too short incubation time for full potency of the competing molecule (a result that could not have been predicted given that our inflammatory cell assays last for 18h).

To go further in characterizing the interactions of **12** in cells, we evaluated its effects in our Caco-2/TC7 cell assay. No significantly inappropriate activity was spotted, but the range of concentrations might have been too narrow.

To conclude on IQGAP1, our results in live-cell microscopy do not exclude it as a putative AHL receptor, especially as other quorum sensing inducers structurally close to AHLs have been recently reported to interact with this protein.⁴¹¹ AHL-FITC signal in live-imaging was observed on cell periphery, which is coherent with a transmembrane 3oxoC₁₂-HSL partner, and proved specific through competitive binding assays in this method. The difference in observation between fixed and live cells is yet to understand : we hypothesized the molecule was not fixed in its active site and diffused, and more work will be required to prove this assumption and develop appropriate tools. Highlighting localised and targeted interactions in live-cell imaging can be rather uneasy, as no antibody-based tools can be employed. Several solutions might be considered : as IQGAP1 is a scaffold protein interacting with tight and adherent junction proteins that rely on calcium, treatment of cells with EDTA to destabilize these junctions could provide further information. Otherwise, cell-engineering might be an option through development of cells without IQGAP1 (stable KO lineage or transient shut down with silencing RNA) or expressing fluorescent IQGAP1.

The group of G. M. Hänsch has rather identified the bitter taste receptor member 38 (T2R38) as an AHL partner in mammalian epithelial cells.^{410,412,413} Bitter taste receptors are

GPCRs widely spread across the human body : on top of taste buds, they have been identified on airway epithelial cells, in the brain, ductal pancreatic cells, enteroendocrine colonic cells and recently in lymphocytes.⁴¹⁴ Using AHL-FITC the group reported close spatial localisation between the AHL probe **12** and immuno-stained T2R38, observed at cell membrane but mostly throughout the cytoplasm in vesicles identified as lipid droplets. Such a localisation would appropriately match our observation with AHL probe **26**, which was observed mostly in the cytoplasm as speckled dots. This synthetic molecule has yet to be further investigated : it proved specific towards its fluorophore control **24**, but has not been tested in competitive assays against AHLs **1** and **2** at the moment.

The interaction between AHL and T2R38 was however not strictly established by Hänsch and co-workers, as none of the employed anti-T2R38 antibody was able to displace the green fluorescence from AHL-FITC. To overcome this technical restriction, the authors operated a pulled-down assay by means of an anti-FITC antibody adsorbed on sepharose beads. Analysis by western blotting returned protein T2R38... and IQGAP1.

Interaction between T2R38 and IQGAP1 is not incoherent because T2R38 is a GPCR ; all GPCRs act by detecting molecules outside the cell and activating internal signaling pathways that rely on scaffolding proteins, such as IQGAP1. A question remains: why did Karlsson and co-workers not identify T2R38 as candidate during their pulled down assay (not even as a background protein) while Gaida *et al.* could? The groups employed similar techniques at similar concentrations (93µM vs. 100µM) but with two important different points: different cell lines were used, and one technique was based on biotin sequestration, while the other relied on FITC targeting.

The specificity of T2R38 protein for *N*-Acyl Homoserine Lactones may also be questioned. Indeed, the groups employed highly different concentrations of AHL-FITC probe in cell imaging to identify their targets : where Karlsson and co-workers used 1µM, Hänsch *et al.* required 50µM of the molecule. T2R38 has furthermore been described as “*broadly tuned for bacterial compounds*”.⁴¹⁵ Using a single-cell calcium imaging assay, Verbeurg *et al.* established the receptor could sense micromolar concentrations of a wide array of bacterial metabolites on top of 3-oxoC₁₂-HSL and C₄-HSL, including quorum sensing molecules Agr D1 thiolactone from *Staphylococcus aureus* and CSP-1 from *Streptococcus pneumoniae*. More generally, bitter taste receptors (T2Rs) have been described to bind amino acid derivatives but also PQS from *Pseudomonas aeruginosa*.^{416,417}

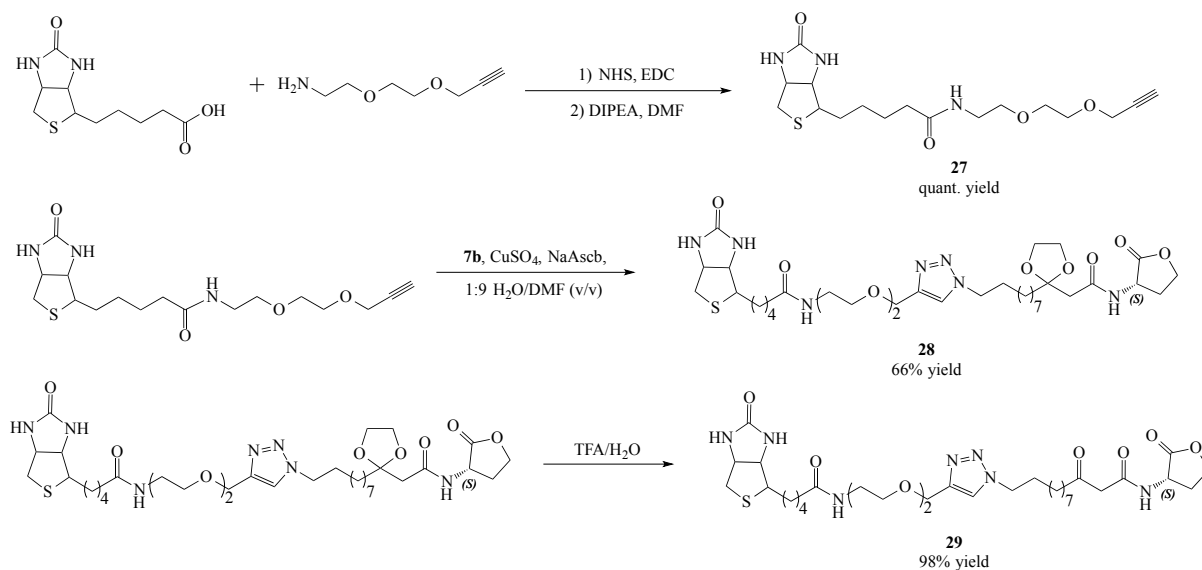
The presence of AHL **1** and its probes in the cell nucleus as observed in fixed-cell imaging is not incompatible either with the hypothesis of PPAR- γ as intracellular receptor, the assumption having been made that AHLs could have several receptors to explain their variety of effects on many cell types. It is yet unclear at the moment why no simultaneous observation has been reported. Because AHL can insert in cell membrane, they may be able to reach intracellular or nuclear receptors without active transport. This insertion phenomenon would however be more impeding at high concentrations.

2.3.2. Design of a biotin-tagged AHL

Biotin-tagged molecules are useful tools in biology, especially to construct experiments such as protein co-immunoprecipitation, flow cytometry, immunohistochemistry... etc. These rely on the high affinity of biotin for streptavidin and avidin, whose strong non-covalent interactions once established require harsh conditions to be broken (highly acidic conditions or high temperatures).

To anticipate future experiments, we thought to construct a biotin-tagged AHL. Previous studies have demonstrated that the addition of a biotin on the HSL headgroup results in loss of activity.^{300,320} Hence, we chose to attach the biotin tag at the acyl tail of 3oxoC₁₂-HSL, using click chemistry and our synthetic azido AHL **7b**. An hydrophilic PEG-based spacer was also inserted in between azido-AHL and biotin, in order to reduce potential steric hindrance, ameliorate water solubility, and increase flexibility to allow multiple conformations and ensure the molecule could accommodate a putative pocket-type active site despite its larger size compared to native AHL.⁴¹⁸

The synthesis of biotin-tagged AHL **29** proceeds in 3 steps (Scheme 17). First, biotin is coupled to 2-[2-(2-propyn-1-yloxy)ethoxy]-ethanamine, used as spacer but also to introduce an alkyne group in the molecule. Intermediate **27** is then clicked to **7b** under aqueous conditions, and the resulting product **28** will be deprotected with TFA to afford final biotin-tagged 3oxoC₁₂-HSL **29**.



Scheme 17 - Three-step synthesis of biotin-tagged 3oxoC₁₂-HSL (compound 29)

The activity of compound **29** was tested in assays on Caco-2/TC7 cell line and luminescent reporter strain *E. coli* pSB1075 (Figure 70). Although not as efficient as natural counterpart **1**, the biotinylated-AHL **29** demonstrated activity for secreted IL-8 reduction in cytokine-stimulated Caco-2/TC7 cells. Especially, one can compare its effects to those of natural 3oxoC₁₂-HSL : on average it appears the biotin-AHL retains 86% of the native AHL capacity to reduce IL-8 secretion in range of concentration 1-25 μM. Activity of **29** is also comparable to that of **1** at 50 and 100μM, but at these dosage neither of the two molecules has anti-inflammatory action of the IL-8 secretion in Caco-2/TC7 cells.

On bacteria strain *E. coli* pSB1075, **29** induces luminescence at much higher concentration than **1**, with an apparent EC₅₀ of 7.6 μM (vs. 9nM for **1**). This result was to be expected as the *Pseudomonas aeruginosa* receptor LasR is highly selective for AHL chain length, as shown by screening of natural AHLs in Table 11.

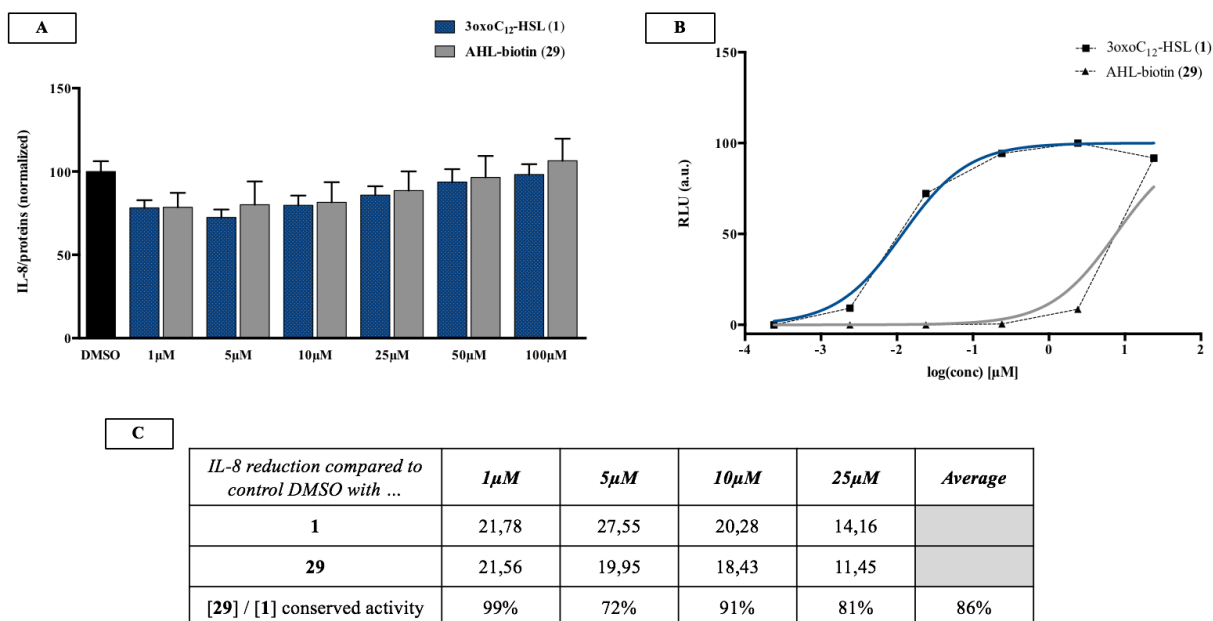


Figure 70 – Biological activity of biotinylated AHL 29

A : Compared IL-8 response of cytokine-stimulated 18-day-old Caco-2/TC7 cells in presence of control DMSO 0.1% or increasing doses of natural AHL **1** or biotin-AHL **29**. No significant difference observed between conditions at same dosage. **B** : luminescent assay on biosensor *E. coli* pSB1075. **C** : summary table of activities of **1** and **29** on Caco-2/TC7 cells.

Our results can be compared with the 2012 study from Karlsson *et al.* and Gaida *et al.*^{320,410} The authors chose to localise the biotin either on the C₃-ketone (turning it into an imine) or on the lactone headgroup ; their compounds are respectively named 3O-C₁₂-HSL-3H-biotin and 3O-C₁₂-HSL-biotin. Comparisons are delicate to established, as both their molecules and protocols differ from ours. The authors use a similar biosensor strain *E. coli* JM109 pSB1075, but compare receptor activation by reading luminescence after incubation at a single dose of 10 ng (neither volume nor concentration is provided). The group nevertheless concludes that 3O-C₁₂-HSL-3H-biotin retains 100% of the native 3oxoC₁₂-HSL activity, while 3O-C₁₂-HSL-biotin exhibits only 65% activity. Our own results lead to a 800-fold increase in EC₅₀.

To record activity in Caco-2 cells, Karlsson *et al.* used a qualitative rather than quantitative tool by comparing the aspect and distribution in confocal laser scan microscopy of junction protein ZO-3 after 5h incubation with 1µM of diverse molecules. The authors conclude no significant difference is observed between native 3oxoC₁₂-HSL and synthetic AHL molecules, which confirms our own conclusions.

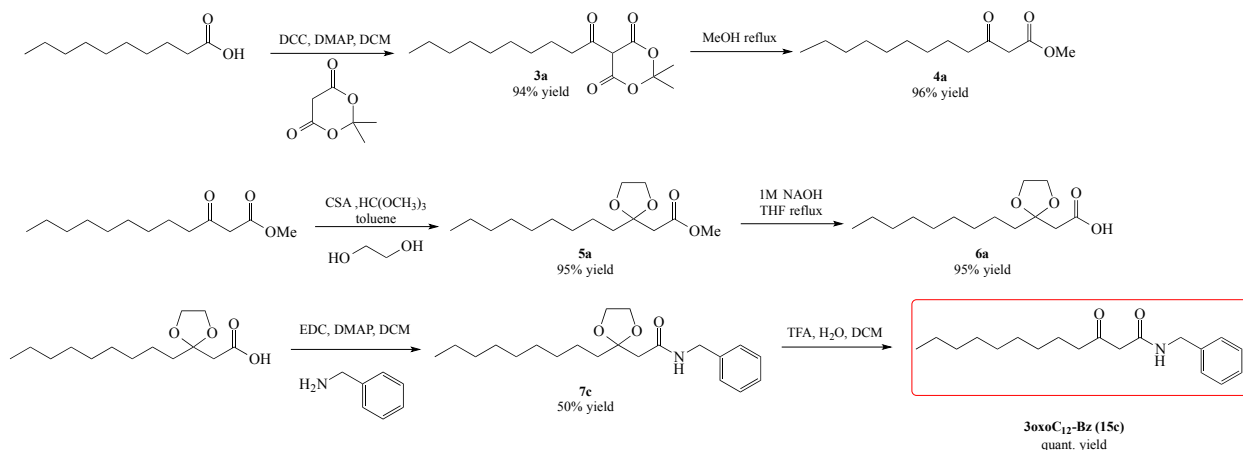
One must deal with protein fishing with care. Indeed, interactions between receptors and biotinylated-molecules can prompt positive outcomes with affinities as high as 10µM, which

denotes a relative low specificity. Furthermore, ligand-protein interactions is not equivalent to biological activity ; it is a requirement, but not an implication.

2.4. AHL, Reactive oxygen species and iron

During the synthesis of clicked molecules we came across a new AHL property : the molecules appears capable to chelate metals. Indeed, Cu-catalysed reactions with the unprotected molecule **15b** kept failing and returned insoluble precipitates. It was then hypothesized that the β -ketoamide structure might be able to chelate the copper in a 1:3 ratio like chelating agent acac (acetylacetonone). No chelating properties of *N*-acyl homoserine lactone have been reported to date ; it has however been shown that tetramic acids were fairly good iron (III) chelators.³²⁸

To study the properties of the β -ketoamide structure, we imagined an AHL analogue with a modified headgroup free of heteroatom to isolate the interactions. A benzyl group was chosen. The analogue **15c** was synthesized according the methodology employed for 3oxoC₁₂-HSL preparation but with a modified step of headgroup coupling (Scheme 18). The overall yield of the synthesis was 14%.



Scheme 18 - Synthesis of AHL analogue 18c

Compound **15c** was employed in cyclic voltammetry. The experiments were performed in collaboration with Dr. Olivier Buriez. This technic studies the electrochemical characteristics of oxidation-reduction transformations in a closed environment. Each resulting curve is specific to a certain redox couple. To investigate the capacity of **15c** to chelate Fe(III), we successively

recorded curves for the metal alone as FeCl_3 , for a solution containing a 1:1 ratio of FeCl_3 and **15c**, and for a solution containing a 1:3 ratio of FeCl_3 and **15c**. The voltammetry experiments were realised in degassed acetonitrile. Although not very physiology-like, this organic solvent was chosen to ease the dissolution of FeCl_3 . Ferric iron is indeed poorly soluble in aqueous solutions at physiological pH, and could only be solubilised in acidic aqueous solutions with pH 2-3 which do not mimic physiological conditions very well either.

The first curve on Figure 71 characterises the redox couples from FeCl_3 . The halogenated iron specie could theoretically form three species, but given that MeCN is not a very coordinating solvent, only one specie predominates, as shown by the reductive wave observed at approximately 0V. This reduction creates two species (at least) in equilibrium, as shown by presence of two oxidation waves at negative intensities.

The addition of one equivalent of ligand induced small but noticeable modifications to the curve, with the apparition of a reduction wave. This new reduction wave is probably linked to the formation of a new complex specie in the medium. The addition of three equivalents of ligand further modifies the curve : the intensity of the new reduction wave increases with the concentration in **15c** and in the newly generated complex specie FeL_x , at the expense of the first reduction wave. Thus, the complexation of Fe(III) displaces the natural equilibria observed in the absence of ligand. Oxidation waves also get modified with the addition of three equivalents of **15c** : the increase in current indicates that the generated complex specie is stable (at least at the time scale of the experiment), and itself stabilises iron into its (III)-oxidation state.

From these results we can assume **15c** has a similar behaviour as acac, and especially a similar hexadentate valence (**Erreur ! Source du renvoi introuvable.**).

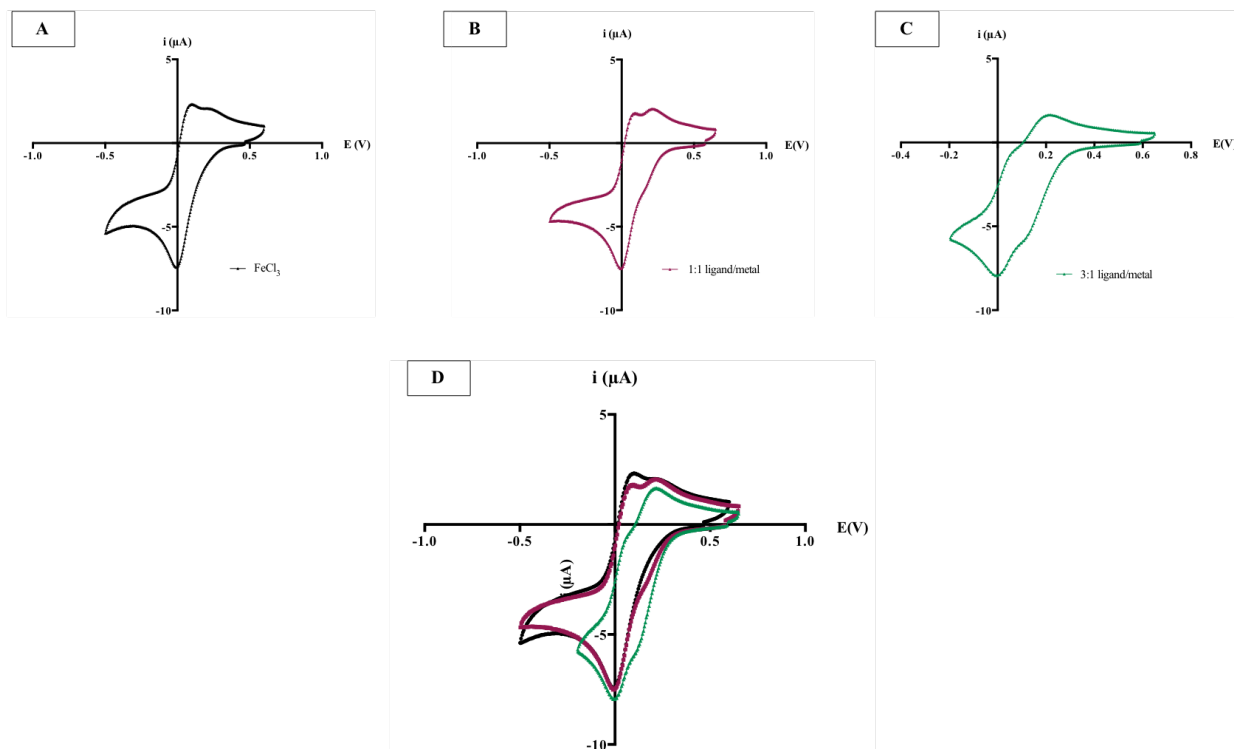


Figure 71 - Cyclic voltammetry of FeCl_3 in presence of several equivalents of ligand

Voltammograms were recorded at room temperature in anhydrous acetonitrile containing 0.1M TBA- BF_4 using a saturated KCl reference electrode, a platinum disk auxiliary electrode and a glassy carbon working electrode. **A** : FeCl_3 alone. **B** : 1 equivalent of FeCl_3 and 1 equivalent of ligand. **C** : 1 equivalent of FeCl_3 and 3 equivalents of ligand. **D** : superimposed curves.

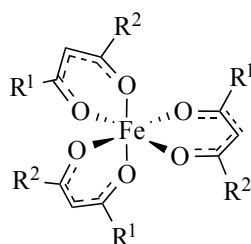


Figure 72 - Structure of an hypothetical 3:1 hexadentate complex between Fe(III) and ligand 15c

R^1 and R^2 are hypothetical substituents.

Living organisms rely on ferric iron for pleiotropic functions, but iron at this oxidation state is poorly available in neutral water (as opposed to iron(II) which is highly soluble in water). Hence, bacteria have developed many strategies to optimize their iron intake by producing siderophores that can directly bind iron (III), or siderophores that can bind iron (II) that will be oxidised to iron (III) once inside the cell.

Assuming AHL are good chelators, they might be able to bring their iron load inside mammalian cells, or participate to the regulation of this iron. In cells, ferric iron can participate to Fenton reactions to produce extremely reactive hydroxyl radicals belonging to the larger class of Reactive Oxygen Species (ROS). Hence, we thought to examine the impact of AHL on ROS production in resting Caco-2/TC7 cells. To do so an intracellular ROS probe was employed, the 2',7'-dichlorodihydrofluorescein diacetate (H₂-DCFDA). This cell permeable probe diffuses inside cells and is diacetylated by cellular esterases into 2',7'-dichlorodihydrofluorescein (H₂-DCF). This specie will then be oxidised in presence of ROS into the highly fluorescent 2',7'-dichlorofluorescein (DCF), with respective excitation and emission wavelengths of 498 and 522nm. The oxidation of H₂-DCF was originally thought to be H₂O₂-specific, but recent evidence have proved the molecule could react with a larger scope of ROS such as hydroxyl radicals, superoxides and peroxynitrites.

Caco-2/TC7 cells grown on dedicated black 12-well plates with glass bottom were incubated with 50µM H₂-DCFDA during 30 min. The medium was removed and the cell rinsed with PBS, and solutions of AHL 1 in phenol-red-free DMEM were distributed. Fluorescence was then recorded over 24h. DMEM and DMSO were used as controls. At first sight, the 5 condition curves display parallel time evolution, but differences appear when we focus on time span 0 – 4h, before a more or less linear behaviour appears (Figure 73). In time frame 0 – 4h, the curves exhibit different behaviours, especially control DMSO which induces a steeper increase in fluorescence, hence in ROS production. The lowest curves are conditions DMEM and 100µM AHL, while curves 1 and 10µM cluster together in an intermediate position. To highlight differences even more, we can define the DMEM curve as a baseline, and study the fold increase from the other curves. With this technique appear two types of behaviour among samples : DMSO, 1µM and 10µM curves show a steep increase in ROS production to reach a maximum after half hour of incubation. The curves slowly normalize to reach the baseline approximatively at 3h, while DMSO will remain at higher level through the course of the whole experiment. The addition of DMSO seems to induce a rapid stress to the cells with lasting effects, that is moderately compensated by the addition of AHL 1 in low concentrations. On the opposite the curve 100µM does not show any fluorescence increase, but goes down to reach baseline within 1h ; this suggests that the DMSO-dependent increase in ROS production is completely rescued by the presence of AHL at high dosage.

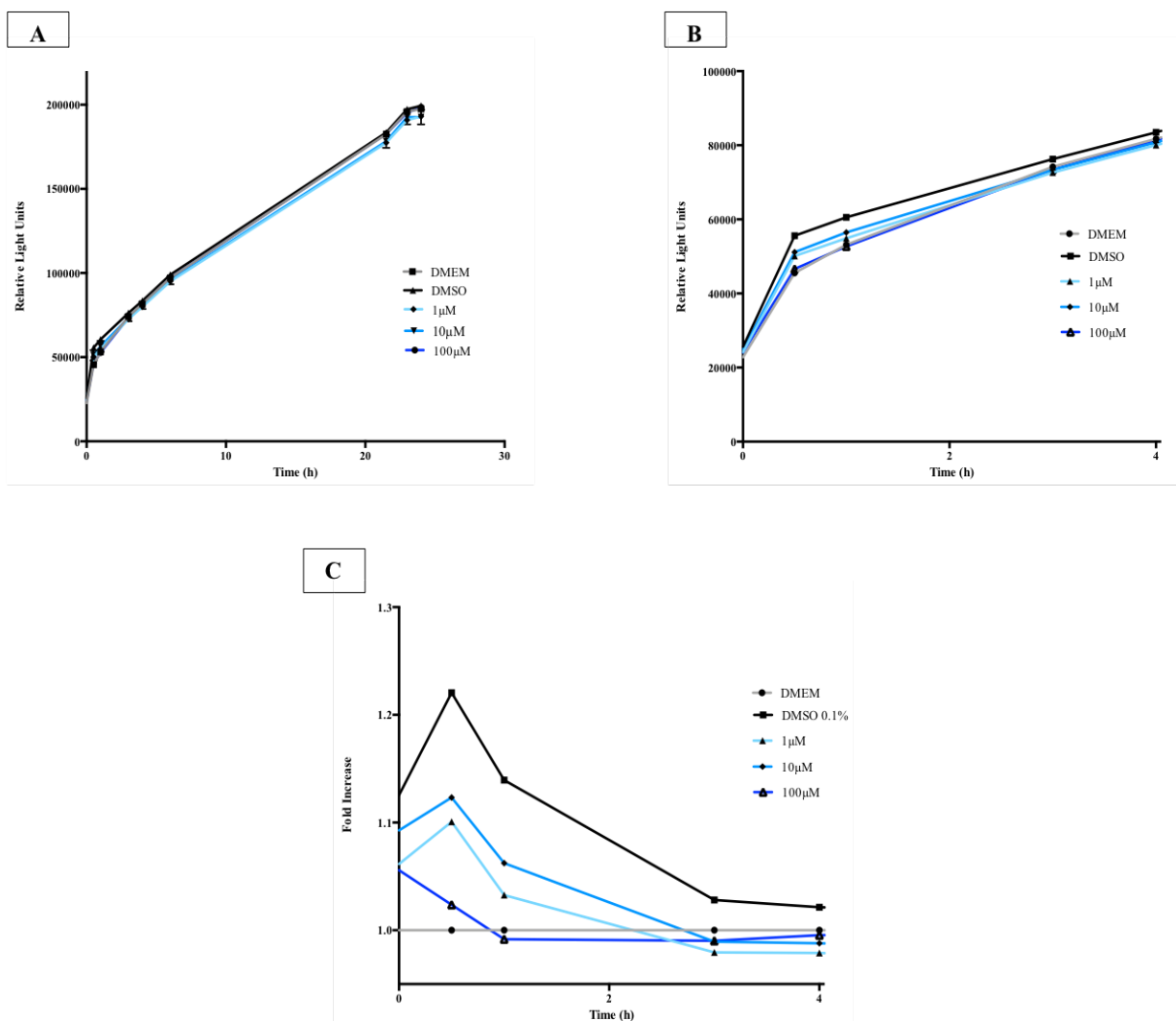


Figure 73 – Fluorescence emitted by probe H₂-DCFDA upon oxidation by intracellular ROS

5-day-old Caco-2/TC7 cells were pre-incubated with 50 μM H₂-DCFDA for 30 min and then exposed to increasing concentrations of 3oxoC₁₂-HSL or controls. **A** : time evolution of fluorescence over 24h. **B** : magnification over 4h. **C** : fold increase in fluorescence over 4h. The points are the mean of several replicates (n = 3) ± SEM.

Although promising these results will need further confirmation via new experiments. The chelating properties of ligand **15c** should be investigated deeper by means of UV-vis spectroscopy, and the related kinetic and thermodynamic constants characterized. The whole study should also be performed using the native AHL **1** to be able to infer biological effects. Similarly, ROS experiments should be repeated. Given the low amount of iron present in basic cell culture medium, iron supplementation might exacerbate our observations. On the opposite, abolition of AHL effects upon addition of iron chelator would corroborate the AHL *in vitro* chelation.

If proved real, the AHL modulation of ROS secretion cannot account for all the reported AHL effects in mammalian cells. (*S*) and (*R*) enantiomers of the 3oxoC₁₂-HSL have very different activities on cell models while they should have similar chelating behaviours ; chelation is indeed independent from the stereochemistry of the lactone ring.

Part II : Structure Activity Relationship

Study & Pharmacomodulation

1. Construction of a library of synthetic natural and non-natural compounds

The previous chapters focused on two *N*-Acyl Homoserine lactones with close structures, both characterised by a twelve-carbon-long acyl chain, an oxo pattern at carbon-3 and a lactone headgroup. We presented a large spectrum of their properties, in terms of mammalian and bacterial biology, but also chemical and metabolic stability. These natural molecules possess interesting anti-inflammatory but certainly too limited to turn them into lead compounds, and are disadvantaged by their instability over time. If in the mindset of a therapeutic agent absorbed by the GI tract, the molecules capacity to act on quorum sensing and modulate phenotypes in the microbiota may also be drawback, especially in a context of IBD patients who already harbour relapsing inflammation and a dysbiotic background.

In order to better identify which chemical features of native AHL were responsible for their biological activity, we performed a Structure-Activity Relationship study using AHL analogues. In the following part we will define molecules as being AHL analogues based on the definition from Galloway R. J. et al. stating them as “*compounds that contain a carbon chain (of any functionality or substitution) or aryl group linked to an amide group [...], the nitrogen atom of which is directly attached to a ring system at a chiral carbon*”¹⁹⁸.

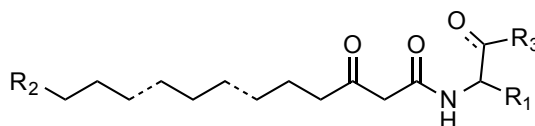


Figure 74 - General frame of *N*-Acyl Homoserine Lactone analogues

Dashed bonds indicate localisation of a potential insaturation. R₁, R₂, R₃ are chemical groups.

Previous publications have defined important requirements for full AHL activity on mammalian cell lines, among which the integrity of the lactone head, an acyl chain ranging from 10 to 14 carbons and an oxo or hydroxyl substitution at carbon-3.^{277,278,294,300}

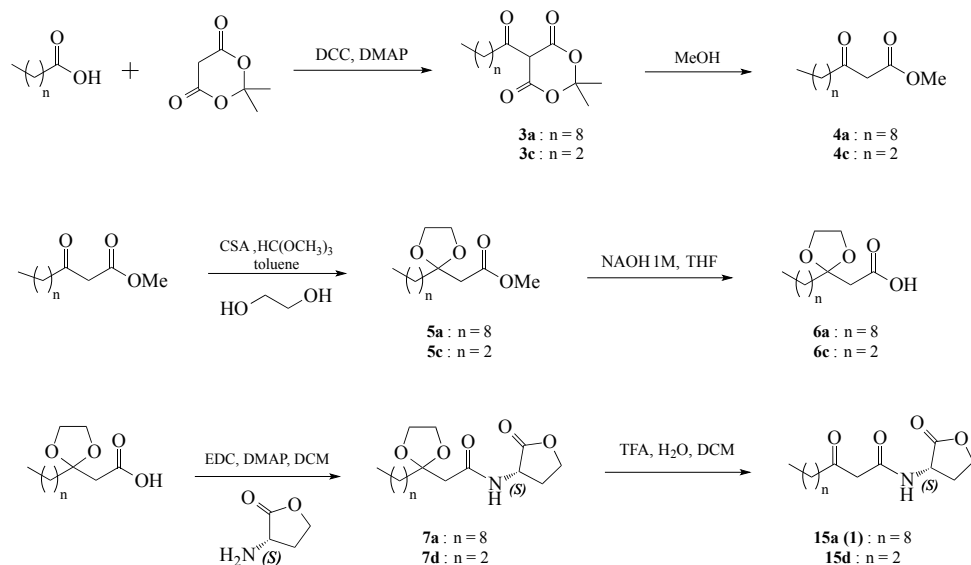
Based on this knowledge and using 3oxoC₁₂-HSL (**1**) as a framework, we designed a library of twenty compounds to study the specific influence on the activity of **1** of the oxidation pattern of carbon-3, the acyl chain and the headgroup. In first intention, the analogues were as far as possible tested in our mammalian and bacterial assays : cytotoxicity, IL-8 and/or IL-6 secretion modulation, and activation of LasR receptor.

1.1. Natural *N*-Acyl-Homoserine Lactones

Many natural *N*-Acyl Homoserine Lactones have been identified to date as secreted by bacterial populations. On top of AHLs **1** and **2** previously studied in chapter 2, we have chosen to work with four extra natural AHLs, among which the *L*-3-oxo-hexanamide-homoserine lactone **15d** (3oxoC₆-HSL), the *L*-dodecanoyl-homoserine lactone **27** (C₁₂-HSL), the *L*-butyryl-homoserine lactone **28** (C₄-HSL), and the *L*-3-oxo-tetradodecanoyl-homoserine lactone **29** (3oxoC₁₄-HSL).

These molecules were chosen to represent the large variety of existing AHLs ; they have various chain lengths from 4 to 14 carbons, and two of them harbour a ketone group at the carbon-3 position, while the other two do not.

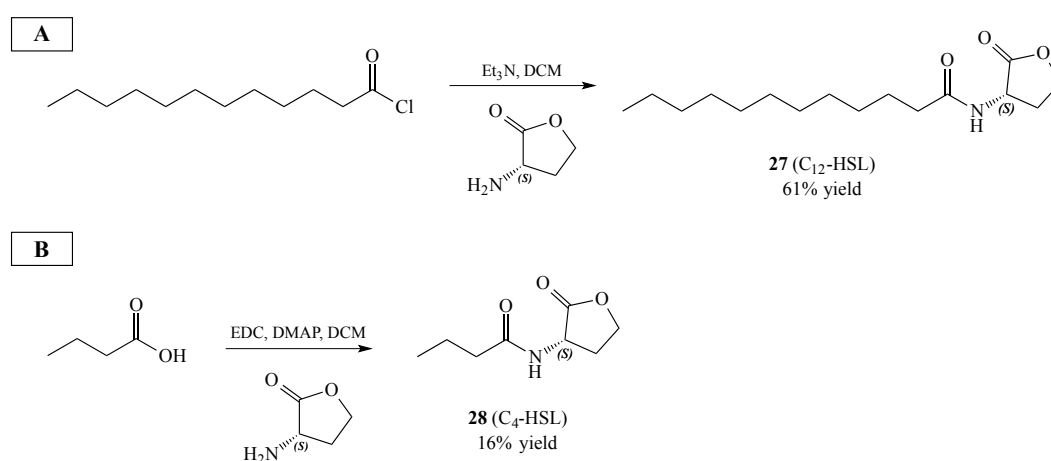
The synthesis of oxo-AHLs relies entirely on the method developed to prepare compound **1** as illustrated in *Part I - 1.1*. The choice of initial carboxylic acid varies depending on the final target molecule, but the methodology remains unchanged (Scheme 19). Of note, the 3oxoC₁₄-HSL (**29**) only was not synthesized but commercially sourced.



Scheme 19 - General methodologies for synthesis of natural 3oxo N-Acyl Homoserine Lactones

Overall yield is 73% for 3oxoC₁₂-HSL **1** (aka **15a**) and xx % for 3oxoC₆-HSL **15d**.

The synthesis of non-3-oxo AHLs is pretty straight forward, and requires only coupling of an appropriate acyl chain precursor with the (*S*)-(-)-(α)-amino-(γ)-butyrolactone hydrochloride headgroup. Two approaches were compared for such coupling: first, an Et₃N-mediated coupling with an acyl chloride to yield C₁₂-HSL **27** (Scheme 20A) ; then the EDC- and DMAP-supported coupling with a carboxylic acid to yield C₄-HSL **28** (Scheme 20B). The second approach gave significantly lower yield (16% vs. 61%), which was to be expected given the reduced reactivity of carboxylic acids versus corresponding acyl chlorides.



Scheme 20 - Compared synthetic routes for non 3-oxo natural AHLs preparation

A : Et₃N mediated strategy. **B** : EDC and DMAP mediated strategy.

1.2. Introduction to AHLs non-natural analogues

To study the involvement of the natural lactone headgroup in the AHL activity in our biological models, a series of 12 synthetic analogues with modified cyclic headgroups but retaining the native pattern of a 12-carbon-long acyl chain and 3-oxo substitution was produced. It was chosen to investigate cyclic headgroups only based on our own experiment ; as demonstrated in *Part I* with the study of analogues bearing amino acids, the headgroup should be polar but not too hydrophilic, and a cyclic conformation is preferred to its extended equivalent (result based on the differences between the alanine and β -alanine analogues).

The non-natural cyclic headgroups were selected with regards to four parameters:

- the stereochemistry of the carbon in α -position to the lactone ring,
- the influence of electron-donating atoms in the ring,
- the ring size,
- the capacity to be hydrolysed.

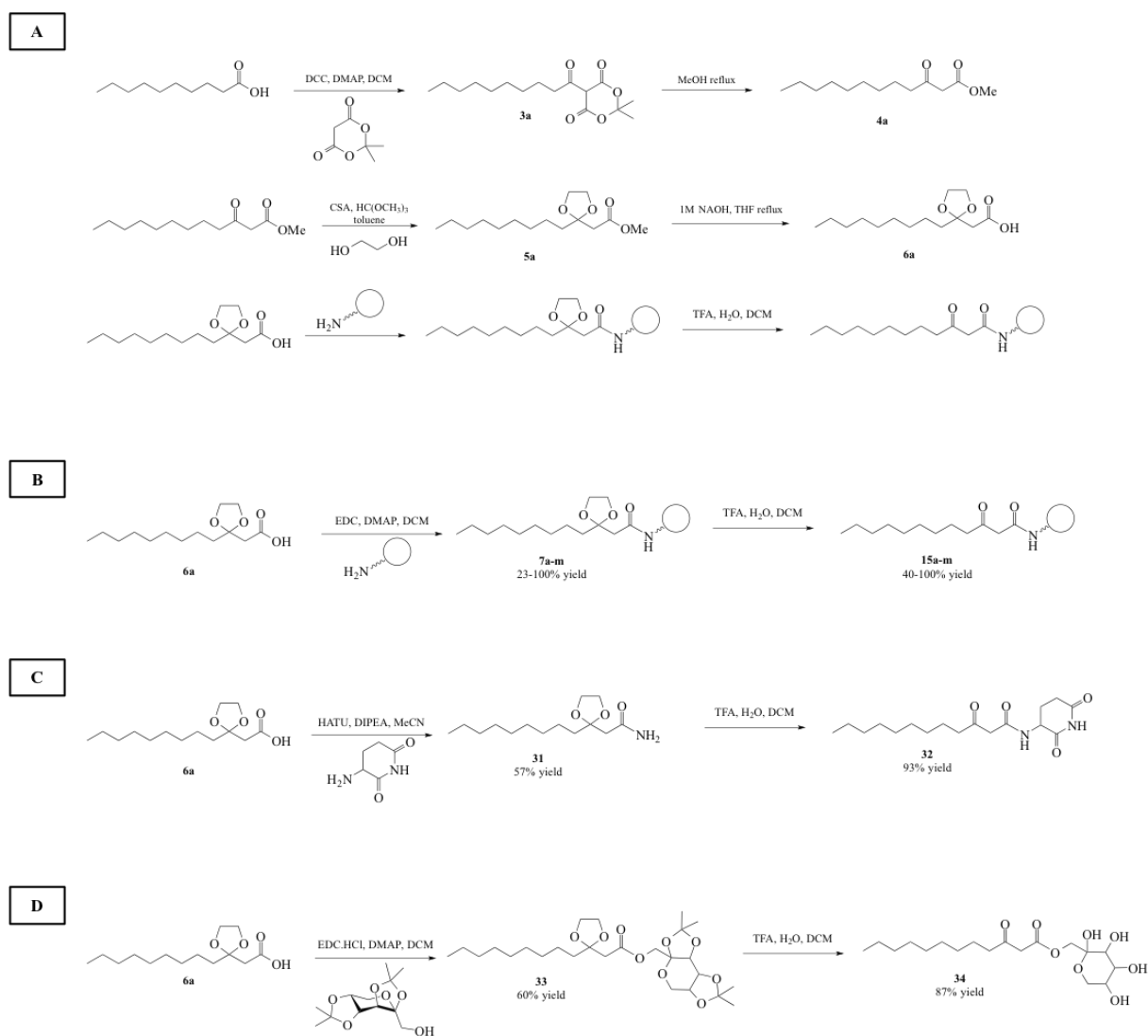
The stereoselective of the carbon in α -position to the lactone is crucial in natural AHLs, where only the (*L*)-enantiomer (hence a α -carbon with a (*S*)-configuration) is active. Chhabra *et al.* have in particular demonstrated in a splenocyte proliferation assay that the immunomodulatory activity of AHL depended critically on their (*L*)-conformation. Where possible the (*S*)-stereochemistry was conserved and the reverse enantiomer was synthesized for comparison. On the opposite side, some headgroups were voluntarily selected for their planar structure, i.e. compounds with aromatic headgroups.

All headgroups but one (**15o**) include electron-donating atoms, whose lone pairs must promote H-bonds formation and non-covalent interactions of the molecule in its active site. These electron-donating atoms and their mode of binding to the ring core have been varied : we included sulphur atoms, diketoamide, hydroxyl and methoxy groups, but also carbohydrate moiety.

The native homoserine lactone contains five atoms. Trying to respect the proportions and 3D-structure of native molecules, we limited the synthetic headgroup sizes to five and six atoms, in order to appropriately mimic the size of the natural ring.

Finally, most of the chosen synthetic compounds cannot be hydrolysed to open forms, thus they are resistant to lactonolysis by both enzymatic and pH-dependent fashions. Three hydrolysable molecules were included : the (*R*)-lactone and thiolactone rings are sensitive to hydrolysis.

The synthesis of non-natural AHL analogues with cyclic headgroups was based on the six-step methodology developed for the preparation of natural 3-oxo AHLs **1** and **2** (Scheme 21), except for the headgroup coupling step, where reagents and coupling conditions were varied based on literature.⁴¹⁹



Scheme 21 - Synthesis for preparation of non-natural AHL analogues with cyclic headgroups

A : general synthetic path. **B** : EDC- and DMAP-mediated coupling, employed for most analogues. **C** : HATU and DIPEA-mediated coupling, employed for the amino-diketopiperidine headgroup. **D** : EDC- and DMAP-mediated coupling employed for protected sugars, affording ester-type linkage of headgroup.

In summary, we have prepared a library of 19 compounds, considered analogues of the 3oxoC₁₂-HSL **1**. These are summarised in the following Table 15, classified by category of modification.

<i>Entry</i>	<i>Category</i>	<i>Usual Name</i>	<i>Structure</i>
1 (15a)	Control	3oxoC ₁₂ -HSL	
2	Modified acyl chain	3oxoC ₁₂ :2-HSL	
15b		12azido-3oxoC ₁₂ -HSL	
15d		3oxoC ₆ -HSL	
28		C ₄ -HSL	
29		3oxoC ₁₄ -HSL	
30		γ-butyrolactone	
7a		Modified lactone	-
27	C ₁₂ -HSL		
15c	Modified cyclic headgroup	-	
15e		(<i>R</i>)-3oxoC ₁₂ -HSL	
15f		(<i>D/L</i>)-3oxoC ₁₂ HTL	
15g		(<i>S</i>)-3oxoC ₁₂ -HTL	
15h		(<i>S,S</i>)-3oxoC ₁₂ -ACH	

15i		(<i>R,S</i>)-3oxoC ₁₂ -ACH	
15j		-	
15k		-	
15l		-	
15m		-	
32		-	
34		-	

Table 15 - Overview of all prepared and employed AHL analogues during the SAR study

2. Structure Activity Relationship study

All the synthetic AHL analogues were tested on mammalian cell lines and bacterial models. All results were compared to the effects obtained with the natural 3oxoC₁₂-HSL as reference compound, which was regarded as a standard to improve. The objective of the Structure Activity Relationship study was to ameliorate the anti-inflammatory properties of the natural molecule on mammalian cell, while decreasing its ability to activate Quorum Sensing receptors in bacteria and increase its stability.

2.1. Compared results on mammalian cell lines

2.1.1. Importance of the keto group

Two molecules were employed to evaluate the influence of the ketone located on carbon-3 of the natural 3oxoC₁₂-HSL : molecules **27** and **7a**.

Compound **27** or C₁₂-HSL is a natural AHL, natively secreted by *Burkholderia vietnamensis* G4, *Pseudomonas fuscovaginae* and *Chromobacterium violaceum* by instance.^{420–422} Its structure is extremely close to that of AHL **1**, except for its oxidation pattern at carbon-3, which carries simple protons. Compound **7a** is the last intermediate in the preparation of **1** (cf. Scheme 19) ; the ketone of the molecule is still protected with a ketal, a much bulkier and less polar group than the native moiety. Together these molecules were used to examine the influence on AHL **1** activity of the absence or the substitution with larger groups of its ketone.

The molecules were tested on both cell lines Caco-2/TC7 and Raw 246.7 according our established protocols (Figure 75). None of the molecules induced significant toxicity in any of the cell lines, and the 10%-secreted-LDH threshold was not exceeded. The activity of the molecules on IL-8 and IL-6 secretions in Caco-2/TC7 cells and Raw 264.7 macrophages respectively, were however impacted by their morphological changes. Compound **7a** shows an overall no activity (secretion on average close to the 100% response), with even pro-inflammatory behaviour at high concentrations, which is 100µM on epithelial cells and 50µM on macrophages. The C₁₂-HSL (**27**) exhibits different behaviours depending on the concerned cell line. On macrophages, similarly to **7a**, its overall effect is rather null. But on epithelial cells it has a less linear behaviour ; in range 1 – 25µM it follows the same variations as **1**, although always with slightly higher IL-8 secretion. In this range of dosage, **27** retains on average 72% (53% - 83%) of the activity from **1**. Surprisingly, at 50 and 100µM **27** is more active than the reference AHL, with respective 4- and 18-fold ameliorations of the inflammation reduction.

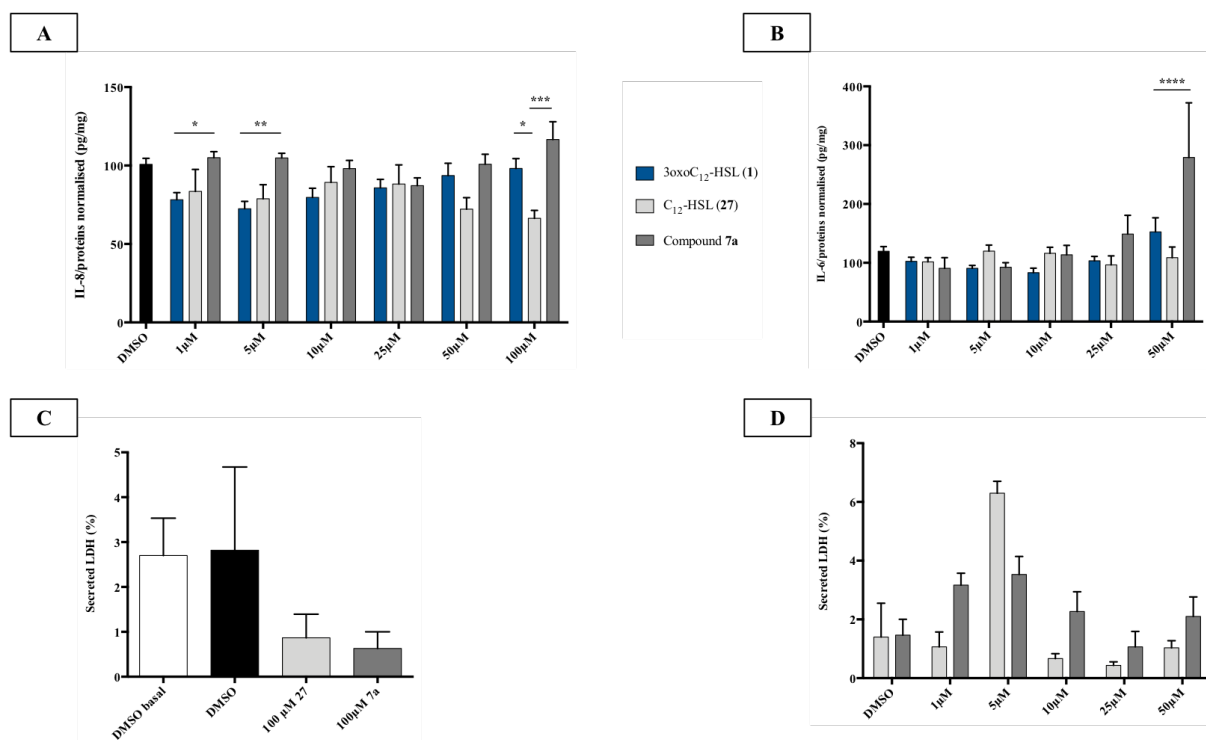


Figure 75 - Compared properties of 3oxoC₁₂-HSL (1), C₁₂-HSL (27) and analogue 7a on our cell models

A : IL-8 response of cytokine-stimulated 18-day-old Caco-2/TC7. *p < 0.05, **p < 0.01, ***p < 0.001 ; two-way ANOVA, Tukey's post- test. **B** : IL-6 response of cytokine-stimulated Raw 264.7 macrophages. ****p < 0.0001 ; two-way ANOVA, Tukey's post- test. **C** (resp. **D**) : secreted LDH (%) under stimulatory conditions in Caco-2/TC7 cells (resp. 264.7 macrophages). The points are the mean of several replicates (n ≥ 6) ± SEM.

Literature is scarce on the effects of compound **7a** in cell assays. Only DiMango *et al.* tested this molecule in the context of IL-8 secretion in resting human airway epithelial cells (IHAEo cells)³⁰⁸. The group demonstrated it had no effect on IL-8 secretion, as opposed to parent 3oxoC₁₂-HSL. This is in line with our own results, where analogue **7a** is inactive in both cell lines, with cytokine secretion certainly due to the presence of DMSO only. The increase in secretion at higher concentrations might be due to the stress provoked by the accumulation of xenobiotics. No data regarding cytotoxicity of **7a** is reported.

More information can be gathered about C₁₂-HSL **27**. Overall the molecule is reported to have no or very moderate effects on immune cell viability, as assayed on mouse macrophage cell line P388D1 and human macrophage cell line U-937.^{276,277} No data is provided on epithelial cells.

Very diverse effects have been reported for compound **27** throughout literature, sometimes describing the molecule as active and other as inactive. Gomi *et al.* described positive-

modulation of pro-inflammatory cytokines and NF- κ B activation in resting immune cells, with increased secretion of TNF- α and IL-1 β in Raw 264.7 macrophages and IL-8 in human monocytes THP1.⁴²⁰ On the opposite, both groups from S. R. Chhabra and E. DiMango found that the C₁₂-HSL exhibited no activity or a significant loss of activity compared to parent 3oxo C₁₂-HSL. Chhabra *et al.* reported a 13-fold increase in the IC₅₀ of **27** compared to **1** (52 μ M vs. 4 μ M) in a splenocyte proliferation assay, while DiMango and co-workers found no significant modulation of IL-8 secretion in resting human airway epithelial cell line IHAEo.^{300,308}

Our own observations can be compared with one or the other of the two theories. On one hand, no significant effect is observed on macrophages with values of IL-6 secretion in the range of action of DMSO at all concentrations. On the other hand, we can see a significant activity on epithelial intestinal cells. We should however keep in mind that our results regard cytokine-activated cells.

2.1.2. Importance of the acyl chain

In total, six molecules were compared to reference AHL **1** in order to identify beneficial/detrimental modifications of its acyl chain : γ -butyrolactone **30** has no acyl chain at all, C₄-HSL and 3oxoC₆-HSL have shorter chains than **1**, 3oxoC₁₄-HSL has a longer chain, and 3oxoC_{12:2}-HSL has an unsaturated chain.

2.1.2.1. Shorter acyl chains

The γ -butyrolactone is used to model the lactone core of the AHL. It is itself a quorum sensing autoinducer for Gram-positive bacteria such as *Streptomyces* (cf. Part I-2.1.2.4.5). C₄-HSL and 3oxoC₆-HSL are two natural short-chain *N*-Acyl Homoserine lactones. The C₄-HSL has no substituent on carbon-3. It belongs to the Quorum sensing triumvirate of *Pseudomonas aeruginosa*, but is also natively secreted by several *Aeromonas* bacteria, *Cedecea neteri* and *Serratia liquefaciens MG1* for example.^{423–427}

The molecules were tested on both cell lines Caco-2/TC7 and Raw 246.7 according our established protocols (Figure 76). None of the molecules induced significant cytotoxicity in the intestinal epithelial cell line. In Raw 264.7 macrophages however, analogues **15d** and **28**

exceeded the 10%-secreted-LDH threshold : C₄-HSL showed increased toxicity from 25μM to reach about 10% secreted LDH at 50μM, while the 3oxoC₆-HSL was toxic from 25μM and above.

The three analogues show overall no effect in the range 1-15 μM on macrophages. At 25μM and 50μM, C₄-HSL and 3oxoC₆-HSL exhibit steep increases in IL-6 secretion, quite certainly linked to the increased toxicity. The γ-butyrolactone has however rather opposite behaviour, with decreases in IL-6 levels about 20% and 27% compared to reference DMSO.

The overall conclusion on cytokine-activated Caco-2/TC7 cells, is that shortening the acyl chain leads to reduced activity. Indeed, in range 1-25μM exhibit little/no effect, and reference 3oxoC₁₂-HSL induces significantly lower IL-8 levels. At higher concentrations (50-100μM) all effects are abolished for the tested molecules, although the γ-butyrolactone shows small but non-significant decrease in IL-8 secretion.

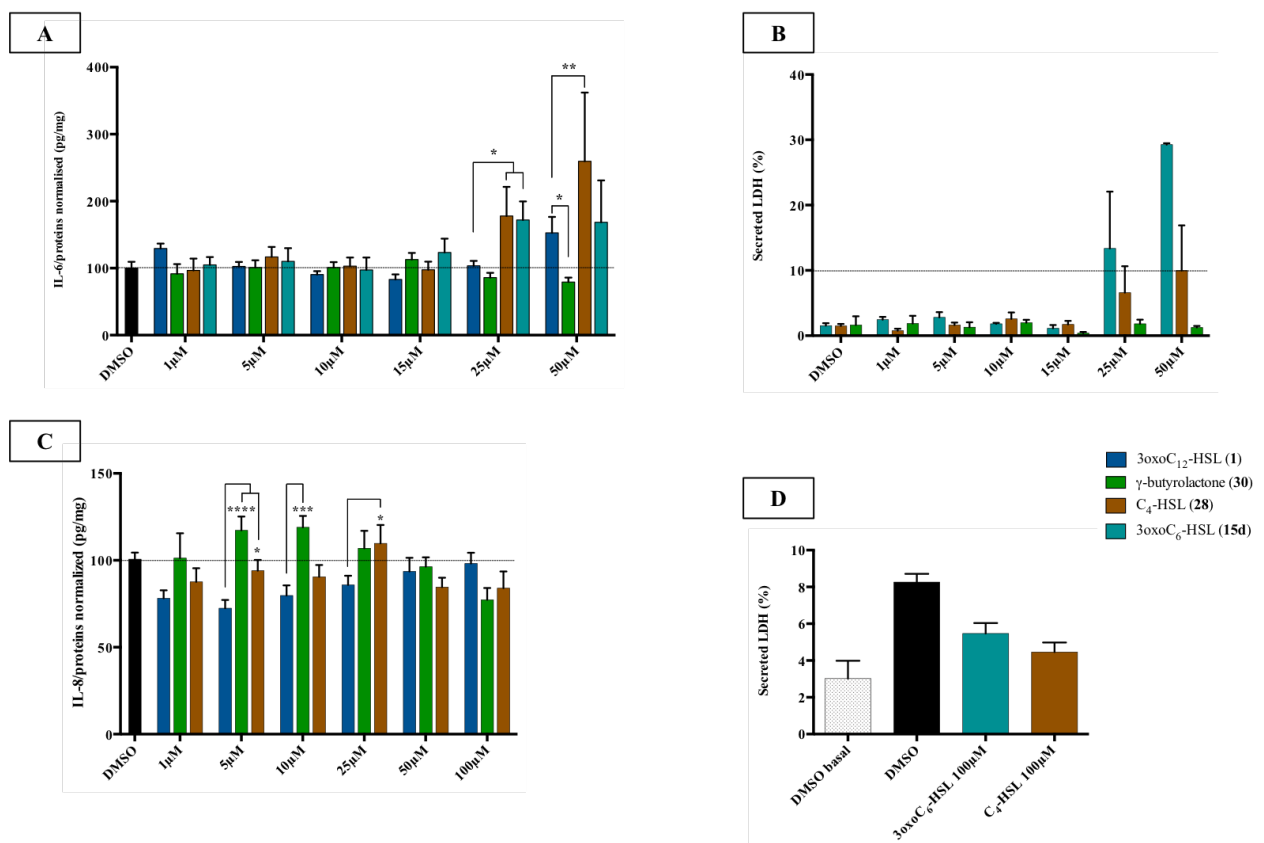


Figure 76 - Compared properties of 3oxoC₁₂-HSL (1) versus short-chain analogues γ-butyrolactone (30), C₄-HSL (28) and 3oxoC₆-HSL (15d) on cell models

A : IL-6 response of cytokine-stimulated Raw 264.7 cells. *p < 0.05, **p < 0.01 ; two-way ANOVA, Tukey's post- test. **B** (resp. **D**) : secreted LDH (%) under stimulatory conditions in 264.7 macrophages (resp. Caco-2/TC7 cells). **C** : IL-8 response of cytokine-stimulated 18-day-old Caco-2/TC7. *p < 0.05, ***p < 0.001, ****p < 0.0001 ; two-way ANOVA, Tukey's post- test. The points are the mean of several replicates (n ≥ 6) ± SEM.

2.1.2.2. Longer acyl chains

Two molecules were compared to reference 3oxoC₁₂-HSL to examine the effect of a moderate increase in acyl chain length : the 3oxoC₁₄-HSL (**29**) and the 12azido-3oxoC₁₂-HSL (**15b**) developed for click chemistry and presented in *Part I-2.3.1.2.1*.

The 3oxoC₁₄-HSL is a natural AHL natively secreted by *Yersinia enterocolitica* and *Burkholderia pseudomallei* among others.^{253,283} It could also be detected in *Pseudomonas aeruginosa* model biofilms.³⁸⁵ This molecule has an acyl chain longer than that of AHL **1** by two carbons, which increases its flexibility and lipophilicity. Analogue **15b** is longer than **1** by the addition of an azido group, which consists of three doubly-bound and charged nitrogen atoms (as the main resonance structure). Because double bonds are shorter than single bonds, his moiety is not much bigger than the ethyl group (CH₂CH₃) added to obtain **29**. Hence the two molecules have sizes of the same order of magnitude ; they however differ greatly in terms of polarity. **15b** have an estimated TPSA of 122.22 Å² when both **1** and **29** exhibit TPSAs of 72.47 Å².

The three molecules – reference AHL and its two analogues – were first tested on Caco-2/TC7 cells (Figure 77). Although very close to **1** in terms of physico-chemical properties, the 3oxoC₁₄-HSL exhibits a very different pattern on cell toxicity. Where no cytotoxicity had been observed with 3oxoC₁₂-HSL in range 1-100µM, the analogue **29** shows increased secreted LDH from 50µM and exceeds the 10%-threshold at 100µM, hence limiting its range of action. On the opposite, analogue **15b** demonstrated toxicity levels very similar to those of reference AHL **1** at 100µM.

Despite this drawback, the 3oxoC₁₄-HSL showed interesting properties in the cell assay, with secreted IL-8 levels of the same order of magnitude than those of AHL **1** in range 1-25µM. Although no significant difference was observed – certainly due to the relatively low number of replicates for **29** (*n* = 6) – molecule **29** showed a constant amelioration of anti-inflammatory properties between 1.3- and 1.7-fold compared to the effects of **1** (Table 16).

The properties of analogue **15b** have already been described in *Part I-2.3.1.2.1*. Overall, the molecule was less active than reference **1**, with more heterogeneous results.

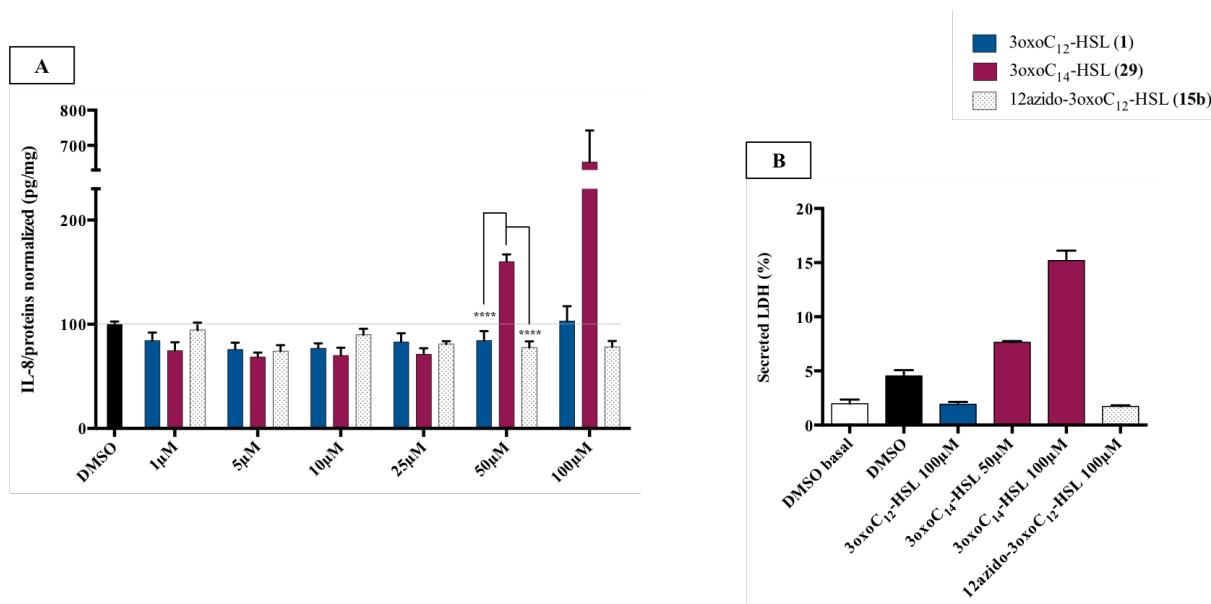


Figure 77 - Compared properties of 3oxoC₁₂-HSL (1) versus long-chain analogues 3oxoC₁₄-HSL (29) and 12azido-3oxoC₁₂-HSL (15b) on cell models

A : IL-8 response of cytokine-stimulated 18-day-old Caco-2/TC7. ****p < 0.0001 ; two-way ANOVA, Tukey's post- test. **B** : secreted LDH (%) under stimulatory conditions in Caco-2/TC7 cells. The points are the mean of several replicates (n ≥ 6) ± SEM.

Dosage (µM)	1	5	10	25
<i>IL-8 secretion with 1</i>	82.24	75.77	76.98	82.99
<i>IL-8 secretion with 29</i>	74.77	68.66	70.14	71.26
<i>Anti-inflammation of 1 (%)</i>	15.76	24.23	23.02	17.01
<i>Anti-inflammation of 29 (%)</i>	25.23	31.34	29.86	28.74
<i>Ratio 29 / 1 (fold variation)</i>	+ 1.6	+1.3	+ 1.3	+ 1.7

Table 16 – Compared efficiency in IL-8 secretion reduction of reference 3oxoC₁₂-HSL (1) and long-chain analogue 3oxoC₁₄-HSL (29)

2.1.2.3. Discussion on acyl chain effects

Overall, the modification of acyl chains have mitigated effects on cellular activity in our models. On one hand, shortening of the chain induced significantly impaired immunosuppressive capacity ; on the other hand, increased chain length showed promising trends for activity but negatively affected the cell viability by increasing cytotoxicity.

In our cell assays, the short-chain AHLs **28** and **15d** but not γ -butyrolactone, appeared inactive. This result is in line with previously published literature, where C₄-HSL and 3oxoC₆-HSL are often used as negative controls to 3oxoC₁₂-HSL. For instance, C₄-HSL exerts no effect on TNF-

α secretion in Raw 264.7 macrophages nor on IL-8 secretion in THP-1 monocytes, and cannot repress cell proliferation of undifferentiated intestinal epithelial cell line IEC-6.⁴²⁰ Similarly, 3oxoC₆-HSL does not affect proliferation of murine leukocytes nor human PBMCs.³⁰⁰ At physiological pH, the γ -butyrolactone (GBL) readily hydrolyses into its open-form counterpart γ -hydroxybutyrate (GHB), a well-known recreational drug. Its effects have been largely investigated on the neuronal system, but data on immune and intestinal cells are scarce, which limits comparison with our own results.

On opposite, the analogues with long acyl chains retained reasonable activity, or were even more active than reference AHL **1**. The 3oxoC₁₄-HSL **29** especially caught our attention as it exerted stronger anti-inflammatory effects on Caco-2/TC7 cells than 3oxoC₁₂-HSL. This result is concordant with literature, where data highlights analogue **29** as an active compound. For instance, Joe et al. reported that 10 μ M of the molecule could reduce IEC-6 cells proliferation in a similar manner to 10 μ M 3oxoC₁₂-HSL, while Chhabra and co-workers revealed **29** was almost as active as **1** on a mouse splenocyte proliferation assay (IC₅₀ of 6.3 vs. 4 μ M) and on human TNF- α release suppression (IC₅₀ of 35 vs. 15 μ M).^{300,428} Valentine et al. studied caspase activation and resulting cell death in Hela and MEFs cells, and demonstrated similar activities of 3oxoC₁₂- and 3oxoC₁₄-HSL in dose range 1-10 μ M.

Overall, data suggest a correlation between acyl chain length and activity on mammalian cells. Davis and co-workers have theorised these observations by demonstrating that acyl chain length positively affects molecular lipophilicity, and by doing so, the AHL capacity to insert in cell membranes. The group established a clear parallel between AHL lipophilicity (modeled by LogP) and insertion in both artificial membrane systems and T-lymphocytes membranes ; in their own words *“increasing AHL acyl chain length from C₈ to C₁₄ increased its immunomodulatory activity in the micromolar range and this was found to negatively correlate with LogP”*.⁴⁰⁹

We have tried to validate this statement on our own library, and computed consensus LogP and TPSA using the SwissADME calculation tool (Table 17). Strikingly, it appears that increasing the chain length at a given number of heteroatoms does not affect TPSA, as opposed to the addition of an azido group for instance, which creates a spike in polarity.

Overall, the predicted results match fairly well the theory for molecules with saturated chains. It is however harder to predict interactions in compounds with insaturations or heteroatoms,

such as **2** and **15b** ; these modifications indeed affect a broad range of physical properties such as flexibility, and not only lipophilicity. Based on Table 17 predictions, it seems that unsaturated chains tend to behave like shorter chains : the LogP prediction for 3oxoC₁₂:2-HSL is closer to that of 3oxoC₁₀-HSL than of 3oxoC₁₂-HSL, while 3oxoC₁₂:1-HSL stands halfway regardless of the localisation of the mono-unsaturation (resp. values : 2.32, 2.19, 2.95 and 2.65/2.63). Although theoretical, this trend may explain our experimental results, where 3oxoC₁₄-HSL is more active than 3oxoC₁₂-HSL, itself better than 3oxoC₁₂:2-HSL.

Little is known on the effects of unsaturated analogues on mammalian cells. Chhabra and co-workers have brought the beginning of an answer by demonstrating that mono-unsaturated AHL analogues had reduced IC₅₀ in a mouse splenocyte proliferation assay, especially if placed midway through the chain. Our own results on cell assays bring new light to this question, as we have demonstrated that carbon double bonds could modulate the apparent EC₅₀, but did not affect the power range of effects.

Molecule	Consensus Log P _{o/w}	TPSA (Å ²)
γ-butyrolactone (30)	0.47	26.30
C ₄ -HSL (28)	0.70	55.40
3oxoC ₆ -HSL (15d)	0.69	72.47
3oxoC ₁₀ -HSL	2.19	72.47
3oxoC ₁₂ :2-HSL (2)	2.32	72.47
12azido-3oxoC ₁₂ -HSL (15b)	2.53	122.22
3oxoC ₁₂ :1-HSL (<i>ω</i> -3 or <i>ω</i> -6)	2.65 / 2.63	72.47
3oxoC ₁₂ -HSL (1)	2.95	72.47
3oxoC ₁₄ -HSL (29)	3.58	72.47

Table 17 – Compared physical properties of reference 3oxoC₁₂-HSL (1**) and several analogues with modified acyl chains**

Overall, the gathered experimental and theoretical data suggest long saturated acyl chains should be preferred for maximal biological activity.

2.1.3. Importance of the cyclic headgroup

2.1.3.1. Chirality and AHL activity

The importance of stereoisomery in native AHL **1** was examined by synthesising its (*R*)-isomer molecule **15e**. This compound is not found in nature. As tested on cell models Caco-2/TC7 and Raw 264.7, the molecule is not cytotoxic, but nevertheless exhibits increased toxicity on intestinal epithelial cells as compared to the native (*S*)-isomer **1** (Figure 78). This

rise in secreted LDH might explain the surge in IL-8 secretion observed at 100 μ M. On both cell lines no significant difference in comparison to control condition DMSO is observed : the molecule is modestly active or even inactive at all concentrations. It is neither pro-inflammatory like **1** on macrophages at 1 and 50 μ M, nor anti-inflammatory like its parent compound on Caco-2/TC7 cells in range 1-10 μ M.

Those results are in accordance with published literature where the (*R*)-isomer of the 3oxoC₁₂-HSL is widely regarded as inactive. No effect on viability of human macrophage cell line U-937 and mouse macrophages p388D1 have been reported after incubation with 50 μ M **15e**. Kravchenko *et al.* studied signal transduction upon incubation with AHL **1** and demonstrated no significant effect was observed when the (*R*)-isomer of the AHL was employed.²⁷⁸

These observations show a real specificity for the (*S*)-isomer of the 3oxoC₁₂-HSL and advocate for the existence of a dedicated receptor, at least at low micromolar concentration. Indeed, if the molecule **1** operated only via lipophilic insertion in membranes, no difference should theoretically be observed between its two enantiomers.

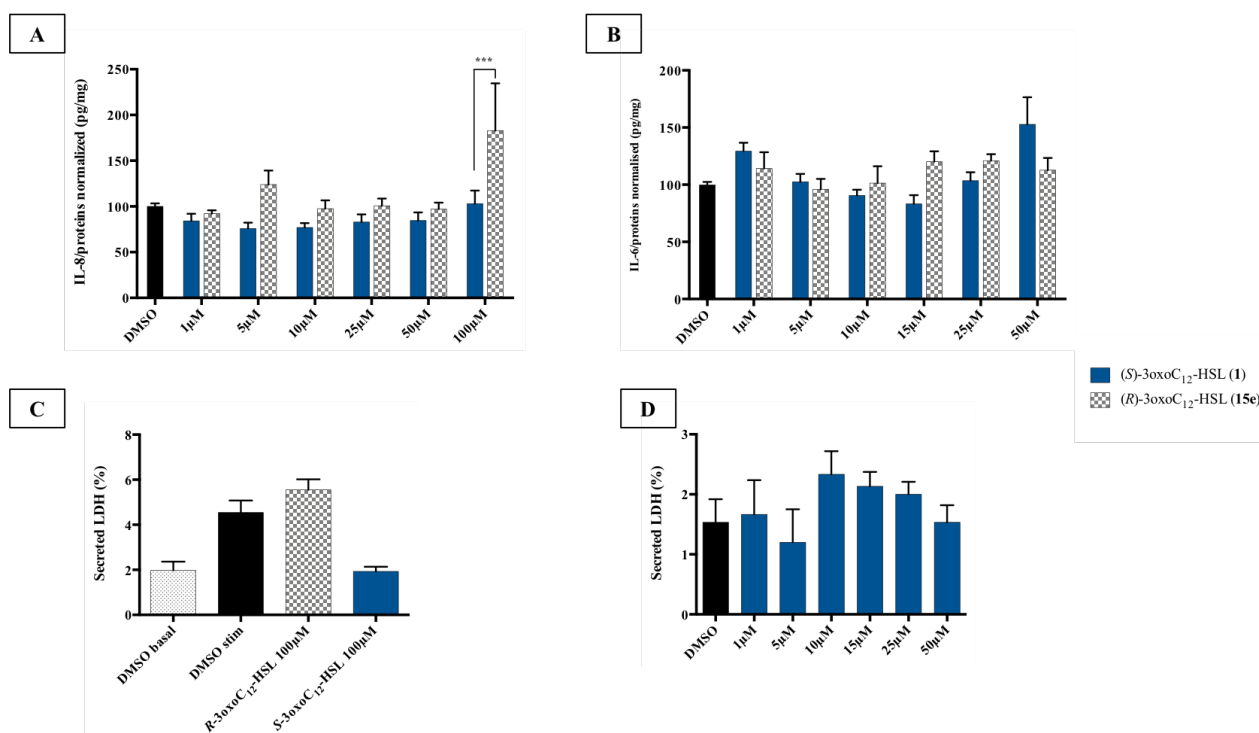


Figure 78 - Compared properties of (*S*)-3oxoC₁₂-HSL (1**) versus its stereoisomer (*R*)-3oxoC₁₂-HSL (**15e**) on cell models**

A (resp. **B**) : IL-8 (resp. IL-6) response of cytokine-stimulated 18-day-old Caco-2/TC7 (resp. Raw 264.7) cells. ****p* < 0.001 ; two-way ANOVA, Sidak's post-test. **C** (resp. **D**) : secreted LDH (%) under stimulatory conditions in Caco-2/TC7 (resp. Raw 264.7) cells. The points are the mean of several replicates (*n* \geq 6) \pm SEM.

2.1.3.2. Thiolactones

We developed analogues where the homoserine lactone ring was replaced by a homocysteine lactone, abusively named “HTL” for homoserine-thiolactone. This analogue headgroup resembles the native homoserine but features a sulphur atom instead of an oxygen, hence turning the ester into a thioester. This molecule retains the capacity to be hydrolysed under basic conditions but also by lactonase activity. Janssens *et al.* have indeed demonstrated the degradation of a 3oxoC₇-HTL molecule by bacterial lactonase AiiA_{soil} ; the rate of degradation was however twice-decreased as compared to the corresponding AHL. Simultaneously, the authors observed the pH-dependent hydrolysis of compound **15g** was as effective as that of **1** in basic conditions ; other groups however described it to be twice slower than that of **1** at physiological pH.⁴²⁹

Two isoforms of the molecule were synthesized : the enantiomerically pure (*S*)-3oxoC₁₂-HTL **15g** and the racemic (*D/L*)- 3oxoC₁₂-HTL **15f**. None of these compounds exhibited significant toxicity in the range of tested concentrations on cell lines Caco-2/TC7 and Raw 264.7 (Figure 79). In terms of activity the two molecules are in the same range of effect as the native homoserine lactone **1** at low micromolar dosage (1-10µM on macrophages and 1-25µM on epithelial cells). Interestingly they revealed more active than the reference AHL at higher doses, reaching a 30%- and 50%-decrease in cytokine secretion on Caco-2/TC7 cells and macrophages respectively.

From our experiments it is hard to decipher whether the (*D*)-enantiomer of the thiolactone analogue is active or not. Indeed differences in activity between **15f** and **15g** are rather small, with the racemic mix **15f** overall less active than the pure enantiomer **15g**. However, if the (*R*)-enantiomer was completely inactive we would expect similar effects of 50µM **15f** and 25µM **15g** for instance, and this is not the case. It is then hard to conclude without synthesizing the (*R*)-enantiomer itself.

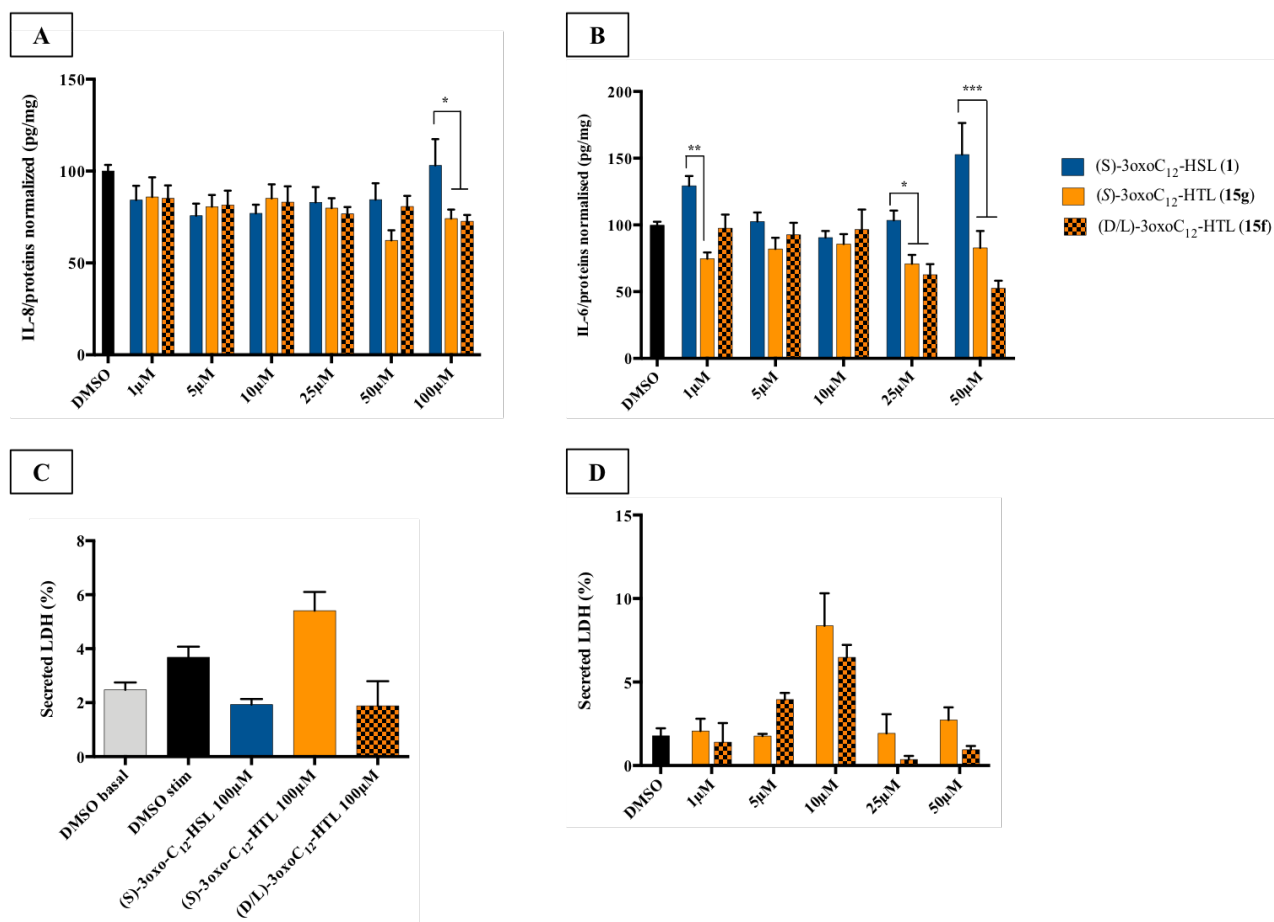


Figure 79 - Compared properties of (S)-3oxoC₁₂-HSL (1) and its thiolactone analogues (S)-3oxoC₁₂-HTL (15g) and (D/L)-3oxoC₁₂-HTL (15f) on cell models

A (resp. **B**) : IL-8 (resp. IL-6) response of cytokine-stimulated Caco-2/TC7 (resp. Raw 264.7) cells. *p < 0.05, ****p < 0.0001 ; two-way ANOVA, Tukey's post- test. **C** (resp. **D**) : secreted LDH (%) under stimulatory conditions in Caco-2/TC7 (resp. Raw 264.7) cells. The points are the mean of several replicates (n ≥ 6) ± SEM.

Across literature it appears that the substitution of the ring oxygen with a sulphur is relatively well tolerated in terms of activity in mammalian cells. Chhabra and co-workers pioneered the domain by demonstrating the enantiomerically pure molecule retained inhibitory properties in a mouse splenocyte proliferation assay, although with higher IC₅₀ than parent AHL.³⁰⁰

On the opposite and surprisingly, Garner *et al.* were unable to observe PARP cleavage and eIF2α phosphorylation upon incubation with **15g**, phenomena described in presence of reference AHL **1**.^{278,430} The authors hypothesized the increased stability of the thiolactone analogue might hinder and slow down its capacity to interact with mammalian partners, hence preventing observation in the time span of their experiment. Such an explanation might coincide with our own observations of increased activity at higher concentration, where the amount of

degraded molecule would be higher. We have furthermore in *Part I* hypothesized that the open-ring form of AHLs might be necessary to mediate their biological activity.

2.1.3.3. The aminocyclohexanol series

The aminocyclohexanol (ACH) is a 6-membered saturated ring with an hydroxyl group on carbon-1 and an amino group on carbon-2. This is not a flat headgroup, and four stereoisomers exist : the (*S,S*), the (*S,R*), the (*R,R*), and the (*R,S*)-configuration. Based on the observation that the (*R*)-enantiomer **15e** of natural 3oxoC₁₂-HSL retained little activity, it was decided to focus on two diastereomers with (*S*)-configuration of the amino group. Hence compounds (*S,S*)-3oxoC₁₂-ACH **15h** and (*R,S*)-3oxoC₁₂-ACH **15i** were synthesized. They only differ by the relative positions of the substituents, in *trans* conformation for **15h** and *cis* conformation for **15i**. This difference may affect their capacity to form stabilising interactions (especially H-bonds) with their mammalian partner(s).

The two compounds are not cytotoxic at low concentrations, but **15i** exhibits an increase in secreted LDH at high concentrations (Figure 80). In epithelial cells, without exceeding the 10%-threshold it still reaches about 9% secreted LDH which is more than its diastereomer **15h** and reference AHL **1**. In the Raw 264.7 cell line, the amount of secreted LDH is consistently higher than with **15h**, and exceeds 10% at 50µM hence limiting the use of the molecule to lower concentrations.

In terms of activity, the substitution of the homoserine lactone by a aminocyclohexanol ring is rather conservative. The two isomers exhibit very similar levels of reduction of IL-8 secretion in Caco-2/TC7 cells, and stand in the same range of efficacy that reference AHL **1**. Their effects are more impressive on Raw 264.7 macrophages where they reveal significantly more effective than the native AHL, reaching about 40 to 50% reduction of IL-6 at 50µM. Although **15i** is cytotoxic at such concentration, the use of **15h** on the opposite could be positively considered. Especially striking is the absence of bell-shaped activity curve on macrophages, while it is maintained on epithelial cells. To examine further the mode of action of **15h** it may be interesting to enlarge the range of tested concentrations up to 100µM or more, to assess whether the bell shape would be observed or a regular dose-dependent activity curve.

As reported in literature, the ACH ring is expected to resist hydrolysis either enzymatic or pH-dependent. Indeed Janssens *et al.* have demonstrated that AHL analogues bearing aminocyclohexanol headgroups remained untouched after incubation with bacterial lactonase AiiA_{soil} or under very basic conditions (pH range 8-12).²⁵⁰

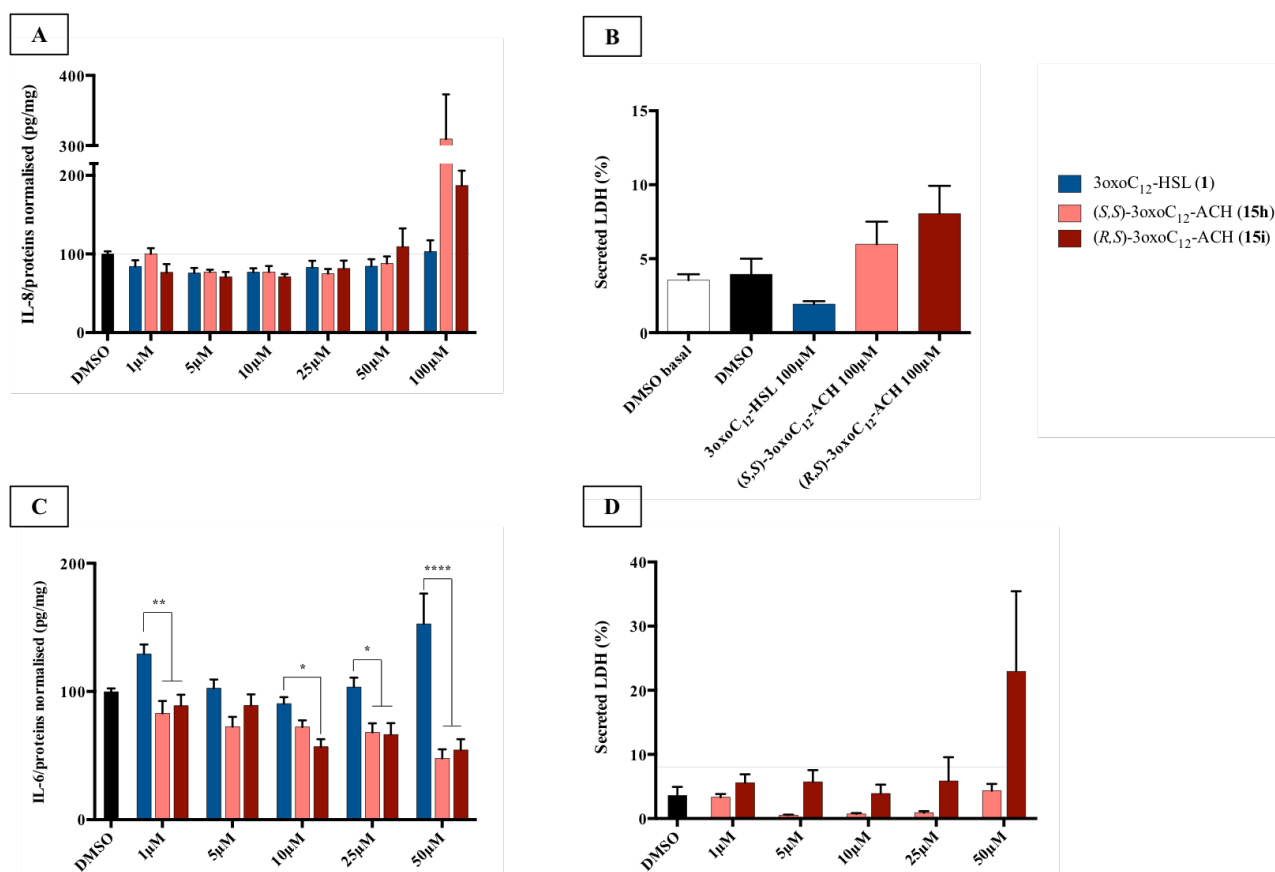


Figure 80 - Compared properties of (S)-3oxoC₁₂-HSL (1) and its cyclohexanol analogues (S,S)-3oxoC₁₂-ACH (15h) and (R,S)-3oxoC₁₂-ACH (15i) on cell models

A (resp. **C**) : IL-8 (resp. IL-6) response of cytokine-stimulated Caco-2/TC7 (resp. Raw 264.7) cells. *p < 0.05, **p < 0.01, ****p < 0.0001 ; two-way ANOVA, Tukey's post- test. **B** (resp. **D**) : secreted LDH (%) under stimulatory conditions in Caco-2/TC7 (resp. Raw 264.7) cells. The points are the mean of several replicates (n ≥ 6) ± SEM.

Little data is found in literature regarding the activity on mammalian models of aminocyclohexanol-bearing AHL analogues. At most, Jadhav *et al.* reported that a mixture of **15h** and **15i** retained good activity on a murine peripheral blood leukocyte proliferation inhibitory assay, while being less cytotoxic than parent AHL **1**.⁴³¹

2.1.3.4. Aromatic headgroups

Aromatic compounds are cyclic planar molecules characterised by a conjugated system that allows delocalisation of π -electrons, hence providing the molecule with increased stability. These characteristics make the advantages of aromatic headgroups : they are flat molecules which solves the problem of active/inactive enantiomer ; their great stability makes them resistant to hydrolysis by both enzymatic and pH-dependent mechanisms ; their particular electronic configuration may create additional constructive interactions with amino acids harbouring an aromatic sidechain (i.e. phenylalanine, tryptophan, tyrosine and histidine) in a putative active site, named π -stacking.

2.1.3.4.1. The methoxy-anilide analogues

The first family of analogues with aromatic headgroups is based on methoxy-anilides. The presence of the methoxy group was thought to mimic the polarity from the ester group in the natural homoserine lactone and to provide stabilising interactions. Three position isomers were prepared, harbouring the methoxy group in *para* (**15j**), *meta* (**15k**) or *ortho* (**15l**) position, in order to identify the most favourable conformations. Indeed, only the *ortho* configuration had been explored with the aminocyclohexanol series.

The three molecules were tested on both cell lines Caco-2/TC7 and Raw 264.7 (Figure 81). Overall the *p*-analogue **15j** elicits cytotoxicity with increasing concentrations. The usual 10%-threshold is not exceeded on epithelial cells, but this molecule shows twice higher levels of secreted LDH than the two other analogues, and three times more LDH than the reference AHL **1**. On macrophages it does exceed the 10%-threshold from 25 μ M and above, while **15k** and **15l** exhibited constant levels of secreted LDH about 6-7% at all doses.

In terms of activity, replacing the homoserine lactone ring with methoxy-anilide is not a conservative substitution at all. The anti-inflammatory properties of **1** observed at low concentration are abolished in **15j-1** : the IL-8 and IL-6 secretion levels oscillate around that of control DMSO in both cell lines in low concentration range, while the behaviour is rather pro-inflammatory at higher dosage.

Given the poor activity of analogues **15j-l** on our cell assays it is hard to identify with ring configuration of substituents could be the most favourable. Obviously the *para*-conformation induces more cytotoxicity, but no frank difference is otherwise observed between the *meta*- and the *ortho*-conformation.

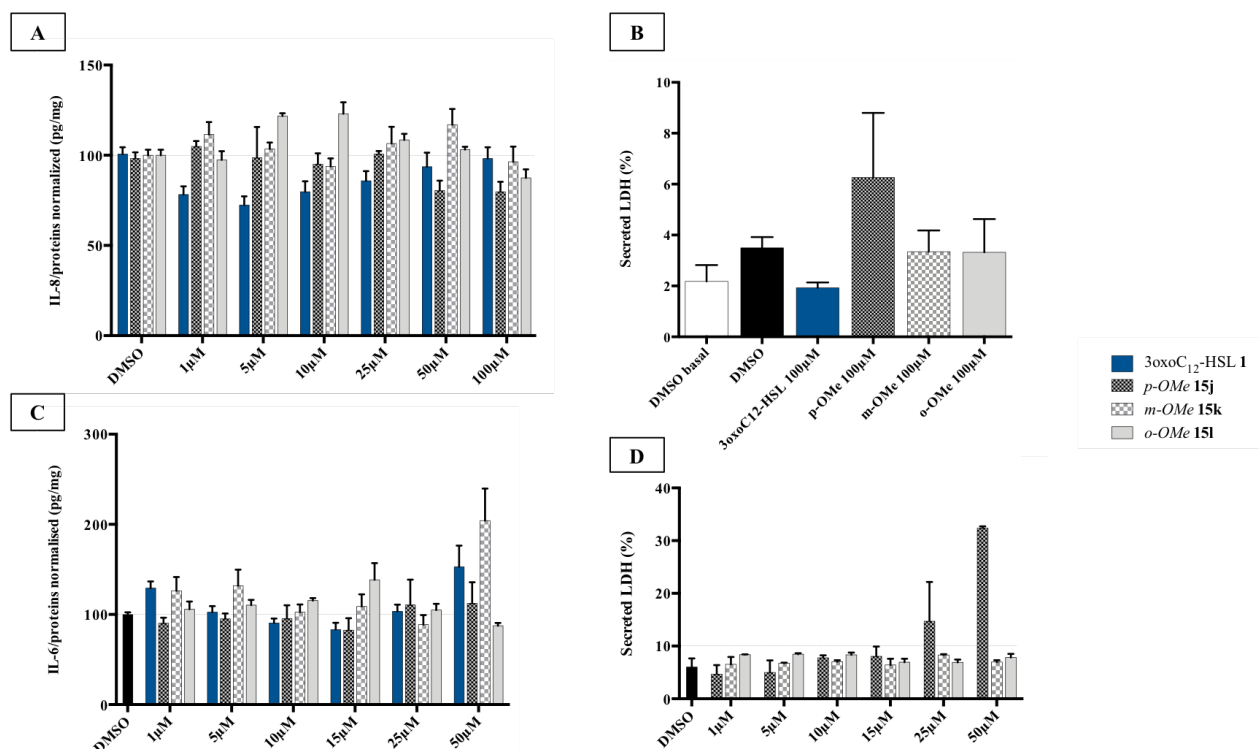


Figure 81 - Compared properties of (S)-3oxoC₁₂-HSL (1) and its methoxy-anilide analogues 15j, 15k and 15l, on cell models

A (resp. **C**) : IL-8 (resp. IL-6) response of cytokine-stimulated Caco-2/TC7 (resp. Raw 264.7) cells. Two-way ANOVA, Tukey's post-test. **B** (resp. **D**) : secreted LDH (%) under stimulatory conditions in Caco-2/TC7 (resp. Raw 264.7) cells. The points are the mean of several replicates ($n \geq 6$) \pm SEM.

The molecule resistance to hydrolysis was verified by reproducing the Caco-2/TC7 cells assay without PON-inhibitor 2-HQ (Figure 82). A similar experiment had been conducted with 3oxoC₁₂-HSL **1** in chapter 2, and a difference in IL-8 response observed depending on the presence or absence of the PON inhibitor. Here we report no significant difference between conditions with or without 2-HQ. The absence of influence of the PON inhibitor is interpreted as inaction of PONs on the molecule, and hence its resistance to hydrolysis.

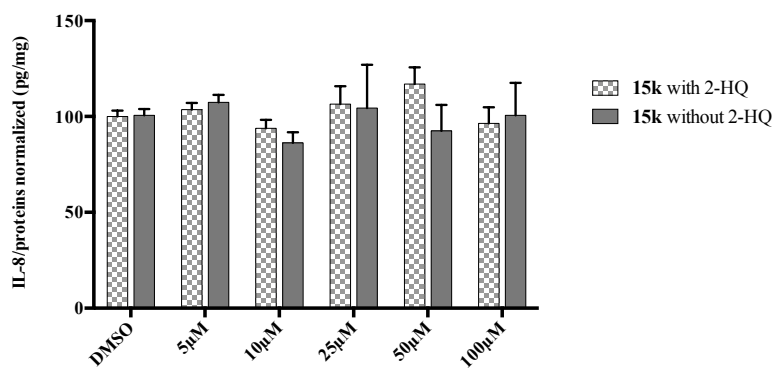


Figure 82 – Compared IL-8 secretion in cytokine-stimulated Caco-2/TC7 cells in presence of increasing doses of methoxy-anilide analogue 15k with and without 100µM PON inhibitor 2-hydroxyquinoline

The points are the mean of several replicates ($n \geq 6$) \pm SEM. No significant difference between conditions, two-way ANOVA, Sidak's post-test.

2.1.3.4.2. The amino-chlorophenol analogue

A second type of aromatic headgroup was employed, the 2-amino-4-chlorophenol. This headgroup retains an *ortho*-conformation of the amino and hydroxyl groups which proved efficient in the aminocyclohexanol series, conjugated to the aromatic properties.

The molecule is not toxic in the range of tested concentrations, on both cell lines. It is as active as reference AHL **1** at low micromolar concentrations (1-10µM) and gets more active than **1** at higher concentration, with a clear dose-dependent effect (Figure 83). The cytokine secretion reduction reaches 50% on epithelial intestinal cells, and 60% on macrophages, which makes this analogue the most active to date.

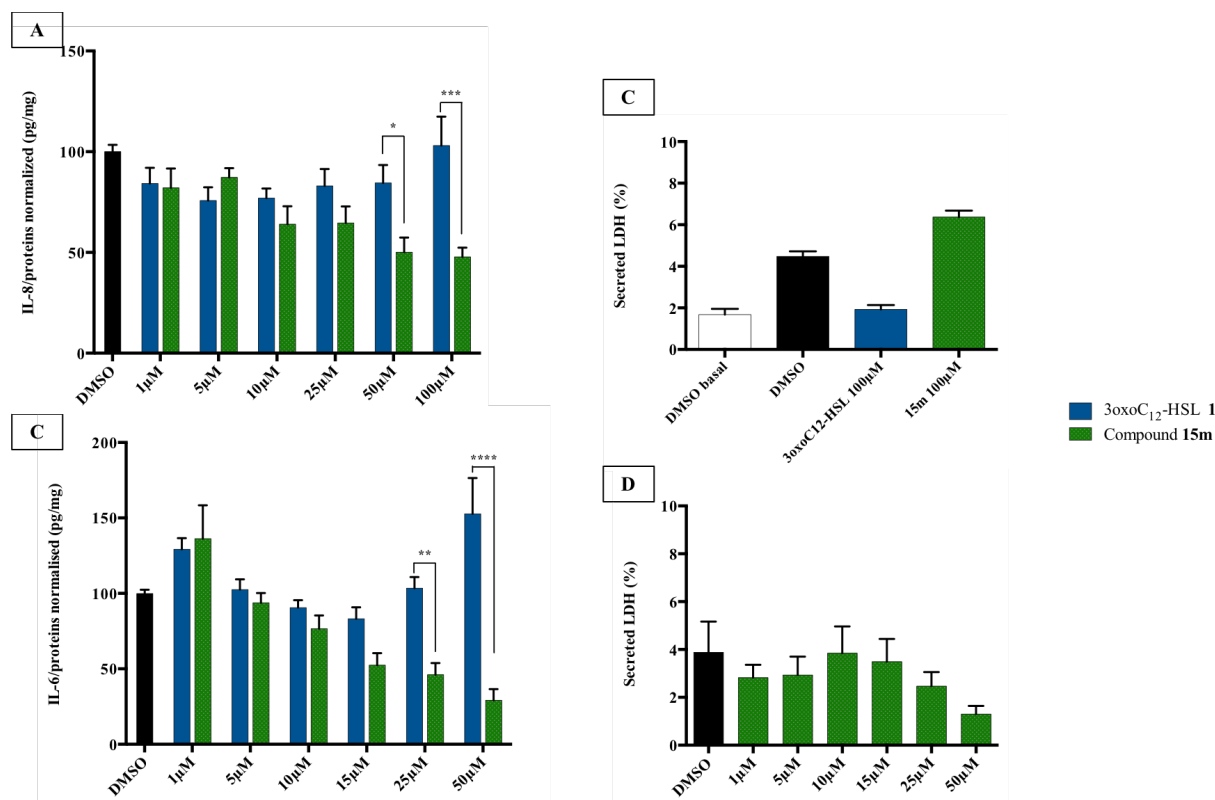


Figure 83 - Compared properties of (S)-3oxoC₁₂-HSL (1) and amino-chlorophenol analogue 15m on cell models

A (resp. **C**) : IL-8 (resp. IL-6) response of cytokine-stimulated Caco-2/TC7 (resp. Raw 264.7) cells. *p < 0.05, **p < 0.01, ***p < 0.001, ****p < 0.0001 ; two-way ANOVA, Sidak's post- test. **B** (resp. **D**) : secreted LDH (%) under stimulatory conditions in Caco-2/TC7 (resp. Raw 264.7) cells. The points are the mean of several replicates (n ≥ 8) ± SEM.

Jadhav *et al.* have described the synthesis and cell assays of an AHL analogue with a very close structure to **15m** : the only difference resides in the presence of a β-diamide instead of a β-ketoamide moiety.⁴³¹ In spite of this modification, the authors report as we do, improved biological properties of the analogue. Their molecule was tested on a leukocyte proliferation assay where it appeared twice more potent than parent AHL **1**, while no toxicity (EC₅₀ > 1000μM) was observed on Jurkat cells where **1** had an EC₅₀ of 250μM.

To study the involvement of the chlorine in this gain of activity, the group concomitantly tested an analogue with an aminophenol headgroup. The latter analogue was not cytotoxic, but its activity was reduced to the level of activity from **1**.

2.1.3.5. Miscellaneous : diverse compounds

Three final analogues were investigated, with very different headgroups : the 3oxoC₁₂-benzyl **15c** that had been synthesized to study metal chelation, an analogue with a diketopiperidine-like headgroup (**32**), and a compound with a fructose headgroup (**34**). Due to their diversity, these molecules will be treated separately ; the last two structures were only tested on the Raw 264.7 macrophage cell line.

The benzyl analogue **15c** carries a very different headgroup from the native homoserine lactone ring, both in terms of structure and physico-chemical properties. In **15c**, the 6-membered ring is not directly linked to the nitrogen atom from the amide, but there is a CH₂ inserted in between. Hence, the structure is bigger but also more flexible than other headgroups. The benzyl furthermore does not contain any heteroatom and is far less polar than the other groups investigated. Compound **15c** is well tolerated at low micromolar concentration, but induces increased levels of secreted LDH at higher dosage (Figure 84). In Caco-2/TC7 cells the quantity of secreted LDH is close to the 10%-threshold at 100μM, while this limit is exceeded at 50μM on macrophages. Simultaneously we observed little effects of the molecule on IL-8 and IL-6 secretion, which makes it a poor analogue of AHL **1**, a result that as rather expected.

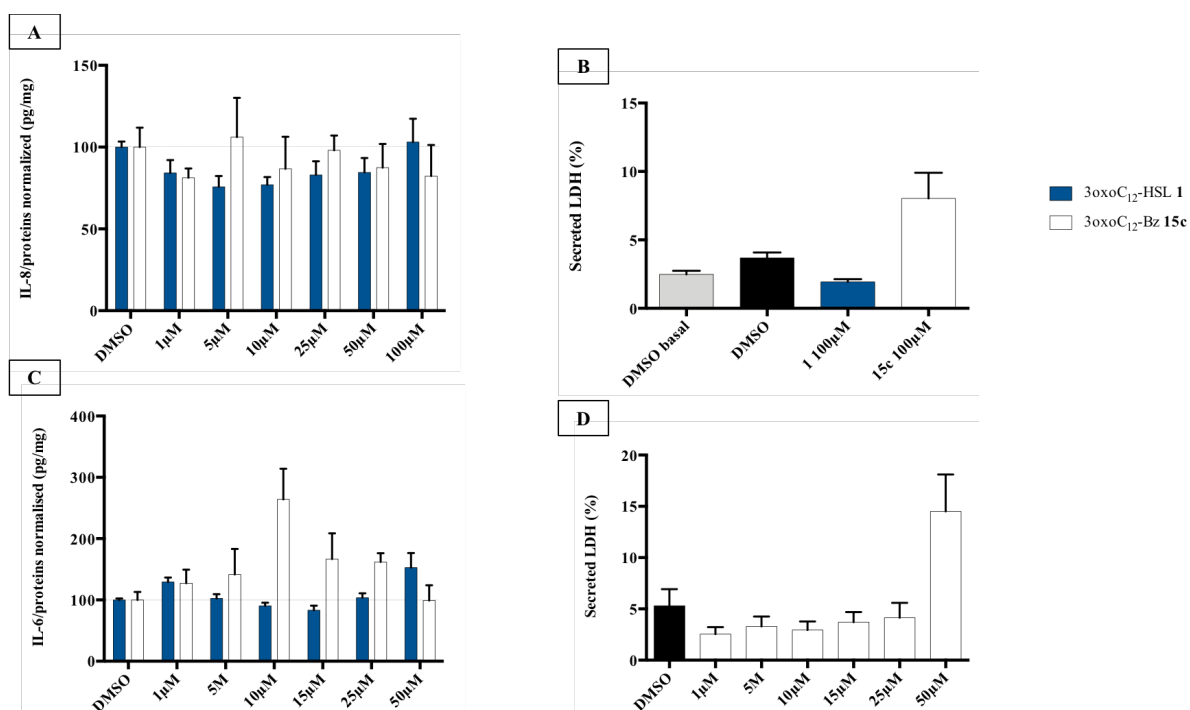


Figure 84 - Compared properties of (S)-3oxoC₁₂-HSL (1**) and benzyl analogue **15c** on cell models**

A (resp. **C**) : IL-8 (resp. IL-6) response of cytokine-stimulated Caco-2/TC7 (resp. Raw 264.7) cells. Two-way ANOVA, Sidak's post-test. **B** (resp. **D**) : secreted LDH (%) under stimulatory conditions in Caco-2/TC7 (resp. Raw 264.7) cells. The points are the mean of several replicates ($n \geq 4$) \pm SEM.

On opposite, analogue **32** is a very polar compound. The headgroup is resistant to PON hydrolysis but could be degraded by other enzymes similarly to the amide linkage bounding head to acyl tail. When tested on Raw macrophages, the molecule increased LDH release and was considered excessively toxic from 25 μ M and above (Figure 85). As a consequence, the levels of IL-6 secretion increased. At lower doses the analogue did not show toxicity and rather increased the cytokine production. Hence, the substitution of homoserine ring with a diketopiperidine-like headgroup hindered the anti-inflammatory properties of native AHL **1** rather than potentializing them.

This molecule had been previously synthesized and tested by Jadhav and co-workers, in comparison to reference 3oxoC₁₂-HSL. In accordance with our results, the authors reported 3-fold decrease in activity on a leukocyte proliferation assay. The group simultaneously studied the diketopiperidine pattern in a 5-membered ring ; reduction of the ring size completely abolished the biological effects of the molecule.

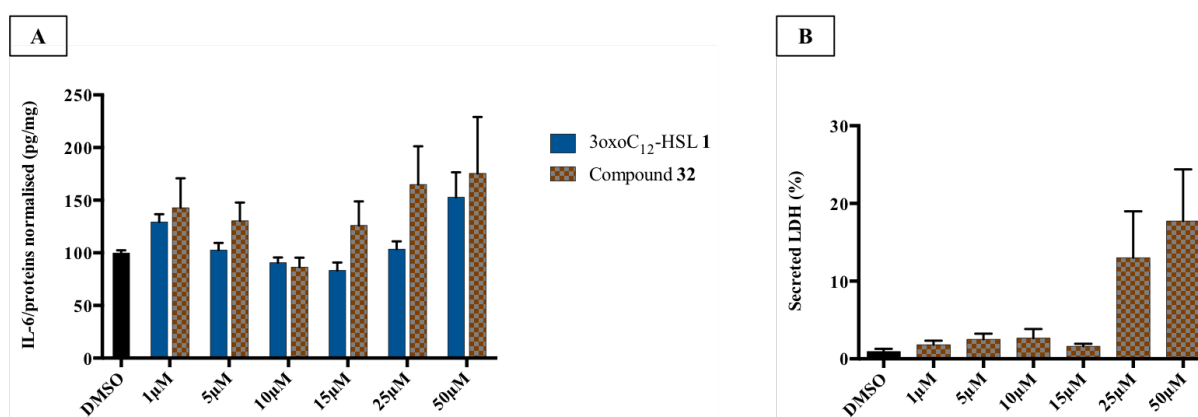


Figure 85 - Compared properties of (S)-3oxoC₁₂-HSL (1**) and analogue **32** on cell models**

A : IL-6 response of cytokine-stimulated Raw 264.7 cells. Two-way ANOVA, Sidak's post- test. **B** : secreted LDH (%) under stimulatory conditions in Raw 264.7 cells. The points are the mean of several replicates (n \geq 5) \pm SEM.

Finally, a carbohydrate ring was grafted as a headgroup on **7a** to prepare molecule **34**. Although carbohydrates are polar compounds that may appropriately mimic the native HSL ring, the choice of linkage employed here brought important modifications to the molecular frame. The β -ketoamide was turned into a β -ketoester, made from coupling between carboxylic acid **7a** and the alcohol moiety on the carbohydrate C-6. Indeed, the other hydroxyl groups were protected with acetylene, and primary alcohols are otherwise more reactive than secondary alcohols. The choice of linkage hence introduced a spacer (CH₂) in between the acyl chain and the actual ring headgroup.

The activity observed with **34** on macrophages is very heterogeneous, but overall the compound is not anti-inflammatory (Figure 86). No toxicity was however observed.

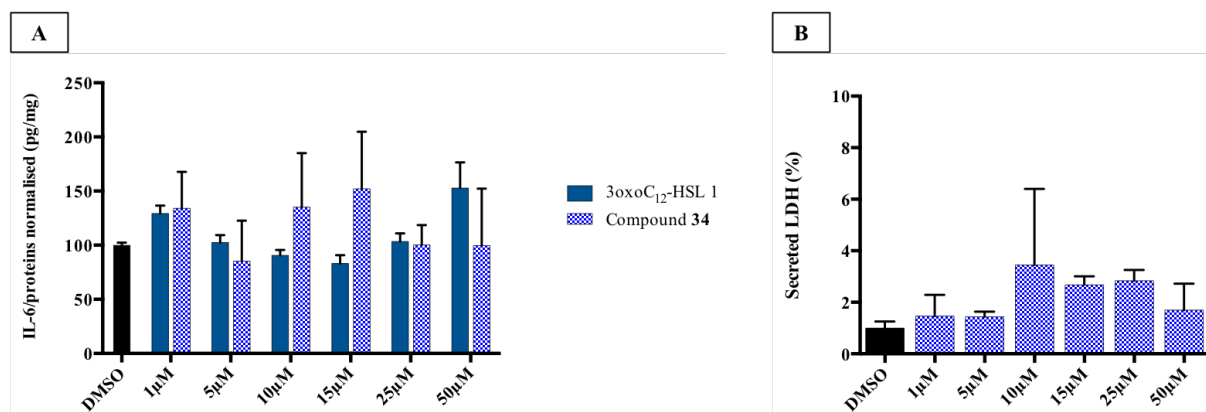


Figure 86 - Compared properties of (S)-3oxoC₁₂-HSL (1) and compound 34 on cell models

A : IL-6 response of cytokine-stimulated Raw 264.7 cells. Two-way ANOVA, Sidak's post- test. **B** : secreted LDH (%) under stimulatory conditions in Raw 264.7 cells. The points are the mean of several replicates (n ≥ 4) ± SEM.

2.1.4. Discussion on AHL modifications

This library of compounds and its biological investigation highlighted conservative and deleterious modifications for AHL activity on our two cell models. Overall, our results confirmed conclusions from literature relative to requirements for acyl chain and carbon-3 substitution. Maximum activity is achieved with relatively long chains of 12-14 carbons, and substitution of carbons with linear heteroatoms has moderate effect on activity as long as it does not impact drastically the chain lipophilicity. The addition of large groups on carbon-3 abolishes the molecule activity, while the complete removal of substituent weakens it. Ketone remained the most favourable group in our experiments, but we lack results with hydroxyl-substituted compounds for complete comparison.

Our results on HSL ring substitution have however widened the spectrum of possibilities, until now believed to be restricted to homoserine groups only. Headgroups that retained activity include homocysteine lactone rings, amino-cyclohexanol and amino-chlorophenol. Surprisingly, the lactone group – closest to native HSL in terms of structure - retained good biological activity but was not the most active. The two lead compounds are molecules **15h** and **15m** ; analogue **15i** must be excluded due to toxicity arising at relatively low concentration.

Both candidates exhibit common features : they are 6-membered rings and harbour an hydroxyl group in *ortho* position to mimic the native carboxyl moiety of HSL. A major difference lies in the different natures of those rings - ACH being a saturated cycle while amino-chlorophenol is aromatic – which impacts their 3D structures and spatial interactions. On one hand aromatic rings are less flexible than their saturated counterparts and cannot accommodate their 3D structure to best fit their receptor, but on the other their locked conformation can confer energetic advantages as less energy is required for interaction with protein partner in the absence of free rotation. This assumption should however be verified by proper docking, which is currently impossible without (a) firmly identified AHL receptor(s) at hand.

The delicate relation between polarity and lipophilicity in AHLs has been highlighted throughout our study as an important modulator of their biological activity. We can try to quantify this parameters in synthetic analogues by computing TPSA as a polarity indicator and a consensus 1-octanol/water partition (Log P_{o/w}) as a lipophilicity indicator (Table 18). Through this models it appears that analogues **15h**, **15i**, and **15m** have similar polarities and are less polar than native AHL **1**. Their lipophilicities are however varied. Analogue **15h** with a *trans* conformation of its amino-cyclohexanol ring is the least lipophilic while its *cis* diastereomer **15i** is the most lipophilic. This striking difference illustrates the importance of spatial conformation. Analogue **15m** shows lipophilicity closest to **1** ; its properties reflect the balance between the hydrophilic OH group and the chlorine atom which increases the lipid solubility of the molecule.

<i>Molecule</i>	<i>TPSA (Å²)</i>	<i>Polar difference to reference AHL 1 (%)</i>	<i>Consensus lipophilicity (Log P_{o/w})</i>	<i>Lipophilic difference to reference AHL 1 (%)</i>
3oxoC ₁₂ -HSL 1	72,47	0	2.95	0
Analogue 15h	66.40	- 8.3	2.84	- 3.7
Analogue 15i	66.40		3.52	+ 19.3
Analogue 15m	66.40		3.02	+ 2,4

Table 18 – Compared physical properties of reference AHL 1 and analogues 15h, 15i and 15m

Considering the good activity of analogue **15m**, one may wonder why the methoxy-anilide analogues exhibited such poor activities. Once again, assumptions can be made based on computations. The three analogues **15j-i** are predicted to be far less polar than **1** and **15m**, but also much more lipophilic. Indeed, their calculated properties show a TPSA decreased by 40% and a Log P_{o/w} increased by 31-34% in comparison to **1**, while **15m** has a TPSA decreased by 8% and a Log P increased by 2% only. On top of these calculated properties, we can compare

the nature of their substituents. When attached to an aromatic ring, both hydroxyl and methoxy moieties can act as electron-donating groups, but they have different behaviours towards H-bond formation. OH can act both as a H-bond donor and acceptor, while OMe can only be a H-bond acceptor. Other hypothesis to explain their very different outcome on cell assays may include size and steric hindrance - indeed, the methoxy-anilide headgroup is significantly larger than native HSL but only slightly bigger than the amino-chlorophenol ring with respective sizes of 97.4 Å³ and 94.4 Å³ vs. 71.3 Å³ ⁴³² – but also inductive effects from the chlorine atom.

Our study highlighted analogues with non-hydrolysable headgroups as the most active candidates on our cell models. One must be cautious with these results ; indeed, these models cannot account for the systemic metabolism of xenobiotics. If the drugs have proved locally efficient, they must be tested at the systemic scale to fully evaluate their distribution and activity. Their incapacity to undergo hydrolysis and degradation might reveal to be a drawback on the long run.

2.2. Further investigation on two hit candidates

Similarly to what had been done with AHLs **1** and **2**, our two lead candidates **15h** and **15m** were tested for modulation of mRNA levels in 18-day-old cytokine-stimulated Caco-2/TC7 cells after 4h incubation. On Figure 87 we can observe a trend towards decreased IL-8 mRNA levels upon incubation with the two analogues. Comparatively to control DMSO the two molecules induce down-regulation at all tested concentrations. In comparison to reference AHL, analogue (*S,S*)-3oxoC₁₂-HSL **15h** is as effective as **1** at 5µM, while **15h** and **15m** are both more effective than **1** at 25µM. These results in mRNA mirror appropriately our observations on secreted protein IL-8, which was not the case with native AHLs. This detectable mRNA modulation is thus a new argument to support the superior efficacy of analogues **15h** and **15m** versus reference 3oxoC₁₂-HSL.

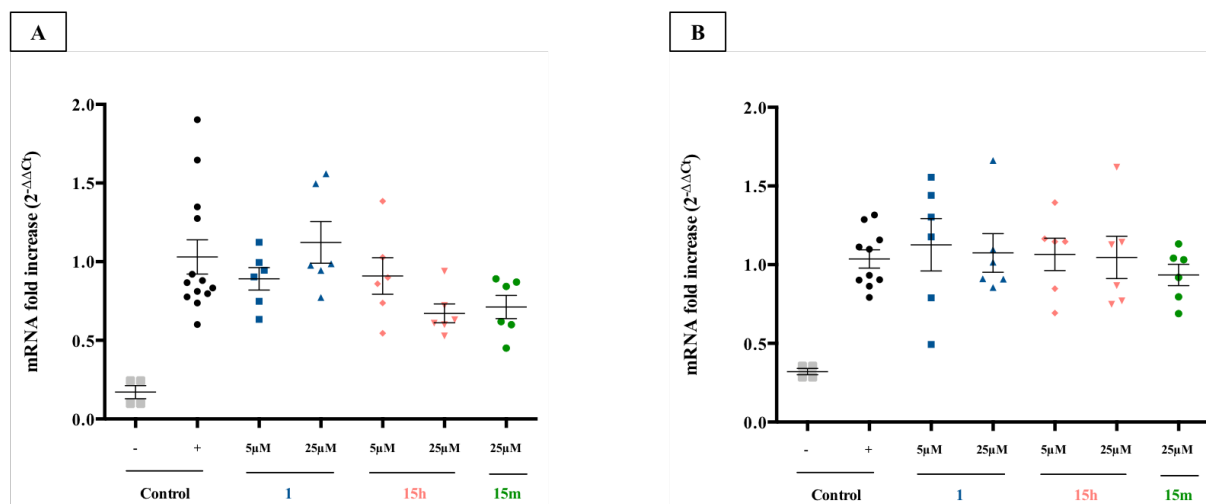


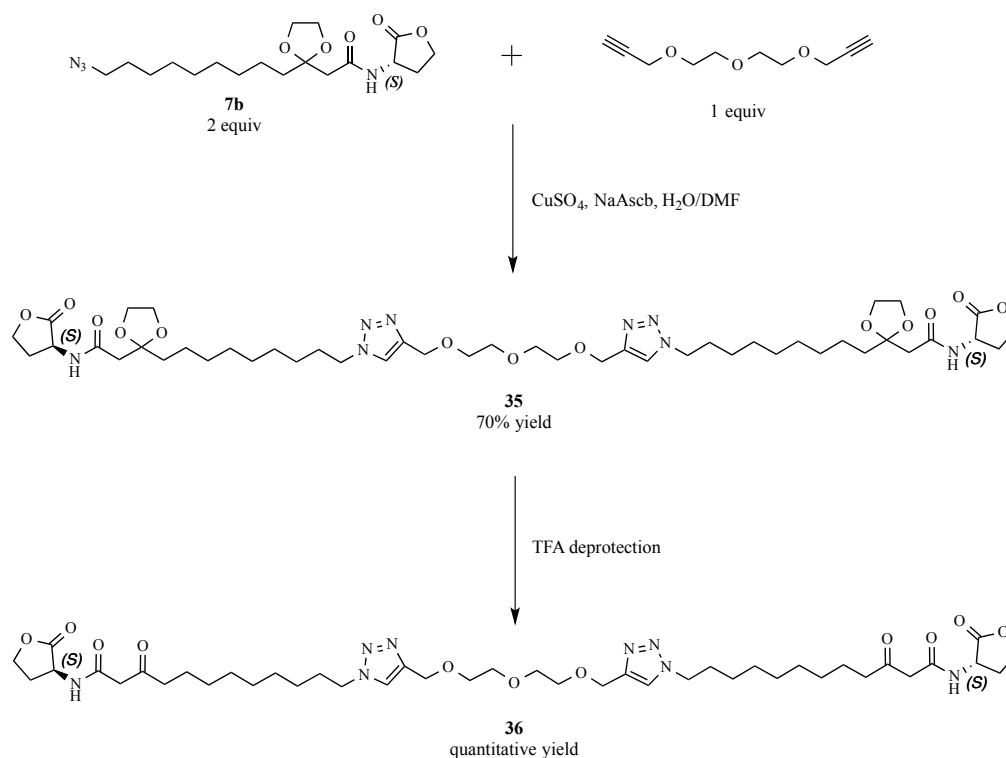
Figure 87 - Compared effects of increasing doses of AHL 1 and two synthetic analogues 15h and 15m on Caco-2/TC7 cells IL-8 and IL-1 β mRNA expression

2-HQ added at 100 μ M in all conditions. **A** : human IL-8 mRNA levels on cytokine-activated cells. Kruskal-Wallis test ($p = 0.0055$), Dunn's post-test. **B** : human IL-1 β mRNA levels on cytokines-activated cells. 2^{- $\Delta\Delta$ Ct} calculated proportionally to house-keeping gene human GAPDH. The points represent different replicates ($n \geq 4$) \pm SEM.

2.3. Development of a dimeric AHL

Receptor clustering has been described to improve apparent ligand affinity via proximity effects and increased rebinding capacity.^{433,434} Receptor clustering is often efficiently achieved by clustering multiple copies of ligands to reach high-affinity interactions. Ligand clustering usually relies on two strategies : ligands are either attached together in a linear form, or can form dendrimers.

Based on the hypothesis of a membrane AHL receptor, we developed a dimeric 3oxoC₁₂-HSL, here molecule **36** (Scheme 22). This molecule contains two AHL entities, connected to their acyl chains by means of a short hydrophilic linker. AHL attachment to the spacer occurs through click chemistry, a technique previously presented in this manuscript, which affords fairly good yields and is orthogonal to the ultimate deprotection step required to recover free ketones.



Scheme 22 - Synthesis of dimeric AHL 36

The dimeric molecule **36** was tested on our mammalian cell assays and results compared to those of native AHL **1** in order to assess any improved effect (Figure 88). Cytokine inductions were compared in terms of “effective concentration” which we understand as the AHL monomer concentration. In other words, where **1** has a concentration λ , the dimer **36** will have the concentration $\lambda/2$ that corresponds to an apparent AHL concentration of λ .

At first sight, the cells exhibit very different tolerances to the new molecule. If the immune cells were more prone to toxicity in presence of **1**, the tendency is increased exponentially with dimer **36**: the molecule is cytotoxic from $10\mu\text{M}$ and above in the macrophage cell line. On opposite, the 10%-secreted-LDH threshold is not crossed in the epithelial cell line, although we can observe an increase in toxicity to stabilise at approx. 8% secreted LDH. As a consequence, the effects observed on cytokine secretion are also very different. On macrophages the dimer rather provokes excessive IL-6 secretion, and does no better than reference AHL **1**. On Caco-2/TC7 cells however, the bell-shape activity curve is observed, and most interestingly the dimer shows increased efficacy than AHL **1** at same effective concentration. This effect reaches significance at $25\mu\text{M}$ concentration of **1**, i.e. $12.5\mu\text{M}$ of **36**.

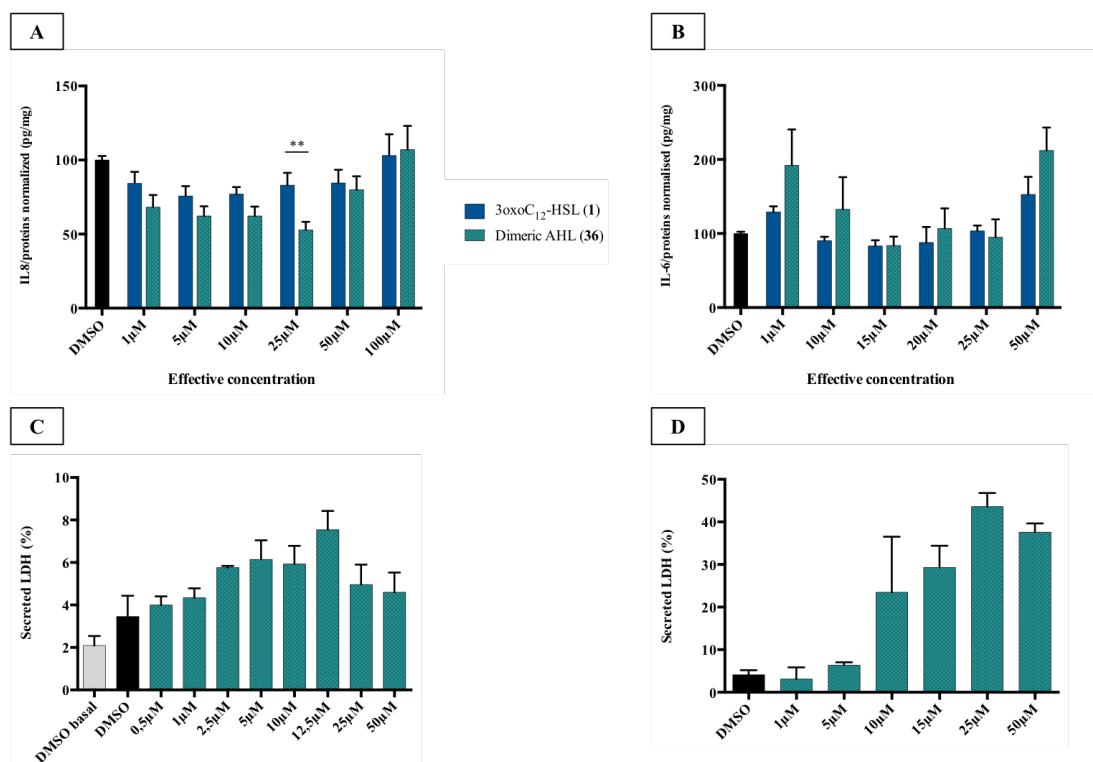


Figure 88 - Compared properties of (S)-3-oxoC₁₂-HSL (1) and compound 36 on cell models

A (resp. **B**) : IL-8 (resp. IL-6) response of cytokine-stimulated Caco-2/TC7 (resp. Raw 264.7) cells. **p < 0.01, two-way ANOVA, Sidak's post-test. **C** (resp. **D**) : secreted LDH (%) under stimulatory conditions in Caco-2/TC7 (resp. Raw 264.7) cells. The points are the mean of several replicates (n ≥ 4) ± SEM.

Although promising, these results have to be considered with precaution. We indeed observe improve effects of the dimeric AHL versus the monomer, but more work shall be achieve to demonstrate it really results from proper receptor clustering effects.

2.4. Results on bacteria strains

As stated in the introduction of this chapter, our gold standard in terms of AHL-inspired synthetic analogue should be a molecule with conserved or improved activity in mammalian cell assays, resistant to ring hydrolysis, and that cannot up-regulate bacterial populations. The SAR study has until now focused on the two first elements ; we report in the following section our results in bacterial cell assays in order to assess to analogue activity for LasR activation, and in some specific cases their bactericidal properties. Similarly to the above-mentioned mammalian cell assays we hereafter divided synthetic compounds in three categories of structural modifications to study their relative impacts.

To make this bacterial SAR study as exhaustive as possible, we also included three extra native AHLs at our disposal: C₇-HSL, 3oxoC₁₀-HSL, and 3-OH-C₁₂-HSL.

2.4.1. Results on LasR bioassay

2.4.1.1. Ketone effects

To assess the influence of the oxidation pattern at carbon-3, four molecules were tested on bacterial strain *E. coli* pSB1075 : 3oxoC₁₂-HSL (**1**), C₁₂-HSL (**27**), analogue **7a** and 3-OH-C₁₂-HSL. These illustrate the natural variety of oxidation patterns in *N*-Acyl Homoserine Lactones (ketone, proton and hydroxyl group), plus the influence of larger substituents (Figure 89).

As expected, AHL **1** best induces luminescence, as native ligand for the *Pseudomonas aeruginosa* AHL receptor LasR. Its hydroxy-counterpart can also induce a 100%-activation, but shows a loss in affinity with a EC₅₀ of 1.8μM. The replacement of ketone with protons similarly results in decreased affinity, with a EC₅₀ of 7.5μM. Intermediate **7a** can be surprisingly recognised by receptor LasR, although with poor affinity (EC₅₀ = 65μM). The half-maximum activation concentrations for **27** and **7a** must however be considered with caution, as they were inverted by analytical modelling. Indeed, the substitutions performed on these molecules impaired their water solubility, which reduced the available concentration range for bacterial assay.

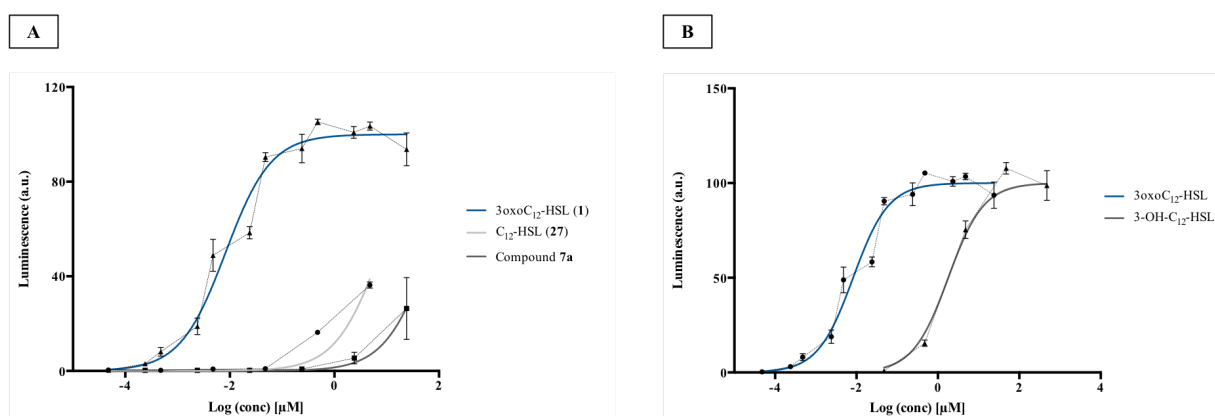


Figure 89 – Influence of carbon-3 substitution on luminescence induction in strain *E. coli* pSB1075

Four hours incubation at 37°C and 70 rpm. **A** : incubation with reference AHL **1**, natural analogue **27** and synthetic intermediate **7a**. **B** : incubation with reference AHL **1** and natural analogue 3-OH-C₁₂-HSL. All points are the mean of several replicates (n ≥ 3) ± SEM. Data normalisation and nonlinear curve fitting achieved on PRISM, GraphPad 6.0.

2.4.1.2. Influence of the acyl chain length

To assess the influence of the acyl chain length on AHL binding to receptor LasR, eight molecules with increasing numbers of carbons were tested on bacterial strain *E. coli* pSB1075: γ -butyrolactone (**30**), C₄-HSL (**28**), 3oxoC₆-HSL (**15d**), C₇-HSL, 3oxoC₁₀-HSL, 3oxoC₁₂-HSL (**1**), 12azido-3oxo-C₁₂-HSL (**15b**), and 3oxo-C₁₄-HSL (**29**). These cover a broad range of chain lengths, from the absence of acyl chain to 14-carbon-long chains.

Three analogues of reference AHL **1** could induce a 100% luminescence activation, and these are the molecules structurally closest to 3oxoC₁₂-HSL : natural AHLs 3oxoC₁₀-HSL and 3oxoC₁₄-HSL, but also synthetic analogue **15b**. 3oxoC₁₀-HSL and 3oxoC₁₄-HSL are however less potent agonists than 3oxoC₁₂-HSL with respective EC₅₀ of 90 and 400 nM, thus 10- and 45-fold increases compared to reference **1**. Analogue **15b** exhibits an EC₅₀ of the same order of magnitude as 3oxoC₁₄-HSL (500 vs. 400 nM). Given that LasR has a narrow specificity for chain length, this proximity in results confirms the assumption we made regarding the size similarity between a 14-carbon chain and a 12-carbon chain extended with an azido group.

On the opposite, the four other analogues induced bioluminescence very poorly, with no detectable EC₅₀. This result is in accordance with LasR specificity for long acyl chain lengths.

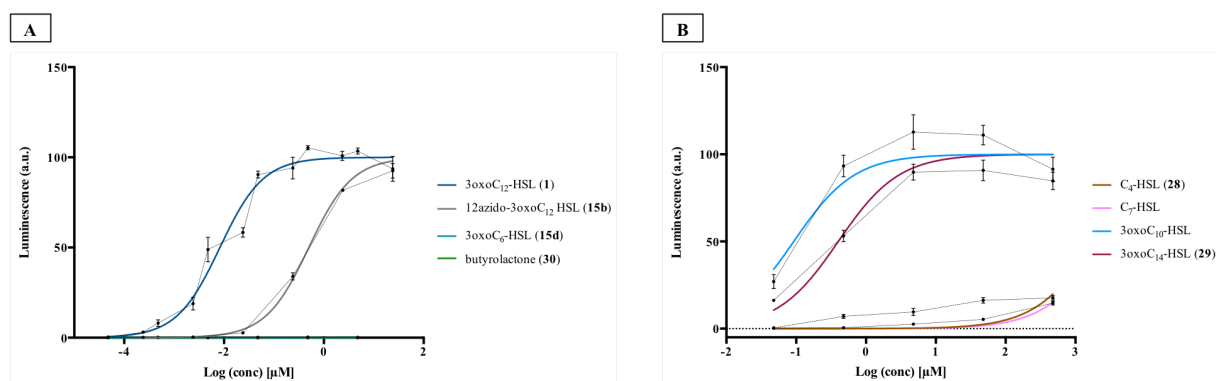


Figure 90 - Influence of acyl chain length on luminescence induction in strain *E. coli* pSB1075

Four hours incubation at 37°C and 70 rpm. **A** : incubation with reference AHL **1**, natural analogue **15d**, γ -butyrolactone **30**, and synthetic analogue **15b**. **B** : incubation with natural AHLs C₄-HSL (**28**), C₇-HSL, 3oxoC₁₀-HSL and 3oxo-C₁₄-HSL (**29**). All points are the mean of several replicates ($n \geq 3$) \pm SEM. Data normalisation and nonlinear curve fitting achieved on PRISM, GraphPad 6.0.

2.4.1.3. Substitution of the headgroup

Finally, 11 analogues were compared to reference 3oxoC₁₂-HSL in order to examine the specificity of LasR for the homoserine lactone ring. We would like to remind that our results on hydrolysed AHLs **1** and **2** and the amino acid analogues **11a-c** have shown a loss of affinity in not cyclic headgroups. Remains to decipher if rings other than HSL could activate the *P. aeruginosa* receptor.

First was investigated the LasR stereochemical specificity, by comparing the luminescence induction in presence of the (*L*) and (*D*) enantiomers of its native ligand 3oxoC₁₂-HSL (Figure 91). Transforming the (*S*) headgroup into its (*R*) enantiomer induces a severe loss of affinity, illustrated by a 1600-fold increase in EC₅₀ (9 nM vs. 14.4μM). We would like once again to highlighted the fact that the exact EC₅₀ value for analogue **15e** must be considered with caution, as it was inverted by analytical modelling. If it is certain that the enantiomeric substitution induced a severe loss of affinity, this could not be fully verified experimentally by lack of water solubility. Indeed, the AHLs critical micelle concentration (CMC) ranges about 200-250μM in aqueous solutions at 37°C.³⁸⁰

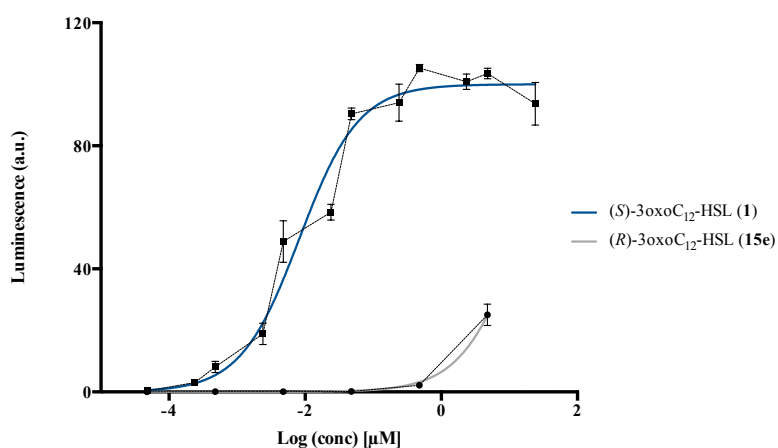


Figure 91 - Influence of stereochemistry on luminescence induction in strain *E. coli* pSB1075 : comparison between the (*S*) and (*R*) enantiomers of the 3oxoC₁₂-HSL

Four hours incubation at 37°C and 70 rpm. All points are the mean of several replicates ($n \geq 3$) \pm SEM. Data normalisation and nonlinear curve fitting achieved on PRISM, GraphPad 6.0.

Among other molecules, the thiolactone analogue **15f** was the best LasR agonist with an EC₅₀ of 130 nM (Figure 92A). Considering its difference with **1** relies on one unique atom, such an increase in affinity shows the remarkable specificity of LasR for its native ligand, and yet ACH analogue **15h** also proves to be an agonist! The latter exhibits an EC₅₀ of 170 nM. On the opposite, diastereomer **15i** does not elicit luminescence (Figure 92B).

Apart from **15h**, all other analogues with 6-membered rings are unable to interact with LasR, as proved by their incapacity to induce luminescence when incubated with the biosensor (Figure 92C).

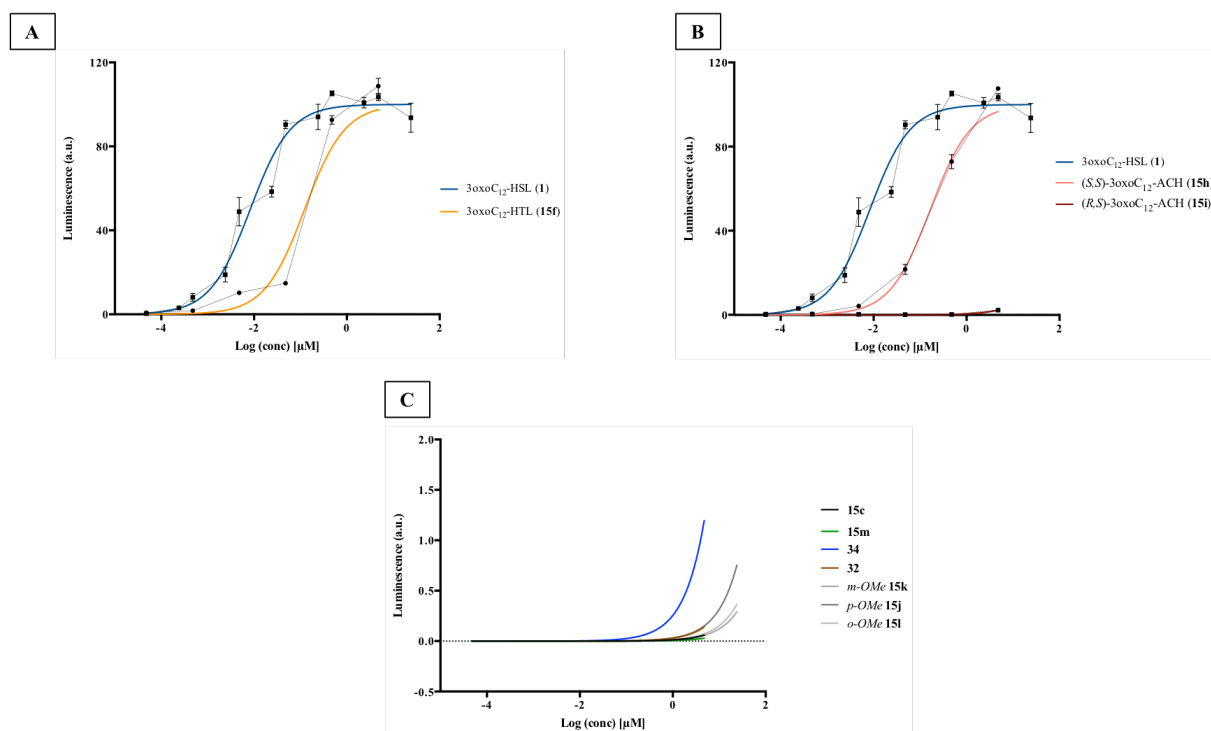


Figure 92 - Influence of cyclic headgroup substitution on luminescence induction in strain *E. coli* pSB1075

Four hours incubation at 37°C and 70 rpm. All points are the mean of several replicates ($n \geq 3$) \pm SEM. Data normalisation and nonlinear curve fitting achieved on PRISM, GraphPad 6.0. **A** : comparison of native AHL **1** and thiolactone analogue **15f**. **B** : comparison of reference AHL **1** and ACH analogues **15h** and **15i**. **C** : other non-luminescence-inducing headgroups.

2.4.2. Bactericidal properties of selected compounds

The capacity of some compounds to induce bacterial cell death was investigated. The absorbance of bacterial culture maintained during 18h in presence of increasing concentrations of tested compounds was recorded at 0 and 18h, and compared to control condition in pure

LYBHI medium. As no significant difference was observed in any experiment (all concentrations and all molecules included), we here only report the data obtained with compounds at 100 μ M (Figure 93). Overall, none of the tested compound is toxic to *E. coli* strain K12.

Especially, we investigated reference AHL **1**, and analogues that occasioned strong decreases and unpredictable results. For instance compounds **15e**, the aromatic **15j-m**, or the two ACH analogues which exhibit completely opposed behaviours.

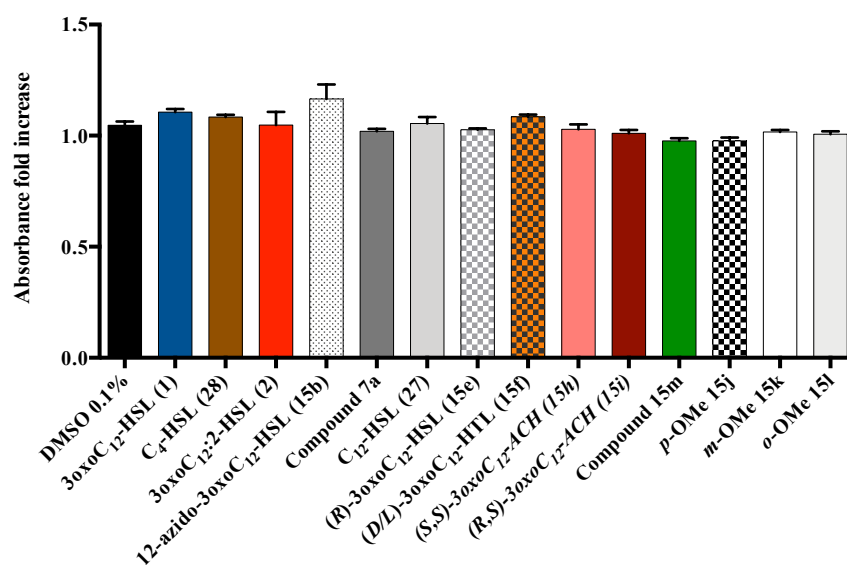


Figure 93 - Screening of analogues for bactericidal properties at 100 μ M and after 18h incubation with *E. coli* strain K12

All points are the mean of several replicates ($n \geq 7$) \pm SEM.

2.4.3. Investigation of inhibitors

The previous section has demonstrated none of the aforementioned compounds was toxic to bacteria at concentration 100 μ M and below. Hence the absence of luminescence observed upon incubation with certain compounds cannot be attributed to bacteria cell death. This should rather be the result of two phenomenon : either the pure absence of ligand interaction with the receptor, or the molecule acting as an antagonist and then inhibiting the production of luminescence.

The aromatic compounds **15j-m** for instance have been reported in literature to behave as LasR antagonists. We tested and confirmed this hypothesis for molecules **15k** and **15m** via inhibition assays (Figure 94). Briefly these experiments rely on the co-incubation of bacteria *E. coli* pSB1075 with constant dose of native ligand 3oxoC₁₂-HSL and increasing concentrations of tested compounds. From the resulting curve can be inverted the half maximum inhibition concentration IC₅₀ which characterises the affinity of a molecule for a protein partner as an antagonist.

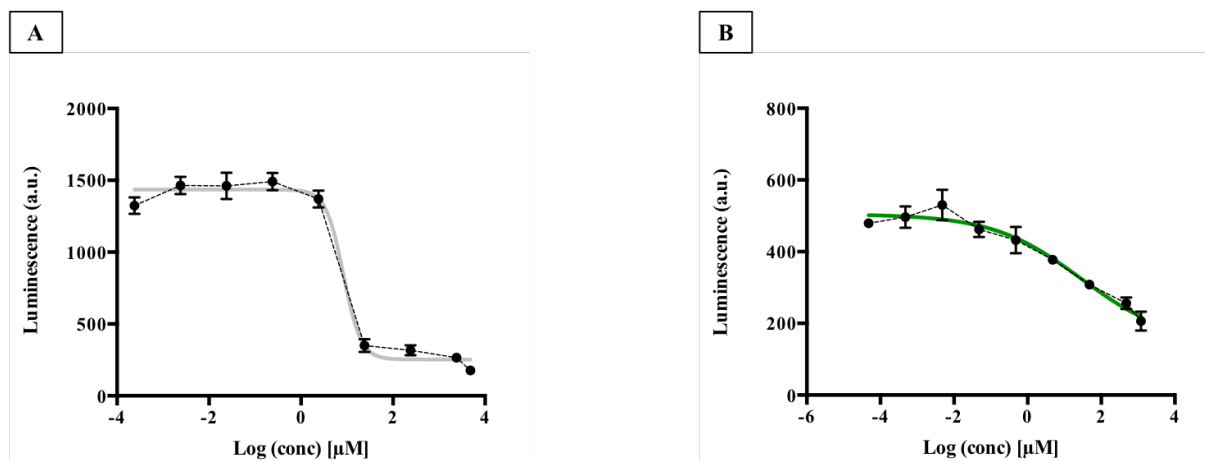


Figure 94 - Inhibition assays on luminescent strain *E. coli* pSB1075

Four hour incubation at 37°C and 70 rpm in presence of 3oxoC₁₂-HSL and increasing doses of tested compound. **A** : tested compound is meta analogue **15k**. **B** : tested compound is 2,4-amino-chlorophenol analogue **15m**. All points are the mean of several replicates ($n \geq 3$) \pm SEM. Data normalisation and nonlinear curve fitting achieved on PRISM, GraphPad 6.0.

The assays confirmed the two analogues were LasR antagonists. The methoxy-anilide **15k** appeared to retain more affinity for the receptor than **15m**, with respective IC₅₀ of 8.3 and 28.2 µM. It was also able to reduce the luminescence by 82%, while the amino-chlorophenol analogue could only reduce it by 71%.

Those results are in accordance with published data, where **15k** – but also **15j** and **15l** - has been shown to inhibit pyocyanin production via LasR antagonism on wild-type *Pseudomonas aeruginosa* strains.^{371,373} Some results were collected on various biosensor strains as well : Moore et al. have highlighted different behaviours of analogue **15k** depending on the strain employed. It can act as a LasR antagonist with an IC₅₀ superior to 200 µM on *P. aeruginosa* reporter strain PAO-JP2, but as a partial agonist on strain *E. coli* JLD271 (inhibitory behaviour with IC₅₀ of 4.7 µM and 40% max. inhibition conjugated to an agonistic behaviour with EC₅₀ superior to 100 µM and 15% max. activation).

Analogue **15m** has been described as a LasR antagonist by several groups, and Kim and co-workers have demonstrated by computational and experimental methods that **15k** was a more potent antagonist of *P. aeruginosa* LasR than **15m**.^{432,435,436}

2.4.4. Discussion on the bacterial properties of the analogue library

The results of this SAR study on bacteria strains have led to conclusions in accordance with published literature. The results for LasR activation in *E. coli* pSB1075 strain are summarised in Table 19.

Modest modifications of the AHL alkyl chain such as variation of the number of carbons or the degree of saturation have already important impacts on the molecule capacity to bind the LasR receptor. Similarly to Iglewski and co-workers we demonstrated that only analogues with tail length ranging from 10 to 14 carbons retained activity in the nanomolar range.⁴³⁷ We could further show that analogues with heteroatom-containing tails whose size fits into this length range also retained activity. On the opposite analogues with chain length outside of this range are either inactive or exhibit dramatic loss of agonistic activity. Besides length requirements, the AHL alkyl chain appears to need flexibility to retain activity. Indeed, the doubly unsaturated AHL **2** shows an 11-fold decrease in efficacy, which correlates to results from Passador and co-workers who demonstrated that AHL analogues with conformationally constrained chains had reduced biological activities.⁴³⁸ This flexibility requirement was later theorized by McCready et al. who identified LasR structural determinants regulating the receptor ligand selectivity.⁴³⁹ We have restrained our library to rather minimal modifications, but several groups have performed drastic changes to the AHL tail and identified potent agonists and antagonists.⁴³⁶

Large libraries of AHL analogues with non-natural headgroups have been synthesized to date. Early studies from Passador et al. identified pure (*S*)-thiolactone analogue as a strong LasR agonist, with activity close to that of native ligand **1**.⁴³⁷ This result was later confirmed by Smith and co-workers, who used the racemic compound in their study on gfp-producing reporter strain *P. aeruginosa* PAO-JP2 harbouring plasmid *plasI-LVA*gfp.⁴³⁵ Surprisingly a compound with a close structure to native homoserine lactone ring appeared inactive in their

work : a HSL where the amide bond had been replaced with an ester. The authors hypothesized the amino group is required for activity, which may partially explain why carbohydrate analogue **34** is inactive in our screening. Janssens et *al.* have also identified racemic analogue **15f** as an agonist of orphan LuxR homolog SdiA from *Salmonella enterica*, although thiolactone-derived AHL analogues with shorter chain were the more potent agonists.²⁵⁰ Finally, McInnis et *al.* firmly confirmed the agonistic behaviour of both **15f** and **15g** using crossed agonism and antagonism assays on two different reporter strains.⁴²⁹ The authors quantified the EC₅₀ of pure enantiomer **15g** as 92 nM on a *E. coli*-based reporter strain, and 3.2 μM on a *P. aeruginosa*-based reporter strain. Considering their strains differ from the one we employed, strict comparisons are hard to establish but the two values obtained on *E. coli* biosensors remain of the same order of magnitude. Interestingly their work also highlighted a thiolactone equivalent of C₁₂-HSL as a reasonably good LasR agonist with respective EC₅₀ of 1.9 and 21 μM. This finding confirms the high proximity between homoserine lactones and homocysteine lactone rings.

Smith et *al.* pioneered the investigation of AHL analogues with aminocyclohexanol headgroup. As soon as 2003, the group described the (*S,S*)-isomer **15h** as a LasR agonist with inducing properties similar to that of native AHL **1**.⁴⁴⁰ Their study also included analogues with ring headgroups 2-aminocyclopentanone, 2-aminocyclopentanol and 2-aminocyclohexanone, structures closer to the native HSL ring. Surprisingly these compounds exhibited poor activities. The same group later demonstrated that the hydroxyl in position adjacent to the amino group was a requirement for activity, as analogues with aminocyclohexane and 4-aminocyclohexanol heads were unable to interact with LasR as agonists.⁴³⁵ To explain these differences the authors hypothesized that the hydroxyl could mimic the carbonyl group of native HSL to participate in H-bonds while the cyclohexane ring mimicked the saturated ring structure of homoserine to perform hydrophobic interaction.

Jog et *al.* brought the investigation on 2-aminocyclohexanol headgroups further and synthesized all four isomers. Among these (*S,S*) analogue **15h** exhibited the highest agonist activity and was nearly comparable to native LasR ligand AHL **1**. Surprisingly its enantiomer the (*R,R*) form was also active, although with an approximate 2-fold lower activity. Based on LasR stereo-preference for the (*L*) isomer of 3oxoC₁₂-HSL versus the (*D*) isomer, this outcome was predictable. The observed difference in activity between (*S,S*)-3oxoC₁₂-ACH and (*R,R*)-3oxoC₁₂-ACH is however much smaller than that between (*S*)-3oxoC₁₂-HSL and (*R*)-3oxoC₁₂-HSL, which indicates greater LasR discrimination for its native ligand than analogues. Among

the four diastereomers analogue **15i** was identified as the least active, which matches our own results.

As previously stated, aromatic AHL analogues **15j-m** have been reported to be LasR antagonist by a great number of groups.^{371,373,431,432,435} Observing that both **15m** and a 2-aminophenol AHL analogue exhibited similar LasR antagonisms, Smith et al. assumed the pattern of adjacent hydroxyl and amino groups was required for activity in aromatic rings like in aminocyclohexanol analogues. The unsaturated carbon bonds would then make the whole difference in behaviour between agonism and antagonism. The activity is however much lower when considering 3-aminophenol. Surprisingly, this hypothesis does not stand when methoxy-anilide derivatives are concerned. Spring and co-workers indeed studied the antagonist effects of series **15j-l** and identified the *para* analogue **15j** as the most powerful LasR antagonist, while the *ortho* agonist **15l** was the weakest. This *ortho* position should however correspond to the criteria suggested by Smith et al.. This finding led the authors to assume an hydrogen-bond acceptor was required in *meta* or *para* position for antagonist activity, whereas with the hydroxyl group that could act either as H-bond donor or acceptor, an *ortho* position was demanded. Those results match our own findings.

<i>Compound</i>	<i>EC₅₀</i> (μ M)	<i>95% CI</i> (μ M)	<i>Max. activation</i> (%)
(<i>S</i>)-3oxoC ₁₂ -HSL 1	0.009	0.007 – 0.010	100
(<i>S</i>)-3oxoC ₁₂ :2-HSL 2	0.10	0.081 – 0.127	100
3dioxalane-C ₁₂ -HSL 7a	65	40 – 110	45
12azido-3oxoC ₁₂ -HSL 15b	0.50	0.42 – 0.59	95
3oxoC ₁₂ -Bz 15c	> 1000	-	0.02
(<i>S</i>)-3oxoC ₆ -HSL 15d	> 1000	-	0.03
(<i>R</i>)-3oxoC ₁₂ -HSL 15e	14.4	12.6 – 16.5	30
(<i>D/L</i>)-3oxoC ₁₂ -HTL 15f	0.13	0.08 – 0.19	100
(<i>S,S</i>)-3oxoC ₁₂ -ACH 15h	0.17	0.13 – 0.21	100
(<i>R,S</i>)-3oxoC ₁₂ -ACH 15i	202	177 – 231	5
<i>p</i> -OMe 15j	> 1000	-	1
<i>o</i> -OMe 15k	> 1000	-	0.5
<i>m</i> -OMe 15l	> 1000	-	0
3oxoC ₁₂ -chlorophenol 15m	> 1000	-	0.08
(<i>S</i>)-C ₁₂ -HSL 27	7.5	6.0 – 9.4	42
(<i>S</i>)-C ₄ -HSL 28	> 1000	-	15
γ -butyrolactone 30	> 1000	-	0.25
3oxoC ₁₂ -aminopiperidine 32	> 1000	-	0.11
3oxoC ₁₂ -sugar 34	393	308 - 501	1.6
C ₇ -HSL	> 1000	-	18
3oxoC ₁₀ -HSL	0.09	0.05 – 0.17	100
3-OH-C ₁₂ -HSL	1.80	1.25 – 2.60	100
3oxoC ₁₄ -HSL	0.40	0.27 – 0.59	90

Table 19 – Summarised properties of analogues on reporter strain *E. coli* pSB1075

It is important to note that molecule **15m** meets the criteria we defined for identification of a lead candidate. On top of demonstrating improved activity on mammalian cell assays and being PON-resistant, this analogue does not positively modulate bacteria in our assays. Indeed, acting as a LasR antagonist, the molecule should not induce the upregulation of *P. aeruginosa* pathogenic phenotypes such as biofilm formation and pyocyanin production. The molecule is furthermore not toxic for bacterial population at 100µM, the maximum dose tested in our eukaryotic assays. Bactericidal properties could for instance be deleterious in dysbiotic and immune-compromised individuals because they would make ecological niches available for colonisation by pathogenic bacterial communities.

On the opposite, analogue **15h** exhibits promising activity on mammalian models, but its LasR agonistic behaviour might prevent it from future *in vivo* experimentation.

Conclusions & Perspectives

This interfacial PhD project has explored many diverse aspects of AHL biology from early cell results to metabolism and the development of bio-inspired synthetic analogues.

Through this work we have confirmed AHL anti-inflammatory results on Raw 264.7 macrophages, and demonstrated for the first time similar properties on an epithelial intestinal cell line under inflammatory conditions. Furthermore, we studied the AHL stability and cell metabolism, a topic often unexplored and neglected in previous biological studies. Our results have demonstrated their poor stability and solubility in biological media (half-life ca 3-4 h), giving rise to several metabolites. The existence of degradation products questions previous literature and conclusions : is the AHL or its hydrolysed form responsible for the observed biological effects? Which form of the molecule interacts with the candidate receptors? So many questions that require a better understanding of the AHL cellular mechanism of action.

The AHL analogues we developed may bring the beginning of an answer. Through our bio-inspired library few compounds retained significant biological activity, except for two. The aminochlorophenol candidate **15m** is to date our lead candidate, and has recently been patented (see Annexe A.3.c). Because this molecule retains LasR activity – although as an inhibitor – we suggest it may have a similar mode of action on mammalian cells as the native 3oxoC₁₂-HSL. This assumption shall be verified through live-cell imaging competitive binding assay. On the opposite to AHL **1**, the analogue **15m** cannot undergo hydrolysis ; it is also more active than the reference AHL on both macrophages and enterocytes. These characteristics make **15m** a good AHL surrogate to perform receptor fishing.

We had developed a biotinylated-AHL to perform protein receptor co-precipitation, but through literature and our experience we found that this was a limited technique. Given the range of AHL concentrations employed for activity, it is plausible that AHLs exhibit low affinity to their protein partners. Low-affinity binding is a serious drawback to protein identification : it either constrains to perform insufficient purification giving rise to a large number of candidates with poor affinity, or the partner may be lost through purification steps making the search fruitless. To illustrate that point, results from Karlsson *et al.* or Hänsch and co-workers are not particularly conclusive ; their investigations returned a very large number of low-affinity

proteins that the authors chose to regard as “background protein hits”.^{320,410} With a ligand of greater affinity however, the protein receptor identification shall have more chances of success. The preparation of a biotinylated version of analogue **15m** shall be easy to perform, given that we have already developed all the necessary building blocks and protocols to prepare the biotinylated AHL **29**.

Meanwhile, the aminochlorophenol candidate **15m** could use further investigation to explore its full potential in broader situations. Its activity could be tested, on new cell models for instance, such as transepithelial permeability or Th17/IL-17 models. AHL **1** has indeed been shown to have deleterious effects on the intestinal epithelium through induction of increased permeability ; the analogue might behave differently. More importantly, *in vivo* assays with small mammals will be carried out. Finally, the SAR study has highlighted interesting anti-inflammatory properties from 14-carbon-long acyl chain ; although preliminary, these experiments should be repeated, and in case of positive outcome the synthesis of a 3oxoC₁₄-aminochlorophenol might reveal an even more powerful analogue. Likewise, our first results with a dimeric AHL are promising. These should be repeated, and the preparation of a dimeric **15m** may be likely.

In terms of mechanism, the exact AHL receptor(s) remain unknown and our work could not confirm any candidate. Apart from T2R38, IQGAP1 and PPAR- γ , recent studies on the physical nature of AHL-binding domain in bacteria have shed new light on putative mammalian receptors. These have especially identified structural similarities between bacterial receptors and widely evolutionary-conserved PAS and GAF domains.^{261,441–444} These domains can be found in a broad array of mammalian proteins such as the aryl hydrocarbon receptor (AhR), but also neuronal carbon monoxide sensor NPAS2 and hypoxia-inducible factor 1 HIF1. We also feel that aquaporins presented in the Introduction, and in particular AQP9, could be plausible candidates as they mediate transport between the intra- and extracellular compartments, and have been implicated in inflammatory disorders.

For the first time, we demonstrated AHL are ionophore molecules, with affinity for iron and copper (and maybe more). We also reported beneficial AHL effects on ROS secretion, which is a novel mechanism of action. In a dose- and time-dependent manner, the 3oxoC₁₂-

HSL is capable of inhibiting the deleterious effects of DMSO on cellular pro-inflammatory mechanisms. These observations also question the dogmatic use of DMSO as a vehicle. Indeed there are several records in literature reporting the non-negligible effects of DMSO itself on biological models.^{415,445,446} Alternative organic solvents could be investigated such as ethanol and acetone. Otherwise to administrate larger doses, formulation in oily solutions (Kolliphor® and Cremophor® are commonly employed in galenic) or gastro-resistant capsules could be an answer.

Finally, and to go back to the start of this project, the origin and exact structure of the 3oxoC₁₂:2-HSL remains unknown. The extremely low amounts of AHLs extracted from faecal samples are the main limitations to the 3oxoC₁₂:2-HSL precise structure assessment. Indeed, extracted quantities are so small that we reached the detection limit, even with high precision mass spectrometry. Despite its correlation to normobiosis, we could not highlight strong beneficial effects of the 3oxoC₁₂:2-HSL on our cell models. Two hypothesis arise to explain those findings : the unsaturated compound might simply be less affine for the AHL receptor and hence less active ; or the isomer we synthesized might not be the one originally extracted from faecal samples. Lipophilicity considerations tend to support the first hypothesis. Indeed, experimental results and computational predictions (*Part II – 2.1.2.3*) suggest insaturations are detrimental to biological activity by rigidifying the structure and decreasing lipophilicity.

This apparent dead-end requires further investigation, and improvement of isolation and sample purification techniques. One could consider for instance a technique to sequestrate ketone-containing compounds ; as a result the samples would be enriched in AHLs, making their detection and characterisation easier. This enrichment may also allow the study of multiple AHL patterns, instead of limiting our investigation to a single molecule as we did.

List of Figures

Figure 1 - General structure of <i>N</i> -acyl homoserine lactones	34
Figure 2 - Non-conventional forms of type-1 autoinducers.....	34
Figure 3 - Type-2 autoinducers (<i>S</i>)-THMF-borate (A) and (<i>R</i>)-THMF (B).....	36
Figure 4 - Chemical structures of Cholerae autoinducer-1 (CAI-1) from <i>Vibrio cholerae</i>	39
Figure 5 - Molecular structure of 3-hydroxypalmitic acid methyl ester.....	39
Figure 6 - <i>Pseudomonas</i> Quinolone Signal (PQS) biosynthetic pathway	40
Figure 7 - Molecular structure of DKPs.....	41
Figure 8 – Chemical structure of γ -butyrolactone.....	41
Figure 9 - Auto-inducing peptides I and II from <i>Staphylococcus aureus</i>	42
Figure 10 - Structure of PON inhibitor 2-hydroxyquinoline (2-HQ).....	54
Figure 11 – Heatmap of found AHLs in faecal samples from IBD patients and healthy subjects as identified by their <i>m/z</i> ratio and the medical status of the donor.....	59
Figure 12 - Growth curve of Caco-2 cells showing the exponential growth phase, the arrest of growth at confluence, and the stationary phase where differentiation occurs.	62
Figure 13 - Atom numbering convention for natural AHL and synthetic analogues	74
Figure 14 - Effects of diverse IL-1 β doses on IL-8 secretion (A) and cytotoxicity (B) in Caco-2/TC7 cells.....	116
Figure 15 - Compared inflammation inductions in Caco-2/TC7 cells with 25 ng/ml IL-1 β stimulation versus combined TNF- α and IFN- γ at 50 ng/ml each.....	116
Figure 16 - Compared effects of activating cocktails on Raw 264.7 macrophages	117
Figure 17 - Effects of DMSO 0,1% and inhibitor 2-HQ on the inflammatory response of Caco-2/TC7 cells (A) and Raw 264.7 macrophages (B).....	117
Figure 18 – Cytotoxicity of AHL treatment on Caco-2/TC7 cells in stimulated state as measured by LDH release	118
Figure 19 - Effects of addition of IL-1 β and DMSO on cytotoxicity in Caco-2/TC7 cells.....	119
Figure 20 - Cytotoxicity of AHL treatment on Raw 264.7 cells in resting and stimulated states as measured by LDH release	120
Figure 21 - IL-8 secretory response of IL-1 β activated Caco-2/TC7 cells in presence of AHL 3oxoC12-HSL (A) and 3oxoC12:2-HSL (B)	121
Figure 22 - IL-8 secretory response of resting Caco-2/TC7 cells in presence of AHL 3oxoC12-HSL (A) and 3oxoC12:2-HSL (B).....	121
Figure 23 - IL-8 secretory response of TNF- α /IFN- γ activated Caco-2/TC7 cells in presence of AHL 3oxoC12-HSL (A) and 3oxoC12:2-HSL (B)	122
Figure 24 – Intracellular IL-8 secretory response of activated Caco-2/TC7 cells after 3-hour incubation in presence of increasing doses of 3oxoC12-HSL.....	123
Figure 25 - IL-8 secretory response of resting or activated Caco-2/TC7 cells with DMSO 0.1% after successive 4-hour pre-incubation with DMSO 0.1%, 5 μ M or 10 μ M 3oxoC12-HSL and 18-hour incubation in presence of increasing doses of 3oxoC12-HSL.....	124

<i>Figure 26 - Compared IL-8 secretory response of activated Caco-2/TC7 cells after successive 4-hour incubation and 18-hour incubation in presence of increasing doses of 3oxoC₁₂-HSL.....</i>	<i>125</i>
<i>Figure 27 - IL-6 secretory response of LPS/IFN-γ activated Raw 264.7 murine macrophages in presence of AHLs.....</i>	<i>126</i>
<i>Figure 28 - IL-1β secretory response of TNF-α/IFN-γ activated Caco-2/TC7 cells in presence of AHL 3oxoC₁₂-HSL (A) and 3oxoC₁₂:2-HSL (B).....</i>	<i>127</i>
<i>Figure 29 – TNF-α secretory response of LPS/IFN-γ activated Raw 264.7 murine macrophages in presence of AHLs.....</i>	<i>127</i>
<i>Figure 30 - Human mRNA levels for cytokines IL-8 (A) and IL-1β (B) in Caco-2/TC7 cells after 4h incubation with AHLs.....</i>	<i>128</i>
<i>Figure 31 – IL-10 secretory response of LPS/IFN-γ activated Raw 264.7 murine macrophages in presence of AHLs.....</i>	<i>129</i>
<i>Figure 32 – Ratio of secreted IL-10 over secreted TNF-α in response to LPS/IFN-γ inflammatory stimulus in Raw 264.7 murine macrophages in presence of AHLs.....</i>	<i>130</i>
<i>Figure 33 - Emission of luminescence by the bacteria reporter strain E. coli pSB1075 in presence of a range of concentrations of AHLs.....</i>	<i>131</i>
<i>Figure 34 - Compared survival and growth of E. coli strain K12 incubated with controls or increasing doses of 1 (A) or 2 (B) as read by absorbance at 600nm.....</i>	<i>132</i>
<i>Figure 35 – Stereoelectronic effects in esters depend on their spatial conformation.....</i>	<i>137</i>
<i>Figure 36 - Standard curve for 3oxoC₁₂-HSL ranging from 300 nM to 100 μM in tandem LC-MS/MS.....</i>	<i>138</i>
<i>Figure 37 - Compared kinetics for AHL decay and degradation products apparition.....</i>	<i>138</i>
<i>Figure 38 - Compared biological effects of tetramic acid 8 on cell lines Caco-2/TC7 cells and Raw 264.7 macrophages.....</i>	<i>140</i>
<i>Figure 39 - Compared emission of luminescence by the bacteria reporter strain E. coli pSB1075 in presence of a range of AHL and tetramic acid concentrations.....</i>	<i>141</i>
<i>Figure 40 - Survival assay of E. coli strain K12 in presence of increasing doses of tetramic acid 8.....</i>	<i>142</i>
<i>Figure 41 - Influence of 0.1% DMSO, PON inhibitor 2-HQ and cytokines on Caco-2/TC7 cells PON-2 mRNA expression.....</i>	<i>144</i>
<i>Figure 42 – Compared effects of increasing doses of AHLs 1 and 2 under various conditions on Caco-2/TC7 cells PON-2 and -3 mRNA expression.....</i>	<i>145</i>
<i>Figure 43 - Compared biological responses to AHLs in presence or absence of PON inhibitor 2-hydroxyquinoline.....</i>	<i>146</i>
<i>Figure 44 – Compared TNF-α responses of LPS/IFN-γ stimulated Raw 264.7 macrophages in presence of natural molecule 3oxoC₁₂-HSL (1) and analogue 3oxoC₁₂-serine (11c).....</i>	<i>150</i>
<i>Figure 45 - Compared TNF-α responses of LPS/IFN-γ stimulated Raw 264.7 macrophages in presence of natural molecule 3oxoC₁₂-HSL (1) and analogues 11a-b.....</i>	<i>151</i>
<i>Figure 46 - Compared LDH secretion (%) of LPS/IFN-γ stimulated Raw 264.7 macrophages in presence of analogues 11a-b.....</i>	<i>151</i>
<i>Figure 47 - 24-hour time evolution of supernatant load in 3oxoC₁₂-HSL, 3oxoC₁₂-HS and C₁₂-TA.....</i>	<i>153</i>

<i>Figure 48 - Partition of PON inhibitor 2-hydroxyquinoline between the extra- and intracellular compartments</i>	155
<i>Figure 49 – Compared proportions of total amount of molecules found in total cell lysate over time</i>	155
<i>Figure 50 – Proportions of homoserine lactone and homoserine forms found in Caco-2/TC7 cell lysates over time</i>	156
<i>Figure 51 – Silica gel TLC plates of 3oxoC₁₂-HSL and 3oxoC₁₂-HS</i>	157
<i>Figure 52 - Time evolution from 0 to 4h of the bioluminescence emitted by strain E. coli pSB1075 in presence of increasing doses of autoinducers and their hydrolysed derivatives</i>	159
<i>Figure 53 – Bioluminescence emitted by strain E. coli pSB1075 in presence of increasing doses of AHL analogues with amino acid headgroups</i>	160
<i>Figure 54 - Spectral properties of fluorescent molecules 12 and 13</i>	164
<i>Figure 55 – Biological activity on Caco-2/TC7 cells in presence of fluorescent molecules 12 and 13</i>	164
<i>Figure 56 - Fixed-cell imaging of control fluorophore 13 and FITC-tagged 3oxoC₁₂-HSL 12</i>	165
<i>Figure 57 – Live-cell imaging with AHL-FITC 12</i>	167
<i>Figure 58 – Competition assay between AHL-FITC 12 and non-tagged AHLs 1 and 2</i>	168
<i>Figure 59 – Compared results with 1μM AHL-FITC 12 after 1h or 24h incubation time</i>	169
<i>Figure 60 – Biological activity of clickable analogue 15b</i>	172
<i>Figure 61 – Compared IL-8 response of cytokine-stimulated Caco-2/TC7 cells incubated with increasing doses of analogue 15b (in white) or natural 3oxoC₁₂-HSL 1</i>	173
<i>Figure 62 - Analogue 15b activity in bacteria lines</i>	173
<i>Figure 63 - Spectral properties of fluorescent molecule 18</i>	175
<i>Figure 64 - Biological activity on Caco-2/TC7 cells in presence of fluorescent molecules AHL-NBD (18) and NBD-Cl</i>	175
<i>Figure 65 - Compared results with 1μM AHL-NBD 18 or 1μM control NBD-Cl after 1h or 24h incubation time</i>	177
<i>Figure 66 - Compared results with 1μM AHL-NBD 18, 1μM control NBD-Cl or 1μM AHL-NBD combined to 50μM 3oxoC₁₂-HSL after 1h incubation time</i>	178
<i>Figure 67 - Spectral properties of fluorescent molecules 20, 23, 24 and 26</i>	182
<i>Figure 68 - Fixed-cell imaging of naphthalimide-tagged AHLs 23 (A) and 26 (B) and their respective controls 20 and 24</i>	183
<i>Figure 69 - Live-cell imaging of molecules 20 (A), 23 (B), 24 (C) and 26 (D)</i>	184
<i>Figure 70 – Biological activity of biotinylated AHL 29</i>	190
<i>Figure 71 - Cyclic voltammetry of FeCl₃ in presence of several equivalents of ligand</i>	193
<i>Figure 72 - Structure of an hypothetical 3:1 hexadentate complex between Fe(III) and ligand 15c</i>	193
<i>Figure 73 – Fluorescence emitted by probe H₂-DCFDA upon oxidation by intracellular ROS</i>	195
<i>Figure 74 - General frame of N-Acyl Homoserine Lactone analogues</i>	197
<i>Figure 75 - Compared properties of 3oxoC₁₂-HSL (1), C₁₂-HSL (27) and analogue 7a on our cell models</i>	205
<i>Figure 76 - Compared properties of 3oxoC₁₂-HSL (1) versus short-chain analogues γ-butyrolactone (30), C₄-HSL (28) and 3oxoC₆-HSL (15d) on cell models</i>	207

Figure 77 - Compared properties of 3oxoC ₁₂ -HSL (1) versus long-chain analogues 3oxoC ₁₄ -HSL (29) and 12azido-3oxoC ₁₂ -HSL (15b) on cell models	209
Figure 78 - Compared properties of (S)-3oxoC ₁₂ -HSL (1) versus its stereoisomer (R)-3oxoC ₁₂ -HSL (15e) on cell models.....	212
Figure 79 - Compared properties of (S)-3oxoC ₁₂ -HSL (1) and its thiolactone analogues (S)-3oxoC ₁₂ -HTL (15g) and (D/L)-3oxoC ₁₂ -HTL (15f) on cell models.....	214
Figure 80 - Compared properties of (S)-3oxoC ₁₂ -HSL (1) and its cyclohexanol analogues (S,S)-3oxoC ₁₂ -ACH (15h) and (R,S)-3oxoC ₁₂ -ACH (15i) on cell models.....	216
Figure 81 - Compared properties of (S)-3oxoC ₁₂ -HSL (1) and its methoxy-anilide analogues 15j, 15k and 15l, on cell models.....	218
Figure 82 – Compared IL-8 secretion in cytokine-stimulated Caco-2/TC7 cells in presence of increasing doses of methoxy-anilide analogue 15k with and without 100µM PON inhibitor 2-hydroxyquinoline	219
Figure 83 - Compared properties of (S)-3oxoC ₁₂ -HSL (1) and amino-chlorophenol analogue 15m on cell models	220
Figure 84 - Compared properties of (S)-3oxoC ₁₂ -HSL (1) and benzyl analogue 15c on cell models.....	221
Figure 85 - Compared properties of (S)-3oxoC ₁₂ -HSL (1) and analogue 32 on cell models.....	222
Figure 86 - Compared properties of (S)-3oxoC ₁₂ -HSL (1) and compound 34 on cell models.....	223
Figure 87 - Compared effects of increasing doses of AHL 1 and two synthetic analogues 15h and 15m on Caco-2/TC7 cells IL-8 and IL-1β mRNA expression.....	226
Figure 88 - Compared properties of (S)-3oxoC ₁₂ -HSL (1) and compound 36 on cell models.....	228
Figure 89 – Influence of carbon-3 substitution on luminescence induction in strain E. coli pSB1075.....	229
Figure 90 - Influence of acyl chain length on luminescence induction in strain E. coli pSB1075	230
Figure 91 - Influence of stereochemistry on luminescence induction in strain E. coli pSB1075 : comparison between the (S) and (R) enantiomers of the 3oxoC ₁₂ -HSL.....	231
Figure 92 - Influence of cyclic headgroup substitution on luminescence induction in strain E. coli pSB1075 ..	232
Figure 93 - Screening of analogues for bactericidal properties at 100µM and after 18h incubation with E. coli strain K12.....	233
Figure 94 - Inhibition assays on luminescent strain E. coli pSB1075.....	234
Figure 95 – LDH-catalysed oxidation of NADH into NAD ⁺	277
Figure 96 - Structures of NADH and NAD ⁺	277
Figure 97 – Structure of copper (I) complex with BCA.....	278
Figure 98 - Description of the ELISA steps.....	279

List of Schemes

<i>Scheme 1 - Biosynthesis of AHL as catalysed by LuxI-type AHL synthases</i>	35
<i>Scheme 2 - Biosynthesis of DPD involving LuxS</i>	37
<i>Scheme 3 - Complex equilibria involving DPD and its derivatives in the AI-2 pool system</i>	37
<i>Scheme 4 - General synthesis of 3oxoC₁₂-HSL (1)</i>	113
<i>Scheme 5 - General synthesis of 3oxoC₁₂:2-HSL (2)</i>	114
<i>Scheme 6 – Hydrolysis of AHL into open-form corresponding acyl homoserine</i>	136
<i>Scheme 7 - Irreversible conversion of AHLs into tetramic acids</i>	137
<i>Scheme 8 - Preparation of tetramic acid 8 from precursor 3oxoC₁₂-HSL</i>	139
<i>Scheme 9 – Equilibrium between closed- and open-ring forms 3oxoC₁₂-HSL and 3oxoC₁₂-HS</i>	147
<i>Scheme 10 - Synthetic pathway for preparation of AHL analogues 11a-c bearing amino acid headgroups</i>	147
<i>Scheme 11 - Common TFA deprotection step of O^tBu- and ketal-protected chemical functions</i>	148
<i>Scheme 12 - Fluorescein-tagged AHL and control</i>	163
<i>Scheme 13 - Synthetic path for preparation of non-natural analogue 12-azido-3oxoC₁₂-HSL (15b)</i>	171
<i>Scheme 14 - Three-step synthesis of NBD-tagged AHL 18</i>	174
<i>Scheme 15 - Synthetic path for the preparation of a naphthalimide-tagged AHL with a free primary amine (compound 23)</i>	180
<i>Scheme 16 - Synthetic path for the preparation of a 4-piperidinyl-naphthalimide-tagged AHL (compound 26)</i> 181	
<i>Scheme 17 - Three-step synthesis of biotin-tagged 3oxoC₁₂-HSL (compound 29)</i>	189
<i>Scheme 18 - Synthesis of AHL analogue 18c</i>	191
<i>Scheme 19 - General methodologies for synthesis of natural 3oxo N-Acyl Homoserine Lactones</i>	199
<i>Scheme 20 - Compared synthetic routes for non 3-oxo natural AHLs preparation</i>	199
<i>Scheme 21 - Synthesis for preparation of non-natural AHL analogues with cyclic headgroups</i>	201
<i>Scheme 22 - Synthesis of dimeric AHL 36</i>	227

List of Tables

<i>Table 1 - Overview of compared clinical, endoscopic and histological characteristics in patients with IBD.....</i>	<i>16</i>
<i>Table 2 - Montreal Classification for Crohn's Disease.....</i>	<i>17</i>
<i>Table 3 - Montreal Classification of extent and severity for Ulcerative Colitis</i>	<i>18</i>
<i>Table 4 - First identified dominant cultivable bacterial genera</i>	<i>24</i>
<i>Table 5 - Main bacterial phyla in the gut microbiota as identified by recent studies</i>	<i>25</i>
<i>Table 6 - General features of dysbiosis in IBD.....</i>	<i>28</i>
<i>Table 7 - Some examples of LuxI/LuxR-type AHL systems.....</i>	<i>33</i>
<i>Table 8 - Summary table of exposed Quorum Sensing molecules.....</i>	<i>42</i>
<i>Table 9 - qPCR well content.....</i>	<i>68</i>
<i>Table 10 - Primers sequences for qPCR</i>	<i>68</i>
<i>Table 11 - Summary properties of diverse natural and commercial AHLs</i>	<i>131</i>
<i>Table 12 - First order kinetic constants for AHL degradation in cell-free medium at r.t.....</i>	<i>139</i>
<i>Table 13 - Compared specific activities of several purified PON proteins for 5-HL and 3oxoC₁₂-HSL hydrolysis</i>	<i>143</i>
<i>Table 14 – Compared predicted physical properties of 3oxoC₁₂-HSL, 3oxoC₁₂-HS, and amino acid analogues.....</i>	<i>149</i>
<i>Table 15 - Overview of all prepared and employed AHL analogues during the SAR study</i>	<i>203</i>
<i>Table 16 – Compared efficiency in IL-8 secretion reduction of reference 3oxoC₁₂-HSL (1) and long-chain analogue 3oxoC₁₄-HSL (29).....</i>	<i>209</i>
<i>Table 17 – Compared physical properties of reference 3oxoC₁₂-HSL (1) and several analogues with modified acyl chains.....</i>	<i>211</i>
<i>Table 18 – Compared physical properties of reference AHL 1 and analogues 15h, 15i and 15m.....</i>	<i>224</i>
<i>Table 19 – Summarised properties of analogues on reporter strain E. coli pSB1075</i>	<i>237</i>

References

1. Ordas, I., Eckmann, L., Talamini, M., Baumgart, D. C. & Sandborn, W. J. Ulcerative colitis. *Lancet* **380**, 1606–1619 (2012).
2. Beaugerie, L. & Itzkowitz, S. H. Cancers Complicating Inflammatory Bowel Disease. *N. Engl. J. Med.* **372**, 1441–1452 (2015).
3. Baumgart, D. C. & Sandborn, W. J. Crohn's Disease. *Lancet* **380**, 1590–1605 (2012).
4. University, J. H. John Hopkins Medical Department course on Crohn's Disease.
5. Strange, E. F. *et al.* European evidence-based consensus on the diagnosis and management of Crohn's disease: definitions and diagnosis. *Gut Suppl* **I**, i1–i5 (2006).
6. Levine, J. S. & Burakoff, R. Extraintestinal manifestations of inflammatory bowel disease. *Gastroenterol. Hepatol. (N. Y.)* **7**, 235–41 (2011).
7. Vavricka, S. R. *et al.* Extraintestinal Manifestations of Inflammatory Bowel Disease. *Inflamm. Bowel Dis.* **21**, 1982–1992 (2015).
8. Podolsky, D. K. The current future understanding of inflammatory bowel disease. *Best Pract. Res. Clin. Gastroenterol.* **16**, 933–943 (2002).
9. Loftus, E. J. *et al.* Crohn's disease in Olmsted County, Minnesota, 1940–1993: incidence, prevalence, and survival. *Gastroenterology* **114**, 1161–1168 (1998).
10. Schwartz, D. A. *et al.* The natural history of fistulizing Crohn's disease in Olmsted County, Minnesota. *Gastroenterology* **122**, 875–880 (2002).
11. Thia, K. T., Sandborn, W. J., Harmsen, W. S., Zinsmeister, A. R. & Loftus, E. V. Risk Factors Associated With Progression to Intestinal Complications of Crohn's Disease in a Population-Based Cohort. *Gastroenterology* **139**, 1147–1155 (2010).
12. Peyrin-Biroulet, L., Loftus, E. V., Colombel, J.-F. & Sandborn, W. J. The Natural History of Adult Crohn's Disease in Population-Based Cohorts. *Am. J. Gastroenterol.* **105**, 289–297 (2010).
13. Loftus, C. G. *et al.* Update on the incidence and prevalence of Crohn's disease and ulcerative colitis in Olmsted County, Minnesota, 1940–2000. *Inflamm. Bowel Dis.* **13**, 254–261 (2007).
14. Satsangi, J., Silverberg, M. S., Vermeire, S. & Colombel, J. F. The Montreal classification of inflammatory bowel disease: Controversies, consensus, and implications. *Gut* **55**, 749–753 (2006).
15. Schwartz, D. A., Pemberton, J. H. & Sandborn, W. J. Diagnosis and treatment of perianal fistulas in Crohn disease. *Ann. Intern. Med.* **135**, 906–918 (2001).
16. Stange, E. F. *et al.* European evidence-based Consensus on the diagnosis and management of ulcerative colitis: Definitions and diagnosis. *J. Crohn's Colitis* **2**, 1–23 (2008).
17. Marchal-Bressenot, A. *et al.* Development and validation of the Nancy histological index for RCH. *Gut* **0**, 1–7 (2015).
18. Ng, S. C. *et al.* Worldwide incidence and prevalence of inflammatory bowel disease in the 21st century: a systematic review of population-based studies. *Lancet* **390**, 2769–2778 (2017).

19. Gower-Rousseau, C. *et al.* Natural History of Adult Ulcerative Colitis in Population-based Cohorts: A Systematic Review. *Clin. Gastroenterol. Hepatol.* **16**, 343-356.e3 (2017).
20. Lophaven, S. N., Lyngge, E. & Burisch, J. The incidence of inflammatory bowel disease in Denmark 1980–2013: a nationwide cohort study. *Aliment. Pharmacol. Ther.* **45**, 961–972 (2017).
21. Kaplan, G. G. The global burden of IBD: from 2015 to 2025. *Nat. Rev. Gastroenterol. Hepatol.* **12**, 720–727 (2015).
22. Berry, D. & Reinisch, W. Intestinal microbiota: A source of novel biomarkers in inflammatory bowel diseases? *Best Pract. Res. Clin. Gastroenterol.* **27**, 47–58 (2013).
23. Kaser, A., Zeissig, S. & Blumberg, R. S. Inflammatory bowel disease. *Annu. Rev. Immunol.* **28**, 573–621 (2010).
24. Satsangi, J., Rosenberg, W. M. C. & Jewell, D. P. The Prevalence of Inflammatory Bowel Disease in Relatives of Patients with Crohn’s Disease. *Eur. J. Gastroenterol. Hepatol.* **6**, 413–416 (1994).
25. Orholm, M. *et al.* Familial Occurrence of Inflammatory Bowel Disease. *N. Engl. J. Med.* **324**, 84–88 (1991).
26. Freeman, H. J. Familial Crohn’s disease in single or multiple first-degree relatives. *J. Clin. Gastroenterol.* **35**, 9–13 (2002).
27. Bengtson, M.-B. *et al.* Familial aggregation in Crohn’s disease and ulcerative colitis in a Norwegian population-based cohort followed for ten years. *J. Crohn’s Colitis* **3**, 92–99 (2009).
28. Peeters, M. *et al.* Familial Aggregation in Crohn’s Disease: Increased Age-Adjusted Risk and Concordance in Clinical Characteristics. *Gastroenterology* **111**, 597–603 (1996).
29. Küster, W. *et al.* The genetics of Crohn disease: complex segregation analysis of a family study with 265 patients with Crohn disease and 5,387 relatives. *Am. J. Med. Genet.* **32**, 105–108 (1989).
30. Meucci, G. *et al.* Familial aggregation of inflammatory bowel disease in northern Italy: a multicenter study. *Gastroenterology* **103**, 514–519 (1992).
31. Tysk, C., Lindberg, E., Järnerot, G. & Floderus-Myrhed, B. Ulcerative colitis and Crohn’s disease in an unselected population of monozygotic and dizygotic twins. A study of heritability and the influence of smoking. *Gut* **29**, 990–996 (1988).
32. Halfvarson, J., Bodin, L., Tysk, C., Lindberg, E. & Järnerot, G. Inflammatory bowel disease in a Swedish twin cohort: A long- term follow-up of concordance and clinical characteristics. *Gastroenterology* **124**, 1767–1773 (2003).
33. Orholm, M., Binder, V., Sørensen, T. I. A., Rasmussen, L. & Kyvik, K. Concordance of inflammatory bowel disease among Danish twins. Results of a nationwide study. *Scand. J. Gastroenterol.* **35**, 1075–1081 (2000).
34. Thompson, N. P., Driscoll, R., Pounder, R. E. & Wakefield, A. J. Genetics versus environment in inflammatory bowel disease: results of a British twin study. *Bmj* **312**, 95–96 (1996).
35. Hugot, J.-P. P. *et al.* Association of NOD2 leucine-rich repeat variants with susceptibility to Crohn’s disease. *Nature* **411**, 599–603 (2001).
36. Girardin, S. E. *et al.* Nod2 is a general sensor of peptidoglycan through muramyl dipeptide (MDP) detection. *J. Biol. Chem.* **278**, 8869–8872 (2003).
37. Inohara, N. *et al.* Host Recognition of Bacterial Muramyl Dipeptide Mediated through NOD2. *J. Biol. Chem.* **278**, 5509–5512 (2003).

38. Yamazaki, K., Takazoe, M., Tanaka, T., Kazumori, T. & Nakamura, Y. Absence of mutation in the NOD2/CARD15 gene among 483 Japanese patients with Crohn's disease. *J. Hum. Genet.* **47**, 469–472 (2002).
39. Croucher, P. J. P. *et al.* Haplotype structure and association to Crohn's disease of CARD15 mutations in two ethnically divergent populations. *Eur. J. Hum. Genet.* **11**, 6–16 (2003).
40. Leong, R. W. L. *et al.* NOD2/CARD15 gene polymorphisms and Crohn's disease in the Chinese population. *Aliment. Pharmacol. Ther.* **17**, 1465–1470 (2003).
41. Kugathasan, S. *et al.* White Children with Crohn's Disease. *Inflamm. Bowel Dis.* **11**, 631–638 (2005).
42. Deuring, J. J. *et al.* Genomic ATG16L1 risk allele-restricted Paneth cell ER stress in quiescent Crohn's disease. *Gut* **63**, 1081–1091 (2014).
43. Hampe, J. *et al.* A genome-wide association scan of nonsynonymous SNPs identifies a susceptibility variant for Crohn disease in ATG16L1. *Nat. Genet.* **39**, 207–211 (2007).
44. Baldassano, R. N., Bradfield, J. P., Monos, D. S., Kim, C. E. & Glessner, J. T. Association of the T300A non-synonymous variant of the ATG16L1 gene with susceptibility to paediatric Crohn's disease. *Gut* **56**, 1170–1171 (2007).
45. Prescott, N. J. *et al.* A Nonsynonymous SNP in ATG16L1 Predisposes to Ileal Crohn's Disease and Is Independent of CARD15 and IBD5. *Gastroenterology* **132**, 1665–1671 (2007).
46. Parkes, M. *et al.* Sequence variants in the autophagy gene IRGM and multiple other replicating loci contribute to Crohn's disease susceptibility. *Nat. Genet.* **39**, 830–832 (2007).
47. TWCCC *et al.* Genome-wide association study of 14,000 cases of seven common diseases and 3,000 shared controls. *Nature* **447**, 661–678 (2007).
48. Henry, S. C. *et al.* Impaired Macrophage Function Underscores Susceptibility to Salmonella in Mice Lacking Irgm1 (LRG-47). *J. Immunol.* **179**, 6963–6972 (2007).
49. Franke, A. *et al.* Replication of signals from recent studies of Crohn's disease identifies previously unknown disease loci for ulcerative colitis. *Nat. Genet.* **40**, 713–715 (2008).
50. Fisher, S. A. *et al.* Genetic determinants of ulcerative colitis include the ECM1 locus and five loci implicated in Crohn's disease. *Nat. Genet.* **40**, 710–712 (2008).
51. Kühn, R., Löhler, J., Rennick, D., Rajewsky, K. & Müller, W. Interleukin-10-deficient mice develop chronic enterocolitis. *Cell* **75**, 263–274 (1993).
52. Uhlig, H. H. *et al.* Characterisation of Foxp3⁺CD4⁺CD25⁺ and IL-10 secreting CD4⁺CD25⁺ T cells during cure of colitis. *J. Immunol.* **177**, 5852–5860 (2006).
53. Sellon, R. K. *et al.* Resident enteric bacteria are necessary for development of spontaneous colitis and immune system activation in interleukin-10-deficient mice. *Infect. Immun.* **66**, 5224–5231 (1998).
54. Parham, C. *et al.* A Receptor for the Heterodimeric Cytokine IL-23 Is Composed of IL-12R 1 and a Novel Cytokine Receptor Subunit, IL-23R. *J. Immunol.* **168**, 5699–5708 (2002).
55. Cua, D. J. *et al.* Interleukin-23 rather than interleukin-12 is the critical cytokine for autoimmune inflammation of the brain. *Nature* **421**, 744–748 (2003).
56. Murphy, C. A. *et al.* Divergent Pro- and Antiinflammatory Roles for IL-23 and IL-12 in Joint Autoimmune Inflammation. *J. Exp. Med.* **198**, 1951–1957 (2003).
57. Chan, J. R. *et al.* IL-23 stimulates epidermal hyperplasia via TNF and IL-20R2-dependent mechanisms with implications for psoriasis pathogenesis. *J. Exp. Med.* **203**, 2577–2587 (2006).

58. Yen, D. *et al.* IL-23 is essential for T cell-mediated colitis and promotes inflammation via IL-17 and IL-6. *J. Clin. Invest.* **116**, 1310–1316 (2006).
59. Kobayashi, T. *et al.* IL23 differentially regulates the Th1/Th17 balance in ulcerative colitis and Crohn's disease. *Gut* **57**, 1682–1689 (2008).
60. Barrett, J. C. *et al.* Genome-wide association defines more than thirty distinct susceptibility loci for Crohn's disease. **40**, 955–962 (2008).
61. Ferguson, L. R. *et al.* Genetic factors in chronic inflammation: Single nucleotide polymorphisms in the STAT-JAK pathway, susceptibility to DNA damage and Crohn's disease in a New Zealand population. *Mutat. Res. - Fundam. Mol. Mech. Mutagen.* **690**, 108–115 (2010).
62. Jostins, L. *et al.* Host–microbe interactions have shaped the genetic architecture of inflammatory bowel disease. *Nature* **491**, 119–124 (2012).
63. Franke, A. *et al.* Genome-wide meta-analysis increases to 71 the number of confirmed Crohn's disease susceptibility loci. *Nat. Genet.* **42**, 1118–1125 (2012).
64. Hindorff, L. A. *et al.* Potential etiologic and functional implications of genome-wide association loci for human diseases and traits. *Proc. Natl. Acad. Sci.* **106**, 9362–9367 (2009).
65. Notarangelo LD, Fischer A, Geha RS, Casanova JL, Chapel H, Conley ME, Cunningham-Rundles C, Etzioni A, H. L. Primary immunodeficiencies: 2009 update. *J. Allergy Clin. Immunol.* **124**, 1161–1178 (2010).
66. Colombel, J. F. IBD - Genes, bacteria and new therapeutic strategies. *Nat. Rev. Gastroenterol. Hepatol.* **11**, 652–654 (2014).
67. Loftus, E. V. Clinical epidemiology of inflammatory bowel disease: Incidence, prevalence, and environmental influences. *Gastroenterology* **126**, 1504–17 (2004).
68. Hou, J. K., El-Serag, H. & Thirumurthi, S. Distribution and manifestations of inflammatory bowel disease in asians, hispanics, and african americans: A systematic review. *Am. J. Gastroenterol.* **104**, 2100–2109 (2009).
69. Benchimol, E. I. *et al.* Asthma, Type 1 and Type 2 Diabetes Mellitus, and Inflammatory Bowel Disease amongst South Asian Immigrants to Canada and Their Children: A Population-Based Cohort Study. *PLoS One* **10**, e0123599 (2015).
70. Joossens, M. *et al.* Contribution of genetic and environmental factors in the pathogenesis of Crohn's disease in a large family with multiple cases. *Inflamm. Bowel Dis.* **13**, 580–584 (2007).
71. Barclay, A. R. *et al.* Systematic Review: The Role of Breastfeeding in the Development of Pediatric Inflammatory Bowel Disease. *J. Pediatr.* **155**, 421–426 (2009).
72. Gent, A. E., Hellier, M. D., Grace, R. H., Swarbrick, E. T. & Coggon, D. Inflammatory bowel disease and domestic hygiene in infancy. *Lancet* **343**, 766–767 (1994).
73. Aamodt, G. *et al.* The association between water supply and inflammatory bowel disease based on a 1990-1993 cohort study in southeastern Norway. *Am. J. Epidemiol.* **168**, 1065–1072 (2008).
74. Kaplan, G. G. *et al.* The inflammatory bowel diseases and ambient air pollution: A novel association. *Am. J. Gastroenterol.* **105**, 2412–2419 (2010).
75. Hou, J. K., Abraham, B. & El-Serag, H. Dietary intake and risk of developing inflammatory bowel disease: A systematic review of the literature. *Am. J. Gastroenterol.* **106**, 563–573 (2011).
76. Mahid, S. S., Minor, K. S., Soto, R. E., Hornung, C. A. & Galandiuk, S. Smoking and Inflammatory Bowel Disease: A Meta-analysis. *Mayo Clin. Proc.* **81**, 1462–1471 (2006).

77. Bastida, G. & Beltrán, B. Ulcerative colitis in smokers, non-smokers and ex-smokers. *World J. Gastroenterol.* **17**, 2740–2747 (2011).
78. Beaugerie, L. *et al.* Impact of cessation of smoking on the course of ulcerative colitis. *Am. J. Gastroenterol.* **96**, 2113–2116 (2004).
79. Odes, H. S. *et al.* Effects of current cigarette smoking on clinical course of Crohn's disease and ulcerative colitis. *Dig. Dis. Sci.* **46**, 1717–1721 (2001).
80. Lunney, P. C. *et al.* Smoking prevalence and its influence on disease course and surgery in Crohn's disease and ulcerative colitis. *Aliment. Pharmacol. Ther.* **42**, 61–70 (2015).
81. Kuenzig, M. E. *et al.* Smoking influences the need for surgery in patients with the inflammatory bowel diseases: a systematic review and meta-analysis incorporating disease duration. *BMC Gastroenterol.* **16**, 1–9 (2016).
82. Andersson, R. E., Olaison, G., Tysk, C. & Ekblom, A. Appendectomy and Protection against Ulcerative Colitis. *N. Engl. J. Med.* **344**, 808–814 (2001).
83. Cheluvappa, R. A novel model of appendicitis and appendectomy to investigate inflammatory bowel disease pathogenesis and remediation. *Biol. Proced. Online* **16**, (2014).
84. Rasmussen, T., Fonnes, S. & Rosenberg, J. Long-Term Complications of Appendectomy: A Systematic Review. *Scand. J. Surg.* **107**, 189–196 (2018).
85. Russel, M. G. *et al.* Appendectomy and the Risk of Developing Ulcerative Colitis or Crohn's Disease: Results of a Large Case-Control Study. *Gastroenterology* **113**, 377–382 (1997).
86. Su, J. W., Ma, J. J. & Zhang, H. J. Use of antibiotics in patients with Crohn's disease: A systematic review and meta-analysis. *J. Dig. Dis.* **16**, 58–66 (2015).
87. Papa, E. *et al.* Non-invasive mapping of the gastrointestinal microbiota identifies children with inflammatory bowel disease. *PLoS One* **7**, (2012).
88. Marteau, P. & Doré, J. *Le microbiote intestinal - Un organe à part entière.* (John Libbey Eurotext, 2017).
89. Adlerberth, I. & Wold, A. E. Establishment of the gut microbiota in Western infants. *Acta Paediatr. Int. J. Paediatr.* **98**, 229–238 (2009).
90. Yatsunenko, T. *et al.* Human gut microbiome viewed across age and geography. *Nature* (2012). doi:10.1038/nature11053
91. Donaldson, G. P., Lee, S. M. & Mazmanian, S. K. Gut biogeography of the bacterial microbiota. *Nat. Rev. Microbiol.* **14**, 20–32 (2016).
92. David, L. A. *et al.* Diet rapidly and reproducibly alters the human gut microbiome. *Nature* **505**, 559–563 (2014).
93. Hungate, R. A role tube method for cultivation of strict anaerobes. in *Methods in Microbiology, Vol. 3B* (eds. Norris, J. & Ribbons, D.) 117 (Academic press, 1969).
94. Freter, R. Interactions between mechanisms controlling the intestinal microflora. *Am. J. Clin. Nutr.* **27**, 1409–1416 (1974).
95. Moore, W. E. & Holdeman, L. V. Human Fecal Flora: The Normal Flora of 20 Japanese-Hawaiians. *Appl. Microbiol.* **27**, 961–979 (1974).
96. Finegold, S., Sutter, V. & Mathisen, G. Normal indigenous intestinal flora. in *Human intestinal microflora in health and disease* (ed. Hentges, D.) 3–31 (Academic press, 1983).

97. Methé, B. A. *et al.* A framework for human microbiome research. *Nature* **486**, 215–221 (2012).
98. Li, K., Bihan, M., Yooseph, S. & Methé, B. A. Analyses of the Microbial Diversity across the Human Microbiome. *PLoS One* **7**, (2012).
99. Hollister, E. B., Gao, C. & Versalovic, J. Compositional and Functional Features of the Gastrointestinal Microbiome and Their Effects on Human Health. *Gastroenterology* **146**, 1449–1458 (2014).
100. Tap, J. *et al.* Towards the human intestinal microbiota phylogenetic core. *Environ. Microbiol.* **11**, 2574–2584 (2009).
101. Eckburg, P. B. *et al.* Diversity of the human intestinal microbial flora. *Science (80-.)*. **308**, 1635–1638 (2005).
102. Qin, J. *et al.* A human gut microbial gene catalogue established by metagenomic sequencing. *Inflamm. Bowel Dis. Monit.* **11**, 28 (2010).
103. Huttenhower, C., Gervers, D., Knight, R. & Consortium, T. H. M. P. Structure, Function and Diversity of the Healthy Human Microbiome. *Nature* **486**, 207–214 (2012).
104. Arumugam, M. *et al.* Enterotypes of the human gut microbiome. *Nature* **474**, 666–666 (2011).
105. Tao, D. & Schloss, P. D. Dynamics and associations of microbial community types across the human body. *Nature* **509**, 357–360 (2014).
106. Zupancic, M. L. *et al.* Analysis of the Gut Microbiota in the Old Order Amish and Its Relation to the Metabolic Syndrome. *PLoS One* **7**, 1–10 (2012).
107. Wang, J. *et al.* Dietary history contributes to enterotype-like clustering and functional metagenomic content in the intestinal microbiome of wild mice. *Proc. Natl. Acad. Sci. U. S. A.* **111**, E2703-10 (2014).
108. Mach, N. *et al.* Early-life establishment of the swine gut microbiome and impact on host phenotypes. *Environ. Microbiol. Rep.* **7**, 554–569 (2015).
109. Vandeputte, D. *et al.* Quantitative microbiome profiling links gut community variation to microbial load. *Nature* **551**, 507–511 (2017).
110. Ley, R. E., Turnbaugh, P. J., Klein, S. & Gordon, J. I. Microbial Ecology: Human gut microbes associated with obesity. *Nature* **444**, 1022–1023 (2006).
111. Hu, S. *et al.* Regional differences in colonic mucosa-associated microbiota determine the physiological expression of host heat shock proteins. *Am. J. Physiol. - Gastrointest. Liver Physiol.* **299**, G1266–G1275 (2010).
112. Skar, V., Skar, A. & Bratlie, J. Beta-glucuronidase activity in the bile of gallstone patients both with and without duodenal diverticula. *Scand. J. Gastroenterol.* **24**, 205–212 (1989).
113. Justesen, T., Nielsen, O. & Hjelt, K. Normal cultivable microflora in upper jejunal fluid in healthy adults. *J. Pediatr. Gastroenterol. Nutr.* **3**, 683–686 (1984).
114. Thursby, E. & Juge, N. Introduction to the human gut microbiota. *Biochem. J.* **474**, 1823–1836 (2017).
115. Lavelle, A. *et al.* Spatial variation of the colonic microbiota in patients with ulcerative colitis and control volunteers. *Gut* **64**, 1553–1561 (2015).
116. Harrell, L. *et al.* Standard colonic lavage alters the natural state of mucosal-associated microbiota in the human colon. *PLoS One* **7**, (2012).
117. Van Den Abbeele, P. *et al.* Butyrate-producing Clostridium cluster XIVa species specifically colonize mucins in an in vitro gut model. *ISME J.* **7**, 949–961 (2013).

118. Musso, G., Gambino, R. & Cassader, M. Obesity, diabetes, and gut microbiota: The hygiene hypothesis expanded? *Diabetes Care* **33**, 2277–2284 (2010).
119. Cook, S. I. & Sellin, J. H. Short chain fatty acids in health and disease. *Aliment. Pharmacol. Ther.* **12**, 499–507 (1998).
120. Corrêa-Oliveira, R., Fachi, J. L., Vieira, A., Sato, F. T. & Vinolo, M. A. R. Regulation of immune cell function by short-chain fatty acids. *Clin. Transl. Immunol.* **5**, 1–8 (2016).
121. Morrison, D. J. & Preston, T. Formation of short chain fatty acids by the gut microbiota and their impact on human metabolism. *Gut Microbes* **7**, 189–200 (2016).
122. Lin, L. & Zhang, J. Role of intestinal microbiota and metabolites on gut homeostasis and human diseases. *BMC Immunol.* **18**, 1–25 (2017).
123. LeBlanc, J. G. *et al.* Bacteria as vitamin suppliers to their host: a gut microbiota perspective. *Curr. Opin. Biotechnol.* **24**, 160–168 (2013).
124. Martens, J. H., Barg, H., Warren, M. & Jahn, D. Microbial production of vitamin B12. *Appl. Microbiol. Biotechnol.* **58**, 275–285 (2002).
125. Pompei, A. *et al.* Folate production by bifidobacteria as a potential probiotic property. *Appl. Environ. Microbiol.* **73**, 179–185 (2007).
126. Staley, C., Weingarden, A. R., Hkoruts, A. & Sadowsky, M. J. Interaction of Gut Microbiota with Bile Acid Metabolism and its Influence on Disease States. *Appl. Microbiol. Biotechnol.* **101**, 47–64 (2017).
127. Brown, A. J. *et al.* The Orphan G Protein-coupled Receptors GPR41 and GPR43 Are Activated by Propionate and Other Short Chain Carboxylic Acids. *J. Biol. Chem.* **278**, 11312–11319 (2003).
128. Kimura, I., Inoue, D., Hirano, K. & Tsujimoto, G. The SCFA receptor GPR43 and energy metabolism. *Front. Endocrinol. (Lausanne)*. **5**, 3–5 (2014).
129. McKenzie, C., Tan, J., Macia, L. & Mackay, C. R. The nutrition-gut microbiome-physiology axis and allergic diseases. *Immunol. Rev.* **278**, 277–295 (2017).
130. Postler, T. S. & Ghosh, S. Understanding the Holobiont: How Microbial Metabolites Affect Human Health and Shape the Immune System. *Cell Metab.* **26**, 110–130 (2017).
131. Reunanen, J. *et al.* Akkermansia muciniphila Adheres to Enterocytes and Strengthens the Integrity of the Epithelial Cell Layer. *Appl. Environ. Microbiol.* **81**, 3655–3662 (2015).
132. Chen, H.-Q. *et al.* Lactobacillus plantarum ameliorates colonic epithelial barrier dysfunction by modulating the apical junctional complex and PepT1 in IL-10 knockout mice. *Am. J. Physiol. Liver Physiol.* **299**, G1287–G1297 (2010).
133. Wrzosek, L. *et al.* Bacteroides thetaiotaomicron and Faecalibacterium prausnitzii influence the production of mucus glycans and the development of goblet cells in the colonic epithelium of a gnotobiotic model rodent. *BMC Biol.* **11**, 61 (2013).
134. Graziani, F. *et al.* Ruminococcus gnavus E1 modulates mucin expression and intestinal glycosylation. *J. Appl. Microbiol.* **120**, 1403–1417 (2016).
135. Varyukhina, S. *et al.* Glycan-modifying bacteria-derived soluble factors from Bacteroides thetaiotaomicron and Lactobacillus casei inhibit rotavirus infection in human intestinal cells. *Microbes Infect.* **14**, 273–278 (2012).
136. Freitas, M. *et al.* A heat labile soluble factor from Bacteroides thetaiotaomicron VPI-5482 specifically increases the galactosylation pattern of HT29-MTX cells. *Cell. Microbiol.* **3**, 289–300 (2001).

137. Quigley, E. M. M. Prebiotics and probiotics; modifying and mining the microbiota. *Pharmacol. Res.* **61**, 213–218 (2010).
138. Littman, D. R. & Pamer, E. G. Role of the commensal microbiota in normal and pathogenic host immune responses. *Cell Host Microbe* **10**, 311–323 (2011).
139. Cani, P. D. *et al.* Metabolic Endotoxemia Initiates Obesity and Insulin Resistance. *Diabetes* **56**, 1761–1772 (2007).
140. Duparc, T. *et al.* Hepatocyte MyD88 affects bile acids, gut microbiota and metabolome contributing to regulate glucose and lipid metabolism. *Gut* **66**, 620–632 (2017).
141. Chassaing, B., Ley, R. E. & Gewirtz, A. T. Intestinal Epithelial cell Toll-like Receptor 5 Regulates the Intestinal Microbiota to Prevent Low-grade Inflammation and Metabolic Syndrome in Mice. *Gastroenterology* **147**, 1363–1377 (2014).
142. Ivanov, I. I. *et al.* Specific Microbiota Direct the Differentiation of IL-17-Producing T-Helper Cells in the Mucosa of the Small Intestine. *Cell Host Microbe* **4**, 337–349 (2008).
143. Round, J. L. & Mazmanian, S. K. Inducible Foxp3⁺regulatory T-cell development by a commensal bacterium of the intestinal microbiota: Commentary. *Proc. Natl. Acad. Sci. U. S. A.* **107**, 12204–12209 (2010).
144. Mazmanian, S. K., Cui, H. L., Tzianabos, A. O. & Kasper, D. L. An Immunomodulatory Molecule of Symbiotic Bacteria Directs Maturation of the Host Immune System. *Cell* **122**, 107–118 (2005).
145. Bäumlner, A. J. & Sperandio, V. Interactions between the microbiota and pathogenic bacteria in the gut. *Nature* **535**, 85–93 (2016).
146. Nibali, L. & Henderson, B. *The Human Microbiota and Chronic Disease*. (Wiley Blackwell, 2016).
147. Kostic, A. D., Xavier, R. J. & Gevers, D. The microbiome in inflammatory bowel disease: Current status and the future ahead. *Gastroenterology* **146**, 1489–1499 (2014).
148. Manichanh, C. *et al.* Reduced diversity of faecal microbiota in Crohn's disease revealed by a metagenomic approach. *Gut* **55**, 205–211 (2006).
149. Sokol, H., Seksik, P. & Rigottier-Gois, L. Specificities of the fecal microbiota in inflammatory bowel disease. *Inflamm. Bowel Dis.* **12**, 106–111 (2006).
150. Baumgart, M. *et al.* Culture independent analysis of ileal mucosa reveals a selective increase in invasive *Escherichia coli* of novel phylogeny relative to depletion of Clostridiales in Crohn's disease involving the ileum. *ISME J.* **1**, 403–418 (2007).
151. Mangin, I. *et al.* Molecular inventory of faecal microflora in patients with Crohn's disease. *FEMS Microbiol. Ecol.* **50**, 25–36 (2004).
152. Becker, C., Neurath, M. F. & Wirtz, S. The intestinal microbiota in inflammatory bowel disease. *ILAR J.* **56**, 192–204 (2015).
153. Lepage, P. *et al.* Twin study indicates loss of interaction between microbiota and mucosa of patients with ulcerative colitis. *Gastroenterology* **141**, 227–236 (2011).
154. Frank, D. N. *et al.* Molecular-phylogenetic characterization of microbial community imbalances in human inflammatory bowel diseases. *Proc. Natl. Acad. Sci. U. S. A.* **104**, 13780–5 (2007).
155. Sokol, H., Seksik, P. & Furet, J. P. Low counts of *Faecalibacterium Prausnitzii* in colitis microbiota. *Inflamm. Bowel Dis.* **15**, 1183–1189 (2009).
156. Sokol, H. *et al.* *Faecalibacterium prausnitzii* is an anti-inflammatory commensal bacterium identified by

- gut microbiota analysis of Crohn disease patients. *Proc. Natl. Acad. Sci. U. S. A.* **105**, 16731–16736 (2008).
157. Nicholson, J. K. *et al.* Host-Gut Microbiota Metabolic Interactions. *Science (80-.)*. **336**, 1262–1267 (2012).
 158. Chassaing, B. & Darfeuille-michaud, A. The commensal microbiota and enteropathogens in the pathogenesis of inflammatory bowel diseases. *Gastroenterology* **140**, 1720–1728 (2011).
 159. Ott, S. J. *et al.* Dynamics of the mucosa-associated flora in ulcerative colitis patients during remission and clinical relapse. *J. Clin. Microbiol.* **46**, 3510–3513 (2008).
 160. Nishikawa, J., Kudo, T. & Sakata, S. Diversity of mucosa-associated microbiota in active and inactive ulcerative colitis. *Scand. J. Gastroenterol.* **44**, 180–186 (2009).
 161. Swidsinski, A. *et al.* Comparative study of the intestinal mucus barrier in normal and inflamed colon. *Gut* **56**, 343–350 (2007).
 162. Png, C. W. C. *et al.* Mucolytic bacteria with increased prevalence in IBD mucosa augment in vitro utilization of mucin by other bacteria. *Am. J. Gastroenterol.* **105**, 2420–2428 (2010).
 163. Sokol, H. *et al.* Fungal microbiota dysbiosis in IBD. *Gut* 1–10 (2016). doi:10.1136/gutjnl-2015-310746
 164. Elson, C. O. *et al.* Experimental models of inflammatory bowel disease reveal innate, adaptive, and regulatory mechanisms of host dialogue with the microbiota. *Immunol. Rev.* **206**, 260–276 (2005).
 165. Bertrand, J.-C., Caumette, P., Lebaron, P., Matheron, R. & Normand, P. *Ecologie microbienne : Microbiologie des milieux naturels et anthropisés.* (2011).
 166. Oleskin, A. V., Botvinko, I. V. & Tsavkelova, E. A. Colonial organization and intercellular communication in microorganisms. *Microbiology* **69**, 249–265 (2000).
 167. Schauder, S. & Bassler, B. L. The languages of bacteria. *Genes Dev.* **15**, 1468–1480 (2001).
 168. Nealson, K. H. & Hastings, J. W. Bacterial Bioluminescence: Its Control and Ecological Significance. *Microbiol. Rev.* **43**, 496–518 (1979).
 169. Tebo, B. M., Linthicum, D. S. & Nealson, K. H. Luminous Bacteria and Light Emitting Fish: Ultrastructure of the Symbiosis. *BioSystems* **11**, 269–280 (1979).
 170. Swaminath Srinivas, H. L. & Guoli Gong, X. H. Quorum Sensing in *Vibrio* and its Relevance to Bacterial Virulence. *J. Bacteriol. Parasitol.* **04**, 1–6 (2013).
 171. Jones, B. W. & Nishiguchi, M. K. Counterillumination in the Hawaiian bobtail squid, *Euprymna scolopes* Berry (Mollusca: Cephalopoda). *Mar. Biol.* **144**, 1151–1155 (2004).
 172. Visick, K. L. & McFall-Ngai, M. J. An exclusive contract: Specificity in the *Vibrio fischeri*-*Euprymna scolopes* partnership. *J. Bacteriol.* **182**, 1779–1787 (2000).
 173. Ruby, E. Lessons From a Cooperative, Bacterial-Animal Association: The *Vibrio fischeri*-*Euprymna scolopes* Light Organ Symbiosis. *Annu. Rev. Microbiol.* **50**, 591–624 (1996).
 174. Eberhardt, A. *et al.* Structural identification of autoinducer of *Phytobacterium fischeri* luciferase. *Biochemistry* **20**, 2444 (1981).
 175. Engebrecht, J., Nealson, K. & Silverman, M. Bacterial bioluminescence: Isolation and genetic analysis of functions from *Vibrio fischeri*. *Cell* **32**, 773–781 (1983).
 176. Engebrecht, J. & Silverman, M. Identification of Genes and Gene Products Necessary for Bacterial Bioluminescence. *Proc. Natl. Acad. Sci. U. S. A.* **81**, 4154–4158 (1984).

177. Pierson, E. A., Wood, D. W., Cannon, J. A., Blachere, F. M. & Pierson, L. S. Interpopulation Signaling via *N*-Acyl-Homoserine Lactones among Bacteria in the Wheat Rhizosphere. *Mol. Plant-Microbe Interact.* **11**, 1078–1084 (1998).
178. McKenney, D., Brown, K. E. & Allison, D. G. Influence of *Pseudomonas aeruginosa* exoproducts on virulence factor production in *Burkholderia cepacia* : evidence of interspecies communication . Influence of *Pseudomonas aeruginosa* Exoproducts on Virulence Factor Production in *Burkholderia cepacia* : Evid. **177**, 6989–6992 (1995).
179. Miller, M. B. & Bassler, B. L. Quorum Sensing in bacteria. *Annu. Rev. Microbiol.* **55**, 165–99 (2001).
180. Kaplan, H. B. & Greenberg, E. P. Diffusion of Autoinducer Is Involved in Regulation of the *Vibrio fischeri* Luminescence System. *Microbiology* **163**, 1210–1214 (1985).
181. Zhu, J. & Mekalanos, J. J. Quorum sensing-dependent biofilms enhance colonization in *Vibrio cholerae*. *Dev. Cell* **5**, 647–656 (2003).
182. Rudner, D. Z., LeDeaux, J. R., Ireton, K. & Grossman, A. D. The *spo0K* locus of *Bacillus subtilis* is homologous to the oligopeptide permease locus and is required for sporulation and competence. *J. Bacteriol.* **173**, 1388–1398 (1991).
183. Winans, S. C. & Bassler, B. L. Mob Psychology. *J. Bacteriol.* **184**, 873–883 (2002).
184. Takano, E., Chakraborty, R., Nihira, T., Yamada, Y. & Bibb, M. J. A complex role for the gamma-butyrolactone SCB1 in regulating antibiotic production in *Streptomyces coelicolor* A3(2). *Mol. Microbiol.* **41**, 1015–1028 (2001).
185. Derzelle, S., Duchaud, E., Kunst, F., Bertin, P. & Danchin, A. Regulation of a Cluster of Genes Involved in Carbapenem Biosynthesis in *Photobacterium luminescens* Identification , Characterization , and Regulation of a Cluster of Genes Involved in Carbapenem Biosynthesis in *Photobacterium luminescens*. **68**, 3780–3789 (2002).
186. Stevens, A. M., Dolan, K. M. & Greenberg, E. P. Synergistic Binding of the *Vibrio fischeri* LuxR Transcriptional Activator Domain and RNA polymerase to the Lux Promoter Region. *Proc. Natl. Acad. Sci. U. S. A.* **91**, 12619–12623 (1994).
187. Ng, W.-L. & Bassler, B. L. Bacterial Quorum-Sensing Network Architectures. *Annu. Rev. Genet.* **43**, 197–222 (2009).
188. Geske, G. D., Neill, J. C. O. & Blackwell, H. E. Expanding dialogues: from natural autoinducers to non-natural analogues that modulate quorum sensing in Gram-negative bacteria. *Chem. Soc. Rev.* **37**, 1432–1447 (2008).
189. Puskas, A., Greenberg, E. P., Kaplan, S. & Schaefer, A. M. Y. L. A quorum-sensing system in the free-living photosynthetic bacterium *Rhodobacter sphaeroides* -- Puskas et al. 179 (23): 7530 -- The Journal of Bacteriology. **179**, 7530–7537 (1997).
190. Tait, K. *et al.* Turnover of quorum sensing signal molecules modulates cross-kingdom signalling. *Environ. Microbiol.* **11**, 1792–1802 (2009).
191. Winzer, K., Hardie, K. R. & Williams, P. Bacterial cell-to-cell communication: Sorry, can't talk now - Gone to lunch! *Curr. Opin. Microbiol.* **5**, 216–222 (2002).
192. Lyon, G. J. & Muir, T. W. Chemical Signaling among Bacteria and Its Inhibition. *2Chemistry Biol.* **10**, 1007–1021 (2003).
193. Williams, P., Winzer, K., Chan, W. C. & Cámara, M. Look who's talking: communication and quorum sensing in the bacterial world. *Philos. Trans. R. Soc. B Biol. Sci.* **362**, 1119–1134 (2007).
194. Schaefer, A. L. *et al.* A new class of homoserine lactone quorum-sensing signals. *Nature* **454**, 595–599

- (2008).
195. Ahlgren, N. A., Harwood, C. S., Schaefer, A. L., Giraud, E. & Greenberg, E. P. Aryl-homoserine lactone quorum sensing in stem-nodulating photosynthetic bradyrhizobia. *Proc. Natl. Acad. Sci.* **108**, 7183–7188 (2011).
 196. Lindemann, A. *et al.* Isovaleryl-homoserine lactone, an unusual branched-chain quorum-sensing signal from the soybean symbiont *Bradyrhizobium japonicum*. *Proc. Natl. Acad. Sci.* **108**, 16765–16770 (2011).
 197. Gerdt, J. P., McInnis, C. E., Schell, T. L., Rossi, F. M. & Blackwell, H. E. Mutational analysis of the quorum-sensing receptor LasR reveals interactions that govern activation and inhibition by nonlactone ligands. *Chem. Biol.* **21**, 1361–1369 (2014).
 198. Galloway, W. R. J. D., Hodgkinson, J. T., Bowden, S. D., Welch, M. & Spring, D. R. Quorum sensing in Gram-negative bacteria: Small-molecule modulation of AHL and AI-2 quorum sensing pathways. *Chem. Rev.* **111**, 28–67 (2011).
 199. Amara, N. *et al.* Covalent Inhibition of Bacterial Quorum Sensing. *J. Am. Chem. Soc.* **131**, 197–201 (2009).
 200. Bachofen, R. & Schenk, A. Quorum sensing autoinducers: Do they play a role in natural microbial habitats? *Microbiol. Res.* **153**, 61–63 (1998).
 201. Sharif, D. I., Gallon, J., Smith, C. J. & Dudley, E. Quorum sensing in Cyanobacteria: N-octanoyl-homoserine lactone release and response, by the epilithic colonial cyanobacterium *Gloeotheca* PCC6909. *ISME J.* **2**, 1171–1182 (2008).
 202. Pearson, J. P., Van Delden, C. & Iglewski, B. H. Active efflux and diffusion are involved in transport of *Pseudomonas aeruginosa* cell-to-cell signals. *J. Bacteriol.* **181**, 1203–1210 (1999).
 203. Fuqua, C. & Greenberg, E. P. Listening in on bacteria: Acyl-homoserine lactone signalling. *Nat. Rev. Mol. Cell Biol.* **3**, 685–695 (2002).
 204. Keller, L. & Surette, M. G. Communication in bacteria: An ecological and evolutionary perspective. *Nat. Rev. Microbiol.* **4**, 249–258 (2006).
 205. Nieto Penalver, C. G. *et al.* *Methylobacterium extorquens* AM1 produces a novel type of acyl-homoserine lactone with a double unsaturated side chain under methylotrophic growth conditions. *FEBS Lett.* **580**, 561–567 (2006).
 206. Lowery, C. A., Dickerson, T. J. & Janda, K. D. Interspecies and interkingdom communication mediated by bacterial quorum sensing. *Chem. Soc. Rev.* **37**, 1337–1346 (2008).
 207. Chen, X. *et al.* Structural identification of a bacterial quorum-sensing signal containing boron. *Nature* **415**, 545–549 (2002).
 208. Vendeville, A., Winzer, K., Heurlier, K., Tang, C. M. & Hardie, K. R. Making ‘sense’ of metabolism: Autoinducer-2, LuxS and pathogenic bacteria. *Nat. Rev. Microbiol.* **3**, 383–396 (2005).
 209. Xavier, K. B. & Bassler, B. L. Interference with AI-2-Mediated Bacterial Cell-Cell Communication. *Nature* **437**, 750–753 (2005).
 210. Ismail, A. S., Valastyan, J. S. & Bassler, B. L. A Host-Produced Autoinducer-2 Mimic Activates Bacterial Quorum Sensing. *Cell Host Microbe* **19**, 470–480 (2016).
 211. Miller, S. T. *et al.* *Salmonella typhimurium* recognizes a chemically distinct form of the bacterial quorum-sensing signal AI-2. *Mol. Cell* **15**, 677–687 (2004).
 212. Gobbetti, M., De Angelis, M., Di Cagno, R., Minervini, F. & Limitone, A. Cell-cell communication in

- food related bacteria. *Int. J. Food Microbiol.* **120**, 34–45 (2007).
213. Surette, M. G., Miller, M. B. & Bassler, B. L. Quorum sensing in *Escherichia coli*, *Salmonella typhimurium*, and *Vibrio harveyi*: a new family of genes responsible for autoinducer production. *Proc. Natl. Acad. Sci. U. S. A.* **96**, 1639–44 (1999).
 214. Xavier, K. B. & Bassler, B. L. LuxS quorum sensing: More than just a numbers game. *Curr. Opin. Microbiol.* **6**, 191–197 (2003).
 215. Thiel, V., Vilchez, R., Sztajer, H., Wagner-Döbler, I. & Schulz, S. Identification, quantification, and determination of the absolute configuration of the bacterial quorum-sensing signal autoinducer-2 by gas chromatography-mass spectrometry. *ChemBioChem* **10**, 479–485 (2009).
 216. Pereira, C. S., Thompson, J. A. & Xavier, K. B. AI-2-mediated signalling in bacteria. *FEMS Microbiol. Rev.* **37**, 156–181 (2013).
 217. Sperandio, V., Torres, A. G., Jarvis, B., Nataro, J. P. & Kaper, J. B. Bacteria-host communication: The language of hormones. *Proc. Natl. Acad. Sci.* **100**, 8951–8956 (2003).
 218. Walters, M. & Sperandio, V. Autoinducer 3 and epinephrine signaling in the kinetics of locus of enterocyte effacement gene expression in enterohemorrhagic *Escherichia coli*. *Infect. Immun.* **74**, 5445–5455 (2006).
 219. Walters, M. & Sperandio, V. Quorum sensing in *Escherichia coli* and *Salmonella*. *Int. J. Med. Microbiol.* **296**, 125–131 (2006).
 220. Walters, M., Sircili, M. P. & Sperandio, V. AI-3 synthesis is not dependent on luxS in *Escherichia coli*. *J. Bacteriol.* **188**, 5668–5681 (2006).
 221. Kelly, R. C. *et al.* The *Vibrio cholerae* quorum-sensing autoinducer CAI-1: analysis of the biosynthetic enzyme CqsA. *Nat Chem Biol* **5**, 891–895 (2009).
 222. Henke, J. M. & Bassler, B. L. Three Parallel Quorum-Sensing Systems Regulate Gene Expression in *Vibrio harveyi*. *J. Bacteriol.* **186**, 6902–6914 (2004).
 223. Milton, D. L. Quorum sensing in vibrios: Complexity for diversification. *Int. J. Med. Microbiol.* **296**, 61–71 (2006).
 224. Higgins, D. A. *et al.* The major *Vibrio cholerae* autoinducer and its role in virulence factor production. *Nature* **450**, 883–886 (2007).
 225. Flavier, A. B., Clough, S. J., Schell, M. A. & Denny, T. P. Identification of 3-hydroxypalmitic acid methyl ester as a novel autoregulator controlling virulence in *Ralstonia solanacearum*. *Mol. Microbiol.* **26**, 251–259 (1997).
 226. von Bodman, S. B., Bauer, W. D. & Coplin, D. L. Quorum Sensing in Plant-Pathogenic Bacteria. *Annu. Rev. Phytopathol.* **41**, 455–482 (2003).
 227. Uroz, S., Dessaux, Y. & Oger, P. Quorum sensing and quorum quenching: The Yin and Yang of bacterial communication. *ChemBioChem* **10**, 205–216 (2009).
 228. Venturi, V. Regulation of quorum sensing in *Pseudomonas*. *FEMS Microbiol. Rev.* **30**, 274–291 (2006).
 229. Reen, F. J. *et al.* The *Pseudomonas* quinolone signal (PQS), and its precursor HHQ, modulate interspecies and interkingdom behaviour. *FEMS Microbiol. Ecol.* **77**, 413–428 (2011).
 230. Bredenbruch, F., Nimtz, M., Wray, V., Morr, M. & Mu, R. Biosynthetic Pathway of *Pseudomonas aeruginosa*. *J. Bacteriol.* **187**, 3630–3635 (2005).

231. Dubern, J. F. J.-F. & Diggle, S. P. S. P. Quorum sensing by 2-alkyl-4-quinolones in *Pseudomonas aeruginosa* and other bacterial species. *Mol. BioSyst.* **4**, 882–888 (2008).
232. Wade, D. S. *et al.* Regulation of *Pseudomonas* Quinolone Signal Synthesis in *Pseudomonas aeruginosa*. *J. Bacteriol.* **187**, 4372–4380 (2005).
233. Xiao, G. *et al.* MvfR, a key *Pseudomonas aeruginosa* pathogenicity LTTR-class regulatory protein, has dual ligands. *Mol. Microbiol.* **62**, 1689–1699 (2006).
234. de Kievit, T. R. & Iglewski, B. H. Bacterial Quorum Sensing in Pathogenic Relationships. *Infect. Immun.* **68**, 4839–4849 (2002).
235. Lequette, Y., Lee, J. H., Ledgham, F., Lazdunski, A. & Greenberg, E. P. A distinct QscR regulon in the *Pseudomonas aeruginosa* quorum-sensing circuit. *J. Bacteriol.* **188**, 3365–3370 (2006).
236. Schertzer, J. W., Boulette, M. L. & Whiteley, M. More than a signal: non-signaling properties of quorum sensing molecules. *Trends Microbiol.* **17**, 189–195 (2009).
237. Camilli, A. & Bassler, B. L. Bacterial Small-Molecule Signaling Pathways Andrew. *Science (80-)*. **311**, 1113–1116 (2006).
238. Holden, M. T. G. *et al.* Quorum-sensing cross talk: Isolation and chemical characterization of cyclic dipeptides from *Pseudomonas aeruginosa* and other Gram-negative bacteria. *Mol. Microbiol.* **33**, 1254–1266 (1999).
239. Nadal Jimenez, P. *et al.* The Multiple Signaling Systems Regulating Virulence in *Pseudomonas aeruginosa*. *Microbiol. Mol. Biol. Rev.* **76**, 46–65 (2012).
240. Bofinger, M. R., De Sousa, L. S., Fontes, J. E. N. & Marsaioli, A. J. Diketopiperazines as Cross-Communication Quorum-Sensing Signals between *Cronobacter sakazakii* and *Bacillus cereus*. *ACS Omega* **2**, 1003–1008 (2017).
241. Du, Y.-L., Shen, X.-L., Yu, P., Bai, L.-Q. & Li, Y.-Q. Gamma-Butyrolactone Regulatory System of *Streptomyces chattanoogensis* Links Nutrient Utilization, Metabolism, and Development. *Appl. Environ. Microbiol.* **77**, 8415–8426 (2011).
242. Ji, G., Beavis, R. C. & Novick, R. P. Cell density control of staphylococcal virulence mediated by an octapeptide pheromone. *Proc. Natl. Acad. Sci.* **92**, 12055–12059 (1995).
243. Kleerebezem, M., Quadri, L. E. N., Kuipers, O. P. & De Vos, W. M. Quorum sensing by peptide pheromones and two-component signal-transduction systems in Gram-positive bacteria. *Mol. Microbiol.* **24**, 895–904 (1997).
244. Rutherford, S. T. & Bassler, B. L. Bacterial quorum sensing: Its role in virulence and possibilities for its control. *Cold Spring Harb. Perspect. Med.* **2**, 1–25 (2012).
245. Atkinson, S. & Williams, P. Quorum sensing and social networking in the microbial world. *J. R. Soc. Interface* **6**, 959–978 (2009).
246. Mayville, P. *et al.* Structure-activity analysis of synthetic autoinducing thiolactone peptides from *Staphylococcus aureus* responsible for virulence. *Proc. Natl. Acad. Sci.* **96**, 1218–1223 (1999).
247. Wood, D. W., Gong, F., Daykin, M. M., Williams, P. & Pierson, L. S. N-acyl-homoserine lactone-mediated regulation of phenazine gene expression by *Pseudomonas aureofaciens* 30-84 in the wheat rhizosphere. *J. Bacteriol.* **179**, 7663–7670 (1997).
248. Dong, Y.-H., Xu, J.-L., Li, X.-Z. & Zhang, L.-H. AiiA, an enzyme that inactivates the acylhomoserine lactone quorum-sensing signal and attenuates the virulence of *Erwinia carotovora*. *Proc. Natl. Acad. Sci.* **97**, 3526–3531 (2000).

249. Lewenza S, Conway B, Greenberg EP & Sokol PA. Quorum sensing in *Burkholderia cepacia*: identification of the LuxRI homologs CepRI. *J. Bacteriol.* **181**, 748–756 (1999).
250. Janssens, J. C. A. *et al.* Synthesis of N-acyl homoserine lactone analogues reveals strong activators of SdiA, the *Salmonella enterica* serovar typhimurium LuxR homologue. *Appl. Environ. Microbiol.* **73**, 535–544 (2007).
251. Michael, B., Smith, J. N., Swift, S., Heffron, F. & Ahmer, B. M. M. SdiA of *Salmonella enterica* Is a LuxR Homolog That Detects Mixed Microbial Communities SdiA of *Salmonella enterica* Is a LuxR Homolog That Detects Mixed Microbial Communities. **183**, 5733–5742 (2001).
252. Soares, J. A. & Ahmer, B. M. M. Detection of acyl-homoserine lactones by *Escherichia* and *Salmonella*. *Curr. Opin. Microbiol.* **14**, 188–193 (2011).
253. Throup, J. P. *et al.* Characterisation of the *yenI/yenR* locus from *Yersinia enterocolitica* mediating the synthesis of two N-acylhomoserine lactone signal molecules. *Mol. Microbiol.* **17**, 345–356 (1995).
254. Atkinson, S., Throup, J. P., Stewart, G. S. A. B. & Williams, P. A hierarchical quorum-sensing system in *Yersinia pseudotuberculosis* is involved in the regulation of motility and clumping. *Mol. Microbiol.* **33**, 1267–1277 (2002).
255. Kaper, J. B. & Sperandio, V. Bacterial Cell-to-Cell Signaling in the Gastrointestinal Tract. *Infect. Immun.* **73**, 3197–3209 (2005).
256. Okuda, J. *et al.* Translocation of *Pseudomonas aeruginosa* from the Intestinal Tract Is Mediated by the Binding of ExoS to an Na,K-ATPase Regulator, FXYD3. *Infect. Immun.* **78**, 4511–4522 (2010).
257. Rumbaugh, K. P. Convergence of hormones and autoinducers at the host/pathogen interface. *Anal. Bioanal. Chem.* **387**, 425–435 (2007).
258. Stilling, R. M. *et al.* The neuropharmacology of butyrate: The bread and butter of the microbiota-gut-brain axis? *Neurochem. Int.* **99**, 110–132 (2016).
259. Barrett, E., Ross, R. P., O’Toole, P. W., Fitzgerald, G. F. & Stanton, C. γ -Aminobutyric acid production by culturable bacteria from the human intestine. *J. Appl. Microbiol.* **113**, 411–417 (2012).
260. Clarke, G. *et al.* Minireview: Gut Microbiota: The Neglected Endocrine Organ. *Mol. Endocrinol.* **28**, 1221–1238 (2014).
261. Hughes, D. T. & Sperandio, V. Inter-kingdom signalling: communication between bacteria and their hosts. *Nat. Rev. Microbiol.* **6**, 111–120 (2008).
262. YAMASHITA, K. *et al.* Inhibitory effect of somatostatin on proliferation in vitro. *Gastroenterology* **115**, 1123–1130 (1998).
263. Chowers, M. Y. *et al.* Human gastrin: A *Helicobacter pylori*-specific growth factor. *Gastroenterology* **117**, 1113–1118 (1999).
264. Chugani, S. & Greenberg, E. P. The influence of human respiratory epithelia on *Pseudomonas aeruginosa* gene expression. *Microb. Pathog.* **42**, 29–35 (2007).
265. Mena, K. D. & Gerba, C. P. Risk Assessment of *Pseudomonas aeruginosa* in Water. *Rev. Environ. Contam. Toxicol.* **209**, 71–115 (2009).
266. Lyczak, J. B., Cannon, C. L. & Pier, G. B. Lung Infections Associated with Cystic Fibrosis. *Clin. Microbiol. Rev.* **15**, 194–222 (2002).
267. Zemanick, E. T., Sagel, S. D. & Harris, J. K. The airway microbiome in cystic fibrosis and implications for treatment. *Curr. Opin. Pediatr.* **23**, 319–324 (2011).

268. Bielecki, P., Glik, J., Kawecki, M. & Martins dos Santos, V. A. P. Towards understanding *Pseudomonas aeruginosa* burn wound infections by profiling gene expression. *Biotechnol. Lett.* **30**, 777–790 (2008).
269. Gambello, M. J., Kaye, S. & Iglewski, B. H. LasR of *Pseudomonas aeruginosa* is a transcriptional activator of the alkaline protease gene (*apr*) and an enhancer of exotoxin A expression. *Infect. Immun.* **61**, 1180–4 (1993).
270. Schuster, M., Lostroh, C. P., Ogi, T. & Greenberg, E. P. Identification, Timing, and Signal Specificity of *Pseudomonas aeruginosa* Quorum-Controlled Genes: a Transcriptome Analysis. *J. Bacteriol.* **185**, 2066–2079 (2003).
271. Schuster, M. & Greenberg, E. P. Early activation of quorum sensing in *Pseudomonas aeruginosa* reveals the architecture of a complex regulon. *BMC Genomics* **8**, 287 (2007).
272. de Kievit, T. R. Quorum sensing in *Pseudomonas aeruginosa* biofilms. *Environ. Microbiol.* **11**, 279–288 (2009).
273. Schuster, M. & Peter Greenberg, E. A network of networks: Quorum-sensing gene regulation in *Pseudomonas aeruginosa*. *Int. J. Med. Microbiol.* **296**, 73–81 (2006).
274. Williams, S. C. *et al.* *Pseudomonas aeruginosa* Autoinducer Enters and Functions in Mammalian Cells. *J. Bacteriol.* **186**, 2281–2287 (2004).
275. Ritchie, A. J. *et al.* The immunomodulatory *Pseudomonas aeruginosa* signalling molecule N-(3-oxododecanoyl)-L-homoserine lactone enters mammalian cells in an unregulated fashion. *Immunol. Cell Biol.* **85**, 596–602 (2007).
276. Tateda, K. *et al.* The *Pseudomonas aeruginosa* Autoinducer N-3-Oxododecanoyl Homoserine Lactone Accelerates Apoptosis in Macrophages and Neutrophils. *Infect. Immun.* **71**, 5785–5793 (2003).
277. Horikawa, M. *et al.* Synthesis of *Pseudomonas* quorum-sensing autoinducer analogs and structural entities required for induction of apoptosis in macrophages. *Bioorg. Med. Chem. Lett.* **16**, 2130–2133 (2006).
278. Kravchenko, V. V. *et al.* N-(3-oxo-acyl)homoserine lactones signal cell activation through a mechanism distinct from the canonical pathogen-associated Molecular PRR Pathways.pdf. *J. Biol. Chem.* **281**, 28822–28830 (2006).
279. Li, L., Hooi, D., Chhabra, S. R., Pritchard, D. & Shaw, P. E. Bacterial N-acylhomoserine lactone-induced apoptosis in breast carcinoma cells correlated with down-modulation of STAT3. *Oncogene* **23**, 4894–4902 (2004).
280. Nicholson, D. W. *et al.* Identification and inhibition of the ICE/CED-3 protease necessary for mammalian apoptosis. *Nature* **376**, 37–43 (1995).
281. Schwarzer, C. *et al.* *Pseudomonas aeruginosa* biofilm-associated homoserine lactone C12 rapidly activates apoptosis in airway epithelia. *Cell. Microbiol.* **14**, 698–709 (2012).
282. Schwarzer, C. *et al.* *Pseudomonas aeruginosa* homoserine lactone triggers apoptosis and Bak/Bax-independent release of mitochondrial cytochrome C in fibroblasts. *Cell. Microbiol.* **16**, 1094–1104 (2014).
283. Valentine, C. D., Anderson, M. O., Papa, F. R. & Haggie, P. M. X-Box Binding Protein 1 (XBP1s) Is a Critical Determinant of *Pseudomonas aeruginosa* Homoserine Lactone-Mediated Apoptosis. *PLoS Pathog.* **9**, (2013).
284. Taguchi, R. *et al.* Mucin 3 is involved in intestinal epithelial cell apoptosis via N-(3-oxododecanoyl)-L-homoserine lactone-induced suppression of Akt phosphorylation. *AJP Cell Physiol.* **307**, C162–C168 (2014).

285. Jacobi, C. A. *et al.* Effects of bacterial N-acyl homoserine lactones on human Jurkat T lymphocytes—OdDHL induces apoptosis via the mitochondrial pathway. *Int. J. Med. Microbiol.* **299**, 509–519 (2009).
286. Zhao, G. *et al.* N-(3-oxo-acyl) homoserine lactone inhibits tumor growth independent of Bcl-2 proteins. *Oncotarget* **7**, 5924–42 (2016).
287. Telford, G. *et al.* The *Pseudomonas aeruginosa* quorum-sensing signal molecule N-(3-oxododecanoyl)-L-homoserine lactone has immunodulatory activity. *Inf. Immun.* **66**, 36–42 (1998).
288. Gardiner, S. M. *et al.* Haemodynamic effects of the bacterial quorum sensing signal molecule, N-(3-oxododecanoyl)-L-homoserine lactone, in conscious, normal and endotoxaemic rats. *Br. J. Pharmacol.* **133**, 1047–1054 (2001).
289. Karlsson, T., Musse, F., Magnusson, K. E. & Vikström, E. Acylhomoserine lactones are potent neutrophil chemoattractants that act via calcium mobilization and actin remodeling. *J. Leukoc. Biol.* **91**, 15–26 (2012).
290. Zimmermann, S. *et al.* Induction of neutrophil chemotaxis by the quorum-sensing molecule N-(3-oxododecanoyl)-L-homoserine lactone. *Infect. Immun.* **74**, 5687–5692 (2006).
291. Khambati, I., Han, S., Pijnenburg, D., Jang, H. & Forsythe, P. The bacterial quorum-sensing molecule, N-3-oxo-dodecanoyl-L-homoserine lactone, inhibits mediator release and chemotaxis of murine mast cells. *Inflamm. Res.* (2016). doi:10.1007/s00011-016-1013-3
292. Wouters, M. M., Vicario, M. & Santos, J. The role of mast cells in functional GI disorders. *Gut* **65**, 155–168 (2016).
293. Hooi, D. S. W., Bycroft, B. W., Chhabra, S. R., Williams, P. & Pritchard, D. I. Differential Immune Modulatory Activity of *Pseudomonas aeruginosa* Quorum-Sensing Signal Molecules. *Infect. Immun.* **72**, 6463–6470 (2004).
294. Ritchie, A. J. *et al.* The *Pseudomonas aeruginosa* Quorum-Sensing Molecule N-3-(Oxododecanoyl)-L-Homoserine Lactone Inhibits T-Cell Differentiation and Cytokine Production by a Mechanism Involving an Early Step in T-Cell Activation. *Infect. Immun.* **73**, 1648–1655 (2005).
295. Ritchie, A. J. *et al.* Modification of In Vivo and In Vitro T- and B-Cell-Mediated Immune Responses by the *Pseudomonas aeruginosa* Quorum-Sensing Lactone Molecule N-(3-Oxododecanoyl)-L-Homoserine Lactone. *Infect. Immun.* **71**, 4421–4431 (2003).
296. Smith, R. S., Harris, S. G., Phipps, R. & Iglewski, B. The *Pseudomonas aeruginosa* Quorum Sensing Molecule N-(3-Oxododecanoyl) Homoserine Lactone Contributes to Virulence and Induces Inflammation In Vivo. *J Bacteriol* **184**, 1132–1139 (2002).
297. Bao, L., Yu, J., Zhong, H., Huang, D. & Lu, Q. Expression of toll-like receptors in T lymphocytes stimulated with N-(3-oxododecanoyl)-L-homoserine lactone from *Pseudomonas aeruginosa*. *Apmis* **125**, 553–557 (2017).
298. Vikström, E., Magnusson, K. E. & Pivoriunas, A. The *Pseudomonas aeruginosa* quorum-sensing molecule N-(3-oxododecanoyl)-L-homoserine lactone stimulates phagocytic activity in human macrophages through the p38 MAPK pathway. *Microbes Infect.* **7**, 1512–1518 (2005).
299. Kravchenko, V. V *et al.* Modulation of Gene Expression via Disruption of NF- κ B Signaling by a Bacterially Small Molecule. *Science* (80-.). **321**, 259–263 (2008).
300. Chhabra, S. R. *et al.* Synthetic Analogues of the Bacterial Signal (Quorum Sensing) Molecule N-(3-oxododecanoyl)-L-homoserine Lactone as Immune Modulators. *J. Med. Chem.* **46**, 97–104 (2003).
301. Thomas, G. L. *et al.* Immunomodulatory effects of *Pseudomonas aeruginosa* quorum sensing small molecule probes on mammalian macrophages. *Mol. Biosyst.* **2**, 132–137 (2006).

302. Miyairi, S. *et al.* Immunization with 3-oxododecanoyl-L-homoserine lactone-protein conjugate protects mice from lethal *Pseudomonas aeruginosa* lung infection. *J. Med. Microbiol.* **55**, 1381–1387 (2006).
303. Glucksam-Galnoy, Y. *et al.* The Bacterial Quorum-Sensing Signal Molecule N-3-Oxo-Dodecanoyl-L-Homoserine Lactone Reciprocally Modulates Pro- and Anti-Inflammatory Cytokines in Activated Macrophages. *J. Immunol.* **191**, 337–344 (2013).
304. Moore, K. W., de Waal Malefyt, R., Coffman, R. L. & O'Garra, A. Interleukin-10 and the interleukin-10 receptor. *Annu. Rev. Immunol.* **19**, 683–765 (2001).
305. Di Santo, E., Adami, M., Bertorelli, R. & Ghezzi, P. Systemic interleukin 10 administration inhibits brain tumor necrosis factor production in mice. *Eur. J. Pharmacol.* **336**, 197–202 (1997).
306. D'Andrea, A. *et al.* Interleukin 10 (IL-10) inhibits human lymphocyte interferon gamma- production by suppressing natural killer cell stimulatory factor/IL-12 synthesis in accessory cells. *J. Exp. Med.* **178**, 1041–1048 (1993).
307. de Waal Malefyt, R., Abarms, J., Bennett, B., Figdor, C. G. & de Vries, J. E. Interleukin 10 (IL-10) Inhibits Cytokine Synthesis by Human Monocytes: n Autoregulatory Role of IL-10 Produced by Monocytes. *J. Exp. Med.* **174**, 1209–1220 (1991).
308. DiMango, E., Zar, H. J., Bryan, R. & Prince, A. Diverse *Pseudomonas aeruginosa* gene products stimulate respiratory epithelial cells to produce interleukin-8. *J. Clin. Invest.* **96**, 2204–2210 (1995).
309. Smith, R. S. *et al.* IL-8 production in human lung fibroblasts and epithelial cells activated by the *Pseudomonas* autoinducer N-3-oxododecanoyl homoserine lactone is transcriptionally regulated by NF-kappa B and activator protein-2. *J. Immunol.* **167**, 366–374 (2001).
310. Smith, R. S., Kelly, R., Iglewski, B. H. & Phipps, R. P. The *Pseudomonas* autoinducer N-(3-oxododecanoyl) homoserine lactone induces cyclooxygenase-2 and prostaglandin E2 production in human lung fibroblasts: implications for inflammation. *J. Immunol.* **169**, 2636–2642 (2002).
311. Shiner, E. K. *et al.* *Pseudomonas aeruginosa* autoinducer modulates host cell responses through calcium signalling. *Cell. Microbiol.* **8**, 1601–1610 (2006).
312. Hartsock, A. & Nelson, W. J. Adherens and Tight Junctions: Structure, Function and Connections to the Actin Cytoskeleton. *Biochim Biophys Acta* **1778**, 660–669 (2008).
313. Vikström, E., Tafazoli, F. & Magnusson, K. E. *Pseudomonas aeruginosa* quorum sensing molecule N-(3-oxododecanoyl)-l-homoserine lactone disrupts epithelial barrier integrity of Caco-2 cells. *FEBS Lett.* **580**, 6921–6928 (2006).
314. Vikström, E., Bui, L., Konradsson, P. & Magnusson, K. E. The junctional integrity of epithelial cells is modulated by *Pseudomonas aeruginosa* quorum sensing molecule through phosphorylation-dependent mechanisms. *Exp. Cell Res.* **315**, 313–326 (2009).
315. Sturm, A. & Dignass, A. U. Epithelial restitution and wound healing in inflammatory bowel disease. *World J. Gastroenterol.* **14**, 348 (2008).
316. Kjøller, L. & Hall, A. Signaling to Rho GTPases. *Exp. Cell Res.* **253**, 166–179 (1999).
317. Evers, E. *et al.* Rho family proteins in cell adhesion and cell migration. *Eur. J. Cancer* **36**, 1269–1274 (2000).
318. Karlsson, T. *et al.* Aquaporin 9 phosphorylation mediates membrane localization and neutrophil polarization. *J. Leukoc. Biol.* **90**, 963–973 (2011).
319. Holm, A., Magnusson, K.-E. & Vikström, E. *Pseudomonas aeruginosa* N-3-oxo-dodecanoyl-homoserine Lactone Elicits Changes in Cell Volume, Morphology, and AQP9 Characteristics in Macrophages. *Front. Cell. Infect. Microbiol.* **6**, (2016).

320. Karlsson, T., Turkina, M. V., Yakymenko, O., Magnusson, K. E. & Vikström, E. The *Pseudomonas aeruginosa* N-Acylhomoserine Lactone Quorum Sensing Molecules Target IQGAP1 and Modulate Epithelial Cell Migration. *PLoS Pathog.* **8**, (2012).
321. Uroz, S. N-Acylhomoserine lactone quorum-sensing molecules are modified and degraded by *Rhodococcus erythropolis* W2 by both amidolytic and novel oxidoreductase activities. *Microbiology* **151**, 3313–3322 (2005).
322. Chowdhary, P. K. *et al.* *Bacillus megaterium* CYP102A1 Oxidation of Acyl Homoserine Lactones and Acyl Homoserines †. *Biochemistry* **46**, 14429–14437 (2007).
323. Gao, A. *et al.* High-resolution structures of AidH complexes provide insights into a novel catalytic mechanism for N-acyl homoserine lactonase. *Acta Crystallogr. Sect. D Biol. Crystallogr.* **69**, 82–91 (2013).
324. Amara, N., Krom, B. P., Kaufmann, G. F. & Meijler, M. M. Macromolecular Inhibition of quorum sensing: Enzymes, antibodies, and beyond. *Chem. Rev.* **111**, 195–208 (2011).
325. Fetzner, S. Quorum quenching enzymes. *J. Biotechnol.* **201**, 2–14 (2014).
326. Utari, P. D., Vogel, J. & Quax, W. J. Deciphering physiological functions of AHL quorum quenching acylases. *Front. Microbiol.* **8**, 1–13 (2017).
327. Lowery, C. A. *et al.* Defining the mode of action of tetramic acid antibacterials derived from *Pseudomonas aeruginosa* quorum sensing signals. *J. Am. Chem. Soc.* **131**, 14473–14479 (2009).
328. Kaufmann, G. F. *et al.* Revisiting quorum sensing: Discovery of additional chemical and biological functions for 3-oxo-N-acylhomoserine lactones. *Proc. Natl. Acad. Sci. U. S. A.* **102**, 309–314 (2005).
329. Murray, E. J. *et al.* Targeting *Staphylococcus aureus* quorum sensing with non-peptidic small molecule inhibitors. *J. Med. Chem.* **57**, 2813–2819 (2014).
330. Hosono Honda, N. *et al.* Roles of *Pseudomonas aeruginosa* Autoinducers and their Degradation Products, Tetramic acids, in Bacterial Survival and Behavior in Ecological Niches. *Microbes Environ.* **26**, 160–164 (2011).
331. Khersonsky, O. & Tawfik, D. S. Structure-reactivity studies of serum paraoxonase PON1 suggest that its native activity is lactonase. *Biochemistry* **44**, 6371–6382 (2005).
332. Billecke, S. *et al.* Human serum paraoxonase (PON1) isozymes Q and R hydrolyze lactones and cyclic carbonate esters. *Drug Metab. Dispos.* **28**, 1335–1342 (2000).
333. Furlong, C. E., Marsillach, J., Jarvik, G. P. & Costa, L. G. Paraoxonases-1, -2 and -3: What are their functions? *Chem. Biol. Interact.* **259**, 51–62 (2016).
334. Ng, C. J. *et al.* Paraoxonase-2 Is a Ubiquitously Expressed Protein with Antioxidant Properties and Is Capable of Preventing Cell-mediated Oxidative Modification of Low Density Lipoprotein. *J. Biol. Chem.* **276**, 44444–44449 (2001).
335. Teiber, J. F. *et al.* Dominant role of paraoxonases in inactivation of the *Pseudomonas aeruginosa* quorum-sensing signal N-(3-oxododecanoyl)-L-homoserine lactone. *Infect. Immun.* **76**, 2512–2519 (2008).
336. Bar-Rogovsky, H., Hugenmatter, A. & Tawfik, D. S. The Mammalian Serum Paraoxonases (PONs) Relate to Bacterial Homoserine Lactonases. *J. Biol. Chem.* **288**, 23914–23927 (2013).
337. Jahoor, A. *et al.* Peroxisome proliferator-activated receptors mediate host cell proinflammatory responses to *Pseudomonas aeruginosa* autoinducer. *J. Bacteriol.* **190**, 4408–4415 (2008).
338. Behrens, M. & Meyerhof, W. Oral and Extraoral Bitter Taste Receptors. in 87–99 (2011).

339. Rozengurt, E. Taste Receptors in the Gastrointestinal Tract. I. Bitter taste receptors and α -gustducin in the mammalian gut. *Am. J. Physiol. Liver Physiol.* **291**, G171–G177 (2006).
340. Carrai, M. *et al.* Association between TAS2R38 gene polymorphisms and colorectal cancer risk: A case-control study in two independent populations of caucasian origin. *PLoS One* **6**, (2011).
341. Lee, R. J. *et al.* T2R38 taste receptor polymorphisms underlie susceptibility to upper respiratory infection. *J. Clin. Invest.* **122**, 4145–4159 (2012).
342. Meyerhof, W. Elucidation of mammalian bitter taste. in *Reviews of Physiology, Biochemistry and Pharmacology* 37–72 (Springer Berlin Heidelberg, 2005). doi:10.1007/s10254-005-0041-0
343. Kim, U. -k. Positional Cloning of the Human Quantitative Trait Locus Underlying Taste Sensitivity to Phenylthiocarbamide. *Science (80-.)*. **299**, 1221–1225 (2003).
344. Bufe, B. *et al.* The Molecular Basis of Individual Differences in Phenylthiocarbamide and Propylthiouracil Bitterness Perception. *Curr. Biol.* **15**, 322–327 (2005).
345. Behrens, M. & Meyerhof, W. Gustatory and extragustatory functions of mammalian taste receptors. *Physiol. Behav.* **105**, 4–13 (2011).
346. Briggs, M. W. & Sacks, D. B. IQGAP proteins are integral components of cytoskeletal regulation. *EMBO Rep.* **4**, 571–574 (2003).
347. Bensenor, L. B. *et al.* IQGAP1 regulates cell motility by linking growth factor signaling to actin assembly. *J. Cell Sci.* **120**, 658–669 (2007).
348. Noritake, J., Watanabe, T., Sato, K., Wang, S. & Kaibuchi, K. IQGAP1: a key regulator of adhesion and migration. *J. Cell Sci.* **118**, 2085–2092 (2005).
349. Brandt, D. T. & Grosse, R. Get to grips: steering local actin dynamics with IQGAPs. *EMBO Rep.* **8**, 1019–1023 (2007).
350. Watanabe, T. *et al.* Interaction with IQGAP1 Links APC to Rac1, Cdc42, and Actin Filaments during Cell Polarization and Migration. *Dev. Cell* **7**, 871–883 (2004).
351. Lichtenstein, A. H. Intestinal Cholesterol Metabolism. *Ann. Med.* **22**, 49–52 (1990).
352. Landman, C. *et al.* Inter-kingdom effect on epithelial cells of the N-Acyl homoserine lactone 3-oxo-C12 : 2 , a major quorum-sensing molecule from gut microbiota. *PLoS One* **13**, 1–18 (2018).
353. Thiel, V., Kunze, B., Verma, P., Wagner-Döbler, I. & Schulz, S. New structural variants of homoserine lactones in bacteria. *ChemBioChem* **10**, 1861–1868 (2009).
354. Ziesche, L. *et al.* Homoserine Lactones, Methyl Oligohydroxybutyrates, and Other Extracellular Metabolites of Macroalgae-Associated Bacteria of the Roseobacter Clade: Identification and Functions. *ChemBioChem* **16**, 2094–2107 (2015).
355. Ziesche, L. *et al.* An unprecedented medium-chain diunsaturated n-acylhomoserine lactone from marine roseobacter group bacteria. *Mar. Drugs* **17**, 1–14 (2019).
356. Zweibaum, A., Laburthe, M., Grasset, E. & Louvard, D. Use of cultured cell lines in studies of intestinal cell differentiation and function. in *Handbook of Physiology :The Gastrointestinal System* (eds. Field, M. & Frizzel, R. A.) 223–255 (American Physiology Society, 1991).
357. Chantret, I. *et al.* Differential expression of sucrase-isomaltase in clones isolated from early and late passages of the cell line Caco-2: evidence for glucose-dependent negative regulation. *J. Cell Sci.* **107 (Pt 1)**, 213–225 (1994).

358. Fogh, J., Fogh, J. M. & Orfeo, T. One Hundred and Twenty-Seven Cultured Human Tumor Cell Lines Producing Tumors in Nude Mice²³. *JNCI J. Natl. Cancer Inst.* **59**, 221–226 (1977).
359. Pignata, S., Maggini, L., Zarrilhi, R., Rea, A. & Acquaviva, A. M. The Enterocyte-like Differentiation of the Caco-2 Tumor Cell Line Strongly Correlates with Responsiveness to cAMP and Activation of Kinase A Pathway'. *Cell Growth Differ.* **5**, 967–973 (1994).
360. Taciak, B. *et al.* Evaluation of phenotypic and functional stability of RAW 264.7 cell line through serial passages. *PLoS One* **13**, 1–13 (2018).
361. Frommberger, M. *et al.* A simple and robust set-up for on-column sample preconcentration ? nano-liquid chromatography ? electrospray ionization mass spectrometry for the analysis of N-acylhomoserine lactones. *Anal. Bioanal. Chem.* **378**, 1014–1020 (2004).
362. Cataldi, T. R. I., Bianco, G., Frommberger, M. & Schmitt-Kopplin, P. Direct analysis of selected N-acyl-L-homoserine lactones by gas chromatography/mass spectrometry. *Rapid Commun. Mass Spectrom.* **18**, 1341–1344 (2004).
363. Cataldi, T. R. I., Bianco, G., Fonseca, J. & Schmitt-Kopplin, P. Perceiving the chemical language of Gram-negative bacteria: listening by high-resolution mass spectrometry. *Anal. Bioanal. Chem.* **405**, 493–507 (2013).
364. Morin, D., Grasland, B., Vallée-Réhel, K., Dufau, C. & Haras, D. On-line high-performance liquid chromatography–mass spectrometric detection and quantification of N-acylhomoserine lactones, quorum sensing signal molecules, in the presence of biological matrices. *J. Chromatogr. A* **1002**, 79–92 (2003).
365. Cataldi, T. R. I., Bianco, G. & Abate, S. Profiling of N-acyl-homoserine lactones by liquid chromatography coupled with electrospray ionization and a hybrid quadrupole linear ion-trap and Fourier-transform ion-cyclotron-resonance mass spectrometry (LC-ESI-LTQ-FTICR-MS). *J. Mass Spectrom.* **43**, 82–96 (2007).
366. Ortori, C. A. *et al.* Comprehensive profiling of N-acylhomoserine lactones produced by *Yersinia pseudotuberculosis* using liquid chromatography coupled to hybrid quadrupole–linear ion trap mass spectrometry. *Anal. Bioanal. Chem.* **387**, 497–511 (2007).
367. Ortori, C. A. *et al.* Simultaneous quantitative profiling of N-acyl-L-homoserine lactone and 2-alkyl-4(1H)-quinolone families of quorum-sensing signaling molecules using LC-MS/MS. *Anal. Bioanal. Chem.* **399**, 839–850 (2011).
368. Wang, J. *et al.* Development of an extraction method and LC-MS analysis for N-acylated-L-homoserine lactones (AHLs) in wastewater treatment biofilms. *J. Chromatogr. B* **1042**, 37–44 (2017).
369. Cataldi, T. R. I., Bianco, G., Abate, S. & Losito, I. Identification of unsaturated N-acylhomoserine lactones in bacterial isolates of *Rhodobacter sphaeroides* by liquid chromatography coupled to electrospray ionization-hybrid linear ion trap-Fourier transform ion cyclotron resonance mass spectrometry. *Rapid Commun. Mass Spectrom.* **25**, 1817–1826 (2011).
370. Giddens, A. C. Studies of Biologically Active Natural Products – Texaline, Pseudopyronines A and B, and Varacin. (2008).
371. Baker, Y. R., Galloway, W. R. J. D., Hodgkinson, J. T. & Spring, D. R. Design and synthesis of a biotinylated chemical probe for detecting the molecular targets of an inhibitor of the production of the *Pseudomonas aeruginosa* virulence factor pyocyanin. *Molecules* **18**, 11783–11796 (2013).
372. Kanchanabanka, C. *et al.* Unusual acetylation-elimination in the formation of tetronate antibiotics. *Angew. Chemie - Int. Ed.* **52**, 5785–5788 (2013).
373. Morkunas, B. *et al.* Inhibition of the production of the *Pseudomonas aeruginosa* virulence factor pyocyanin in wild-type cells by quorum sensing autoinducer-mimics. *Org. Biomol. Chem.* **10**, 8452 (2012).

374. Biswas, N. N. *et al.* Indole-based novel small molecules for the modulation of bacterial signalling pathways. *Org. Biomol. Chem.* **13**, 925–937 (2015).
375. Pinto, A., Ciesla, J. H., Palucci, A., Sutliff, B. P. & Nomura, C. T. Chemically Intractable No More: In Vivo Incorporation of ‘click’-Ready Fatty Acids into Poly-[(R)-3-hydroxyalkanoates] in *Escherichia coli*. *ACS Macro Lett.* **5**, 215–219 (2016).
376. Hodgkinson, J. T. *et al.* Robust routes for the synthesis of N-acylated-l-homoserine lactone (AHL) quorum sensing molecules with high levels of enantiomeric purity. *Tetrahedron Lett.* **52**, 3291–3294 (2011).
377. Alagely, A. *et al.* *Quorum Sensing: Methods and Protocols*.
378. Yamaguchi, T. *et al.* Turn-ON fluorescent affinity labeling using a small bifunctional O-nitrobenzoxadiazole unit. *Chem. Sci.* **5**, 1021–1029 (2014).
379. Huang, D., Yang, G., Feng, X., Lai, X. & Zhao, P. Triazole-stabilized gold and related noble metal nanoparticles for 4-nitrophenol reduction. *New J. Chem.* **39**, 4685–4694 (2015).
380. Davis, B. M., Richens, J. L. & O’Shea, P. Label-free critical micelle concentration determination of bacterial quorum sensing molecules. *Biophys. J.* **101**, 245–254 (2011).
381. Al-Sadi, R. M. & Ma, T. Y. IL-1 β Causes an Increase in Intestinal Epithelial Tight Junction Permeability. *J. Immunol.* **178**, 4641–4649 (2007).
382. Al-Sadi, R., Ye, D., Said, H. M. & Ma, T. Y. Cellular and molecular mechanism of interleukin-1 β modulation of Caco-2 intestinal epithelial tight junction barrier. *J. Cell. Mol. Med.* **15**, 970–982 (2011).
383. Beguin, P., Errachid, A., Larondelle, Y. & Schneider, Y. J. Effect of polyunsaturated fatty acids on tight junctions in a model of the human intestinal epithelium under normal and inflammatory conditions. *Food Funct.* **4**, 923–931 (2013).
384. Erickson, D. L. *et al.* *Pseudomonas aeruginosa* quorum-sensing systems may control virulence factor expression in the lungs of patients with cystic fibrosis. *Infect. Immun.* **70**, 1783–1790 (2002).
385. Charlton, T. S. *et al.* A novel and sensitive method for the quantification of N-3-oxoacyl homoserine lactones using gas chromatography-mass spectrometry: application to a model bacterial biofilm. *Environ. Microbiol.* **2**, 530–541 (2000).
386. Murray, T. S., Egan, M. & Kazmierczak, B. I. *Pseudomonas aeruginosa* chronic colonization in cystic fibrosis patients. *Curr. Opin. Paediatr.* **19**, 83–88 (2007).
387. Singh, P. K. *et al.* Quorum-sensing signals indicate that cystic fibrosis lungs are infected with bacterial biofilms. *Nature* **407**, 762–764 (2000).
388. Pearson, J. P. *et al.* Structure of the autoinducer required for expression of *Pseudomonas aeruginosa* virulence genes. *Proc. Natl. Acad. Sci.* **91**, 197–201 (1994).
389. Huang, Q. *et al.* IL-17 Promotes Angiogenic Factors IL-6, IL-8, and Vegf Production via Stat1 in Lung Adenocarcinoma. *Sci. Rep.* **6**, 1–12 (2016).
390. Hirata, T. *et al.* Interleukin (IL)-17A stimulates IL-8 secretion, cyclooxygenase-2 expression, and cell proliferation of endometriotic stromal cells. *Endocrinology* **149**, 1260–1267 (2008).
391. ZHANG, J., GONG, F., LI, L., ZHAO, M. & SONG, J. *Pseudomonas aeruginosa* quorum-sensing molecule N-(3-oxododecanoyl) homoserine lactone attenuates lipopolysaccharide-induced inflammation by activating the unfolded protein response. *Biomed. Reports* **2**, 233–238 (2014).
392. Camps, J., Pujol, I., Ballester, F., Joven, J. & Simó, J. M. Paraoxonases as Potential Antibiofilm Agents: Their Relationship with Quorum-Sensing Signals in Gram-Negative Bacteria. *Antimicrob. Agents*

- Chemother.* **55**, 1325–1331 (2011).
393. Clayden, J., Greeves, N. & Warren, S. *Organic chemistry (2nd edition)*. (Oxford University Press, 1988). doi:10.1086/278635
394. Yates, E. A. *et al.* Lactones Undergo Lactonolysis in a pH-, Temperature-, and Acyl Chain Length-Dependent Manner during Growth of. *Society* **70**, 5635–5646 (2002).
395. Shamir, R. *et al.* Paraoxonases (PONs) 1, 2, and 3 are expressed in human and mouse gastrointestinal tract and in Caco-2 cell line: Selective secretion of PON1 and PON2. *Free Radic. Biol. Med.* **39**, 336–344 (2005).
396. Gaidukov, L. & Tawfik, D. S. The development of human sera tests for HDL-bound serum PON1 and its lipolactonase activity. *J. Lipid Res.* **48**, 1637–1646 (2007).
397. Gonzalvo, M. C. *et al.* Human Liver Paraoxonase (PON1): Subcellular Distribution and Characterization. *J. Biochem. Mol. Toxicol.* **12**, 61–69 (1998).
398. Losa, D. *et al.* Airway epithelial cell integrity protects from cytotoxicity of pseudomonas aeruginosa quorum-sensing signals. *American Journal of Respiratory Cell and Molecular Biology* **53**, 265–275 (2015).
399. Horke, S. *et al.* Novel Paraoxonase 2-Dependent Mechanism Mediating the Biological Effects of the Pseudomonas aeruginosa Quorum-Sensing Molecule N-(3-Oxo-Dodecanoyl)-L-Homoserine Lactone. *Infect. Immun.* **83**, 3369–3380 (2015).
400. Devarajan, A. *et al.* Role of PON2 in innate immune response in an acute infection model. *Mol. Genet. Metab.* **110**, 362–370 (2013).
401. Stoltz, D. A. *et al.* Drosophila are protected from Pseudomonas aeruginosa lethality by transgenic expression of paraoxonase-1. *J. Clin. Invest.* **118**, 3123–3131 (2008).
402. Tao, S. *et al.* Paraoxonase 2 modulates a proapoptotic function in LS174T cells in response to quorum sensing molecule N-(3-oxododecanoyl)-L-homoserine lactone. *Sci. Rep.* **6**, 1–12 (2016).
403. Glansdorp, F. G. *et al.* Synthesis and stability of small molecule probes for Pseudomonas aeruginosa quorum sensing modulation. *Org. Biomol. Chem.* **2**, 3329 (2004).
404. Liang, L. & Astruc, D. The copper(I)-catalyzed alkyne-azide cycloaddition (CuAAC) ‘click’ reaction and its applications. An overview. *Coord. Chem. Rev.* **255**, 2933–2945 (2011).
405. Li, L. & Zhang, Z. Development and applications of the copper-catalyzed azide-alkyne cycloaddition (CuAAC) as a bioorthogonal reaction. *Molecules* **21**, 1–22 (2016).
406. Kolb, H. C., Finn, M. G. & Sharpless, K. B. Click Chemistry: Diverse Chemical Function from a Few Good Reactions. *Angew. Chemie - Int. Ed.* **40**, 2004–2021 (2001).
407. Speers, A. E. & Cravatt, B. F. Profiling Enzyme Activities In Vivo Using Click Chemistry Methods. *Chem. Biol.* **11**, 535–546 (2004).
408. Garner, A. L. *et al.* Synthesis of clickable acylhomoserine lactone quorum sensing probes: Unanticipated effects on mammalian cell activation. *Bioorganic Med. Chem. Lett.* **21**, 2702–2705 (2011).
409. Davis, B. M., Jensen, R., Williams, P., Shea, P. O. & O’Shea, P. The Interaction of N-Acylhomoserine Lactone Quorum Sensing Signaling Molecules with Biological Membranes : Implications for Inter-Kingdom Signaling. *PLoS One* **5**, 1–10 (2010).
410. Gaida, M. M., Dapunt, U. & Hänsch, G. M. Sensing developing biofilms: the bitter receptor T2R38 on myeloid cells. *Pathog. Dis.* **74**, 1–10 (2016).

411. Simon, S. *et al.* Inter-kingdom Signaling by the Legionella Quorum Sensing Molecule LAI-1 Modulates Cell Migration through an IQGAP1-Cdc42-ARHGEF9-Dependent Pathway. *PLoS Pathog.* **11**, 1–30 (2015).
412. Maurer, S. *et al.* Tasting *Pseudomonas aeruginosa* Biofilms: Human Neutrophils Express the Bitter Receptor T2R38 as Sensor for the Quorum Sensing Molecule N-(3-Oxododecanoyl)-L-Homoserine Lactone. *Front. Immunol.* **6**, 369 (2015).
413. Gaida, M. M. *et al.* Expression of the bitter receptor T2R38 in pancreatic cancer: localization in lipid droplets and activation by a bacteria-derived quorum-sensing molecule. *Oncotarget* **7**, (2016).
414. Tran, H. T. T., Herz, C., Ruf, P., Stetter, R. & Lamy, E. Human T2R38 Bitter Taste Receptor Expression in Resting and Activated Lymphocytes. *Front. Immunol.* **9**, (2018).
415. Verbeurgt, C. *et al.* The human bitter taste receptor T2R38 is broadly tuned for bacterial compounds. *PLoS One* **12**, (2017).
416. Pydi, S. P. *et al.* Amino acid derivatives as bitter taste receptor (T2R) blockers. *J. Biol. Chem.* **289**, 25054–25066 (2014).
417. Freund, J. R. *et al.* Activation of airway epithelial bitter taste receptors by *pseudomonas aeruginosa* quinolones modulates calcium, cyclic-amp, and nitric oxide signaling. *J. Biol. Chem.* **293**, 9824–9840 (2018).
418. Matsuyama, A., Yashiroda, Y. & Yoshida, M. Chemical Proteomics: A Global Study of Protein–Small Molecule Interactions. in *Chemical Genomics* (ed. Fu, H.) 26–36 (Cambridge University Press, 2012). doi:<https://doi.org/10.1017/CBO9781139021500.005>
419. Hodgkinson, J. T. *et al.* Design, synthesis and biological evaluation of non-natural modulators of quorum sensing in *Pseudomonas aeruginosa*. *Org. Biomol. Chem.* **10**, 6032–6044 (2012).
420. Gomi, K. *et al.* Mouse and human cell activation by N-dodecanoyl-DL-homoserine lactone, a *Chromobacterium violaceum* autoinducer. *Infect. Immun.* **74**, 7029–7031 (2006).
421. Conway, B.-A. & Greenberg, E. P. Quorum-Sensing Signals and Quorum-Sensing Genes in *Burkholderia vietnamiensis*. *J. Bacteriol.* **184**, 1187–1191 (2002).
422. Mattiuzzo, M. *et al.* The plant pathogen *Pseudomonas fuscovaginae* contains two conserved quorum sensing systems involved in virulence and negatively regulated by RsaL and the novel regulator RsaM. *Environ. Microbiol.* **13**, 145–162 (2011).
423. Swift, S. *et al.* Quorum sensing in *Aeromonas hydrophila* and *Aeromonas salmonicida*: Identification of the LuxR homologs AhyR and AsaR and their cognate N-acylhomoserine lactone signal molecules. *J. Bacteriol.* **179**, 5271–5281 (1997).
424. Swift, S. *et al.* Quorum sensing-dependent regulation and blockade of exoprotease production in *Aeromonas hydrophila*. *Infect. Immun.* **67**, 5192–5199 (1999).
425. Tan, K. H., How, K. Y., Tan, J. Y., Yin, W. F. & Chan, K. G. Cloning and characterization of the autoinducer synthase gene from lipid-degrading bacterium *Cedecea neteri*. *Front. Microbiol.* **8**, 1–10 (2017).
426. Pearson, J. P., Pesci, E. C. & Iglewski, B. H. Roles of *Pseudomonas aeruginosa* las and rhl quorum-sensing systems in control of twitching motility. *J. Bacteriol.* **197**, 5756–5767 (1997).
427. Eberl, L. *et al.* Involvement of N-acyl-L-homoserine lactone autoinducers in controlling the multicellular behaviour of *Serratia liquefaciens*. *Mol. Microbiol.* **20**, 127–136 (1996).
428. Joe, G. *et al.* Acyl-homoserine lactones suppresses IEC-6 cell proliferation and increase permeability of isolated rat colon permeability of isolated rat colon. **8451**, (2014).

429. McInnis, C. E. & Blackwell, H. E. Thiolactone modulators of quorum sensing revealed through library design and screening. *Bioorganic Med. Chem.* **19**, 4820–4828 (2011).
430. Garner, A. L. *et al.* Immunomodulation and the quorum sensing molecule 3-oxo-C12-homoserine lactone: The importance of chemical scaffolding for probe development. *Chem. Commun.* **49**, 1515–1517 (2013).
431. Jadhav, G. P. *et al.* Immunosuppressive but non-LasR-inducing analogues of the pseudomonas aeruginosa quorum-sensing molecule N-(3-Oxododecanoyl)-l-homoserine Lactone. *J. Med. Chem.* **54**, 3348–3359 (2011).
432. Kim, C. K. C. C. K. C. *et al.* Structural understanding of quorum-sensing inhibitors by molecular modeling study in *Pseudomonas aeruginosa*. *Appl. Microbiol. Biotechnol.* **83**, 1095–1103 (2009).
433. Caré, B. R. & Soula, H. A. Impact of receptor clustering on ligand binding. *BMC Syst. Biol.* **5**, (2011).
434. Liu, J., Liu, M., Zheng, B., Yao, Z. & Xia, J. Affinity enhancement by ligand clustering effect inspired by peptide dendrimers-shank PDZ proteins interactions. *PLoS One* **11**, 1–12 (2016).
435. Smith, K. M., Bu, Y. & Suga, H. Library screening for synthetic agonists and antagonists of a *Pseudomonas aeruginosa* autoinducer. *Chem. Biol.* **10**, 563–571 (2003).
436. Mattmann, M. E. & Blackwell, H. E. Small molecules that modulate quorum sensing and control virulence in *pseudomonas aeruginosa*. *J. Org. Chem.* **75**, 6737–6746 (2010).
437. Passador, L. *et al.* Functional analysis of the *Pseudomonas aeruginosa* autoinducer PAI. *J. Bacteriol.* **178**, 5995–6000 (1996).
438. Kline, T. *et al.* Novel Synthetic Analogs of the *Pseudomonas* Autoinducer. *Bioorg. Med. Chem. Lett.* **9**, 34447–3452 (1999).
439. McCready, A. R., Paczkowski, J. E., Henke, B. R. & Bassler, B. L. Structural determinants driving homoserine lactone ligand selection in the *Pseudomonas aeruginosa* LasR quorum-sensing receptor. **116**, (2019).
440. Smith, K. M., Bu, Y. & Suga, H. Induction and Inhibition of *Pseudomonas aeruginosa* Quorum Sensing by Synthetic Autoinducer Analogs. *Chem. Biol.* **10**, 81–89 (2003).
441. Vannini, A. The crystal structure of the quorum sensing protein TraR bound to its autoinducer and target DNA. *EMBO J.* **21**, 4393–4401 (2002).
442. Yao, Y. *et al.* Structure of the *Escherichia coli* Quorum Sensing Protein SdiA: Activation of the Folding Switch by Acyl Homoserine Lactones. *J. Mol. Biol.* **355**, 262–273 (2006).
443. Ho, Y.-S. J. Structure of the GAF domain, a ubiquitous signaling motif and a new class of cyclic GMP receptor. *EMBO J.* **19**, 5288–5299 (2000).
444. Gu, Y.-Z., Hogenesch, J. B. & Bradfield, C. A. The PAS Superfamily: Sensors of Environmental and Developmental Signals. *Annu. Rev. Pharmacol. Toxicol.* **40**, 519–561 (2000).
445. Jamalzadeh, L. *et al.* Cytotoxic Effects of Some Common Organic Solvents on MCF-7, RAW-264.7 and Human Umbilical Vein Endothelial Cells. *Avicenna J. Med. Biochem.* **In press**, 10–33453 (2016).
446. Hollebeeck, S. *et al.* Dimethyl sulfoxide (DMSO) attenuates the inflammatory response in the in vitro intestinal Caco-2 cell model. *Toxicol. Lett.* **206**, 268–275 (2011).
447. Lü, Y. *et al.* Synthesis and sensing applications of a new fluorescent derivative of cholesterol. *New J. Chem.* **40**, 1817–1824 (2016).
448. Morisaki, T. *et al.* An N-sulfanylethylanilide-based traceable linker for enrichment and selective

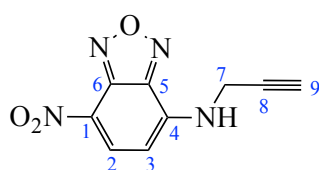
- labelling of target proteins. *Chem. Commun.* **52**, 6911–6913 (2016).
449. Ouadahi, K., Allard, E., Oberleitner, B. & Larpent, C. Synthesis of azide-functionalized nanoparticles by microemulsion polymerization and surface modification by click chemistry in aqueous medium. *J. Polym. Sci. Part A Polym. Chem.* **50**, 314–328 (2012).
450. Ahn, B., Rhee, S. G. & Stadtman, E. R. Use of fluorescein hydrazide and fluorescein thiosemicarbazide reagents for the fluorometric determination of protein carbonyl groups and for the detection of oxidized protein on polyacrylamide gels. *Anal. Biochem.* **161**, 245–257 (1987).
451. Key, J. A., Li, C. & Cairo, C. W. Detection of cellular sialic acid content using nitrobenzoxadiazole carbonyl-reactive chromophores. *Bioconjug. Chem.* **23**, 363–371 (2012).

ANNEXES

A.1. Synthesis

a. Molecule(s) not prepared in person

Synthesis of 7-nitro-*N*-2-propyn-1-yl-2,1,3-benzoxadiazol-4-amine **16** [1201012-14-7]



$C_9H_6N_4O_3$
(Mw: 218.17)

Prepared according published procedure⁴⁴⁷ by *M. Laurent Cattiaux* with 48% yield. 1H NMR (300 MHz, $CDCl_3$): δ 8.54 (dd, $J = 8.5, 0.5$ Hz, 1H, NH), 6.35 (d, $J = 8.5$ Hz, 2H, C(2)HC(3)H), 4.30 (dd, $J = 5.8, 2.5$ Hz, 2H, C(7)H₂), 2.43 (t, $J = 2.5$ Hz, 1H, C(9)H). ^{13}C NMR (75 MHz, $CDCl_3$): δ 149.55, 146.70, 136.47 (CH benzene), 135.91 (CH benzene), 131.15, 100.10 (C₉), 94.94, 74.32 (C₈), 33.54 (C₇). HRMS (ESI): exact mass calculated for $C_9H_6N_4O_3Na$ ($[M+Na]^+$): 241.0332. Found: 241.0333.

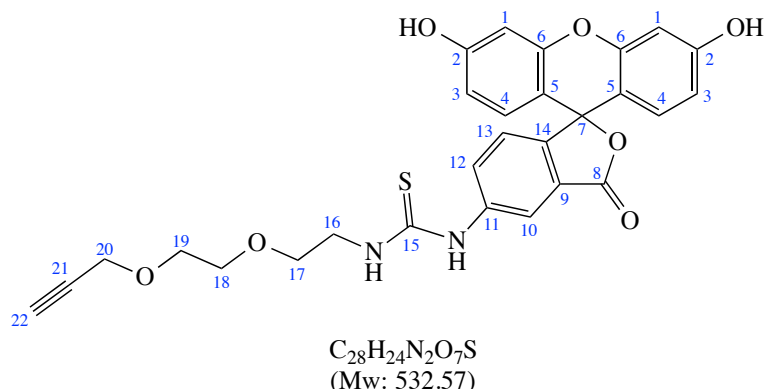
b. Molecules prepared for this project but not employed

The following molecules were prepared in link to this PhD project but were not employed. Indeed, we wished to prepare several tagged AHLs : one with a fluorescein standing at tail end of the AHL, another with a fluorescein linked at ketone, and a third with the NBD linked at ketone. Unfortunately and despite several attempts, the linkages of AHL and fluorophore were unsuccessful.

Coupling of 5-FITC to 2-[2-(2-propynyloxy)ethoxy]ethylamine⁴⁴⁸

To a stirred solution of 5-FITC (1.0 equiv) in 1:1 THF/EtOH v/v (approx. 3 ml/0.1 mmol FITC) were successively added Et_3N (2.0 equiv) and the 2-[2-(2-propynyloxy)ethoxy]ethylamine (2.0 equiv). The reaction mixture was stirred overnight. At completion, the reaction mixture was evaporated to dryness

before purification by Flash chromatography in EtOAc/MeOH/H₂O with gradient a elution from 90:5:3 to 50:5:3.

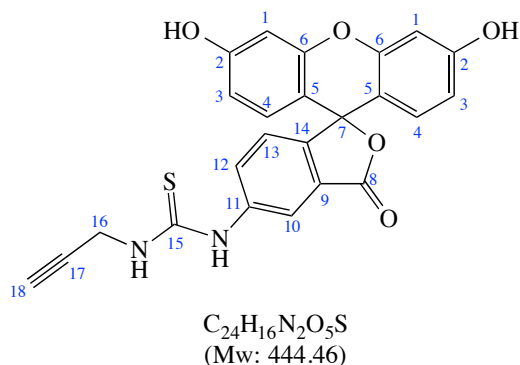


Prepared with quantitative yield. ¹H NMR (300 MHz, MeOD-*d*₄): δ 8.14 (dd, *J* = 2.1, 0.6 Hz, 1H, C(10)**H**), 7.78 (dd, *J* = 8.3, 2.1 Hz, 1H, C(12)**H**), 7.16 (dd, *J* = 8.2, 0.6 Hz, 1H, C(13)**H**), 6.71 (d, *J* = 8.7 Hz, 2H, C(1)**H**), 6.67 (d, *J* = 2.4 Hz, 2H, C(4)**H**), 6.55 (dd, *J* = 8.7, 2.4 Hz, 2H, C(3)**H**), 4.17 (d, *J* = 2.4 Hz, 2H, C(20)**H**₂), 3.83 (d, *J* = 10.9 Hz, 2H), 3.73 – 3.68 (m, 6H), 2.82 (t, *J* = 2.4 Hz, 1H, C(22)**H**). ¹³C NMR (75 MHz, MeOD-*d*₄): δ 183.03 (C₈), 171.31 (C₁₅), 154.30 (C₂), 130.48, 125.82, 113.78, 111.61, 103.65, 76.22 (C₂₂), 71.28 (C₂₁), 70.29, 59.22 (C₂₀), 45.60. R_f (30:5:3 EtOAc/MeOH/H₂O): 0.65. HRMS (ESI): exact mass calculated for C₂₈H₂₅N₂O₇SH ([M+H]⁺): 533.1377. Found: 533.1377.

Coupling of 5-FITC to propargylamine

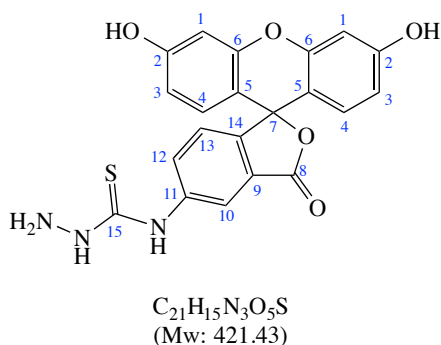
To a stirred solution of 5-FITC (1.0 equiv) in dry DMF were successively added propargylamine (1.5 equiv) and triethylamine (4 equiv). The reaction mixture was stirred at r.t. for 12h. At completion, the reaction mixture was evaporated to dryness and used crude.

1-(3',6'-dihydroxy-3-oxo-3H-spiro[isobenzofuran-1,9'-xanthen]-5-yl)-3-(prop-2-yn-1-yl)thiourea⁴⁴⁹
[944721-38-4]



Prepared with quantitative yield. ^1H NMR (300 MHz, MeOD- d_4): δ 8.21 – 8.13 (m, 1H), 7.64 (dd, J = 8.4, 2.1 Hz, 1H), 7.07 (dd, J = 8.3, 0.6 Hz, 1H), 6.70 – 6.60 (m, 4H), 6.53 (dd, J = 8.7, 2.4 Hz, 2H), 5.29 – 5.24 (m, 1H), 5.17 (td, J = 2.8, 1.6 Hz, 1H), 4.95 (s, 4H), 4.75 (t, J = 2.6 Hz, 2H). ^{13}C NMR (75 MHz, MeOD- d_4): δ 171.59 (C₈), 161.62 (C₁₅), 154.26 (C₂), 147.25, 130.24, 129.44, 127.68, 125.78, 115.29, 113.71, 111.76, 103.50 (C₁₈), 87.97 (C₁₇), 58.32 (C₁₆). MS (ESI): exact mass calculated for C₂₄H₁₅N₂O₅S⁻ ([M-H]⁻): 443.08. Found: 443.0.

Synthesis of Fluorescein-5-thiosemicarbazide⁴⁵⁰ [76863-28-0]



To a 0.25 M solution of hydrazine in distilled water (6 equiv) was added dropwise a 0.2% fluorescein isothiocyanate solution in bicarbonate-carbonate buffer pH 9.0 (1 equiv) with stirring.

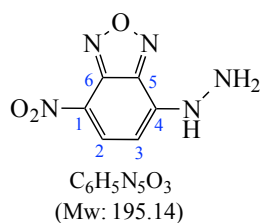
The mixture was stirred at r.t. for 1h, after what pH was adjusted to 3-4 with 2N HCl, and the resulting precipitate was collected by filtration and dried. Prepared with 56% yield.

^1H NMR (300 MHz, DMSO- d_6) δ 10.23 – 10.15 (m, 3H, 2xNH and OH), 9.40 (s, 1H, OH), 8.50 (s, 1H, C(10)H), 8.04 – 7.95 (m, 1H, C(12)H), 7.18 (dd, J = 14.1, 8.3 Hz, 1H, C(13)H), 6.67 (d, J = 2.1 Hz, 2H, C(1)H), 6.58 (d, J = 2.0 Hz, 4H, C(3)H and C(4)H), 2.02 (d, J = 8.1 Hz, 2H, NH₂). MS (ESI): mass calculated for C₂₁H₁₄N₃O₅S ([M-H]): 420.43. Found: 420.40.

Synthesis of (NBD-H) by coupling of NBD-Cl and hydrazine⁴⁵¹

NBD-Cl (1.0 equiv) was dissolved in chloroform (0.5 ml/mg). A 1% hydrazine solution (48.3 equiv, 0.77ml hydrazine in 50 ml MeOH) was then added and the reaction mixture was stirred at r.t. for 2h. A brown precipitate formed, that was isolated by filtration and used without further purification.

4-hydrazinyl-7-nitro-2,1,3-benzoxadiazole [90421-78-6]



Prepared with 72% yield. ¹H NMR (300 MHz, D₂O): δ 7.07 (dd, *J* = 10.6, 0.6 Hz, 1H), 6.48 – 6.37 (m, 1H).

c. Side project molecule : the ketone trap

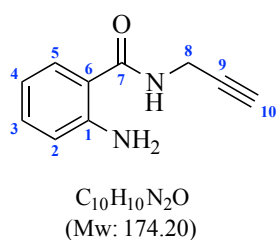
As stated in the *Conclusions & perspectives*, we have imagined a strategy to extract ketone-containing molecules from biological samples and concentrate them. As preliminary work, we have synthesized the compound below. This molecule has many advantages : it can give off blue fluorescence to be traced easily, it bears an alkyne moiety to be immobilised (on solid phase or beads) via click chemistry linkage, and its free amine could react with ketones to form imines later reduced to amines hence permanently trapping ketone-containing molecules.

Procedure for the preparation of 2-amino-*N*-prop-2-ynylbenzamide

Isatoic anhydride (1 equiv) was dissolved in DMF (approx. 3ml/mmol substrate) and heated to 50°C. Propargylamine (1.52 equiv) was then added and the mixture was stirred at 50°C for 3h. The reaction could be followed by TLC, revealed under UV light ($\lambda = 254$ nm).

At completion the solvent was removed. The resulting orange oil was taken up in H₂O (approx. 10ml/mmol substrate), and the pH adjusted to 9 with 1M NaOH. Organics were extracted with DCM (x3), dried over MgSO₄, and the solvent removed. The crude product could be purified by flash Chromatography with gradient elution from 1:4 to 4:1 EtOAc/Cyhex.

2-amino-*N*-prop-2-ynylbenzamide **37** [4943-83-3]



Prepared with 71% yield. ^1H NMR (300 MHz, CDCl_3): δ 7.33 (dd, $J = 7.9, 1.5$ Hz, 1H), 7.22 (dd, $J = 7.2, 1.5$ Hz, 1H), 6.71 – 6.61 (m, 2H), 6.23 (s, 1H, NH), 5.54 (s, 2H, NH_2), 4.20 (d, $J = 2.6$ Hz, 2H, NHCH_2), 2.27 (t, $J = 2.6$ Hz, 1H, $\text{C}\equiv\text{CH}$). ^{13}C NMR (75 MHz, CDCl_3): δ 169.02 (C_7), 149.06 (aromatic C), 132.80 (aromatic C), 127.34 (aromatic C), 117.51 (aromatic C), 115.10 (aromatic C), 79.81 (C_9), 71.85 (C_{10}), 29.55 (C_8). HRMS (ESI) : exact mass calculated for $\text{C}_{10}\text{H}_{10}\text{N}_2\text{O}$ ($[\text{M}+\text{H}]^+$): 175.0866. Found: 175.0865.

A.2. Usual Biochemical Assays

LDH release assay

The assay is based on the catalysis of the reduction of pyruvate into lactate in presence of NADH by the LDH contained in the sample (cell lysate or supernatant). As shown in Figure 95, NADH is oxidized in NAD^+ through this reaction, hence by following the decrease in absorbance at 340 nm due to NADH consumption one can relate the slope of decrease to the LDH concentration.

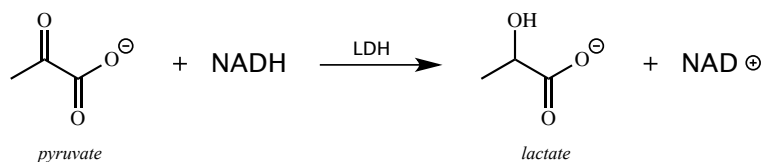


Figure 95 – LDH-catalysed oxidation of NADH into NAD^+

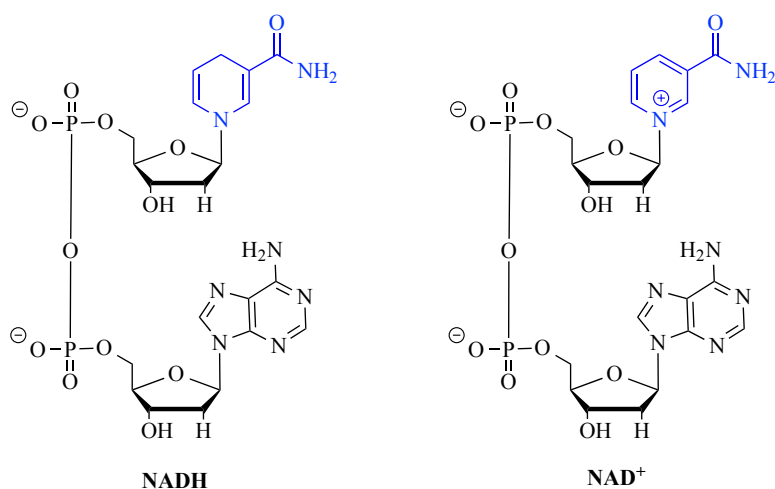


Figure 96 - Structures of NADH and NAD^+

Protein concentration determination in cell lysate by BCA assay

This assay is used to determine proteins concentration in a sample, which is linked to the number of cells initially present. It relies on the ability of proteins to transform Cu(II) into Cu(I) under basic conditions. The released Cu(I) ion will then form a stable complex with bicinchoninic acid (BCA), whose apparition and accumulation in the medium can be measured by monitoring absorbance at 560 nm. To quantify the amount of complex formed, a calibration curve is previously established using bovine serum albumin (BSA) as a reference compound to correlate amount of protein content (μg) and observed absorbance.

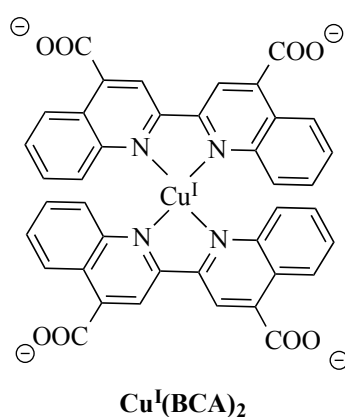


Figure 97 – Structure of copper (I) complex with BCA

ELISA immunoassay

The Enzyme-Linked Immunosorbent Assay (ELISA) is an analytical biochemistry assay based on a solid-phase enzyme immunoassay to quantitatively detect the presence of a ligand (usually a protein) in a liquid sample. Most commonly in the “sandwich” ELISA method, the surface of the well is coated with a primary antibody (capture antibody), and non-specific binding sites are blocked with a solution of non-reacting proteins such as bovine serum albumin. The ligand-containing sample is then added to the well, and captured by the antibody. A secondary antibody (the detection antibody) specific to the target ligand and bearing a biotin is added to the well, forming a sandwich complex in which the ligand is trapped in between the two antibodies. The biotin is then detected by addition of a streptavidin attached to horseradish peroxidase enzyme (Sav-HRP), which catalyses the oxidation of TMB tetramethylbenzidine) in presence of

hydrogen peroxide to produce a blue compound. The reaction is finally quenched by addition of sulfuric acid H₂SO₄ that turns the reaction yellow and absorbance is read at 450 nm.

A calibration curve is always inserted in the plate with known amounts of the target ligand to determine the quantitative relation between Optical Density and ligand concentration.

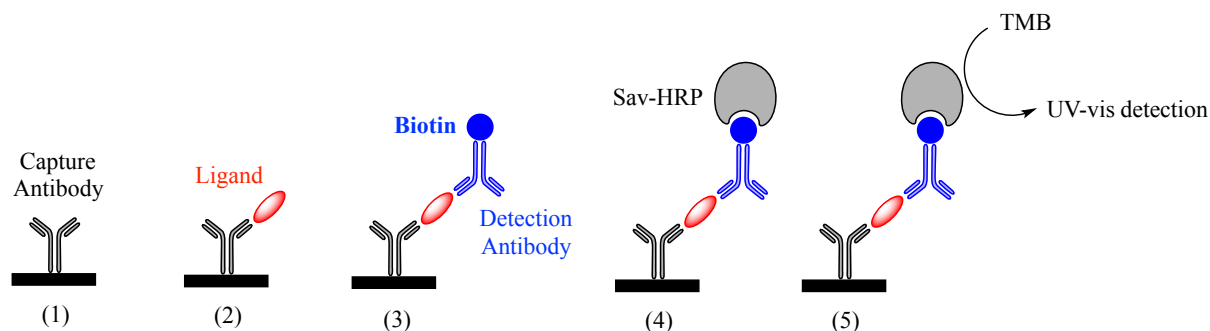


Figure 98 - Description of the ELISA steps

A.3. Scientific communications related to this PhD work

a. Oral communications

The following communications were achieved during the course of the PhD:

- “*Implications of N-Acyl Homoserine Lactones in Inflammatory Bowel Diseases*”, ENS 2018 Young Researchers Day. 05/03/2018, Paris, France.
- “*Chemical Modulation of Quorum Sensing Molecules from the Gut Microbiota & Impact on Gastrointestinal Epithelial Cells*”, Journée de la Montagne Ste-Geneviève 2018. 05/06/2018, Paris, France.
- “*Chemical Modulation of Quorum Sensing Molecules from the Gut Microbiota & Impact on Intestinal Epithelial and Immune Cells*”, Journées de l’Ecole Doctorale 394 2019. 20-21/05/2019, Paris, France.

b. Posters

The following posters were presented during the course of the PhD:

- “*Implications of N-Acyl Homoserine Lactones in Inflammatory Bowel Diseases*”, Journées de l’Ecole Doctorale 394 2017. 27-28/04/2017, Paris, France.
- “*Chemical Modulation of N-Acyl Homoserine Lactones and Impact on Intestinal Epithelial Cells*”, Journées de l’Ecole Doctorale 394 2018. 22-23/05/2018, Paris, France.
- “*Chemical Modulation of N-Acyl Homoserine Lactones and Impact on Intestinal Epithelial and Inflammatory Cells*”, 55th International Conference on Medicinal Chemistry (RICT 2019). 3-5/07/2019, Nantes, France.
- “*Chemical Modulation of N-Acyl Homoserine Lactones and Impact on Intestinal Epithelial and Inflammatory Cells*”, IUPAC International Conference 2019. 5-12/07/2019, Paris, France.

c. Publications

The results from this PhD are currently undergoing review as part of a patent submission. Consequently they have not yet been divulged through scientific publication. This patent is entitled « ANALOGUES DE N-ACYL-HOMOSERINE LACTONES ET COMPOSITION PHARMACEUTIQUE LES COMRENANT » and is registered under the reference number FR 1911861.

In parallel, a review “*The Microbiome in IBD*” dealing with gut microbiota and its modifications during the course of IBD has been published as a book chapter of “Biomarkers in Inflammatory Bowel Diseases” from Nik Sheng Ding & Peter De Cruz, 2019.

The review can be found below.



Agathe Peyrottes, Phillippe Seksik, Joël Doré,
and Philippe Marteau

Abstract

In individuals with IBD, the microbiome occupies an integral juncture between their genetics and disease profile and may participate to the manifestations of the disease and the severity of its course. This chapter will highlight major microbiome research studies showing the pathobionts and symbionts in the human micro-

biome associated with IBD. It will also include a brief outline of various bacterial, viral and fungal sequencing techniques, including 16S rRNA and hiSeq, along with a post-processing interpretation of the data to arrive at potential biomarkers of IBD. It will also cover the major microbial signatures found in association with IBD, including postoperative recurrence of Crohn's and the occurrence of pouchitis.

A. Peyrottes
Sorbonne Université, École normale supérieure,
CNRS, INSERM ERL 1157, APHP Laboratoire des
Biomolécules (LBM), Paris, France

Laboratoire des Biomolécules, Département de
chimie, École normale supérieure, UPMC Univ. Paris
06, CNRS, PSL Research University, Paris, France

Sorbonne Université, École normale supérieure,
CNRS, Laboratoire des Biomolécules (LBM),
Paris, France

P. Seksik · P. Marteau (✉)
Sorbonne Université, École normale supérieure,
CNRS, INSERM ERL 1157, APHP Laboratoire des
Biomolécules (LBM), Paris, France

Sorbonne Université, École normale supérieure,
CNRS, Laboratoire des Biomolécules (LBM),
Paris, France

Services d'Hépatologie, de Gastroentérologie et
nutrition, APHP, Hôpital Saint Antoine, Paris, France
e-mail: philippe.marteau@aphp.fr

J. Doré
MGP MetaGenoPolis et Micalis Institute, INRA,
AgroParisTech, Université Paris-Saclay,
Jouy-en-Josas, France

24.1 Introduction

Microorganisms present in the gastrointestinal tract (the microbiome) interact with each other and with host cells in both health and disease (including IBD). Their death, survival and development are controlled by environmental factors such as diet, antibiotics and inflammation. Hence, the presence or absence of certain microorganisms may be used as a bioindicator of ecological selective pressures, including those resulting from disease. Molecular methods have revolutionised our ability to describe changes in the microbiota. Microorganisms (which include bacteria, archaea, yeast, fungi and viruses/bacteriophages) have many functions. They secrete bioactive molecules, transform exogenous or endogenous molecules and are sensed by host cell receptors, such as NOD-like and Toll-like receptors. There is thus great value in the pursuit of

disease markers in (or from) the microbiome and as therapeutic targets in IBD, which we review in the present chapter. To date, ecological description tools are not used in clinical practice but are only available to researchers. Individual data on qualitative and quantitative measurements of microbiota (“microbial profiles”) are not sufficiently standardised to guarantee their accuracy and reliability, although this may happen soon.

24.2 Overview of the Gut Microbiome in IBD: Description and Potential Role in Pathogenesis

Many tools can be used to describe the microbiota, its genetic potential and its metabolic activity (respectively, the metagenome, transcriptome, proteome and metabolome). Most studies of the bacterial composition of the gut microbiome have used a 16S rRNA gene-based approach. This allows characterisation of the microbiome at the family or genus level and includes the quantitative polymerase chain reaction (qPCR) and restriction fragment length polymorphism (RFLP) or pyrosequencing. A higher resolution can be reached using shotgun sequencing (brands such as Illumina, Ion Proton, PacBio, etc.). Microbial diversity can be assessed within a day for numerous samples in parallel for costs that have steadily diminished, currently reaching approximately 50€ for 16S rDNA and 500€ for shotgun sequencing. In the context of research, it is commonly applied to assess the microbiome in cohort studies and clinical trials.

The microbiota differs between niches in the gastrointestinal tract. This is because segments vary in their ecological conditions as measured by pH, gastrointestinal transit time, the availability of nutrients and the presence of bile acids and substrates for adhesion. The microbial composition of faeces varies from chime microbiota in the right colon [27] to mucosa-adherent microbiota present in the ileum and entire colon of both healthy people and those with IBD [15, 19, 22]. Micro-biomarkers of IBD have been found in both faecal and mucosal biopsy samples.

The role of the microbiota in IBD pathogenesis has been approached through interventional studies and descriptive studies in human and animal models. Interventional studies have tested the influence of candidate microorganisms on cells, tissues or animals. They have also studied the consequences of altering the microbiota in patients or animals by administering antibiotics, prebiotics, fibres or probiotics and faecal transplantation. The main features that suggest the microbiota’s role in the pathogenesis of IBD are summarised in Table 24.1. The main dysbiotic characteristics repeatedly observed in IBD cases are shown in Table 24.2.

Pathogens or pathobionts are rarely observed in IBD, and treatments that attempt to eradicate or limit them have little effect on IBD symptoms and lesions. Some microbes are significantly less represented in IBD, especially those from the *Firmicutes* phylum [15, 36, 46]. The dominant *Firmicutes* from the *Clostridium* cluster IV, *F. prausnitzii*, belongs to the core microbiota in the vast majority

Table 24.1 Main arguments for the role of the microbiota in IBD

	Animal models	Humans
Arguments	<p>Researchers have not been able to induce experimental IBD in germ-free animals</p> <p>Some microbiota are more colitogenic than others [28]</p>	<p>IBD lesions predominate where bacteria are most abundant (at the end of the ileum and the colon)</p> <p>Genetic polymorphisms associated with IBD risk factors include genes involved in bacterial recognition and/or autophagy [17, 20, 35, 39]</p> <p>The microbiota of IBD patients differs from that of healthy participants (dysbiosis)</p> <p>Metronidazole and ciprofloxacin are effective treatments for pouchitis</p> <p>The probiotic mixture VSL #3 is effective in preventing the recurrence of pouchitis</p> <p>The transfer of faecal microbiota is an effective treatment for UC</p>

Table 24.2 Main dysbiotic features repeatedly observed in IBD

Rate of occurrence	Dysbiotic features
Very often	Unstable composition of the dominant microbiota over time Decreased microbial richness Restricted biodiversity, especially among <i>Firmicutes</i> Decreased proportions of <i>Faecalibacterium prausnitzii</i> , <i>Roseburia</i> spp., <i>Butyricoccus pullicaecorum</i> or <i>Akkermansia</i> spp.
Often	Increase in <i>Enterobacteriaceae</i> including adherent invasive <i>Escherichia coli</i> (AIEC) associated with the ileal mucosa in ileal CD Increase in H ₂ S producers [31] Increase in fusobacteria in patients with UC
Sometimes	Acquisition of <i>Clostridium difficile</i> Presence of <i>Mycobacterium avium paratuberculosis</i> during CD

of healthy humans. Research has shown that it is lower in individuals with UC and CD [45]. However, this finding was more significant in CD, especially ileal CD. The concentration of *F. prausnitzii* often mirrors that of *Enterobacteriaceae* [23], and the ratio of *E. coli* to *F. prausnitzii* is a proposed method for assessing dysbiosis in CD [3, 45]. The microorganism *F. prausnitzii* can lower the production of pro-inflammatory cytokines IL-12 and IFN- γ and can increase IL-10 secretion in peripheral blood mononuclear cells. It can also block the NF- κ B pathway in intestinal cell lines. Its in vivo anti-inflammatory effects and that of its culture supernatant have been demonstrated in mice with TNBS-induced colitis [43].

Levels of butyrate-producing bacteria are often lower in people with IBD compared with healthy controls. These groups encompass *Roseburia* [24, 38], *Eubacterium* [38] and *F. prausnitzii* [24]. Butyrate has several anti-inflammatory effects on the intestine [7, 9, 41, 47, 50]. Levels of *Akkermansia muciniphila*, a member of the phylum *Verrucomicrobia*, may be low in individuals with UC. Experimental studies have shown that it reinforces the epithelial barrier at tight junctions and has very little pro-inflammatory effect on epithelial cells.

Several studies have shown differences in the microbiota (either faecal or mucosa-associated) between UC, ileal CD and colonic CD. In addition to different genetic risk factors and phenotypes, this strongly suggests that these are three different diseases [15, 21, 24, 32]. For instance, several groups have reported that levels of *F. prausnitzii* were lower and levels of *Enterobacteriaceae* were higher in ileal CD than in colonic CD [32], regardless of the biopsy site.

Ecological alterations in IBD affect archaea, bacteriophages and fungi in addition to bacteria [14]. Sokol and colleagues studied the bacterial and fungal compositions of samples of faeces from 235 participants (IBD patients and healthy controls) using 16S and ITS2 sequencing. They observed that the fungal microbiota was skewed in IBD, with an increased *Basidiomycota/Ascomycota* ratio, a decrease in *Saccharomyces cerevisiae* and an increase in *Candida albicans* [44].

The microbiota and host cooperate to transform endogenous and exogenous substrates; hence candidate metabolites and the metabolome are sources of potential micro-biomarkers. For example, the faecal concentrations of conjugated bile acids (BA) were found to be significantly higher in active colonic IBD, whereas that of secondary BA were significantly lower. Additionally, in IBD, decreased concentrations of isomerised forms of BA, including isolithocholic acid (iso-LCA), isodeoxycholic acid (iso-DCA) and ursodeoxycholic acid (UDCA), are observed. The ratio of iso-LCA to LCA in faeces has been shown to have a strong correlation with dysbiosis, IBD activity and IBD diagnosis [4].

24.3 Microbial Signatures and Other Microbial Biomarkers in Clinical Situations of IBD

The presence or absence of a single microorganism or metabolite is not specific enough to be a signature of IBD, but some combinations of microbial variables described below have interesting biomarker characteristics.

24.3.1 Associations with Crohn's Disease

Gevers et al. conducted a pioneering and impressive work on a large series of children with previously untreated IBD. They studied the faecal- and mucosa-associated microbiota and inferred a taxon–taxon interaction network [15]. After observing that some groups tended to exhibit co-occurrence while others exhibited co-exclusion, the authors proposed a microbial dysbiosis index (MD-index). They chose to calculate this arbitrarily as the log of the total abundance of organisms increased in CD over the total abundance of organisms decreased in CD. They took samples at different sites to evaluate how well the MD-index classified the CD state of participants using a receiver-operating characteristic (ROC) analysis. The best performances were obtained for ileal mucosa biopsy samples (AUC = 0.85) and rectal biopsy samples (AUC = 0.78), while faecal samples did not perform that well (AUC = 0.66). In another paediatric series with prospective longitudinal microbial follow-up, the MD-index was significantly correlated with severity of IBD, but not with treatment response [42].

Further evidence of the association between specific microorganisms and CD was from studies by V. Pascal and colleagues. They analysed faecal samples from a large cohort of IBD and non-IBD participants using 16S rRNA sequencing with the aim of developing an algorithm to discriminate between those who had CD and those who did not [36]. Eventually, the algorithm retained samples that did not contain “*Faecalibacterium* or *Peptostreptococcaceae* and *Anaerostipes* and *Christensenellaceae*” or those that contained “*Fusobacterium* and *Escherichia* but not *Collinsella* and *Methanobrevibacter*”. The algorithm was tested on several data banks and obtained an average of 77.7% true positives for CD detection and an average of 7.3% and 12.8% false positives for healthy controls and UC patients, respectively. However, when applied to a French cohort, its accuracy was only 64% when discriminating between CD and UC (60% sensitivity and 68% specificity) and 77% when discriminating between CD and healthy controls (60%

sensitivity and 94.8% specificity). There is therefore clear hope that consensual micro-biomarkers will soon be found, although the critical step of standardising methods is not yet complete [10].

24.3.2 Association with Early Recurrence of Ileal Crohn's Lesions After Surgery

In CD, lesions may recur early after surgery (i.e. less than 1 year) in a large proportion of patients, and several authors have wondered if microbial characteristics at the time of surgery (especially in the surgical specimen) could help predict this outcome. Only a small series of patients have been studied.

A study of 21 participants by H. Sokol and colleagues found that a higher level of *F. prausnitzii* in the ileal mucosa of surgical specimens was associated with a lower risk of early postoperative recurrence [43]. In a study of six participants, at the time of surgery, the microbiota of CD patients who remained in remission had more richness and was more similar to controls than that of patients with subsequent recurrence [13]. In a series of studies on 12 participants, De Cruz and colleagues showed that patients with recurrent disease harboured more *Enterococcus* and *Veillonella* spp., while those maintaining remission had higher levels of *Bacteroides*, butyrate-producing *Firmicutes* and *Prevotella* and *Parabacteroides* spp. [12]. Mondot and colleagues studied whether the microbiota composition of faeces collected from 20 participants just before surgery could help predict recurrence [30]. They found that four specific molecular species had biomarker potential. The presence of *Coprococcus catus* and a relative of Clostridiales bacterium (*Butyricicoccus* genus) were significantly associated with the absence of recurrence. The presence of *Proteus mirabilis* and a relative of *Eubacterium rangiferina* were associated with future postoperative recurrence. Wright and colleagues studied the differences in taxa observed in the surgical specimens of 34 participants. Patients who had early endoscopic recurrence had higher levels of members of the *Firmicutes*

phylum, the *Bacteroides* genus and the *Bacteroidaceae* and *Pasteurellaceae* families than those without recurrence [52].

24.3.3 Associations with IBD Activity and Severity

Some authors have investigated the correlation of faecal microbial profiles as biomarkers to distinguish between CD patients in remission and those with active disease. For example, Tedjo D.I. and colleagues conducted a longitudinal study in which they collected faecal samples from CD patients in remission and during active disease. A random forest analysis highlighted 50 OTUs (or bacterial taxa) as able to discriminate between remission and active disease, with a sensitivity of 0.79 and a specificity of 0.73. As expected, *F. prausnitzii* was associated with remission [48]. Varela and colleagues used quantitative real-time PCR to determine the total faecal bacteria counts of *F. prausnitzii* in 116 UC patients in remission, 29 first-degree relatives and 31 healthy controls [49]. They found lower counts of *F. prausnitzii* in UC patients and their unaffected relatives compared to healthy controls (faecal counts of 1.4×10^8 copies/g and 1.7×10^8 copies/g vs 6.5×10^8 copies/g). Patients who had experienced a disease flare less than 12 months before the study had lower counts of *F. prausnitzii* compared to patients with longer remission. Faecal counts of *F. prausnitzii* $< 10^8$ copies/g increased the probability of having a relapse within 12 months fourfold ($p < 0.001$).

24.3.4 Prediction of Pouchitis

Machiels and colleagues collected faecal samples from 21 patients with UC before colectomy and ileal pouch anal anastomosis (IPAA) and at regular intervals for the following 12 months. They observed that the presence of *R. gnavus*, *B. vulgatus* and *C. perfringens* and the absence of *Blautia* and *Roseburia* in faecal samples before surgery were associated with a higher risk of developing pouchitis [25]. In line with this,

N. Maharshak and colleagues used 16S rRNA gene pyrosequencing to analyse the faecal microbiota of 20 patients with a normal pouch after IPAA. They compared samples collected before the development of pouchitis in some patients ("pre-pouchitis group", $n = 7$) with those collected from patients who did not develop pouchitis ($n = 13$). Genera *Ruminococcus*, *Lachnospira* and *Coprococcus* were significantly lower in pre-pouchitis patients than in the other group [26].

24.3.5 Microbial Markers of Primary Sclerosing Cholangitis (PSC)

Bajer and colleagues reported that PSC was associated with specific gut microbes independently of concomitant IBD. They analysed the faecal composition of 31 healthy controls, 32 UC patients without PSC and 43 patients who had PSC with concomitant IBD ($n = 2$) and without ($n = 11$). They found that *Rothia*, *Enterococcus*, *Streptococcus*, *Veillonella* and three other genera were markedly overrepresented in PSC regardless of concomitant IBD. They tracked *Rothia*, *Veillonella* and *Streptococcus* to the species level, and this allowed them to identify *Rothia mucilaginoso*, *Streptococcus infantis*, *S. alactolyticus* and *S. equi* along with *Veillonella parvula* and *V. dispar*. The microbiome in PSC was also characterised by decreased abundance of *Adlercreutzia equolifaciens* and *Prevotella copri*. A decrease in the genus *Phascolarctobacterium* was linked to the presence of colonic IBD. In patients with UC, *A. muciniphila*, *Butyrivococcus pullicaecorum* and *Clostridium colinum* were decreased along with the genus *Roseburia* [2].

24.3.6 Theragnostics

S. Rajca and colleagues studied the composition of gut microbiota in patients from a prospective cohort trial designed to identify predictive factors of clinical relapse after discontinuation of infliximab in CD. They collected faecal samples from 33 patients with CD at baseline, at 2 months, at 6 months and at the end of the follow-up period. Of these, 19

relapsed and 14 did not. Low percentages of *F. prausnitzii* and *Bacteroides* were associated with a high risk of relapse independently of a high concentration of serum C-reactive protein (CRP) [37]. Ananthkrishnan and colleagues conducted a prospective study with CD and UC patients starting vedolizumab therapy. Community α -diversity was significantly higher, and *Roseburia inulinivorans* and a species of *Burkholderiales* were more abundant at baseline in CD patients who later entered remission with Vedolizumab treatment [1].

24.4 Therapeutic Strategies to Manipulate the Gut Microbiota in IBD

Researchers have documented four ways of influencing the microbiota in IBD [5], which include the use of antibiotics, prebiotics and fibres, probiotics and faecal microbiota transplantation (FMT). The current use of these approaches is very limited (Table 24.3), but randomised controlled trials (RCTs) are increasing, and some of these have yielded positive results. During these treatments, the endogenous microbiota is influenced by ecological selection pressure. After this has occurred, the microbiota may either keep some of its new characteristics or move back to its dysbiotic composition (resilience). These findings are summarised below.

24.4.1 Antibiotics

Antibiotics may promote dysbiotic features including *Clostridium difficile* infection and the promotion of antibiotic resistance. The use of antibiotics early in life has been reported as a significant risk factor of IBD in the western world and a protective factor in Asia [33]. The (few) indications for antibiotics in IBD are shown in Table 24.3.

24.4.2 Prebiotics and Fibres

As *F. prausnitzii* is reduced in patients ingesting low amounts of fibre, it is quite possible that low

Table 24.3 Indications of treatments targeting the microbiota in IBD (according to ECCO guidelines) [16, 18]

IBD type	Indications
Crohn's disease	<p>Antibiotics are considered appropriate for septic complications, perineal disease or symptoms due to small bowel bacterial overgrowth</p> <p>Anti-mycobacterial treatment cannot be recommended based on the results of controlled trials</p> <p>A double-blind clinical trial recently tested rifaximin in patients with moderately active CD. A dose of 800 mg of rifaximin appeared to be more effective than a placebo in achieving remission, but dosages of 400 and 1200 mg did not. No confirmation of this data is available</p> <p>Ciprofloxacin has been shown to significantly increase the efficacy of adalimumab in the healing of perianal fistulas. Other data has confirmed its utility in perianal disease</p> <p>Trials testing probiotics and prebiotics have been negative</p>
Ulcerative colitis	<p>Antibiotics are recommended only when an infection is suspected (i.e. in a short-term first attack, after recent admission to hospital or after travel to an amoebiasis-endemic area) or immediately before surgery</p> <p>There is some evidence for the therapeutic benefit of probiotics when added to standard therapy to induce remission, particularly VSL #3</p> <p>Results of RCTs evaluating faecal microbiota transfer are encouraging. These support the use of FMT to induce remission in active UC</p> <p>Data on the use of antibiotics to maintain remission was considered to be insufficient by the ECCO consensus (2016)</p> <p>A total of three RCTs comparing <i>E. coli</i> Nissle 1917 to 5-ASA suggested that this probiotic was not inferior to 5-ASA for the maintenance of remission in UC</p> <p>No evidence has been reported that any other probiotic is effective for maintaining remission</p>
Pouchitis	<p>The majority of patients respond to metronidazole or ciprofloxacin, but the optimal modality of these treatments is not clearly defined</p> <p>In chronic pouchitis, a treatment combining these antibiotics is effective</p> <p>The probiotic mixture VSL #3 is effective in maintaining antibiotic-induced remission and in preventing pouchitis</p>

Table 24.4 Methods and efficacy of FMT in active UC (results of four RCTs)

	Rossen et al. [40]	Moayeddi et al. [29]	Paramsothy et al. [34]	Costello et al. [11]
N° of patients (verum/ placebo)	23/25	38/37	41/40	38/35
Placebo	Autologous faeces	Water	Coloured water	Autologous faeces
Treatment duration (weeks)	12	6	8	8
N° of FMT	2	6	40	3
Route of administration	Nasoduodenal	Enemas	Coloscopy then enemas	Coloscopy then enemas
Donor(s)	Single	Single	Pool of 3 to 7	Pool of 3 to 4
Remission verum vs placebo	30%/20% $p = 0.51$	24%/5% $p = 0.03$	27%/8% $p = 0.02$	32%/9% $p < 0.01$
Response verum vs placebo	48%/52% $p = 0.58$	39%/24% $p = 0.16$	54%/23% $p < 0.01$	55%/20% $p < 0.01$

fibre diets (which are often recommended to patients suffering from IBD) participate in dysbiosis. A prebiotic is a substrate (usually a sugar but some polyphenols are also of interest) that is undigested in the small intestine that increases the populations of microorganisms supposedly beneficial in the colon [51]. The most studied have been fructans (fructo-oligosaccharides (FOS) and inulin). The few therapeutic trials of these agents in IBD have shown poor tolerance and no efficacy [5, 6, 51]. Such drawbacks were expected considering that these substances are fermentable oligosaccharides, disaccharides, monosaccharides and polyols (FODMAPs). This should not discourage researchers, and studies for other products and/or doses are ongoing.

24.4.3 Probiotics and Faecal Microbiota Transplantation

In RCTs on probiotics, researchers have shown that VSL #3 is effective in preventing pouchitis and that *E. coli* Nissle 1917 is effective in preventing relapse of UC. Studies testing probiotics in patients with CD have been negative [5]. Receipt of FMT from a healthy donor or from a pool of donors is effective in patients with recurrent *Clostridium difficile* infection [8]. The results of controlled trials in participants with active UC are encouraging, as shown in Table 24.4 [11]. However, there are many issues for researchers to resolve before patients, clinicians

and society can validate or refute this treatment. Currently, there are only few examples of the use of this technique in IBD, but this could soon change. Studies targeting pathogens or pathobionts such as *Mycobacterium avium paratuberculosis* or AIEC should be performed in patients carrying these microorganisms (and probably not on those who do not carry them).

24.5 Unmet Needs and Future Directions

Microorganisms living in the inflammatory environment seem to be good bioindicators that integrate the ecological disturbances of IBD. Researchers should not consider the candidate markers presented here in relation to causality in IBD. Instead, they should consider only their marker characteristics. We have shown here that several candidates could be “micro-biomarkers” of IBD, but proper validation requires large-scale studies with longitudinal assessment of candidate markers and the consideration of potential confounders. As the microbiota is influenced by diet, age, ethnicity, etc., it is possible that micro-biomarkers could vary between countries. This should be anticipated, properly assessed and should not discourage research and development. We must also guarantee that the medical value of these markers will not be affected by drugs, antibiotics and bowel preparation. It is likely that

markers with a suspected link to disease causes or mechanisms will also be used as surrogate markers for clinical trials. For example, trying to improve *F. prausnitzii* concentration, restore richness and diversity or robustness makes sense for intestinal ecologists. To improve their sensitivity/specificity, future predictive models of IBD could encompass a combination of both microbiomarkers and bio-clinical parameters.

Summary Points

- Alterations of the microbiota (dysbiosis) occur in IBD, and some features differ significantly between healthy participants, patients with ileal CD, patients with colonic CD, patients with UC and patients with primary sclerosing cholangitis (PSC).
- These may serve as bioindicators (as they integrate ecologic pressure due to disease burden) and may be used to develop diagnostic algorithms.
- Confounding factors, including ethnicity, diet and medical treatments must be studied.
- The Dysbiosis Microbiota Index for identifying ileal CD from rectal biopsies (even when the rectum is normal) and the Pascal Index for CD are promising.
- Large-scale international studies with proper controls and phenotyping of specific situations are required.

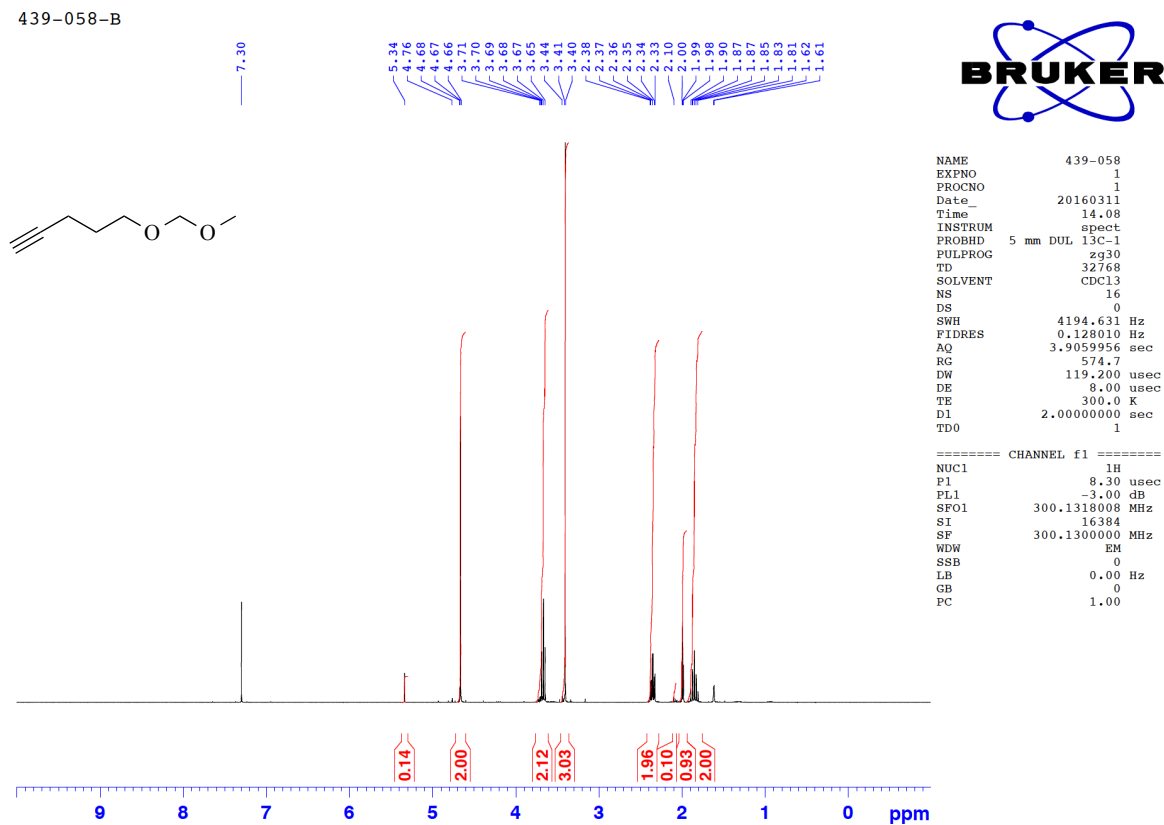
References

1. Ananthakrishnan A, et al. Gut microbiome function predicts response to anti-integrin biologic therapy in inflammatory bowel diseases. *Cell Host Microbe*. 2017;21(5):603–10.
2. Bajer L, et al. Distinct gut microbiota profiles in patients with primary sclerosing cholangitis and ulcerative colitis. *World J Gastroenterol*. 2017;23(25):4548–58.
3. Balzola F, et al. Connecting dysbiosis, bile-acid dysmetabolism and gut inflammation in inflammatory bowel diseases. *Inflammatory Bowel Disease Monitor*. 2012;13(2):73.
4. Bazin T, et al. A simple biomarker for IBD associated dysbiosis: the ratio of Iso-LCA/LCA indicates alteration of isomeration of bile acids in the intestinal lumen. *Gastroenterology*. 2015;148(4 Suppl 1):S–718.
5. Bejaoui M, Sokol H, Marteau P. Targeting the microbiome in inflammatory bowel disease: critical evaluation of current concepts and moving to new horizons. *Dig Dis*. 2015;33(Suppl 1):105–12.
6. Benjamin JL, et al. Randomised, double-blind, placebo-controlled trial of fructo-oligosaccharides in active Crohn's disease. *Gut*. 2011;60(7):923–9.
7. Blottière HM, et al. Molecular analysis of the effect of short-chain fatty acids on intestinal cell proliferation. *Proc Nutr Soc*. 2003;62:101–6.
8. Cammarota G, et al. European consensus conference on faecal microbiota transplantation in clinical practice. *Gut*. 2017;66(4):569–80.
9. Canani RB, et al. Potential beneficial effects of butyrate in intestinal and extraintestinal diseases. *World J Gastroenterol*. 2011;17(12):1519–28.
10. Costea PI, et al. Towards standards for human fecal sample processing in metagenomic studies. *Nat Biotechnol*. 2017;35(11):1069–76.
11. Costello SP, et al. Systematic review with meta-analysis: faecal microbiota transplantation for the induction of remission for active ulcerative colitis. *Aliment Pharmacol Ther*. 2017;46(3):213–24.
12. De Cruz P, et al. Association between specific mucosa-associated microbiota in Crohn's disease at the time of resection and subsequent disease recurrence: a pilot study. *J Gastroenterol Hepatol*. 2015;30(2):268–78.
13. Dey N, et al. Association of gut microbiota with post-operative clinical course in Crohn's disease. *BMC Gastroenterol*. 2013;13(131):1–11.
14. Filyk HA, Osborne LC. The microbiome: the intestinal ecosystem's influence on immune homeostasis, health, and disease. *EBioMedicine*. 2016;13:46–54.
15. Gevers D, et al. The treatment-naïve microbiome in new-onset Crohn's disease. *Cell Host Microbe*. 2014;15(3):382–92.
16. Gomollón F, et al. 3rd European evidence-based consensus on the diagnosis and management of Crohn's disease 2016: part 1: diagnosis and medical management. *J Crohn's Colitis*. 2017;11(1):3–25.
17. Hampe J, et al. A genome-wide association scan of nonsynonymous SNPs identifies a susceptibility variant for Crohn disease in ATG16L1. *Nat Genet*. 2007;39(2):207–11.
18. Harbord M, et al. Third European evidence-based consensus on diagnosis and management of ulcerative colitis. Part 2: current management. *J Crohn's Colitis*. 2017;11(7):769–84.
19. Harrell L, et al. Standard colonic lavage alters the natural state of mucosal-associated microbiota in the human colon. *PLoS One*. 2012;7(2):e32545.
20. Hugot JP, et al. Association of NOD2 leucine-rich repeat variants with susceptibility to Crohn's disease. *Nature*. 2001;411(6837):599–603.
21. Imhann F, et al. Gene-microbiome interactions underlying the onset and the clinical phenotypes

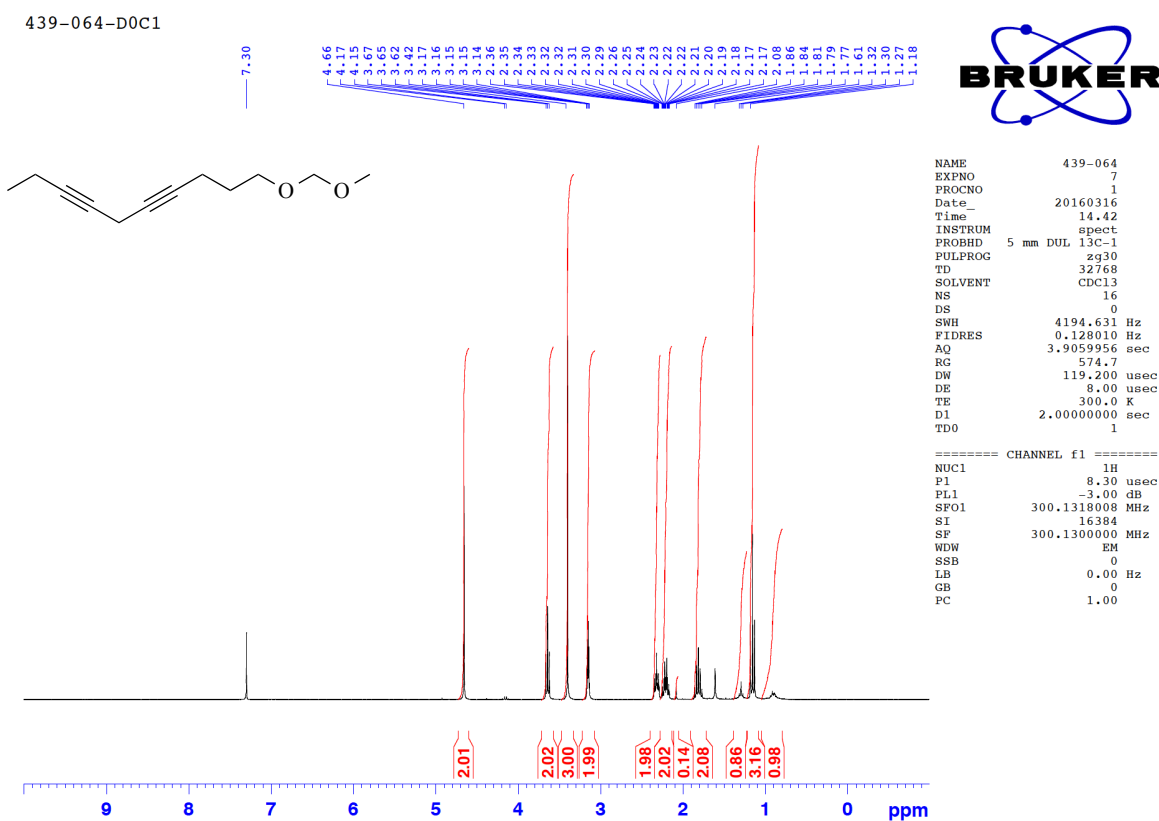
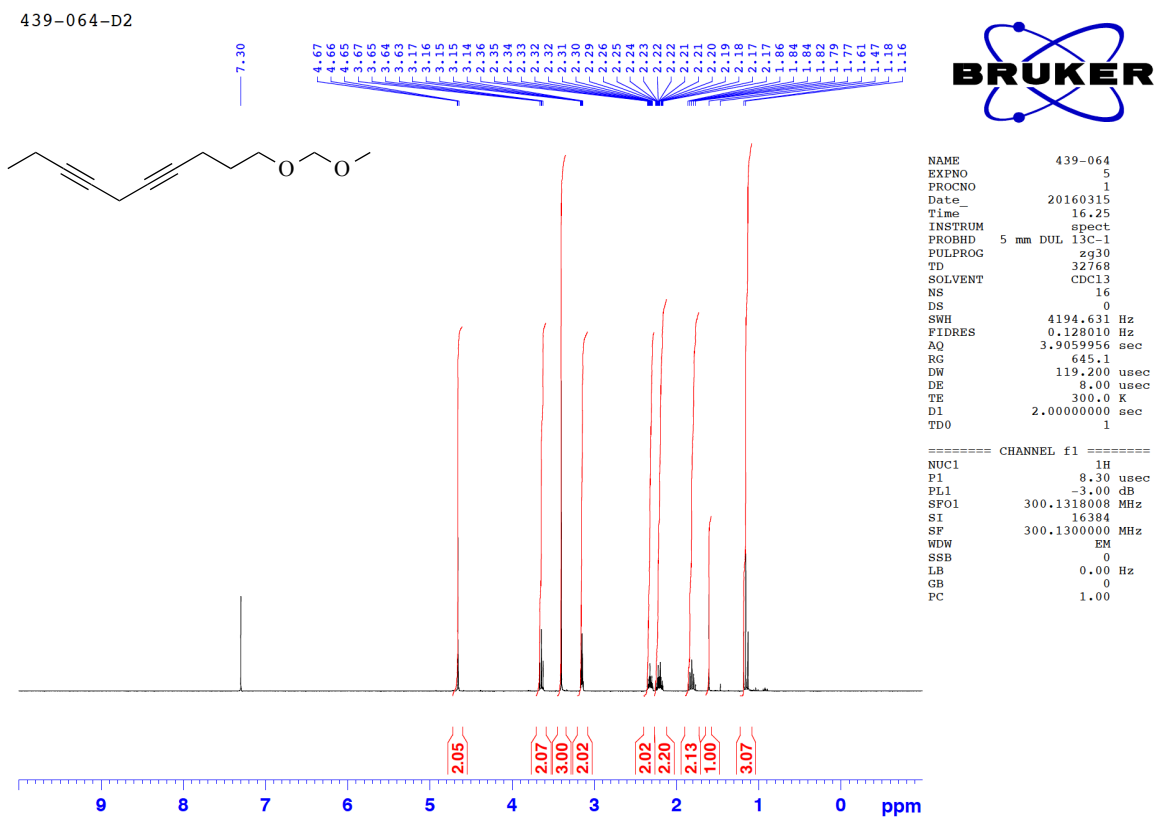
- of inflammatory bowel disease. *Gastroenterology*. 2016;150(4):S22.
22. Lepage P, et al. Biodiversity of the mucosa-associated microbiota is stable along the distal digestive tract in healthy individuals and patients with IBD. *Inflamm Bowel Dis*. 2005;11(5):473–80.
 23. Lepage P, et al. Twin study indicates loss of interaction between microbiota and mucosa of patients with ulcerative colitis. *Gastroenterology*. 2011;141(1):227–36.
 24. Machiels K, et al. A decrease of the butyrate-producing species *Roseburia hominis* and *Faecalibacterium prausnitzii* defines dysbiosis in patients with ulcerative colitis. *Gut*. 2014;63(8):1275–83.
 25. Machiels K, et al. Specific members of the predominant gut microbiota predict pouchitis following colectomy and IPAA in UC. *Gut*. 2017;66(1):79–88.
 26. Maharshak N, et al. Alterations of enteric microbiota in patients with a normal ileal pouch are predictive of pouchitis. *J Crohn's Colitis*. 2017;11(3):314–20.
 27. Marteau P, et al. Comparative study of bacterial groups within the human cecal and fecal microbiota comparative study of bacterial groups within the human cecal and fecal microbiota. *Appl Environ Microbiol*. 2001;67(10):4939–42.
 28. Metwaly AA, et al. Identification of disease-relevant bacterial signatures in gnotobiotic IL-10 deficient mice using fecal samples from IBD patients undergoing hematopoietic stem cell transplantation. *Gastroenterology*. 2017;152(5):S989.
 29. Moayyedi P, et al. Fecal microbiota transplantation induces remission in patients with active ulcerative colitis in a randomized controlled trial. *Gastroenterology*. 2015;149(1):102–9.
 30. Mondot S, et al. Structural robustness of the gut mucosal microbiota is associated with Crohn's disease remission after surgery. *Gut*. 2016;65(6):954–62.
 31. Mottawea W, et al. Altered intestinal microbiota-host mitochondria crosstalk in new onset Crohn's disease. *Nat Commun*. 2016;7:13419.
 32. Naftali T, et al. Distinct microbiotas are associated with ileum-restricted and Colon-involving Crohn's disease. *Inflamm Bowel Dis*. 2016;22(2):293–302.
 33. Ng SC, et al. Worldwide incidence and prevalence of inflammatory bowel disease in the 21st century: a systematic review of population-based studies. *Gastroenterology*. 2017;152(5):S970–1.
 34. Paramsothy S, et al. Multidonor intensive faecal microbiota transplantation for active ulcerative colitis: a randomised placebo-controlled trial. *Lancet*. 2017;389(10075):1218–28.
 35. Parkes M, et al. Sequence variants in the autophagy gene IRGM and multiple other replicating loci contribute to Crohn's disease susceptibility. *Nat Genet*. 2007;39(7):830–2.
 36. Pascal V, et al. A microbial signature for Crohn's disease. *Gut*. 2017;0:1–10.
 37. Rajca S, et al. Alterations in the intestinal microbiome (dysbiosis) as a predictor of relapse after infliximab withdrawal in Crohn's disease. *Inflamm Bowel Dis*. 2014;20(6):978–86.
 38. Rajilić-Stojanović M, et al. Phylogenetic analysis of dysbiosis in ulcerative colitis during remission. *Inflamm Bowel Dis*. 2013;19(3):481–8.
 39. Rioux JD, et al. Genome-wide association study identifies new susceptibility loci for Crohn disease and implicates autophagy in disease pathogenesis. *Nat Genet*. 2007;39(5):596–604.
 40. Rossen NG, et al. Findings from a randomized controlled trial of fecal transplantation for patients with ulcerative colitis. *Gastroenterology*. 2015;149(1):110–8.
 41. Segain J, et al. Butyrate inhibits inflammatory responses through NFκB inhibition: implications for Crohn's disease. *Gut*. 2000;47(3):397–403.
 42. Shaw KA, et al. Dysbiosis, inflammation, and response to treatment: a longitudinal study of pediatric subjects with newly diagnosed inflammatory bowel disease. *Genome Med*. 2016;8(1):75.
 43. Sokol H, et al. *Faecalibacterium prausnitzii* is an anti-inflammatory commensal bacterium identified by gut microbiota analysis of Crohn disease patients. *Proc Natl Acad Sci U S A*. 2008;105(43):16731–6.
 44. Sokol H, et al. Fungal microbiota dysbiosis in IBD. *Gut*. 2016:1–10. Available at: <http://gut.bmj.com/content/early/2016/02/03/gutjnl-2015-310746?paperoc>.
 45. Sokol H, Seksik P, Furet JP. Low counts of *Faecalibacterium prausnitzii* in colitis microbiota. *Inflamm Bowel Dis*. 2009;15(8):1183–9.
 46. Sokol H, Seksik P, Rigottier-Gois L. Specificities of the fecal microbiota in inflammatory bowel disease. *Inflamm Bowel Dis*. 2006;12(2):106–11.
 47. Tedelind S, et al. Anti-inflammatory properties of the short-chain fatty acids acetate and propionate: a study with relevance to inflammatory bowel disease. *World J Gastroenterol*. 2007;13(20):2826–32.
 48. Tedjo DI, et al. The fecal microbiota as a biomarker for disease activity in Crohn's disease. *Sci Rep*. 2016;6:35216.
 49. Varela E, et al. Colonisation by *Faecalibacterium prausnitzii* and maintenance of clinical remission in patients with ulcerative colitis. *Aliment Pharmacol Ther*. 2013;38(2):151–61.
 50. Vinolo MAR, et al. Regulation of inflammation by short chain fatty acids. *Nutrients*. 2011;3(10):858–76.
 51. Wong C, Harris PJ, Ferguson LR. Potential benefits of dietary fibre intervention in inflammatory bowel disease. *Int J Mol Sci*. 2016;17(6).
 52. Wright EK, et al. Microbial factors associated with postoperative Crohn's disease recurrence. *J Crohn's Colitis*. 2017;11(2):191–203.

A.4. NMR characterisation of the 3oxoC₁₂:2-HSL as provided by the commercial supplier DIVERCHIM

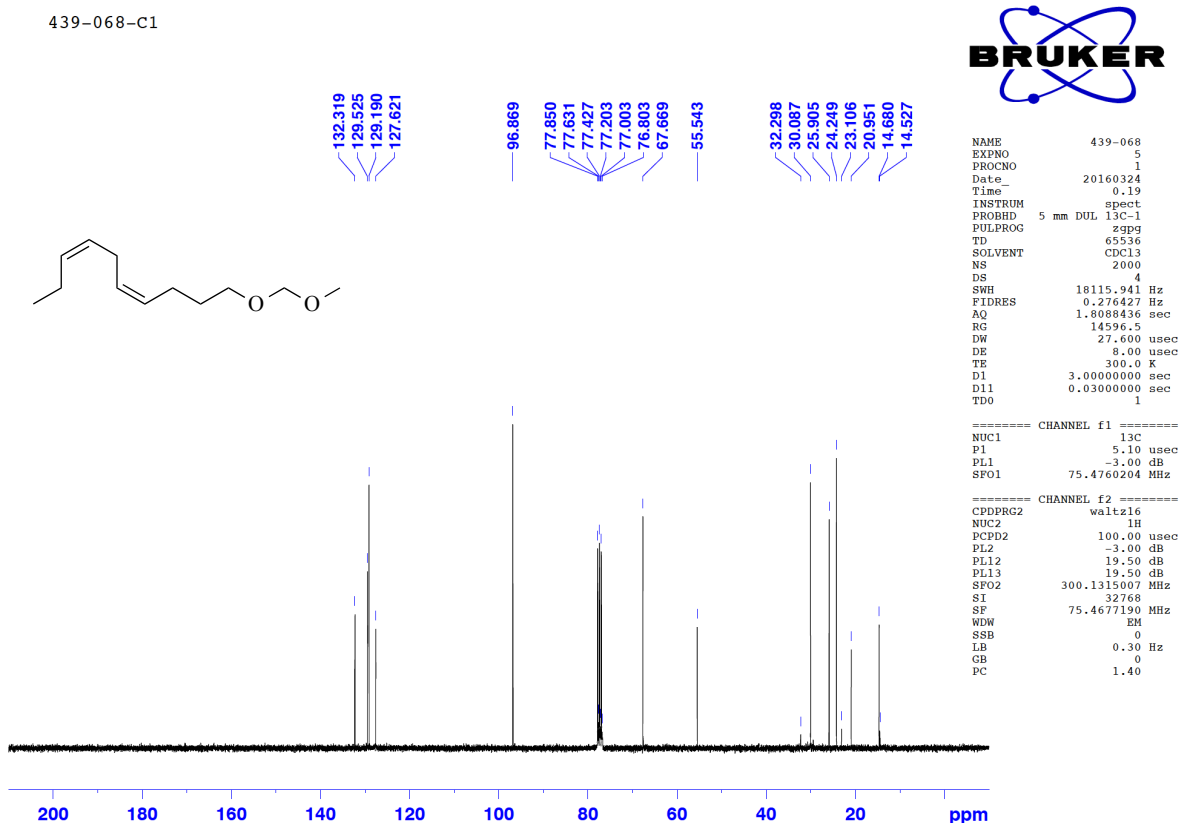
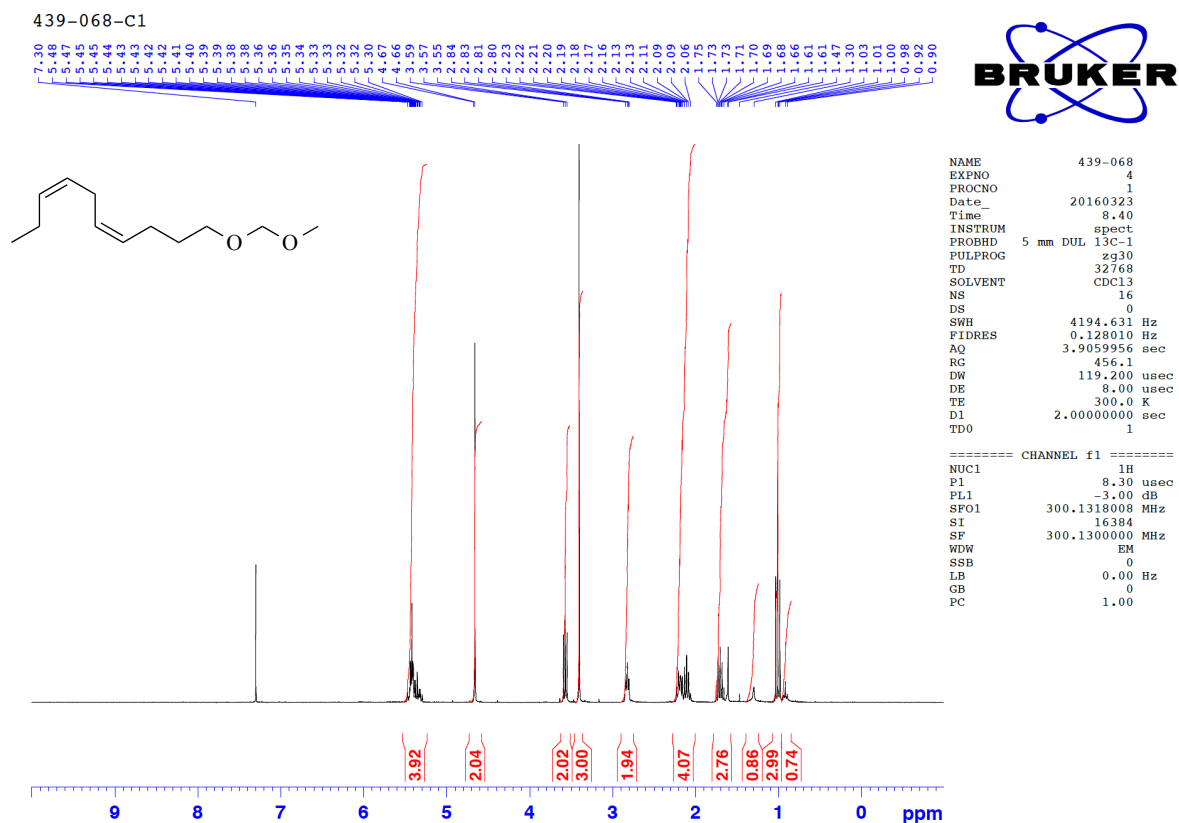
First intermediate : Formula C₇H₁₂O₂. Mw = 128.17 g/mol. Batch 439-058-B.



Second intermediate : Formula C₁₂H₁₈O₂. Mw = 194.28 g/mol. Batch 439-064-D2 & 439-064-D0C1.

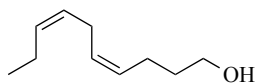


Third intermediate : Formula C₁₂H₂₂O₂. Mw = 198.31 g/mol. Batch 439-068-C1.



Fourth intermediate : Formula C₁₀H₁₈O. Mw = 154.25 g/mol. Batch 439-078-B.

439-078-B

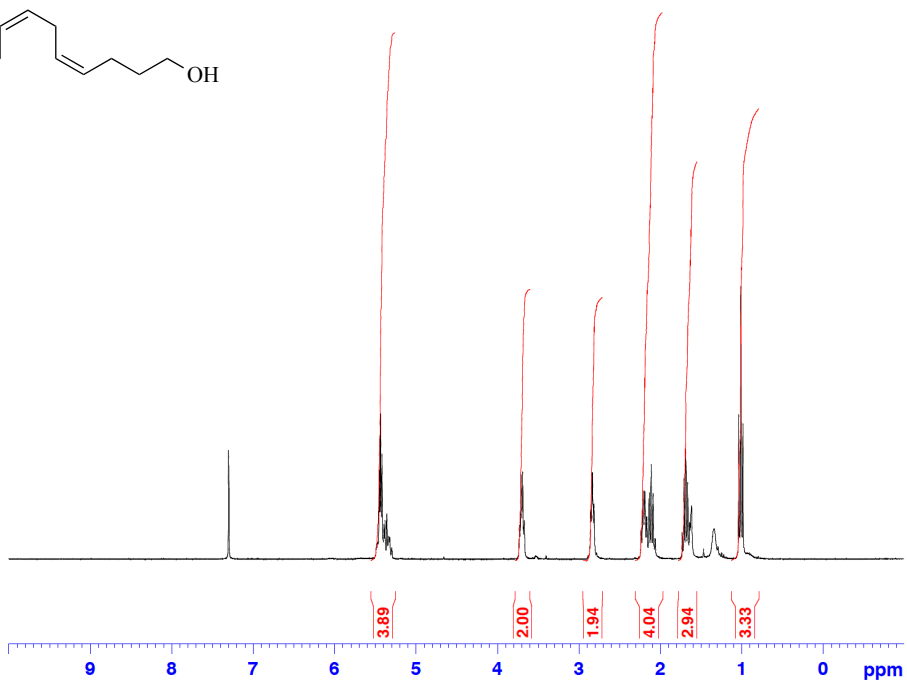


7.20
5.49
5.47
5.45
5.44
5.42
3.80
3.36
3.34
5.33
4.66
3.71
3.69
3.67
3.53
3.52
3.51
3.48
2.84
2.82
2.79
2.27
2.24
2.21
2.19
2.17
2.14
2.11
2.09
2.07
1.72
1.71
1.69
1.66
1.64
1.62
1.52
1.50
1.47
1.34
1.29
1.27
1.22
1.20



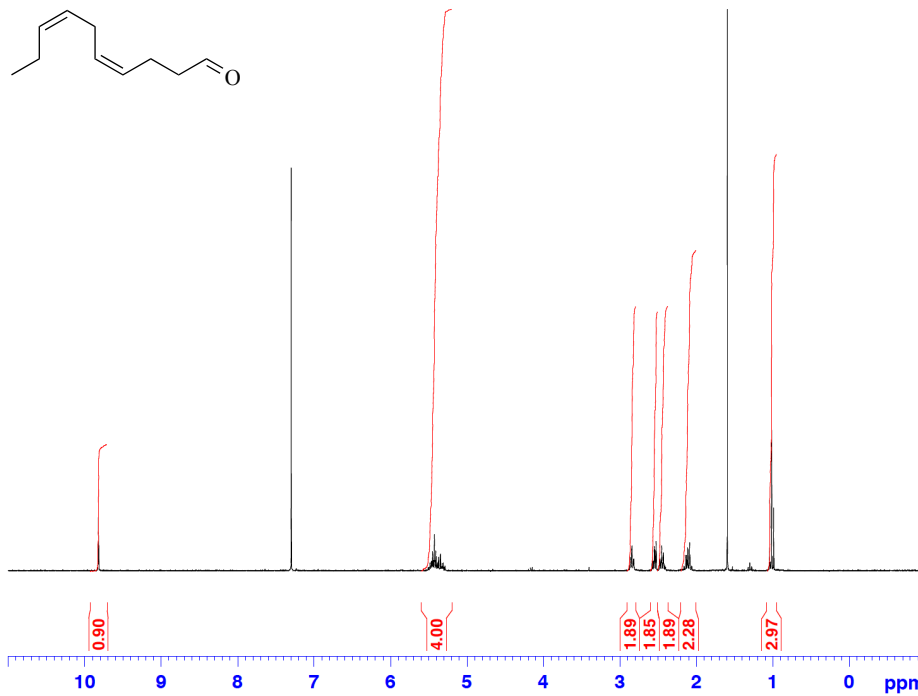
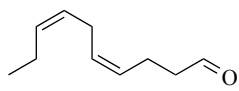
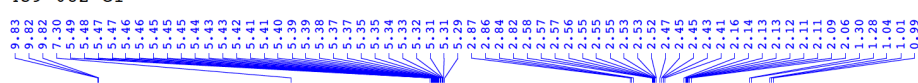
NAME 439-078
EXPNO 1
PROCNO 1
Date_ 20160324
Time 9.59
INSTRUM spect
PROBHD 5 mm DUL 13C-1
PULPROG zg30
TD 32768
SOLVENT CDCl3
NS 16
DS 0
SWH 4194.631 Hz
FIDRES 0.128010 Hz
AQ 3.9059956 sec
RG 574.7
DW 119.200 usec
DE 8.00 usec
TE 300.0 K
D1 2.00000000 sec
TDO 1

===== CHANNEL f1 =====
NUC1 1H
P1 8.30 usec
PL1 -3.00 dB
SF01 300.1318008 MHz
SI 16384
SF 300.1300000 MHz
WDW EM
SSB 0
LB 0.00 Hz
GB 0
PC 1.00



Fifth intermediate : Formula C₁₀H₁₆O. Mw = 152.24 g/mol. Batch 439-082-C1.

439-082-C1



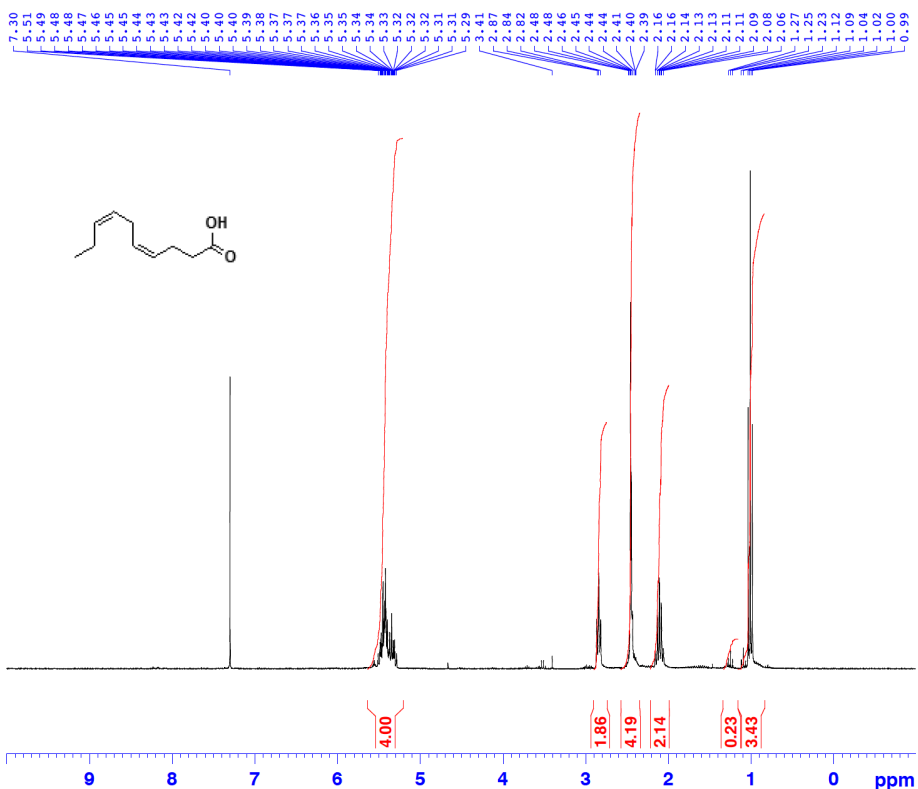
```

NAME          439-082
EXPNO         3
PROCNO        1
Date_         20160325
Time          16.32
INSTRUM       spect
PROBHD        5 mm DUL 13C-1
PULPROG       zg30
TD            32768
SOLVENT       CDCl3
NS            16
DS            0
SWH           4194.631 Hz
FIDRES        0.128010 Hz
AQ            3.9059956 sec
RG            1625.5
DW            119.2200 usec
DE            8.00 usec
TE            300.0 K
D1            2.00000000 sec
TD0           1

===== CHANNEL f1 =====
NUC1          1H
P1            8.30 usec
PL1           -3.00 dB
SFO1          300.1318008 MHz
SI            16384
SF            300.1300000 MHz
WDW           EM
SSB           0
LB            0.00 Hz
GB            0
PC            1.00
    
```


Sixth intermediate : Formula $C_{10}H_{16}O_2$. Mw = 168.24 g/mol. Batch 439-091-B.

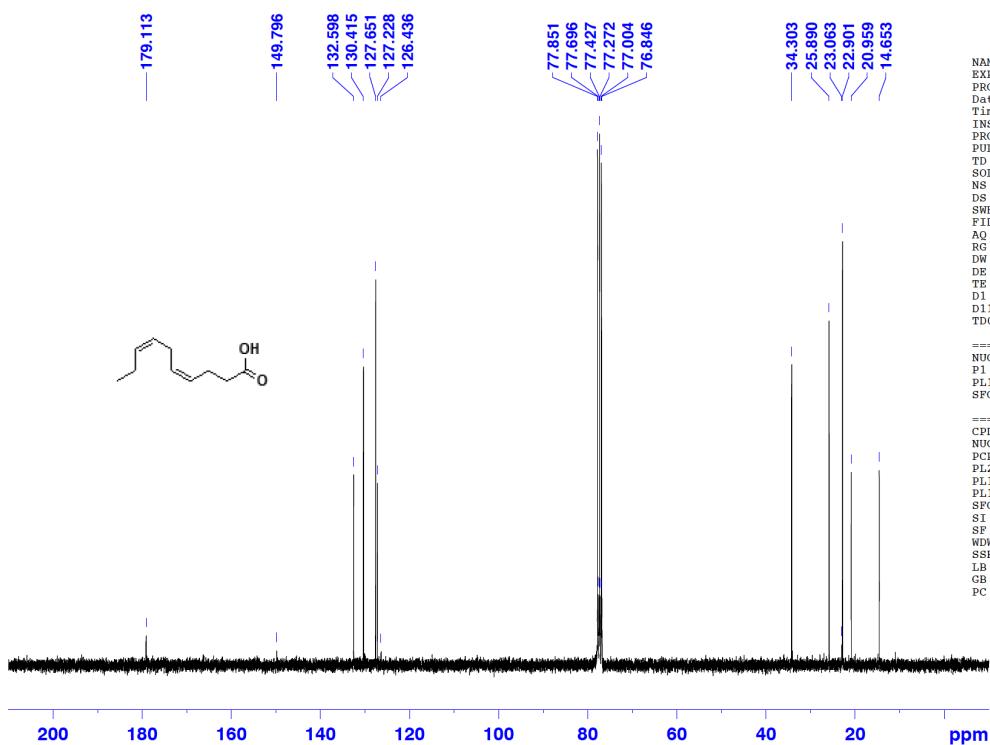
439-091-B



NAME 439-091
EXPNO 1
PROCNO 1
Date_ 20160330
Time 15.29
INSTRUM spect
PROBHD 5 mm DUL 13C-1
PULPROG zg30
TD 32768
SOLVENT CDCl3
NS 16
DS 0
SWH 4194.631 Hz
FIDRES 0.128010 Hz
AQ 3.9059956 sec
RG 574.7
DW 119.200 usec
DE 8.00 usec
TE 300.0 K
D1 2.00000000 sec
TD0 1

===== CHANNEL f1 =====
NUC1 1H
P1 8.30 usec
PL1 -3.00 dB
SFO1 300.1318008 MHz
SI 16384
SF 300.1300000 MHz
WDW EM
SSB 0
LB 0.00 Hz
GB 0
PC 1.00

439-091-B

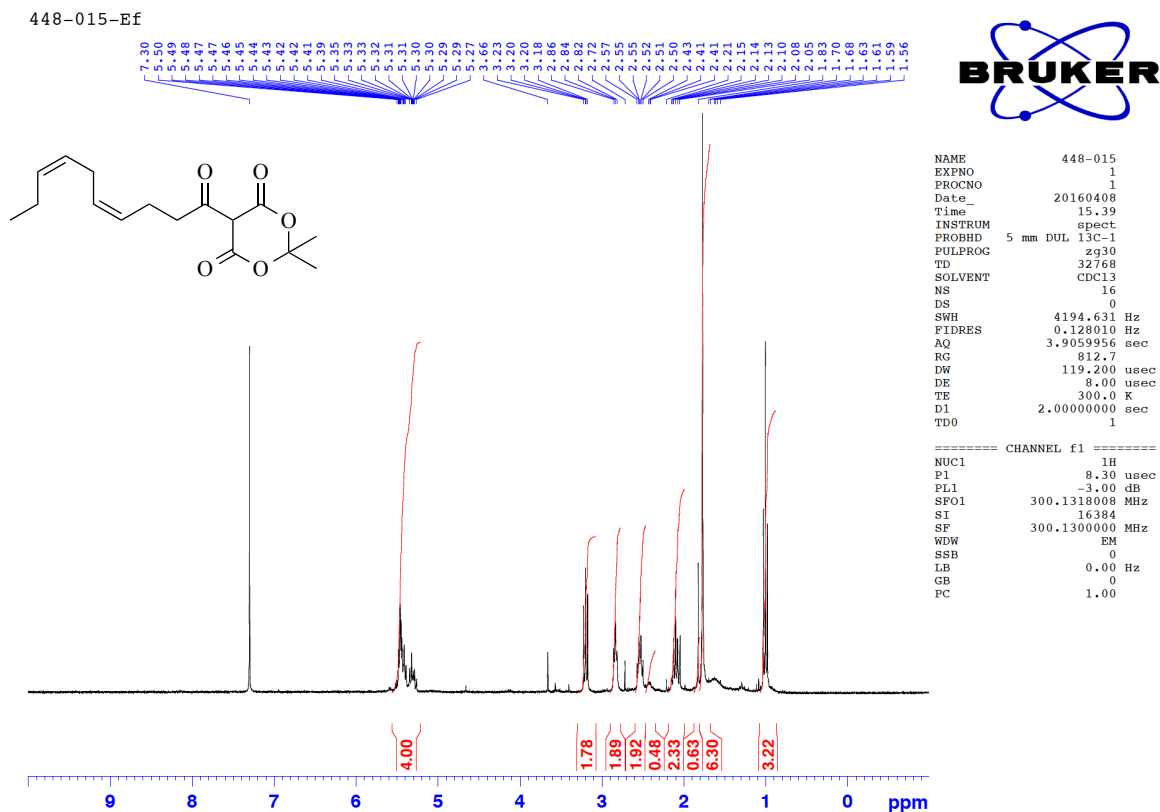


NAME 439-091
EXPNO 2
PROCNO 1
Date_ 20160330
Time 21.28
INSTRUM spect
PROBHD 5 mm DUL 13C-1
PULPROG zgpg
TD 65536
SOLVENT CDCl3
NS 2500
DS 4
SWH 18115.941 Hz
FIDRES 0.276427 Hz
AQ 1.8088436 sec
RG 16384
DW 27.600 usec
DE 8.00 usec
TE 300.0 K
D1 3.00000000 sec
D11 0.03000000 sec
TD0 1

===== CHANNEL f1 =====
NUC1 13C
P1 5.10 usec
PL1 -3.00 dB
SFO1 75.4760204 MHz

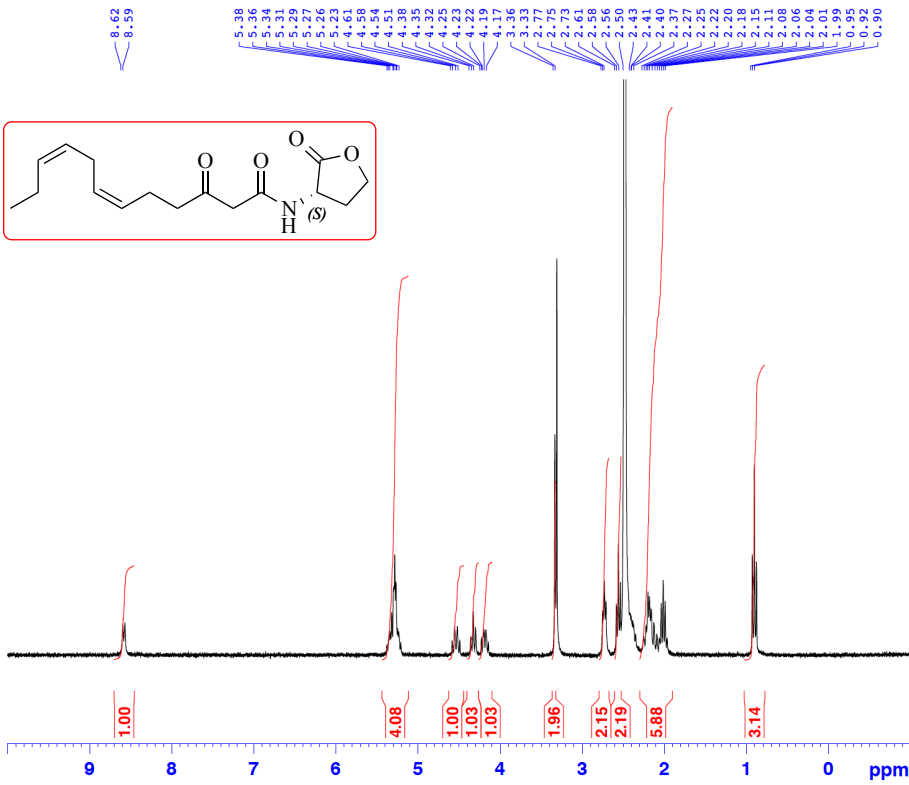
===== CHANNEL f2 =====
CPDPRG2 waltz16
NUC2 1H
PCPD2 100.00 usec
PL2 -3.00 dB
PL12 19.50 dB
PL13 19.50 dB
SFO2 300.1315007 MHz
SI 32768
SF 75.4677190 MHz
WDW EM
SSB 0
LB 0.30 Hz
GB 0
PC 1.40

Seventh intermediate : Formula C₁₆H₂₂O₅. Mw = 294.35 g/mol. Batch 448-015-Ef.



Eighth intermediate (final compound 3oxoC₁₂:2-HSL) : Formula C₁₆H₂₃NO₄. Mw = 293.37 g/mol. Batch 448-018-C1Es.

448-018-C1Es



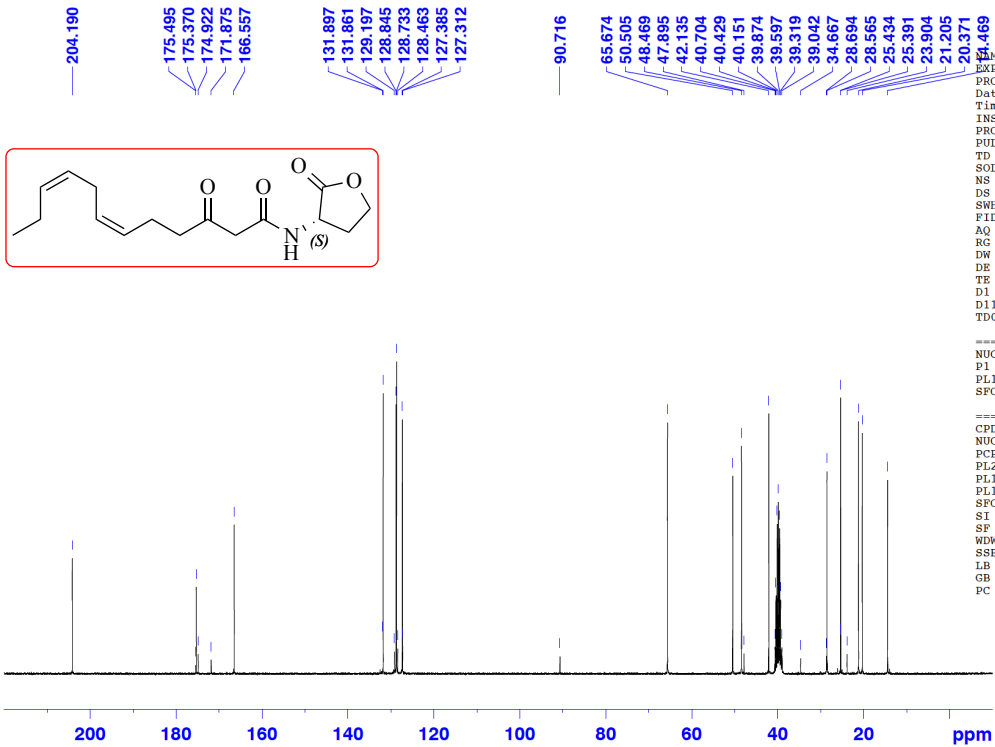
```

NAME      448-018
EXPNO     5
PROCNO    1
Date_     20160418
Time      12.16
INSTRUM   spect
PROBHD    5 mm DUL 13C-1
PULPROG   zg30
TD         32768
SOLVENT   DMSO
NS         16
DS         0
SWH       4194.631 Hz
FIDRES    0.128010 Hz
AQ        3.9059956 sec
RG         574.7
DW        119.200 usec
DE         8.00 usec
TE        300.0 K
D1        2.00000000 sec
TD0       1
  
```

```

===== CHANNEL f1 =====
NUC1      1H
P1        8.30 usec
PL1       -3.00 dB
SF01     300.1318008 MHz
SI        16384
SF        300.1300063 MHz
WDW       EM
SSB       0
LB        0.00 Hz
GB         0
PC        1.00
  
```

448-018-C1Es



```

NAME      448-018
EXPNO     6
PROCNO    1
Date_     20160420
Time      0.51
INSTRUM   spect
PROBHD    5 mm DUL 13C-1
PULPROG   zgpgg
TD         65536
SOLVENT   DMSO
NS         5000
DS         4
SWH       18115.941 Hz
FIDRES    0.276427 Hz
AQ        1.8088436 sec
RG         8192
DW        27.600 usec
DE         8.00 usec
TE        300.0 K
D1        3.00000000 sec
D11       0.03000000 sec
TD0       1
  
```

```

===== CHANNEL f1 =====
NUC1      13C
P1        5.10 usec
PL1       -3.00 dB
SF01     75.4760204 MHz

===== CHANNEL f2 =====
CPDPRG2   waltz16
NUC2      1H
PCPD2     100.00 usec
PL2       -3.00 dB
PL12     19.50 dB
PL13     19.50 dB
SF02     300.1315007 MHz
SI        32768
SF        75.4677567 MHz
WDW       EM
SSB       0
LB        0.30 Hz
GB         0
PC        1.40
  
```